FINAL SYSTEM REPORT

TIROS OPERATIONAL VERTICAL SOUNDER
BACIS SOUNDER UNIT

A
PROPOSAL
FROM

GULTON INDUSTRIES INC.

DATA SYSTEMS DIVISION • 15000 CENTRAL EAST, ALBUQUERQUE, N. M. 87112

73040501

QC
879.25
G8

FINAL SYSTEM REPORT

TIROS OPERATIONAL VERTICAL SOUNDER
BACIS SOUNDER UNIT

DESIGN DEFINITION STUDY

Contract No. 2-35402

February 28, 1973

ATMOSPHERIC SCIENCES
LIBRARY

MAY 1975

N.O.A.A.
U. S. Dept. of Commerce

Prepared for:

U. S. Department of Commerce
National Oceanic and Atmospheric Administration
National Environmental Satellite Service
P. O. Box 9227
Suitland, Maryland 20233

Robert H. Maschhoff, Project Manager
Gulton Industries, Inc.
Data Systems Division

15 1969

National Oceanic and Atmospheric Administration
TIROS Satellites and Satellite Meteorology

ERRATA NOTICE

One or more conditions of the original document may affect the quality of the image, such as:

Discolored pages
Faded or light ink
Binding intrudes into the text

This has been a co-operative project between the NOAA Central Library and the Climate Database Modernization Program, National Climate Data Center (NCDC). To view the original document contact the NOAA Central Library in Silver Spring, MD at (301) 713-2607 x124 or Library.Reference@noaa.gov.

HOV Services
Imaging Contractor
12200 Kiln Court
Beltsville, MD 20704-1387
January 26, 2009

FORWARD

This report summarizes the results of a design definition study of the TIROS Operational Vertical Sounder-Basic Sounder Unit (TOVS/BSU). The study was conducted by Gulton Industries, Incorporated, Data Systems Division, and by Beckman Instruments, Incorporated, Advanced Technology Operations, for the National Oceanic and Atmospheric Agency, National Environmental Satellite Service.

The principal objective of the study was to demonstrate that the stringent performance and reliability requirements for an operational sounder could be met. Although the TOVS/BSU is similar to the Infrared Temperature Profile Radiometer, now in orbit on NIMBUS 5, the accuracy requirements are more stringent and the orbit is more demanding from a radiometric point of view.

The principal conclusion of the study is that improvements in detector and interference filter technology, and a unique thermal approach make it possible to meet the performance requirements with a reliable design.

CONTENTS

SECTION 1 - SUMMARY 1-0

SECTION 2 - STUDY PROGRAM 2-0

SECTION 3 - OPTICAL SUBSYSTEM DESIGN 3-0

Subsection - Configuration 3-0
Subsection - Optical Design 3-12
Subsection - Mechanical Design Optics Subassembly 3-24

SECTION 4 - ANALYSIS OF OPTICAL PERFORMANCE 4-0

SECTION 5 - OPTICAL TESTING 5-0

Subsection - Description of Test Program 5-0
Subsection - Results of Tests Performed 5-8

SECTION 6 - DETECTORS AND ANALOG PROCESSING 6-0

SECTION 7 - SCANNER SUBSYSTEM DESIGN 7-0

Subsection - Summary 7-0
Subsection - Scan Mechanism Desing 7-10
Subsection - Design Verification 7-22
Subsection - Mechanical Details of the Scanner 7-32

SECTION 8 - DESCRIPTION OF ELECTRONICS SUBSYSTEMS 8-0

SECTION 9 - DESIGN OF POWER SUPPLY 9-0

SECTION 10- THERMAL ANALYSIS 10-0

SECTION 11- ANALYSIS OF RADIOMETRIC ACCURACY 11-0

SECTION 12- DESIGN OF INSTRUMENT PACKAGE 12-0

SECTION 13- STRUCTURAL DESIGN OF THE TOVS-BSU 13-0

SECTION 14- RELIABILITY PROGRAM 14-0

APPENDIX 1- RADIATION EFFECTS ON THE TIROS SPACECRAFT ELECTRONICS

APPENDIX 2- OUTLINE OF INTERFACE INTEGRATION DATA BETWEEN THE BASIC SOUNDING UNIT OF THE TOVS INSTRUMENT AND THE TIROS-N SPACECRAFT

APPENDIX 3- HARMONIC ANALYSIS OF TIROS SOUNDER SYSTEM, A SELF DOCUMENTING MATH MODEL PROGRAM

APPENDIX 4- DESIGN STUDY OF DICHROICS

APPENDIX 5- TOVS IMMERSED DETECTOR STUDY

SECTION 1
SUMMARY

Purpose and Functions of the Instrument 1-0
Summary of Principal Design Requirements..... 1-2
Key Features of the Instrument Design 1-4
Arrangement of the Instrument 1-8
Relation to Previous Instrument..... 1-12

PURPOSE AND FUNCTIONS OF THE INSTRUMENT

The proposed TIROS Operational Vertical Sounder-Basic Sounding Unit (TOVS/BSU) is a high-reliability spaceflight instrument for making radiometric measurements for the deduction of global atmospheric temperature profiles from the surface to 10 millibars pressure altitude.

The TOVS-BSU will fly aboard the TIROS-N satellite on a 906-nautical mile sun-synchronous orbit. The instrument performs a step scan perpendicular to the satellite's earth track which, in conjunction with the earth's rotation, provides complete earth coverage. The instrument field-of-view is small, providing the high resolution required to obtain useful soundings in the presence of partial cloud coverage. The intended useful lifetime of the instrument is two years.

The BSU measures radiation leaving the earth's atmosphere in the near and intermediate infrared regions of the electromagnetic spectrum. The instrument measures the radiation emerging from the top of the atmosphere in several spectral intervals ranging from the center of a molecular absorption band out to the wing of the band. Thermal energy measured near the opaque band center arises from higher altitudes because of the atmospheric absorption of the energy emitted at lower levels. Energy measured in the wing of an absorption band comes from lower altitudes because of the higher transparency of the upper atmosphere. If the distribution of the absorbing gas is known, the measured variation of outgoing radiation with wavelength can be interpreted in terms of the variation of atmospheric temperature with altitude.

The table opposite indicates the spectral regions of interest. Measurements made in the 15 μm CO_2 absorption band provide the basic radiance data for generating a temperature sounding. The relatively large number of channels in this region (7) provides compatibility with multi-layered atmospheric modeling programs. Measurements in other spectral regions provide for certain corrections to be made to the above radiance measurements. The effect of ozone absorption at 14.3 μm can be corrected by determining atmospheric ozone content using radiance data from the 9.6 μm band. Measurements in the water vapor rotation bands allow determination of a moisture profile which is in turn useful for further corrections.

The window channels function in conjunction with the small, half-power (FOV) of 1.125 degrees to provide for sounding in the presence of partial cloud cover. Smith has shown that if adjacent FOV elements have a different percentage of cloud cover (likely for small FOV's) then a solution for the average "clear column" radince may be obtained. When clouds exist in a FOV the 3.8 μm and 11 μm brightness temperatures differ. Small FOV's are necessary to make it likely that the average does not differ much from either FOV "clear column" radiance. The detector-signal processing system must provide data from adjacent FOVs that is statistically independent in order for the above solution to be valid.

SPECTRAL REGIONS OF INTEREST

Radiometric measurements in the listed spectral regions allow the deduction of an atmospheric temperature profile at pressure altitudes from 10 to 1000 millibars.

λ (μm)	Band	Function
3.8	IR Atmospheric Window	Surface Temperature
4.3	CO_2 Absorption	Temperature Profile
9.6	O_3 Absorption	Ozone Profile
11.1	IR Atmospheric Window	Surface Temperature
15	CO_2 Absorption	Temperature Profile
18-30	Water Vapor Rotation Bands	Moisture Profile

SUMMARY OF PRINCIPAL DESIGN REQUIREMENTS

Very accurate radiometric measurements in 14 channels which cover the important spectral bands with accurate registration of the fields of view of each channel must be made to obtain satisfactory atmospheric soundings.

Spectral radiance measurements are required at 14 different wavelengths to obtain soundings of the atmospheric temperature and moisture profiles. The 14 channels used to obtain the soundings lie in the spectral wavelength range from 3.8 to 29 μm, and have the closely specified center wavenumber and spectral bandwidths given in Table 1. From 11 to 15 μm (channels 4-11) the required spectral bandwidth is only about 2 percent. Channel 11 is located at the narrow maximum of the CO_2 absorption (Q-branch). Because of the high absorption at this wavelength, this channel can see only the highest altitudes. The channel bandwidth must be made small to correspond to the narrowness of the absorption band.

The moisture profile channels (12, 13, 14) have longer wavelengths (18.8 - 29.0 μm). Especially at 29 μm, advanced interference filter technology and the use of somewhat different imaging techniques are necessary to provide the desired selection.

The most important design requirement is the stability and accuracy with which the measurements in these channels must be made. Measurements in each channel must be made with the accuracy listed in Table II. Because the full-scale radiance is specified to be that of a 330°K blackbody, the accuracy typically required corresponds to only 0.05-0.1% of full scale, or to a noise-equivalent temperature difference of about 0.08°K (worst case, channel 4).

To eliminate errors from detector sensitivity changes, stray light, and mirror emissions, provision must be made for periodic calibration by the viewing of space and the calibration blackbody.

The optical system is required to maintain a precise alignment because the relative error between the pointing direction of the various channels must be less than 0.01 degree to attain the desired registration and independence of measurements. The optics and the electronics must be designed to prevent detectable crosstalk between channels or memory from scene to scene.

To achieve the required accuracy within the stated constraints on field of view, weight, and envelope, it is necessary to design a light collection and detection scheme having a very low noise-equivalent spectral radiance and a very high rejection of stray light. It is also necessary to pay close attention to thermal effects which might induce errors between channels after the in-flight calibration. The location of the BSU on the sunny side of the spacecraft allows the sunlight to enter directly into the scanner cavity during a substantial portion of the TIROS orbit at certain times of the year, leading to temperature variations within the instrument. Stability and accurate measurement of the in-flight calibration blackbody temperatures are essential, and the thermal and optical design must assure that other temperature variations do not lead to unacceptable drifts. The scanner must step and settle accurately in a fraction of the allowed 100-ms measurement interval and must retrace at nearly 100 pulses per second to provide the 8.0-second line period required. It must operate continuously for two years.

The detailed performance requirements for the Basic Sounder Unit are contained in NOAA/NESS Specification 10040-101, Technical Specification for a Design Study of the TIROS Operational Vertical Sounder (TOVS), Revision B, dated 1/31/72. The reader should consult this specification for further details.

TABLE I. TOVS-BSU SPECTRAL CHANNEL ASSIGNMENTS

The narrow bandwidth at the absorption maximum at 669 cm^{-1} is a particularly critical requirement, since it permits accurate high-altitude soundings.

Channel No.	Centroid Wave Number cm^{-1}	Spectral Bandwidth cm^{-1}	Function
1	2700 ±10	300 ± 50	Infrared Atmospheric Window
2	2350 + 4	50 ± 5	Temperature Profile
3	1030 ± 4	25 ± 3	Ozone Correction
4	899 ± 2	15 + 4, -1	Infrared Atmospheric Window
5	750 ± 1	15 + 4, -1	Temperature Profile
6	735 ± 1	15 + 4, -1	Temperature Profile
7	715 ± 1	15 + 4, -1	Temperature Profile
8	700 ± 1	15 + 4, -1	Temperature Profile
9	690 ± 1	15 + 4, -1	Temperature Profile
10	675 ± 1	15 + 4, -1	Temperature Profile
11	669 ± 0.5	3.5 +1.0, -0.5	Temperature Profile
12	532 ± 2	25 ± 5	Moisture Profile
13	432 ± 2	25 ± 5	Moisture Profile
14	340 ± 2	25 ± 5	Moisture Profile

TABLE II. DESIGN REQUIREMENTS FOR TOVS-BSU

Very high radiometric accuracy is required to get satisfactory temperature profiles.

• Full-Scale Radiance	Equivalent to that from 330°K. blackbody.
• Noise Spectral Radiance, Relative Error Between Channels, Scene-to-Scene Memory	0.15 Ch 3-14, 0.02 Ch 2, 0.003 Ch 1, (mW/m^2-sr-cm^{-1})
• Absolute Accuracy	±1.0 required (mW/m^2-sr-cm^{-1}) ±0.5 design goal (mW/m^2-sr-cm^{-1})
• Field of View	1.125 degrees (50% power) 1.25 degrees (99% power)
• Relative Field-of-View Alignment	1% of 50% FOV, or 0.01125 degree
• Channel-to-Channel Cross Talk	-60 dB
• Maximum Weight	45 lb
• Maximum Envelope	24 x 12 x 14 in.
• In-Flight Calibration Method	Space and calibration blackbody look.
• Scanner	
- No. of Steps	36 steps, each 1.125 degrees, on each side of nadir
- Step and Dwell Period	100 ms
- Scan and Retrace	8.0 s
• Digital Resolution	11 bits, with sign and parity

KEY FEATURES OF THE INSTRUMENT DESIGN

The optics and electronic design of the TOVS-BSU follow the approach proven on the ITPR instrument on NIMBUS-5. The design of the scanner is improved, although similar in concept. These designs result in an instrument that provides the desired performance.

As shown in the instrument block diagram that follows, light reflected from the scan mirror enters one of seven reflecting telescopes which image the distant scene onto a field stop that determines the FOV. This light is chopped by a rotating disc. Each telescope contains a dichroic beam splitter to divide the chopper light into two beams which are separately filtered and imaged on uncooled, but temperature-stabilized, pyroelectric detectors.

To avoid possible scene-to-scene variations in chopping, the chopper makes a complete rotation once each 100-ms scene time (shaft speed 600 rpm). To achieve a chopping frequency which provides the lowest detector noise, the telescopes are arranged in two rings, each having four positions, so that a 40-Hz chopping frequency is attained with two tracks of four apertures each. There is one spare position. To optimize the channel sensitivities, one group of four telescopes has an 80-mm aperture, while the other group of three has a 61-mm aperture. To achieve a stable zero reference, the chopper is not made black but rather reflects the light of a reference blackbody onto the detector during the period when the scene is blocked. This proven design is necessary to prevent errors from chopper temperature variation on the sun-drenched TIROS orbit.

The required angular resolution and stray light rejection are attained by use of a Cassegrainian telescope. The secondary mirror of the telescope is imaged on the detector by a lens. The central zone of the secondary mirror (which faces the aperture in the primary mirror) is made concave to image the detector on itself and reject stray radiation from the field stop.

The low noise-equivalent radiance desired is attained by the use of triglycine sulfate pyroelectric detectors with integral preamplifiers. The temperature of these detectors is controlled at 35°C. The chopper signal is amplified, demodulated, and filtered using a separate integrator for each channel. The demodulation is synchronized by a signal derived from an optical phase-reference pickup on the chopper. Particular attention is paid to the elimination of memory effects by selection of time constants in the signal-handling chain. The data is digitized by an 11-bit bipolar converter.

The scanning mechanism employs a size-15 motor and a size-3C harmonic drive to achieve the desired stepping performance. This design is different in detail from that used in the ITPR, but similar in concept. Important differences include the use of a low-inertia drive to reduce torque requirements, a new design for the electronic drive circuit, and a new assembly procedure which allows easy assembly of the position-sensing shaft encoder and which provides shafts for use in checking motor torque in place.

Data processing operations are synchronized with the scanner. The chopper is also synchronized to the scanner by means of a phase-locked loop which assures constant phasing of the signals and readout. The integration period is 75 milliseconds. A scanner settling time of 37.5 milliseconds is obtained by making use of the scene-blocking of the 40-Hz chopper.

Thermal control of the instrument is particularly critical because of entrance of sunlight into the mirror cavity. A sunshade carried by the scan mirror prevents the sun from reaching the calibration blackbody, and nearly completely shields the mirror itself. Even with this shade, the housing must be made heavier to conduct heat to radiator panels used to reject the solar heat and the heat from the electronics, which is all located in the radiometer housing.

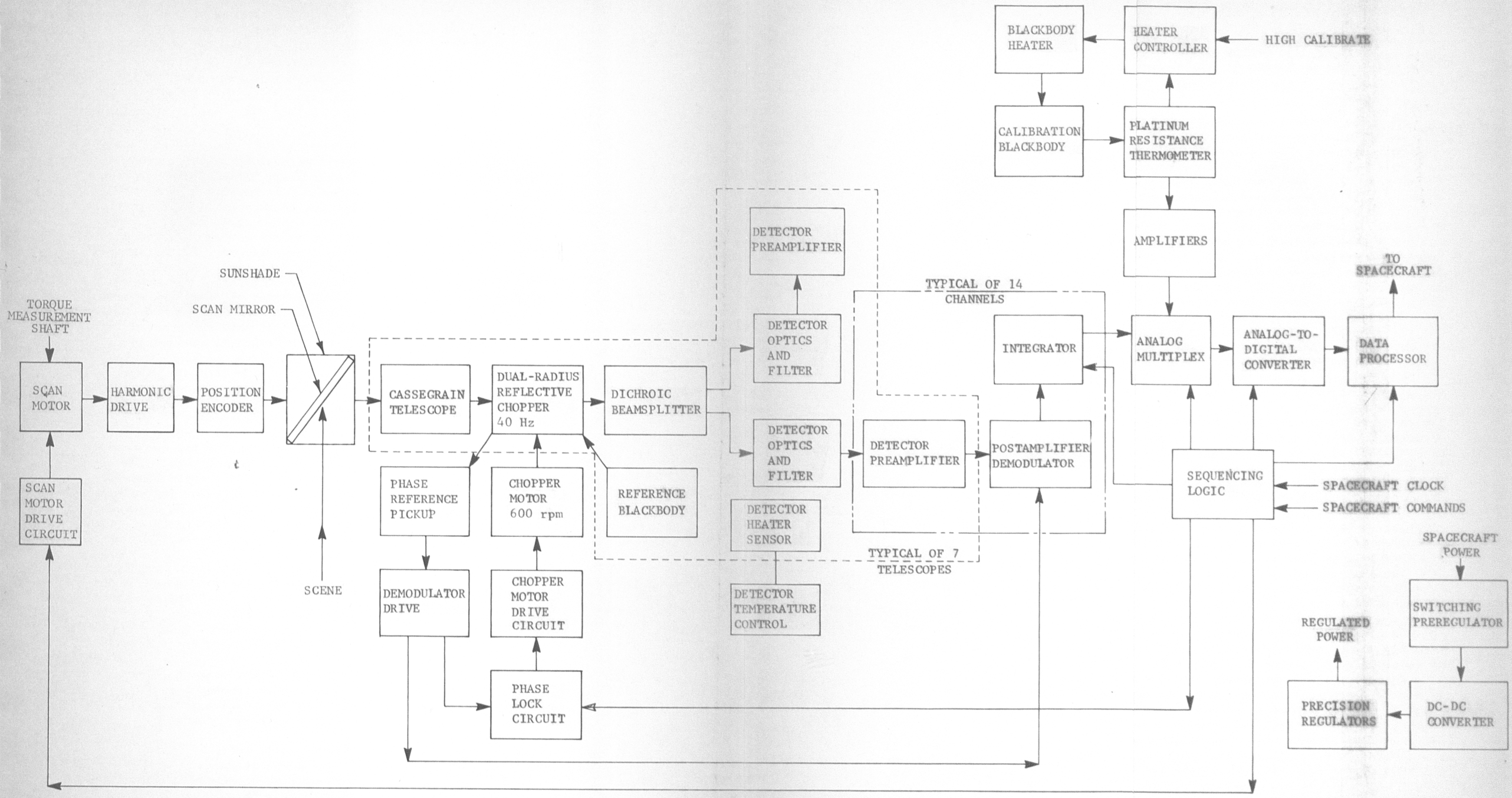
BLACKBODY HEATER
HEATER CONTROLLER
HIGH CALIBRATE
CALIBRATION BLACKBODY
PLATINUM RESISTANCE THERMOMETER
AMPLIFIERS
TO SPACECRAFT
DETECTOR PREAMPLIFIER
TYPICAL OF 14 CHANNELS
SUNSHADE
SCAN MIRROR
TORQUE MEASUREMENT SHAFT
DETECTOR OPTICS AND FILTER
INTEGRATOR
ANALOG MULTIPLEX
ANALOG-TO-DIGITAL CONVERTER
DATA PROCESSOR
SCAN MOTOR
HARMONIC DRIVE
POSITION ENCODER
CASSEGRAIN TELESCOPE
DUAL-RADIUS REFLECTIVE CHOPPER 40 Hz
DICHROIC BEAMSPLITTER
DETECTOR OPTICS AND FILTER
DETECTOR PREAMPLIFIER
POSTAMPLIFIER DEMODULATOR
SEQUENCING LOGIC
SPACECRAFT CLOCK
SPACECRAFT COMMANDS
SCAN MOTOR DRIVE CIRCUIT
PHASE REFERENCE PICKUP
CHOPPER MOTOR 600 rpm
REFERENCE BLACKBODY
DETECTOR HEATER SENSOR
TYPICAL OF 7 TELESCOPES
SPACECRAFT POWER
SCENE
DEMODULATOR DRIVE
CHOPPER MOTOR DRIVE CIRCUIT
DETECTOR TEMPERATURE CONTROL
SWITCHING PREREGULATOR
REGULATED POWER
PHASE LOCK CIRCUIT
PRECISION REGULATORS
DC-DC CONVERTER

Functional Diagram of TOVS/BSU. This design approach has been proven on the ITPR instrument on NIMBUS-5.

ARRANGEMENT OF THE INSTRUMENT

The TOVS-BSU, which is a scanning radiometer, consists essentially of a cantilevered structure mounted on the underside of the spacecraft flight. A large viewing port on its bottom permits the instrument to perform a step-wise scan back and forth about the spacecraft suborbital track. The instrument also has a space-look function during which it looks at space above the limb of the earth, on its right or anti-sun side.

A cross-sectional view of the TOVS-BSU is shown in the accompanying figure. It consists essentially of a main frame to which various functional subassemblies are attached. The instrument is organized with the optical subassembly at the front end and the scanner subassembly at the rear. The scanner subassembly consists of a large 45-degree mirror that rotates incrementally about an axis parallel to the roll axis, a drive mechanism, and an encoder for mirror position sensing. The elliptical scan mirror is of beryllium, with a gold reflective coating. Because of the insulation problems presented by the TIROS N orbit, the scan mirror has a sunshield which is essentially a large, thin-walled cylinder with cutouts for the entrance and exit beams.

The mirror shaft is carried in bearings in a housing attached to the rear portion of the instrument. The drive source is a permanent magnet stepper motor of 90-degree step angle. Speed reduction between the drive motor and the mirror shaft is achieved by the use of a harmonic drive gear reducer. This is a unique power transmission device which yields high-speed reduction in a single pass with extremely low backlash at the output shaft. It is a commercially manufactured product and has been proven in both industrial and aerospace applications, such as in the Apollo Lunar Rover. In addition to the harmonic drive, the scanner housing contains the shaft encoder, which gives scanner position information.

For calibration, the scanner can be commanded to step to both the previously described space look position and an internal calibration position. In this position the scanner looks straight up at the upper portion of the instrument housing. In this area is mounted an array of blackbody cavities. These consist of an isothermal monometallic plate whose temperature is accurately monitored. The pattern of the blackbodies matches the pattern of the parallel telescopes in the optics deck.

The optics subassembly is a separable unit mounted in the front of the instrument. It consists of the telescope array (for optics) and the thermally controlled aft optics housing, on which are mounted the detector-preamplifier units and their associated optical components. Between the fore and aft optics is located the reflective chopper wheel.

The reflective chopper wheel, like the other reflective elements, employs a gold coating. Because of the two diameters of the telescope array, the chopper wheel has two active diameters. Each diameter consists of a toroidal reflecting surface, with equally spaced cutouts. The toroidal reflective surfaces image the blackbody cavities on the detectors. The blackbody cavities are blackened holes machined in the housing, which are accurately temperature-controlled.

The instrument housing is an aluminum casting, designed primarily for rigidity and thermal stability. It has surfaces for mounting the subassemblies that have been discussed, as well as the instrument electronics. The electronics are mounted in convenient areas, primarily in the upper part of the instrument housing where pockets are provided for this use. The upper part of the housing also has ears for mounting the package to the spacecraft, and an area for spacecraft interface electrical connectors.

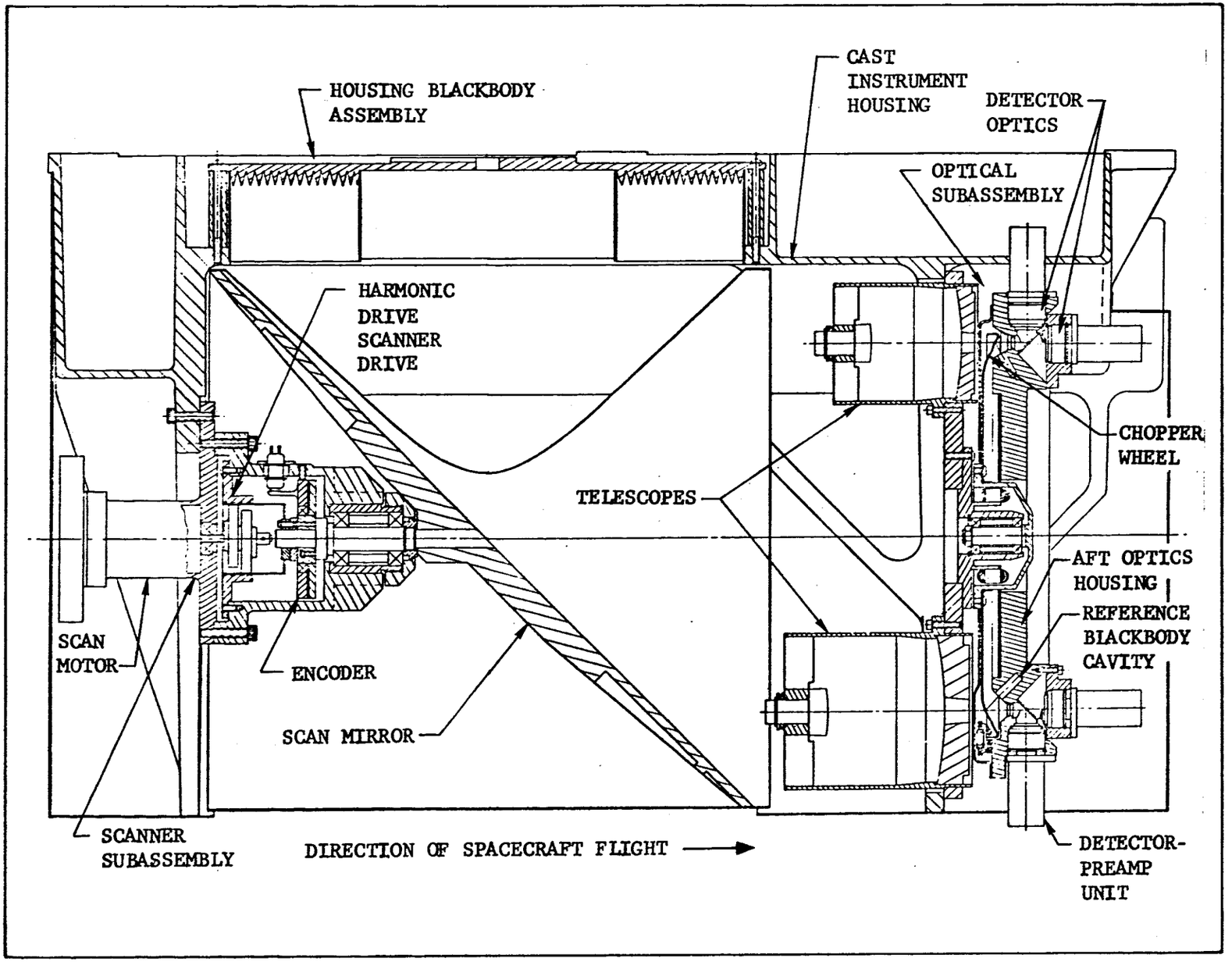

Layout of TOVS Basic Sounder Unit

Gulton Industries, Inc.
Data Systems Division
Beckman Instruments, Inc.
Advanced Technology Operations

TOVS-BSU INSTRUMENT WEIGHT BREAKDOWN

The basic dimensions of the instrument package are: 24 inches long, 14 inches deep, and 12 inches wide, with a wider (14-inch) area at the top for the mounting tabs. A target weight of 45.0 pounds can be reached for the complete BSU, allocated to the various assemblies itemized.

Unit	Weight (lb)
Housing	13.5
Scanner Subassembly	7.3
Optics Subassembly	12.4
Housing Blackbody Subassembly	1.5
Electronics	7.0
Covers	1.3
Hardware, Connectors, Cabling	2.0
Total	45.0

RELATION TO PREVIOUS INSTRUMENT

The TOVS is a radiometer based on the Infrared Temperature Profile Radiometer (ITPR) design. The ITPR is a seven-channel instrument operating aboard the NIMBUS 5 spacecraft. While the designs are conceptually similar, the detailed designs differ because of different environmental and spacecraft constraints.

Each ITPR channel simultaneously views a 1.8-degree FOV, which corresponds to a 20-nautical-mile-diameter field at the subsatellite point. A cross-course step-scan mirror assembly covers three grids, each consisting of 14 FOVs and 10 scan lines. One is to the left of the subsatellite track, one about the center, and the third to the right. The scan drive uses a permanent magnet stepper motor and harmonic drive to provide 1.8-degree step increments. An 11-bit encoder resolves all look angles, including space and housing calibration positions.

The ITPR optical system consists of one Cassegrainian telescope per channel, except for channels 1 and 2, which share one telescope with a dichroic beam splitter for channel separation. The seven channels are separated into two "window" channels, one water vapor channel, and four carbon dioxide absorption channels for temperature profiling. The channel assignment, spectral band and comparison with the TOVS requirements are shown in the facing table.

In the ITPR, scene radiances are modulated at 25 Hz by a rotating chopper. Secondary optics focus the scene radiance onto triglycine sulphate (TGS) pyroelectric detectors. During the blocked portion of the chopped scene, the detector views a reference blackbody cavity, which is maintained at the same temperature as the detector assemblies.

Instrument calibration is achieved by viewing "space" and housing blackbodies.

The major portion of the ITPR electronics is in a separate 3/3 NIMBUS module. Only detector amplifiers and chopper drive electronics are in the radiometer housing.

The TOVS instrument will include all the electronics and the radiometer in one structure. The ITPR radiometer and electronics weighed 37 pounds. The TOVS weight objective is 45 pounds.

While the ITPR and TOVS are similar in configuration and function, there are major differences in operating environment which will affect the TOVS design. The ITPR operates in a nominal 500-nautical-mile, sun-synchronous polar orbit with a 12 noon ascending node. In this orbit the ITPR is exposed to the sun only briefly, over the poles. The TOVS will operate in a 906-nautical-mile orbit with an inclination of 103 degree and a 3-pm ascending node. In its orbit, unlike the ITPR, one side of the TOVS can be exposed to the sun at all times, and the sunlight can directly enter the mirror cavity over a large portion of the orbit. The higher thermal loading from the sun and the inclusion of the electronics in the radiometer unit impose severe design requirements on the TOVS.

COMPARISON OF TOVS AND ITPR CHANNEL REQUIREMENTS

TOVS Channel No.	Central Wave Number $\nu(cm^{-1})$	Bandwidth $\Delta\nu(cm^{-1})$	ITPR Channel (νcm^{-1})
1	2700	300	2675
2	2350	50	
3	1030	25	
4	899	15	900
5	750	15	747.5
6	735	15	
7	715	15	716
8	700	15	
9	690	15	691
10	675	15	
11	669	3.5	668.5
12	532	25	505
13	432	25	
14	340	25	

SECTION 2
STUDY PROGRAM

Summary of Study Program 2-0
Summary of Optical and Radiometric Study..... 2-2
Description and Results of the Detector Study 2-4
Approach to Analog Signal Handling 2-6
Study of the Scan Mechanism and Drive Circuit..... 2-8
Design of the Sequencing and Control Logic 2-10
Summary of Thermal Design and Analysis 2-12
Outline of the Systems Study..... 2-14

SUMMARY OF STUDY PROGRAM

The principal purpose of the study was to examine the feasibility of a conceptual design of the TOVS-BSU. All study goals were accomplished, and the detailed conclusions show that a viable operational instrument can be built using parallel telescopes and dichroic beamsplitters.

Purpose and Scope of the Study— The purpose of the TOVS-BSU study was to establish a conceptual design for a sounder instrument using parallel telescopes and spectral selection by means of interference filters and dichroic beamsplitters, as well as to examine the feasibility of that design by means of tests and analyses directed at uncovering critical design problems.

Although the study did not include a detailed design of the entire instrument, detailed design of the optics, scanner, detector preamplifier, and analog signal channel was required. The detector preamplifier, one optical telescope with appropriate filters, and the scan mechanism were fabricated and tested.

Study Subtasks— The study was organized into subtasks as shown in the Table I. Separate subtask reports were submitted for six subtasks, as shown. The present report summarizes and updates the essential results of these subtask study reports. Several subtasks were deemphasized during the course of the study, and their results are included in other reports. The scan pattern was found to be almost uniquely specified by the requirements of the Global Atmospheric Research Program. The scan pattern described in the report was adopted early in the study by agreement between the contractors and NOAA. The systems interface study required only a preliminary definition of the mechanical, thermal and electrical interface, since the detailed spacecraft design has not been chosen.

Significant Accomplishments of the Study— All of the study subtasks were completed. Extensive detector and FET testing established the present limits of pyroelectric detector technology for the TOVS-BSU application.

A complete analysis of the optical design was verified by tests made on a precision mockup of two channels; critical filters and beamsplitters were procured and tested. A preamplifier and analog channel design was completed as well as designs of the scan drive circuit and the control logic. The scan mechanism was designed, breadboarded, and tested. A thermal design and analysis was completed, and radiometric effects from optical component temperature changes were computed. All other electronic and mechanical systems were studied. Particular attention was paid to the design of the housing and structure to obtain accurate weight estimates, and to a complete description of the electronics to obtain accurate power estimates. The results were reported in the six subtask reports. A preliminary version of this report was provided as input to a design review held 13 and 14 February 1973, at Albuquerque, New Mexico.

Principal Conclusions of the Study— The principal qualitative conclusions of the study are shown in Table II. Because of improvements in FET technology, pyroelectric detector sensitivity is now limited by internal mechanisms rather than by electronic noise (at an optimum chopping frequency). The optical design images enough light on these detectors to come very close to the design goal (within a factor of 1.11). The thermal analysis shows that the temperature changes of components can be controlled well enough that barely detectable changes in signal levels occur between calibrations. The operating and nonoperating temperatures of critical components are also within specifications. The scan mechanism design and test effort shows that it is possible to build a lightweight, relatively low power scanner which meets the stepping requirements. Finally, the electronic and mechanical systems design shows that these goals can be met with the allotted weight and power.

TABLE I. STUDY SUBTASKS

The present report summarizes the results of the following subtasks.

Subtask	Notes
Detector Study	*
Optical and Radiometric Design	*
Analog Electronic Channel	*
Scan Program and Pattern	
Scan Mechanism and Drive Circuit Design	*
TOVS Control Logic	*
Thermal Design	*
Systems Interface Study	
Systems Design Study	

*Separate study report submitted

TABLE II. SIGNIFICANT CONCLUSIONS OF THE STUDY

These results show that the TOVS-BSU is a viable operational instrument.

• Filter and Dichroic Performance	Satisfactory
• Detector Noise	Intrinsic, acceptable
• Radiometric Error	Close to design goal
• Thermal Behavior	Satisfactory
• Calibration Frequency	Adequate
• Scanner Performance	Satisfactory
• Weight Allowance	Adequate
• Power Allowance	Adequate

SUMMARY OF OPTICAL AND RADIOMETRIC STUDY

The manufacturer's estimates of detector, interference filter, and dichroic beamsplitter performance were used to establish a baseline optical configuration consisting of a multiple telescope array. Analyses of the performance of this baseline design were confirmed by tests performed on an optical mockup, an engineering model of the most difficult telescope arrangement. The radiometric performance of the instrument was calculated using this test data and the results of the detector and thermal design studies, and was found to be close to the design goal. Improvements in the design to provide improved performance are feasible.

Scope – The design study for the TOVS-BSU was limited to optical configurations using multiple telescopes, each viewing the same scene, with interference filters and dichroic beamsplitters in each telescope to separate the light into 14 spectral channels. The advantages of this approach are explained in detail later; the principal advantage is that all detectors view the same scene for most of the scan dwell time. Chopping is performed independently of spectral selection, leading to reduced radiometric offsets and lower crosstalk between channels. The principal disadvantage of the approach is that the individual telescopes in a multiple telescope array are smaller and gather less light. The telescopes use more optical components, and must be carefully aligned to view the same scene. The study was performed to see if these disadvantages could be overcome to realize the advantages of the configuration. Analyses were verified by tests made on an optical mockup, consisting of one telescope with the most difficult combination of filters and dichroic beamsplitters. The principal tasks performed in the study are listed in the table opposite.

Filter and Dichroic Study – Because it was decided that the optical mockup would be an engineering model of a flight design, it was necessary to establish an early design baseline using predictions of dichroic and filter performance available shortly after the start of the study. These estimates were obtained by means of a survey of thin-film filter and dichroic manufacturers to determine their current capabilities.

Configuration Study – With the filter and dichroic performance data in hand, a configuration study was performed to find the telescope and dichroic arrangement which provided the best division of scene energy between the 14 spectral channels, taking into account geometric and chopping constraints. The study showed that the best arrangement consisted of four large (80 mm) telescopes and three small (61 mm) telescopes arranged in two concentric rings with one spare position. Each telescope need contain only one dichroic beamsplitter in this arrangement. The sizes of the telescopes were chosen to make use of all of the clear aperture of the instrument available within the allotted envelope for the instrument. Application of this ground rule led to a baseline design.

Implementation of Baseline Design – The details of the baseline design were then worked out by ray-trace to establish the exact dimensions and layout of the optical components, first for the mockup telescope and then for the rest of the instrument. The mockup was built to released drawings and specifications prepared with the aid of these ray-traces. The mockup detected channel 11 (Q-branch, 669 cm^{-1}) and channel 14 (340 cm^{-1}).

Optical Analysis – Ray-trace analyses were performed to predict the aberrations and to determine the sensitivity of the position of the focal point to telescope parameter variations and optical component mounting errors. The movements of the focal point were then used to calculate the errors in the sharpness and the centroid of the field-of-view. Optical mounting tolerances required were found to be tight but achievable. An analytical calculation of the diffraction

from the annular aperture was performed, which showed that the diffraction in all channels should be acceptable, although the longest wavelength channel was nearly diffraction-limited.

Optical Test.— Tests which were made on the filters and dichroics purchased for the mockup and on the optical mockup itself, confirmed the predictions of the analyses. Diffraction in the longest-wavelength channel appeared to be larger than calculated, probably because the calculation did not account for the diffraction from telescope mirror spiders.

Radiometric Analysis.— Using the results of the detector study and improved data on filters and dichroics obtained near the end of the study program, as well as the results of the thermal analysis of the instrument, an analysis of the statistical and systematic radiometric errors was performed, allowing for the influence of in-flight calibration errors and optical component temperature changes. This analysis showed that because of the orbital temperature variations produced by solar radiation on the TIROS orbit, frequent calibration of the TOVS-BSU or any similar instrument is necessary, but the required accuracies can be attained. The noise spectral radiance design goals can be met within a few percent. Further optimization of the baseline design using recent filter dichroic and detector data will lead to improved performance.

Conclusions.— The optical design and analysis showed that the TOVS-BSU design goals can be met, or very closely approached, within the envelope and weight constraints of the TIROS spacecraft, and that further improvements are possible.

TASKS IN THE OPTICAL AND RADIOMETRIC DESIGN STUDY

The following detailed studies were performed to show that the optical and radiometric design goals are attainable.

- Filter and dichroic survey
- Optical configuration study
- Detailed baseline design
- Filter and dichroic procurement and test
- Optical mockup design, fabrication, and test
- Optical analysis
- Radiometric analysis

DESCRIPTION AND RESULTS OF THE DETECTOR STUDY

Uncooled pyroelectric detectors can be used in the TOVS-BSU because the required noise level is larger than the fundamental limit imposed by thermal background radiation, and also because they provide adequate detectivity if the detector material, input FET, and chopping frequency are correctly selected. Tests performed during the design definition program showed explicitly that the necessary NEP's are attainable for the instrument design described herein.

The noise equivalent power of any detector is subject to a fundamental lower limit arising from the noise produced by the random absorption and emission of photons. This limit for a black detector in equilibrium with the surrounding cavity is given by the equation:

$$NEP > (16\ k\ \sigma T^5 A)^{1/2}$$

where k is Boltzmen's constant, T is the absolute temperature, σ is the Stefan-Boltzman constant, and A is the detector area. For a 2 mm circular detector at 300°k, the limit is 1.0×10^{-11} W/ Hz.

The NEP required by a TOVS detection channel can be estimated from the aperture (80 mm), the FOV (1.125°), and the overall transmission including spider and secondary blockage, filter and lens losses, and ac-dc conversion. For a 2 mm detector, the NEP required in the most sensitive channel is 1.0×10^{-10} W/ Hz, which is a factor of 10 larger than the photon background limit.

Because the detector time constants and temperature coefficients should be the same for all channels, it is desirable to use the same kind of detector for all channels. No non-thermal detectors are known which will cover the wide spectral range of the instrument. The only thermal detector which also provides the required detectivity is the pyroelectric detector. Pyroelectric detectors of TGS or doped TGS can be obtained which provide the NEP required to meet or closely approach the sensitivity design goals. Very low noise Fet input amplifiers are required to realize the performance potential of the detectors.

It was reaffirmed that to attain the lowest NEP, it is necessary to operate the detector at a low chopping frequency preferably below 50 Hz. Chopping is required because at very low frequencies, amplifier 1/f noise causes degraded performance. From 15 Hz to about 75 Hz NEP degrades as the square root of frequency above that the voltage noise produced by the input FET dominates, and the narrowband NEP increases linearly with frequency. At 40 Hz, the NEP is limited by the dielectric loss of the detector (loss tangent noise). Since this noise mechanism is intrinsic, the NEP varies as the square root of the detector area, giving a constant detectivity D* of about 1.5×10^9 cm-$\sqrt{Hz}$/W. Amplifier noise is still a contributer but not significant if the Fet has been properly selected.

Because pyroelectric detectors exhibit their optimum NEP over a narrow temperature range, and also because the temperature coefficient of responsivity is fairly large (~1%/°C for TGS at 35°C), it is necessary to control the detector temperature. The detail detector study showed that the detector temperature should be between 25°C and 35°C controlled to ±1°C, with a drift rate between calibrations of 0.1°C or less.

Tests designed to simulate the most severe in orbit radiation environment show that only slight degradations in NEP can be expected. The attendent fact established is that thin detectors work best in the radiation field.

Detector systems considerations reveal a basic compatibility between a parallel channel system and pyroelectric detectors. A parallel system allows the use of small detectors at very reasonable angles of incidence on the detectors. Acceptance angle tests have shown that for the large telescope of the system detector diameters of 1.5 mm work well. For a larger telescope as might be required in a color sequential system the detector becomes commensurately larger holding f numbers constant. Maintaining the necessary thinness for detectors of no more than double the above diameter verges on impossibility. When operated in a high sensitivity mode, pyroelectric detectors are basically slow devices. Channel-to-channel or color-to-color mixing by thermal smearing is avoided by going to a parallel channel system.

HIGHLIGHTS OF THE DETECTOR EVALUATION STUDY

The following items were established or verified during the study.

- Uncooled detectors can be used
- TGS based pyroelectrics offer best performance
- Only thin elements provide necessary performance
- Low frequency chopping enhances NEP
- Temperature control is needed
- Radiation effects are not severe
- Detectors have large acceptance angles
- Compatibility with FET amplifiers exists

APPROACH TO ANALOG SIGNAL HANDLING

The primary problem in the signal handling area is achieving the necessary amplifier noise level. A secondary problem is the requirement that signals coming from one scene or FOV are not to be contaminated by signals from any combination of previous scenes.

Achieving the necessary amplifier noise level is made difficult by virtue of the high impedance nature of the detector source. An amplifier is required that has a normally low voltage noise and an extremely low current noise. The problem is further aggravated by the fact that at the high impedance levels microphone noise can be severe. This requires a carefully designed interface between the detector and pre-amplifier.

The scene-to-scene independence problem is made somewhat difficult by the fact that optical chopping must occur at a relatively low frequency for best detector performance. The optimum chopping frequency falls at 40 Hz or less. If however, it is made too low then the frequencies resulting from chopping mix with scene-to-scene induced signal components which can have a fundamental component as high as 5 Hz resulting in crosstalk or "memory errors".

The spectrum or bandwidth of the scene radiance signal is a function of the time per scene and the number of colors viewed in that time. Fortunately, for a parallel channel system this bandwidth is minimized. Frequency domain analysis has shown that the spectrum falls to a negligible level above 20 Hz thus allowing a chopping frequency of 40 Hz without mixing effects if the passbands are properly designed. Following the necessary demodulation, integration over an integral number of scene chops minimizes any residual mixing effects.

A FET testing program revealed that an adequate source of supply for suitable devices exists. Devices from at least four manufacturers were found to provide acceptably low current noise, i.e. in the range of 5×10^{-16} A/$\sqrt{\text{Hz}}$ or less. Voltage noises of less than 25 nV/$\sqrt{\text{Hz}}$ are quite common.

The use of matched Fet pairs is recommended for the input stage combined with the pre-amplifier circuit developed and used on the ITPR. The design forces the dc potential of the detector active terminal to within a few multivolts of ground and surroundings. This minimizes microphonic problems due to motion of the very small element electrode lead.

A reliable source for the necessary large valued bias resistors has been established. It has been determined that resistors whose resistance must be close to 10^{12} ohms can be safely described noisewise by the Johnson relationship. They are physically very small and fit into most detector packages quite easily.

Voltage mode amplification is recommended at the chopping frequency to control the responsivity temperature coefficient. Operating point stabilization such as used in the ITPR pre-amplifiers is suggested.

Computer modeling and other analysis has shown that a scene integration time of 75 msec can be used if proper phasing is employed within the instrument system. With proper scan step and chopper phasing 37.5 msec is still available for the scan step and settle. Accurate full wave demodulation is required to keep scene-to-scene crosstalk at the lowest possible level.

KEY FEATURES AND FACTS

- Parallel system avoids channel crosstalk
- Scene-to-scene crosstalk can be controlled
- Gains are easily customized to channel
- Adequate availability of low noise FETS
- Detector-FET interface is critical
- Voltage mode amplification is recommended
- Full wave demodulation is needed
- A 75 msec integration time can be used
- Power required for signal handling is low
- Parallel system parts count is relatively high
- A channel failure does not render instrument worthless

STUDY OF THE SCAN MECHANISM AND DRIVE CIRCUIT

After the scan pattern was selected, the torque and speed requirements for the scanner were derived and were used as the input to a comparison of different drive mechanisms. The comparison favored the use of a stepper motor and harmonic drive, with a single-phase bipolar drive circuit. Tests on a breadboard of this scanner show that the baseline performance is attained. Analysis indicates that improved performance can be attained, making possible a longer signal integration period.

Scan Pattern— Early in the study, it was realized that the Global Atmospheric Research Program (GARP) scan grid requirements, together with the instrument requirements, implied an essentially unique scan pattern, consisting of 72 scene elements (36 on each side of nadir). When the angular interval between these elements is 1.125 degrees, complete earth coverage is obtained. With a scene dwell-time of 100 milliseconds, each scan line can be completed in 8.0 seconds, of which 7.2 seconds is used for the forward step-and-dwell and 0.72 seconds (of the 0.8 second available) is used for retrace at 100 steps per second. With a half-power field of view of 1.125 degrees (equal to the step interval), there is some scene-to-scene overlap, but the line widths are such that spacecraft motion provides suitable line-to-line spacing. One scan line of each 32-line frame is used for in-flight calibration, and there is enough time available to make statistically accurate calibration measurements.

Derivation of Torque and Speed Requirements— The moment of inertia of the elliptical scan mirror is determined by its density, area, and by the thickness required for rigidity and thermal uniformity. At the beginning of the study, it was decided to allow 50 milliseconds for the mirror to step and settle. The torque and damping requirements were then determined. The drive mechanism also had to be capable of stepping under load at the retrace rate of 100 steps per second.

Comparison of Alternative Drive Mechanisms— Alternative drive mechanisms, including stepping motors with various speed-reducing devices as well as a direct-drive servo, were compared as shown in Table II. The accuracy, wear, weight, power, ease of assembly, behavior in the launch environment, reliability, and complexity of each alternative was considered. The comparison showed that the stepper-motor harmonic-drive combination used on the Infrared Temperature Profile Radiometer remains the best choice, primarily because of its simplicity, low weight, low wear rate, and high inherent reliability. At this time, it appears that difficulties experienced with the ITPR drive cannot be attributed to any basic flaw in the stepper-motor harmonic-drive mechanism.

Detailed Design and Component Selection— A detailed design of a stepper-motor harmonic-drive mechanism was performed. Components, including a pin-type shaft encoder, were selected for performance in the TIROS environment. The selected drive circuit is a bipolar single-phase (bridge) circuit which provides the required torque at lower power than the circuit used on ITPR. While a study of lubricants was outside the scope of the study (the use of silicone lubricants was specified, as on ITPR), a reexamination of the approach to lubrication was performed since analysis indicates that lubricant degradation may have contributed to the ITPR failure.

Testing of Scanner Breadboard— A breadboard of the scan mechanism was built using components as close as possible to those required for the flight design. By reducing the input inertia of the harmonic drive, and with the use of the breadboard drive circuit, it proved possible to meet the retrace requirements and to step and settle in 50 milliseconds. Temperature tests with the breadboard showed that this performance was attained over a wide temperature range (-20 to +60°C) even with the commercial motor and lubricants used.

Conclusions. The scan mechanism and drive circuit study showed that the required performance can be attained with a mechanism weighing 2.5 pounds (exclusive of the mirror) which consumes an average power of less than 8 watts measured at the input to the driver. With further optimization of the motor and drive circuit, analysis indicates that the drive will be capable of stepping and settling within 37.5 milliseconds, which would allow use of a 75-ms signal integration period, and would lead to a 22-percent improvement in the noise-equivalent spectral radiance.

TABLE I. SCAN PATTERN PARAMETERS

These parameters are determined by GARP pattern and instrument field-of-view and data frame requirements

• Step size	1.125 degrees
• Step interval	100 milliseconds
• Steps per line	72
• Time per line	8.0 seconds
• Step and dwell time	7.2 seconds
• Retrace times available	0.8 second maximum
• Actual retrace time	0.72 second at 100 steps per second
• Lines per frame	32
• In-flight calibration	Once per frame (Two measurements, each 2.4 seconds)

TABLE II. ALTERNATIVE DESIGNS CONSIDERED

These designs were evaluated using the criteria listed in the text

- Stepper-motor and harmonic drive
- Stepper motor and gear train
- Responsyn
- Direct-drive servo

TABLE III. PROPERTIES OF THE SELECTED DRIVE

The selected stepper-motor harmonic-drive combination has the following performance

• Weight	2.5 pounds
• Power: less than	8.0 watts
• Settling time: less than	50 milliseconds
• Maximum retrace rate	125 steps per second
• Fatigue safety factor	3.7

DESIGN OF THE SEQUENCING AND CONTROL LOGIC

A totally synchronous system is required in regard to scanning, optical chopping, signal integration, digitization, and data readout.

The requirement for total synchronism arises first of all from the rather precise nature of the scan pattern. Due to the small amount of time per scene and resultant small number of optical chops, it is important that scanning, chopping, and integration window be phase locked. The allowable phase error is 5° and can be reasonably implemented digitally. Since the chopper motor starts at random phase positions depending on where it last stopped, the drive to it must be variable in phase over ±180° relative to a reference derived from the TIP clock.

The study has shown that special care is required in regard to generating the drive pulses for the step scan and retrace. Damping and therefore settling time is determined by time shaping the drive pulses.

A special dual instrument operating mode is required during the interval of switchover from one instrument to the other. This is accomplished by doubling the time per scene resulting in an identical output data rate to that of a single instrument in normal mode. During this mode as well as in normal mode the start of a scan line is synchronized with major frame sync pulses.

A requirement for a "super major frame" sync pulse was defined. In order to minimize dead time between the BSU and SSU from uncorrelated calibration interruptions it is suggested the TIP provide in effect a "cal sync" pulse every 256 seconds or some other convenient number in this range.

Simultaneity of data readout from the 14 colors is obtained by converting the 14 integrators to hold circuits in synchronism. Subsequently their contents are digitized in sequence and where necessary placed in storage to provide a reasonably smooth output data flow.

SUMMARY OF THE THERMAL DESIGN AND ANALYSIS

The thermal design and analysis study showed that the range and orbital variation of orbital temperatures could be controlled within acceptable limits with the allotted instrument weight and power and with the agreed-upon thermal interface.

Objectives of the Thermal Design and Analysis. The TOVS-BSU is an instrument subject to inherent thermal control problems, not only because of its relatively high power consumption and the fact that solar radiation enters the scanner cavity, but also because it is a precision radiometer operating in the thermal infrared region, so that it is potentially sensitive to minute temperature variations of optical components. The objectives of the study were to design a thermal control system to assure that the range and orbital variations of instrument temperature were acceptable, and to verify the design by analysis.

Nature of Problems Encountered. Because the instrument power is larger than the power which can flow across the spacecraft interface, the excess power must be radiated to space. Because there are some TIROS orbits on which the sun never sets, while for orbits at other times of the year there is an appreciable time spent in the earth's shadow, the variation of the solar heat input into the scanner cavity is large. On some orbits, sunlight will strike the scan mirror, optical telescopes, and even the calibration blackbodies if no precautions are taken. The gold-coated scan mirror could become very hot, since the solar absorptivity of gold is much higher than the thermal emissivity. Pyroelectric detectors are temperature-sensitive, and must be temperature-controlled to stabilize the responsivity.

Approach to the Thermal Design. Preliminary analysis showed that the excess heat can be conducted through the instrument structure and dissipated by passive radiators located on both sides of the instrument. To prevent the sunlight from raising the temperature of the scan mirror and from disturbing the temperatures of the optical components and calibration blackbodies, a sunshade is required; this shade is attached to the scan mirror and rotates with it, serving both to shade the critical components and to dissipate the incident solar energy by radiation. An actively controlled heater can then be used to stabilize the temperature of the detectors, detector optics, and chopper-reference blackbodies.

Detailed Thermal Design and Analysis. The details of this scheme were worked out and its performance verified by use of a 20-node computer model analysis which took into account the principal thermal effects. The results of these model calculations helped determine the mechanical design of the instrument housing, which took into account the thermal conductance requirements and the thermal gradients which must be withstood without introducing significant optical misalignments.

Conclusions of the Study. The thermal design study showed that a passive temperature control method could control the instrument temperatures so that the temperatures of critical components (such as motors) did not exceed their specified ranges. Active control of the detector temperatures can be accomplished with a small heater. The variations in optical component temperatures lead to barely detectable changes in spectral radiance between calibrations so that corrections derived from the in-flight calibrations are small. The warmup time and the power required to hold the motors above 0°C in the nonoperating condition were also calculated and are given in the detailed thermal discussion later in this report.

Beckman Instruments, Inc.
Advanced Technology Operations
J. O. Maloy

PRINCIPAL OBJECTIVES OF THE THERMAL DESIGN STUDY

- Design of thermal control system to limit instrument temperature excursions
- Verify design by analysis

MAJOR THERMAL DESIGN FEATURES

These design features assure adequate control of instrument temperatures.

- Excess heat dissipated by passive radiators
- Sunshade carried on scan mirror keeps sun off optics, calibration blackbodies, and most of scan mirror
- Active heater stabilizes detector temperature

SELECTED ANALYTICAL RESULTS

- Motor temperatures lie within acceptable range (-25 to +70°C)
- Interface heat transfer is less than the 15 watts allowed
- Optical and blackbody orbital temperature variations between calibration produce barely detectable change in background radiance.

SECTION 3
OPTICAL SUBSYSTEM DESIGN

CONFIGURATION

Selection of Radiometer Configuration 3-0
Method of Spectral Selection 3-2
Constraints on Choice of Optimum Telescope Configuration 3-4
Selection of Preferred Configuration 3-6
Optimization of the Preferred Configuration 3-8
Expected Performance of Baseline and Revised Configuration 3-10

OPTICAL DESIGN

Selection of Optical Channel Configuration 3-12
Design of the Telescope 3-14
Design of Detector Optics 3-16
Optical Design of Chopper and Reference Blackbody 3-18
Design of the Phase Reference Pickup 3-20
Properties of Optical Components 3-22

MECHANICAL DESIGN OPTICS SUBASSEMBLY

Arrangement of the Optics Subassembly 3-24
Construction and Support of the Telescopes 3-26
Mounting of Detector Optics 3-28
Mounting of Detector-Preamplifier Modules 3-30
Details of Chopper Disc and Drive 3-32
Structural Analysis of the Optics 3-34
Nature of Optical Subsystem Interface Requirements 3-36

SELECTION OF RADIOMETER CONFIGURATION

The selected approach for making radiometric observations is to measure all 14 spectral channel radiances in parallel with individual detectors. The advantages over a series approach are that errors in measurement caused by channel-to-channel crosstalk are eliminated, and pyroelectric detectors that have a flat spectral response and need not be cooled can be used.

The required radiometric observations could be taken either in parallel or in series during each scan scene. If taken in parallel, 14 individual detectors, one for each channel, view the scan scene simultaneously. If taken in series, one or more detectors sense energy from a spectral scan made during the time frame of each scan scene. In this mode, each detector would be time-shared, measuring energy in several spectral channels at various times during each scan scene. The advantages and disadvantages of each technique are considered in the following discussion.

Accuracy Considerations - The calculation of an atmospheric temperature profile is critically dependent upon the accuracy of the spectral radiometric measurements. Radiometric observations made in each of the 14 spectral channels must be taken from essentially the same field-of-view (FOV). In addition, the measurement of a spectral channel radiance must be independent of the radiance outside of the bandpass of that channel; that is, there must be no crosstalk between channels.

The parallel approach to data collection can satisfy both criteria: 1) individual channel FOVs were aligned within the necessary accuracy on a similar parallel-channel radiometer, the ITPR now flying on the NIMBUS-5 satellite; 2) use of individual detectors for each channel eliminates a major source of channel-to-channel crosstalk.

A series approach to data collection requires some form of image motion compensation to correct spectral observations for the satellite orbital velocity because the FOV changes between observations. Such compensation mechanisms increase the relative channel pointing errors, which should not exceed 0.01 degree. Memory in the detection circuitry can give rise to channel-to-channel crosstalk in the series approach. Even in the absence of detector memory, there are electronic memory effects (arising from capacitative elements, for example) that can introduce unacceptable crosstalk and radiometric error.

Calibration Considerations - The use of individual detectors to make parallel observations requires careful calibration to establish relative channel gains. Experimentation associated with the ITPR indicated that satisfactory calibration was readily achieved. In addition, the detectors used on ITPR and TOVS-BSU have been proven to have very stable response and gain characteristics. Relative channel gain is not eliminated in a series approach because the optical element producing the spectral scan must be calibrated and also must be stable.

Additional Advantages of Parallel Detection Technique - An additional advantage results from the use of a parallel detection technique. Observations taken in parallel during the entire scan scene interval allow sufficient energy to be collected for detection by relatively slow thermal detectors. Pyroelectric detectors have a flat spectral response over the near and intermediate infrared region. They need not be cooled and, therefore, lend themselves to simple instrument design and high reliability.

MAJOR CONSIDERATIONS IN SELECTING RADIOMETER CONFIGURATION

- Negligible channel crosstalk.
- Satisfactory calibration to establish relative channel gains.
- Flatness of detector response.
- Uncooled detectors.

METHOD OF SPECTRAL SELECTION

A nondispersive system incorporating dichroic beamsplitters and bandpass filters is chosen for channel separation and spectral selection in the TOVS-BSU, providing a simple and redundant optical system with adequate sensitivity independent of scene polarization.

The TOVS-BSU collects energy from the scan scene with a telescopic optical system which defines the field-of-view (FOV). After collection, the energy is chopped, segregated into 14 spectral channels, and detected. The separation of energy is accomplished by the detector optics. The separation may be accomplished by either dispersive or nondispersive techniques; that is, by use of a grating(s) or a combination of reflecting and transmitting thin-film interference filters.

A factor that greatly affects the choice of technique for spectral selection is the requirement that the BSU should not be sensitive to the polarization of incoming radiation. The temperature profile theory assumes the use of a radiometer insensitive to polarization. Even if the polarization caused by atmospheric scattering were accurately measurable, the available temperature profile theory could not make use of the additional information without complex and as yet unproved extensions. To achieve an accurate profile, it is essential that the instrument readings differ by not much more than the noise level when the polarization state of incoming radiation is changed. This requirement implies that very low sensitivity to polarization ($\sim$1%) is an important design constraint.

Dispersive Technique - The use of a grating in the design of a space flight temperature profile radiometer has been exhaustively studied at Beckman. While it is feasible to build such an instrument, the use of a single grating imposes severe constraints on the detector configuration and produces ill-defined, yet extreme, polarization sensitivity in the instrument response. The limitation on available space for a grating instrument requires that detection of closely-spaced spectral channels incorporates detectors in close juxtaposition. Pyroelectric detectors must be packaged with their respective amplifiers for optimum operation. These requirements imply that a relatively inflexible and costly detector-amplifier array must be developed.

Although the polarizing properties of diffraction gratings have been given extensive study, prediction of performance is qualitative in nature. Quantitative evaluation must be carried out experimentally and is quite sensitive to the fabrication techniques used in the manufacture of the grating.

Nondispersive Technique - The use of nondispersive techniques allows the mechanical design of the detector optics systems to be both simple and compact. The technique is based upon the use of thin-film technology. Bandpass filters employing thin-film interference determine the spectral properties of the individual channels. In order for a channel filter to be effective, it must reject all spectral energy except for the bandpass of interest. The spectral region of overlap between the spectral response of the pyroelectric detector and the expected spectral radiance of the scan scene is 2.5 μm to 50 μm. State-of-the-art in thin-film technology dictates that the channel filter be composed of two elements in order to provide this sideband rejection: (1) a bandpass filter to determine the spectral characteristics of a particular channel, and (2) a blocker filter to reject all sideband energy not rejected by the bandpass filter. Bandpass rejection is accomplished both by the thin-film coatings and the spectral transmittance of the bandpass and blocker filter substrates.

To use the light collected by a telescope more effectively, it may be separated by dichroic beamsplitters into two or more beams which are subsequently passed through interference filters. The dichroic beamsplitter, by virtue of its

thin-film coatings, reflects or transmits energy located spectrally on either side of a cut-on/cut-off wavelength. The wavelength of the cut-on/cut-off point depends on the state of polarization of the incident light. The dichroic, therefore, tends to be polarization-sensitive in the region spectrally close to the cut-on/cut-off. The design and fabrication of a dichroic with high transmittance and reflectance at points very far removed from cut-on/cut-off are difficult. The selection of spectral channels to be separated by a dichroic is, therefore, important. The channels must be sufficiently far apart to ensure a lack of polarization sensitivity, but be close enough to allow high transmittance and reflectance. Use of several dichroic beamsplitters in series enhances these difficulties.

The proper placement of channels with dichroic beamsplitters makes it possible for a nondispersive system to achieve adequate sensitivity independent of polarization. Nondispersive elements allow for a simple and compact mechanical design with a simple detector configuration. Above all, a nondispersive system provides redundancy in the form of individual spectral defining optics for each channel.

KEY FEATURES OF NONDISPERSIVE DETECTOR OPTICS

These features provide the rationale for the selection of a nondispersive approach to channel spectral selection.

- Simple and compact mechanical system.
- Simple detector configuration.
- Well-defined polarization rejection.
- Adequate sensitivity.

CONSTRAINTS ON CHOICE OF OPTIMUM TELESCOPE CONFIGURATION

The size, number, and arrangement of telescopes used for collection of scene radiation are optimized to meet the channel $(NER)_\nu$ design goals without introducing sensitivity to scene polarization. The constraints of that optimization are: (1) the instrument clear aperture available, (2) the chopper configuration and frequency, (3) the energy balance among channels allowing for filter losses, and (4) the performance of available dichroic beamsplitters.

To meet the design goals for noise equivalent spectral radiance $(NER)_\nu$ and to maintain instrument insensitivity to scene polarization, it is necessary to choose the optimum sizes, number, and arrangement of telescopes.

Constraints on Telescope Sizes and Arrangement. The telescopes used for collection of scene radiation reflected from the scan mirror must be contained within the circular instrument clear aperture (CA) defined by the projection of the rotating scan mirror's surface area normal to the telescope optical axis. The diameter of the instrument CA is 10.75 inches, based upon the BSU size limitation.

The use of a rotating chopper to modulate the output of the telescopes requires that the telescopes be placed in one or more rings, each corresponding to a chopper track. All channels must have the same chopping frequency and phasing so that their integration and scan sequencing are identical. In order for all channels to have the same chopping frequency, each ring must have the same number of telescope positions, whether the positions are used or not.

The telescopes need not have the same diameter. Use of different telescope diameters allows the balancing of energy among channels which require different telescope energy outputs because the channel transmittances and $(NER)_\nu$ design goals are different. Since the use of different sizes of telescopes increases design and fabrication costs, the number of different sizes should be minimized commensurate with the satisfaction of $(NER)_\nu$ design goals.

Chopping Frequency Considerations. The accurate calculation of temperature profiles in the presence of partial cloud coverage necessitates the elimination of scene-to-scene variations in instrument response. Slight variations in chopper window widths will occur in fabrication. To eliminate scene-to-scene errors due to this variation, the chopper must rotate an integral number of revolutions in each 100-ms scene frame time. The minimum angular velocity for the chopper corresponds to one revolution-per-scan frame time, 0.1 second, or 10 r/s.

The signal chopping frequency for a given chopper angular velocity increases with the number of telescope positions on each ring of telescopes. Based on a chopper rotation frequency of 10 r/s, the chopping frequency for N telescope positions is 10 x N Hz. Since the optimum chopping frequency for pyroelectric detectors is about 40 Hz, the use of fewer telescope positions on each ring is desirable. The optimum frequency of 40 Hz results from a low frequency for low detector noise, but not so low as to introduce scene-to-scene crosstalk resulting from detector transient response.

Critical Properties of Dichroic Beamsplitters - The optical properties of dichroic beamsplitters which are critical in instrument optimization are the transmittance, sensitivity to polarization, and ability to effectively separate two closely spaced wavelengths.

Due to the stringent $(NER)_\nu$ design goals, channel transmission losses must be minimized. Although the peak reflectance of a dichroic is relatively high (~95%), peak transmittance is ~80 percent or less at wavelengths greater than 15 μm. To maintain as high a channel transmittance as possible, the number of dichroics placed in the optical path of that channel must be kept as small as is feasible.

Due to the difficulties in the design of wide-band dichroics, transmittance and reflectance are significantly degraded at wavelengths far removed from the transition point midway between peak transmittance and peak reflectance; "far removed" as established by the state-of-the-art is about 50 percent of the transition point wavelength.

A dichroic beamsplitter's sensitivity to polarization is related to its limited ability to effectively separate closely spaced wavelengths. The spectral region between peak reflectance and peak transmittance is finite. The width of this transition region is established by the state-of-the-art at about 10 percent of the wavelength of the cutoff point. This limitation alone limits a dichroic's ability to effectively separate wavelengths. In addition, the spectral location of the cutoff region is sensitive to the state of polarization of the incident energy, thereby effectively widening the region by a factor which is critically dependent upon the coating process, so that it must be fabricated and tested for insensitivity to polarization.

Due to the inherent optical properties of the dichroic, it is imperative that the dichroic be required to separate only channels spaced greater than 10 percent and less than 50 percent in wavelength.

CRITICAL ASPECTS CONSTRAINING THE CHOICE OF OPTIMUM TELESCOPE CONFIGURATION

Telescopes

- Limited to instrument clear aperture.
- Centered on one or more rings.
- Same number of telescope positions per ring.

Chopping Frequency and Phase

- Same for all channels.
- Determined by number of telescope positions on each ring.
- Optimum for low detector noise and low scene-to-scene crosstalk is about 40 Hz.

Dichroic Beamsplitters

- Cannot effectively separate wavelengths spaced closer than 10 percent nor farther apart than 50 percent.
- Limited to transmittance of about 80 percent.
- Exhibit polarization sensitivity.

SELECTION OF PREFERRED CONFIGURATION

The preferred configuration consists of seven telescopes: three telescopes on one ring and four telescopes on a second ring. Telescopes are located at four positions on each ring, leaving an unfilled position on the outer ring of three telescopes. This configuration results in an optimum chopping frequency of 40 Hz.

Examination of Extremes - To see the need for the use of dichroics, consider for example the use of 14 telescopes containing no dichroics at all. Fourteen telescopes, nested within the instrument CA, would not, however, provide sufficient energy transfer to satisfy $(NER)_\nu$ goals even if 100-percent transmittance could be achieved. It follows then that dichroic splitters are needed.

The opposite extreme -- the use of only one telescope -- is obviously not feasible. Thirteen dichroics would be required to separate all fourteen channels. The total transmittance of thirteen dichroics would not provide sufficient energy throughput to satisfy $(NER)_\nu$ design goals. In addition, several dichroics would ultimately be required to separate wavelengths far less than 10 percent apart, resulting in degraded transmittance and severe polarization sensitivity. Use of an intermediate number of telescopes might satisfy both the polarization insensitivity and $(NER)_\nu$ design goals. This is, in fact, the motivation for instrument optimization.

Influence of Dichroic Properties - As stated in the previous topic, the state-of-the-art imposes a limitation on the ability of dichroics to separate closely spaced wavelengths without introducing polarization effects and degradation of transmittance and reflectance. This aspect is especially critical because of the close proximity of seven spectral channels detecting the CO_2 absorption band between 13.3 μm and 14.9 μm.

Due to the close proximity of the seven channels detecting the 15 μm CO_2 absorption band, use of fewer than six telescopes would require the dichroic beamsplitter to separate spectral channels closer than 10 percent or 1.6 μm. This requirement is too stringent for the state-of-the-art. A 6-telescope configuration would require one beamsplitter to separate the 13.3 μm and 14.9 μm channels. Although such a dichroic could be fabricated, it would be expected to exhibit severe polarization sensitivity. This undesirable feature eliminates a 6-telescope configuration from futher consideration.

The use of a configuration involving six or fewer telescopes is precluded by limitations on dichroic performance. This limitation can be avoided by placing one of the seven channels detecting the 15 μm CO_2 band on each of seven telescopes. Critical aspects influencing the optimization of a seven-telescope configuration are discussed in the following paragraphs.

Influence of Chopper Frequency on a Seven-Telescope Configuration - A 7-telescope configuration avoids problems arising from limitations on dichroic performance. Consideration must now be given to the satisfaction of $(NER)_\nu$ design goals. Channel $(NER)_\nu$ bears a direct relationship to chopping frequency since $(NER)_\nu$ is directly proportional to detector noise which increases appreciably for chopping frequencies in excess of 40 Hz.

A configuration comprising seven equal diameter telescopes positioned on a single ring is a poor choice because of detector noise resulting from a high, 70-Hz chopping frequency. Two rows of telescopes - four telescopes and three telescopes each, positioned in separate rings - provide an optimum chopping frequency of 40 Hz. Although a 40-Hz chopping frequency results from the location of four telescopes on one ring, the requirement that all channels have the same chopping

frequency dictates that the three remaining telescopes be located at four telescope positions (leaving an unfilled position on the second ring), resulting in a 40-Hz chopping frequency for that ring also.

REASONS MOTIVATING THE SELECTION OF A PREFERRED CONFIGURATION OF SEVEN TELESCOPES CENTERED ON TWO DIFFERENT RINGS -- FOUR TELESCOPES ON ONE RING, THREE ON THE OTHER.

- Inability of dichroic beamsplitters to separate channels in a five or fewer telescope configurations.
- Polarization sensitivity of dichroic needed for a six-telescope configuration.
- Optimum use of dichroics in a seven-telescope configuration.
- High, and therefore unsuitable, chopping frequency resulting from seven telescopes centered on a single ring.
- Optimum chopping frequency of 40 Hz resulting from seven telescopes centered on two different rings.

OPTIMIZATION OF THE PREFERRED CONFIGURATION

The preferred configuration of seven telescopes consists of four large and three small telescopes whose diameters are chosen to provide the energy transfer to the spectral channels in order to best satisfy the NER_ν design goals. For the baseline design, the ratio of the telescope diameters was 1.31. Later data on filter transmission and detector sensitivites leads to a ratio of 1.60.

The seven-telescope configuration chosen avoids problems arising from limitations on dichroic performance and allows use of the optimum chopping frequency. This configuration can be optimized further by use of two different diameter telescopes in order to balance the distribution of energy to the spectral channels. The result of this optimization is the selected optimum configuration illustrated in the facing figure. The optimization procedure described below provides a ratio of large-to-small telescope-diameters; geometric calculation based upon the instrument reduces that ratio to the diameters shown in the figure.

The optimization procedure operates on the thesis that the energy output of the telescopes must be balanced to meet the channel NER_ν design goals. Calculations are based upon channel bandpass, $\Delta\nu$, NER_ν design goals, and expected channel transmittance, T. The channel NER_ν is related to telescope diameter D, detector NEP, $\Delta\nu$, and T as follows:

$$NER_\nu \sim NEP/(\Delta\nu \times T \times D^2).$$

The baseline design described in detail in this report was assumed the use of detectors whose NEP amplifier current-noise limited and was therefore independent of the detector diameter.

With this assumption the telescope diameter, required to provide sufficient energy transfer to satisfy each channel NER_ν design goal, varies according to the relation,

$$D \sim \left[NER_\nu \times \Delta\nu \times T\right]^{(-1/2)}.$$

Channel placement on the telescopes, as listed in the opposite table, is established on the basis of D values calculated initially without regard to dichroic transmittance or reflectance. The ratio of diameters of large and small telescopes required for an optimum configuration is determined by the ratio of the D values of the most critical channel associated with a large telescope and the most critical channel associated with a small telescope. Since dichroic transmittance and reflectance are not equal and vary with wavelength, the total channel transmittance must take into account the transmittance and reflectance of the dichroic for the final baseline configuration optimization presented in the table. Proper placement of channels, after final calculation of D values incorporating dichroic transmittance, is verified by the table.

Once the diameter ratio is determined, it is simple to determine the actual maximum telescope diameter. For an instrument clear aperture of 10.75 inches, the telescope diameters are 80 mm and 61 mm.

It has been established by the study subtask that pyroelectric detector noise varies directly as the square root of the detector area since the noise is loss-tangent limited. Because detector and telescope diameters are directly related by optical design, detector noise is directly proportional to telescope diameter, and will therefore vary between channels placed on large and small telescopes.

For detectors whose sensitivity is internally limited with constant detectivity, D*, the telescope diameter varies as follows with NER_ν, T, and $\Delta\nu$:

$$D \sim \left[NER_\nu \times \Delta\nu \times T\right]^{-1} .$$

This version implies that a larger variation in optimum diameter ratio is to be expected.

Following through the same channel assignment and optimization procedure given above, we find that the channel assignment is different. Since channel 1 is the most important channel, it is placed on a large telescope to provide a lower NER_ν channel at the expense of channel 13 which is placed on a small telescope. The optimum telescope diameter ratio becomes 1.60, corresponding to telescope diameters in a 10.75-inch clear aperture of 87.5 and 56 mm. These changes require some minor redesign of the chopper and detector optics and the telescopes.

PARAMETERS CRITICAL TO ENERGY BALANCE

The values of channel transmittance, bandpass, and NER_ν determine the relative telescope diameters required to satisfy NER_ν design goals.

Channel	Bandwidth	Transmittance Dichroic	Transmittance Filter & Lens	NER_ν +	Baseline D	Baseline Tele.	Revised D	Revised Tele.
1	300	0.95	0.68	0.003	1.30	S.	1.72	L
2	50	0.95	0.43	0.02	1.56	L	2.45	L
3	25	0.95	0.34	0.15	0.91	S	0.83	S
4	15	0.95	0.35	0.15	1.16	S	1.34	S
5-7	15	0.80	0.35	0.15	1.26	S	1.59	S
8-10	15	0.80	0.35	0.15	1.26	L	1.59	L
11	3.5	0.95	0.21	0.5	1.70	L	2.31*	L
12	15	0.80	0.14	0.15	1.15	L	2.38	L
13	15	0.80	0.14	0.15	1.15	L	2.38	S
14	15	0.75	0.14	0.15	1.16	L	2.54	L

+ $mW/m^2 - sr - cm^{-1}$.

* Based upon a revised filter and lens transmittance of 0.26.

1110-104-236

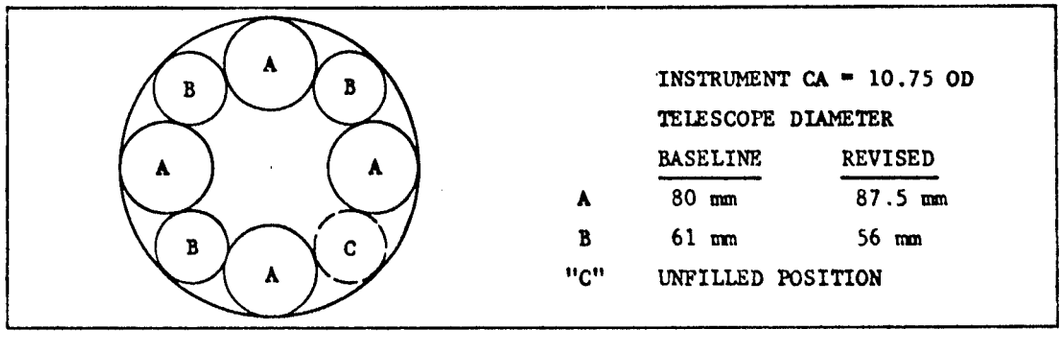

Nesting of Telescopes Within the Instrument Clear Aperture. A proper proportion in large and small telescope diameters allows optimization of channel throughput to channel NER_ν design goals.

EXPECTED PERFORMANCE OF BASELINE AND REVISED CONFIGURATION

The baseline configuration can be reoptimized in light of revised optical design, detector NEP values, and improved channel transmittance. Calculation of NER_ν values resulting from that reoptimization indicate an improvement in the satisfaction of NER_ν design goals.

A baseline configuration was established at an early stage of the TOVS-BSU design study to facilitate the construction of the optical mock-up. Although the baseline configuration was optimized for energy balance, revised channel transmittances and detector NEPs, resulting from investigation made in the study program, required a reoptimization. Reoptimization of the baseline configuration was discussed in the previous topic. Evaluation of the performance of the baseline and optimized configuration are as follows:

Optimization of the optical configuration, centers around satisfaction of NER_ν design goals. The calculation of NER_ν values is carried out in the section on detector NEP, and channel transmittance and bandwidth. The data listed in the opposite table are based on that calculation. The ratio between the calculated and design goal NER_ν provides a means of assessing the performance of the baseline and revised configurations.

The calculated performance of the baseline configuration, in terms of the design goal NER_ν values, was satisfactory enough to allow its use in further study and testing of the BSU. The improvement in performance gained by a reoptimization of the baseline configuration is particularly notable in channels 1, 2, 11, and 14. Due to this improvement, the revised configuration becomes the foundation for the development of BSU flight instrumentation.

Satisfaction of NER_ν design goals is indicated in the table opposite for both the baseline and revised configurations. The NER_ν values are based on initial and revised values of channel transmittance and detector diameter and NEP.

RATIO BETWEEN THE CALCULATED AND THE DESIGN GOAL NER_ν VALUES FOR ALL FOURTEEN CHANNELS

Channel	Baseline Configuration	Revised Configuration
1	1.25	0.76
2	1.39	1.09
3	0.62	0.56
4	0.99	0.94
5	1.13	1.11
6	1.13	1.11
7	1.13	1.11
8	0.90	0.70
9	0.90	0.70
10	0.90	0.70
11	1.25	0.98
12	0.94	0.74
13	1.01	1.24
14	1.17	0.91

SELECTION OF OPTICAL CHANNEL CONFIGURATION

Analysis of the radiometric and field-of-view requirements leads to an optical configuration which employs a reflecting telescope, reflecting chopper at the field stop, and a detector optical relay which images the detector on the secondary mirror.

The primary object of the optical design is to provide the desired angular resolution with minimum radiometric error. To meet this objective, the optical train, consisting of the collecting optics, field stop, chopper, dichroic splitter, filter, and detector must be designed for high rejection of stray light and thermal emissions.

A telescopic optical system must be used to collect enough light from the small field of view. This telescope must be folded to achieve the desired long focal length in a short space.

The Cassegrainian reflecting telescope configuration, consisting of a concave primary mirror and a convex secondary mirror, provides the required focal length and folded geometry.

An optical chopping scheme must be used to achieve the desired systems sensitivity. The use of a reflective collecting telescope with low-emittance mirror surfaces permits location of the chopper at the rear of the telescope near the telescope focus. The small size of the beam near the focus makes it easy to provide an accurate radiometric reference by imaging a small, constant-temperature blackbody directly on the detector with a low-emittance reflecting surface on the chopper. An aperture located at the focus of the telescope just behind the chopper can then accurately define the field of view.

An optical system is necessary to relay the light through to a dichroic beamsplitter and, from there, through a filter to the detector. The dichroic and filter are not perfectly efficient and do emit thermal radiation; therefore, these components must, in any case, be located after the chopper where their unchopped emissions will not be detected except as constant background. Because low emissivity is not required, a simple refractive lens system can be used for the relay optics. Germanium lenses perform best in the short wavelength channels, while the use of silicon lenses is necessary for the long-wave channels.

The detector relay optics must not image the detector on the field stop because the accuracy of the field alignment could be destroyed by a detector misalignment or nonuniformity in responsivity across the detector.

Stray light control requires the use of baffles if light scattered into the field stop is imaged onto the detector. Such baffles contribute to diffraction and may contribute new sources of scattered light.

To eliminate stray light and reduce the effects of detector nonuniformity, it is better to focus the detector on the aperture-defining surface. By making this surface the secondary mirror, all need for baffles or hoods is eliminated.

The central zone of the secondary mirror is unused. To eliminate chopper radiation from behind the field stop from being reflected and imaged on the detector, the center of the detector must be masked off. The optical mockup built for the study employed a concave central zone on the secondary mirror, a less effective approach. The masked-detector approach was used in the ITPR.

A layout of the optical system which results from application of these principles is shown on the opposite page. The details of the system design are discussed next.

CONSIDERATIONS LEADING TO CHOICE OF OPTICAL CONFIGURATION

Problem	Approach to be Used
Light collection from small FOV	Telescopic collecting optics
Low emission	Reflecting telescope
Short geometry	Cassegrainian telescope
High sensitivity	Optical chopper
Accurate radiometric reference	Reflective chopper with blackbody
Accurate field definition	Field stop not at detector
Inclusion of dichroic and filter	Detector relay optics
Elimination of stray light	Image detector on secondary mirror

1110-104-213

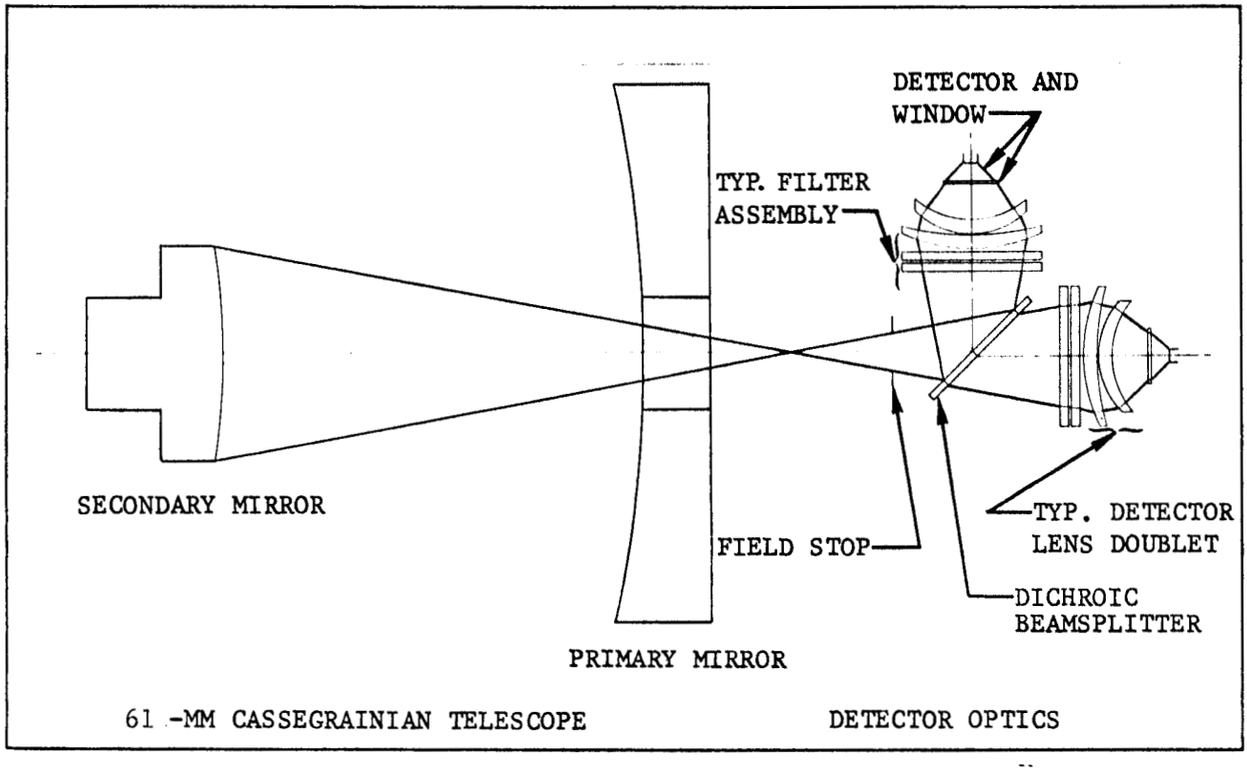

Optical Layout of a 61-mm Telescope With Detector Optics. The telescopes selected for use in the BSU are of the sphere-sphere Cassegrainian type. The detector optics consist of nondispersive elements, filters and dichroic, defining the channel spectral characteristics and detector lens doublets imaging the aperture stop of the system onto the surface of the detectors.

DESIGN OF THE TELESCOPE

The Cassegrainian reflecting telescopes employ spherical mirrors for ease of manufacture, finishing, and alignment. Parameters are chosen to provide minimum secondary mirror obscuration consistent with good image quality, and practical dimensions for the field stop and detector optics components.

The Cassegrainian telescope configuration, consisting of a concave primary mirror and convex secondary, permits the effective telescope focal length to be many times greater than its physical length. It allows very small angular fields-of-view to be greatly magnified at the prime image plane with a very short telescope structure. The circular field stop opening, located precisely on the prime image plane of the telescope, completely defines the angular field-of-view of the radiation from the earth scene.

The dimensions of the telescope mirrors and field stops are determined by computer ray-trace using the following rationale:

- The primary mirror diameter is made as large as possible, consistent with instrument size and weight constraints.
- The primary and secondary mirrors are made spherical, to permit economical manufacture, test, and alignment, and to make it easier to give the mirrors a high polish to reduce emission and scattering.
- The relative aperture at the field stop is chosen to be f/4, so that the beam passing through the interference filters is not too divergent.
- The diameter of the field stop is then chosen so that dichroics, lenses, and filters are of easily manufactured sizes.
- To minimize the diameter of the field stop, the secondary mirror is placed as close as possible to the field stop, consistent with an acceptable level of aberration.

A drawing of the resultant design is shown on the facing page. The table (opposite) itemizes some of the more important telescope parameters together with the corresponding values used in the NIMBUS-5 ITPR, and it compares BSU and ITPR double-sphere telescope dimensions and performance characteristics.

While spherical mirrors cannot produce the image quality which a paraboloid primary mirror and hyperboloid secondary mirror or other aspheric mirror combinations can produce, this spherical-mirror Cassegrainian telescope meets all the angular field-of-view specifications.

The corresponding spherical mirrors of the different telescopes can be economically matched in radius of curvature and sphericity, and can be aligned easily to their own optical axis to give the specified alignment of field-of-view centroids between all channels. Spherical mirrors can also economically be given a very high quality surface polish which is necessary to permit less than 1-percent emissivity and less than 1-percent diffuse scatter after coating. Paraboloids, hyperboloids, ellipsoids, and higher-degree aspheric optical surfaces are much more expensive to produce and to match in quantities. It is also difficult to produce high-quality surface polish on aspherics.

The central zone of the secondary mirror is not used, since those rays which would theoretically use this area are physically blocked by the secondary mirror before they ever reach the primary mirror. This zone of the secondary mirror can reflect stray radiation to that central part of the detector which is an image of this central zone of the secondary mirror.

To keep stray radiation from reaching the detector, a mask may be used in the image plane of the secondary mirror, located at the detector.

In the design of the optical mockup, an alternative but less effective approach was taken. The unused central zone of the secondary mirror was given a concave spherical surface with a radius of curvature exactly equal to the secondary mirror field-stop spacing, as shown in the drawing opposite. This concave dimple in the secondary mirror then precisely images the corresponding central zone of the detector back on itself. Although this approach helps eliminate incident stray light, it allows thermal radiation from the field stop and detector optics to be chopped and then reflected to the detector. Because the detector optics are to be temperature-stabilized, the radiometric error is acceptable, but not desirable.

Radiometric analysis shows that the masked-detector approach used on ITPR is superior and its use is recommended.

1110-102-214

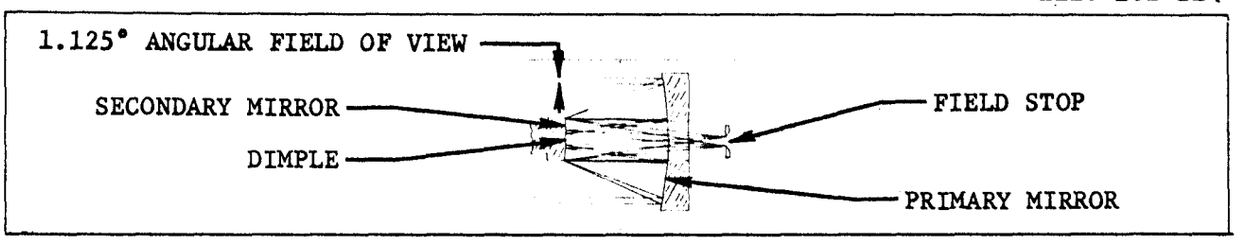

Ray Trace Drawing of Cassegrain Telescope. Spherical mirrors provide adequate definition and are used for ease of manufacture and test. The center of the secondary is deliverately made concave.

SELECTED TELESCOPE PARAMETERS

	BSU 61-mm Dia.	BSU 80-mm Dia.	ITPR 53.249-mm Dia.
PRIMARY MIRROR RADIUS OF CURVATURE (MM)	148.20	194.50	121.6073
SECONDARY MIRROR RADIUS OF CURVATURE (MM)	78.70	103.20	64.5231
PRIMARY-SECONDARY MIRROR SPACING (MM)	47.70	62.60	39.100
SECONDARY MIRROR FIELD STOP SPACING (MM)	74.86	98.44	61.100
SECONDARY MIRROR DIAMETER (MM)	19.52	25.60	16.000
PRIMARY MIRROR DIAMETER (MM)	61.0	80.0	53.249
PRIMARY MIRROR USED AREA DIAMETER (MM)	58.452	76.654	45.708
FOCAL LENGTH (MM)	218.062	286.709	178.571
FIELD STOP DIAMETER (MM)	4.282	5.630	4.6
HALF-POWER FOV DIAMETER (DEGREES)	1.125	1.125	1.4760
NUMERICAL APERTURE (NA) AT FIELD STOP	0.131*	0.131*	0.131*
PERCENT OBSCURATION	14.46	14.00	14.95
CIRCLE OF CONFUSION (DEGREES)	0.077	0.077	0.11
TOTAL AREA OF ACCEPTANCE WITH SPIDER AND SECONDARY OBSCURATION (CM^2)	20.87	35.99	13.9525

*FOR IMAGE AT CENTER OF FIELD-OF-VIEW.

DESIGN OF DETECTOR OPTICS

Each of the 14 channels uses a doublet lens system to sharply image its telescope secondary mirror on the detector, making the secondary mirror the aperture stop of the telescope. Only three different lens designs are used for the 14 channels.

The detector optical systems commence at the field stop and include, in order, a dichroic filter beamsplitter, spectral filters, the doublet lenses, a window to seal the detector, and the detector itself. The figure is an optical schematic of two typical detector channels following the field stop of a telescope.

The dichroic filter is mounted at 45 degrees to the telescope axis. It must be designed specifically for maximum reflectance at 45-degree incidence for the spectral bandwidth required by the reflective channel, and for maximum transmittance at 45-degree incidence for the spectral bandwidth of the transmitted channel. The dichroic filters for all channels have the same physical dimensions.

Two spectral filters with blockers are required by each channel in addition to the dichroic filter in order to properly define the spectral bandwidth. These spectral filters immediately follow the dichroic filter in both the reflecting and transmitting channels. The spectral filters have the same mounting diameter for all 14 channels. In their optical position, the maximum incident angle for any ray at these filters is less than 8 degrees. Thus, near-maximum spectral performance can be expected from these filters.

A doublet lens (a two-element lens system) follows the two spectral filters of each channel and sharply images the telescope secondary mirror on the detector. The doublet lenses for all 14 channels have the same physical diameters. The doublet lenses for channels 1 through 11 are made from germanium, and require two different sets of surface radii, depending on whether the lenses are used with a 61- or 80-mm OD telescope. The doublet lenses for channels 12, 13, and 14 are made from silicon and require a third set of surface radii. These three sets of lens surface radii have been optimized by automatic computer ray-trace procedures for the same numerical aperture (NA) at the detector, and are able to image the circular edge of the secondary mirror at the surface of the detector with aberrations which are less than 1/200 of the detector diameter, or 1/200 of the secondary mirror diameter for that matter, since they are images of one another. The detector is manufactured with a sensitive diameter just slightly smaller than the secondary mirror image; thus, it cannot receive stray radiation from the edges and outside of the secondary mirror. If channel 12 or 13 is placed on a 61-mm telescope (as considered in an alternative design), design of a silicon lens for a 61-mm telescope will be required.

The imaging scheme also has the advantage that the image of the detector at the field stop is defocused so that nonuniformities in detector response do not produce corresponding nonuniformities in sensitivity across the field-of-view.

A thin window is mounted several millimeters in front of each of the 14 detectors. The windows are germanium for channels 1 through 12, and silicon for channels 12, 13, and 14. They are soldered to the detector housing as a seal. The spectral filters and the doublet lenses can be mounted in a separate housing isolated from the detector, which provides convenient mounting and servicing of these elements. The detector housing is adjustable, relative to the filter and lens housing, in the event any final detector adjustment is needed. The final adjustment will be made with machined adapters which will remain stable.

The detailed design data for the detector optics is given in an appendix to the optical subtask report.

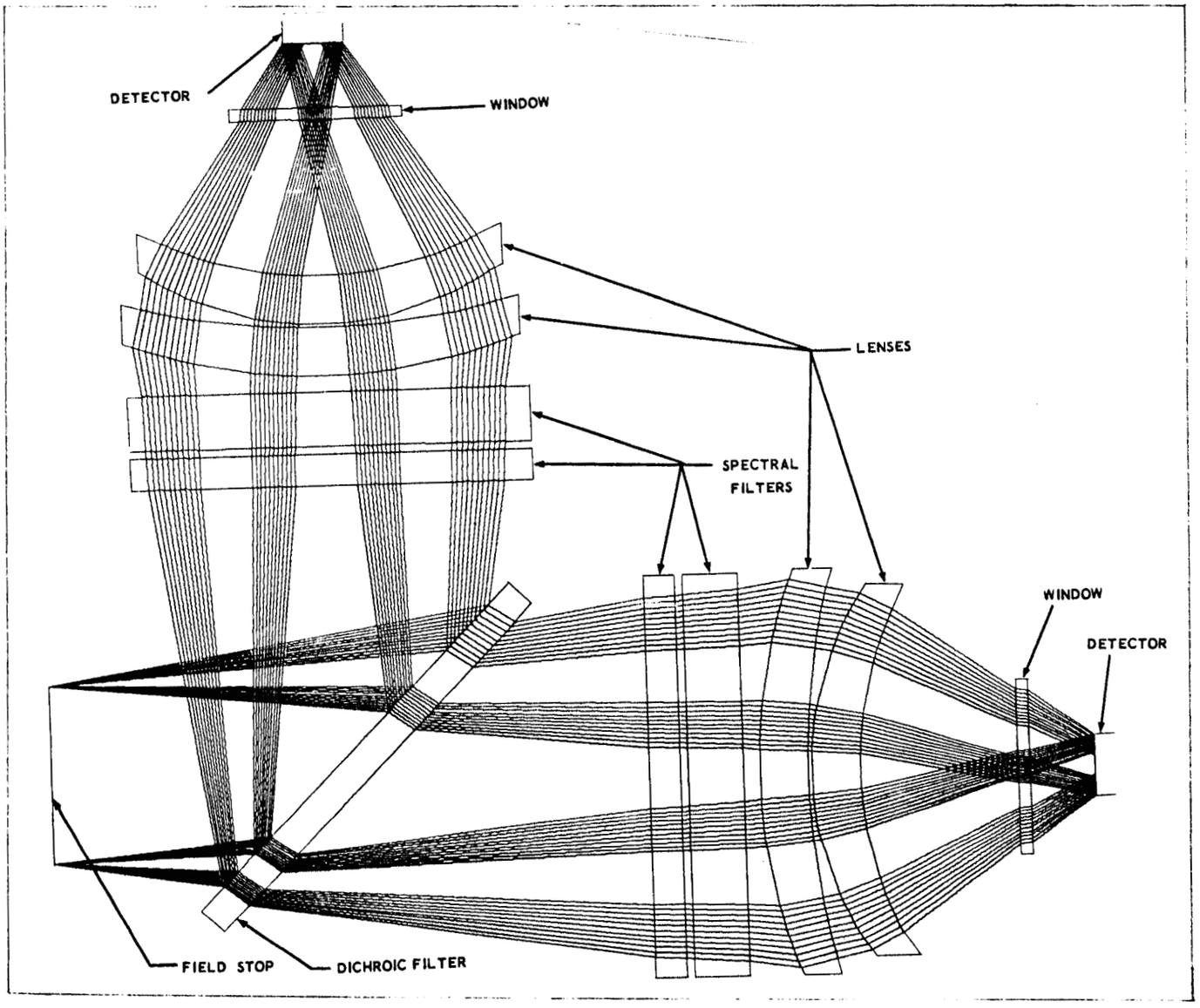

Ray Trace of Detector Optics. Notice how a point on the field stop is imaged uniformly into an area on the detector.

OPTICAL DESIGN OF CHOPPER AND REFERENCE BLACKBODY

A reflective chopper is used to image the detector of each channel into a thermally controlled and measured reference blackbody cavity to eliminate radiometric error from chopper temperature variations.

A highly reflective chopper, in conjunction with an efficient blackbody cavity, can provide a higher blackbody emittance and better blackbody temperature control and measuring accuracy than can a black chopper wheel, the temperature of which must be stable and uniform to better than 0.08°K while it is rotating to avoid detectable radiometric error. Consequently, a reflective chopper is used for all channels.

The light-chopper chops the entering radiation just before it reaches the field stop. The chopper surface facing the field stop is a sector of a concave toroid with a circular cross-section; it has four equally spaced windows in two rings to give four chopping cycles per chopper rotation for each set of telescopes. The concave toroid surface is highly polished and gold-coated for preferably less than 1-precent emissivity and less than 1-percent diffuse scatter. During the chopping cycle, when the chopper blocks the field stop, the toroidal mirror images the detectors of both channels into a small, blackbody cavity located on the chopper side of the field stop.

Separate toroidal mirror chopper surfaces have been designed by computer ray-tracing for the channels following the 61 and 80-mm telescopes, since these telescopes are mounted at different radii. These ray-traces have shown that such toroidal chopper mirrors mounted on a single chopper disc can image the detectors completely within cavities having relatively small openings and relatively large internal areas, for a high, effective emissivity.

Separate but identical cavities are used as the reference blackbody for each telescope. The cavities are temperature-controlled to ±1°C, and are accurately temperature-monitored.

Shown on the facing page is a ray-trace drawing showing how light coming from the detector through the field stop is imaged in the blackbody. The blackbody cavities were made cylindrical in the optical mockup, as shown. The walls of the cavities were coated with 3M black paint.

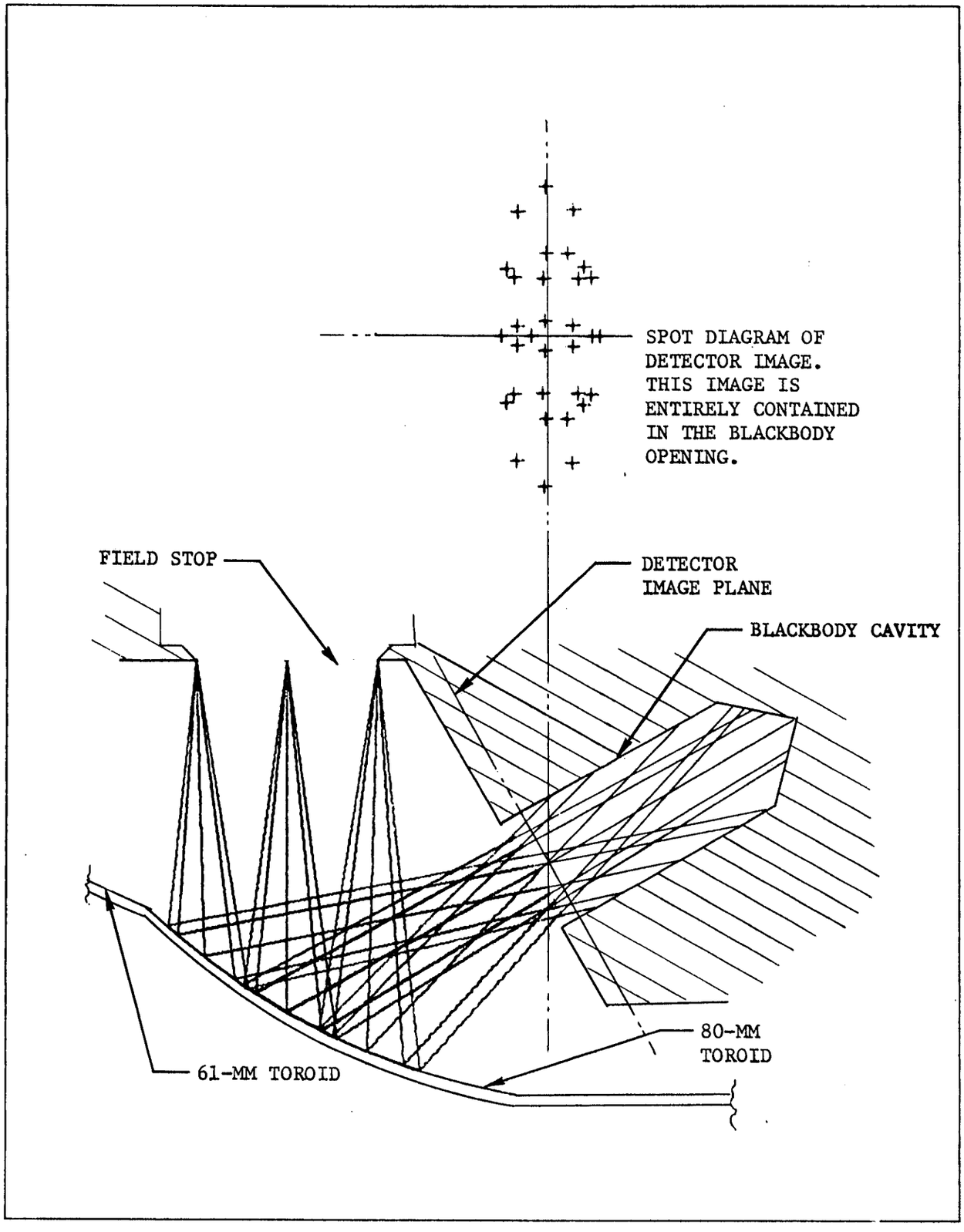

Image Characteristics of Toroidal Chopper Mirror. A mirror chopper and blackbody must be used to provide radiometric reference of adequate stability.

DESIGN OF THE PHASE REFERENCE PICKUP

The phase-reference pickup provides reference for synchronous demodulation of detector signals and synchronization of the chopper with the data system. A narrow beam is interrupted by an edge on the chopper wheel to provide a reference signal with rapid and unambiguous light-dark transitions. The design has been confirmed by mockup testing.

To achieve the required noise performance, the TOVS-BSU employs synchronous demodulation of detector signals. The rotation of the optical chopper is synchronized with the scanner and integrator sequence by means of a phase-locked loop. The synchronizing signal is derived from an optical phase-reference pickup which is sensitive to the angular position of the chopper. The pickup must provide an indication of chopper position which is stable to a fraction of a degree.

Difficulties were experienced with the optical pickup used in the ITPR instrument because the finite beam size and scattering of light caused the signal to make a gradual transition from light to dark. As a result, the duty cycle and phasing were not well defined. This difficulty has been corrected by a design (shown in Figure A) which has been incorporated into the optical mockup.

The beam from a gallium arsenide light-emitting diode (LED) is collimated by a small hole to achieve a beamwidth of about 0.005 of an inch. This beam is alternately interrupted and transmitted at 40 Hz by the chopper wheel, on a 27-inch circumference, and is detected by a phototransistor. This choice of beamwidth is equivalent to 0.27 electrical degree in one cycle of the 40-Hz reference signal. The waveform produced as the chopper interrupts the beam is thus very nearly square.

The phototransistor signal is amplified by circuits which are located at the chopper in the optics subassembly. Because the light transmitted by the defining aperture is small, it is important to shield the phototransistor from stray light to reduce the background signal. When this is done, the phototransistor can be operated into a dc-coupled electrometer, as shown in Figure B. This electrometer is followed by an ac-coupled amplifier as shown. In the optical mockup, this amplifier was made to have such a high gain that it functioned as a ±15 V limiter used to drive the reference input of a lock-in amplifier. The observed switching time was 80 μs, which corresponds to 1.15 electrical degrees. This value is larger than that defined by the optics because of the finite slew rate of the low-power operational amplifier used; however, it is quite acceptable.

For flight, the amplifier gain need only be large enough to drive a comparator located in an electronics subassembly to convert the analog signal to a logic level. The reduction in slew rate will assure that the optically-defined resolution is attained.

The phase-reference pickup electronics dissipates about 60 mW when the LED draws 10 mA from +5 V.

The phase reference pickup is easily made redundant, since there are four stations where such pickups can be placed.

1110-104-207

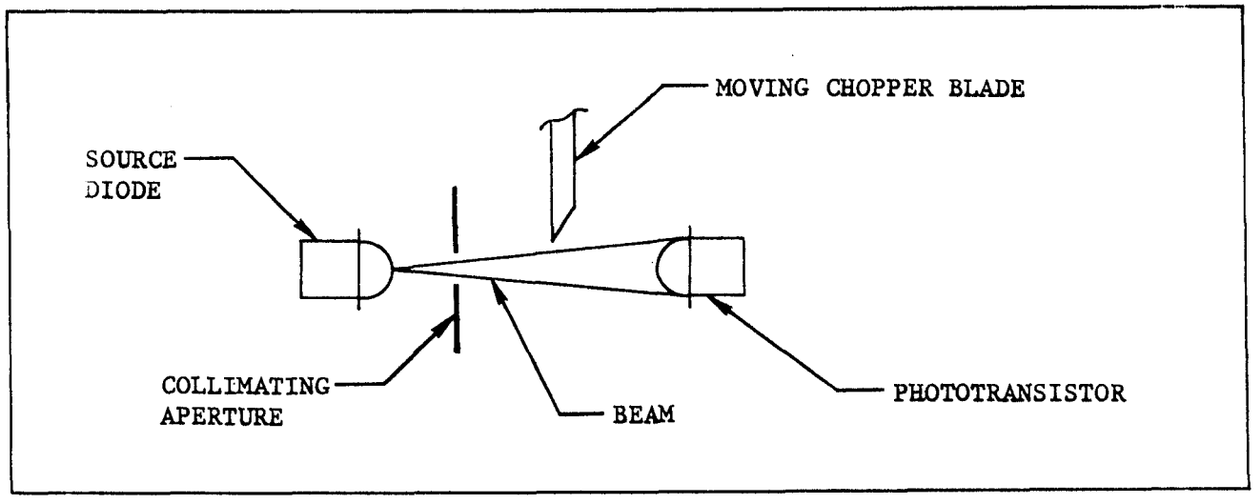

Figure A. Optical Concept of Phase Reference Pickup. The narrow beam defined by an aperture is cut by the chopper to provide a sharp transition.

1110-104-208

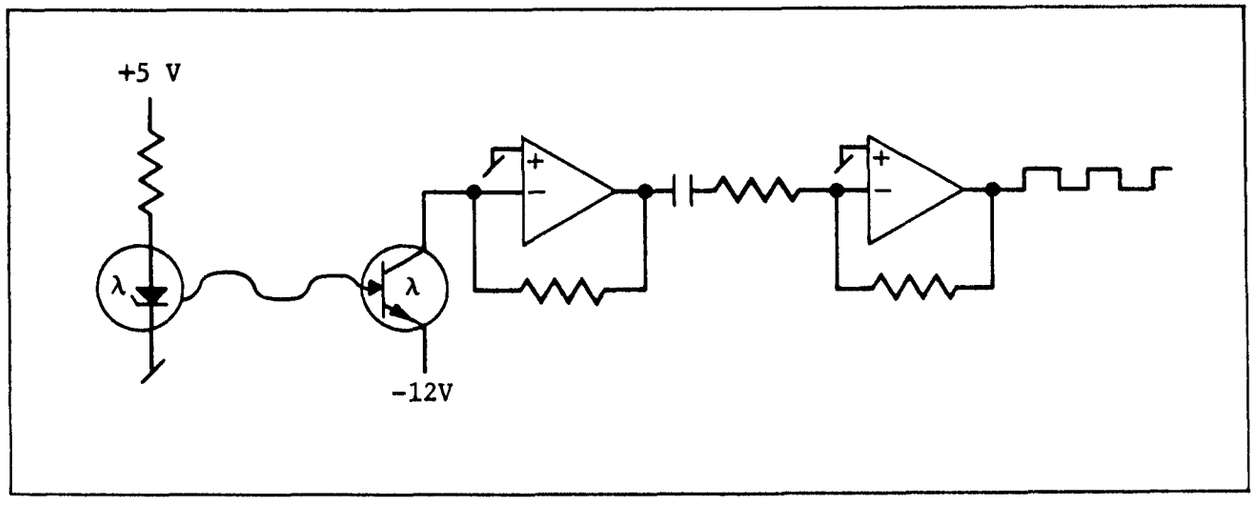

Figure B. Electronic Concept of Phase Reference Pickup. The photo-transistor current is amplified by a dc electrometer and an ac-coupled buffer amplifier.

PROPERTIES OF OPTICAL COMPONENTS

The optical components used in the TOVS-BSU must be suitable for space flight and must be of a quality suitable for accurate radiometric measurements in the near and intermediate infrared region. Key properties of components are summarized here.

Telescope mirror blanks shall be of fused silica so as to provide thermal stability of the mirror figures. Fused silica can be polished to provide an ultrahigh reflectivity of the coated surface, yielding a low emissivity. Fused silica offers an advantage over other high thermal stability glasses; that is, metallic coatings, if defective, can be dissolved without etching the substrate surface. Such rework cannot be accomplished with CERVIT materials.

Lens, dichroic beamsplitters, and filter-blocker substrates shall be of a material suitable for the wavelengths of interest. Suggested materials are listed in Table I. They shall be fabricated from optical grade material, free of inhomogeneities, and shall be annealed. The index of refraction of the material used in the fabrication of the blanks shall be sufficiently well defined to provide proper data for optical design.

The polished surfaces of the mirrors shall be of 10-20 surface quality (or better if practical) to provide low emissivity of the final coated surface. Other optical elements shall be of a 40-60 surface quality to avoid scatter. Optical surfaces shall exhibit no grayness or orangepeel.

The figure of the optical surfaces shall be defined by the optical design and shall be specified on control drawings. All figures shall be verified by testing against test glasses. The radius of test glasses shall be certified by independent testing laboratories. Test glasses shall be deliverable items.

The thin-film coating of optical elements shall meet the spectral requirement established by their application. The metallic coatings of mirrors shall provide high reflectivity throughout the near and intermediate infrared region, 2.5 μm to 30 μm. Antireflection coatings of lenses shall be optimized for wavelengths of interest and shall be as uniform as practical, minimizing run off. Spectral requirements of dichroic, filter, and blocker elements shall be in accordance with the application and shall be thermally stable as outlined in their specifications.

Thin-film coatings shall not deteriorate under the environmental conditions normal to space flight applications as outlined in Table II. Degradation is defined as a change in spectral properties beyond tolerances established by the specification or adhesion or surface quality of the coatings. Nondegradation during cleaning shall not be applicable to mirror coatings. Test specimens shall be fabricated in a manner identical to that of the elements they represent. Environmental testing of the qualification test specimens shall indicate conformance to the environmental requirements. All optical components shall be subjected to screening tests to eliminate failures caused by infant mortality. These tests shall be developed by optical engineering and reliability personnel and shall be monitored by Quality Assurance.

TABLE I. SUGGESTED MATERIALS FOR OPTICAL ELEMENTS

The materials listed are suggested as suitable for the wavelengths indicated.

Element	Wavelength Region	Suggested Material
Mirror	N/A	Fused Silica
Lens, Dichroic, & Filter	3.7 μm to 15 μm 18.8 μm to 29 μm	Germanium Silicon located
Blocker	--	As required

TABLE II. OUTLINE OF ENVIRONMENTAL TESTS

The coatings on optical elements shall not be permanently degraded by testing under the listed environmental conditions.

Condition	Abbreviated Description of Test
Humidity	Requirements of MIL-C-675
High Temperature	+50°C for a period of 24 hours
Low Temperature	-25° in 10^{-5} torr, +5°C in maximum humidity test
Adherence	Requirements of MIL-M-13508 prior to humidity test
Radiation	Irradiation by bremsstrahlung in accordance with specification
Cleaning	Isopropyl alcohol with cotton tipped applicator (n/a to mirror coatings)

ARRANGEMENT OF THE OPTICS SUBASSEMBLY

The TOVS optics subassembly consists of the assembly of the telescopes, the telescope mounting plate, and the temperature-controlled detector optics housing with the detectors, filters, dichroics, blackbodies, and detector optics. This subassembly is a primary structural element of the instrument which is separately aligned and tested.

As shown in the facing figure, the optics subassembly has two main parts: the telescope mounting plate with attached telescopes and chopper motor; and the detector optics housing with its detectors, detector optics, filters, dichroics, blackbodies, and thermal control heater. The telescope mounting plate is machined from aluminum alloy with an intermediate thermal stabilization treatment before final machining. It is basically a flat plate with a cutout for the chopper motor and a circular array of cutouts for the telescope barrels. In the area of the telescope cutouts, there is a thickened section for added strength in the cusp area between the telescopes. Accurately-machined pads and tapped holes to accommodate the optics housing are provided at the outer periphery of the telescope mounting plate. The rotating optical chopper wheel and its heat shield are accommodated in the area between the telescope mounting plate and the optics housing. The optics housing is a primary mount for all aft optics and all detectors as well as the site of the reference blackbodies; its thermal mass makes possible accurate temperature control of detectors and blackbodies.

Critical Thermal Areas - The critical thermal areas in the optics assembly have to do with the detectors, the reference blackbodies, and the chopper wheel. The detectors and the reference blackbodies must be made thermally stable. Their temperatures should not vary more than a few hundredths of a degree between calibrations if interpolation between calibrations is to be avoided.

This control is achieved by thermally coupling these elements to a stable mass, namely, the detector optics housing whose temperature is controlled by use of a heater. The blackbody cavities are machined directly in the beryllium housing, while the detector-preamplifier housings are mated to the housing with joints of low thermal resistance. It is also necessary to avoid channel-to-channel temperature variations. This is accomplished by ensuring that the heat flow in the thermally stable mass is symmetrical. Accordingly, the detector optics housing is basically circular with the heat input distributed to avoid gradients in the structure. To minimize these gradients, the detector optics must be isolated from the rest of the instrument. Isolation is achieved in the TOVS instrument by thermally tailoring the structural contact points between the optics housing and the telescope mounting plate. A cross-sectional view of one of the mounting points is shown in Figure B. The thermal properties of the joint are accurately determined by controlling the material cross-sectional area and thermal path length of the mounts.

Temperature Control of Chopper - Since this instrument employs thermally stable references and a reflective chopper wheel, the temperature stability requirement on the chopper is far less stringent than it would be otherwise, but the chopper temperature must still be reasonably uniform and stable; the requirement is about 2°C. Uniformity is achieved by stabilizing the chopper wheel at the temperature of the optics housing and by making it of a thermally conductive material. The primary mechanism is radiative coupling. Except for the reflective toroidal areas, the side of the chopper wheel that faces the aft optics housing is black, as is that side of the optics housing. A heat shield, thermally grounded to the optics housing, is interposed between the chopper wheel and the telescope mounting plate. Thus, the chopper wheel is surrounded by material at optics housing temperature. It receives a very small heat input from its hub

because all of the chopper motor's heat dissipation occurs in its stationary stator and not in the rotor to which the chopper wheel is attached.

1110-104-211

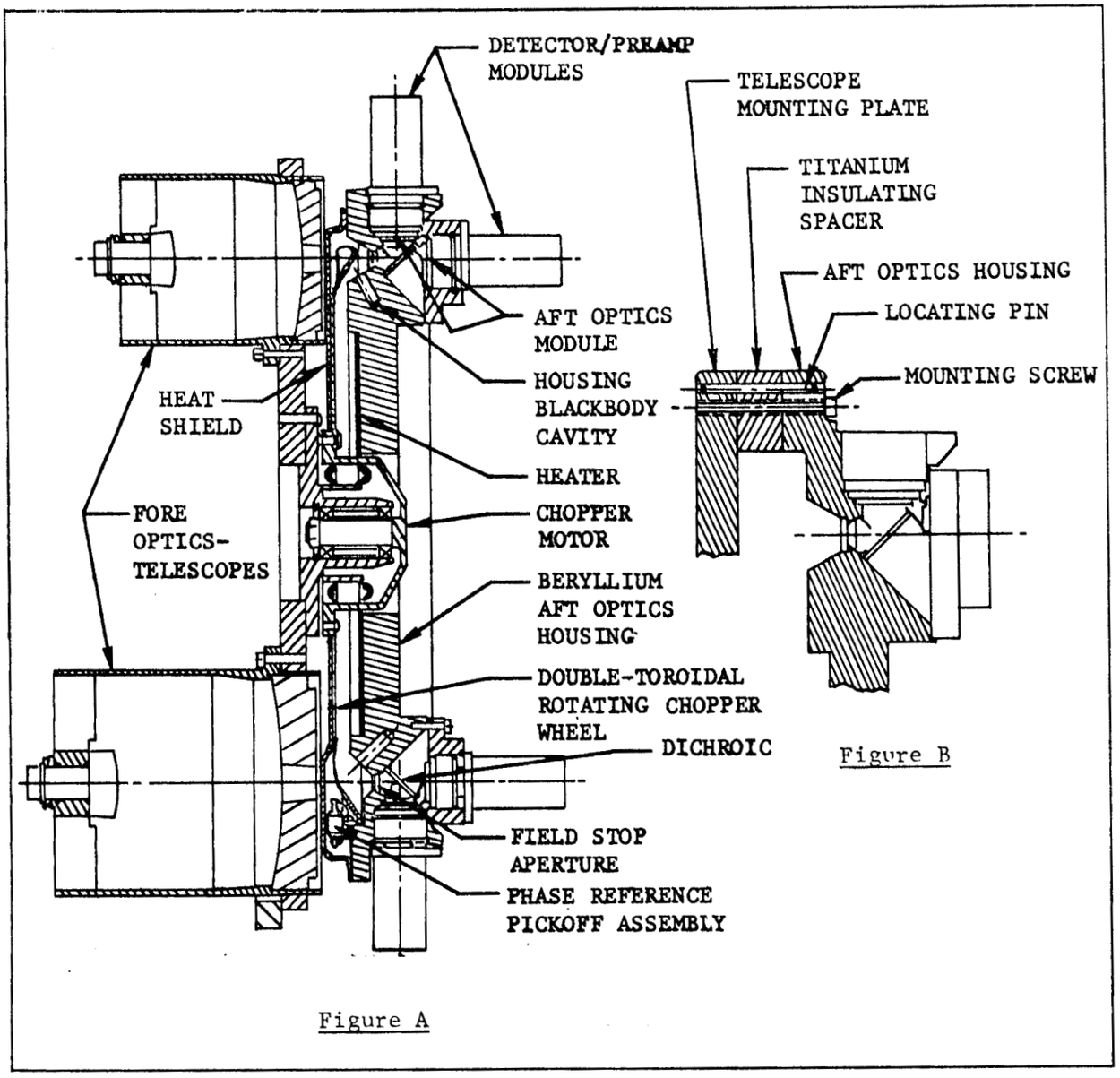

Figure A. Arrangement of the TOVS Optics Subassembly. The filters, dichroics, detectors, and reference blackbodies are mounted on a temperature-controlled plate.

Figure B. A Cross-Sectional View of one of the Mounting Points. Temperature control of the plate is achieved by thermally tailoring the structural contact points between the optics housing and the telescope mountingplate.

CONSTRUCTION AND SUPPORT OF THE TELESCOPES

The light-collecting telescopes are subassemblies which are individually mounted on a baseplate. Cylindrical panels space the primary and secondary mirrors which are mounted with wave springs. The mounting plate is aligned to the aft optics by pins.

The baseline design chosen for study employs individually-mounted telescopes because this approach has been successful in the past. The telescope layout is shown in Figure A.

Primary Mirrors - The spherical telescope primary mirrors are front-surface mounted in the telescope barrels. The seats against which the mirrors are held cover the full periphery of the mirror and are precision-machined in the metal of the telescope barrel. The mirrors are held firmly against their seats by wave springs of circular form. The contact area of the springs against the mirror is the same as the projected contact area at the mirror seat to avoid bending stresses in the material of the mirror. Retainers pinned in place at the aft end of the telescope barrels offer a reaction surface for the spring force and keep the entire assembly together. The preload of the wave springs is chosen so as to keep the mirrors against their seats under the worst conditions of environmental loading.

The preloading springs locate the mirrors in the axial direction. In the radial direction, a small amount of clearance is necessary because of the difference in temperature coefficient of the fused silica mirrors and the aluminum telescope barrels (3.1×10^{-7} per °F and 12.9×10^{-6} per °F, respectively). Taking into consideration the greatest possible temperature swings, the clearance that must be allowed on the diameter is 0.006 in. Slight movement of a spherical mirror on a spherical seat produces no changes in the optical parameters, so such motion is of no concern. The impact forces which may exist between the mirrors and the walls of the telescope tubes are not easily calculated; however, the damping produced by the mirror clamping forces will attenuate this greatly, or even prevent the relative motion altogether. This discussion is based on the 80-mm mirror; the diametral clearance required for the 61-mm objective is smaller.

Secondary Mirrors - The telescope secondary mirrors are mounted in the same manner for both the 80- and 61-mm telescopes. These mirrors are centered on the optical axis at the mounts of the telescope tubes by three spider arms. These mirrors are also held in place by spring pressure. However, the optical design does not allow first-surface mounting of the secondaries, as their peripheries must be kept clear to avoid excessive blockage. Therefore, the mirrors are second-surface mounted, the second surface being a shoulder which bears on the metal of the spider mount. The length from the shoulder to the figured surface of the mirror must be accurately controlled; however, the convex shape allows this to be done easily. Wave springs similar to those used for the telescope objectives, although much smaller, are used to provide the seating force for the secondaries. Retention and a reacting surface for the springs are given by retaining rings assembled into grooves ground into the rear part of the mirror bodies. The fused silica material is sufficiently strong to allow this procedure. For the cases at hand, the maximum calculated tensile stress in the material is 17 psi for the large telescope secondary. In order to ensure stable positioning of the telescope secondary, and to reduce temperature differences between the mirrors and the spider mounts, the mirrors are located by beveled indium rings--a technique that was employed successfully in the ITPR instrument.

Telescope Mounting - The aluminum telescope mounting plate locates and supports the telescope barrels. It also carries the chopper motor, and serves as the main structural support member for the entire optics subassembly. The

telescope mounting plate has a pattern of large cutouts on two diameters to accommodate the telescope barrels, and a hole at the center for the chopper motor. The size of the telescope apertures is so large that there is little material left in the cusp areas where adjacent telescope cutouts meet. Since rigid mounting of the telescopes is a necessity, an annular thickened section was added to the plate in the cusp area, thereby achieving adequate structural rigidity while retaining the optimized optical design. The thickening is shown opposite in the side view of the plate (Figure B).

Threaded holes for mounting the aft optics housing on its insulating spacers are provided at the periphery of the telescope mounting plate. Holes also are provided for mounting the telescope mounting plate (and thus the entire optics subassembly) to the instrument housing. Space is provided for the installation of locating dowel pins through to the aft optics housing. These pins, installed when the optics subassembly is initially adjusted, are necessary to preserve optical alignment.

The chopper motor is mounted in the center of the telescope mounting plate, which shunts the motor's heat flow to the instrument housing. The increase in the thickness of the plate in the cusp area reduces the thermal impedance.

1110-104-217
1110-104-216

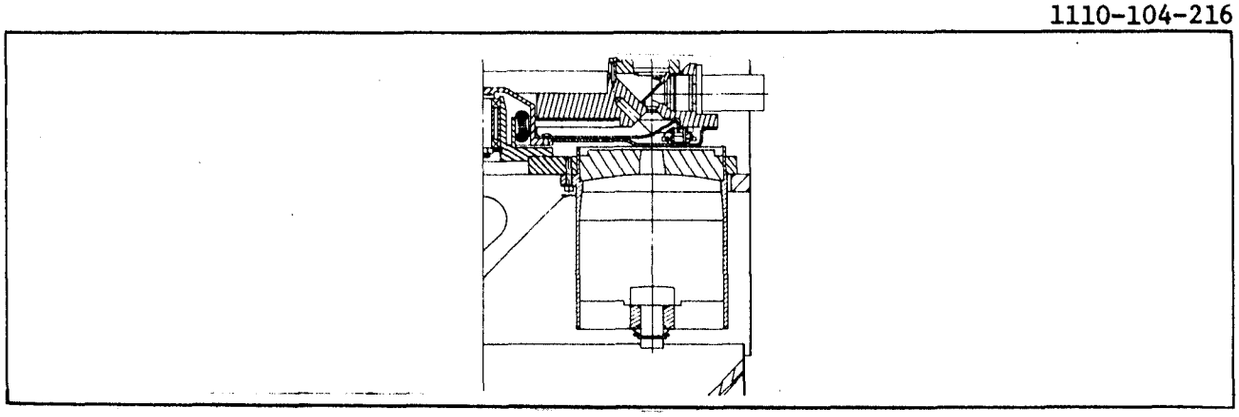

Figure A. Telescope Detail. The mirrors are mounted to precisely machined surfaces in individual barrels using wave washers for compression.

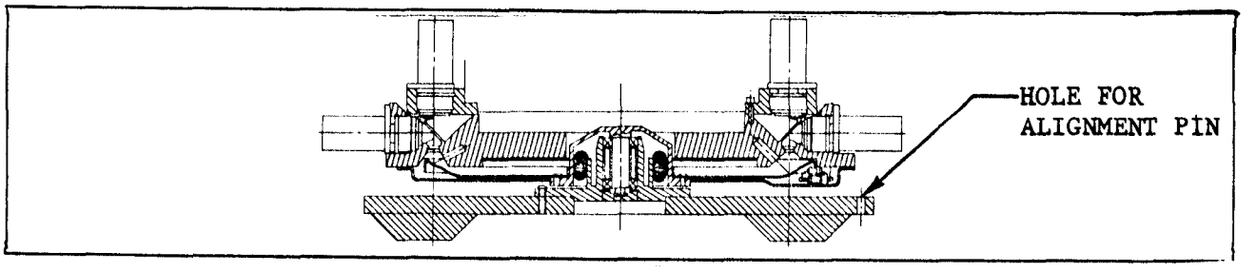

Figure B. Side View of Telescope Baseplate. The baseplate is thickened for strength where each telescope is mounted and is aligned to the detector optics assembly by means of pins.

MOUNTING OF DETECTOR OPTICS

The detector optics is mounted on a single temperature-controlled housing into which is machined the field stops and the mounting surfaces for dichroic mirrors, filter and lens modules, and detectors.

The detector optics housing provides a circular array of detector optics mounting points. With each mounting point is associated one reference blackbody (a blackened cavity machined into the metal of the housing), one dichroic mounting surface, and two lens/filter mounting cavities. Each mounting point is used by two channels, with the split between the two channels occurring at the dichroic mirror. Thus, the dichroic mirror, field stop, and reference blackbody cavity are shared by both channels, as shown in the detector optics layout opposite.

Field Stops - The field stops are machined into the detector optics housing which is accurately aligned to the telescope mounting plate with pins.

Dichroic Mirrors - The dichroic mounting surfaces, set at an angle of 45 degrees to the incoming optical axis, are machined directly into the metal of the optics housing, permitting the dichroic mirrors to be first-surface mounted. This technique enhances the optical accuracy and stability of the system. However, a large pocket which must be provided to allow installation of the dichroics interferes with the placement of the lenses and filters for the axial channel. To eliminate this problem, final machining of the bores for mounting the axial channels' lenses and filters is not done until the lens and filter separable modules are installed and pinned in place. This improved dichroic mounting technique assures that the accuracy of lens and filter mounting is not compromised.

Mounting of Dichroic Mirrors - The dichroic mirrors are held against the accurately machined seats in the optics housing by beryllium copper spring clips. The spring clips employ the same material and precision as that specified for the other optics mounting springs. Each dichroic is held against its seat with a force of 1.0 lb, and a generous clearance is allowed around the periphery of the dichroic since slight lateral movement is of no concern.

Dichroic mirrors are readily accessible when their corresponding axially mounted housings are removed.

Transmitting Detector Optics - The transmitting detector optics (blocking filters, bandpass filters, and lenses) of the TOVS instrument are mounted in a modular fashion. For each channel there are two modules containing these elements--one for the filters and one for the lenses. Spring pressure is used to restrain and accurately locate the elements in much the same manner as is done with the telescope mirrors. For every channel there is a cavity in the optics housing at the detector mounting flange. Into this cavity is inserted the filter module, which is located against a shoulder at the bottom of the cavity. A pre-loading spring is placed at the top of the cavity. The lens housing is inserted next, followed by a retaining ring which fits into a machined groove in the housing. The spring force seats the components against the shoulder and the retaining ring, respectively, thus locating them accurately (accuracy of location is essential for the lenses though not so important for the filters). The layout of one of the lens mounting modules is shown in Figure B; a filter mounting module is shown in Figure C.

1110-104-221 1110-104-222 110-104-223

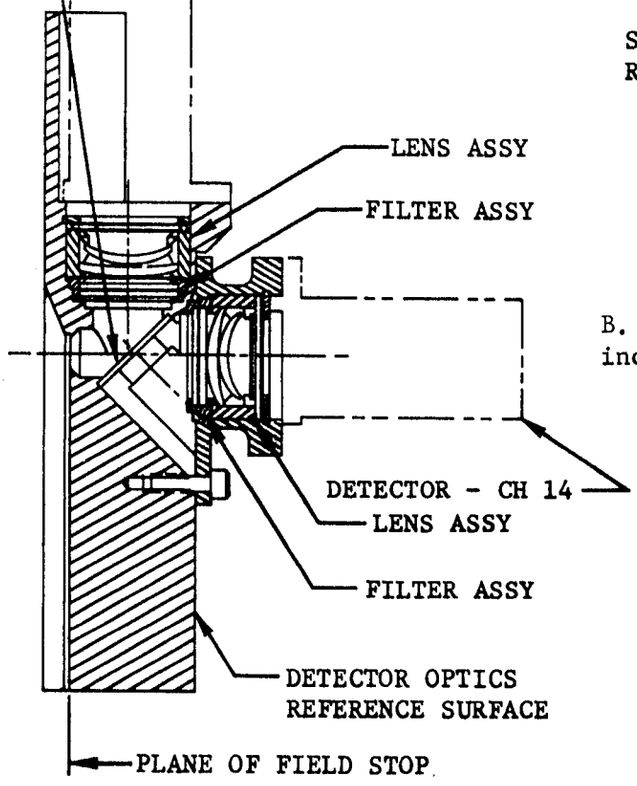

A. Typical Detector Optics Layout. All components are located by reference to machined surfaces

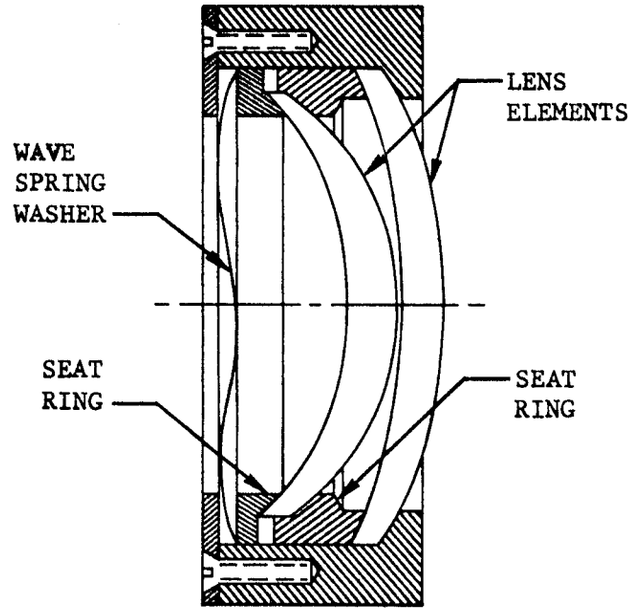

B. Typical Lens Module. Modules allow independent testing of each lens system

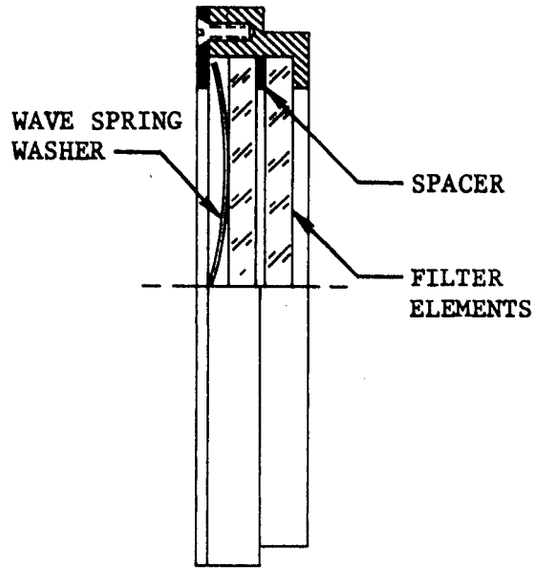

C. Filter Module. Modular mounting allows filter and blocker to be tested together in final configuration

MOUNTING OF DETECTOR-PREAMPLIFIER MODULES

The TOVS detectors and preamplifiers are mounted in a standard housing which is the same for all 14 channels. Important considerations in the design and mounting of these housings are accuracy, optical stability, thermal stability, and ease of access.

Housing Types - The detector-preamplifier housings are made of aluminum and are about 3/4 of an inch in diameter by 1-1/2 inches long. They are flange-mounted on the optics housing in the pattern shown in the figure opposite. There are basically two types of housings: those placed axially in the package (transmitting channels) and those placed circumferentially (reflected channels). It is desirable that all be readily accessible for service. The axial housings are removed directly from the end of the instrument after the cover is removed. The circumferentially located housings can be removed from the sides and bottom of the package, with the exception of one channel which may be removed through a hole in the electronics tray. All may be removed with equal facility when the optics deck is dismounted.

Mounting Accuracy Considerations - Detector-preamplifier housings must be designed to ensure accurate mounting both with respect to focus and to placement in the optics field. Accurate placement along the optical axis (focus) is achieved by mounting to optimized dimensions determined by computer ray-trace and by the use of interface adapters of selected thickness at the housing interface. The advantage of this method of placing the detectors and detector optics axially is that there are no adjustments which can creep after final assembly.

Lateral Placement - Proper lateral placement of the active areas of the detectors at the field-of-view is achieved by individually adjusting each detector housing. To facilitate this, the detector housing mounting flanges and their mating areas on the optics housing are precision-lapped to a flatness of ±0.0005 of an inch which permits the detector housings to be moved laterally in such a manner that no change of focus takes place. Thus, any energy changes seen when the adjustment is made are due solely to the lateral movement of the detector chip in the field. When optimum position is achieved, the detector mounting screws are tightened. The theoretical location of the optical axes of the various channels is held with sufficient accuracy that a great range of adjustment for the detectors is not necessary. Accordingly, the latitude allowed is ±0.005 inch.

Achieving Optical and Thermal Stability - Ensuring long-term optical stability of the detectors is primarily a matter of ensuring that they do not move about once initial adjustment is made. There are two pilot holes in the flanges of all detector housings, and these are used to drill and ream holes for two locating pins which prevent any movement of the detector housings. Once the pins are installed, it is possible to remove a complete detector housing and then repeat its location back on the optics housing.

Thermal stability of the detectors is very important to radiometric accuracy. The maximum desirable channel-to-channel temperature variation is about 1°C, and the maximum temperature variation between calibrations (every 256 seconds) is about 0.1°C. These thermal specifications are met by controlling the temperature of the housing with a proportional temperature controller. The success of this scheme obviously depends upon having the detectors and detector housings isothermal with the optics housing. This is done by providing a low thermal resistance between detector housings and the optics housing. It should be noted that the detectors are intentionally located on the optics housing in a symmetrical fashion, and dummy detector housings are mounted at the spare channel locations. This tends to avoid channel-to-channel temperature gradients.

1110-104-209

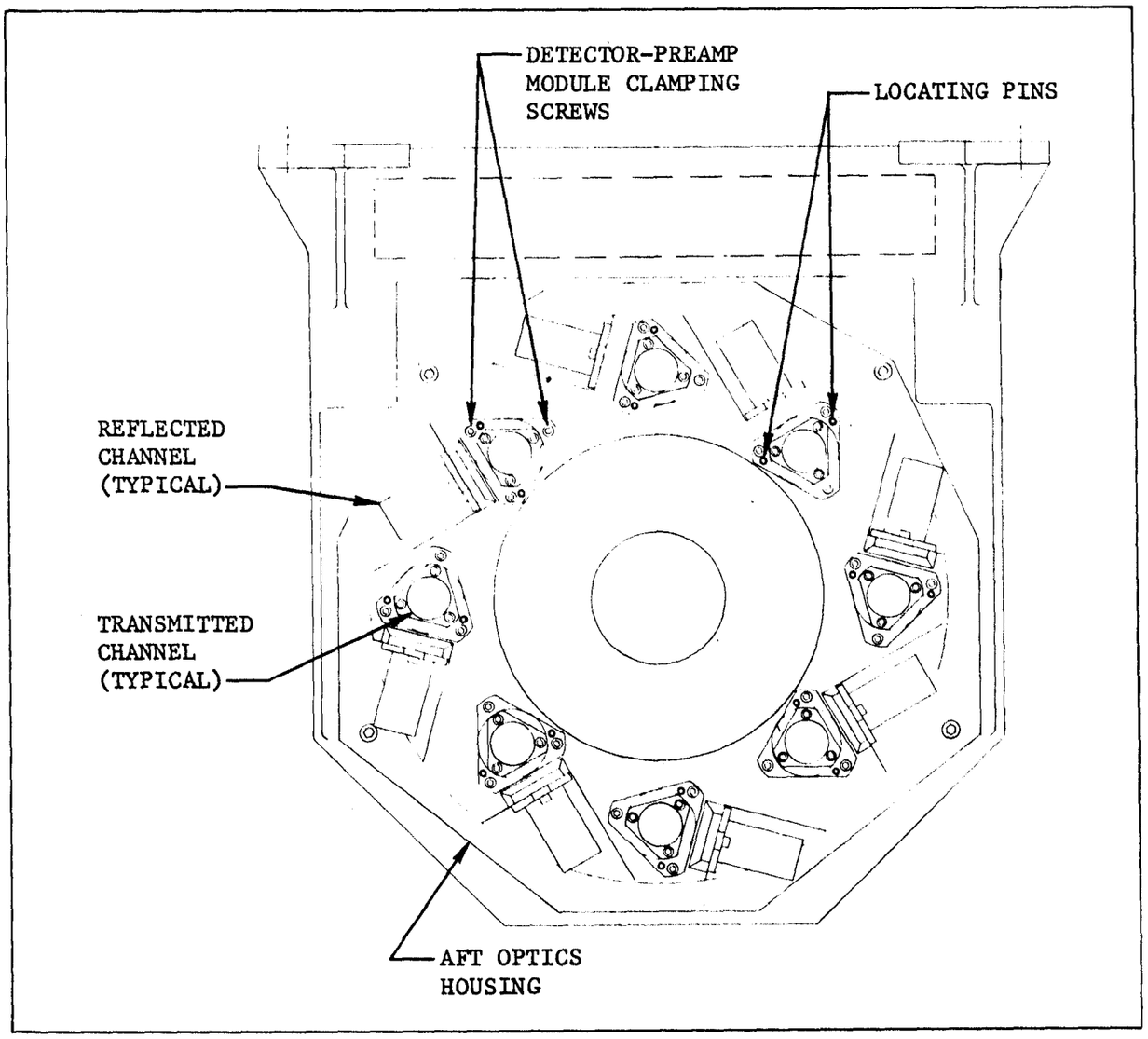

Detector Mounting Locations. The detectors are mounted to machined surfaces without adjustments except a machined shim.

DETAILS OF CHOPPER DISC AND DRIVE

The chopper disc is designed for good mechanical and thermal stability, and is direct-driven by a 20-pole hysteresis synchronous motor at 600 r/min.

The chopper is a disc with toroidal reflecting surfaces which image the detector onto the temperature-controlled reference blackbodies.

The chopper disc is attached directly to the motor rotor and driven at synchronous speed. The 40-Hz chop, required by the system design, is accomplished with a four-bladed chopper disc driven at 600 r/min. The blades and cutouts are equal in size since a symmetrical chopping pattern is desired.

There are two rings of cutouts in the chopper, corresponding to the two rings of telescopes. A view of the chopper disc is shown in Figure A. The reflective surfaces between rings are polished and gold-coated, while the rest of the chopper is black for good radiation coupling to the temperature-stabilized detector optics housing.

The disc is made of electroformed nickel, a desirable material and process for this part since the material is stable, has a high elastic modulus, and polishes well. The process allows it to be formed in very thin sections in a strain-free manner with detail features, such as strengthening ribs, easily produced.

Thermal emission from even the polished gold surfaces of the mirrors can be detected; therefore it is important that the chopper temperature be stable and uniform within 2-4°C so that the effects of emission can be calibrated out.

Because of the need for a thermally stable chopper, the thermal conductivity of the disc material is important. The conductivity of nickel is quite good--more than half that of aluminum--and better than the common austenitic stainless steels by a factor of more than 5.

It is necessary to strengthen the rim of the chopper wheel with a continuous band of material to compensate for the large cutouts which would otherwise tend to weaken it. This continuous rim is also used to create the phase reference signal. The phase reference pickup (see Figure B) is an optical transmitting device with a very narrow beam, which is interrupted by the passage of notches in the rim of the chopper wheel, thereby generating a precise phase reference signal.

The chopper drive motor is a 20-pole hysteresis synchronous unit driven by 100-Hz pulses from the power supply. It is very similar in design to a previous unit flown on another satellite instrument. The unit had a rated torque of 0.8 oz-in, and its weight was 7.5 oz.

The motor is primarily of titanium construction. The chopper drive motor is of inverted design, wherein the stator is actually located inside the rotor. This helps to reduce weight with this type of motor, since its weight is mostly in the copper and iron of the stator. In this application it is also very easy to provide a large-diameter hub to which the chopper disc can be mounted; thus, the problem of securely attaching it to a small-diameter shaft with taper pins and such hardware is avoided. To avoid an inertia problem, the rotor is of titanium. (A thin ring of magnetic alloy pressed into the periphery of the titanium part completes the magnetic circuit.) A strong point of the multipole design is velocity stability; the motor inherently has a very low velocity ripple (flutter), therefore the chopper disc need not be a flywheel--it can be designed for as low an inertia as possible.

1110-104-219

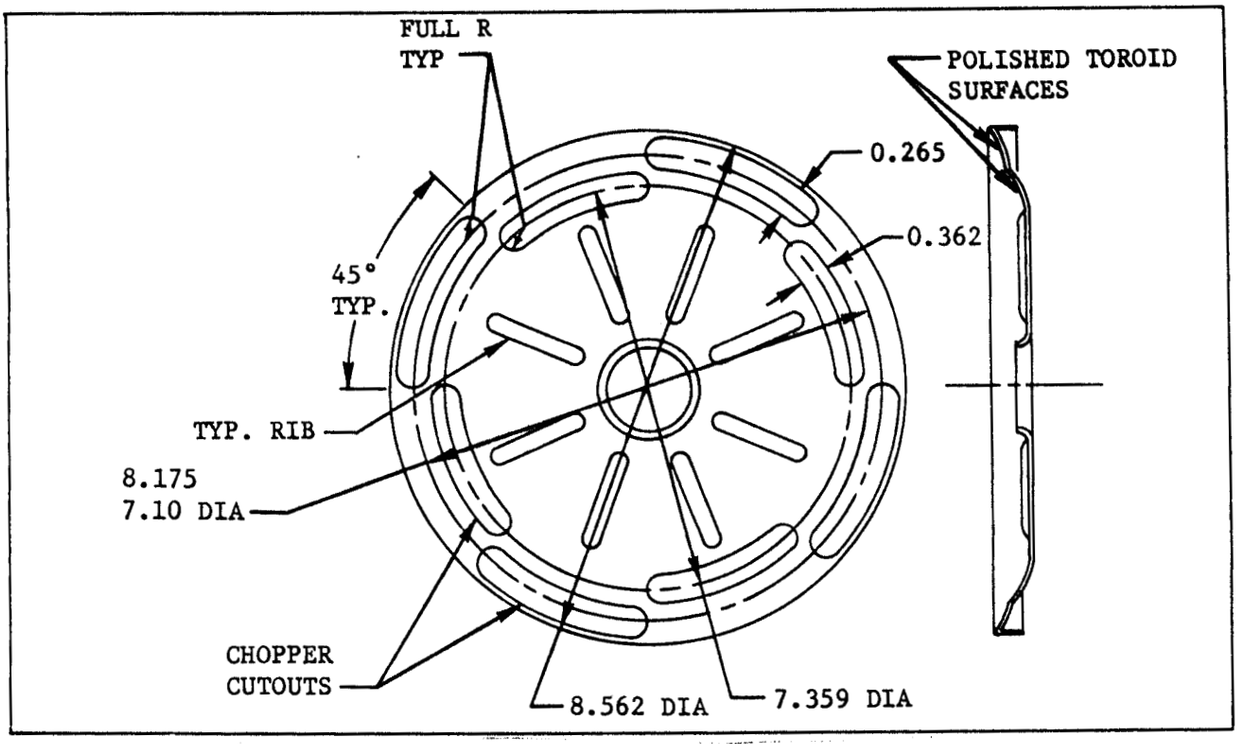

Figure A. Plan View of Chopper Showing Cutouts. Two rows of cutouts are needed to chop the light for each of two rings of telescopes.

1110-104-220

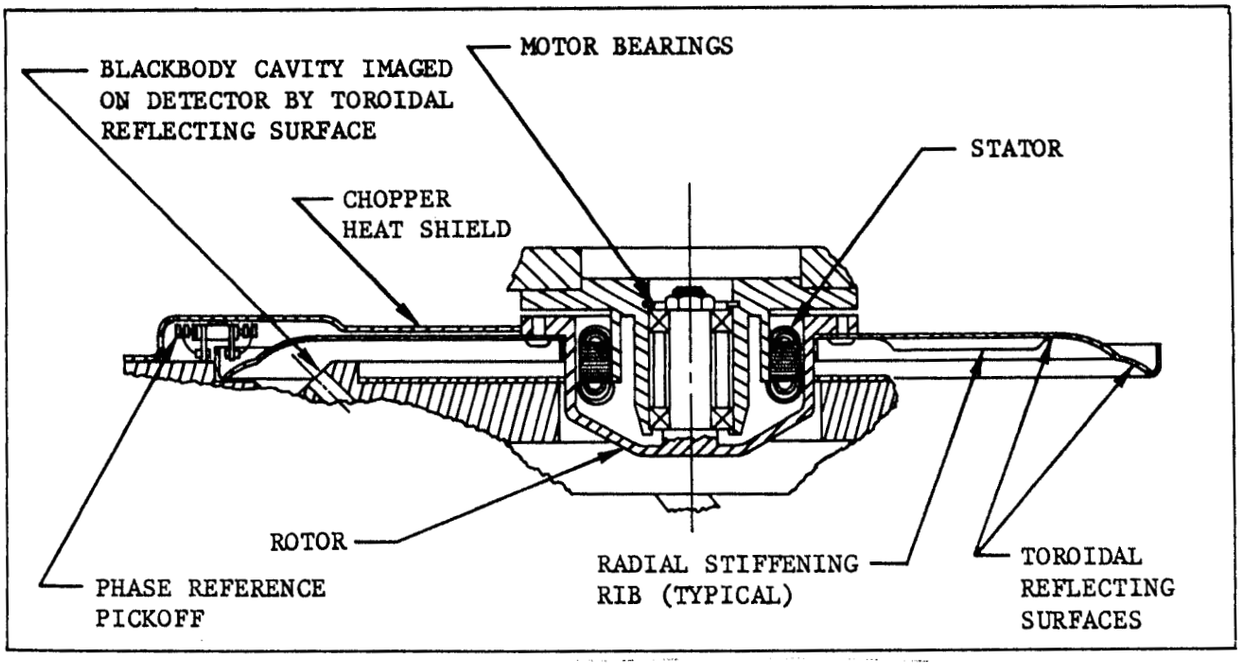

Figure B. BSU Chopper Disc and Drive. The chopper disc is attached directly to the rotor of the drive motor.

STRUCTURAL ANALYSIS OF THE OPTICS

Structural areas which are seen as potentially troublesome in the optics subassembly are: bending of the telescope tube, bending of the detector preamplifier assembly, and inertial movement of spring-retained optical components.

The telescope tubes were treated as tip-loaded cantilevered beams. The maximum stress and deflection in the material of the telescope tubes are 51 lb/in^2 and 6×10^{-6} inches, respectively. The calculated natural frequency of 3140 Hz indicates that there will be no resonance problems. (Testing does not go above 2000 Hz.) A similar analysis of the detector preamplifier assemblies gives stress and deflection values of 141 lb/in^2 and 21×10^{-6} inches. The natural frequency of these components is about 5300 Hz, which is well above the exciting frequencies.

The telescope mirrors, dichroics, filters, and detector lenses are held against their seats by spring pressure, since it is desirable that these components remain against their seats under the worst conditions of loading. Accordingly, an analysis was made to ensure that the required seating forces would not be overly large.

The applicable random vibration testing spectrum for the BSU is shown in the facing figure. It shows only white noise at 0.2 g^2 per Hz to 2000 Hz, with sharp rolloff above that point. This yields an rms figure of 20 g, and the design point is taken as three times the rms, or 60 g. Springs for seating pressure at 60 g, +20 percent, for manufacturing tolerance. The results are shown in the table opposite. Unit stresses on the optical components are negligible.

TOVS OPTICAL COMPONENTS -- SEATING FORCES

	Weight (lb)	Required Spring Force (lb)	Stress (lb/in^2)
Telescope Primary Mirror	0.37	26.6	24
Telescope Secondary Mirror	0.38	2.8	17
Dichroic	0.003	0.8	16

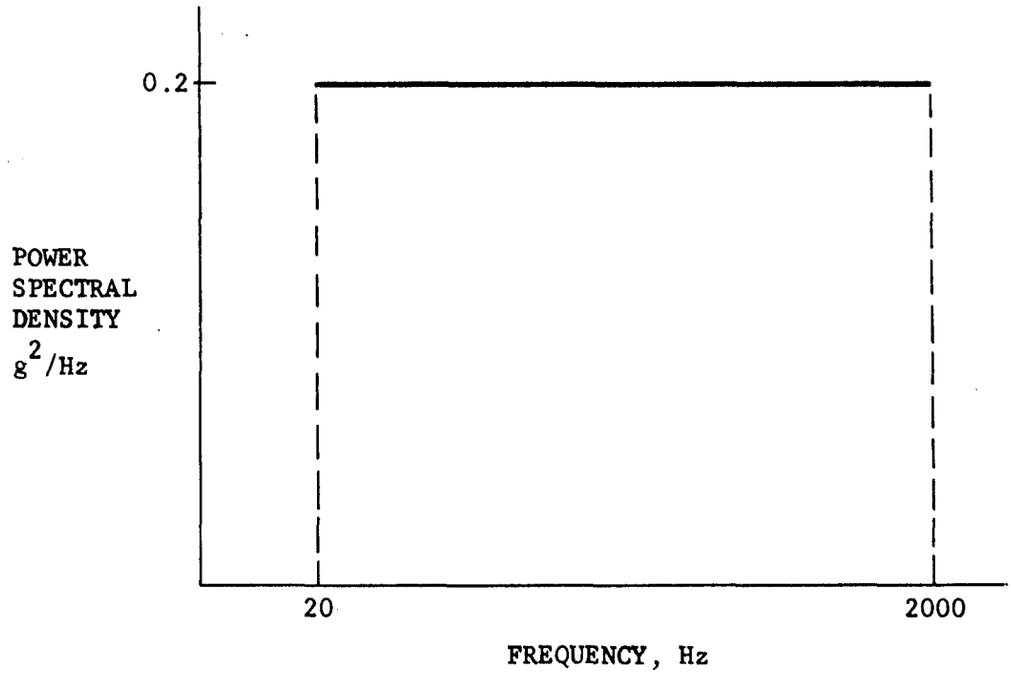

Applied Random Vibration, TOVS Basic Sounder Unit. Survival of random vibration with this spectral density is an instrument design requirement.

NATURE OF OPTICAL SUBSYSTEM INTERFACE REQUIREMENTS

Interface constraints for the optical subsystem exist in several areas: mechanical, optical, structural, and thermal. The mechanical requirement is primarily one of size and also has to do with ease of access. Optically, the primary consideration is stability -- the optical axis of the instrument relative to the spacecraft is determined by the fit-up of the optics deck. The structural requirement has to do primarily with environmental stress; however, because of thermal requirements it also is necessary that a high-conductance path to the instrument frame be provided.

The mounting of the optics deck must be sufficiently stable and strain-free to ensure pointing accuracy. Although there is no stated requirement for absolute pointing accuracy, it is considered desirable that the instrument exit beam be within 0.1 degree of true nadir. Also, there should be no long-term change in the instrument's pointing angle. Of greater importance are channel-to-channel errors. It is essential that all channels view the same scene with an accuracy of 0.1 degree maximum channel-to-channel pointing angle variation. What this means is that the telescopes, when assembled to the optics deck, must be aligned accurately and must not lose this alignment as a result of being bolted to the instrument or because of long-term drift. These conditions are met by using proven thermal treatments to stabilize both the instrument frame and the optics deck components and by machining the mating surfaces to sufficient flatness. For thermal reasons, a minimum area of contact of about 22 in.^{2} is necessary; and for mechanical reasons, it is desirable that clamping pressures not be too high. With such a large area of contact, of course, the latter condition is easily met. In fact, it is necessary to increase the number of screws for thermal reasons so that sufficiently intimate thermal contact is assured.

There is a mechanical strength requirement on the optical subsystem interface relating to environmental stress. The total weight of the optics deck is 12.6 lb, with the center of gravity located as shown in the facing figure. Environmental stresses applied to this unit -- due to both shock and vibration -- can result in tensile, compressive, and shear loading at the interface. Since the moment arm of the center of gravity about the mounting plane is only 0.37 inch, the loading is primarily direct tensile and shear loads -- high loads due to bending cannot develop.

Thermal design of the instrument requires a minimum contact area at the optical subsystem interface of about 22 in.^{2}. Additionally, the use of thermal compound at the joint to lessen contact resistance is necessary. Silicone rubber is specified for this purpose. This material is applied to the faying surfaces and then the joint is made up in the normal manner with the excess thermal compound being wiped away. Experience has proved this technique. A continuous silicone film on the order of 0.003- to 0.005-inch thick can be expected. Because of the elasticity of the cured silicone material, screw preload does not relax with time. Thus, the mechanical properties of the joint are not affected.

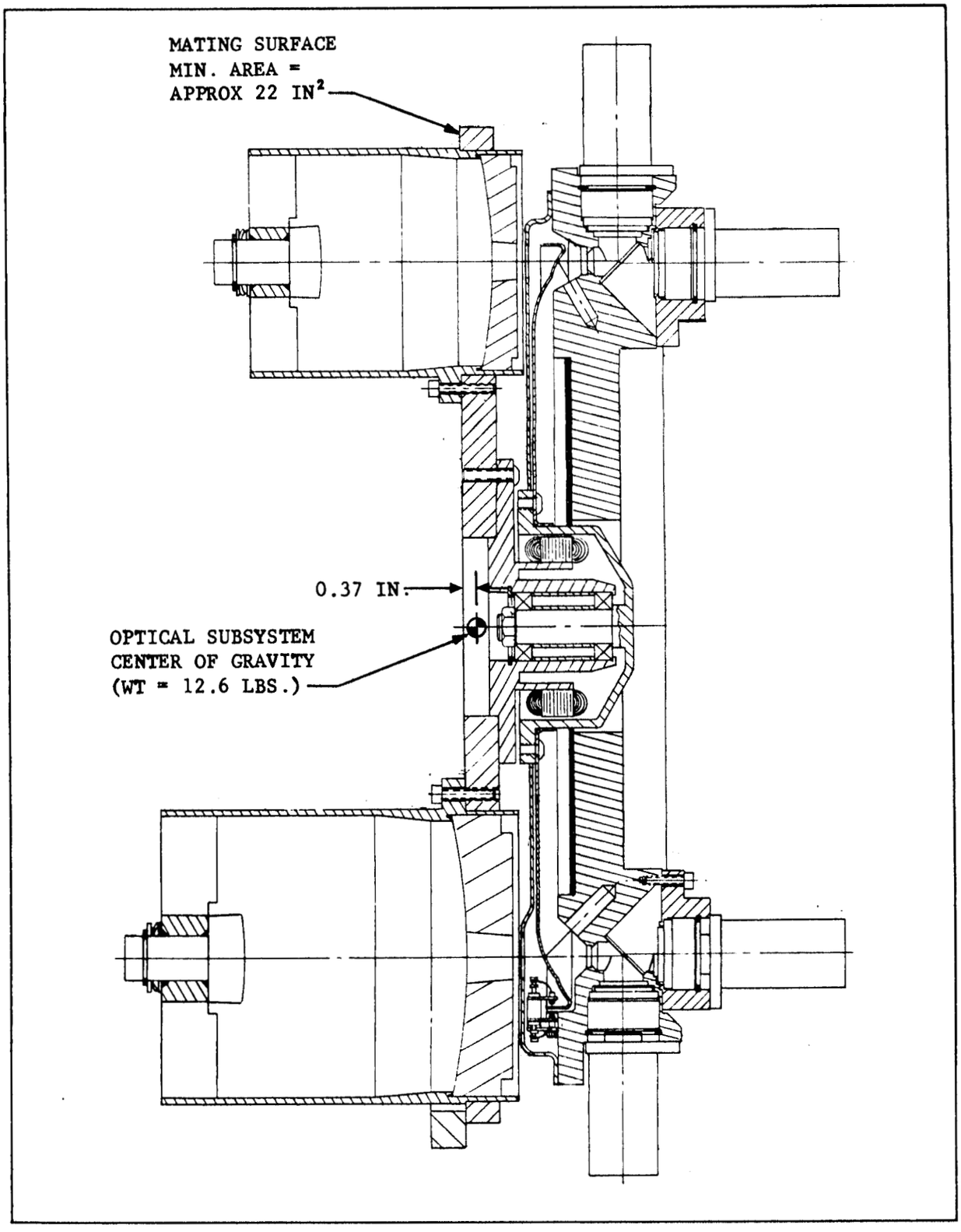

TOVS Optical Subsystem. This assembly requires a rigid mounting with a high thermal conductance.

SECTION 4
ANALYSIS OF OPTICAL PERFORMANCE

Summary of Optical Performance Analysis 4-0
Analysis of Geometric Image 4-2
Calculation of Diffraction Effects 4-4
Sensitivity to Detector Nonuniformity 4-6
Influence of Misalignments on the Accuracy of the Field of View 4-8
Estimates of Scene-to-Scene Correlation and Channel Centroid Matching 4-10

SUMMARY OF OPTICAL PERFORMANCE ANALYSIS

To make the fields of view of the different channels match, and to avoid cross-talk between neighboring scenes, the centroids of the fields of view of each channel must be accurately matched and the edges of the fields must be sharp. An analysis program has been carried out to show that the BSU baseline design provides the required performance.

The orbital atmospheric sounding technique depends on a high degree of correlation between the readings taken in the different spectral channels. Each channel must view almost exactly the same scene. It is also necessary to make each scene radiance measurement independent of the radiance of neighboring scenes, both to minimize error and to reduce the number of data-processing steps required in real-time.

Control of Image Quality - Sharp FOV edges are attained by providing good image quality, which is affected (see listing opposite) not only by aberration and diffraction, but also by errors in the alignment of the telescopes and the tolerance in component mounting.

Matching of FOV Centroids - To attain the required matching, it is necessary that the centroids of the FOV of the various channels match each other within 1 percent of the half-power FOV, or within 0.01125 degree. The list opposite shows there are three principal effects which tend to result in variations of the FOV centroid from channel to channel. The first is the attainment of the required mechanical alignment by means of the control of mechanical tolerances in the placement of the telescopes and detector optics as well as the proper positioning of each component. Second and third are the effects of nonuniformities in detectors and lenses.

Nature of Analysis Performed - All of these effects, except diffraction, have been investigated by precision ray-trace techniques whose details are reported in an appendix.

The effect of misalignment of optical componenets on the location of the FOV centroid and the size of its circle of confusion were investigated by perturbing the location of each optical element in turn. Ray-traces run with the perturbed values were compared to unperturbed traces to determine the required sensitivity, which then provides a specification for mechanical tolerances in manufacture.

The effects of nonuniformity of detectors has been investigated by means of a ray-trace showing the intensity at the detector of on- and off-axis radiation. The effects of lens and filter nonuniformity should be similar and, therefore, were not separately investigated.

Aberration was estimated by use of a spot diagram of the angular distribution of rays in object space originating from the center and edges of the field stop.

Because time did not permit the completion of a computer program to provide a simultaneous calculation of aberration and diffraction, diffraction of the annular aperture was estimated analytically by integrating the Fraunhofer diffraction pattern over the field stop and circular field of view.

The results of the analyses, described in detail in the appendix, are briefly discussed in the following topics.

CONTROL OF IMAGE QUALITY

Scene-to-scene cross talk is influenced by the following factors:

- Aberration
- Diffraction
- Telescope alignment and tolerance

MATCHING OF FOV CENTROIDS

Three principal sources of error must be controlled to match the channel FOV's to the required tolerance of 0.01125 degree.

- Alignment of each telescope to common centerline
- Nonuniformity of detectors
- Nonuniformity of lenses

ANALYSIS OF GEOMETRIC IMAGE

The double-sphere telescope design meets the 50 and 99 percent FOV design goals. No rays from outside the 99-percent FOV enter the field stop. Resolution is excellent, with a nearly constant aberration both on and off axis, and with a circle of confusion whose half-power width is 0.077 degree.

The telescope field stops were selected to provide the desired 1.125-degree half-power FOV, since NER_ν calculations showed this FOV is attainable. The effect of geometric aberrations is to round off the edge of the ideal 1.125 degree FOV. In the absence of diffraction, this rounding off does not affect the specified rejection of off-axis radiation unless the aberrations allow the acceptance of radiation which is outside the 99-percent FOV. The total half-width of the bundle of rays emanating from the edge of the field stop should then be narrower than the difference between angular radii of the half-power and 99-percent FOV. The specified values are:

- Radius of 99 percent FOV 0.6250 degree
- Radius of 50 percent FOV 0.5625 degree
- Difference 0.0625 degree

The aberration characteristics of the 61-mm and 80-mm diameter telescopes were evaluated by two quite different ray-trace methods. In one, a large number of parallel rays enters the telescope with a given angular FOV, and their point-spread image function is analyzed at the prime image plane. In the second, a large number of rays starts from a single point on the prime image plane and fills the aperture stop with rays. Their angular field-spread function is evaluated in object space. The latter approach can yield the image quality in the object space and is more easily compared with the BSU specification. The figure opposite shows the actual spot diagrams obtained by this method for two points: one at the center of the field stop and one at the edge. The aberration is mostly spherical, with some coma evident at the edge of the FOV. The spot diagrams are, of course, identical for the 80-mm and 61-mm telescopes which have the same relative dimensions. The maximum angular spread for all rays is found to be 1.248 degrees, just inside the 99-percent FOV specification, while the half-power FOV is calculated to be 1.120 degrees, slightly less than the 1.125 degree design goal. The full width at half maximum (half-power) radial width of the spot diagram at the edge of the field is 1.35 mrad, or 0.077 degree; the rms width is 0.059 degree.

Because all geometric rays originate within the 99-degree FOV, only diffraction and the effects of misalignments can cause energy to be received from outside this field. The Cassegrainian telescope, designed for minimum secondary diameter and maximum useful aperture with spherical mirrors thus provides adequate image quality.

TOVS DOUBLE SPHERE TELESCOPE F/3.82. 286.709 MMFL--80 MM OD 8-14-72

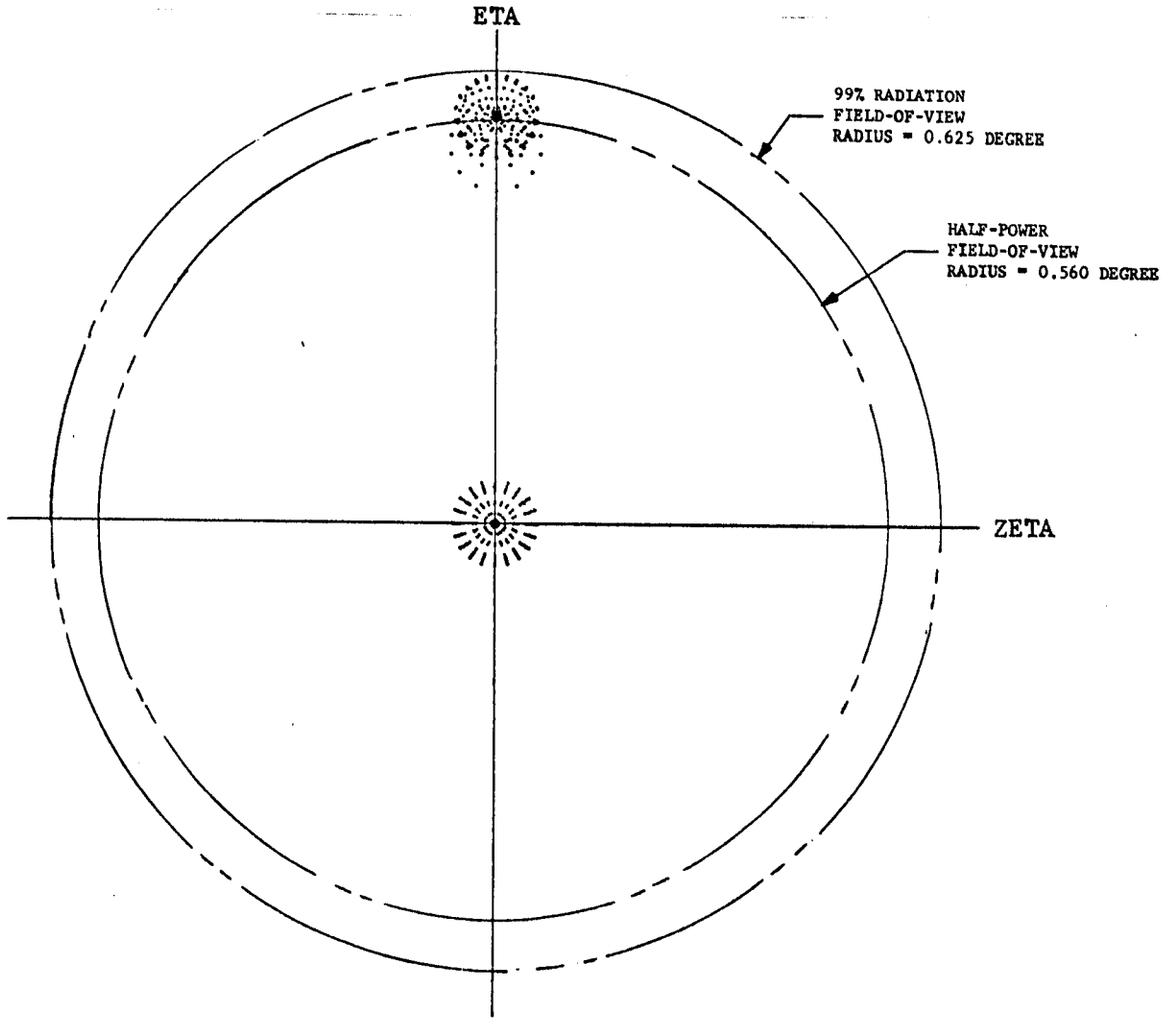

IMAGE PARAMETERS

These values apply to both the 80-mm and 61-mm telescopes.

Half-Power FOV	1.120 degrees
Full FOV	1.248 degrees
Half-Power Width of Point Image	0.077 degree

Angular Field-of-View 200-Ray Diagrams for Ray Starting Points at Edge and Center of Field Stop

CALCULATION OF DIFFRACTION EFFECTS

Fraunhofer diffraction from the annular telescope aperture has been calculated for a circular field-of-view by use of an analytical approximation. The calculation predicts that all channels should meet the 99-percent FOV specification.

The importance of diffraction in determining the response at wide angles can be seen by examining the analytical form for Fraunhofer diffraction from a circular aperture. The intensity function at the image plane for a point object is

$$I_o(\theta) = 4J_1^2(x)/x^2 ,$$

where J_1 is the Bessel Function of the first order and

$$x = 2\pi a\theta/\lambda$$

where a is the radius of the aperture, λ is the wavelength, and θ is the angle equivalent to the geometric position on the field stop. For large angles so that $x \gg 1$, this intensity function varies as

$$I_o(\theta) \sim (8/\pi x^3) \cos^2 (x - 3\pi/4)$$

The rapidly varying cosine term is smoothed out in practice by imperfect definition of edges and by aberrations, so that the average value is

$$I_o(\theta) = 4\pi/x^3$$

The inverse cube dependence does not fall off all that rapidly. When one integrates this point response over the field-of-view to obtain the energy distribution, and then integrates again to find the energy outside a given angle, it is found that this energy falls off quite slowly, thus diffraction is by no means a negligible source of stray radiation, even though the angular radius of the first diffraction ring is much less than the aberration point spread (0.44 mrad compared to 1.4 mrad even in channel 14).

For an annular disc, the diffraction function, normalized to unit total energy when integrated over solid angle, is:

$$I_o(\theta) = \frac{(kb)^2}{\pi} \frac{1}{\left(1 - \frac{a^2}{b^2}\right)} \left[\frac{J_1(kb\theta)}{kb\theta} - \frac{a^2}{b^2} \frac{J_1(ka\theta)}{ka\theta} \right]^2$$

where b is the outer radius, a is the inner radius, and $k = 2\pi/\lambda$. This formula is derived by I.L. Goldberg and A. W. McCulloch[1] who used to perform a numerical integration to find the energy falling outside a circular field with a given size of circular field stop. One first calculates the actual angular sensitivity by integrating the above distribution over the field stop, and then calculates the energy outside a given radius. Unfortunately, Goldberg and McCulloch do not give results in the angular region needed.

Rather than a numerical method, the approximate analytical method of Steel, De, and Bell[2] was used to perform the integration. The method employs an approximation to the convolution of field stop and source, and also employs the asymptotic expansion of the Bessel function for large arguments.

This approach leads to the following equation for the fractional energy which passes through a field stop of angular radius r from a diffuse source at angles s or larger:

$$E = \frac{\lambda}{2\pi^2(b-a)r} \log \frac{s+r}{s-r}$$

A plot of this function is shown in the figure for $\lambda = 29$ m, b = 76.6 mm, a = 25.6 mm, and r = 9.77 milliradians (all ray-trace values). The calculated diffraction from outside the specified 99 percent FOV is less than 1 percent, namely, 0.77 percent.

An improved calculation, which takes into account the influence of aberrations on diffractions as well as the influence of the secondary mirror spiders, requires a fast ray-trace/integration computer solution specialized for this purpose. The Beckman ray-trace program, because of its generality and high precision, cannot be adapted directly to perform such an integration, although it is being modified to calculate the point-spread function.

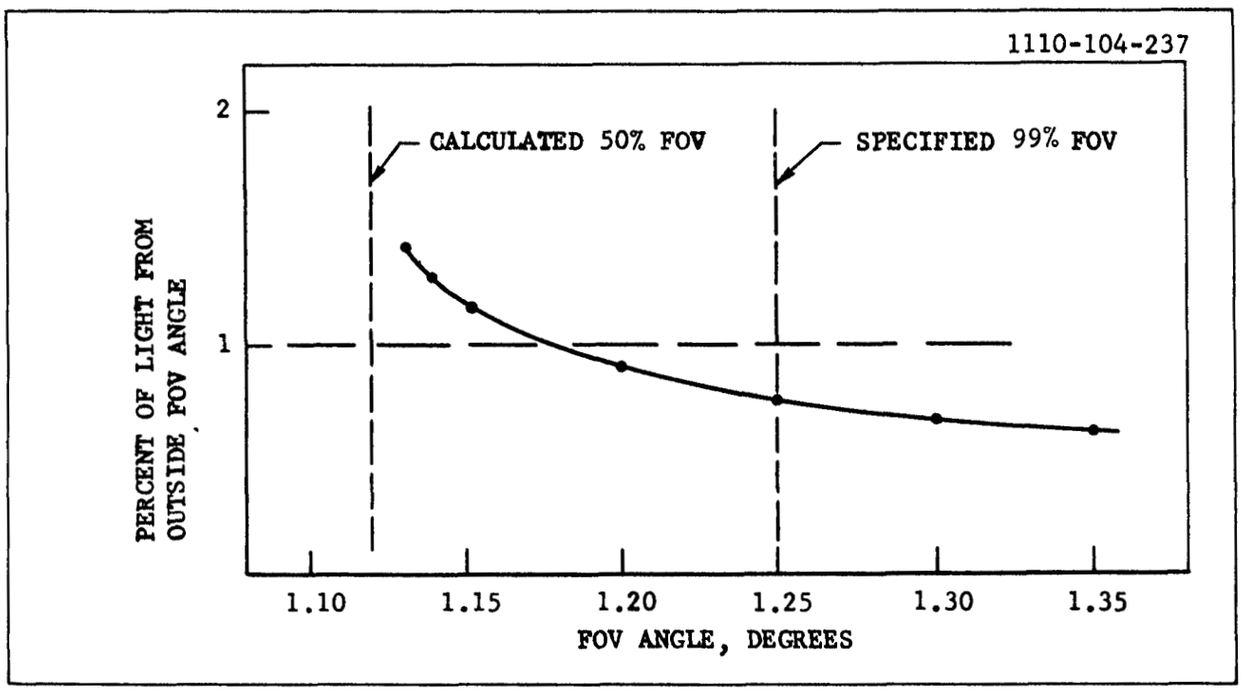

Fraunhofer Diffraction From Annular Aperture for Channel 14 (29μm). The 99% FOV specification is met.

(1) I. L. Goldberg and A. W. McCulloch, Applied Optics 8, 145, (1962).

(2) W. H. Steel, M. De, and J. A. Bell, J. Opt. Soc. Am. 62, 1099, (1972).

SENSITIVITY TO DETECTOR NONUNIFORMITY

A major advantage of the BSU optical configuration is the insensitivity of the centroid of the field of view to detector nonuniformities, which has been confirmed by a detector ray-trace.

Because the detector is imaged upon the secondary mirror and not upon the field stop, the image of a point source is defocused. This effect limits the sensitivity to detector nonuniformity.

The residual sensitivity was checked with a ray trace. To make the ray trace, 200 parallel rays which uniformly filled the entrance aperture were traced from the entrance aperture to the detector for two cases: one with the rays parallel to the optic axis, and one with the rays at an angle corresponding to the half-width of the half-power FOV.

Spot diagrams at the detector were obtained which showed that the detector was uniformly illuminated in a circular spot. The motion of an image point across the FOV causes this spot to be slightly moved and distorted, as shown in the ray-trace spot diagram opposite. (The darker spots correspond to the object point at the center of the FOV.) The motion of the object across the FOV corresponds to a motion of the centroid of the sensitive area by much less than 1 percent. This effect matters very little, since the detector is overfilled by the image of the secondary mirror. At most, the detector need only be about 1 percent undersize to eliminate nearly all of this effect. If we assume the outer 1 percent of the detector to be completely insensitive on one side only, then the corresponding shift in the FOV centroid would be much less than 1 percent.

The design is thus very insensitive to detector nonuniformity. A specification of ±10 percent variation across the detector is not only acceptable but conservative.

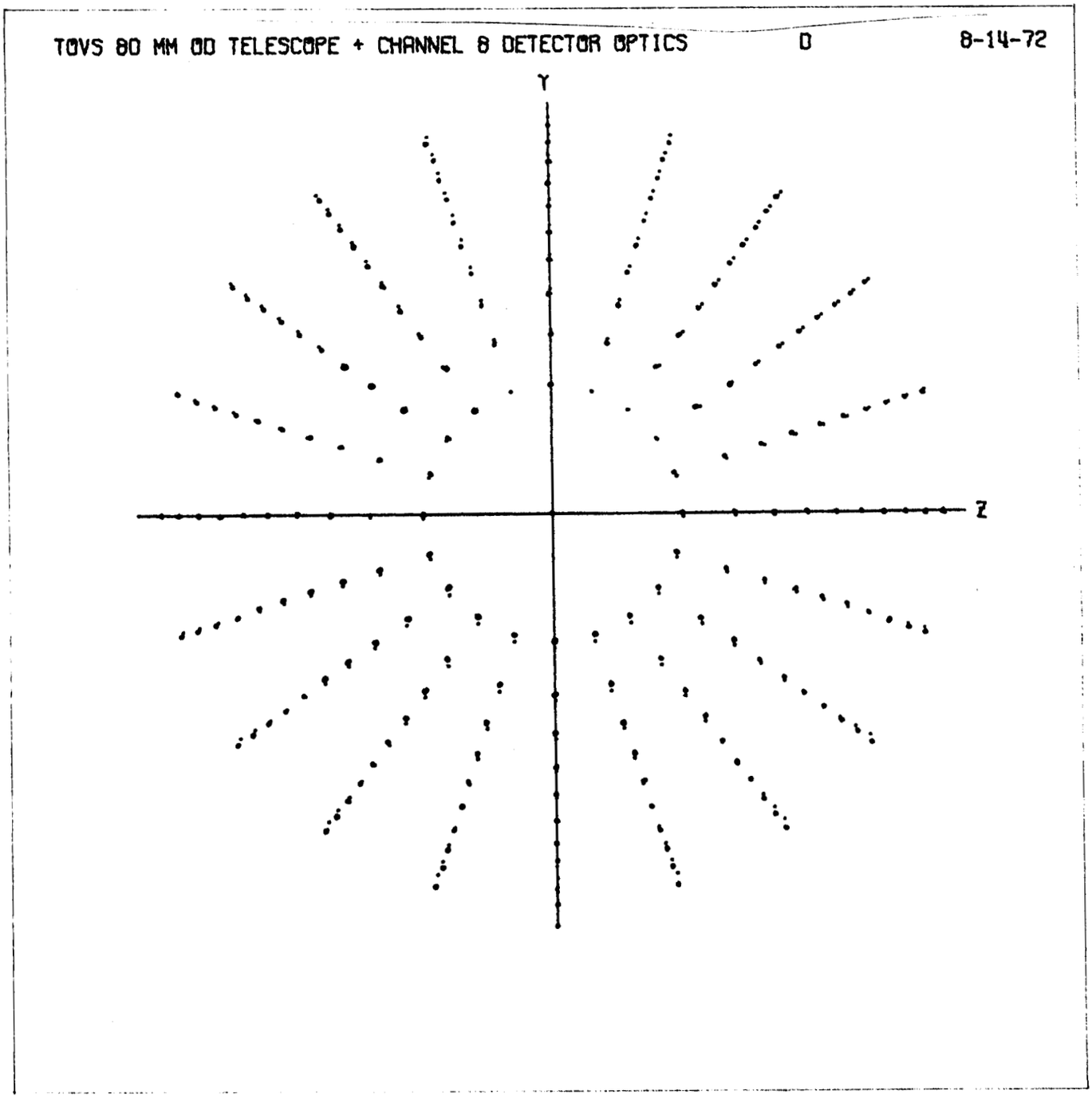

Ray Trace of Detector Image for Object Point at Center of FOV (Dark Spots) and Edge of FOV (Light Spots). The centroid of the image, which overfills the octal detector, moves less than 1 percent of the detector diameter, so that the effect of detector nonuniformities on the FOV centroid is negligible with detectors uniform to ±10 percent or better.

INFLUENCE OF MISALIGNMENTS ON THE ACCURACY OF THE FIELD OF VIEW

An analysis of the influence of optical component mounting errors and misalignments shows that tolerances of less than 0.001 inch must be maintained in mirror mounting to achieve the desired FOV accuracy.

To determine the effect of optical component positioning errors on the centroid and size of the field-of-view, the ray-trace program was used to find the changes in the position of the telescope focus as a function of telescope position errors. A ray-trace using two extreme rays was made to determine the location of the unperturbed focus. Then one mounting parameter was perturbed at a time and the trace was repeated to determine the longitudinal and lateral shift in the focal point. With each ray-trace, the computer automatically adjusts the spacing between the secondary mirror and the field stop until the two rays precisely focus on the image.

The positioning errors studies were the types of errors listed opposite, which are the spacing between the primary and secondary mirrors, the lateral shifts of one spherical mirror relative to the next surface, and changes in spherical mirror radii. Each type of error was ray-traced for three different magnitudes, covering two decades, 0.0025 mm, 0.0250 mm, and 0.250 mm, which are roughly equivalent, respectively, to 0.0001 inch, 0.0010 inch, and 0.0100 inch.

A plot of the focus shift as a function of the perturbation is given in the appendix along with the computer-generated data. It was found that the errors in focus are linearly related to the perturbations in the range investigated.

The longitudinal focus shifts were related to the change in the field-of view as a result of defocusing as follows: if x is the position of the focus, p is the component location parameter, d is the field stop diameter, and F is the F number, then the FOV broadening is given by

$$\left[\frac{\partial\ (\mathrm{FOV})}{\partial p}\right]_{\mathrm{width}} = \frac{1}{d}\left(\frac{\partial x}{\partial p}\right)\ \frac{1}{F}$$

The derivative $\partial x/\partial p$ was determined from the ray-trace results.

The movement of the centroid caused by lateral motion in the y direction normal to the optic axis is

$$\left[\frac{\partial\,\mathrm{FOV}}{\partial\,p}\right]_{\mathrm{centroid}} = \frac{1}{d}\ \frac{\partial y}{\partial p}$$

where again the partial derivative is determined from the ray-trace.

The results of this analysis are shown in the table opposite. To attain the required FOV image sharpness, it is necessary to control the primary-secondary spacing to 0.0008 inch. To meet the centroid alignment requirement, it is necessary to keep lateral shifts in the primary mirror location to less than 0.0006 inch. Other tolerances are less critical. Meeting these tolerances requires the customary degree of care in mounting optical components-an aspect discussed in the Subsection on Mechanical Design of Optics Subassembly.

A similar error analysis was performed for the detector optics. The analysis primarily determined the margins required on the secondary mirror size, detector size, and detector positioning. This analysis is reported in the appendix to the optics subtask report.

DIMENSIONAL TOLERANCES FOR 1% FOV IMAGE ERROR
Calculations are for the smaller (more critical) 61mm telescope.

SOURCE OF ERROR DESCRIPTION	FOCAL ERROR		LATERAL ERROR	
	(mm)	(Inches)	(mm)	(Inches)
Primary to Secondary Spacing	0.020	0.0008	>0.250	>0.0100
Lateral Shift of Primary	>0.250	>0.0100	0.0151	0.0006
Lateral Shift of Secondary	>0.250	>0.0100	0.025	0.0010
Primary Radius	0.040	0.0016	>0.250	>0.0100
Secondary Radius	0.100	0.0040	>0.250	>0.0100

ESTIMATES OF SCENE-TO-SCENE CORRELATION AND CHANNEL CENTROID MATCHING

Because the scan step is equal to the width of the half-power field-of-view, and not the 99-percent field-of-view, the correlation between adjacent scenes is relatively large. The centroids of the fields can be matched within specifications if extreme care is taken.

Scene-to-Scene Correlation - Part way through the study program, it was agreed that the scan step would be made equal to 1.125 degrees, which is equal to the half-power field-of-view of the baseline design. This choice of step angle is a natural result of the scan geometry and readout timing. Because of the geometric aberrations, there will be an overlap of the fields-of-view, as shown in the figure opposite.

The 50-percent FOV is the full-width-at-half-maximum of the response function obtained when a point source moves across a diameter of the FOV. Much more than half the total energy lies within this FOV. To estimate the energy which lies outside the 50-percent FOV, a convolution calculation was performed, assuming a triangular point-spread function with a base width of 2.2 mrad, which is a good fit to the ray trace. With care in mounting, the contribution of additional blurring from defocusing can be made negligible. The resulting distribution has a quadratic tail which extends out to the 99-percent FOV. The solid angle under this tail is approximately

$$\Delta\Omega = \frac{2\pi}{3} \times \Theta_1 \times \frac{(\Theta_2 - \Theta_1)^3}{\Delta\Theta^2} = 5.6 \times 10^{-6} \text{ sr}$$

where Θ_1 = radius of 50-percent FOV = 9.8 mrad

Θ_2 = radius of 90-percent FOV = 10.9 mrad

$\Delta\Theta$ = base width of spread function = 2.2 mrad

Since the solid angle of the entire FOV is 3.02×10^{-4} sr, the fraction of the solid angle in the outer annulus is 1.9 percent. About 1/8 of the energy overlaps one adjacent scene, so that the scene-to-scene correlation is 0.2 percent.

While the geometric aberrations dominate inside the 99-percent FOV, diffraction contributes outside that field. For channel 14, 0.8 percent of the energy comes from outside the 99-percent FOV. The added contribution of diffraction in channel 14 is an eighth of this 0.1 percent. The contribution in other channels is directly proportional to the wavelength and inversely proportional to the telescope diameter.

It follows that the scene-to-scene correlation may be as large as 0.3 percent in channel 14. This value is about three times larger than that implied by the TOVS-BSU specification, which requires that the correlation be less than the noise equivalent spectral radiance, which is about 0.1 percent of a full-scale signal.

Relative Channel Centroid Matching - The centroids of the channel fields-of-view can be matched with the required accuracy of 0.01125 degrees, provided that the detectors are uniform to about ±10 percent, the lenses and filters are properly rotated for best alignment, and telescope mirrors are stably mounted with certain critical tolerances held to a few ten-thousandths of one inch.

REQUIREMENTS FOR CHANNEL CENTROID MATCHING

- Detectors uniform to ±10%
- Lenses and filters rotated for best alignment
- Telescope mirrors must have precision optical mounts.

1110-104-239

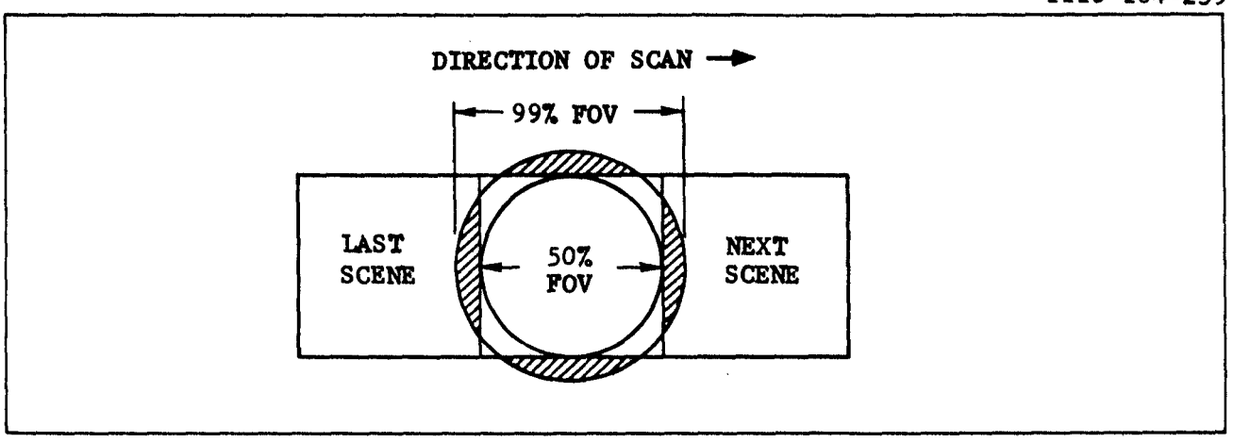

Overlap of Circular Fields in Rectangular Scan Grip. Because the step angle is equal to the 50 percent FOV, there is overlap between adjacent scenes and scan lines.

EFFECTS OF POLARIZATION

Radiometric error due to polarization effects is dependent upon the degree of polarization of the scan scene radiation, the scan angle with respect to nadir, and the variation of dichroic beamsplitter transmittance and reflectance with the polarization state of the incident radiation. The effect should be less than five percent of the degree of polarization of scene radiation and less than 0.1 percent for essentially unpolarized scene radiation.

Degree of Polarization - The degree of polarization of electromagnetic energy radiated into space from the earth's surface, the troposphere, and the stratosphere is ill-defined. Radiation transmitted through the earth's atmosphere is partially polarized by scattering, a physical process which is inherently polarization sensitive. The degree of scattering, however, varies inversely as the fourth power of the wavelength of the scattered radiation except in regions of stray absorption. Thus, polarization becomes a less critical consideration in the description of longer wavelength radiation, so that the channel most likely to be affected is the 3.8 μm channel (Channel 1). The degree of polarization of radiation detected by the BSU may, however, present a problem if the instrument transmittance is a function of the state of polarization of that radiation.

Scan Angle - Energy radiated from a given scan scene will be partially polarized as the result of reflection off the metallic surface of the scan mirror. The degree of polarization is a function of the angle of incidence and complex indices of refraction for the metallic surface of the scan mirror. The polarizing properties of a metallic reflector are, however, much less than those of dielectric reflectors. The facing graph provides estimates of the reflectance of high-reflectivity gold in the infrared as a function of BSU scan angle. The estimates presented are based upon the complex index of refraction of a gold coating at 4 μm given by the American Institute of Physics Handbook. The graph shows a maximum difference in reflectance of 2.6 percent for light polarization in parallel and perpendicular planes.

An optical element possessing a circular symmetry and inclined normal to the incident radiation will not contribute to the polarization of that radiation. Although the angle of incidence of radiation on the telescope mirror is not 90 degrees, circular symmetry will average out any polarization effect. This characteristic is also true of the detector lenses. Bandpass and blocking filters are oriented normal to incident radiation and, therefore, do not act as polarizers. Although detector lenses and filters may exhibit some birefringence (and, therefore, exhibit polarizing properties), as a result of mechanical stresses, this effect can be minimized, if not eliminated, by annealing the substrates prior to fabrication and by properly mounting the optical elements. Other than the scan mirror, the only optical element with potentially-critical polarizing properties is the dichroic beamsplitter.

Dichroic Beamsplitter Variation - The polarizing properties of a dichroic beamsplitter critically depend upon the design and fabrication of the thin film coatings. In particular, the spectral location of cut-off and cut-on points varies with the state of polarization of incident radiation. If the spectral channels separated by the dichroic are sufficiently far removed from each other (by more than 2 μm), the dichroic can be designed so that the cut-off and cut-on points are quite distant from the spectral regions of interest, thus minimizing the polarization effects.

With proper design and fabrication, a dichroic beamsplitter can have a transmittance and reflectance, for channels sufficiently separated in wavelength,

that are virtually independent of the state of polarization of the incident radiation. Tests conducted in the present study, as well as calculations performed by Optical Coating Laboratories, Incorporated, under a subcontract, have shown that the variation of reflectance with polarization is undetectable, while the variation in transmittance is less than 5 percent. These results are reported in detail in an appendix.

1110-104-210

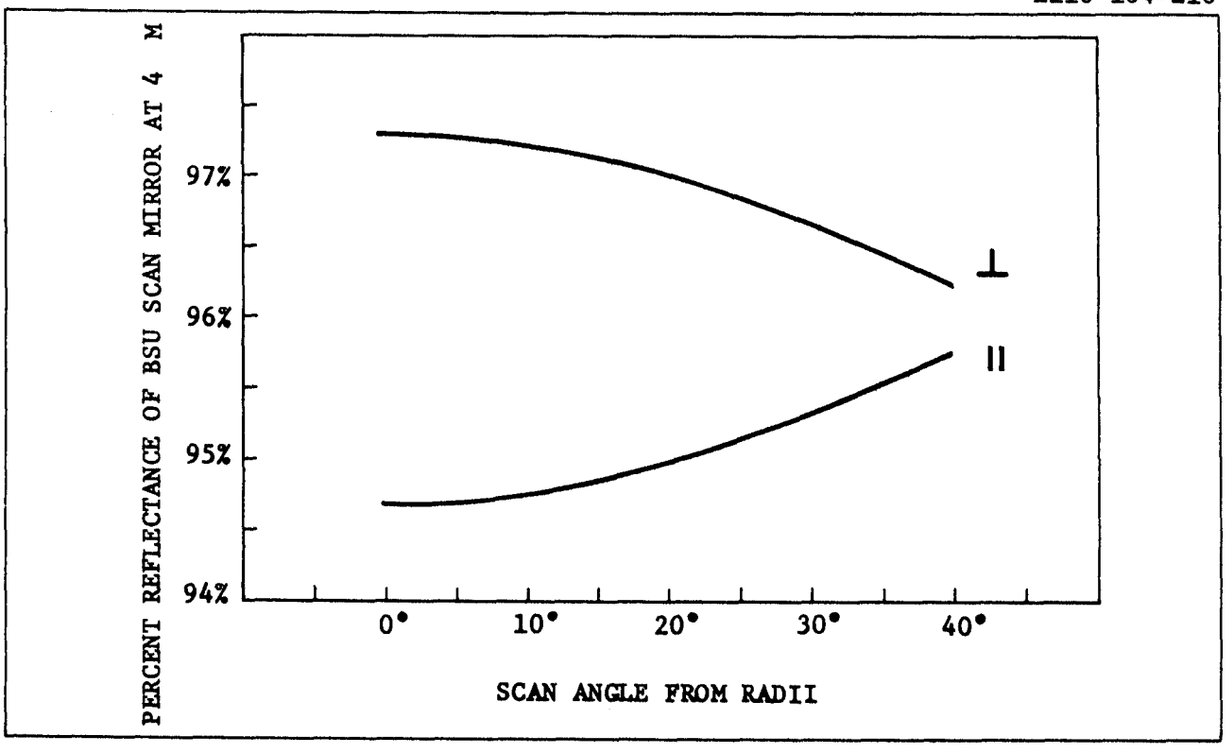

⊥ Radiation Polarized Normal to the Plane of Incidence
II Radiation Polarized Parallel to the Plane of Incidence

Reflectance at 4 μm of a Gold Coating on the BSU Scan Mirror as a Function of Scan Angle. This graph indicates data calculated from the BSU scan geometry, and is based upon complex indices given in the American Institute of Physics Handbook.

SECTION 5
OPTICAL TESTING

DESCRIPTION OF TEST PROGRAM

Discussion of Testing Goals and Philosophy 5-0
Description of Optical Mockup 5-2
Discussion of Tests Performed 5-4
Test Equipment and Calibration 5-6

RESULTS OF TESTS PERFORMED

Summary of Optics Testing. 5-8
Testing of Filters 5-10
Procurement and Testing of Dichroics 5-14
Fabrication and Testing of Lenses. 5-16
Results of Field-of-View Testing 5-18
Results of Spectral Transmittance Tests. 5-20
Results of Polarization Testing. 5-22
Results of Diffraction Testing 5-24
Out-of-Band Energy Testing 5-26

DISCUSSION OF TESTING GOALS AND PHILOSOPHY

A test procedure was developed to verify the predicted performance of the components and optical test assembly, and to estimate the performance of the TOVS-BSU.

The testing of the optical test assembly was designed to verify calculated data, explore aspects such as polarization sensitivity and diffraction effects, and investigate the practical aspects of component manufacturing and their influence on instrument performance.

Some aspects of the TOVS-BSU testing are duplications of ITPR tests. Wherever possible, the techniques developed for the ITPR tests were applied and the equipment utilized. For other tests such as diffraction effects, new equipment was designed and constructed and new measurement techniques developed. The same applied for the polarization sensitivity measurements of optical components and the completed optical test assembly. The polarization measurements were particularly troublesome since the test equipment itself is highly polarization-sensitive.

The design goal was, for both tests, to explore the phenomena as thoroughly as time allowed on this study. Some of the effects observed were expected to produce signal changes of only one percent (diffraction effect).

An important aspect of this study was the manufacture and testing of optical components, utilizing silicon as substrate material. This wavelength region is not as well known with respect to component fabrication as the germanium range. The goal was the development of fabrication techniques to produce components which would pass all the applicable specifications for environmental exposures and produce components with the highest possible bandpass transmission and greatest sideband rejection.

A dual-channel, single-telescope optical test assembly was constructed to test the two channels with the most difficult overall requirements, namely, channel 11 (668.5 wave numbers) and channel 14 (340 wave numbers). This optical test assembly was also constructed in such a way that ITPR filters could be used. This permitted testing in the 3- to 10-micrometer region to measure polarization sensitivity. The TOVS-BSU filters were replaced by ITPR filters of channel 1 and 5. The anti-reflection coatings of the TOVS-BSU lens assembly transmit enough energy in these bands to perform these particular measurements.

The testing was performed in three major steps, the component testing, the evaluation of the subassemblies, and the system testing on the assembled optics test assembly. Throughout the testing sequence, all parameters with a possible influence on the final test results were investigated.

The majority of the testing was performed on two instruments--a Beckman IR-12 infrared spectrophotometer and a specially constructed test collimator with a blackbody source. The IR-12 was modified to permit polarization and transmission measurements on individual optical components as well as on the complete optics test assembly. The collimator was utilized for alignment and integrated measurements of stray light, polarization sensitivity, and response versus temperature level. Both instruments had been used for ITPR measurements and needed only minor modifications to perform the TOVS-BSU testing.

The complete test sequence is discussed in this section. Parameters of component and subassembly testing are discussed in detail. Also included is a summary of the test results of the subassembly testing and the possible influence which these results may have on the system testing. The system testing served several purposes. One of the more important of these was to investigate how well theoretical data could be translated into actual hardware. It also permitted evaluation of how the combination of the tolerances of individual elements could be arranged to minimize errors in the final result, such as the orientation of the lenses with respect to each other to average possible transmission differences.

The location and the orientation of components were changed to evaluate tolerance brackets as well as the effect of extreme tolerances on system performance. Testing of the complete optics test assembly permitted evaluation of hard-to-analyze optical parameters such as polarization sensitivity and diffraction.

As a result of all the testing performed, it is possible to estimate with considerable accuracy the performance of the remaining channels. To achieve as accurate an estimate as possible, the amount of test data obtained and the exploration of applicable cases went beyond the normal test concept. The primary goal of the total test sequence was also verification of predicted performance, which is discussed in detail in a later topic.

TESTING GOALS AND PHILOSOPHY

The testing proceeded in stages beginning with individual components and ending with the main assembly.

- Test every aspect of components, subassemblies, and main assembly
  - Dimensional Tolerances
  - Spectral Characteristics
  - Alignments
  - Diffraction Effects
  - Polarization Sensitivity
  - Stray Light
- Test sequentially to be able to use data of previous tests.
- Test for verification of predicted performance of channels 11 and 14.
- Test to obtain enough data to predict performance of the remaining channels.
- Utilize proven test methods where possible.
- Use existing test equipment where possible.

DESCRIPTION OF OPTICAL MOCKUP

An optical mockup consisting of one telescope was constructed to permit verification of the theoretical predictions through spectral and geometrical testing (alignment). The design and construction was as close to that of a flight model as possible.

The optical mockup is depicted in the photographs opposite; it consists of an 80-mm "large" telescope and has two optical channels. All optical components and subassemblies are constructed as discussed in Section 3 Optical Design. A rotating reflective chopper is included in the mockup which modulates the diverging incident radiation just prior to the field stop. The outer rim of this chopper also interrupts the beam of an optical phase-reference pickup (PRP). This PRP provides the phase reference signal for lock-in amplifiers used to read out signal energy. The chopper motor is a 400-Hz hysteresis synchronous motor which provides 40-Hz signal modulation through the chopper disc.

The two optical channels are designed to place the Channel 14 (29 micrometers, 340 wavenumbers in the transmitted beam, and Channel 11 (15 micrometers, 668 wavenumbers) in the reflected beam. These two channels represent the channels with the most difficult overall requirements.

The components for Channel 14 are silicon substrates with appropriate coatings; components for Channel 11 are germanium substrates. The filter from the ITPR instrument can also be accommodated. These filters have greater bandwidth for higher energy throughput for field-of-view testing and are located in the 3.8 - to 14 μm region which is utilized to test the polarization sensitivity of the mockup.

The Optical Mockup is mounted on an auxiliary mount which permits installation on a collimator-blockbody test fixture or an external platform for a Beckman IR-12 Infrared Spectrophotometer.

The optical mockup can be fitted with several types of detectors; testing was performed with two types of pyroelectric detectors, a triglycinesulfate (TGS) and double oxide detectors with various coatings.

1110-104-224

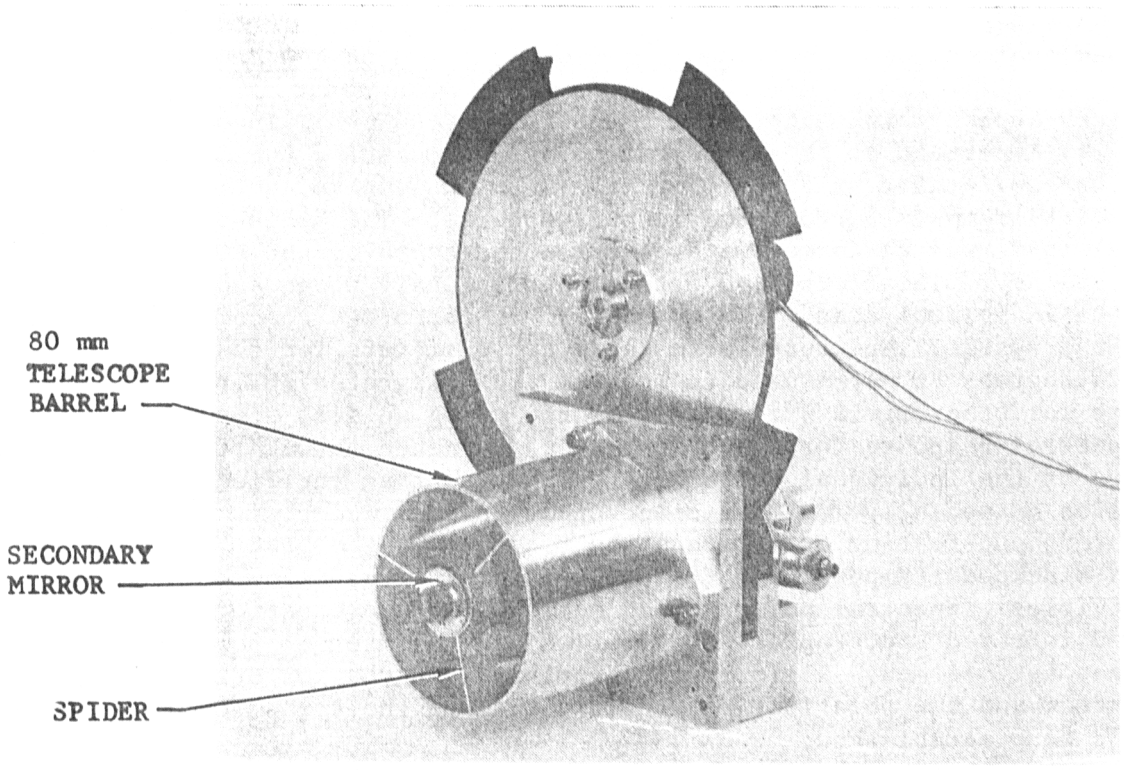

1110-104-225

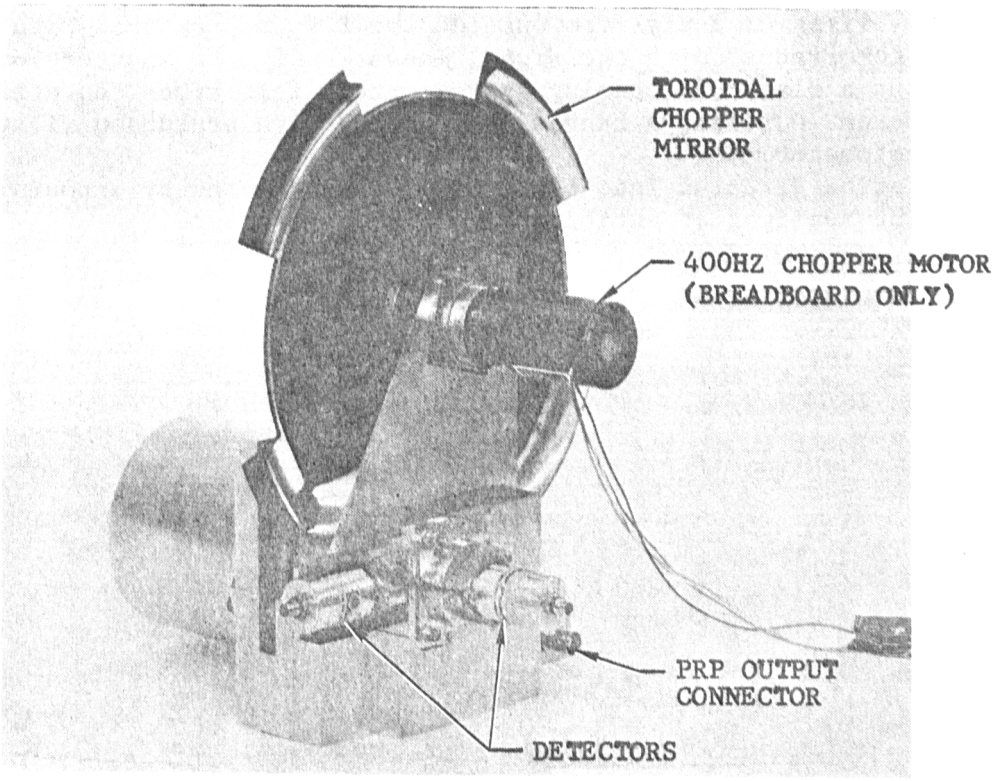

Optical Mockup: 80-mm Telescope (Channel 11) and Channel 14 Aft Optics

DISCUSSION OF TESTS PERFORMED

To establish a high degree of confidence in the test results, testing was performed at the individual component level on subassemblies and on the completed system.

Every aspect which might affect the final result was investigated. This was especially important at the subassembly level in testing the lens assemblies and filter assemblies for uniformity of transmission over the entire effective aperture.

A list of tests performed is shown opposite. The field-of-view (FOV) test, in final form, was performed with a source one-tenth of the FOV to measure response across the FOV. This test also establishes the half power and full FOV points across an individual scan. Enough scans were performed to completely cover the FOV of the system. Apertures with the exact diameters for the half-power points and 1.25 degrees FOV were used to measure the integrated FOV response, while the response for other field sizes was measured using an iris diaphragm.

Spectral response for all channels was obtained through transmission measurements of the individual components which were then verified for the completed channel on a specially modified spectrophotometer.

Throughput-testing establishes the response of the assembled channels to various blackbody temperatures for comparison with the calculated channel sensitivities. Spectral polarization measurements were performed on a specially modified infrared spectrophotometer for which the internal polarization properties have been established. All operational mirror and channel orientations were duplicated, and the polarization sensitivities of the transmitted and reflected channels were established.

Stray light contributes to the detector signal from a variety of sources, optically from imperfect components system and reflection of radiation into the FOV from structures and housings.

Stray light directly from outside the FOV was measured with a blackbody at elevated temperature with the signal measured with an aperture of correct FOV size versus a blackbody opening approximately four times the area. Stray light from different wavelength ranges is measured with broadband filters and on a spectrophotometer.

Radiation directed into the FOV was investigated by exposing the instrument to incident sunlight at anticipated angles of exposure.

LIST OF SYSTEM TESTS PERFORMED ON MOCKUP

- Field-of-view (FOV) to establish response across FOV.
- Field-of-view (FOV) to establish response to circular fields of varying sizes.
- Spectral response to measure transmission of assembled channels 11 and 14.
- Throughput (sensitivity) of assembled channels 11 and 14.
- Polarization sensitivity of assembled channels 1 and 5 (ITPR).
- Diffraction effects in channel 14.
- Stray light from outside FOV.
- Stray light from different wavelength ranges.
- Stray light from scattered radiation incident on structures.

LIST OF COMPONENT AND SUBASSEMBLY TESTS PERFORMED

- Spectral transmission of filters and dichroic versus temperature, angle of incident radiation, and polarization.
- Transmission uniformity of filter and lens assemblies.

TEST EQUIPMENT AND CALIBRATION

The test equipment for the optical mockup is carefully designed and constructed for optimum performance. All instruments are maintained in calibration and alignment during the test phases; all important parameters are monitored and recorded.

Most of the tests described in the previous section are performed on two instruments--an infrared collimator with a blackbody source and a specially modified Beckman IR-12 spectrophotometer (see figure opposite). The infrared collimator is a Newtonian type telescope of 1250-mm focal length. The focal plane is located outside the main body and serves as a mounting plane for a variety of accessories. These accessories are:

- Aperture plates of various diameters for integrated field-of-view (FOV) measurements.
- Movable aperture plate to scan across the FOV with a small opening in front of the blackbody.
- A continuously variable iris aperture for diffraction studies.

All apertures are aligned within 0.025 mm at the collimator image plane.

With the optical mockup installed on the collimator, the collimator image plane is focused on the field stop with a 4.7-to-1 reduction. The accuracy of the aperture plate orientation is therefore within 0.0053 mm at the field stop of the mockup.

The mockup itself is aligned on the collimator in such a way that the backlighted field stop projects a perfectly centered image on the collimator image plane.

The blackbody is maintained at an elevated temperature (approximately 950°C) 24 hours a day and the temperature maintained with a thermocouple readout.

Stray light measurements are performed with ITPR long-wave and short-wave pass filters. These filters have been measured on a Beckman IR-12 spectrophotometer for leaks. The filters are installed in front of the mockup telescope spinning to minimize heating from the blackbody.

The second major test instrument is a specially modified Beckman IR-12 spectrophotometer with a wavelength range of 2.5 mm to 50 mm. This instrument is equipped with an external platform for spectral transmittance measurements (single beam) on the assembled optical mockup. The exit slit of the instrument is focused essentially on the mockup field stop which is verified by removing one of the order-sorting filters, and projecting visible radiation from the grating onto the field stop.

For polarization measurements, a silver bromide wire-grid-type polarizer is installed directly behind the slit. The optical mockup is mounted in such a way that it can be rotated around the optical axis to simulate scan mirror rotation of an operational instrument.

All component transmission measurements are performed in double-beam mode with a polarizer aligned in a common optical path to minimize grating polarization influence on the measurements.

Reflectance measurements are performed with a reflectance accessory.

The wavelength calibration of the spectrophotometer is periodically checked, utilizing absorption peaks of the CO_2 and H_2O bands.

The test setup for the optical mockup includes a Princeton Applied Research look-in amplifier whose reference signal is provided by the phase-reference pickup (PRP) signal from the mockup.

Phasing of the signal output is adjusted for maximum output and verified and monitored with an oscilloscope.

Throughout the testing phase, all aspects which can possibly influence the results, such as purging, local heating, stray light, cleanliness of equipment, and maintenance of calibration, are carefully observed and monitored.

1110-104-227

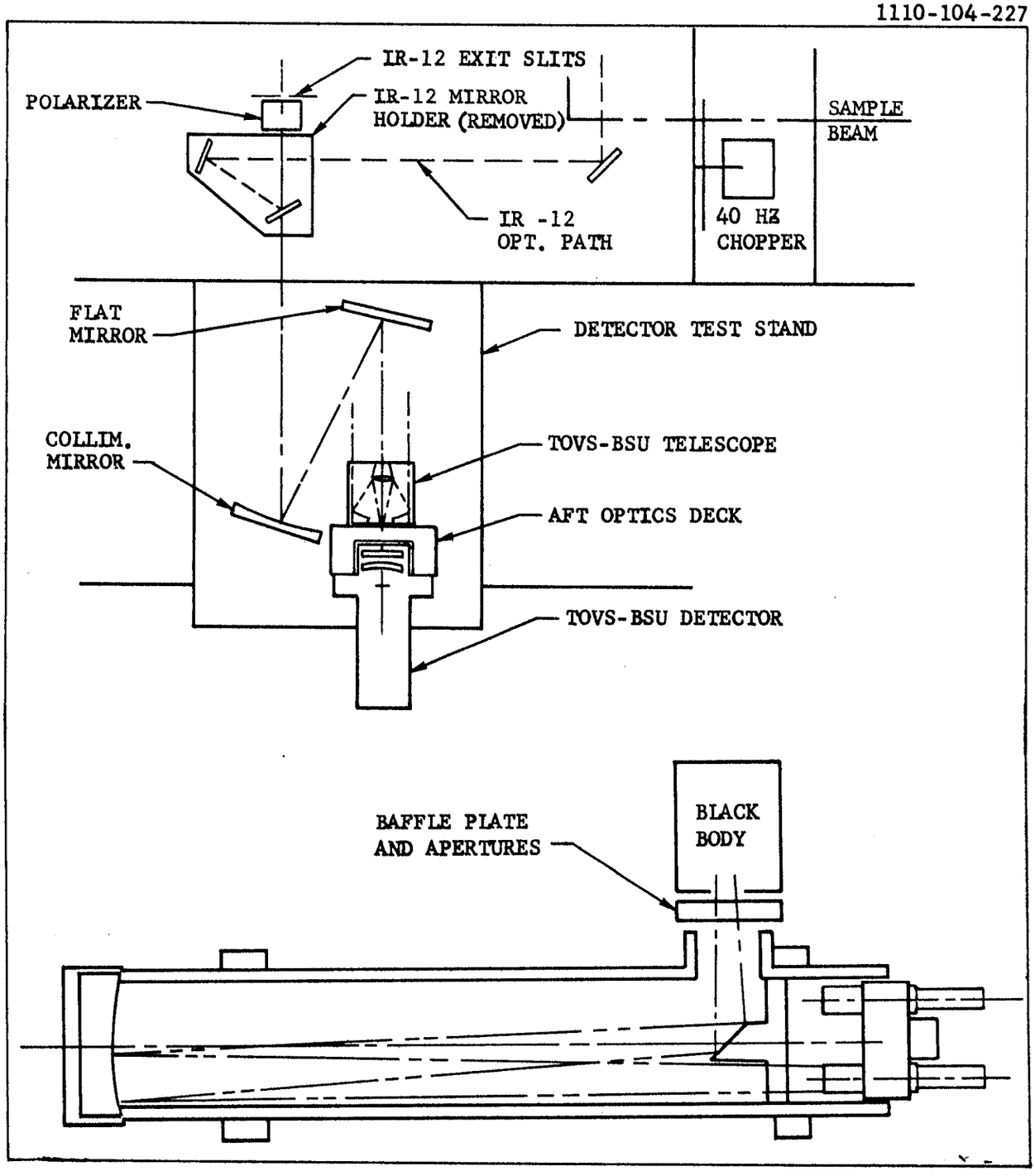

Beckman IR-12 Spectrophotometer With External Test Platform (Top)
Newtonian Infrared Collimator With Blackbody Source (Bottom)

SUMMARY OF OPTICS TESTING

Results of the optics testing show that the essence of optical requirements has been met. Testing indicated that the FOV for channel 14 is diffraction-limited but that the 99% requirement can only be approximated to within 0.6 percent.

An optical mock-up of an 80-mm telescope was constructed, incorporating channel 11 (668.5 wave numbers) in the reflected mode and channel 14 (340 wave-numbers) in the transmitted mode, for component and system testing. Testing of the components, subassemblies, and the assembled system was completed. The following is a summary of the results.

Silicon filters and dichroics for channel 14 were fabricated to obtain practical manufacturing experience. They met all applicable environmental test specifications. The transmittance of the filter was improved from 15 to 26 percent. The dichroic had optimum reflectance for channel 11 and 65 percent transmittance for channel 14. This is somewhat less than the expected 75 percent. The manufacturer, however, is confident of achieving 75 percent transmittance. Transmittance varies by approximately 4 percent for different states of polarization.

The individual lenses for channels 11 and 14 were manufactured from germanium and silicon, respectively, and had transmittance values of 89 and 83 percent. Transmittance values of the double-lens assemblies, with the lenses oriented at random with respect to each other, are on the order of 3 percent. Experience on the ITPR indicates that uniformity can be improved by selective orientation of the lenses. The field-of-view (FOV) tests performed at 2630 cm^{-1} and 691 cm^{-1} show that the requirements for the half-power points at 1.125 degrees FOV and the containment of 99 percent of the energy in 1.25 degrees FOV can be met. At 340 cm^{-1} (channel 14), diffraction effects reduce the energy contained in the 1.25 degrees FOV to 98.4 percent.

It was shown that FOV flatness was influenced to a greater extent by variations in detector lens transmittance than by variations in responsitivity over the sensitive area of the detector. Orientation of the detectors to meet the 1 percent FOV alignment specification was not difficult to perform.

The total transmittance value for channel 14, approximately 12 percent, is much better than the originally estimated 7 percent. The spectral transmittance scan of the assembled channel 14 shows no alteration of the spectral characteristics due to the influence of other components.

Polarization tests on the mock-up indicate about a 3-percent modulation of instrument response by variations in the state of polarization of energy detected in channel 11 at 669 cm^{-1}.

The stray-light tests performed show less than 1 percent of stray light contributed from outside the FOV. No stray light could be measured from wavelength regions below the channel bandpasses to beyond 50 micrometers.

TEST RESULTS

- Half-power points are within the required 1.125 degrees (FOV).
- 99 percent of energy is contained within the required 1.25 degrees FOV for channels 1 to 13.
- 98.4 percent of energy is contained within the required 1.25 degrees FOV for channel 14.
- Asymmetry of radiometric FOV is within the required 1 percent.
- Transmittance value of channel 14 is 12 percent.
- Polarization sensitivity of channel 11 is acceptable.
- Stray light from outside the FOV is less than 1 percent.
- Response from other wavelength regions is less than 1 percent.

TESTING OF FILTERS

The filters for channel 14 (340 wavenumbers) were fabricated to obtain practical manufacturing experience. Testing of the filters shows that all required specifications have been met or exceeded.

The filter for the reflected channel (Channel 11) is a germanium 668.5 wavenumber filter with 5.5 wavenumber bandwidth purchased to ITPR specifications. Its properties were thoroughly investigated for the ITPR program and they also pass TOVS-BSU specifications. This filter is not discussed in this topic. The filter for the transmitted channel (Channel 14) is a silicon filter which was fabricated to obtain practical manufacturing experience. The combined properties of substrate and coating are not as well known as those of germanium especially with respect to environmental conditions such as humidity, vacuum, and temperature. Still, all required specifications have been met by the filter.

Listed in the table are the filter characteristics as established by the filter supplier.

Of special interest is the transmission of the filter which was originally estimated to be 15 percent. As shown in the facing figure, this transmission was almost doubled (Beckman scans).

The scans of the individual filter elements also show adequate sideband rejection with only a minute leak at 1580 wavenumbers as discernible from the scans.

Sideband rejection was specified to 200 wavenumbers. No spectral transmittance scans have been performed beyond this point.

Transmittance of the filter assembly was also measured with the elements oriented at 4 degrees to the incident radiation to simulate the BSU optics. There was no measurable change observed from the transmittance curve in the figure (zero degrees to incident energy).

The two filter elements (bandpass and blocker) are mounted in a separate subassembly (see the figure). This approach facilitates alignment of the filter elements with respect to each other and maintaining this alignment during spectral testing and installation in the aft optics deck. The filter elements are held in place in the subassembly by a spring washer.

It has been shown that the silicon filters for Channel 14 (340 wavenumbers) can indeed be fabricated to meet all desired specifications. The manufacture and testing of the silicon filter supplements the extensive data gathered with the ITPR filters (manufactured from germanium). It can be concluded that the filter requirements for the entire TOVS-BSU wavelength range can be met successfully.

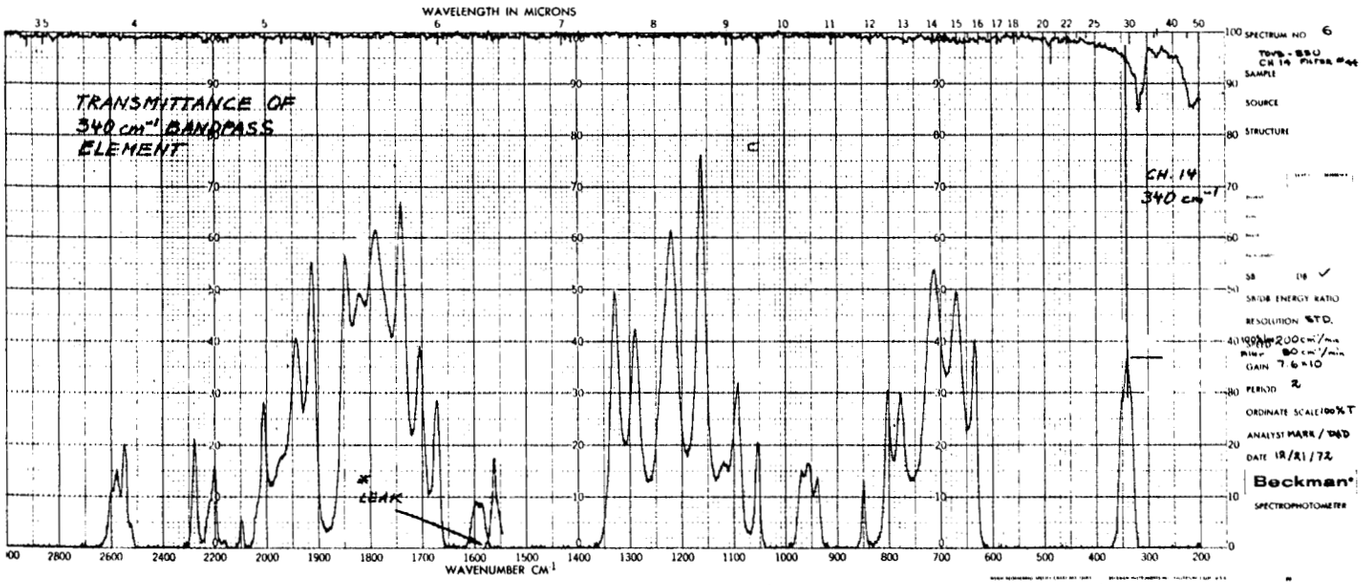

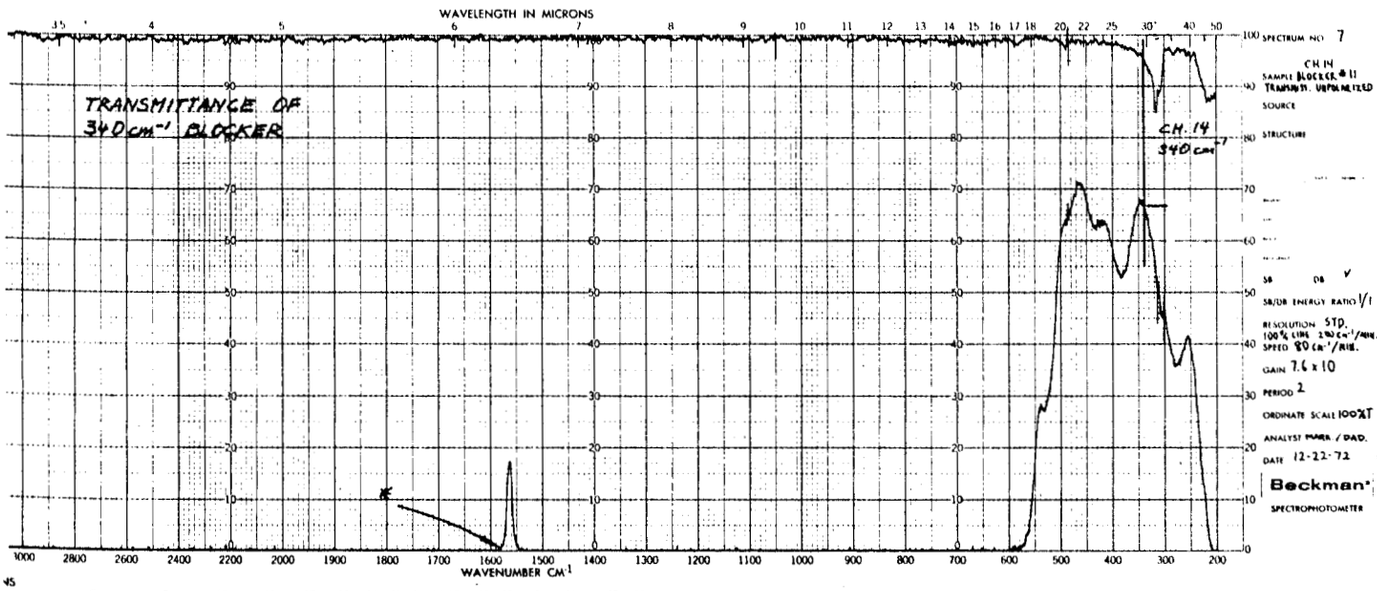

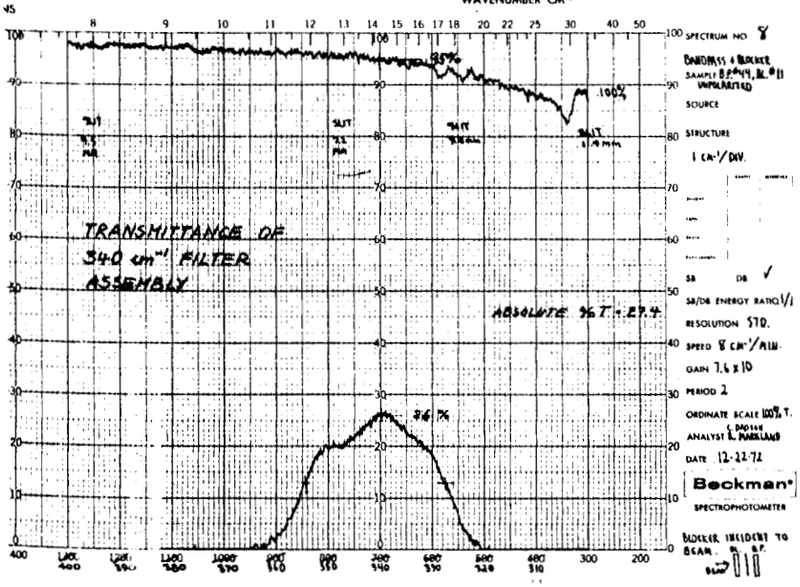

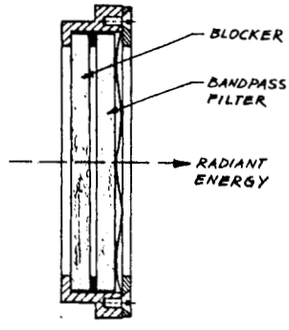

FILTER ASSEMBLY

Spectral Scans of the TOVS-BSU Dichroic Beamsplitter

FILTER DATA SHEET
(19 Dec. 1972)

	Observed	Filter Properties Specified
Channel Number	14	14
Filter Serial Number	44/11	
Filter Center Wavenumber (cm^{-1})	340.6	340 ± 2
Half Bandwidth (cm^{-1})	27.8	25 ± 5
Filter Transmission (percent)	28	25
Half Bandwidth Centering Point (cm^{-1})	341.4	
1% Absolute Transmission Points	363.5/319.7	370/310
Center Wavenumber Shift vs Temperature (cm^{-1})	0.4 per 25°C	+14, -6 for 0-50°C
Filter shifts to lower wavenumbers with decrease in temperature.		
Integrated Out-of-Band Transmission	0.4%	1%
Coating Batch Numbers		
Bandpass:	21121272/21121572	
Blockers:	21120172/21120472	
Material of Filter Element:	proprietary	
Material of Blocker Element:	proprietary	

PROCUREMENT AND TESTING OF DICHROICS

The dichroic filter was manufactured to obtain practical manufacturing experience. The dichroic meets all specifications with satisfactory results.

The beam splitter (dichroic) for the TOVS-BSU mockup reflects channel 11 (668.5 wavenumbers) and transmits channel 14 (340 wavenumbers); the substrate material is polycrystalline silicon with some doping element. The transmittance and reflectance scans of the dichroic are shown in the facing figure. The transmittance of the 340 wavenumber band is approximately 64 percent which is somewhat below the expected goal of 75 percent. However, according to the manufacturer, this goal can be reached. The reflectance at 668.5 wavenumbers is near maximum.

The transmittance versus temperature at 340 wavenumbers is shown below.

TEMPERATURE	TRANSMITTANCE
$0^{o}C$	61.5 percent
$25^{o}C$	65.5 percent
$50^{o}C$	65.0 percent

The 6-percent change in transmittance between $0^{o}C$ and $25^{o}C$ indicates a decrease in transmittance with a decrease in temperature at low temperatures. There is no detectable wavelength shift with temperature change.

The transmittance of the dichroic with varying angle of incidence is also established. The incident radiation of from 40 to 50 degrees to the normal does not measurably change transmittance but produces a small wavelength shift of approximately 4 wavenumbers at the 370-wavenumber peak.

The polarization sensitivity of the dichroic was measured on a Beckman IR-12 spectrophotometer with a wire-grid polarizer in double-beam mode. The dichroic was oriented at 45 degrees with respect to the sample beam such that the plane of incidence was normal to the slit. The transmittance of the dichroic changed from 60 percent to 56 percent absolute with polarization states of 0 and 90 degrees, respectively. The location of the wavelength peak did not seem to change with change in polarization states.

All environmental specifications such as humidity, vacuum, and temperature are met by the dichroic.

The dichroic which was investigated and used in the mock-up is manufactured by Spectrum Systems, Waltham, Mass.

Another dichroic which transmits channel 11 (668.5 wavenumbers) and reflects channel 14 (340 wavenumbers) could not be investigated due to lack of time. This dichroic is manufactured by OCLI, Santa Rosa, Calif. The OCLI test results are discussed in the topic on system polarization sensitivity.

The manufacture of this most difficult dichroic can be accomplished with either channel 11 or channel 14 in the transmitted or reflected channel. The tested dichroics meet all required specifications. It can be concluded therefore that all anticipated dichroic combinations for the TOVS-BSU can be fabricated to meet the desired performance specifications.

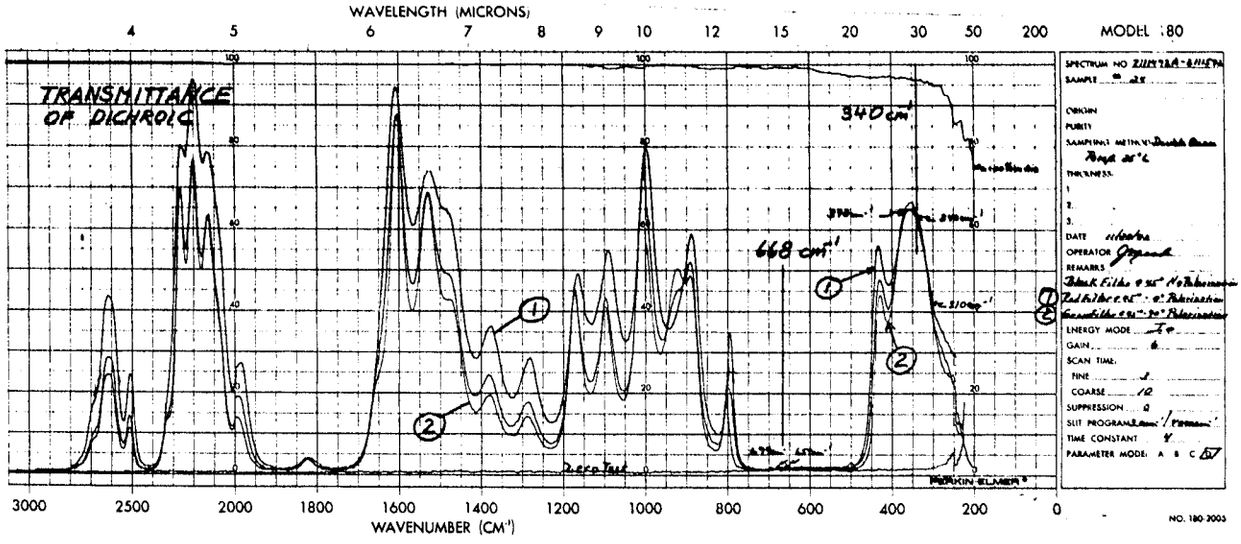

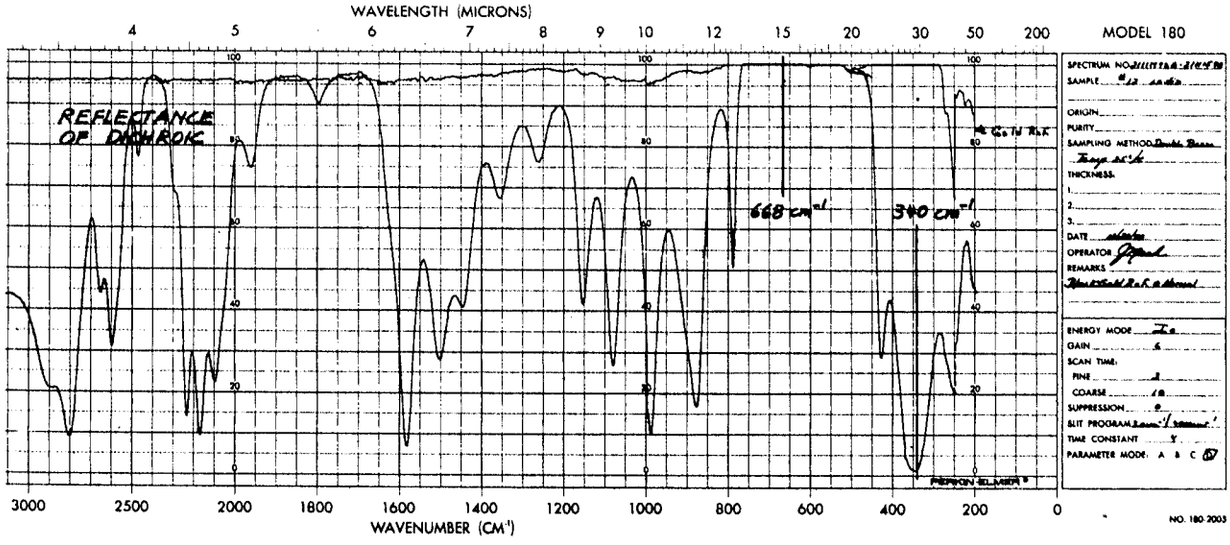

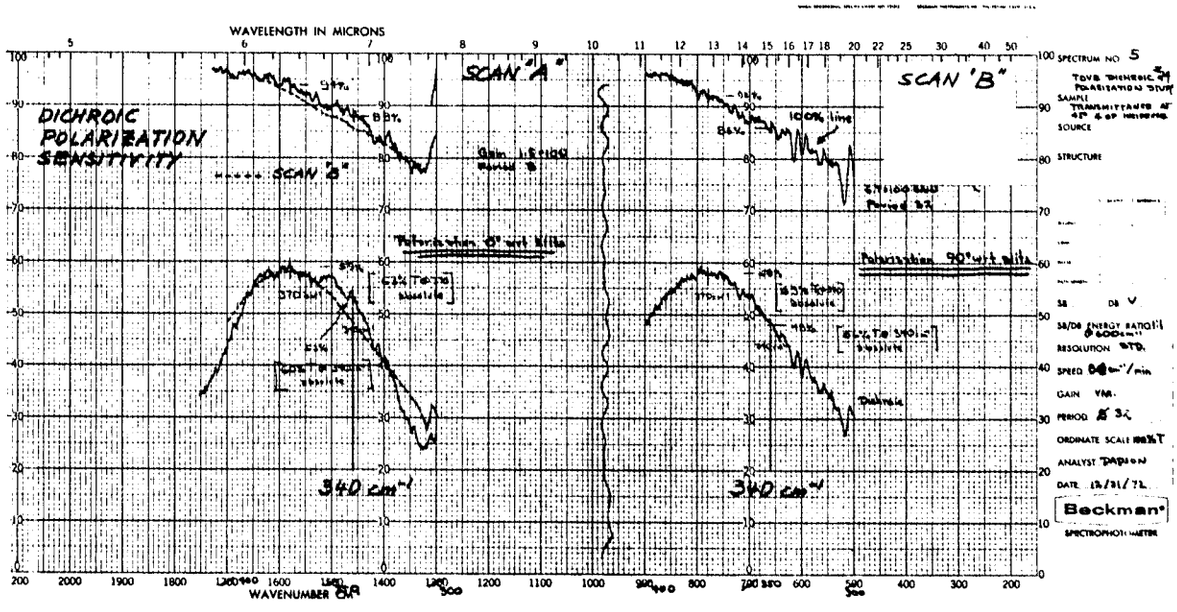

Spectral Scans of the TOVS-BSU Dichroic Beamsplitter

FABRICATION AND TESTING OF LENSES

Coated silicon and germanium lenses for the mockup were fabricated, assembled, and tested for transmittance and uniformity. The lenses met the specifications for transmittance and uniformity.

The lens assemblies for channel 11 and channel 14 consist of two lenses each which are mounted in a separate housing as shown in Figure A, facing. This type of mounting facilitates testing, handling, and mounting of the lenses in the aft optics deck; it also preserves alignment of the two lenses with respect to each other. The lenses are held in place in this subassembly by a spring washer.

The lenses for channel 11 (668.5 wavenumbers) were manufactured out of germanium; those for channel 14 (340 wavenumbers), out of silicon. All lenses are suitably coated with antireflection coatings to obtain maximum transmission at the respective wavelength. The following transmittance values were obtained:

668.5 wavenumbers - 89 percent
340 wavenumbers - 83 percent

Both types of lenses are manufactured out of polycrystalline material and all radii are checked with test glasses calibrated to 0.025 mm.

The germanium lenses pass all environmental specifications. Exception was taken for humidity and the scotch tape test on the silicon lenses. However, the manufacturer indicates that these specifications could have been met as well as the transmission improved if more time had been allowed for manufacture.

Uniformity tests were performed on the complete lens assembly in the mockup. The filter assembly for these tests was replaced consecutively by three discs with 3-mm holes located as shown in Figure A. With these discs stationary, the lens assembly was rotated and 16 individual readings were taken for one complete revolution. The graphs of these tests are shown in Figure B.

The percentage variations for a complete revolution for the silicon lenses in the three individual tests are as follows:

Test ① center hole	2.76 percent
Test ② hole 1 diameter off-center	2.84 percent
Test ③ hole 2 diameter off-center	5.55 percent

The results for the germanium lenses were similar. A knowledge of the transmission uniformity is important since it influences field-of-view uniformity.

If necessary, the lenses can be tested individually and then aligned with respect to each other. Coating "run-off" can also be determined with these measurements but was not attempted in these tests.

The germanium and silicon lenses passed all dimensional and transmittance specifications, with the exception stated previously in the text. It can be concluded, therefore, that the lenses for all TOVS-BSU can be fabricated.

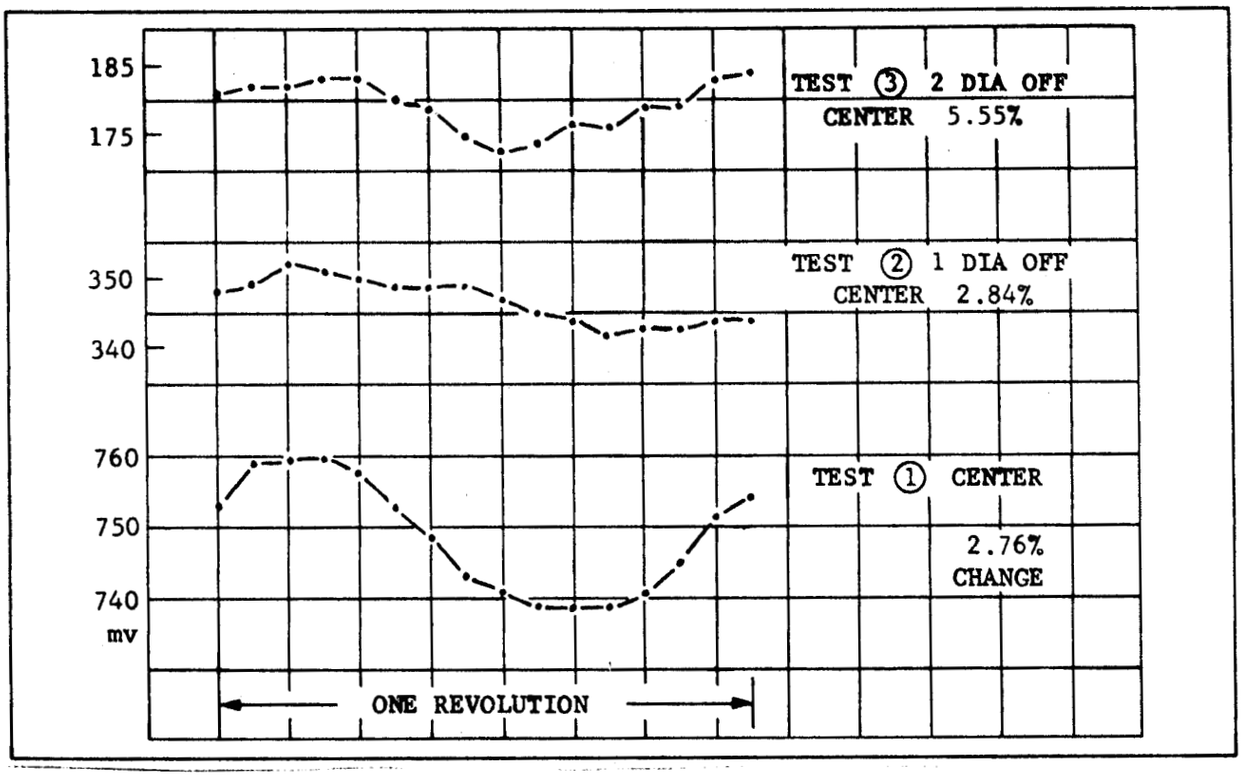

Figure A. Transmission Sensitivity of Silicon Lens Assembly

1110-104-229

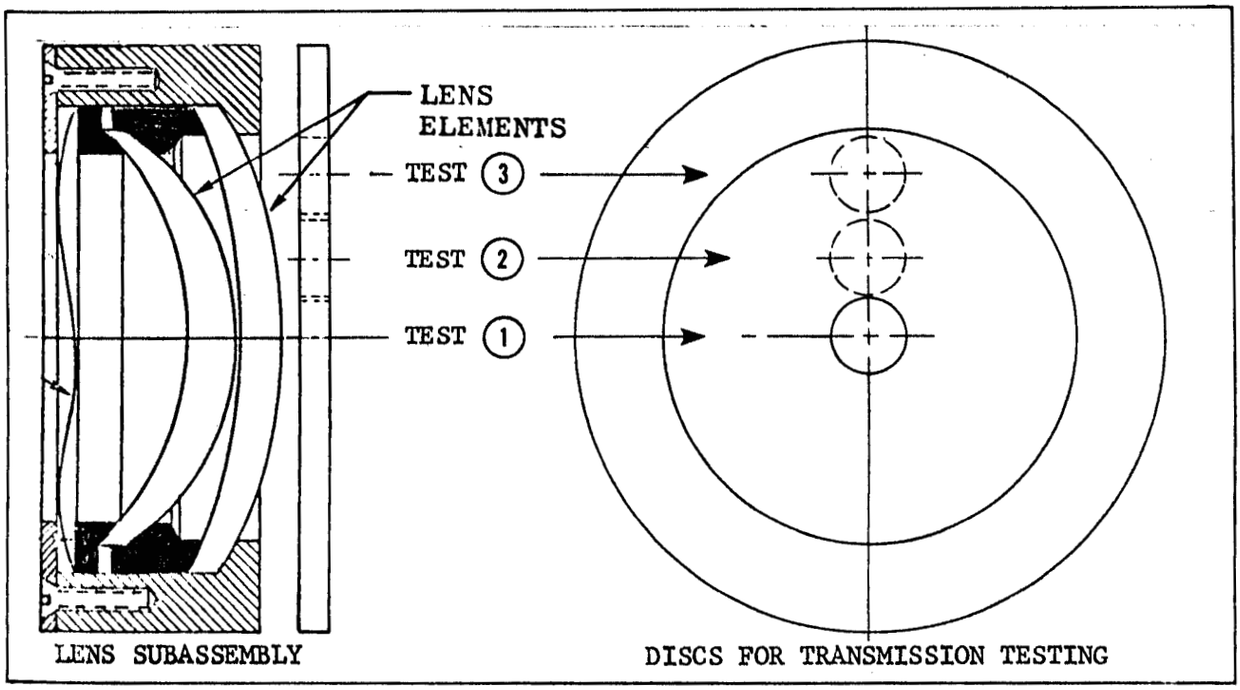

Figure B. Apparatus for Testing Uniformity of Lens Transmittance

RESULTS OF FIELD-OF-VIEW TESTING

The field-of-view (FOV) tests of channel 11 and 14 show that the design goals for half-power points and full FOV have been met. Stray light acceptance is less than 2 percent for each channel.

The field-of-view (FOV) requirements for the individual channels are as follows: The FOV shall not exceed 1.20 degrees at the half-power points; reduction of the half-power FOV to 1.125 degrees shall be a design goal. Ninety-nine percent of the total energy observed shall emanate from a circular FOV not greater than 1.125 degrees considering a continuous uniform target.

The ITPR filter of channel 1 (center wavenumber 2675, half-bandwidth 450 wavenumbers) was installed in the transmitting channel of the optical mockup (channel 14, center wavenumber 340) to provide adequate energy throughput for the FOV measurements. The measurements are performed with a source which subtends about one-fourth of the FOV. The resultant FOV response is shown in the facing figure which illustrates that the design goal of reducing the half-power point to less than 1.125 degrees has been realized. The energy outside the 1.25 degree FOV is 3.3 percent, as calculated from the scan data. This value is large because of the large source used.

With the channel 14 filter (340 wavenumbers) installed, the FOV scan is similar but somewhat harder to obtain due to the lower signal-to-noise ratio. The FOV scans for channel 11 are similar to the ITPR filter (channel 1) response. It appears to be not at all difficult to realize a 1-percent positioning accuracy with the detectors.

Another test measuring the energy contained in the 1.25-degree FOV is the response from an aperture which subtends 1.25 degrees at the opening of a blackbody, versus no aperture at the blackbody opening. The apertures are 26.8 mm versus 76.2 mm, respectively. With a blackbody temperature of 900°C, there is approximately a 2-percent increase in response between the two measurements (channel 14, 340 wavenumbers).

The nonuniform response across the FOV was originally attributed to varying detector response across the detector sensitive area.

It was found, however, that by rotating the lens assembly 180 degrees, the slope of the top could be reversed (see the figure). This amount of response change has not yet been correlated with the measured transmittance changes of the lens assembly.

It is further possible that transmission nonuniformities of the filter assembly and dichroic will contribute to this effect.

By rotating these components to relative positions determined from transmission scans of the subassemblies, it should be possible to obtain a perfectly flat FOV top.

The shift of the FOV centroid calculated from the data shown in the lower figure opposite is 0.04 percent of the 50-percent FOV, a value which meets the 1 percent centroid matching specification.

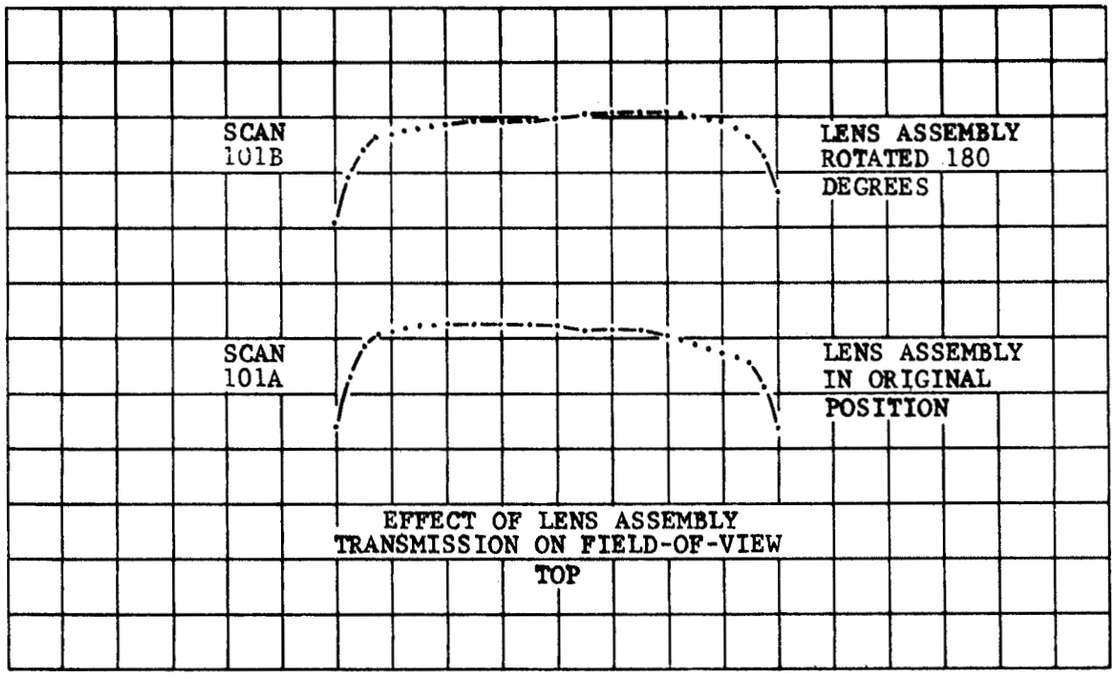

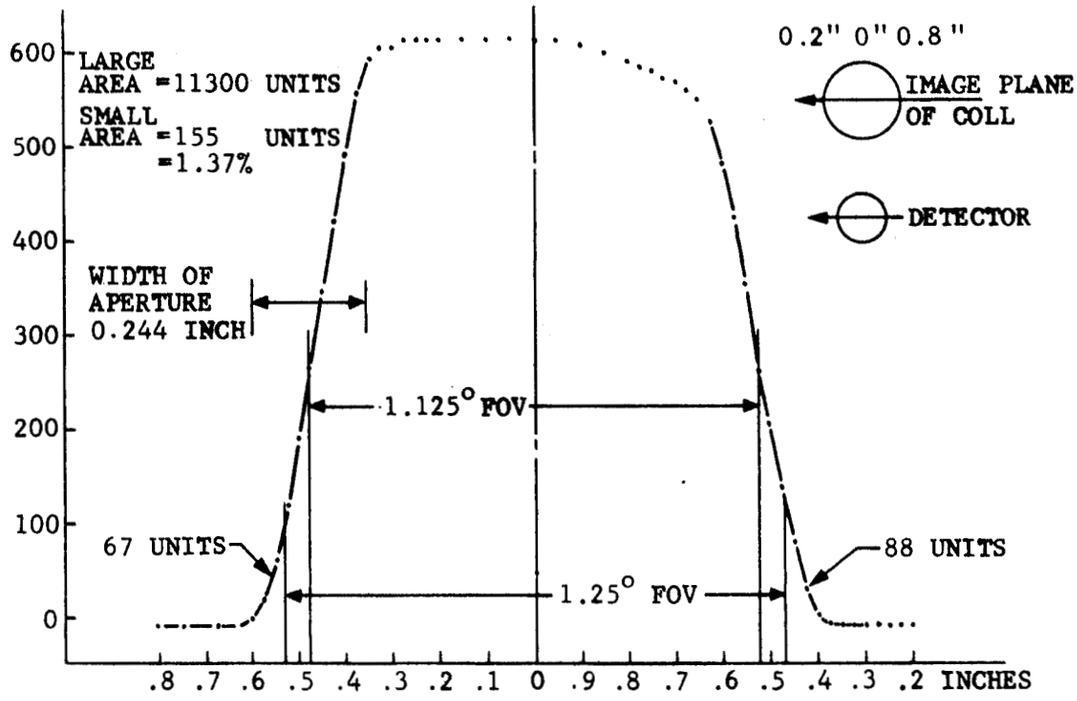

Field-of-View Channel 14 (With ITPR Channel 1 Filter)

RESULTS OF SPECTRAL TRANSMITTANCE TESTS

The spectral transmittance scans for the completely assembled optical mockup show that the optical elements do not influence channel transmittance.

There are 12 optical component surfaces between telescope opening and detector sensitive areas. They all can contribute to the final energy bandpass "seen" by the detector. All components have been tested individually and the final bandpass can be predicted accurately. A check on this prediction can be performed by scanning the bandpass with a high-resolution source. A Beckman IR-12 spectrophotometer is used in the single-beam mode to furnish this source. The complete optical mockup is mounted on an outboard platform and the energy is directed out of the instrument through an opening in the cover. The platform is covered with a housing which permits purging the entire optical path.

The scans of channel 11 (with ITPR channel 5 filter) and channel 14 are shown in the figure opposite. The reflected scan of channel 11 will not be discussed since dichroic and lenses are not optimized for this wavelength region.

Channel 14 (340 wavenumbers) unfortunately is located in a very low-energy region of the spectrophotometer which results in low signal-to-noise ratio for the pyroelectric detector. The scan shown in the figure is performed with a slit width of 5 wavenumber resolution (versus 25 wavenumber bandwidth for channel 14).

A transmittance scan of the channel 14 filter is superimposed over the channel response scan. The scan clearly shows that the transmittances of the individual optical elements do not appreciably influence the bandpass of the completed channel.

This scan is a test to verify the shape of the bandpass only. The shape of the filter transmission curve, which ultimately should determine the total channel transmittance, is well preserved as is the location of the half-bandwidth points.

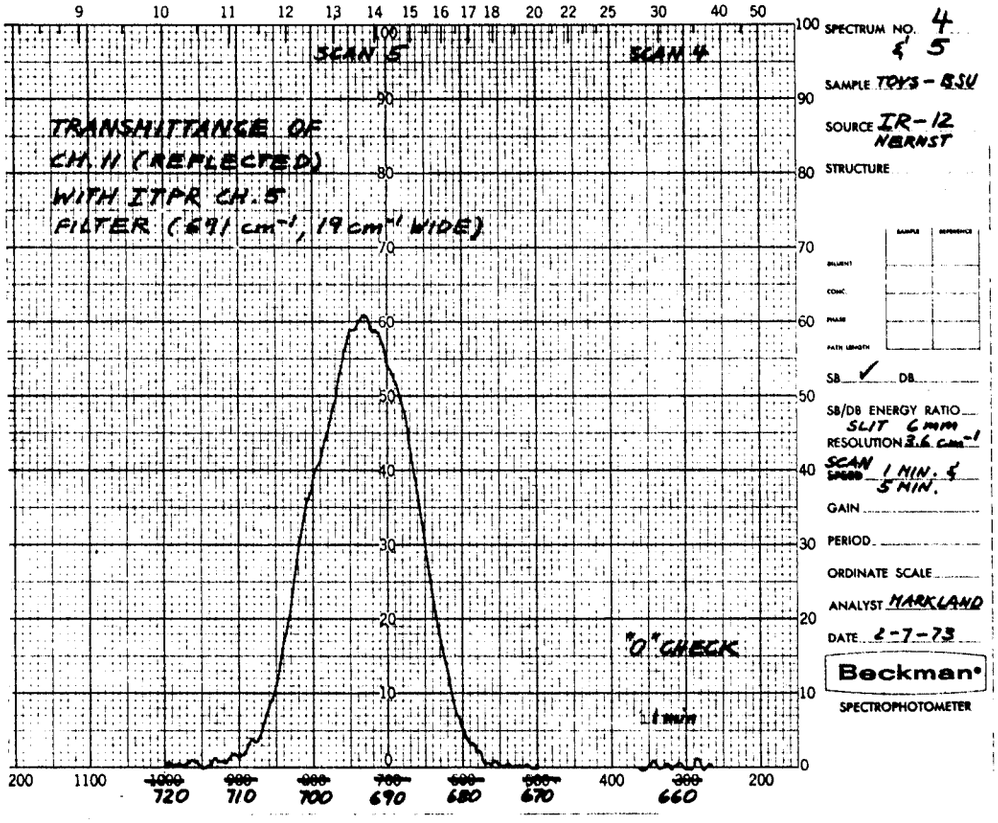

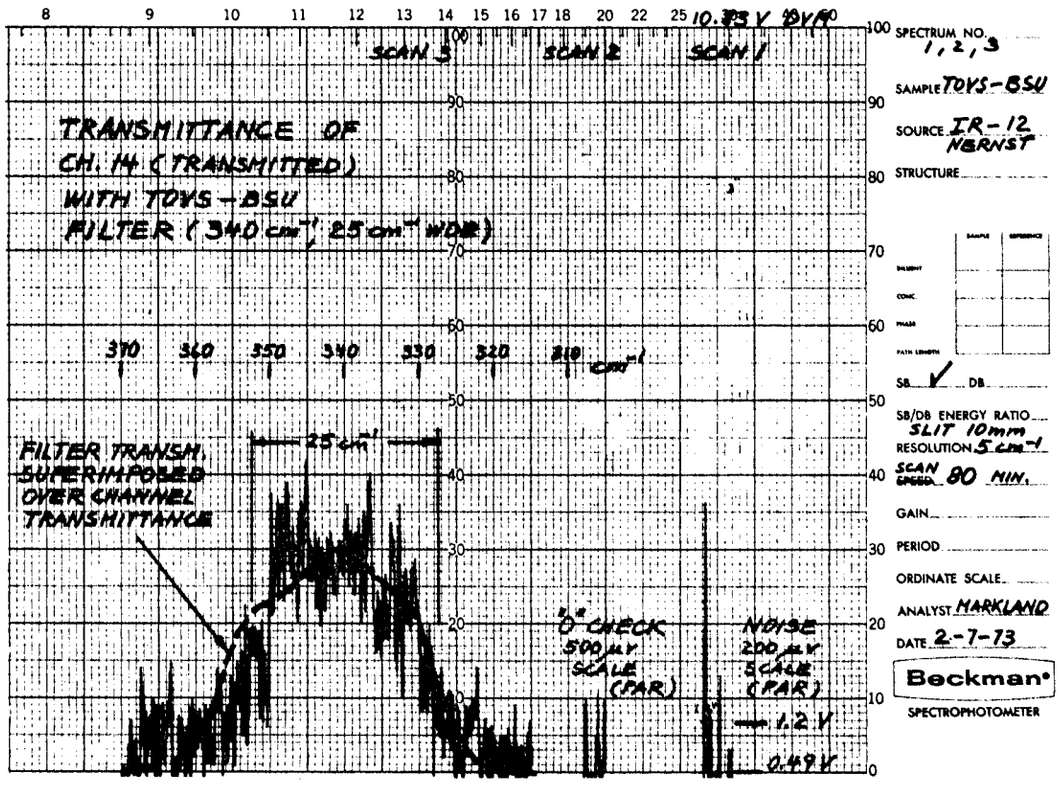

Spectral Scans of Optical Mockup Transmittances

RESULTS OF POLARIZATION TESTING

Testing of ITPR filters and TOVS-BSU filter and dichroic verifies their insensitivity to polarization. The ITPR dichroic transmittance varies 15 percent with the state of polarization. All polarization testing indicates that components fabricated for this study are sufficiently free from polarization sensitivity to assure accurate radiometric measurements by both channels 11 and 14.

Complete prediction of the TOVS-BSU performance requires determination of the instrument response to variations in the degree of polarization of energy radiated and scattered by the scene. To estimate instrument response to scene polarization, the optical mock-up as well as its constituent components were tested for variations in response and transmittance, respectively, with the state of polarization of incident energy. In addition, the polarization sensitivity of several ITPR components was tested to predict such sensitivity.

Variations in transmittance and reflectance with the state of polarization of bandpass filters and blockers, as well as dichroic beamsplitters were measured in a double-beam mode on a Beckman IR-12 infrared spectrophotometer with a polarizer attachment.

Optical mock-up response to polarized light was measured using the optical test platform attached to the IR-12. As discussed in the topic on test hardware and calibration, the IR-12 was altered to allow every output from the monochrometer to leave the instrument through a hole in its cover. This energy was linearly polarized with a silver chloride pile-of-plates polarizer prior to folding and collimating by the optical test platform optics.

The TOVS channel-14 filter and ITPR channels 1 and 2 filters were measured for variation in transmission with state of polarization of energy incident, normal to the plane of the filters. No polarization sensitivity was detected.

The TOVS-BSU channel 11-14 dichroic and an ITPR channel 1 and 2 dichroic were tested for variation in transmittance and reflection with the state of polarization of energy incident at 45 degrees. The dichroics were placed in the sample compartment and inclined to the incident beam at 45 degrees, with the plane of incidence normal to the IR-12 monochrometer slits. The results of the testing are presented in the opposite table. They indicate little polarization sensitivity in reflectance for either dichroic. In transmission, however, the ITPR dichroic had approximately 15 percent higher absolute transmittance at 900 cm^{-1} (ITPR channel 2) for energy linearly polarized in the plane of incidence. The TOVS-BSU dichroic exhibited about 4-percent higher absolute transmittance at 340 cm^{-1} for energy polarized in the plane of incidence and 1-percent absolute transmittance at 370 cm^{-1} (the point of peak transmittance). The reflectance of either dichroic was insensitive to state of polarization within the variation in the experimental error of 5 percent. Theoretical polarization transmittance curves from OCLI (ITPR dichroic) and experimental curves from Spectrum Systems (BSU dichroic) verify the above testing within the expected accuracy of measurement, ± 2 percent.

The optical mock-up was tested for response to linearly polarized energy utilizing the IR-12 and an accessory optical platform as discussed above. The experimental setup simulated the BSU scanning operation by utilizing a stationary scan mirror (aluminized flat, inclined at 45-percent with respect to incident collimated energy) and rotating the optical mock-up to simulate a 360-degree scan pattern.

The monochromatic energy incident on the simulated scan mirror was linearly polarized in its plane of incidence. Variation in instrument response with rotation of the optical mock-up, then corresponded to an instrument sensitivity to scene polarization.

The transmittance of the silver chloride polarizer limited testing to the BSU reflected channel 11 (as simulated by a channel 5 ITPR bandpass filter in conjunction with the TOVS-BSU channel 11-14 dichroic). Instrument response was found to be modulated sinusoidally with a peak-to-peak amplitude of 4 percent of average response by rotating the optical mock-up through 360 degrees. The 4-percent variation in response places an upper limit on the polarization sensitivity of the dichroic which is in agreement with testing of the dichroic reflectance.

As discussed in the topic on Effect of Polarization, and as verified by testing, the dichroic beamsplitter is responsible for the polarization sensitivity of the BSU. Tests on the TOVS-BSU channel 11 through 14 dichroic indicate that dichroic beamsplitters can, in fact, be fabricated which are sufficiently insensitive to polarization to assure accurate radiometric measurements.

RESULTS OF COMPONENT POLARIZATION TESTING

Experimental data indicate that the filters and the TOVS-BSU dichroics tested are insensitive to polarization. The ITPR dichroic transmittance varies 15 percent with the state of polarization.

	ITPR		TOVS-BSU		
	Channel 1 Filter	Channel 2 Filter	Channel 1-2 Dichroic	Channel 4 Filter	Channel 11-14 Dichroic
Center Wave Number	2675 cm^{-1}	900 cm^{-1}	R-2675 cm^{-1} T-900 cm^{-1}	340 cm^{-1}	R-669 cm^{-1} T-340 cm^{-1}
$T_{\parallel} - T_{\perp}$	<0.01	<0.01	0.15	<0.01	0.04
$R_{\parallel} - R_{\perp}$			<0.05		<0.05

T: Transmittance
R: Reflectance

$\parallel$: polarized parallel to plane of incidence
$\perp$: polarized normal to plane of incidence

RESULTS OF DIFFRACTION TESTING

The diffraction measurements indicate that the requirement to pass 99 percent of the channel energies through a 1.25-degree field-of-view can be met with the possible exception of channel 14.

An attempt was made to measure the effect of diffraction on the field-of-view response of the TOVS-BSU optical mockup in channel 14 (340 wavenumbers) and channel 14 with an ITPR filter (2630 wavenumbers).

The infrared collimator was used with an iris diaphragm (continuously variable aperture) installed at the collimator image plane. The aperture was varied from an opening of less than 1.125 degrees field-of-view (FOV) to more than 1.25 degrees until an increase in opening did not produce a higher signal from the detector. This setting was used as the 100-percent response in the graph of the figure opposite. The graph plots percent response versus opening of the iris. The 1.25 and 1.125 degrees FOV are marked at the corresponding iris openings. The scan for channel 14 (340 wavenumbers) was performed with a blackbody temperature of 970°C, the collimator was purged with nitrogen gas which also cooled the blades of the iris diaphragm. The response curve shows 98.4 percent at 1.25 degrees FOV which is close to the requested 99 percent. In a previous measurement, a 98-percent response was obtained on the basis of an opening of double the diameter used for setting the 100 percent level for the above measurements.

The second scan shown on the graph was again obtained with channel 14, only the 340 wavenumber filter was replaced with a 2630 wavenumber filter and the temperature changed to 635°C to get "on scale." The 99-percent response point is well within the 1.25 degrees FOV. This agrees with a previous measurement which did not show an increase in signal between an aperture of the correct 1.25 degree FOV size versus an aperture double the diameter used to set 100 percent for the above measurement.

The second series of points on the 2630 wavenumber graph is a second set of measurements. Diffraction effects would result in a broadening of the cut on at the 100-percent point and an increase of signal at the 1.25-degree FOV. Broadening and signal increase (stray light) should be more pronounced with the 340 wavenumber filter than with the 2630 filter. This is clearly evident from the graphs.

The diffraction measurements are difficult to perform since very small signal changes have to be measured, and a multitude of factors can influence the results.

It appears, however, that the diffraction effects can be measured. The measurements were performed at the extreme wavelength points of the TOVS-BSU. The results indicate that the 99-percent energy requirement for the FOV can be met for most channels with the exception of channel 14 which is reduced to 98.4 percent.

1110-104-238

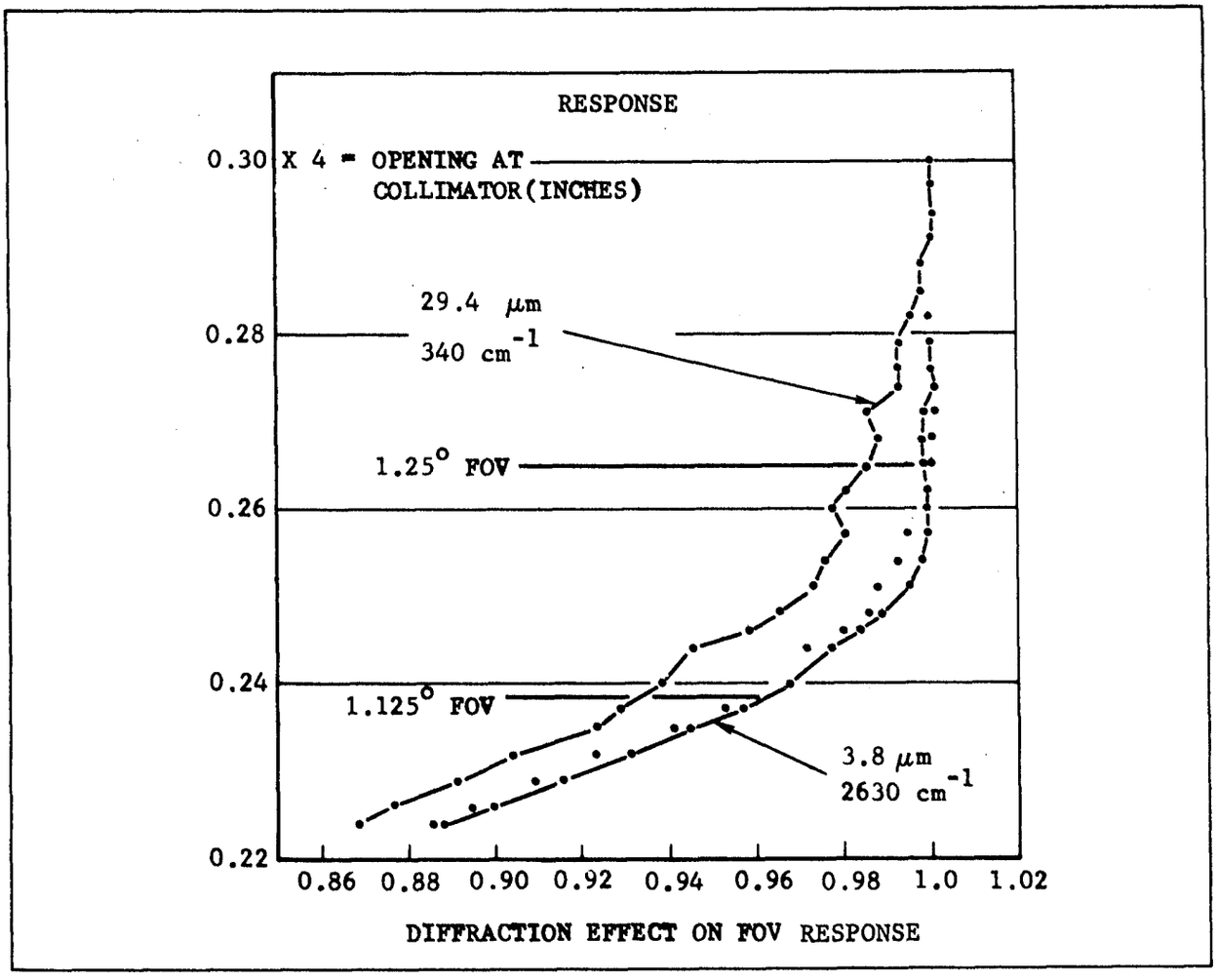

The second set of points at 3.8 μm were taken in a second run.

OUT-OF-BAND ENERGY TESTING

The out-of-band energy testing was performed with broadband filters for selected wavelength regions. Results indicate excellent out-of-band rejection for most wavelength bands.

Energy which reaches the detector from outside the FOV is stray light and affects the accuracy of the measurement. This type of stray light was investigated during the FOV testing and the diffraction effect measurements. Results indicate excellent out-of-band rejection from this source with less than 1-percent influence on the bandpass signal.

A different out-of-band test is described in this section. Energy from the blackbody source is passed through broadband filters located directly in front of the telescope openings. The filters selectively pass energy below and above the bandpass of the respective channel for an integrated measurement of stray light outside the channel bandpass, but within the FOV, and transmitted through all optical elements through "leaks."

These out-of-band energy tests were performed on the transmitted channel with an ITPR 2630 wave number filter installed and reflected channel with an ITPR 691 wave number filter. The graph in the facing figure shows the location of the channel bands and the transmission ranges of the various testing filters.

The facing table shows the response of the channels with the various testing filters; the blackbody is at 635°C for ITPR filters.

The crystal quartz is, in effect, a far infrared filter transmitting past 200 wave numbers. It is interesting to note that none of the absorption filters (Ca F_2, OW-1 and quartz) indicate the presence of out of band. The long-wave pass (LWP) filters, which are coated KRS-5 substrates, may have leaks or pin holes themselves which would contribute to the apparent stray light in both channels. Pin holes would contribute more stray light to the 2630 wave number channel than to the other channel, which is indeed the case. Since none of the out of band that the channels will ever see is at this elevated temperature, it was concluded, from the measurements performed, that the channels have excellent out-of-band rejection for the shorter and far infrared wavelength regions. Results on stray light rejection for longer regions up to 200 wave numbers are less conclusive.

The TOVS-BSU channel 11 (reflected), 668.5 cm^{-1}, and channel 14 (transmitted) 390 cm^{-1}, filters were also tested for long wavelength out-of-band energy transmittance. These filters were tested against quartz to provide data regarding transmittance of energy of wavenumber 200 cm^{-1}. Tests on both BSU filters indicate out-of-band energy rejection to a level less than 1 percent.

RESPONSE OF THE CHANNELS WITH VARIOUS STRAY-LIGHT FILTERS

	ITPR		TOVS/BSU	
	2630 Wave Numbers	691 Wave Numbers	668.5 Wave Numbers	340 Wave Numbers
Short-Wave Pass				
Shutter (30°C)	4	13	–	–
Open (Blackbody)	932	768	–	–
OW-1 plus PYREX	4	–	–	–
Ca F_2	–	13	–	–
Long-Wave Pass				
Shutter	3	17	71	36
Open	932	764	750	736
LWP "A"	12	–	–	–
LWP "C"	–	21	–	–
Crystal Quartz	–	17	72	40
	Relative Values			

1110-104-240

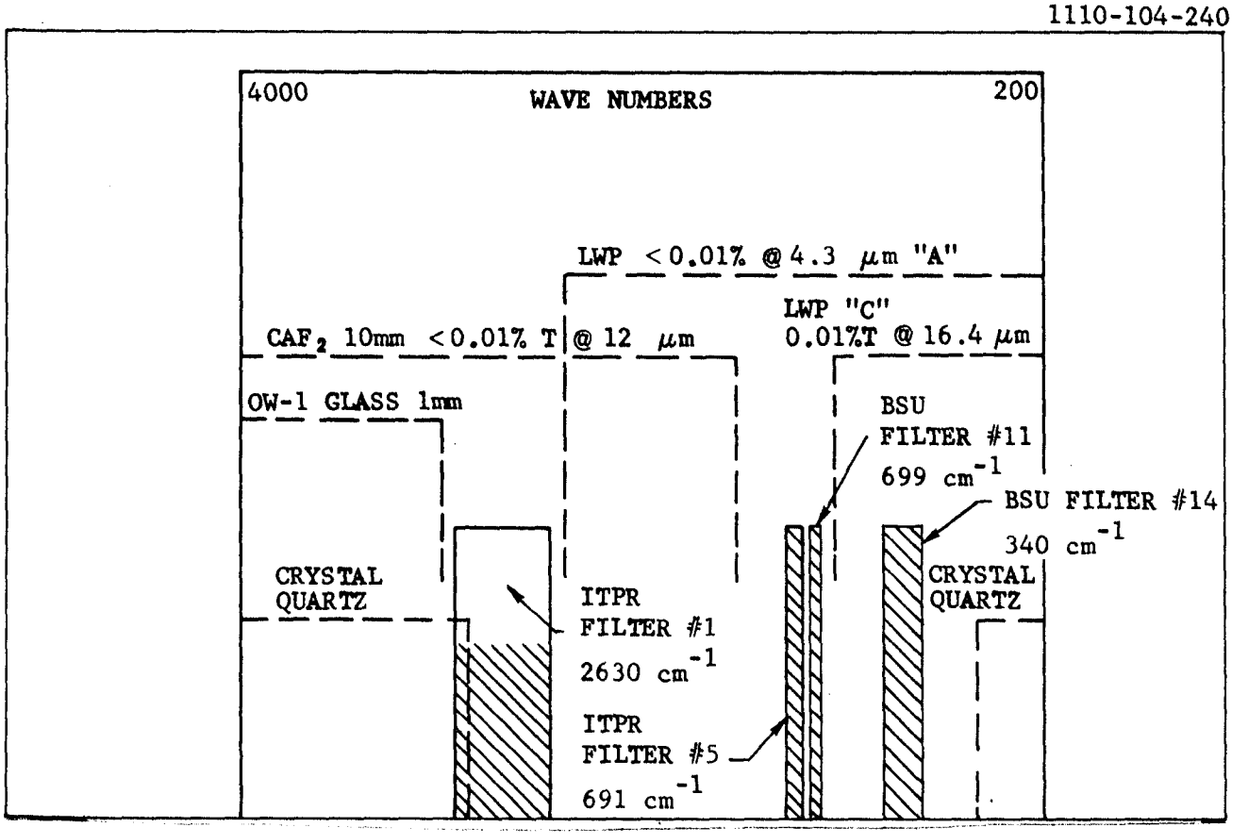

Pictorial Graph Showing Location of the Channel Bands and Filter Transmittances

SECTION 6
DETECTORS AND SIGNAL PROCESSING

System Considerations..... 6-0
Detector Selection..... 6-2
Basic Detector Performance Considerations..... 6-6
The Pre-amplifier..... 6-8
The Detector/Pre-amplifier Noise Equivalent Circuit..... 6-12
Detector/Pre-amplifier Test Results..... 6-14
ITPR Detector Performance..... 6-18
Detector Performance vs. Size..... 6-20
Post Amplification..... 6-24
Demodulation and Integration..... 6-26
Analog Multiplexer Requirement..... 6-30
Analog Multiplexer Description..... 6-32
Analog Multiplexer Circuits..... 6-34
Analog-To-Digital Conversion Method..... 6-36
ADC Error Analysis..... 6-38
Description of the ADC Circuits..... 6-40
Radiation Considerations 6-42

SYSTEM CONSIDERATIONS

Consistent with the optical design a detection/signal processing system is required involving a detector per channel; parallel amplification, demodulation and integration, followed by a time shared 12 bit ADC system.

Among the starting parameters and requirements, the use of uncooled detectors and a total available time of 100 msec per scene or FOV are the most significant. Following close behind are the requirements of scene-to-scene independence and simultaneity of measurement for all colors or channels.

The Figure depicts the processing block diagram which yields the required results given all the constraints. The multiplexer and A/D converter although part of the analog processing is not included in the diagram. Discussion of these areas follow later. The building of the block diagram starts with the proper definition of detector characteristics which are quite special.

One of the tasks of this design definition study was to find the best possible uncooled detector consistent with sensitivity requirements and optical interface requirements and at the same time properly characterizing it in operation. The result of this investigation showed that alanine doped TGS pyroelectric detectors offer the best performance. Among pyroelectric detectors triglycene sulphate (TGS) has the best sensitivity for detectors in the 1 to 2 mm diameter range as well as appropriate spectral characteristics. Basically, a pyroelectric detector works by outputting a charge when the element is exposed to radiant energy. Radiant energy when absorbed by the element causes a change in its temperature which, in turn, is responsible for generating the charge.

A very low noise pre-amplifier is required to convert the detector signals to levels necessary for subsequent processing. At the heart of the pre-amplifier is an input stage consisting of carefully specified field effect transistor (FET). The second stage of the pre-amplifier is suggested to be an LM108A or equivalent on the basis of low power consumption and adequately low noise. The recommended circuit is virtually identical to that used on ITPR.

Additional gain and frequency shaping are provided by the post-amplifier prior to a synchronous demodulator and integrator. All the operational amplifiers used to implement these functions should be LM108A as well. Although some circuit details are given here most of them are included in the Analog Channel Report.

Analog to Digital conversion to 12 bits is suggested; while the present detectors do not warrent more than 11 bits the temperature monitoring circuits can use 12 bits to advantage. Also, should there be detector improvements between instrument inception and its execution (as was the case in the ITPR) maximum benefit can be gained only with a 12 bit system.

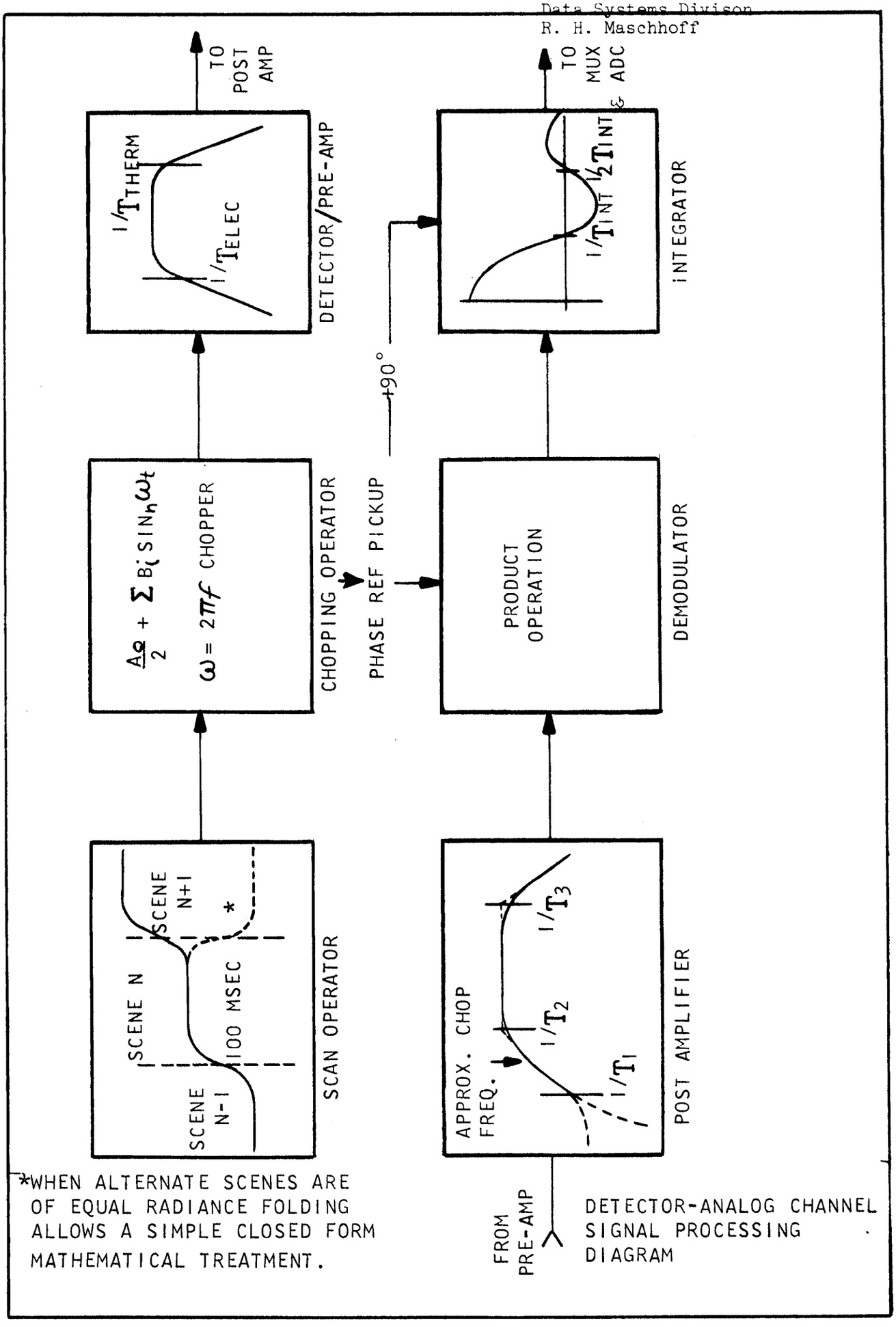

*WHEN ALTERNATE SCENES ARE OF EQUAL RADIANCE FOLDING ALLOWS A SIMPLE CLOSED FORM MATHEMATICAL TREATMENT.

DETECTOR-ANALOG CHANNEL SIGNAL PROCESSING DIAGRAM

DETECTOR SELECTION

Building a good detector involves first of all the proper choice of material for the sensing element followed by proper mounting techniques

The point of departure in terms of finding the best material was pure TGS used very successfully on the ITPR program. This section discusses some of the significant findings in the search for the best material or detector.

Triglycene Sulphate (TGS) has been found to be generally the best material for detectors when high sensitivity is of paramount importance. It is particularly good in situations where relatively large detectors are required for optical reasons. This is because it has a low dielectric constant relative to most other materials and at the same time exhibits a good pyroelectric coefficient. Pure TGS, however, suffers several disadvantages for general usage. One is a relatively low Curie temperature (i.e., 49°) above which the pyroelectric effect vanishes. This is not a significant problem for the TOVs because of temperature control. More serious is the possibility of pure TGS spontaneously depoling over the time scale of months, especially in a radiation environment, necessitating an in-flight means of repoling. Several variations of TGS have been proposed which address one or both of these problems. The Table contains a listing of TGS and some of its derivatives. Included are parameters of importance in determining detector performance. In addition to TGS, several other good detector materials are included.

During the design definition study the following types of detectors were tested: irradiated TGS, deuterated TGS(DTGS), alanine doped TGS(αTGS), a combination of TGS and TGSe, SBN(50,50), and $PbTiO_3$. The parameters of interest were responsivity, noise, acceptance angle, and sensitivity to radiation damage. With the results information is also presented for representative TGS detectors on board ITPR in orbit.

Preliminary optical throughput calculations indicated that NEPs of less than $10^{-10} W/\sqrt{Hz}$ at no less than a 40 Hz chopping rate would be required. Further, the detector size had to be about 2.0 mm in diameter. The exact size depended a great deal on the useful acceptance angle of the detector. A design constraint limit of 35° from normal was set for the optical breadboard simply because there was little information available on the acceptance angle. Two channels in the ITPR had detectors with a maximum incidence angle of 28° and appeared to have a responsivity nearly as good as those that had a 14° maximum angle was about the best input available.

For the TOVS, TGS or its derivatives offer the advantage of being inherently absorbing over the entire spectral range of interest. A uniform construction technique consisting of a semi-transparent front electrode can be employed. Qualitatively, if the electrode is too opaque, most of the energy will be reflected; if the electrode is too tenuous, the detector series resistance becomes too high and introduces noise.

The active area for a detector can be determined by either the front or rear electrode. It is most convenient to use the rear electrode then the takeoff lead for the front electrode can be out of the active area.

GULTON INDUSTRIES, INC.
Data Systems Division
R. H. Maschhoff

Strontium Barium Niobate (SBN) has long attracted the interest of investigators in search of pyroelectric detector materials. Varying proportions of the first two elements can be considered but most of them spontaneously depole with time. A 50%/50% combination exhibits stable poling with a moderately large dielectric constant. However, loss tangents run unacceptably high on the order of 1 to 2%. The same objection holds for Lead Titanate $PbTiO_3$. This is only available as a ceramic because of the difficulty of growing large enough single crystals. Loss tangents are in the vicinity of 1%. Both materials do not provide intrinsic absorption at wavelengths below about 6 microns. This introduces the need for front surface absorbers which are difficult to make uniform and yet not degrade responsivity.

The possibility of immersing one of the higher dielectric constant materials in a germanium hemisphere was considered because of the factor of sixteen area reduction it offered. The techniques and improvements of immersion were demonstrated by Laser Precision Corp., but the needed performance for TOVS was still not realized. This was due to the high loss tangent of the SBN used in the experiment.

A detector fabricated of KT4000, a low dielectric constant material, was tested and found not to provide the needed performance either because of the low capacitance unit that resulted. A material with an intermediate value of dielectric constant and moderate loss tangent would appear to be the best candidate for immersion. Appendix -5- contains a report on the various findings uncovered during the immersion effort.

Material	Curie Temp °C	Dielectric Constant	Pyroelectric Coeff C cm^{-2} $^{o}K^{-1}$	Specific Heat J cm^{-3} $^{o}K^{-1}$	Loss Tangent	Source
TGS	49	40	3.5	2.5	5×10^{-4} to 5×10^{-3}	Various
DTGS	62.9	20	2.5	Est. 2.5	5×10^{-4} to 5×10^{-3}	Barnes/Mullard
α_1 TGS	50	25	3.7	2.5	10^{-3} to 5×10^{-3}	Mullard α_1 10% alanine in solution
α_2 TGS	51	20	3.9	2.5	10^{-3} to 10^{-2}	Mullard α_2 20% alanine in solution
Irradiated TGS	48	30	3.8	2.5	5×10^{-4} to 1×10^{-2}	Mullard & Barnes
SBN 50/50	115	380	6.5	2.1	.01 to .02	Barnes Rpt.
Lithium Tantalate	660	47	1.9	3.16	2×10^{-4}	Molectron
$PbTiO_3$	470	200	6.0	3.36	.01	Matsushita

GULTON INDUSTRIES, INC.
Data Systems Division
R. H. Maschhoff

BASIC DETECTOR PERFORMANCE CONSIDERATIONS

It is useful and perhaps necessary to review some fundamental considerations involving pyroelectric detectors and their use in systems.

If the detector is represented in terms of a voltage generator the responsivity (R_V) can be written as: $R_V = \frac{\Omega}{\omega \; ShC}$

where

ω	=	$2 \pi f$	f	=	Chopping Frequency
Ω	=	Pyroelectric Coefficient	-		Coulombs/^{o}Kcm^2
S	=	Specific Heat	-		Joules/^{o}Kcm^3
h	=	Element Thickness	-		cm
C	=	Capacitance	-		$\frac{\varepsilon\varepsilon' A}{h}$

As long as the element absorbs all the energy responsivity is independent of thickness because the capacitance term has thickness in its denominator. Inserting values for TGS yields a theoreticl responsivity of 800V/w at 25Hz for the ITPR detector size of .0256cm^2. Measured values of 650 to 700 V/w indicate reasonable agreement. Direct ratioing to 40Hz yields a first cut responsivity of 420V/w for this size detector.

Before discussing electrical or circuit type noise a review of some basic thermal performance limitations is in order. Before an uncooled detector can be considered, the radiative exchange noise must not be exceeded. We are approximately an order of magnitude away from the intrinsic radiative noise limit of a 300°K element of the size of interest as seen below.

$$NEP = (4KT^2 \, G_{TR})^{1/2}$$

$$NEP = 4 \, T^2 (K \, A_d \, \sigma T)^{1/2}$$

$$NEP = 6.9 \times 10^{-12} \, W/\sqrt{Hz}$$

$G_{TR} = 4 \, A_d \, \sigma T^3 \varepsilon$

σ = Stefan-Boltzmann Constant

$= 5.67 \times 10^{-12} \, W/cm^2 T^4$

$A_d = 1.76 \, mm^2$ for d = 1.5 mm

ε = emissivity

K = Boltzmann's Constant

Thermal conduction noise likewise is not limiting if reasonable thermal isolation of the element is retained after mounting. In practice, if the detector thermal time constant is on the order of 100 msec or longer, conduction noise is not a limiation.

$$NEP = (4 \, KT^2 G_{TC})^{1/2}$$

G_{TC} = Thermal Conductance

We can estimate G_{TC} from knowledge of the thermal time constant.

$$G_{TC} = \frac{H}{T} = \frac{SA_d h}{T}$$

$$NEP = \left(\frac{4\ KT^2 S\ A\ h}{T_{TH}}\right)^{1/2}$$

S = Specific Heat
= 1.5 J/°K cm^3
h = Detector thickness
= 10 to 50 μm

NEP = 3.62×10^{-11} W/$\sqrt{Hz}$ for 10 μm elements.

The remaining detector noises are frequency dependent and are perhaps easiest to grasp if first expressed in terms of a voltage noise. Then using the expression $NEP = \frac{\tilde{e}_n}{R_V}$ we can relate them to the necessary noise level. A finite de conductance across the element electrodes yields the following noise:

$$\tilde{e}_n = \sqrt{\frac{4KT\ G}{\omega^2 C^2}}$$

C = 25pf 40 μm thick
100pf 100 μm thick

Typically it is possible to attain a conductance of 10^{-12} mho for the size element in question. This yields a noise of 21 nv/$\sqrt{Hz}$ at 40 Hz for the 1.8mm dia detector 40 μm thick or 5.25 nv/$\sqrt{Hz}$ for a 10 μm thick element of the same area. These correspond to NEPs of 5×10^{-11} W/$\sqrt{Hz}$ and 1.25×10^{-11} W/$\sqrt{Hz}$ respectively.

Loss tangent noise typically includes dielectric losses and series resistance in the electrodes. For TGS reported values range from $\tan\delta = 5 \times 10^{-3}$ to 5×10^{-4}. Voltage noise due to it is:

$$\tilde{e}_n = \sqrt{\frac{4KT \tan\delta}{\omega C}}$$

C = 25 pf 40 μm
100 pf 10 μm

This yields a noise of 115nV/$\sqrt{Hz}$ for a 40 μm thick element and 57 nV/$\sqrt{Hz}$ for a 10μm thick element 1.8 mm dia if $\tan\delta = 5 \times 10^{-3}$. Corresponding NEPs are 2.73×10^{-10} W/$\sqrt{Hz}$ and 1.37×10^{-10} W/$\sqrt{Hz}$. For the lower loss tangent these results would be divided by a factor of 3.16.

Quite clearly a thin detector offers the best performance. The only proviso is that it must be thick enough to absorb the energy. Subsequent test data will show that this is the case even for 10 μm elements.

Attainment of an NEP of 10^{-10} W/$\sqrt{Hz}$ with responsivities between 500V/W and 800 V/W requires a total input equivalent noise of 80 nV/$\sqrt{Hz}$ or less. Since noises add quadratically there is a reasonable allowance available for amplifier noise.

THE PRE-AMPLIFIER

In a properly designed circuit the amplifier may use either voltage or current feedback or none without changing the S/N ratio. The detector responsivity temperature coefficient is lowest in the voltage mode of operation.

Secondary considerations such as stability and microphonic properties tend to dictate the exact configuration. The ITPR preamplifier used voltage feedback at high frequencies and current feedback at dc. This combines several desirable features including driving the dc potential of the detectors active terminal to within a few millivolts of ground. This yields good microphonic performance as well as rapid recovery from overload. See Figure.

The key to good S/N performance depends on concurrent low voltage and low current noise in the input stage. Junction Fets as of this writing are the only acceptable devices to fill this need. Most existing systems employing pyroelectrics are amplifier noise limited because very low noise Fets are just becoming available.

It was essential then to establish the availability of suitable Fets if the TOVS objectives were to be met. In general, one has the choice of either low voltage noise or low current noise from the standard offerings of manufacturers. These correspond to large geometry and small geometry devices respectively. Intermediate geometry devices have been found to yield satisfactory compromises; usually some selection is required for one or both noise parameters.

The Table presents a summary of Fets tested; and the final results of importance. More complete data is found in the analog channel report. An adequate selection of Fets is available.

Retaining the voltage equivalent representation started earlier, the voltage noise is defined as that obtained with a short circuited input. It is written directly as $\tilde{e}_n$. Generally $\tilde{e}_n$ is flat with frequency above 50 Hz for a large range; below this it exhibits a usually serious 1/f characteristic and is in reality one big reason for a chopped system. Current noise is found by inserting an impedance Z_s in series with the input noting the increased noise and performing a quadratic subtraction. $\tilde{i}_n = \frac{\text{e difference}}{Z_s}$. Having found the current noise its effect with a detector in place yields a voltage noise

$$\tilde{e}_n = \frac{\tilde{i}_n}{\omega C}$$

Once again a thin detector shows an advantage as seen when a typical current noise of 5×10^{-16} A/ $\sqrt{\text{Hz}}$ is applied.

$$\tilde{e}_n = 79.5\text{nv}/\sqrt{\text{Hz}} \quad \text{40 μm thick x 1.8 mm dia @ 40 Hz}$$

$$= 20 \ \text{nv}/\sqrt{\text{Hz}} \quad \text{10 μm thick x 1.8 mm dia @ 40 Hz}$$

Corresponding NEPs are 1.9×10^{-10} and 4.75×10^{-11} W/$\sqrt{\text{Hz}}$

Voltage noises of 20 to 25 $nV/\sqrt{Hz}$ are readily available especially if current noise is not so critical as with thin detectors. It can be observed that the input capacitance of the amplifier was not allowed for in determining R_V. It turns out that first order, NEPs are not effected because noise as well as R_V go down with extra circuit capacitance.

A bias resistor is needed for operating point stability or for a path for Fet leakage currents. Resistors of 5 x 10" ohm or greater offer no noise problem.

In order to realize the noise performance possible with the above Fets, several other potential problems must be avoided. Noise on the power supply line must be well controlled. The optimum method of supplying pre-amp power requires further detailed engineering.

Microphonic noise of at least two types can occur. One due to relative motion of the detector signal lead with respect to the case can be avoided or greatly reduced by arranging that this lead is near dc ground potential. Using current mode amplification is one way of accomplishing this. The other source of microphonics arises in the crystal itself. All pyroelectric materials are piezoelectric which demands the maximum isolation possible for the detector element. Suppliers of detectors have developed mounting techniques which control microphonics quite well. Any design which demands a new mounting technique would be inviting disaster unless adequate time for testing its microphonic characteristics is available.

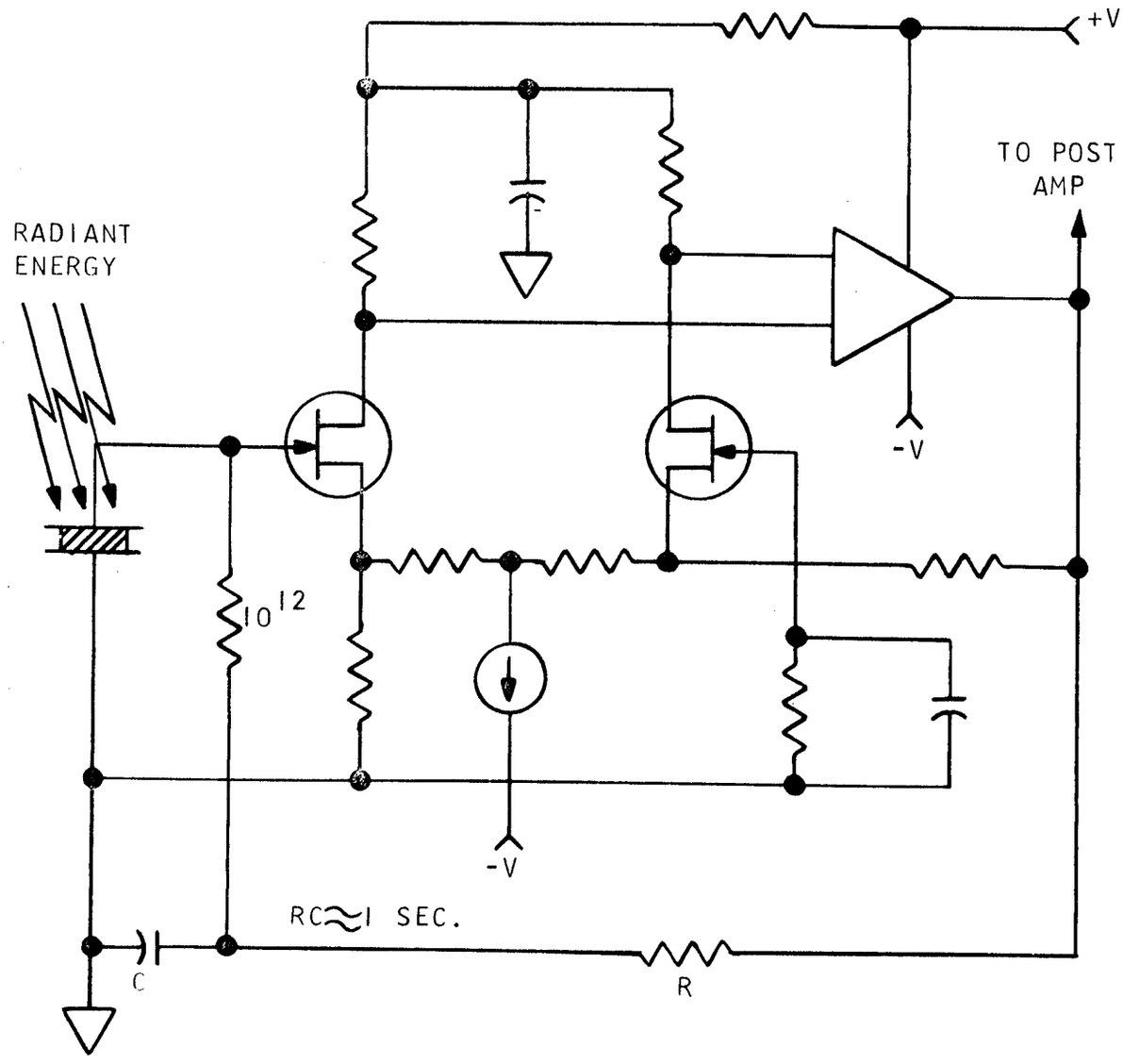

DETECTOR/PRE-AMPLIFIER

13961-840

FET Designation	$nV/\sqrt{Hz}$ Total Noise in Pre-amp With A 30pf Cap. Simulating Detector			Removing Noise of a 2×10^{11} Load Resistor		Derived* Current Noise
	20Hz	40Hz	80Hz	40Hz	80Hz	$\times 10^{-16}$ $A/\sqrt{Hz}$
2N5199-1	94	52	32	46	29	4.67
2N5199-2	174	65	43	60	41	5.74
2N5199-3	280	104	44	101	42	12.0
2N5199-4	103	52	25	45.6	21.6	5.26
2N5199-5	122	55	29	49	26	5.44
2N5454-1	165	68	39	63	37	6.68
DN1154-2	90	42.5	28	34	25	3.02
DN1154-3	94	42	24	38	20	4.23
DN1154-4	103	52	36.5	46	34	4.06
2N5521-1	112	52	26	46	22.8	5.24
2N5521-3	85	50	28	43	25	4.58
AD841-1	106	62	36.5	57	34	5.99
AD841-2	108	50	36.5	43	34	3.45

$$* \quad \tilde{i}n = \frac{1}{C}\sqrt{\frac{e_{40}^{2}-e_{80}^{2}}{(2\pi 40)^{2}-(2\pi 80)^{2}}}$$

THE DETECTOR/PRE-AMPLIFIER NOISE EQUIVALENT CIRCUIT

A noise equivalent circuit is a convenient tool which can be used to gain full benefit from the test results presented later. The figure depicts the two forms of a noise equivalent circuit for the detector plus the pre-amplifier.

The first thing that should be noticed is that the voltage response varies inversely with frequency and the current response is independent of frequency. If this fact is ignored it is easy to lose the proper perspective in regard to signal-to-noise ratio. Although most references in this report are in terms of the voltage equivalent noise it is useful to include the current representation as well.

The most significant result of the testing and evaluation program is that intrinsic detector noise in form of the loss tangent is the performance limiting factor for this application.

The limiting factor in the ITPR situation was amplifier or Fet current noise. The combination of a higher chopping frequency, thinner elements and better Fets is responsible for the change.

In view of this it is instructive to examine the loss tangent effect to make sure we have made a proper choice of amplification type. When the signal-to-noise ratio is formed for the two cases it is seen that the result is identical.

$$S/N = \frac{I_s}{\sqrt{4KT \text{ Tan } \delta\omega C_d}}$$

Inspection of some of the other noise sources reveals similar results. Only when a particular frequency situation, combined with a particular geometry and available Fets might one approach emerge better than the other.

Selection of the voltage mode for TOVS as was done for ITPR is justified because of the lower temperature coefficient of the voltage responsivity. This minimizes the detector temperature control requirements but does not eliminate them.

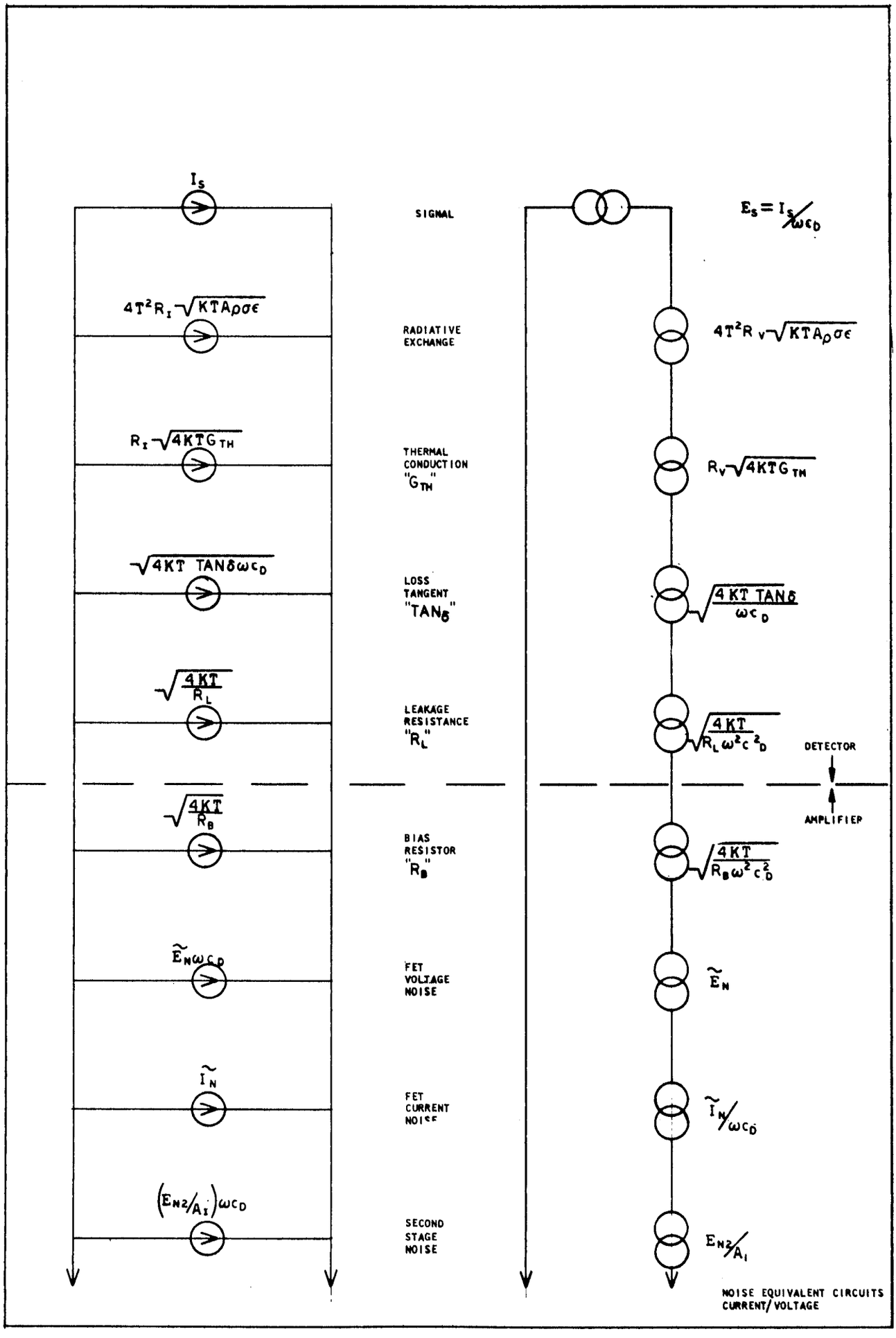

NOISE EQUIVALENT CIRCUITS
CURRENT/VOLTAGE

DETECTOR/PRE-AMPLIFIER TEST RESULTS

At the outset of the testing program a decision was made to do the critical testing of detectors and amplifiers were mated.

Fets of known quality were incorporated into a package also containing the detector element and the large bias resistor. The impetus for this came from difficulties encountered in trying to evaluate bare element detectors under the ITPR program. The difficulties of controlling microphonics and extraneous pickup when the high impedance leads needed to be routed through connectors are serious. In addition, this facilitated more realistic radiation testing because of the close similarity to final packaging techniques.

One of the rules of the testing program (easily enforced with the above packaging approach) was that responsivity and noise were to be measured with the same amplifier. The resultant measured NEPS have virtually no uncertainty about them arising from amplifier gain uncertainties.

Measurements were made of the input characteristics of the type of pre-amplifier circuit employed on the ITPR. Because of the high loop gain of the circuit (provided by the operational amplifier) there should be virtually no Miller multiplication of the drain gate capacitance of the input Fet. Using a 2N5197 for the input Fet a simple test consisted of injecting a small signal from a low impedance source on the ground side of a 17 pf capacitor simulating the detector. The amplifier output was noted and then also noted when the capacitor was shorted. The ratio of the output voltages resulted from an amplifier input capacitance of 15 pf. Several signals at frequencies between 10 Hz and 200 Hz were used to verify that the impedance was indeed capacitive in nature.

In addition to Responsivity and Noise tests, the response as a function of incident angle was determined. The detector viewed an extended source through a small aperture. By rotating the detector case about an axis passing through the element, a cosine response is the ideal result. The detailed results are presented in the detector report. No significant departure from the cosine response was noted. In each case the response at small angles from the normal were greater than at normal incidence. As far as the detector response is concerned, incident angles up to 45° offer no problem. A compromise however must be made in setting the peak of the anti-reflection coating response; the optimum point would be at the controid of the ray angle over an annular field. Alternately the window could be a dome of appropriate radius and then anti-reflection coated for optimum throughput.

The results in regard to NEP are shown in the Table; they require some discussion. Only detectors 4 and 5 provide acceptable performance for the TOVS. They were very thin detectors of α alanine TGS employing a Mullard developed mounting method. Detectors 1 through 3 were electroded and mounted in a manner virtually identical to the ITPR detectors, which were of pure TGS, epoxy sealing rather than solder was used. Sealing the capsule with epoxy was agreed on to expedite delivery and might have been a mistake. Another difference from ITPR was that poling was accomplished by radiation except in the case of the deuterated element. Inspection of the data sheets supplied with the low performance units revealed measured loss tangents between 0.7 and 1.0%. This indicated possible incomplete poling. The irradiation induced poling was annealed out of two units and were then subsequently repoled. The responsivity went up between 5 and 10% confirming suspicions. However, the noise did not go down indicating permanent damage. The manufacturer agreed that the damage was likely permanent and fresh start would be needed to obtain data on non-irradiated material.

Detector Identification	Element Size	Fet Type	Operating Temp.	NEP at 40 Hz w/ $\sqrt{Hz}$	NEP at 90 Hz w/ $\sqrt{Hz}$
Irradiated TGS #1	1.5 mm dia. x 40 μm	2N5199	25°	2.3×10^{-10}	3.3×10^{-10}
Irradiated TGS #1	1.5 mm dia. x 40 μm	2N5199	35°C	2.2×10^{-10}	-
Irradiated TGS/TGSe #2	1.5 mm dia. x 40 μm	DN1154	25°C	1.6×10^{-10}	2.04×10^{-10}
Irradiated TGS/TGSe #2	1.5 mm dia. x 40 μm	DN1154	35°C	2.0×10^{-10}	3.0×10^{-10}
DTGS #3	1.5 mm dia. x 40 μm	DN1154	25°C	2.3×10^{-10}	3.7×10^{-10}
α TGS #1 #4	1.5 x 1.5 mm x 10 μm	11006B	25°C	9.4×10^{-11}	1.4×10^{-10}
α TGS #1 #4	1.5 x 1.5 mm x 10 μm	11006B	35°C	8.4×10^{-11}	-
α TGS #5	1.5 x 1.5 mm x 10 μm	11006B	25°C	1.30×10^{-10}	2.0×10^{-10}
Immersed* KT4000	.7 mm x .7mm** (2.8 mm x 2.8 mm effective)	DN1154	25°C	2.0×10^{-10}	-
ITPR TGS	2.56 mm x 50 μm	FN2081	37°C	2.0×10^{-10} @ 25Hz	-
Lead Titanate	1.0 mm dia		25°C	6×10^{-10}	1×10^{-9}
SBN 50/50	2.02 mm^2 x 100 μm		25°C	4.8×10^{-10}	

* See Appendix on Immersion Studies for more detail
** Approximate area needed for TOVS

DETECTOR/PRE-AMPLIFIER TEST RESULTS - CONTINUED

Examining the shape of the NEP vs. frequency curve for a thick detector and a thin detector as shown in the figure is revealing. From a normalization point at 40 Hz curves depicting $1/\sqrt{f}$ behavior are constructed. Over a large portion of the frequency range the noise follows the $1/\sqrt{f}$ curve. Recalling the noise equivalent circuit, we find only one element which produces this behavior; namely, the loss tangent. Since we do not have a measure of the loss tangent for the mounted element, it must be obtained indirectly. We subtract the noises contributed by known sources and make a trial assignment of the remainder to loss tangent. Solving the equation

$$e_n^2 = \frac{4KT \tan \delta}{\omega C}$$

for tan δ yields 3×10^{-3} and 8×10^{-3} for the 10 μm and 40 μm thick elements, respectively. The thin element offers the best performance; this is of course not a new result but verifies what has been predicted by many expositors on pyroelectric detectors. The thin detector has of course also reduced contributions from current noise because of its increased capacitance. Also consistent is the derived loss tangent for the thick units with direct measurements of this parameter made by the manufacturer. The difference in loss tangent does not derive from differences in thickness but in the materials treatment. The detector evaluation has shown that at least one modification of TGS, that of α alanine doping, provides the necessary performance for the TOVS. Significantly this material represents the company's standard product and can be expected to be reproducible. Detectors of pure TGS as used on the ITPR were not retested specifically under this program. Analysis of the performance of these detectors in the completed ITPR shows that by decreasing the thickness from 50 μm to 25 μm will also yield useable detectors for the TOVS. The TOVS is not limited then to either one detector supplier or material.

This testing program as well as results from the ITPR program showed that there is a small improvement i.e. 10% in NEP when going from 25°C to 35°C. Within limits then the detector mounting plate temperature can be allowed to be set by thermal constraints.

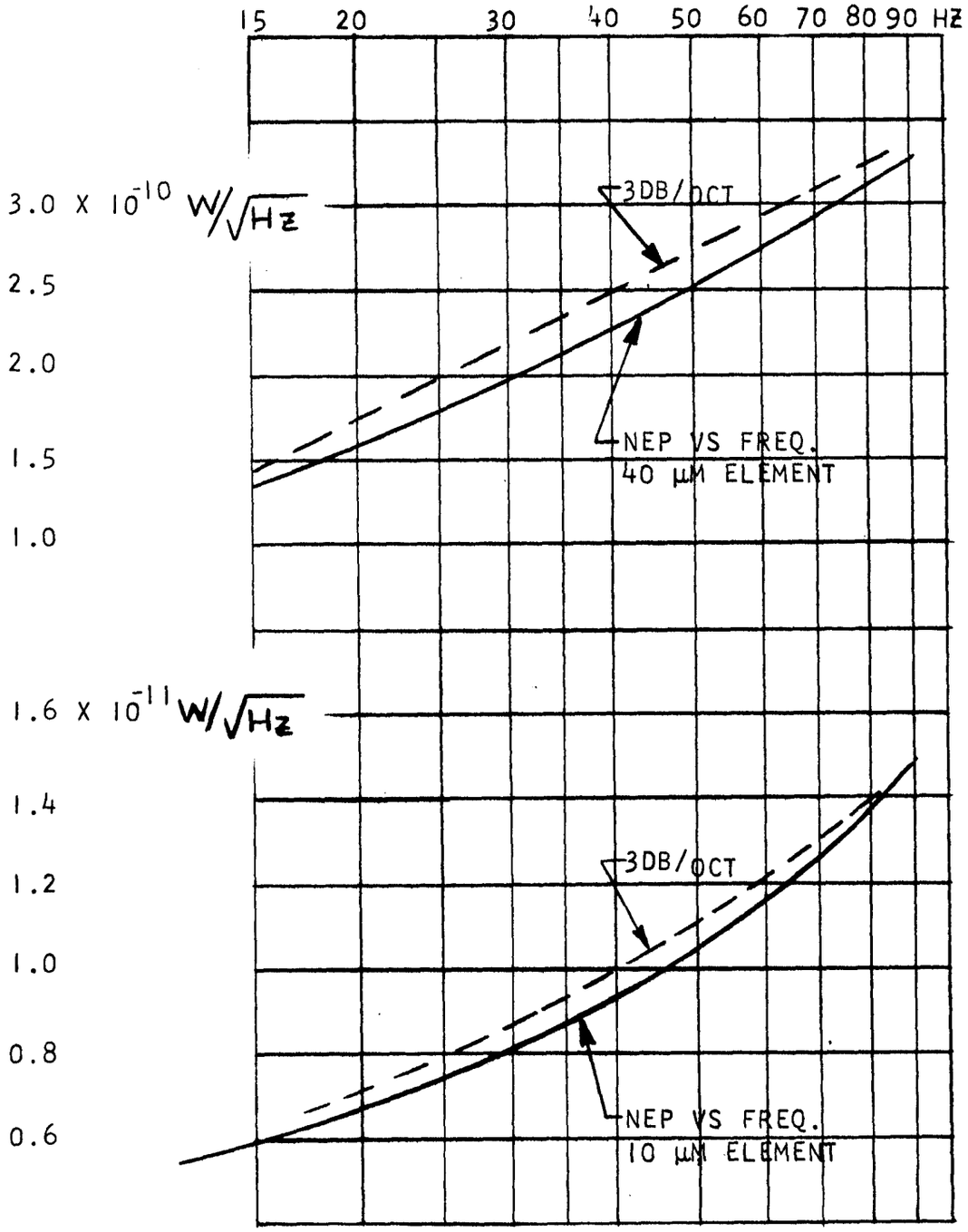
15
20
30
40
50
60
70
80
90
HZ
3.0 X 10^-10 W/√HZ
2.5
2.0
1.5
1.0
3DB/OCT
NEP VS FREQ.
40 μM ELEMENT
1.6 X 10^-11 W/√HZ
1.4
1.2
1.0
0.8
0.6
3DB/OCT
NEP VS FREQ.
10 μM ELEMENT

ITPR DETECTOR PERFORMANCE

An analysis based upon ITPR NEN performance follows.

An almost direct carry over of results is possible here because geometrical requirements for TOV's detectors are almost identical to ITPR units. The larger of the two TOVs telescopes requires a detector with an O.D. of 2 mm (the ITPR size), the center 17% of area being desensitized. This size is consistent with an aft optics f/no. of 0.7. Changing the f/no. to say 0.6 would reduce the diameter to 1.7 mm.

Final system performance data for Channel 1 (the 3.8 μ channel) showed NEN's of 0.0035 and 0.0030 $mw/m^2\text{-}sr\text{-}cm^{-1}$ for the prototype and flight units, respectively. This performance has been verified for the prototype unit now in orbit. Several other channels exhibited equivalent performance but is not evident in the data because of quantizing limitations.

Using the relationship

$$NEN = \frac{NEP\ (\Delta f)^{1/2}}{\pi A_{fs}(NA)^2 T_1 T_2 \Delta\nu}$$

where

Δf = system noise bandwidth = 2.05Hz

A_{fs} = area of field stop = 16.6 mm^2

NA = numerical aperture = 0.129

T_1 = transmission of optics = 47%

T_2 = chopping factor = 0.5

$\Delta\nu$ = 415 cm^{-1}

yields a detector NEP of 2.0×10^{-10} $W/\sqrt{Hz}$ at the attendent chopping frequency of 25 Hz and operating temperature of 35°. The average responsivity of the detectors used on ITPR was 700 V/ω which yields a total input equivalent noise of 140 $nv/\sqrt{Hz}$.

The following easily demonstrated sources of noise can now be removed from the above noise.

FET voltage noise = $2 \times 25\ nv/\sqrt{Hz} = 35\ nv/\sqrt{Hz}$

(Both FET's in preamp contribute voltage noise.)

FET current noise effect = $i_n/\omega C$ C = 45 pf

$= 2eI_G = 113\ nv/\sqrt{Hz}$

e = electron charge I_G = 2 pa (average for ITPR FET's @35°C)

The load resistor of 2×10^{11} ohms contributes 40 nv/$\sqrt{\text{Hz}}$ of noise at 25 Hz. There are some additional small sources of noise such as second-stage noise which we will neglect because we want to establish an upper limit of the loss tangent induced noise. Quadratic subtraction of these known noises from the total noise leaves 63 nv/$\sqrt{\text{Hz}}$ for the worst possible loss tangent noise. Using the expression developed earlier for this noise

$$e_n = \sqrt{\frac{4\ KT \tan \delta}{\omega C}}$$

where

$T = 308^{\circ}K$

$K = 1.38 \times 10^{-23}$

$\omega = 2\ \pi\ 25$

$C = 45$ pf

We find that $\tan \delta$ becomes 1.65×10^{-3}. This compares to currently reported loss tangents between 2 and 3×10^{-3} by Barnes Engineering, as well as others. The difference is credited to the biasing arrangement of the pre-amplifier which removes all but a few millivolts of dc voltage across the detector.

DETECTOR PERFORMANCE VS. SIZE

We are now in a position to generate information which will make it possible to do trade-off studies involving detector size and NEP.

This is necessary to provide inputs for final design interactions relating instrument size and NEN's. Figure A shows a curve of NEP vs. detector size for detectors of the Mullard construction. Only when the size goes below 1 mm in diameter do sources of noise other than loss tangent become limiting. Figure B shows a curve for pure TGS detectors such as used on ITPR except that the thickness has been decreased to 25 μm. In addition, the performance of FET's with the following specifications are included.

$V_{DS} = 6$ V $\quad I_D = 100$ μa

$I_{GS} = 0.3$ pa

$BV_{GSS} = 50$ V

$V_{GS(off)} = 1.5$ V

$I_{DSS} = 150$ μa

$Y_{fs} = 200$ μmho

e_n 10 Hz $= 25$ nv $Hz^{-1/2}$

e_n 100 kHz $= 12$ nv $Hz^{-1/2}$

We use an operating point of 35°C for this development. Starting with ITPR detector size, a 2 mm diameter annular detector with an area of 0.0256 cm^2 which had an average responsivity of 700 V/W at 25 Hz. In the voltage mode responsivity is invariant with thickness but varies directly with frequency.

We can then state a responsivity of 437.5 V/W at 40 Hz. This is very conservative because the amplifier relative capacitance loading is less for thin detectors. At 35°C pure TGS has a relative dielectric constant of 75. This yields a detector capacitance of 67.5 pf and a total circuit capacitance of 77.5 pf. Using the above FET as the input stage yields an amplifier with about 10 pf of input capacitance. The loss tangent available for pure TGS is conservatively 2×10^{-3} (ITPR was 1.65×10^{-3}).

We write the following noise voltages

loss tan noise	-	42 nv $Hz^{-1/2}$
voltage noise	-	25 nv $Hz^{-1/2}$
current noise	-	23 nv $Hz^{-1/2}$
load resistor	-	10 nv $Hz^{-1/2}$
rms total		55 nv $Hz^{-1/2}$

$$NEP = \frac{\tilde{e}_n}{R_v} = 1.25 \times 10^{-10} W/Hz^{-1/2}$$

For use in subsequent NEN calculations the detector NEPs used were 1.2×10^{-10} W/$\sqrt{Hz}$ for 2 mm OD detectors and 9×10^{-11} W/$\sqrt{Hz}$ for 1.5 mm OD detectors. This corresponds to that needed for 80 mm and 61 mm dia telescopes and f .7 aft optics. Note this includes a safety factor of about 25% over the best 10 μm unit tested. A good yield of useable devices can be expected. The NEP is not expected to degrade for f numbers down to 0.5.

An overview of the pyroelectric detector situation at this point reveals that the performance exists to meet the previously estimated TOVS requirements. The prediction, based on first principle considerations, that thin detectors work better than thick detectors was verified explicitly. The data also shows that the various modifications of TGS are not much better than pure TGS as far as sensitivity is concerned. Although bulk material properties of the modified versions of TGS look very good, these same properties are not always retained when fabricated into actual elements. They do, of course, have other advantages such as immunity to depoling and higher operating temperatures. Several non-TGS materials were found to be good detectors, in particular $PbTiO_3$ and SBN 50/50, but not good enough for application to the TOVS. Their ruggedness and high temperature capabilities recommend them for more severe environments.

This program also addressed itself to obtaining better information as to the space radiation susceptibility of detectors which might be flown on the TOVS. The question of total dose survival had basically been answered during ITPR testing (for TGS detectors), but the magnitude of induced noise was really an open question. Tests designed to simulate the noise situation showed that only nominal increases could be expected. This was greatly reinforced by data from ITPR and VTPR in orbit showing similar results. What the simulated tests showed was that thin detectors are less susceptible than thick detectors.

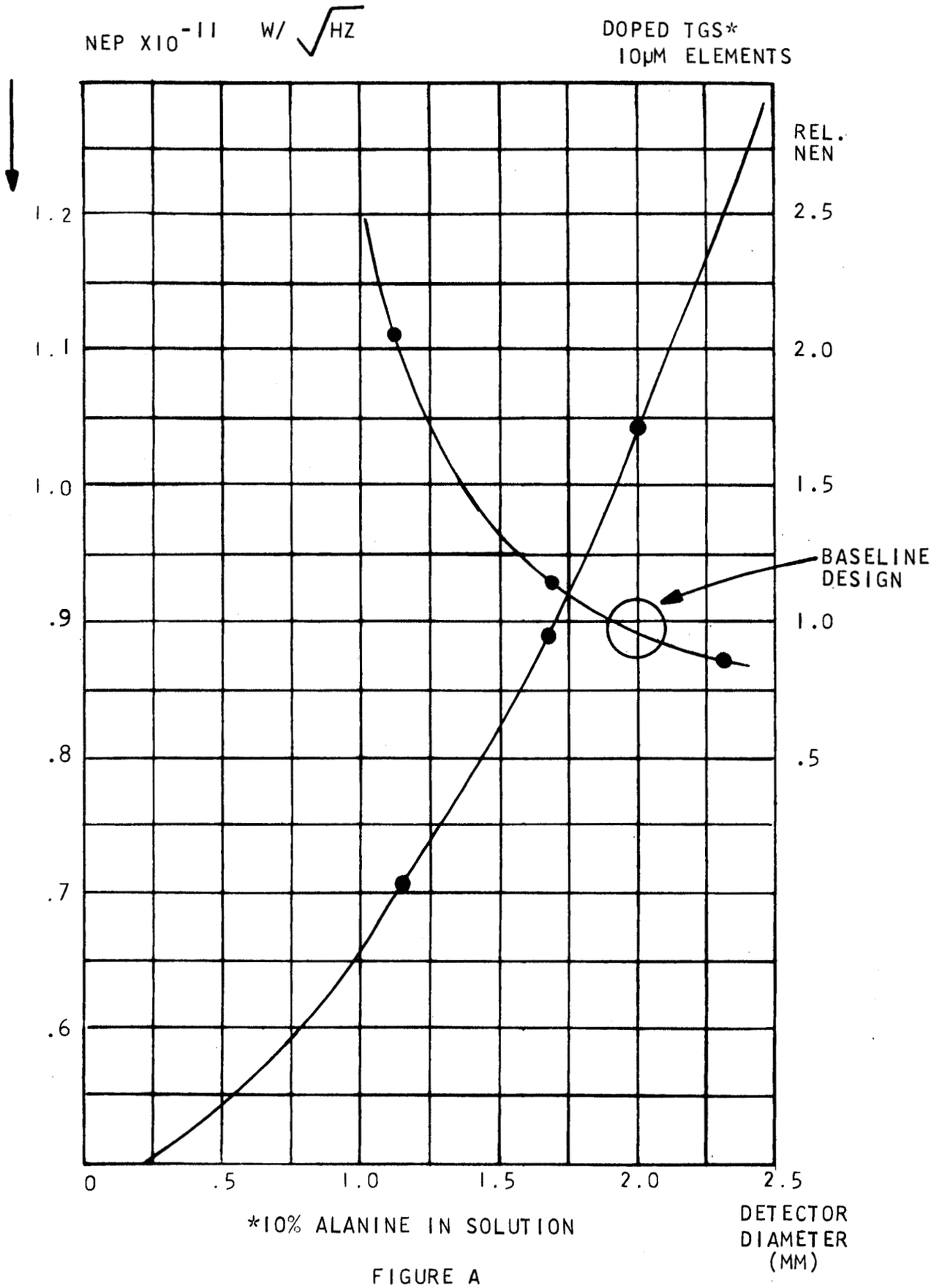

*10% ALANINE IN SOLUTION

FIGURE A

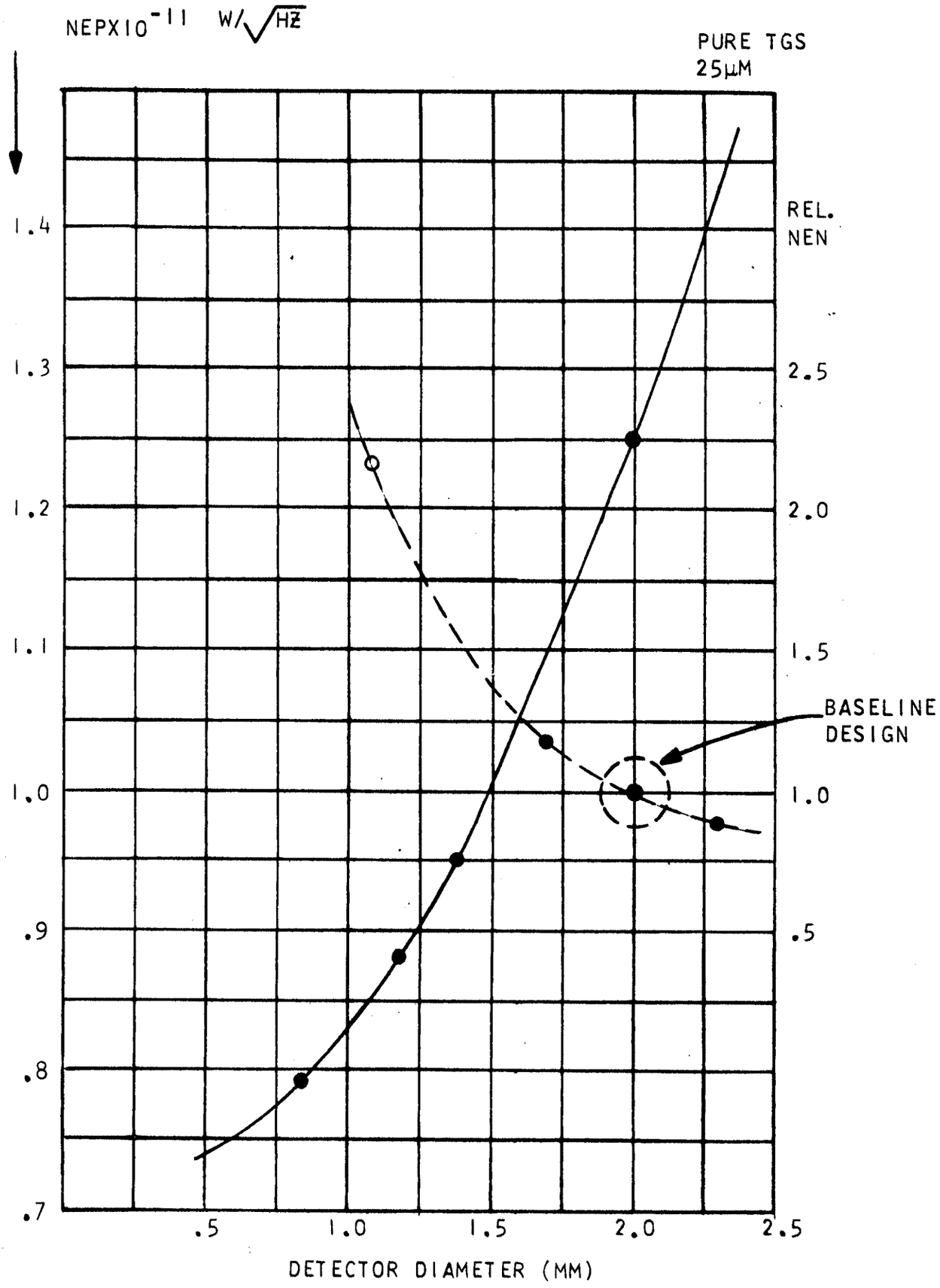
NEPX10^{-11} W/$\sqrt{HZ}$
PURE TGS
25μM
REL.
NEN
1.4
1.3
1.2
1.1
1.0
.9
.8
.7
2.5
2.0
1.5
1.0
.5
BASELINE
DESIGN
.5
1.0
1.5
2.0
2.5
DETECTOR DIAMETER (MM)

FIGURE B

POST AMPLIFICATION

The post amplifier has the important function of shaping the frequency passband which, when properly designed, controls scene-to-scene crosstalk.

A thorough analysis of this is developed in the Analog Channel Report and Math Model Appendix. Because of the 1/f noise characteristics of useable amplifiers a chopping system must be employed. Practically, since it is difficult to provide a stable detector dc response, optical chopping is very appropriate. There are, of course, radiometric advantages to optical chopping as well. Now, if one assumes varying scene-to-scene irradiances, it is seen the detector is exposed to radiation having frequency components arising from changing scenes as well as chopping. Chopping-induced and scene-induced frequencies must be separated or large errors can arize in subsequent demodulation. The post amplifier is a convenient place to suppress the scene-to-scene frequency components; gain is almost a byproduct.

The facing page indicates some approximate waveforms which on first considerations would appear to yield error free results. What they in fact represent is a detector amplifier system which has a flat response. Two situations must be discussed in view of at least two detector possibilities.

The detectors fabricated by Mullard Ltd. have thermal time constants of approximately 100msec. This relatively short time constant is due to a fairly tight thermal bond with a massive mounting header. It is almost in variant with pressure or type of gas in the capsule. An amplifier zero located so as to cancel the thermal pole is a reasonable solution in this case. It must be done carefully because any lack of flatness in the response around the maximum scene induced frequencies will result in scene-to-scene crosstalk.

Detectors of the ITPR construction had thermal time constants on the order of 2 seconds. Moreover, there was considerable unit to unit variation, making cancellation of the detector thermal time constant with an amplifier zero an individual adjustment proposition for each channel. Further, the long time constant is not stable with changes in the state of vacuum in the capsule. To avoid this problem in the ITPR program the amplifier passband was not designed to have a flat response but rather the low frequencies (below the chopping frequency) were suppressed with an extra amplifier high pass coupling. This, when coupled with an appropriate selection of integrator start times eliminated the problem. The prime purpose of developing the math model (see appendix 3) is to optimize the amplifier passband to achieve a similar result with the TOVS.

The demodulator output for the alternating scene case is symmetrical about zero. This is a very special case statistically not likely to happen; a random scene sequence will result in wandering dc levels which are acceptable as long as the subsequent demodulation is full wave. Since the detectors do not have a dc response the dc level will never get out of control for any immaginable sequence of scenes.

One can consider a chopping arrangement where there is in effect one chop per each scene (a 5 Hz chop rate in this case). Corrections for the lack of dc response could be made by clamping the signal during the blocked beam period. The question of what is the correct level to clamp to immediately arises (1) because there is noise on the detector output, and (2) the lack of high frequency response in the detector distorts the waveform so that the reference plateau cannot be accurately identified. Only by individual optimization and adjustment of each detector and its pre-amplifier can this be made to work. This is not consistent with an easy reproducibility. Far worse is the sensitivity of such fine tuning to component drift and change with time and radiation in space.

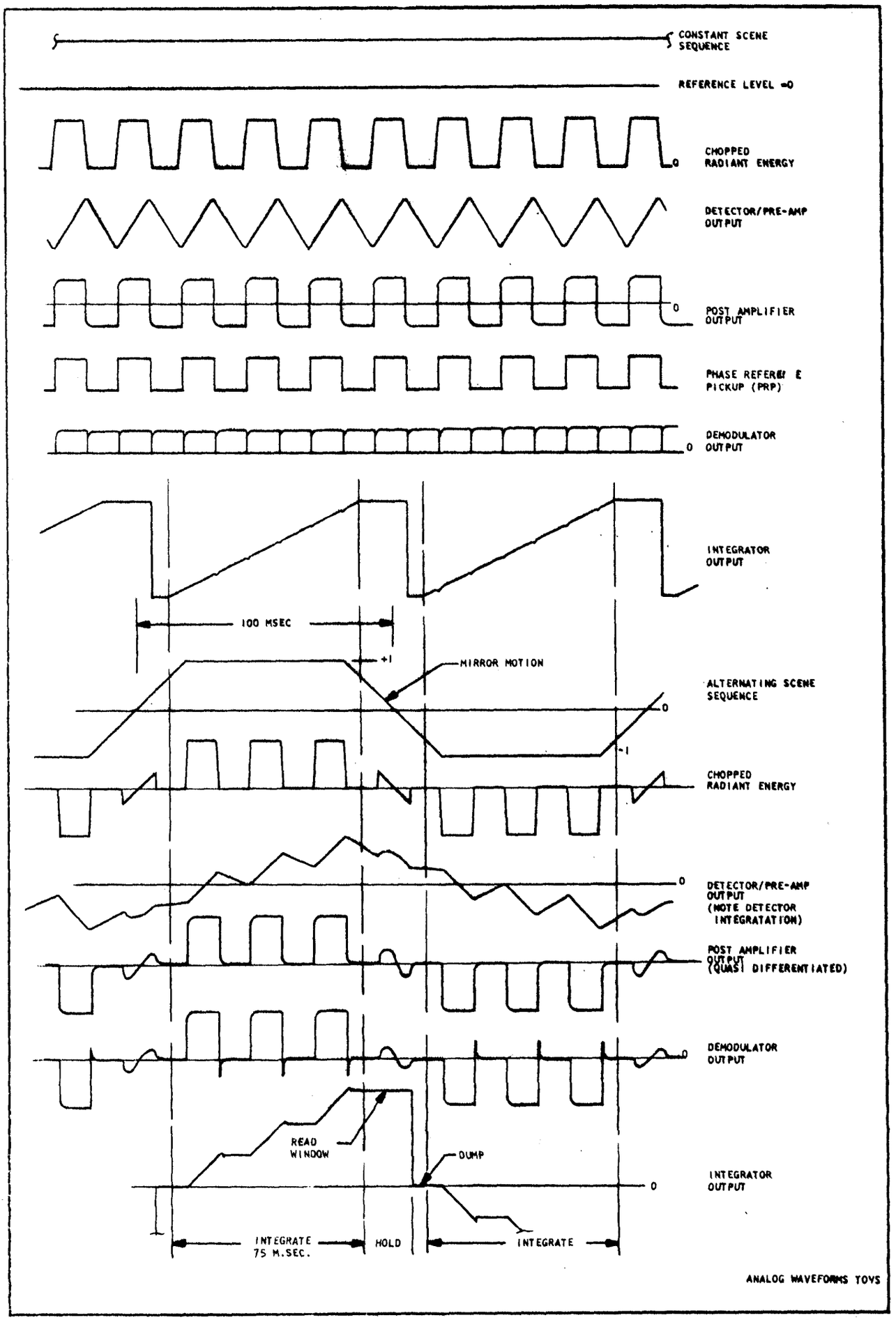
CONSTANT SCENE SEQUENCE
REFERENCE LEVEL =0
CHOPPED RADIANT ENERGY
DETECTOR/PRE-AMP OUTPUT
POST AMPLIFIER OUTPUT
PHASE REFERENCE PICKUP (PRP)
DEMODULATOR OUTPUT
INTEGRATOR OUTPUT
100 MSEC
+1
MIRROR MOTION
ALTERNATING SCENE SEQUENCE
-1
CHOPPED RADIANT ENERGY
DETECTOR/PRE-AMP OUTPUT (NOTE DETECTOR INTEGRATATION)
POST AMPLIFIER OUTPUT (QUASI DIFFERENTIATED)
DEMODULATOR OUTPUT
READ WINDOW
DUMP
INTEGRATOR OUTPUT
INTEGRATE 75 M.SEC.
HOLD
INTEGRATE
ANALOG WAVEFORMS TOYS

13961-830

DEMODULATION AND INTEGRATION

In order to realize the low scene-to-scene memory effect presented in the previous section, full-wave demodulation and integration is required.

The reference for demodulation is obtained from an auxiliary optical phase reference pickup located on the chopper wheel.

Because of the relatively small number of chops per scene (i.e., 4 chops at 40 Hz), the chopper drive and therefore the resultant PRP must be phase locked to the scan drive timing. This can be accomplished within an acceptable tolerance of $\pm$ 5.0° by totally digital means and is discussed in the control section.

The full-wave demodulator consists of a phase splitter and a FET switche per phase in which the switches are driven by the PRP and $\overline{\text{PRP}}$ signals, respectively. The most important requirement of the phase splitter is that the inverted signal not have an offset relative to the non-inverted signal. If this dc symmetry is not maintained, then any residue of the slow scene induced component that appears at the post amplifier output will produce errors in the output. A review of the mathematical operation performed by the demodulator will quickly reveal this. Lack of symmetry appears as an admixture of full-wave and half-wave demodulation; the results are quite apparent.

Fourier Series Representations:

$$\text{Signal } (e_s) = \frac{a_o}{2} + \sum_{n=1,3,5,7,\cdots} (a_n \cos n\,\omega t + b_n \sin n\,\omega t)$$

$$\text{PRP}(e_{ref}) = \sum_{n=1,3,5,7,\cdots} b_n' \sin n\,\omega t \qquad \text{(Full Wave)}$$

$$= \frac{A}{2} + \sum b_n' \sin n\,\omega t \qquad \text{(Half Wave)}$$

Forming the products on a term by term basis reveals the terms which contribute to the desired output are of the form $b_n b_n' \sin^2 n\omega t$.

This can be rewritten as: $\dfrac{b_n b_n'(1-\cos 2n\omega t)}{2}$. All other products yield purely ac terms which are subsequently smoothed. The exception is when the $\frac{A}{2}$ term is not zero; then there is the obvious product of $(\frac{a_o}{2})$ K $(\frac{A}{2})$ where K denotes the strength of the half-wave contamination. Pure full wave demodulation is needed.

It is assumed throughout that the PRP is perfectly symmetrical which, of course, will never be exactly true. Tolerances on chopper blade edge positions and the width of the PRP optical beam produce some uncertainty. The effect of lack of time symmetry in the PRP also adds a dc component to its series representation. It is important to minimize any lack of symmetry.

GULTON INDUSTRIES, INC.
Data Systems Division
R. H. Maschhoff

One of the prime requirements imposed by meteorologists is that there be independence between fields of view. In other words, a lack of scene-to-scene crosstalk. Prior to and during the ITPR program, a rigorous investigation was conducted aimed at establishing whether it was better in integrate or low pass filter subsequent to demodulation. Selecting the cutoffs of various filters to meet the independence requirements yielded the result that integration was the best.

The noise bandwidth of an integration type system comes out as 1/2T where T is the integration interval. However, unlike a low pass filter, the noise rejection it offers against more discrete types of interference is less than ideal. Figure A shows the amplitude vs. frequency response of a 40 Hz chopped system and a 50 msec integration time. Figure B shows the same result for a 75 msec integration. Note the difference in response to 60 Hz for the two cases. For the suggested 75 msec integration time greater care will be needed in shielding from 60 Hz during ground checkout. Alternately, the clock frequency during ground checkout could be changed slightly so 60 Hz would fall on a null point. There existed some lack of tolerance to 60 Hz interference in ITPR for the same reason. But once in orbit the channel noise in fact went below any attained during checkout.

Both periods of integration presented provide a null response to the second harmonic of the chopping frequency of 80 Hz. This is of course due to the fact that the integrations are over an integral number of chops. Quite clearly any integration over a non-integral number of chops is inviting disaster.

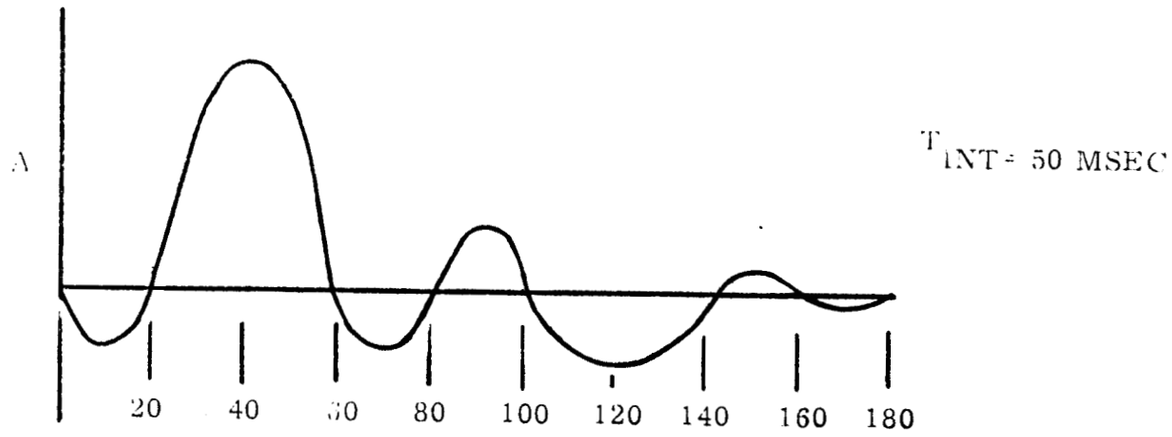

Figure A

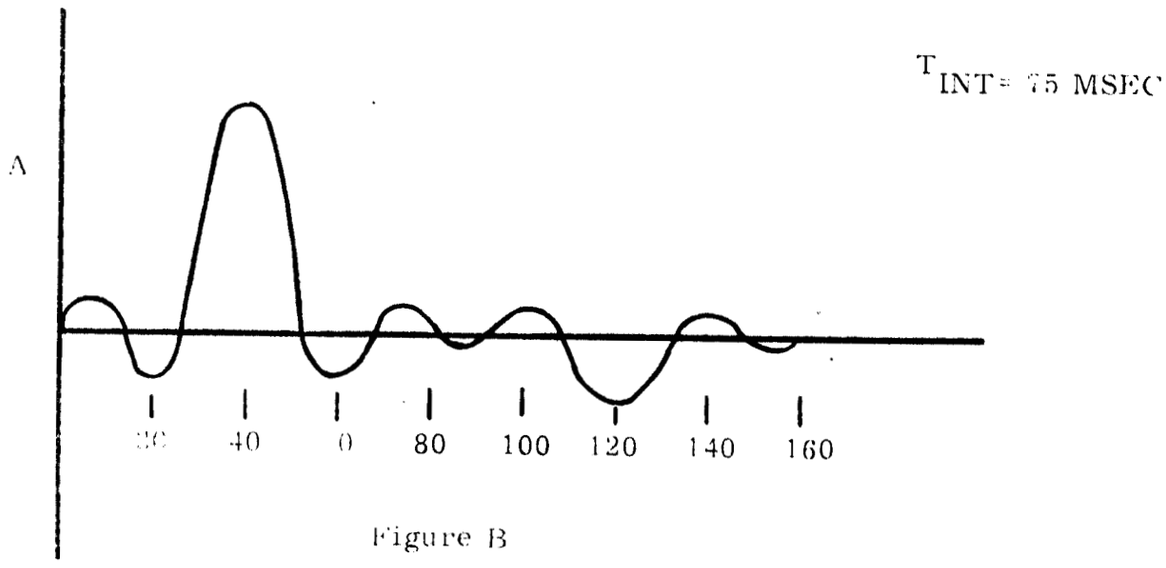

Figure B

ANALOG MULTIPLEXER REQUIREMENTS

A study of the analog multiplexer requirements for TOVs was conducted to determine the performance requirements and components to be used in the construction.

Basic Requirement: A precision analog multiplexer is required to provide the means of time sharing of the ADC between thirty eight (38) input data sources. Requirements imposed upon the multiplexer are summarized in Table A. The electrical requirements are not very stringent since each of the input data channels are driven from a low impedance source (0.1 Ω typical) and the output interfaces directly with a high input impedance buffer.

Approaches: Two (2) basic approaches to synthesizing the multiplexer were considered; i.e. (1) junction FET type and (2) MOS FET type. The switch elements and associated driver circuits for both of these approaches are different and therefore provide different advantages and disadvantages. A summary of the MOS and JFET multiplexer characteristics is shown in Table B.

Junction FET: A junction FET type multiplexer was utilized on the ITPR and exhibited excellent performance characteristics. JFETs are inherently stable devices with good radiation tolerance, since their characteristics are based on bulk conduction. The control circuitry necessary to turn the switches ON and OFF add components to the basic multiplexer which is a disadvantage in the areas of reliability and volumn. ON resistance of the JFET is low and reasonably constant at 100 ohms. Temperature variations reflect a chance in ON resistance of approximately 5 ohms.

MOS FET: The MOS FET multiplexer utilizing a P channel, enhancement mode, monolithic, MOS FET switching element was considered. Typical specifications for the device include; 500 Ω ON resistance, 1000 MΩ OFF resistance, 2.2pf input capacitance and 1.0nA leakage current. Integrated switches in a variety of configurations are available including, four (4), five (5) and six (6) analog switches per chip. Advantages of this type of multiplexer include, high packaging densities, simple drive circuit requirements, and no external biasing components. Although the MOS FET is more sensitive to radiation than the JFET, it is a suitable device for operation on the TOVs instrument.

Recommendation: The JFET type multiplexer is recommended for the TOVs experiment. Factors leading to this recommendation are listed below:

a) Space savings advantage of the MOS FET multiplexer is not too significant due to the relative small number of analog inputs.
b) Radiation tolerance of the JFET give it an advantage over the MOS FET.
c) Electrical performance characteristics and operational reliability of both devices are adjudged to be equivalent.

TABLE A: Multiplexer Requirements

Characteristics	Requirements
Analog Voltage Range	+ 10VDC to -10VDC
Type of Input	Analog Voltage, Single Ended
Number of Data Point	14
Number of Temperature Monitors	23
Number of Special Monitors	1
Operating Mode	Sequential
Redundancy	Non-Redundant
Transfer Error, Maximum	0.1 mV
Power Consumption	0.2 Watts
Sampling Rate	2.0 ms/channel
ON Resistance	500 Ω, max.
OFF Resistance	100 Ω, min.

TABLE B: Comparison of MOS & JFET Characteristics

ITEM	MOS FET	JFET
Input Voltage Range (TOVs Requirement)	+10VDC to -10VDC	±10VDC to -10VDC
Type of Analog Switch	P Channel Enhancement Mode	N Channel Depletion Mode
Type of Driver	Integrated Circuit	Discrete Component
Number of Bias Components	None	2
Relative Power (OFF/ON)	3mw/25mw	1 mw/32mw
Relative Volume	1	6
Switch Resistance (ON)	500 Ω	100 Ω
Leakage Current @25°C	1.0nA	0.1nA
Breakdown Voltage	35 VDC	40 VDC

ANALOG MULTIPLEXER DESCRIPTION

A twenty (20) channel prime multiplexer coupled with a twenty-four (24) channel submultiplexer will provide the necessary TOVs analog gating.

Multiplexer Configuration: A simplified block diagram of the analog multiplexer is shown in Figure A, and consists of a twenty (20) point prime multiplexer, a twenty-four (24) point submultiplexer, and associated control logic. Sampling rate for the prime multiplexer is 10 sps/channel, while the subcommutated channels are sampled at a 10/12 sps/channel. Note that the submultiplexers are arranged into two gating structures, each of which has its own respective amplifier.

Prime Multiplexer: A 4 x 4 matrix configuration is recommended for the analog prime multiplexer. First level switches are arranged as four (4) groups with four (4) switches/group. Second level switch outputs are connected together at a common mode and provide the switching to connect one (1) switch from the first level to the multiplexer output. This configuration provides some advantages in failure mode effects, reduces errors due to leakage current, and provides some sharing of switch drives.

Channel numbers 1 thru 14 are reserved for the infrared energy data, while channels 15 and 16 are dedicated to submultiplexer A and B.

Submultiplexer: Two (2) submultiplexers consisting of twelve (12) channels each are required to commutate the twenty-four (24) instrument monitor points. A two level switching matrix of size 6 x 2 is recommended. First level switches are connected to form two (2) groups of gates consisting of six (6) switches/group. Second level switching is used to select one of the first level groups. Amplifiers are required to provide gain for the precision temperature bridges and buffer isolation for the thermister monitors.

Sampling Format: A recommended sampling format is tabulated below:

CH. NO.	DATA
1	IR Channel 1
2	IR Channel 2
3	IR Channel 3
4	IR Channel 4
5	IR Channel 5
6	IR Channel 6
7	IR Channel 7
8	IR Channel 8
9	IR Channel 9
10	IR Channel 10
11	IR Channel 11
12	IR Channel 12
13	IR Channel 13
14	IR Channel 14
15	Subcommutator A
16	Subcommutator B

NOTE:

1) Subcommutator A consists of 12 channels of temperature monitors denoted as TM1-TM12.

2) Subcommutator B consists of 11 channels of temperature monitors denoted as TM13-TM24, plus the bridge excitation voltage. Refer to the interface document for additional information.

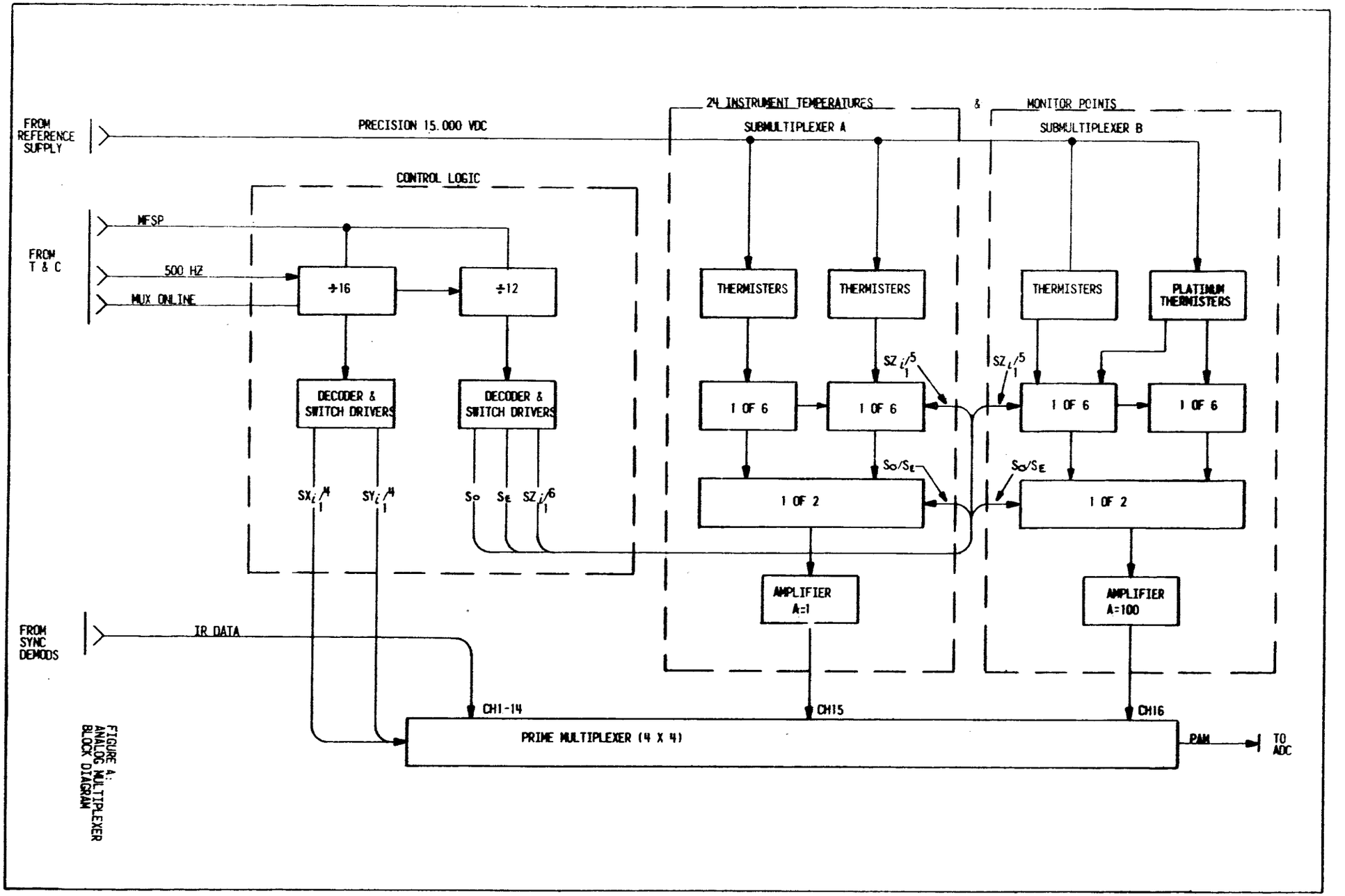

FIGURE A: ANALOG MULTIPLEXER BLOCK DIAGRAM

ANALOG MULTIPLEXER CIRCUITS

Analog multiplexer circuits are well defined and use the same type of components as the ITPR instrument. Errors contributed by this circuitry is neglibible.

General: A single path thru the analog multiplexer is shown in Figure A to illustrate the first and second level switch circuits and a typical switch driver.

Note that the first level switch uses a resistor diode network to control the Fet while a boot strap connection is recommended for the second level switch.

Analog Switch: The basic switch element is an N channel, silicon, junction, field effect transistor, part number 2N4393. This device has excellent electrical characteristics; including R_{DS} (ON) of 100 maximum, V_P of -3Vdc max., I_D (OFF) of 0.1 nA @ 25°C, and BV_{GS} of -40 V minimum. Alternate devices of equivalent quality are also acceptable. Selection of a high quality, space qualified part is no longer a difficult task. Control of the switch is provided by establishing these conditions:

Switch On: $Vg = Vs$

Switch Off: $Vg < Vs\ (min) - V_p$

Switch Driver: A two stage transistor switch driver is used to translate the matrix control signals from logic levels (0 to +5 Vdc) to voltages of -20 Vdc (OFF) to +15 Vdc (ON). Circuit is similar to the one used on the ITPR and is recommended because of the low power consumption characteristic. Integrated circuit type drivers were consisted; but were rejected.

Buffer Amplifier: A precision, unity gain, voltage follower type amplifier is required at the output of the prime multiplexer. An integrated operational amplifier, Type LM108 is recommended. This choice was based upon offset stability, low bias currents and low power consumption considerations. The LM108 is specified at 3.0 mV maximum dc offset and typical drifts of 3.0 μV/°C; bias current is 3.0 nA maximum, and dc offset current is 0.4 nA with a TC of 2.5 pA/°C. Power consumption is 40 mW maximum.

Multiplexer Errors: The analog multiplexer contributes errors which degrade the quality of the analog data. Main error sources include JFet ON resistance, leakage current, cross talk, offset current drift and offset voltage dirft due to the buffer amplifier. Errors were computed; the results of which summarized below:

Error Source	Value
a. Error due to delta change of r_{ds}	0.006 mV
b. Error due to offset current of A1	2.4 μV
c. Error due to offset voltage of A1	0.09 mV
d. Error due to leakage currents of switches	2.4 μV
e. Error due to cross talk thru switches	1.2 μV
TOTAL ERROR (LINEAR SUM)	0.113 mV
TOTAL RMS ERROR	0.091 mV
	(0.0009% FS)

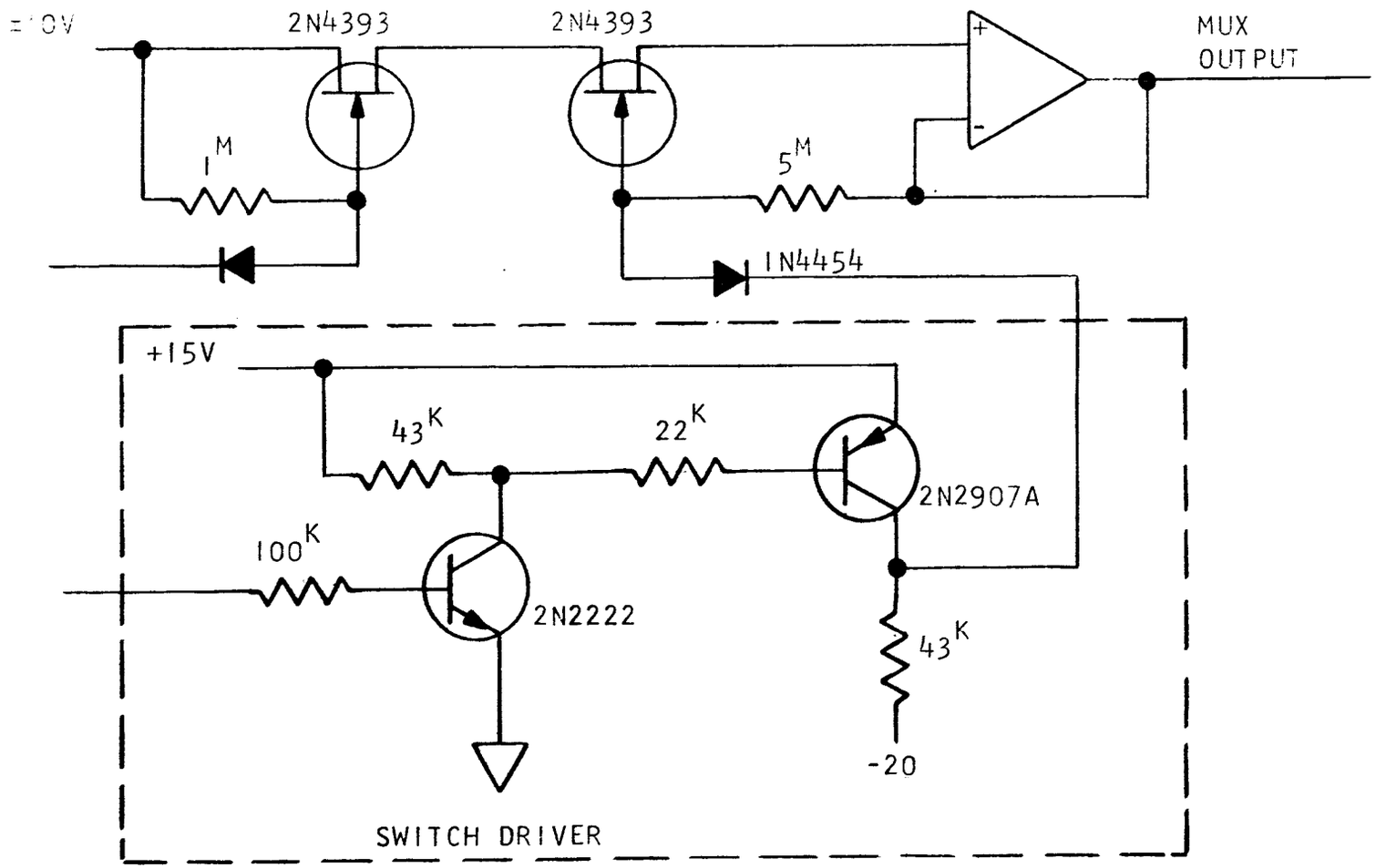

FIGURE A
A PATH THRU THE
ANALOG MULTIPLEXER

BUDCO INDUSTRIES, Inc.
Data Systems Division
S. G. Day

ANALOG-TO-DIGITAL CONVERSION METHOD

Evaluation of several conversion techniques shows that the successive approximation, trail current type converter, utilizing an offset binary code is the most suitable for the TOVS instrument.

General Requirement: Analog data generated within the TOVS system must be converted to a digital number for subsequence data transmission. Data processed thru the ADC includes all infrared energy channels, selected temperature monitors, and calibration voltages.

Conversion Methods: Several different approaches to performing the conversion were investigated, including 1) dual slope integration, 2) ramp comparator, and 3) successive approximation.

The dual slope integration technique is a very accurate conversion method. A two step integration process is employed where the analog input is integrated for a fixed time T1, after which the integrated is discharged at a precision rate over the period T2. A measurement of the time interval T2 yield the digital value of the analog input. The major characteristics of this type of converter are listed below:

- Yields a very accurate conversion value.
- Very insensitive to noise.
- Utilizes very simple circuitry.
- Consumes very little power.
- Relatively slow conversion rate.

While this conversion technique has many good characteristics, the slow conversion rate is not compatible with the TOVS requirement. This characteristic eliminates the dual slope integrator type ADC.

The ramp comparator is similar to the slope integrator in that a time interval proportional to the input voltage provides the conversion value. Conversion rate is faster than the dual slope technique, but is slower than the TOVS requirement.

Two (2) successive approximation techniques were considered; i.e., (1) voltage mode and (2) current mode. Both of these techniques overcame the speed limitations of the dual-slope and ramp comparators but are more complex than either. A comparison of the current and voltage mode conversion technique is shown in Table A. The ADC used on the ITPR provides an example of the voltage mode technique, while the current mode converter is modeled after that employed on the ERB program. The main differences between them is the D/A method used to develop the trail voltage/current steps.

Recommended Conversion Method: The successive approximation, current summing type is recommended for use on the TOVS. An offset binary code is recommended in lieu of the sign magnitude in order to eliminate the absolute value amplifier and obtain gains in accuracy and simplicity.

FIGURE A: TOVS & ITPR ADC CHARACTERISTICS

ITEM	ITPR CONVERTER	TOVS CONVERTER
Input Voltage Range	+10 Vdc to -10 Vdc	+10 Vdc to -10 Vdc
Number of Bits	11 Bits (10 Data + Sign)	12 Bits
Output Code	Sign/Magnitude	Offset Binary
Conversion Method	Successive Approximation, Trial Voltage	Successive Approximation, Trail Current
Bit Trial Period	1.0 ms	125 μs/Bit
Power Consumption	2.10 Watts	0.95 Watts
Relative Volumn	1.0	0.9

ADC ERROR ANALYSIS

Circuitry employed in the analog to digital converter will contribute an error of less than 0.032% to the encoded value under the worst case conditions.

A comprehensive error analysis has been performed on all ADC circuits. This work, together with all supporting data and computation is on file at Gulton Data Systems Divison. The background work is not included in this report; however, a summary of the result is shown in Table A of the adjacent page.

A linear summation of all the tabulated errors yields a maximum, worst case value of 0.0889% of full scale or 8.89 mV. This is a very pessimistic approach to error.

The RMS summation of all the tabulated errors yields a maximum value of 0.058% of full scale or 5.8 mV. This figure is the worst case maximum RMS value and is computed for severe environmental conditions and wide variations of circuit component tolerances.

A more realistic case is to compute the RMS which occurs in each circuit and to obtain the system error via the RMS summation approach. This computation yields values of 0.032% of full scale or 3.2 mV absolute. A very reasonable number.

TABLE A Tabulation of ADC Errors

CIRCUIT	ERROR SOURCE	ERROR, %
Current Switches & Resistor Network	Offset Voltage Match (Switches)	0.0166
	TC of Tracking (Switches)	0.0100
	Leakage Current (Switches)	0.0025
	Tolerance & TC (Resistors)	0.0213
	Total Error (Linear Sum)	0.0504
Comparator	Bias Current	0.0025
	Offset Voltage Drift	0.0050
	Sensitivity Error	0.0005
	Long Term Drift	0.0175
	Total Error (Linear Sum)	0.0255
Reference Supply	Input Voltage Changes	0.0001
	TC of Reference Diode	0.0010
	TC of Zener Current	0.0040
	Offset Drift of Current Amplifier	0.0049
	Long Term Drift	0.0030
	Total Error (Linear Sum)	0.0130
ADC	System Error (RMS)	0.058

DESCRIPTION OF THE ADC CIRCUITS

The ADC is comprised of precision analog circuits designed with intergrated networks and supplemented where necessary with discrete components.

General Description: A simplified block diagram of the ADC is shown on the adjacent page and consists of an input buffer amplifier, a precision reference supply, ladder network, comparator circuit and control logic.

Quad Current Switches and Resister Network Circuit: Three quad current switches, a precision resister network and an amplifier are used to generate accurate binary weighted currents. Recommended part numbers for resister network and three quad current switches are HCN-28 (Hy Comp), ICL8018A (Intersil), ICL8019A and ICL8020A respectively. Integrated amplifier A1 should be an LM108 or equivalent part.

In the circuit, a stable constant voltage drop across all eleven emitter resisters of current switching transistors is obtained. This is done by using the reference transistors of quad with an operational amplifier and a high precision current source. By amplifier feedback theory the collector current of the reference transistor (Q6) is equal to $V_{REF}/(R7 + R8 + R9)$. The amplifier output voltage is forced to be equal to the value of the base voltage necessary to make the emitter current of Q6 equal to $I_{REF} \times (1 + \beta)/\beta$. The base current is supplied by the amplifier output. Since the bases of all eleven current switching transistors are tied to the base of Q6 and the switching transistors track the reference in β and V_{BE}, the voltage drops across emitter resisters are equal.

Because of the constant emitter voltage drops and the precision resisters at the emitter, the quads generate exact bit currents. To maintain the progression of binary weighted bit currents, a set of four matched resisters (10K, 20K, 40K and 80K) is used at the switching transistor of each quad and the current outputs of the second and third quads are precisely attenuated by 1/16 and 1/256 respectively.

Precision Reference Source: The reference current generator circuit consists of a stable reference diode and a precision resister. The circuit generates a reference current of 125 μ amps.

The reference diode CR1 used in the circuit has a voltage temperature coefficient of .0005%/°C and t.c. of the precision resistor R7 is 5 ppm/°C. Due to this, error in the reference current is less than 0.01% over the operating temperature range of 0°C to 40°C.

A stable, precision voltage source is provided by the positive voltage regulator, which uses an LM105 integrated circuit. Its function is to take the +15 VDC unregulated voltage directly from the TOVs power supply and to output a stable +12 VDC.

In the circuit, the output voltage is set by Resistors R3 and R5. With a proper selection of the resistor values of R3 and R5, exact +10 volts output is obtained. Resistor R1, connected between current limit and output terminals of the LM105, provides the short circuit protection. Capacitor C1 is the frequency compensating capacitor and it stabilizes the LM105. C2 on the reference by-pass terminal helps to reduce the output noise.

Comparator Circuit: An integrated-circuit comparator is recommended. National Semiconductors LM-111H will perform this function. Specifications for this device include low bias current (0.06 μ A), good voltage gain (200 V/mV), low input offset current (0.04 μ A) maximum, and low power consumption (80 mW). Response time is not too impressive at 200 ns; but the sensitivity and stability about the threshold level more than compensate for the slower speed.

In the circuit, two clamp diodes, CR1 and CR2, at the input are used to improve the comparator response. Resistor R8 provides positive feedback which produces hysterisis in the transfer characteristic. This hysterisis is required to reduce the sensitivity of the comparator to the input noise.

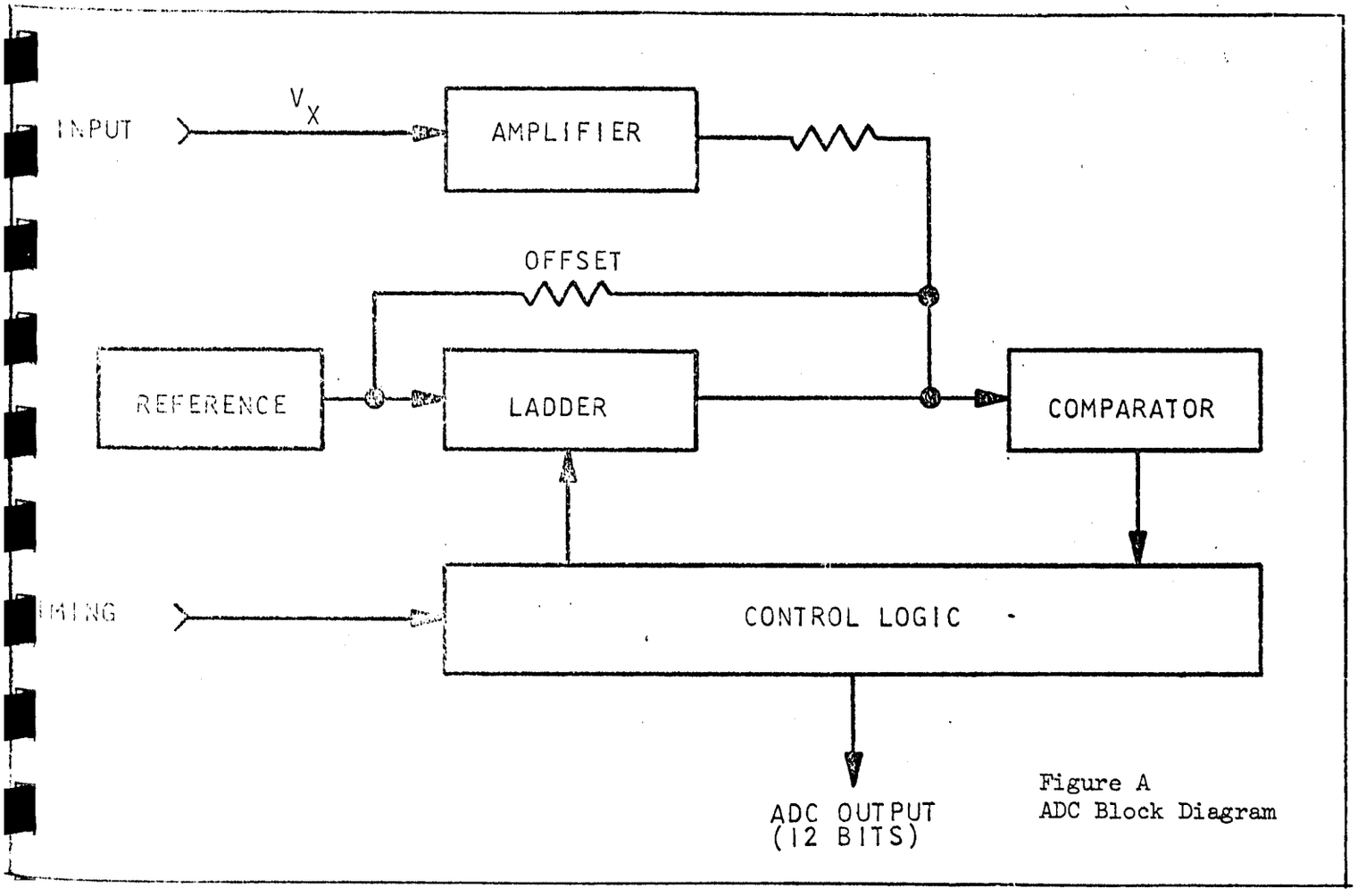

Figure A
ADC Block Diagram

RADIATION CONSIDERATIONS

Radiation simulation tests as well as data from ITPR and VTPR in orbit show a small noise increase over portions of the orbit. Total dose survival is not a problem as evidenced by electron bombardment tests on ITPR and constant calibrations in orbit.

There are two distinct effects on the pyroelectric detector/amplifiers due to inner Van-Allen radiation. Both are transient effects, and both defy shielding within any reasonable limits of space and weight. One is the noise increase due to conductivity changes in and on (bulk and surface effects) the detectors and semiconductors due to bremsstrahling, the x-ray production due to the deceleration of <5 Mev electrons. This amounts to an approximate 20% increase in the noise level of the detector/amplifier, over the range of expected inner Van-Allen belt electron flux and spectrum. The other effect is noise spikes due to >45 Mev protons, occurring randomly from a few per second to once per few seconds. These spikes may be best handled by ignoring the errant data point. Data from orbit shows this is a valid procedure for the high gain Q branch channel in particular

Both of these effects have been deduced analytically and verified experimentally. See the Appendix on Radiation Effects for details of the analysis and experimental data. The most significant finding in tests performed was that thin detectors are less susceptible than thick detectors. This supports the recommendation coming from the other noise evaluations that the TOVS should use the thinnest practical detector elements.

In other portions of the analog channel, such as the multiplexer and ADC where conductivity modulation may occur with incident radiation, impedances are at safe low levels. Even if the off impedance of a switch degrades, little or no error occurs because the source impedance of other points tying to the mode are so low (an op amp output) that no effect is to be expected. Amplifier gains are resistively determined and are nearly oblivious to transient effects in the constituent operational amplifiers.

SECTION 7
SCANNER SUBSYSTEM DESIGN

SUMMARY

Review of Objectives and Requirements for the Scanner Design and Test Program 7-0
Nature of Scan Pattern and Sequence 7-2
Impact of Scan Sequence on Scanner Design 7-4
Summary of Flight Scanner Design Features 7-6
Discussion of ITPR Scanner Performance..... 7-8

SCAN MECHANISM DESIGN

Analysis of Scan Drive Mechanism Requirements 7-10
Summary of Drive Mechanism Comparison..... 7-12
Description of Harmonic Drive 7-14
Choice of Scanner Configuration 7-16
Selection of Motor and Drive Ratio for Retrace 7-18
Approaches for Controlling the Settling Characteristics 7-20

DESIGN VERIFICATION

Math Model Describing Scanner Motion 7-22
Performance Predictions Based on the Math Model..... 7-24
Summary of Scanner Breadboard Testing 7-26
Mechanical Layout of the Scanner..... 7-28
Estimates of Physical Characteristics 7-30

MECHANICAL DETAILS OF THE SCANNER

Selection of Flight Scanner Components 7-32
Structural Problems in the Scanner..... 7-34
Selection of Scanner Lubricants 7-36
Nature of Scanner Subsystem Interface Requirements 7-38

REVIEW OF OBJECTIVES AND REQUIREMENTS FOR THE SCANNER DESIGN AND TEST PROGRAM

A scan mechanism design and test program was conducted as part of the Basic Sounder Unit (BSU) instrument study with the objective of establishing a scanner design that is compatible with the BSU instrument and that meets performance specifications. Following the design selection, a laboratory mockup of the scanner (including electronics) was built and tested.

The BSU is part of the TIROS Operational Vertical Sounder (TOVS), an instrument system that will be flown on the TIROS-N spacecraft. TOVS, in turn, is part of an operational meteorological data gathering system that has a performance requirement of two years. As a consequence of the operational lifetime, as well as the instrument mission, the scanner subsystem must meet the requirements listed in the table on the facing page, with respect to performance, physical characteristics, and environmental factors. This topic discusses those overall requirements and the major considerations in meeting them.

The scanner performance requirements were derived from the given parameters of the scan program and from the mirror characteristics. The scan mirror, which is designed for accurate manufacture and optical stability, has certain physical characteristics. However, for the purpose of the scanner design, the only characteristic necessary to consider is the moment of inertia, since it is this feature of the mirror that affects scanner performance. The other scanner performance requirements resulted from the scan program study; they represent scanner output functions which must be achieved.

The physical characteristics of the scanner subassembly are impacted most by space, weight, and power requirements implied by the BSU instrument system design. The environmental requirements are derived from the testing and service stresses which the BSU instrument will experience.

Although all requirements are important and affect successful scanner performance, it is specified performance which has the greatest impact upon design feasibility. Accordingly, it was the performance requirements which primarily were addressed by the scanner study. This emphasis also determined that it was more important to simulate scanner dynamics rather than be an exact copy of flight hardware.

Hardware requirements were also addressed by the study. Of significance to the hardware design was the experience gained from building, testing, and flying the ITPR instrument, which had many requirements similar to those of the BSU. Accordingly, the design phase of the scanner study was an opportunity to optimize scanner subsystem hardware based upon ITPR experience, and to define requirements for scanner components.

SCANNER REQUIREMENTS

The step, dwell, and retrace requirements are extremely critical.

Performance	
• Inertia Load	25.2 gm cm^2 at motor
• Step Angle and Accuracy	1.125° ±0.1°
• Step and Settle Time	50 ms
• Retrace Speed	100 steps/s
• Angular Range	360°
Physical Characteristics	
• Space Envelope	11.25 in. dia x 15 in. long
• Weight	2.5 lb*
• Drive Power	8 W*
Environmental	
• Operating Temperature Range	-25°C to +70°C
• Acceleration	22 g
• Vibration	5 - 2000 Hz Sine, 10 g all axis 20 - 2000 Hz Random, 20 g runs

* Design Goals

NATURE OF SCAN PATTERN AND SEQUENCE

The scan pattern requirements for the TOVS-BSU can be derived almost uniquely from the need for complete geographical coverage, the desired field of view, grid size, and orbital period.

Specified Requirements. The TOVS instrument must have a scan pattern which provides complete geographical coverage. The design shall include selection of scan dwell time, space and housing blackbody viewing periods, and scanning transit times. Each scan grid shall be comprised of approximately 80 scan elements (1.125° FOVs) or less in a square area. The scan grid projection on the earth's surface shall cover a geographic area whose dimensions are nominally 400 x 400 km, based on a satellite altitude of 1678 km. The scan transit time will be chosen to allow successive scan grids to be separated by no more than one field of view based upon a satellite ground speed of 5.56 km/s. The TOVS shall sample data from regions extending out to at least 36 FOVs on each side of the spacecraft track. The maximum area overlap of the 99-percent FOV limits shall not exceed three percent of the instantaneous FOV (IFOV) area for elements in successive scan strips.

Derived Requirements. Based upon a nominal 120-minute orbital period, full global coverage requires that the angle subtended by a scan line at the earth's center be 30°. Scan angle about nadir, ϕ, is determined then by the geometry presented on the facing page. Solution to the geometry yields a value of $\phi = 41.06$ degrees Seventy-two IFOVs of 1.125 degrees can be obtained in an 81-degree scan line. Therefore, data will be sampled from 36 IFOVs on each side of nadir, corresponding to a scan pattern of ±40.5 degrees. The area subtended by the IFOV at the ends of the scan will resemble an ellipse. The minor diameter of this ellipse will determine the line-to-line spacing within a 400-km square grid. Geometric calculation indicates that the proper number of scan lines for contiguous coverage at the edge of the scan is 8.22 scan lines per 400 km. The number of scan lines must be a whole number. If eight lines are selected, significant gap between scan lines will occur. If nine lines are chosen, then there is some overlap at outer IFOV of the scan with less gap at nadir. This would be the preferred scan coverage.

Vertical raster of the grid is generated by the forward velocity of the spacecraft.

$$V_F = \frac{2\pi a}{120 \times 60} = 5.56 \text{ km/s}$$

Time required to cover 400 km is

$$t_{grid} = \frac{400}{5.56} = 72 \text{ s}$$

Time required to advance 1 scan line is eight seconds. This scan time allows satisfaction of the maximum three precent area overlap of instantaneous 99 percent FOVs in successive scan strips.

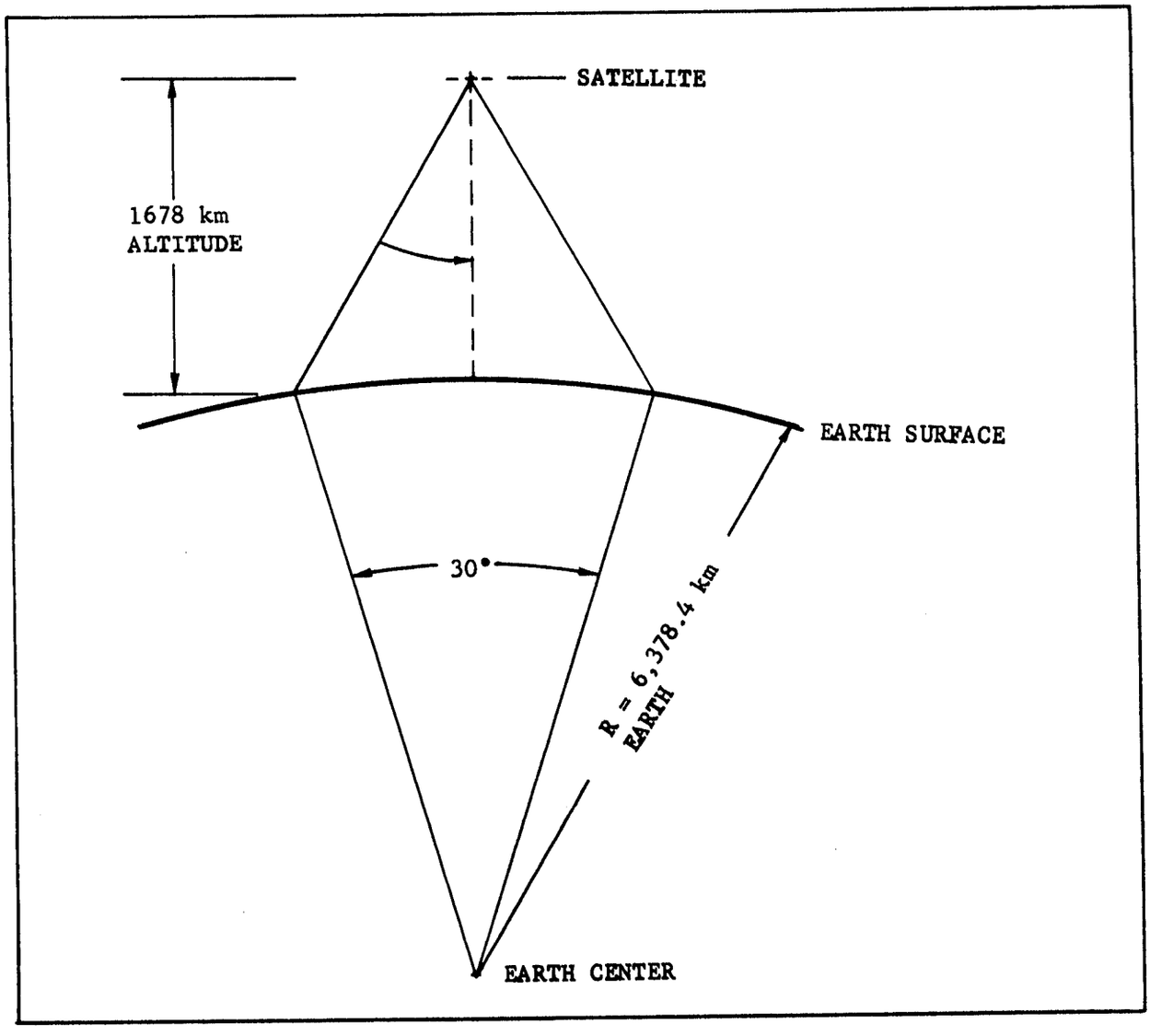

Scan Geometry Related to Earth-Spacecraft Relationship

IMPACT OF SCAN SEQUENCE ON SCANNER DESIGN

The TOVS instrument scanning sequence is the single most important factor affecting the design of the scanner. To cover the desired field, the scanner must perform rapid stepping under fixed control, with fixed timing. The time allotted for scene viewing affects the remaining time available for stepping and settling, and thus impacts scanner dynamics.

The scanning program has three distinct phases: step-dwell, retrace, and calibrate. The timing of each of these functions is shown in the figure. One step-dwell cycle is of 100-ms duration, and consists of a dwell period of 75 ms followed by a step-and-settle period of 37.5 ms *. The chopper function is shown to the same time base to illustrate the synchronization of scanning, chopping, and signal integration. One integration period consists of three scene chops and three reference chops. The step is initiated during a chopper reference phase when the scene is blocked, so the amount of data lost during scanner stepping is minimized.

A scan line consists of 72 scenes viewed serially. This requires 72 scanner steps, or 7.2 s at 100 ms/step. An additional 800 ms is allowed for retracing, bringing the total allotted time for one scan line to 8.0 s. Since the scanner drive input for retracing is 100 pps, the 72-step interval is actually retraced in only 72 ms, leaving an 8-ms cushion before the next scan line is begun.

The third illustration in the figure shows the scanner sequencing for a complete data grid of 32 scan lines as well as how the calibration functions fit into the scan program. Calibration, which is performed at the end of each scan grid, consists of a space look and a housing blackbody look. The space look, in terms of scanner rotational angle, is 70 degrees above nadir; the housing blackbody look is 180 degrees above nadir.

The specified scan sequence imposes two demands on the scanner design: stepping and settling, and slewing. Of the 100 ms for each data frame, only 37.5 are available for stepping and settling, which impacts the torque and damping of the scan drive motor. Slewing involves the retrace and the movement to calibration positions. The requirement is that a 100-pps input to the scanner must be followed without error so that the commanded positions will be reached in time, which impacts the motor slew rate of the loaded motor.

The step-and-settle requirement affects the choice of three system parameters: motor output torque, system inertia, and damping. The torque must be sufficiently high to get the motor rotor and connected inertias out of its detented position quickly. Stepping and settling together must consume no more than 37.5 ms.

The system slewing rate must be high enough to allow movement between the commanded positions in the times shown in the sequencing diagram. The required output slew rate is 100 steps of 1.125 degrees/s, or an angular rate of 1.96 rad/s. This affects the stepper motor parameter of no-load speed, or step rate, and also impacts the motor's detent torque, since high detent torque tends to lower the no-load step rate. Balancing of these two parameters to achieve adequate speed while keeping good damping is one of the tradeoffs that must occur in the motor design process.

* The system design shows that it is desirable that the scanner step and settle in 37.5 ms. This value appears to be attainable, but the baseline mechanical design subjected to breadboard testing was based on a 50-ms step-and-settle interval.

1110-102-9

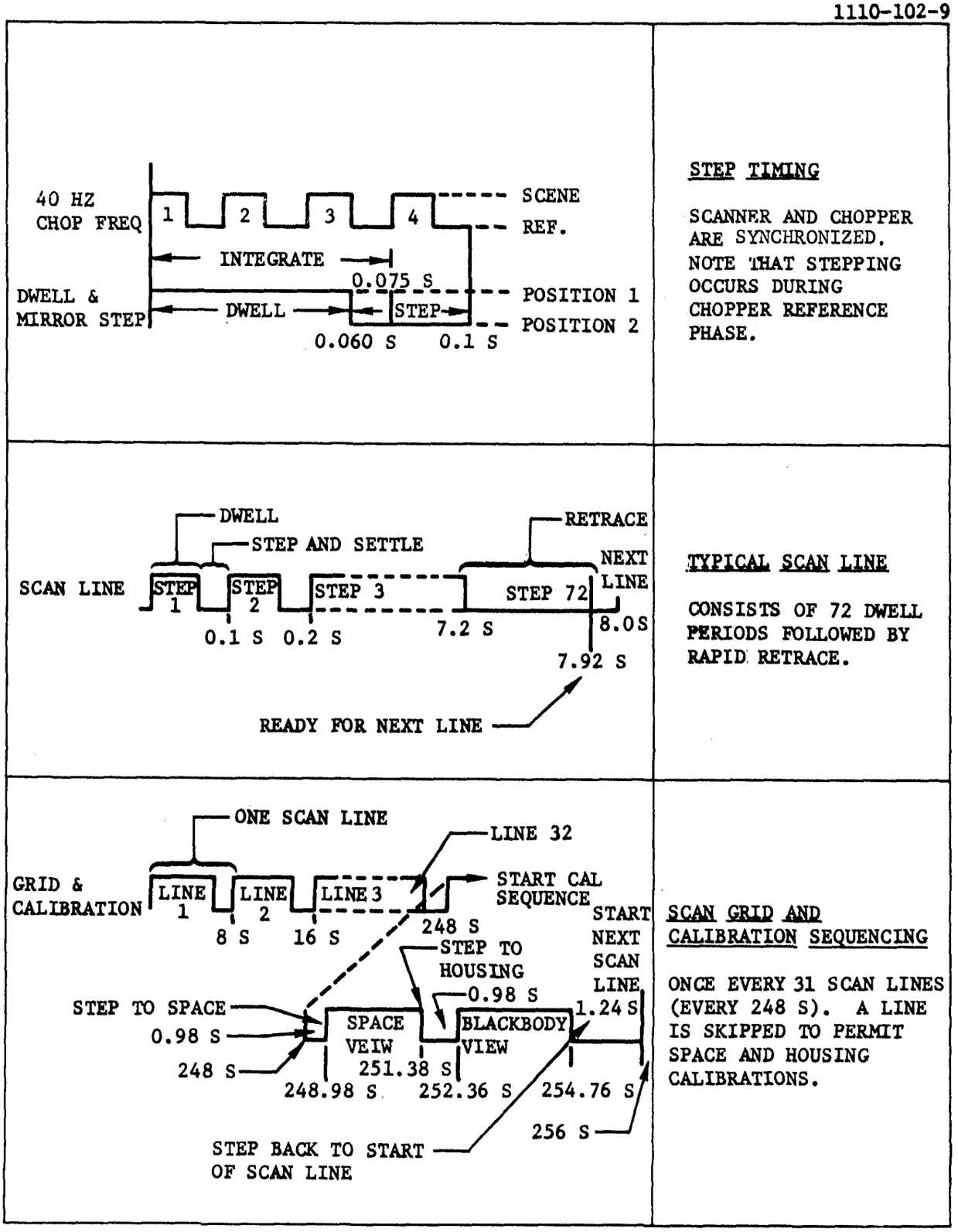

TOVS Scan and Calibration Sequencing. A 75-ms integration period permits the use of three chops per scene, increasing the instrument signal-to-noise ratio. The steppping and settling required impacts the scanner dynamics.

SUMMARY OF FLIGHT SCANNER DESIGN FEATURES

The TOVS-BSU scanner design is a simple, straightforward configuration that meets the performance objectives. It is similar to the ITPR design, but has been improved to avoid assembly problems, and to provide better thermal stability and increased life.

The scanner, a major functional part of the BSU instrument, is constructed as a self-contained, separately checkable subassembly. In addition to being designed to the demanding parameters of the BSU application, the scanner is configured to ensure ease of producibility and the high reliability needed for an operational instrument.

The major design features of the in-line scanner assembly are shown in Table I. Since the instrument performs a stepped scan, a stepper motor was chosen as the source of motive power. Because of its simplicity, low wear rate, light weight, and extremely accurate transmission of motion, a harmonic drive was selected as the speed reducing element of the mechanism. The encoder is a seven-track pin contact type. It is similar to that used in the ITPR instrument, but major improvements have been incorporated. The main structure of the subassembly is aluminum. The scan mirror shaft is supported on pre-loaded ball bearings whose larger size and increased number reflect the greater size of the BSU scan mirror.

The BSU is similar in concept to the ITPR instrument. Some features and arrangements of features carry over directly, but the practical design of the instrument and of the scanner subsystem is impacted by the increased speed, coverage, and life requirements of the BSU.

A number of features in the BSU scanner represent significant design improvements over the techniques used in the ITPR. Some specific details are shown in Table II. The design of the drive motor is changed to incorporate a large flange on its front end, eliminating a joint that existed previously and allowing greatly improved concentricity between motor and harmonic drive, which improves the accuracy and smoothness of motor transmission. The non-metallic motor mount that was used for ITPR has been eliminated to improve the rigidity of the motor mounting and to conduct heat directly to the instrument housing. The increased scanner dynamical performance required that inertias at the motor shaft be reduced by changing the harmonic drive to a low inertia design.

The design improvement most significant for checkout and assembly is the use of a unitized shaft encoder. This device was changed from the ITPR design so that it is pre-assembled before being placed in the scanner assembly, which allows the unit to be checked out and shipped by the manufacturer as an assembled unit. Reliability is greatly enhanced and assembly problems that existed with the ITPR are completely absent. The method of wiring the encoder also was changed, to incorporate a connector. This again is a great improvement over the hard wiring used on the ITPR encoder. Both the scan mirror and the encoder are indexed to the main shaft by means of precision Woodruff keys, allowing easy phasing of encoder to mirror at initial assembly. Finally, the method of mounting the main shaft bearings was changed. To avoid any possible thermal problems which might occur with the pre-loaded bearings, a monometallic bearing mount was designed. This involves a stainless steel sleeve pressed into the aluminum scanner housing. The gradual loosening of the bearing outer races in their bores that is sometimes encountered cannot happen with this design.

The design generated by the scanner study was based on both past experience and analysis. To prove out the key design features of the scanner, particularly as regards scanner dynamics, a laboratory breadboard model was constructed and tested.

TABLE I. MAJOR DESIGN FEATURES

• Assembly	-In-line
• Motor	-90-degree PM Stepper
• Reduction Drive	-Size 1C Harmonic Drive
• Encoder	-Pin Contact, 7-track
• Structure	-Aluminum for Thermal Conduction
• Bearings	-Tandem Pair Front, Single Rear - preloaded

TABLE II. IMPROVEMENTS IN BSU OVER ITPR INSTRUMENT

The TOVS-BSU scanner design incorporates improvements based on problems encountered in the ITPR assembly.

• Drive Motor Mounting	- Integral mounting flange for improved concentricity
• Harmonic Drive	- Low-inertia wave generator
• Encoder Design	- Pre-assembled
• Bearing Mounting	- Monometallic Design
• Encoder Wiring	- Connector
• Mirror-Encoder Alignment	- Keyway
• Motor Thermal Circuit	

DISCUSSION OF ITPR SCANNER PERFORMANCE

Present understanding of the failures that have been experienced with the ITPR scanner does not appear to invalidate the similar TOVS-BSU scanner design. The failures appear to have been caused by reduced motor torque and lubricant degradation rather than by a basic design flaw, and both of these conditions can be prevented by improving motor and lubricant manufacturing controls.

The scan mechanism in the Infrared Temperature Profile Radiometer (ITPR) on NIMBUS-5 is very similar in design to that recommended for the TOVS-BSU. It met the somewhat less demanding transient response and retrace requirements for ITPR and was extensively tested in engineering model, prototype, and flight unit tests prior to spacecraft integration.

The scanner on the ITPR flight unit for NIMBUS-5 malfunctioned in thermal-vacuum testing, failing to follow the commanded sequence reliably. Disassembly of the scanner failed to show any obvious mechanical failure or source of increased torque load, although there was some evidence of wear and a glassy particle was found in the harmonic drive lubricant, but at an uncritical location. Motor torque was lower than nominal. The failure was attributed primarily to low temperatures which increased lubricant viscosity, although the scanner was overheated during testing.

The prototype instrument was then successfully tested in thermal vacuum, integrated with the spacecraft, and launched in December 1972. After several weeks of successful operation of the entire instrument, the scanner again began to behave erratically, as the other unit had done. Later it was found that the instrument could be turned back on, and that the scanner would operate normally; but, after a period of time, the erratic operation would again occur. This behavior pattern has been more or less consistent. There is no obvious correlation between erratic behavior and operating temperature, although the scanner temperature has exceeded the qualification limit of 45°C.

Investigation of these failures is in progress, and the investigation is not complete. So far, the results of the investigation are as follows:

- Mechanical and structural analysis conducted during the TOVS scanner design effort has not disclosed any source of bearing failure, excessive drive wear, or other fundamental mechanical design flaw.
- Glassy particles have been found, not only in the harmonic drive, but recently also were found in the unused G-300 grease used to lubricate the motor. These particles were found deep in the squeeze tube and were evidently either in the grease when delivered or were the result of aging that occurred since the motor was greased.
- The grease used to lubricate the harmonic drive was purchased separately by the drive supplier.
- The tendency to form such particles is a known property of some silicone greases.
- The permanent magnet motors were operated above the 45°C qualification temperature. Conceivably, demagnetization could have resulted from repeated thermal cycling. The motor involved in the first failure was sent to the supplier, who found it to be partially demagnetized.
- The motor supplier did not test the motor with the single-phase drive circuit used in the instrument but rather used a two-phase circuit which provided more torque. The torque becomes marginal when a single-phase drive is used.

At this point in the investigation, it appears that the failure was caused by improper testing and inadequate screening of the motors, which allowed use of motors of marginal torque capability. This problem may have been aggravated by contamination of the grease and overheating of the motors. To prevent recurrence it is evidently necessary to increase the controls used in procurement of scan drive components, a precaution which would be taken in any case for an operational instrument.

A number of improvements have been made in the TOVS scanner design to facilitate assembly and testing and to provide greater performance margins. The ITPR encoder was of separable design--one part was affixed to the output shaft and the other to the scanner drive housing. Because of the encoder location, the assembly was blind and verification of proper assembly was difficult. Encoder wiring was also difficult in that there was hard wiring to the pin cage, and it was possible to over-strain the cable. The TOVS encoder is a unitized, pre-assembled design and has its own electrical connector, thus avoiding these problems. A potential problem was noted with the ITPR mirror shaft bearings, which were mounted directly into the aluminum of the scanner housing. This has been fixed in the TOVS scanner by adding a pressed-in stainless steel sleeve into which the bearings are seated. The immediate area of the bearing mounting is thus monometallic and differential thermal expansion problems are avoided. The bearing size has been increased because of the greater mass of the TOVS scan mirror. The use of different lubricants is being considered.

In addition to the above improvements, the following steps should be taken with the TOVS scanner to assure reliability in orbit: motor qualification to higher temperatures, improved materials and process controls, and improved implementation of supplier reliability and quality programs to assure adequate screening and acceptance testing of motors, drives, and other devices.

IMPROVEMENTS IN BSU SCANNER DESIGN AND MANUFACTURE

These improvements are a direct result of ITPR experience.

- Motor is heat-sunk to instrument housing.
- Encoder is a unitized assembly.
- Use of connectors.
- Monometallic shaft bearing design.
- Increased manufacturing controls.
- Use of more reliable lubricants.

ANALYSIS OF SCAN DRIVE MECHANISM REQUIREMENTS

Analysis of the speed, accuracy, and weight requirements for the BSU showed that only a few alternative designs are suitable.

The primary requirements of the scan drive are response time, accuracy, and ability to operate for two years in orbit. The scanner operates in two modes: step-dwell, and retrace. The requirements are intended to ensure that operation is satisfactory in both modes. The life requirement, of course, is vital to instrument success.

The necessary motor torque and speed characteristics can be derived from the response-time requirements. The mechanism design analysis shows that there are two torque conditions to be met: the motor peak torque must be at least 8 oz-in., and the average or running torque at 100 pps must be 2.6 oz-in. minimum.

The detailed dynamic analysis also defined the necessary system damping. The step-dwell transient response should be slightly underdamped to achieve a minimum response time and to reduce losses which would increase torque requirements during retrace if the motor were critically damped. Detailed analysis shows that a damping factor of 0.4 to 0.6 is needed.

The accuracy requirement relates to the step-dwell mode of operation. The accuracy of the instrument's look angle is determined directly by how accurately the scanner steps. The overall pointing accuracy requirement for the instrument is 0.1 degree, which also means a scanner positioning accuracy of 0.1 degree, as there is no optical doubling in the scanner. If half of this total allowable system error is allotted to the scanner, the required output shaft positioning accuracy would be 0.05 degree. For an 80:1 speed-reduced system, the accuracy requirement at the motor shaft then would be decreased to 4 degrees; and, similarly, for other speed reduction ratios. Positioning accuracy required of a direct-drive system would still be 0.05 degree.

The life requirement is a fundamental part of the operational instrument specification. If it is assumed that one BSU has to operate continuously for the entire two-year period, the scanner output shaft will experience an equivalent of 4×10^6 revolutions total. Geared-up parts of the system would experience correspondingly higher total revolutions; thus, for the case of an 80:1 speed-reduced system, motor total revolutions would be 3×10^8 revolutions.

Several systems which could meet the requirements are listed in Table II on the facing page. First is a 90-degree stepper motor with 80:1 harmonic-drive speed reduction. The next system--the Responsyn--is a variation of the harmonic drive principle wherein the rotating wave generator is replaced by the rotating magnetic field, and there is no physical high-speed shaft. The Responsyn is also a stepper. The third alternative is a stepper motor driving through conventional gears rather than the harmonic drive. Finally, the direct drive servo referred to would be a "pancake" type dc torque motor directly coupled to the scanner output shaft. It would have both rate and position feedback.

The following sections of this report will examine the alternative designs discussed above in detail.

TABLE I. SCAN DRIVE MECHANISM REQUIREMENTS

The derived requirements were established and taken as firm constraints on design.

SPECIFIED REQUIREMENTS	DERIVED REQUIREMENTS
Response Time	
• Step and settle in 1.125 degrees in 0.04 s	- Peak Motor Torque = 8 oz-in. - Avg Motor Torque = 2.6 oz-in. at 100 pps - Damping Ratio = 0.4 - 0.6
Accuracy	
• Each step +0.05 degree	
Repeatability	
• Start each successive scan line at same point ±0.05 degree	
Life	
• 2 years, + 2000-hr testing	- 3 x 10^8 revs at input shaft
Power	
• Less than 10 W average	- 30 W peak
Weight	
• Minimum possible, consistent with weight budget	- 2.5 lb

TABLE II. CANDIDATE SYSTEMS

Each system is analyzed in the next topic.

• Stepper Motor - Harmonic Drive	- Accuracy easily met; select system parameters to meet response time requirements
• Responsyn	- Equals performance of stepper/harmonic drive, but has no holding torque
• Stepper Motor - Gear Drive	- Difficult to meet accuracy requirements. Dynamics about same as those above
• Direct Drive Servo	- Mechanically simple, but heavy. Much system complexity to meet accuracy requirement

SUMMARY OF DRIVE MECHANISM COMPARISON

The stepper motor-harmonic drive design was selected for the scanner of its simplicity, low backlash, low weight, low wear, low stress factors, and power-off holding torque.

Several candidate designs for the TOVS-BSU scanner were compared to select the best design. The candidates were: a permanent magnet stepper-harmonic drive combination, a stepper driving through conventional gears, a direct-driving dc torquer type motor with feedback, and the "Responsyn" device, which also incorporates a harmonic drive.

Several selection criteria were used. Foremost was accuracy, since this is vital to instrument success. Both output accuracy and backlash were tabulated. System complexity is indicated by feedback requirements, electronic complexity, ball bearing count, and total electromechanical or mechanical device count. The best indicator of expected life is the stress on the mechanism; this was tabulated as contact stress in the speed reduction elements. Also examined were weight, whether or not application of electrical power was necessary to achieve holding torque, and potential lubrication problems.

Since each design can be made to achieve the desired characteristics, selection is based primarily on maximum reliability and maintenance of specified performance after two years in orbit. Quantification of these considerations was accomplished by weighting the selection criteria. Then, when the candidate designs were ranked, they could be "scored" by multiplying rank figures and weighted values of the criteria. The resultant figures are shown in the table on the facing page.

The geared stepper motor design has a number of drawbacks. The most serious one is questionable life due to the high Hertzian contact stresses in the gear teeth. This is a problem inherent in involute gearing which cannot be avoided in weight-optimized systems. Lubrication, too, promised to be a problem--the backlash requirement would dictate such a tight mesh that there would be no room for the copious lubricant films needed for good gear life. The gear drive was therefore disqualified.

There are three primary disadvantages to the direct drive, closed loop motor: excessive weight, system complexity, and high power consumption because of the control electronics required. The projected weight of this system was three to five times the projected weight of the other candidates; and there would be the need for an auxiliary angular rate feedback device to close the loop--a device not required by any of the other systems. Power must be kept on at all times to keep the servo loop locked. The direct drive system does, of course, offer mechanical simplicity; hence the need to consider it.

The Responsyn drive is basically a harmonic drive and stepper motor integrated into one device. There is no mechanical element to deform the flexible member; instead, this is accomplished by the rotating magnetic field of the electrical stator. The device is attractive for the same reasons that recommend the stepper-harmonic drive combination. However, it has one fault: there is no physical contact between the flexspline and its mating member except in the presence of electrical excitation, so that there is no power-off holding torque. In fact, this device would require continuous application of power, and this high power requirement is sufficient to disqualify this drive.

The remaining design--the combination of stepper motor and harmonic drive speed reducer--was the one selected. This system offers the best combination of performance, low weight and power, and favorable life factors. This subjective evaluation is reinforced by the "score" figures resulting from the numerical tradeoff exercise detailed in the table.

COMPARISON OF SCAN DRIVE CANDIDATE MECHANISMS

Only the open loop stepper-harmonic drive meets design objectives with acceptable weight, power, and projected life.

Criteria	Stepper Motor/ Harmonic Drive	Rank	Stepper Motor/Gear Train	Rank	Direct Drive w/Feedback	Rank	Responsyn	Rank	Relative Importance of Criteria
Accuracy	0.1 degree	4	0.1 degree	1	0.1 degree	2	0.1 degree	3	3
Electronic Complexity	low	4	low	4	high	1	low	4	3
Feedback requirements for 0.05 degree resolution	none used	4	none used	4	required	1	none used	4	2
Backlash	2 min	3	6 min	1	0	4	2 min	2	3
Total bearings required	8	2	10	1	5	4	5	3	1
Holding Power required	No	4	No	4	Yes	1	Yes	1	3
Weight*	2.5 lb	4	3.5 lb	3	8-10 lb	1	3.5 lb	3	2
Contact Stress	2,000 psi	3	30,000 psi	1	0	4	2,000 psi	3	3
Device Count	4	2	5	1	4	3	3		1
Potential Lubrication Problems	Minor	3	Severe	1	Minor	4	Minor		3
Total "Score"**	83	—	52	—	59	—	69	—	—

*Not including scan mirror
**(Rank) X (Relative Importance)

BECKMAN INSTRUMENTS, INC.
Advanced Technology Operations
J. C. Hammond

DESCRIPTION OF HARMONIC DRIVE

The harmonic drive is an aerospace proven power transmission device that uses the elastic properties of metals to effect a differential motion between engaging members and thus achieve a high velocity ratio. Its outstanding features are great torsional rigidity, and the ability to achieve a very high speed ratio without intermediate shafts.

Harmonic Drive - Harmonic drive 10 years ago by USM Corporation has been engineered for both industrial and aerospace/military applications, such as missiles, satellites, the Apollo Lunar Rover, and others. It is available in stock designs in a wide range of sizes.

An illustration of the harmonic drive principle is shown in Figure A. It consists of three primary elements: a flexible spline which appears as a normal gear, a circular spline which is similar to an internal gear, and a wave generator. The flexible spline is deflected by the wave generator into an elliptical shape and contacts the circular spline in two areas. Rotation of the wave generator causes the major axis of the ellipse to rotate. The resultant progressive meshing of flex spline and circular spline teeth leads to differential action, because of the differing tooth numbers. A slow rotation of the flex spline--that output member-- results. The direction of rotation is opposite to that of the wave generator.

The outward action of this assembly is identical to that of a differential epicyclic gear train. However, the harmonic drive's load carrying capacity is greater than for a conventional gear train because the load is carried at two opposite areas in the spline mesh and is distributed over a number of spline teeth at each area of contact. Unlike a gear which uses an involute profile resulting in rolling contact--which is necessary because of the relative motion between the mating teeth--the harmonic drive has essentially zero velocity at the point of contact. Therefore, where gear teeth have rolling action which is essentially line contact, harmonic drive teeth have area contact.

Because of the lower contact stresses and near-zero relative velocity between the flex spline and the circular spline (it is estimated that only a maximum of two percent slip occurs between the two members under full load), a more optimum lubrication system than for other drives is feasible. The circular spline can be gold-plated to provide a low-stress shear surface, and the mating teeth can be coated with a vacuum grease. A reservoir can be located adjacent to the gear mesh, assuring molecular flow across the meshing splines, support bearings, and out to the labyrinth seals.

Another advantage of the harmonic drive is that, since the flexible spline can be a non-rotating element, the stepper motor and wave generator can be packaged as a hermetically sealed unit, offering improved bearing life as a result of optimum lubrication techniques. This unique feature has been exploited in a number of applications.

One of the limitations of the harmonic drive is the tendency to seek a preferential position of the flexible spline. Due to residual stresses and grain orientation, the flexible spline tends to seek an elliptical position at a fixed angular location. Therefore, when the drive is stopped at some other position, there is a tendency to spring back. Since a permanent-magnet stepper motor is being used, the motor restoring forces will oppose the torque generated by the flexible spline. This torque input is a measurable value and is included in the harmonic drive specification to assure that the position accuracy is well within the allotted tolerance band. Typically, the maximum preferential positioning torque is 0.3 oz-in. or less.

An application of the harmonic drive to the BSU scanner is described in detail in the following topics.

Responsyn - Another harmonic drive device considered in the scan drive comparison was the Responsyn. This device is a variation of the basic harmonic drive, and is also made by the USM Corporation. It incorporates the harmonic drive into a stepper motor. The mechanical wave generator is replaced by a rotating magnetic field which flexes the internal spline. This greatly simplifies the assembly and provides a minimum weight actuator as well as the highest response and damping characteristics. The Responsyn, however, requires power to retain position, and the driving power and average holding power combined are excessive and exceed the allotted power budget.

1110-102-7

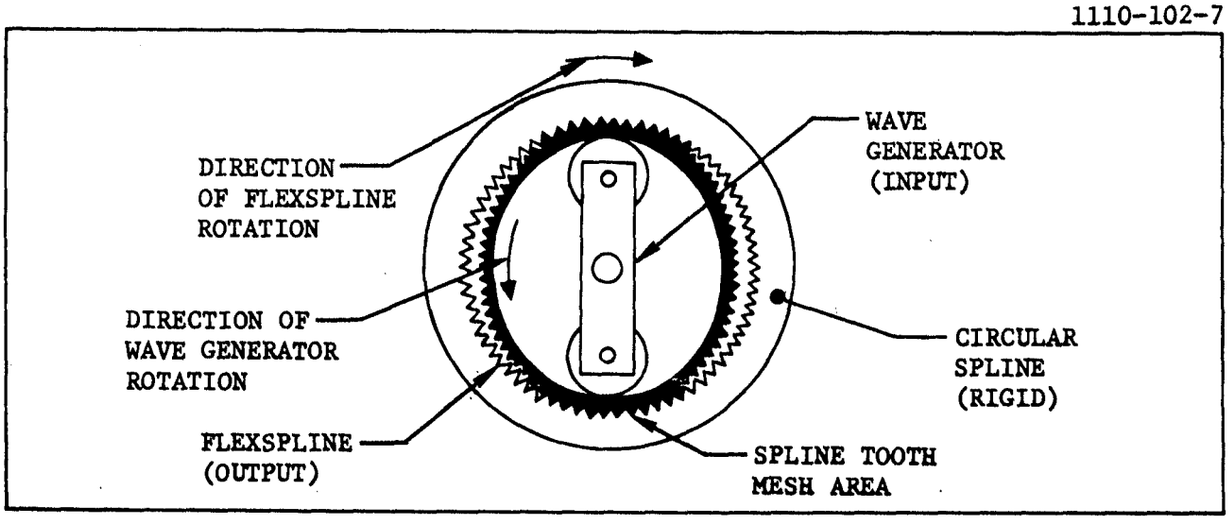

Figure A. Illustration of Harmonic Drive Principle. A small difference in the number of teeth on flexspline and circular spline causes slow CW rotation of flexspline when wave generator is rotated CCW.

1110-102-12

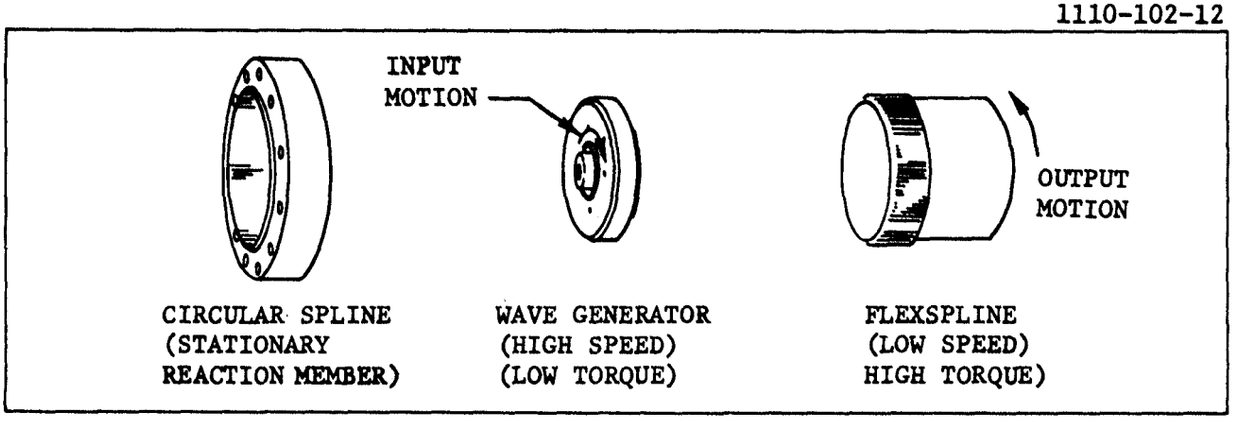

Figure B. Harmonic Drive Components. This figure shows a conventional high-inertia wave generator consisting of an elliptical bearing.

CHOICE OF SCANNER CONFIGURATION

Arrangement of the scanner components resulted in a simple axial design. The only tradeoff necessary involved the location of the encoder, which was located on the output shaft for phasing accuracy, size constraints, and negligible reflected inertia to the drive motor.

Several configurations were considered to provide a scanner which assured component alignment, minimum support structure (for weight considerations), and checkout of drive performance at final assembly.

The scanner has several design constraints derived from the instrument configuration and required by the harmonic drive.

- Size of the scan assembly--11.0-in. diameter by 16.5-in. length.
- Phasing of encoder and mirror.
- Motor load--reduce all inertia loads to the motor to enable use of minimum size motor.
- Provide for motor output torque tests.

The packaging constraints are shown in Figure A. Considering the space required for bearing and scan housing, only 3 in. are available for the motor and its support structure. This, in turn, becomes a constraint on selecting the motor and encoder. Selection of the harmonic drive permits all components to be located on a common axis, simplifying the structure and assembly.

A shaft encoder is required to read out mirror positions throughout the scan and calibration sequence. The 9-bit encoder, mirror, and instrument optical axis must be in phase to determine the viewing angle of the 1.125-degree field of view.

There are two possible locations of the encoder: on the output shaft, or at the motor. The encoder at the output shaft is a single disc multitrack unit. If located on the motor, the encoder either must be geared down to the same ratio as the harmonic drive or must use a multi-turn encoder. To keep the inertia loading at 10 percent or less of the motor requires a small diameter with more turns to resolve 9 bits. The typical size of a unit that will meet these requirements is such that the combined motor and encoder assembly could not be packaged in the available space.

One feature to be included in the operational scanner design is the ability to check motor performance after assembly and environmental testing. Access to the free end of the motor shaft is necessary to couple to a dynamic torque test fixture.

The drive assembly is shown in Figure B. The components shown were selected based upon the drive analysis described in the remainder of this section.

The detailed features of this layout are discussed later.

1110-102-14

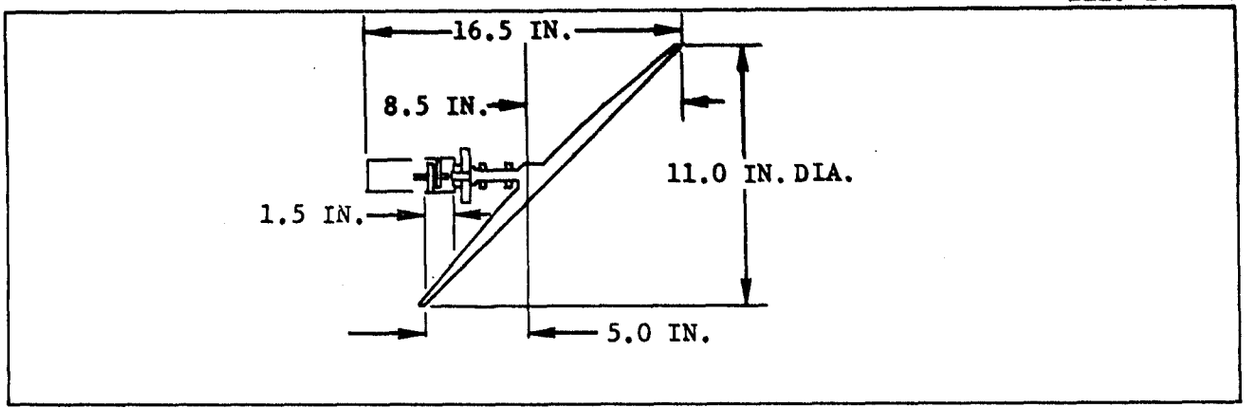

Figure A. Outline of Scan Drive Assembly Showing Packaging Constraints of Mirror, Harmonic Drive, and Motor.

1110-102-15

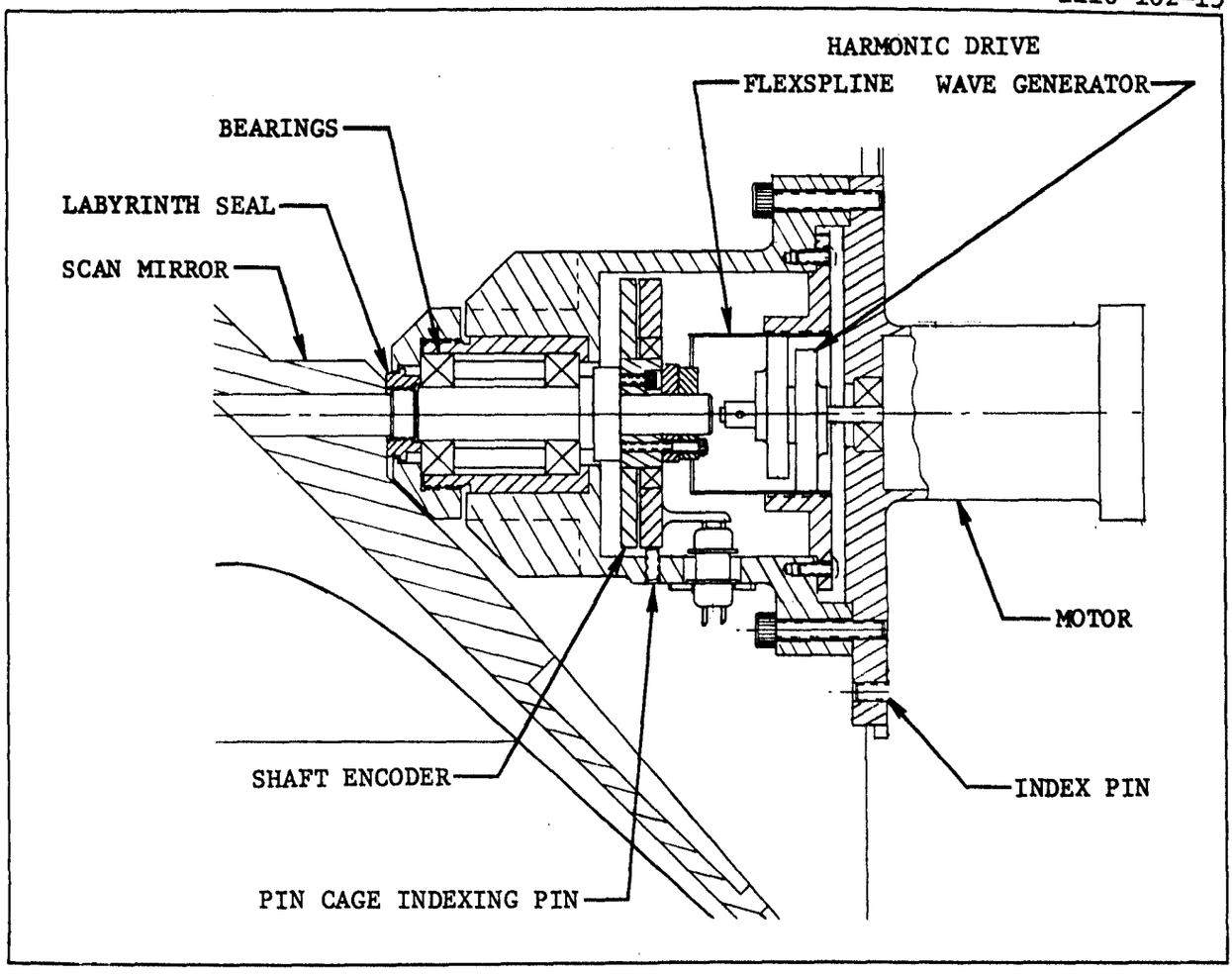

Figure B. BSU Harmonic Drive Scanner Mechanism

SELECTION OF MOTOR AND DRIVE RATIO FOR RETRACE

A permanent-magnet, 90-degree stepper motor with an output torque of 3.0 oz-in. at 100 pps and an 80:1 reduction ratio drives the mirror 81 degrees in 0.72 s, as required by the scan sequence. Selection of the motor, drive ratio, and step rate is based upon satisfying the calculated torque-speed curve.

Motor and Drive Ratio Requirements - The scan motor must drive the scan mirror under two different loading conditions. The step-dwell period requires the motor to drive the mirror 1.125 degrees in 0.05 s every 0.1 s and retrace 81 degrees in 0.72 s, or 1.125 degrees every 0.01 s. The retrace determines motor acceleration requirements, while the step-settling determines the damping. The mechanism is first designed to satisfy the retrace rate and then checked for damping characteristics.

Permanent-magnet stepper motors are available with either 45-degree or 90-degree step angles. For a mirror step angle of 1.125-degrees, drive ratios of 40, 80, 120, or 160:1 are required, with corresponding step rates (50, 100, 150, etc.).

Basis for Motor Selection - Selection of the stepper motor is based upon two requirements: (1) the torque required to accelerate the load, and (2) the average torque required to drive the load at a specific pulse rate. Although the retrace rate is 1.125-degrees every 0.010 s, the characteristics of the stepper motor do not require the motor to travel one step angle in 0.01 s to accelerate the load to constant velocity. It is necessary only to rotate through half the step angle during the first pulse. The next pulse will increase motor acceleration since the mass now has angular momentum in the direction of rotation. Typically the motor "locks in" at the pulse rate within two or three steps. This characteristic will reduce the motor torque required.

Determining Average and Peak Torque Requirements - The average torque required to drive the motor at 112.5 degrees per second is the difference between the acceleration and the equivalent torque provided by the angular momentum of the mass, as shown in equation (1). Added to this value are torques necessary to overcome friction and detent torque, as shown in equation (2).

$$T_{peak} = J\ddot{\theta} = \left[\frac{J_L}{(N)^2} + J_{W.G.}\right] \frac{\theta}{\left(\frac{t}{2}\right)^2} \qquad (1)$$

$$T_{avg} = T_{peak} - 1/2\ J_s\ \dot{\theta}^2 + T_F + T_{DT} \qquad (2)$$

where J_L = scan mirror inertia, $J_{W.G.}$ = wave generator inertia, $J_s = J_L + J_{W.G.}$ θ = motor step angle, N = drive ratio, t = time, T_F = friction torque, and T_{DT} = detent torque.

The results are plotted in the figure for a 90-degree step angle. For a 45-degree step angle and twice the step rate, the peak torques would double. The average torque would also increase.

Selection of Drive Ratio - A harmonic drive is used in the scan drive mechanism for drive reduction. The space and weight budgets necessitate selecting the smallest harmonic drive that will meet the required torque and drive ratio. However, a tradeoff must be made between required torque and drive ratio, since use of a higher drive ratio, and, therefore, a higher step rate,

requires less torque.

The required torque (based upon a step rate of 100 pps and a drive reduction ratio of 80:1) is well within the range of the smallest harmonic drive (size 1C). Although an increase in step rate and drive ratio would reduce the torque required to drive the scan mirror, an increase beyond the drive ratio range available for a 1C harmonic drive would require a larger harmonic drive, with a corresponding increase in weight, size, and wave generator inertia. Such an increase would provide no system advantage.

Selection of Motor - From the data presented in the figure, the selected drive ratio of 80:1 based upon a 90-degree stepper at 100 pps requires 8 oz-in. peak torque and 2.6 oz-in. average torque. Motors are available that meet or exceed these requirements; e.g., the 15 P-03 from Computer Devices. The ratings are for single-phase drive at 28V.

1110-102-1

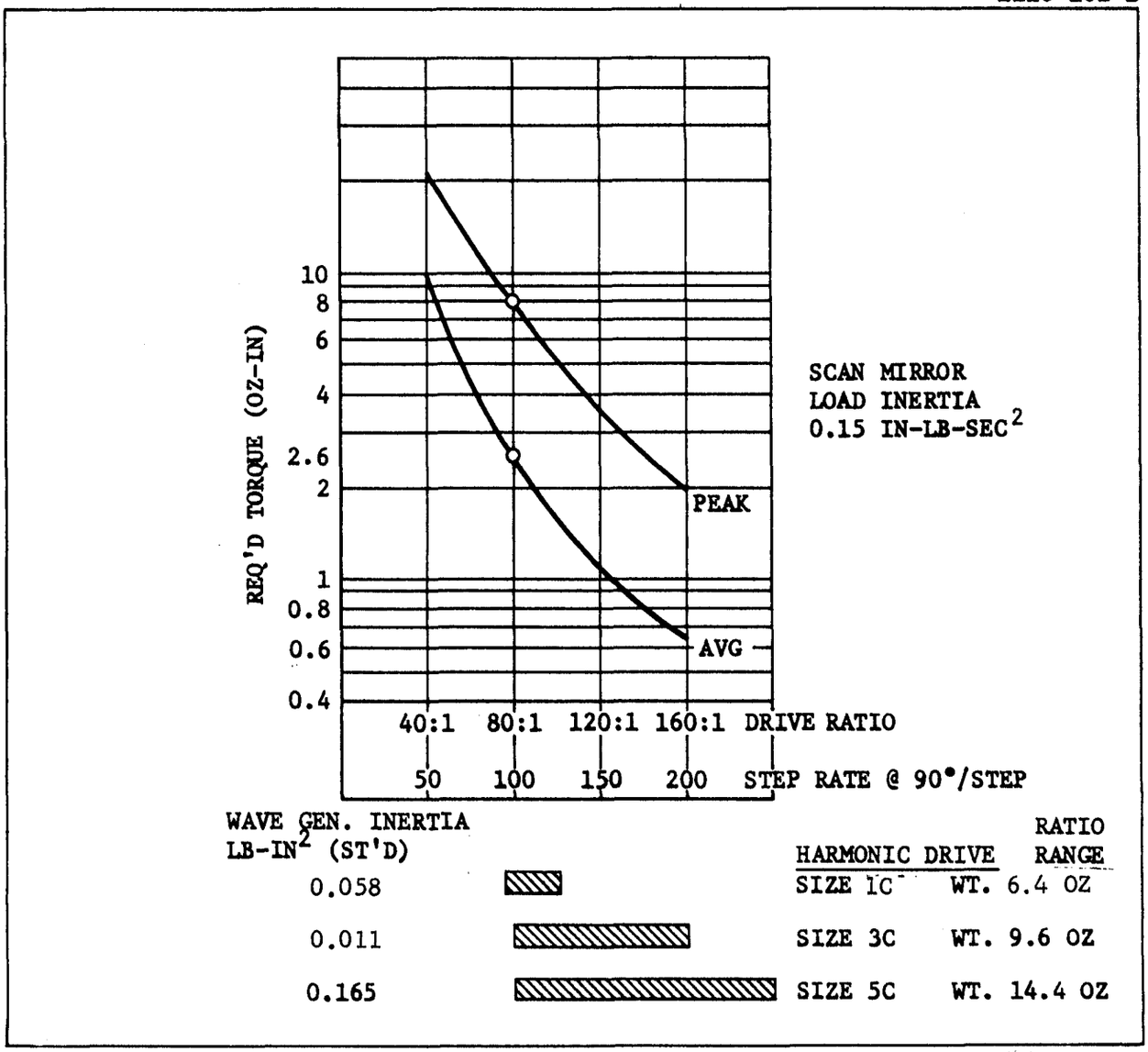

Required Torque - Speed Curve to Drive Scan Mirror During Retrace Period. Selection of reduction ratio, step rate, and drive size can be determined from the data presented.

APPROACHES FOR CONTROLLING THE SETTLING CHARACTERISTICS

To achieve the desired response with minimum weight and power, the characteristic response curve of the step dwell period should be underdamped, with the last crossover of the ±0.1 degree error band occurring before 50 ms. To control the settling characteristics, the slope of the motor performance curve can be selected to provide the required damping. Other possibilities are modulation of the applied voltage or the use of dynamic braking.

A motor capable of driving the load at the 100-pps retrace rate can obviously single-step in 0.05 s. How the rotor arrives at its final position (1.125 degrees) is dependent upon the damping. The response curve can be any shape between the underdamped and the critically damped curve and even slightly overdamped if the angle is within the error band at 0.05 s. From typical curves plotted in Figure A, only an underdamped response similar to curve B (which also travels approximately half the step angle in 0.010 s) can be considered, unless the torque, weight, and power are unnecessarily increased.

The motor torque-speed curves corresponding to the response curves are shown in Figure B. The motor must provide the acceleration and average torque requirements shown by curve B. The motor performance curve is a function of the air gap only (assuming all other parameters are the same). The smaller the air gap, the greater the magnetic coupling between stator and rotor, which produces a higher stall torque and detent torque. The maximum step rate is reduced since the higher detent force reduces motor output torque.

The scanner drive damping is a function of velocity dependent parameters such as the slope of the torque-speed curve, viscous damping, and external electronic circuit features (e.g., dynamic braking, retro-torquing, and modulation of the applied voltage during the single-step period). The damping sources are listed in the table below.

A model of the motor load combination describing the motion and damping characteristics is required. Once confirmed by analysis, a drive breadboard can be assembled and tested.

DAMPING SOURCES

• Motor Damping Factor*	- (in-oz-s/rad)
• Viscous Damping	- Not predictable; should be less than 10% of total damping to avoid changes in response.
• Dynamic Braking*	- All motor windings are grounded after power pulse to dissipate currents generated from the rotor magnetic field.
• Retro-Torquing	- Momentarily applying a reverse pulse to the last phase to limit overshoot.
• Controlled Velocity Gradient*	- Applies voltage modulation within the 0.050-s period to control motor velocity, reducing overshoot.

*The motor damping factor can be selected, and the dynamic braking and controlled velocity gradient are readily implemented.

1110-102-2

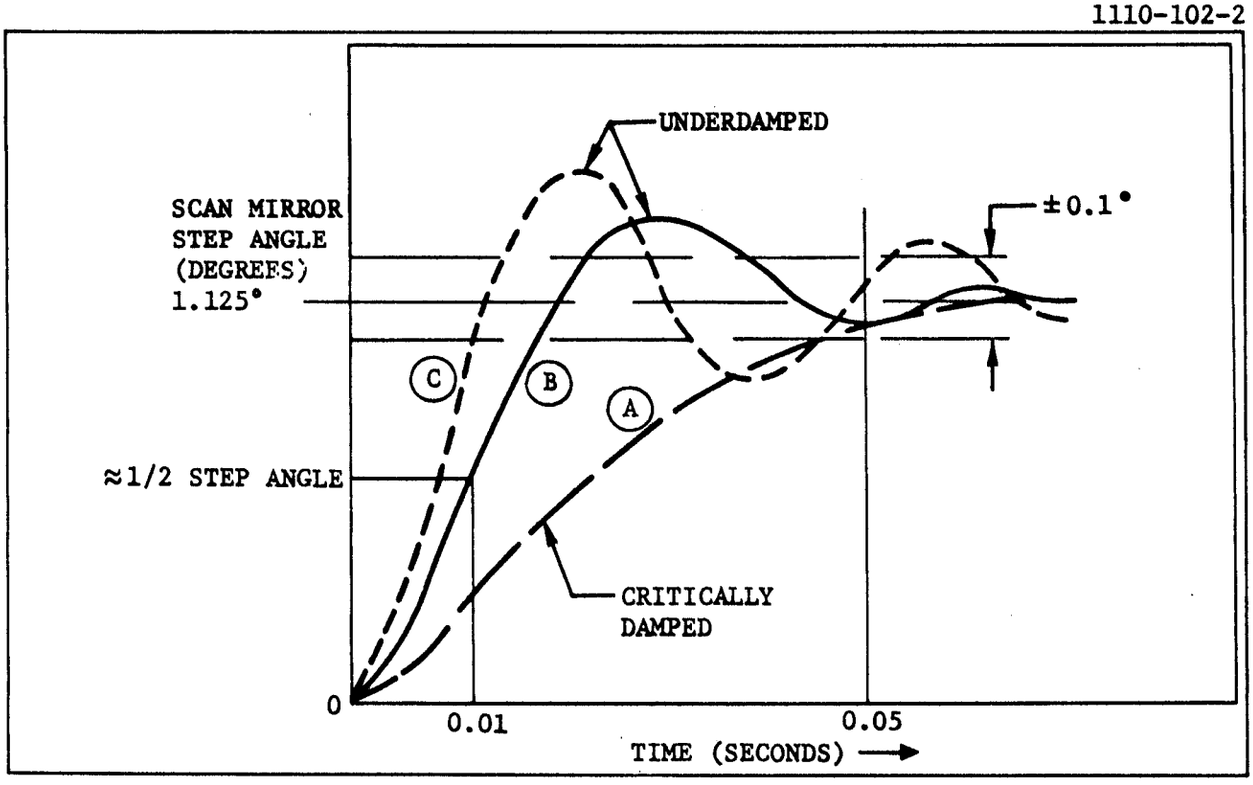

Figure A. Scan Mirror Response Curve Relating Settling Characteristics and Acceleration for Retrace.

1110-102-3

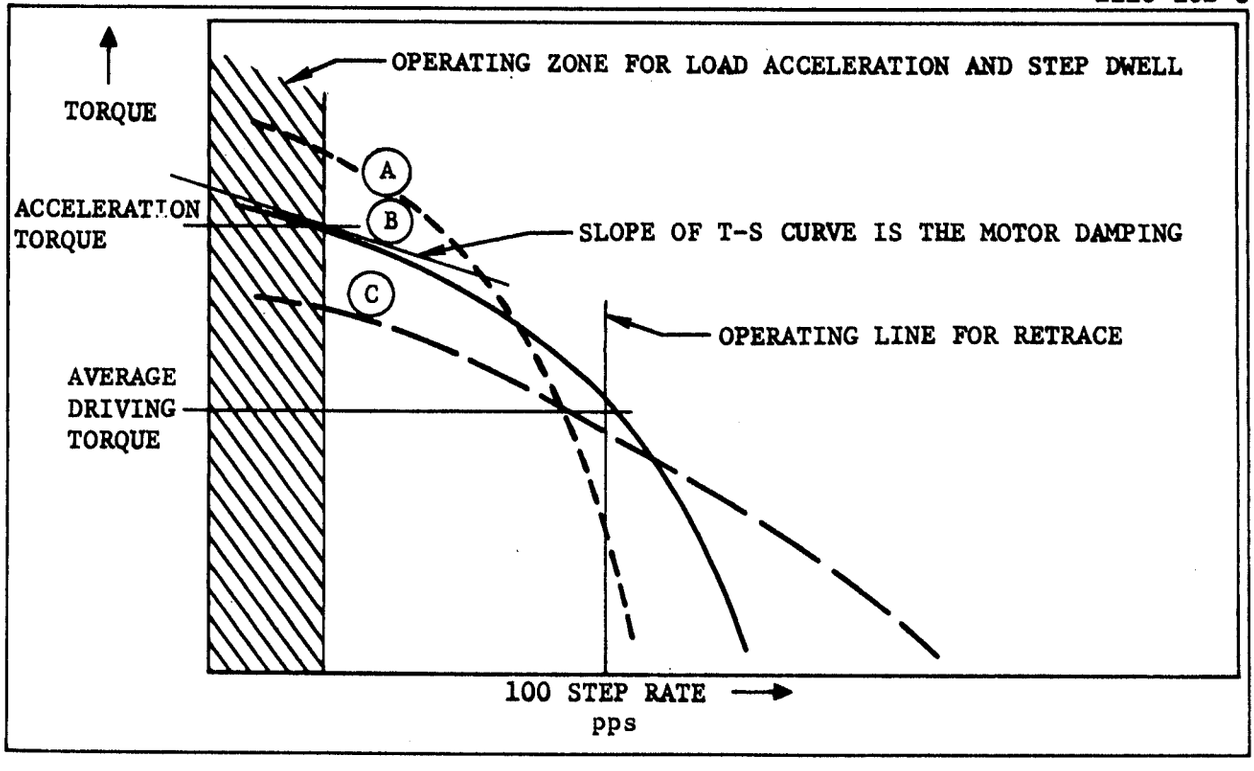

Figure B. Typical Motor Torque-Speed Performance Curves Slowing Relative Behavior. The motors are identical except for air gap.

MATH MODEL DESCRIBING SCANNER MOTION

A linearized second order equation describing the step settle motion of the scanner was developed on the ITPR program. The model predicted performance within 10 percent of test data. A similar analysis of the BSU scanner shows that the selected motor and harmonic drive are capable of driving the scan mirror and meeting the single step response and retrace rate.

The math model is used to determine whether a specific motor will meet the step-dwell requirements. The scanner breadboard will establish actual operating conditions.

The model is based on the equation of motion of the motor shaft (symbols are defined opposite):

$$J\ddot{\theta} + F\dot{\theta} = T_o \tag{1}$$

As soon as the motor rotates, the motor generates a reverse torque. Therefore, the output torque, T_o, is equal to the applied torque minus the restoring torque

$$J\ddot{\theta} + F\dot{\theta} = T_M - T_R \tag{2}$$

Substituting motor characteristics

$$JR\ddot{\theta} + FR\dot{\theta} - K_tE + K_tK_e\dot{\theta} + K_rR\theta = 0 \tag{3}$$

This is

$$\ddot{\theta} + \left(\frac{F}{J} + \frac{K_t K_e}{JR}\right)\dot{\theta} + \frac{K_r}{J}\theta = E\frac{K_t}{JR} \tag{4}$$

This second order differential equation is the same as that of the common spring-mass-damper system. In operational form, the step response is

$$\theta(s) = \frac{1}{s}\left[\frac{E\frac{K_t}{RJ}}{s^2 + \left(\frac{K_tK_e + FR}{JR}\right)s + \frac{K_r}{J}}\right] \tag{5}$$

Of all the model parameters, only the small viscous damping component of the damping factor is unknown. Estimates from the past test data were used for this parameter. The 1/s term is the transform of a step input. The denominator represents the characteristic form

$$s^2 + 2\zeta\omega_n s + \omega_n^2 \tag{6}$$

where ω_n is the natural frequency and ζ is the damping factor. From this equation we can calculate the response to a step input and determine the damping factor ζ required of the motor. The required damping factor is 0.4 or greater. With the motor characteristics substituted in the denominator of equation (5), the natural frequency and damping can be calculated.

The math model is for the continuous power condition only, but is a good, worst-case approximation of the motor dynamics. How the response curve is modified with voltage modulation is dependent on the duty cycle, detent torque, and dynamic braking.

DEFINITION OF SYMBOLS USED IN TEXT

s	Laplace transform variable (complex frequency)
J	total system moment of inertia at the motor shaft
θ	angle of rotation of motor shaft (dot indicates time derivative)
F	viscous damping constant
E	applied voltage
T_o	total torque
T_M	applied torque
T_R	restoring torque
K_t	applied torque constant
K_e	electrical damping torque constant
K_r	restoring torque constant
R	winding resistance
ζ	damping factor
ω_n	undamped natural frequency of oscillation

1110-102-4

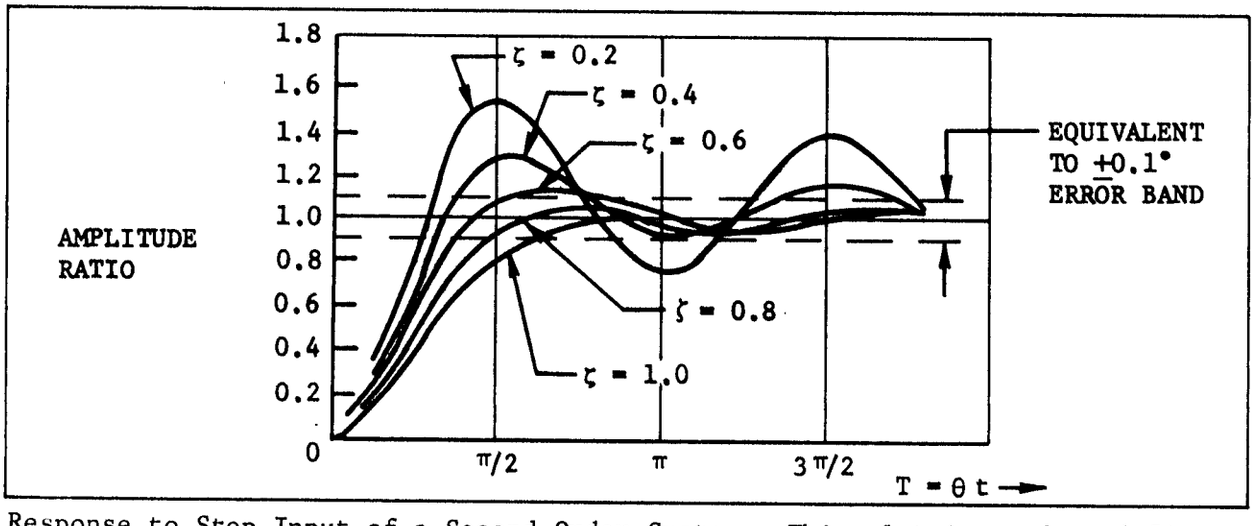

Response to Step Input of a Second Order System. This plot is used to define the minimum damping required to settle.

PERFORMANCE PREDICTIONS BASED ON THE MATH MODEL

Using the math model and the characteristics of a commercially available size-15 stepper motor driven in a single-phase series mode, the behavior of the scanner is predicted to meet the step and settle, and retrace requirements.

The transform of the motion equation developed in the previous topic must be corrected for a single-phase series drive, since motor constants are tabulated assuming single-phase center-tapped operation. The winding impedance is doubled, changing the motor constants proportionally to obtain the transformed step response:

$$\theta(s) = \left[\frac{E}{s} \quad \frac{2\,\frac{K_t}{J}}{s^2 + \left[\frac{K_t K_e + FR}{RJ}\right] 2s + \frac{2K_r}{J}} \right]$$

In this equation, E is the applied voltage. Other symbols are defined in the table. The selected motor performance curve and characteristics are shown in Figure A. The corresponding natural frequency and damping are given by

$$\omega_n^{\,2} = \frac{2K_r}{J}$$

$$\zeta = \left[\frac{K_t K_e + FR}{RJ}\right] \left(\frac{t}{2K_r}\right)^{1/2}$$

Substituting the motor parameters given in the table leads to a value of ω_n = 109 s^{-1} and ζ = 0.43, close to the values desired.

The solution of the transfer equation was done with the G.E. Time Share program "Laplace Transform Inversion." The program computes the response in the domain of a linear system whose Laplace transform is as the ratio of two polynomials. The calculated response curve is shown in Figure B. The curve shows that the motor will accelerate the load to constant velocity within a few milliseconds and is damped to within plus and minus 0.1 degree in less than 50 ms. At the retrace rate of 100 pps, the motor will be capable of driving the scanner at 157 rad/s average velocity measured at the motor shaft.

This analysis is based on the assumption that motor power is kept on during the entire 100-ms step interval. Power can be removed during the step at the point where the acceleration is zero, to be reapplied just as the desired angle is reached. It can then again be removed after the mirror settles within the desired error band.

MOTOR PARAMETERS

K_t = torque constant = 0.246 in.-lb/A (per phase)

K_e = electrical damping constant = 0.1115 V/rad/s

K_r = restoring torque constant = 0.2185 in.-lb/rad (per phase)

J = total inertia = 30×10^{-6} in.-lb-s^2 (includes rotor and wave generator inertia and reflected mirror inertia at the motor)

R = winding resistance = 20 ohms per phase

F = damping constant = 8.7×10^{-4} in.-lb-s/rad (slope of the motor response curve at acceleration torque)

1110-102-5

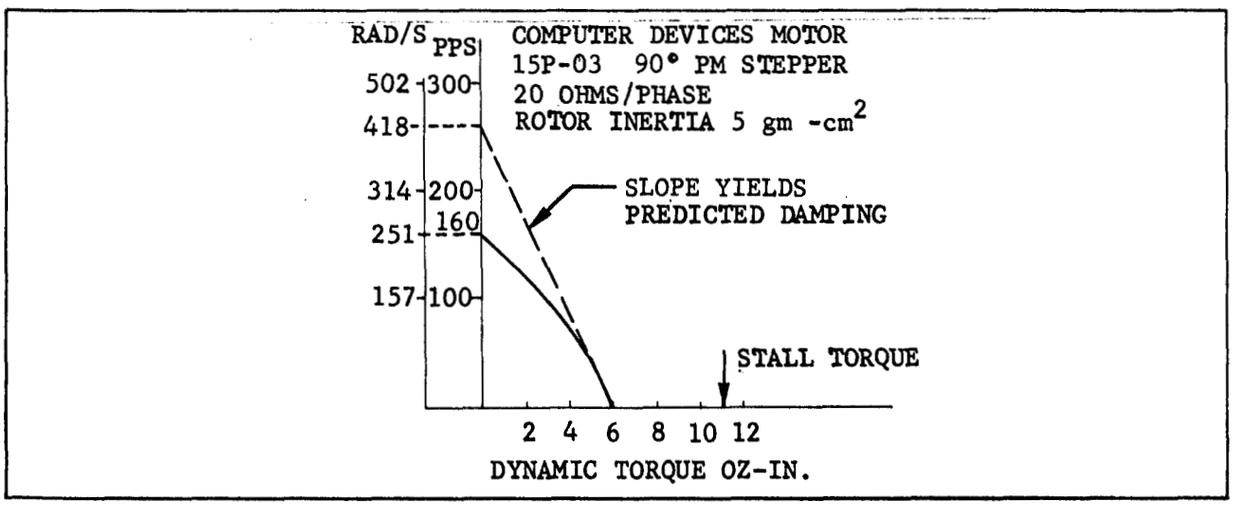

Figure A. Motor Performance Curve at 28-V and Single-Phase Excitation

1110-102-6

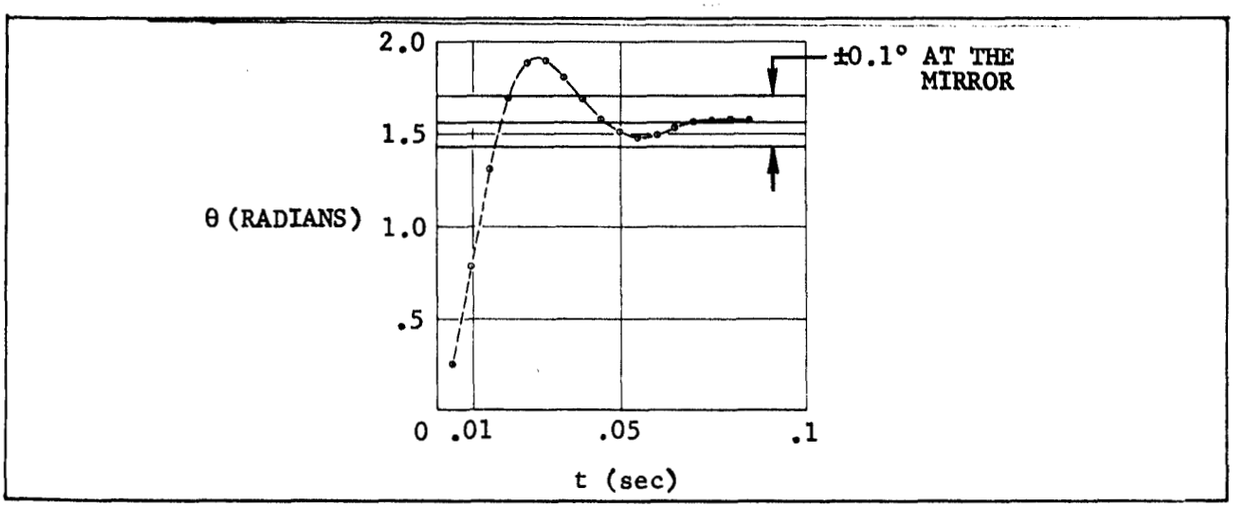

Figure B. Calculated Single-Step Response of the 90-Degree Stepper Motor. The amplitude ratio of 1.22 corresponds to a damping factor of 0.42 (minimum required value).

SUMMARY OF SCANNER BREADBOARD TESTING

The BSU scanner breadboard was constructed to investigate the dynamics of the selected scanner. The scanner mockup tests demonstrated that the scan assembly is capable of meeting operational flight performance, and confirmed the performance analysis.

Construction and testing of a laboratory mockup scanner device (scanner breadboard) was required as part of the TOVS-BSU design study. The objectives of the breadboard testing were to demonstrate system transient response, simulating dynamically important scanner characteristics such as inertias, motor torque, and system damping. Another objective was to verify scanner system power requirements and to define the optimum scanner drive circuit and drive waveform.

The scanner mockup consisted of a size-15 motor having the approximate performance characteristics required, a standard harmonic drive unit of the proper size (although with different ratio), a balanced mass to simulate mirror inertia, and a resolver to permit readout of output shaft position. The drive circuit used was a breadboard version of the flight drive circuit design. Mode of operation of the driver circuit was single phase, with full winding excitation at 28 V. Details of the scanner breadboard hardware and drive circuit are presented in a later section.

A comparison of the test performance versus the calculated response is shown in the table. The acceleration, velocity gradient, and crossover compare very well. The peak amplitude and damped response differ and can be attributed to the difference in the time period that power is applied to the motor. The math model assumes power applied continuously. The mockup test was run with power applied only during the first 10 ms.

A recording of an isolated step dwell period during the scan sequence is shown in the figure. Power was applied only for the first 10 ms. The damped response is attributed only to the magnetic detent and viscous damping of the motor and wave generator bearings. This test data was from the latest drive modification, which incorporated a double-eccentric wave generator rather than the standard elliptical bearing configuration. Earlier tests with the standard wave generator resulted in a severely underdamped response with out-of-band overshoots occurring well beyond 50 ms. The high inertia load also limited retrace rate to 85 pps.

Design verification by actual test, as was done with the BSU scanner breadboard reinforces the confidence resulting from a rigorous design analysis. Potential problem areas as well as areas where further improvement may be achieved are spotlighted, and the detail design approach that must be taken to insure good quality and manufacturing characteristics is made more clear.

CALCULATED DATA VS. TEST DATA FOR SCANNER MOCKUP

	Calculated	Test Data
Velocity Gradient	117	100
First Crossover	17 ms	27 ms
Peak Amplitude	1.9 rad	1.78 rad
Damping Ratio	0.6	0.8
Settling Time	40 ms	50 ms

1110-102-16

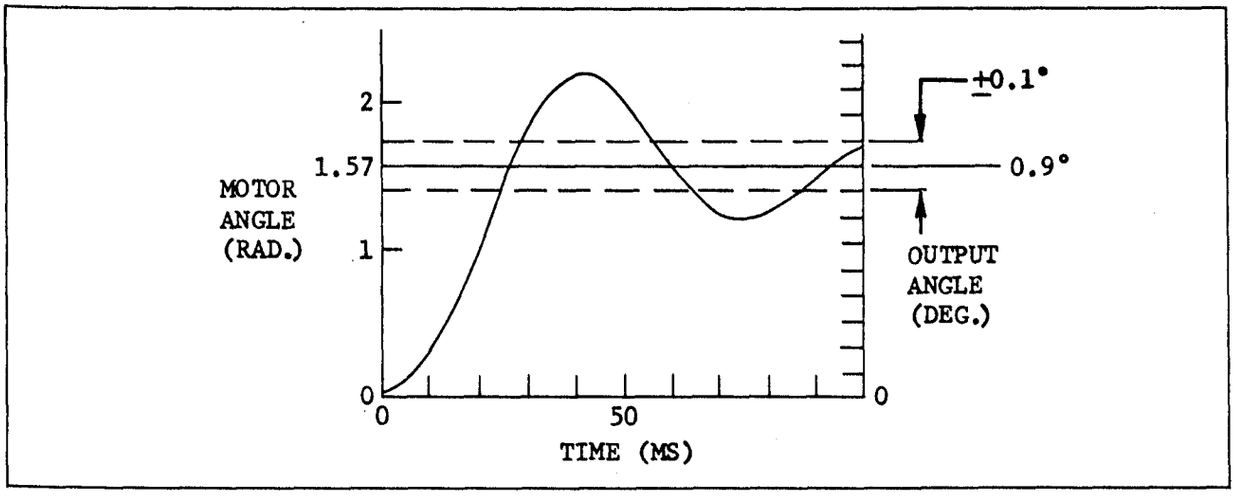

Figure A. Response of Mockup Scanner With Standard Wave Generator

1110-102-17

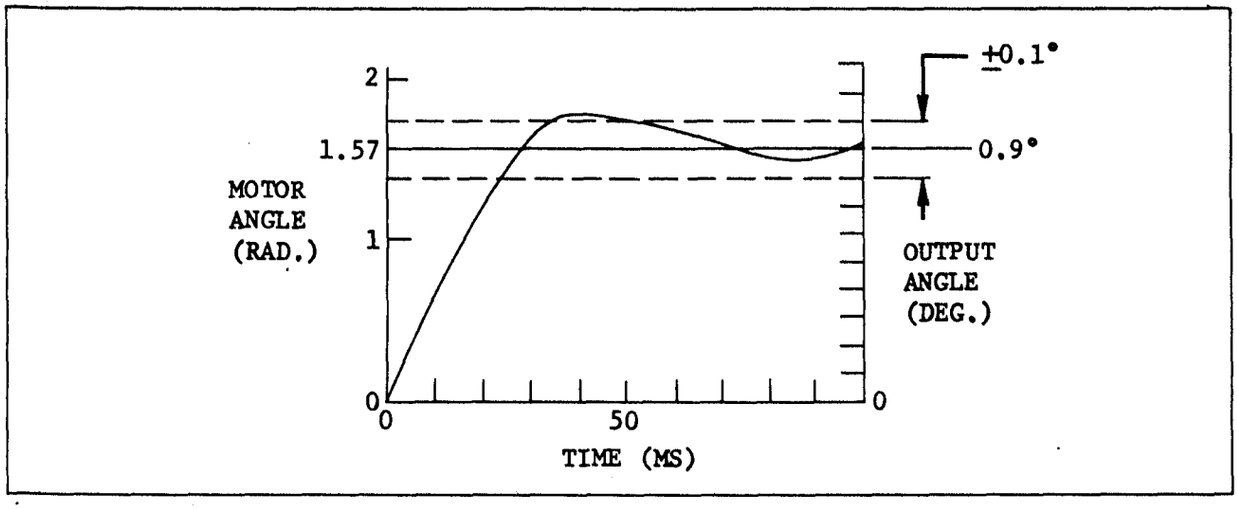

Figure B. Response of Mockup Scanner With Low-Inertia Wave Generator

MECHANICAL LAYOUT OF THE SCANNER

The BSU scanner assembly consists of a coaxial arrangement of the scan mirror, shaft, encoder, harmonic drive, and scan motor--preassembled into a cylindrical aluminum housing that mates with the instrument frame. In addition to being simple, lightweight, and economical of space, this arrangement is easy to assemble.

The layout of the scanner assembly is shown in the figure on the facing page. Note that the scanner housing utilizes space that would otherwise be wasted because of the mirror configuration. The cantilevered aluminum housing which supports the whole assembly has mounting surfaces for the shaft support bearings and the motor mounting flange, and contains the harmonic drive and the encoder in the completed assembly.

The scan mirror, shaft encoder, and flex spline of the harmonic drive are mounted to the mirror shaft. The scan mirror and shaft encoder are located on opposite ends of the mirror shaft by Woodruff keys precisely aligned with respect to one another. The scan mirror is secured by a roll pin; the shaft encoder by three screws. The mirror shaft is supported in the scan mirror subassembly housing by ball bearings that are preloaded by two sleeves threaded to the shaft and the housing hub. Preloading is against precision spacers and is therefore insensitive to the torque placed on the sleeves.

The shaft encoder is indexed to the housing by means of a pin cage indexing pin installed from without the housing. The pin contains a spring to limit excessive loading of the mirror shaft bearings. The scanner housing does not mate directly to the instrument frame, but rather to the large flange on the front of the stepper motor. This flange is provided directly on the motor housing in order to improve concentricity between the motor and the harmonic drive, and to promote good heat transfer from the motor to the instrument frame.

The wave generator used in the scanner is not the elliptical-bearing type which is standard for these units, but a special eccentric, double-roller type. In addition to offering greatly reduced inertia as well as the resultant dynamic performance advantages that have been discussed, this wave generator design is also somewhat easier to assemble into the flex spline.

When the wave generator is inserted into the bore of the flex spline, it must be determined that proper assembly has taken place, since the fine-pitch teeth could engage plus or minus one tooth from the theoretical elliptical center line. Operating the drive in this condition for a prolonged time would destroy the teeth. The drive is checked by recording the torque over several revolutions. The peak torque recorded should be equal to the motor detent torque. Peaks greater than 50 percent of the detent torque indicate improper operation of the drive; and it must be disassembled, checked, and reassembled.

1110-102-18

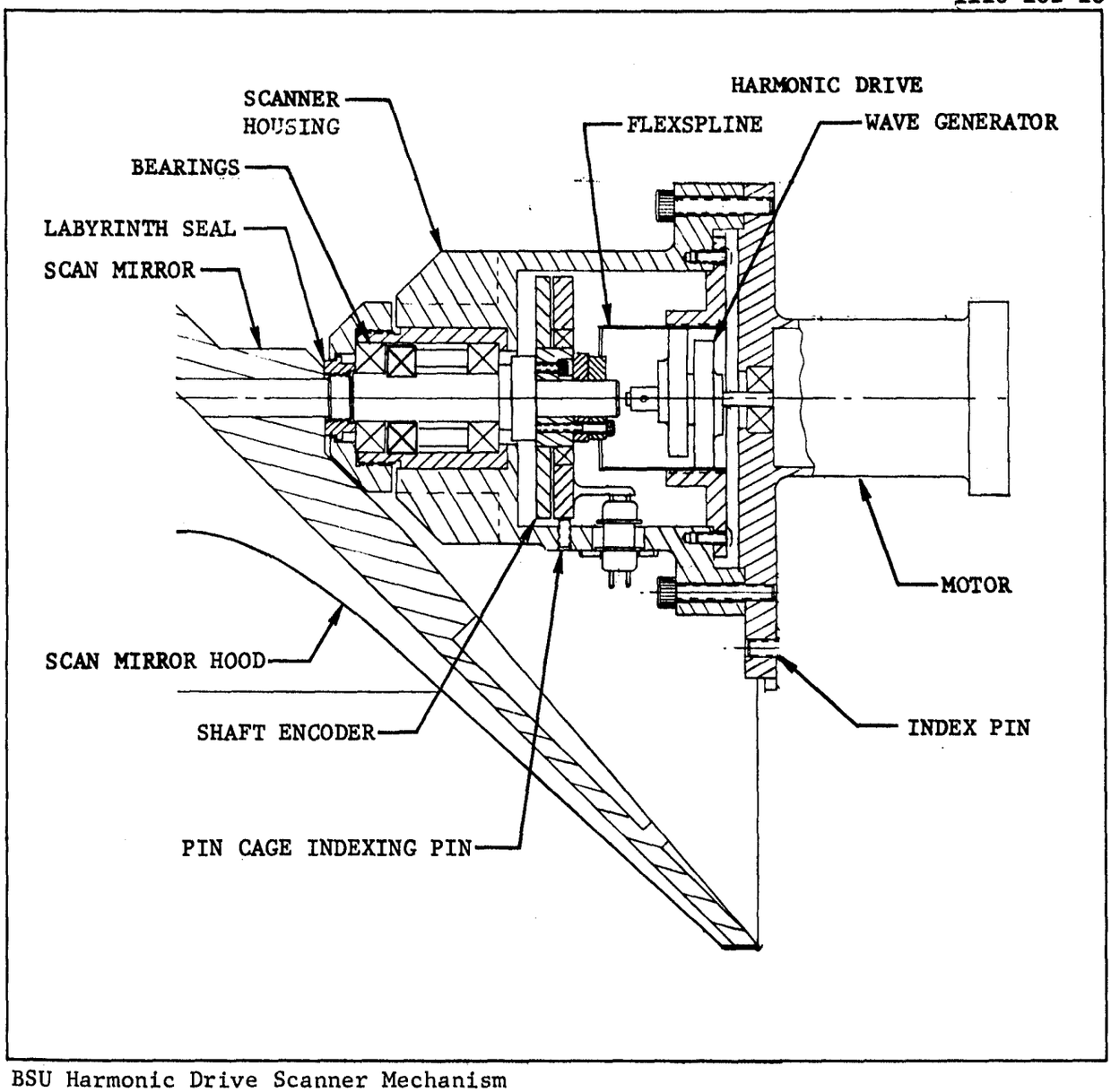

BSU Harmonic Drive Scanner Mechanism

ESTIMATES OF PHYSICAL CHARACTERISTICS

The BSU scanner fits within the overall instrument layout and meets the derived requirements of space envelope, weight, and power.

In the instrument weight budget, 3.06 lb was allotted to the scanner subsystem, exclusive of the scan mirror and sunshield. This total weight is comprised of the individual component weights listed in the table.

Scanner drive power has been discussed extensively in this report. A goal of 10 W for the average motor power was set in the study. This goal has been met, since the average power is only 7.7 W.

The scanner's instantaneous uncompensated angular momentum about the spacecraft roll axis is 0.0375 lb-in-s for the step-dwell phase; and 0.375 lb-in-s for the retrace, or slewing, phase. Over any 8-s multiple of step-dwell and retrace operation, this integrates to zero, since the period of oscillatory motion is 8 s. Every 256 s there is a calibration sequence, however, and at that time the scanner output shaft describes a complete revolution. Each calibration sequence, therefore, results in an increased angular momentum to the instrument; but this momentum, in turn, can be used against the steady opposite rotation of the chopper disc to yield a decreased momentum to the spacecraft.

An alternative approach, which would result in a zero long-term angular momentum input, is to slew back from the calibration positions to the scan sector rather than to describe a complete revolution. The total angular movement is greater for this scheme, so that time must be taken away from the calibration dwells. Each calibration would then be 2.0 s rather than the 2.4 s available with the scan program discussed above.

Pertinent parameters of the scanner's electrical drive circuit are shown in the table.

ESTIMATES OF BSU SCANNER PHYSICAL CHARACTERISTICS

Long-term angular momentum input to the instrument from the scanner depends on which way the calibration functions are mechanized.

WEIGHT

Component	Weight	Source*
Motor	0.62 lb	M
Harmonic Drive	0.20 lb	M
Encoder	0.38 lb	E
Output Shaft	0.24 lb	C
Output Bearings	0.24 lb	M
Structure	1.38 lb	E
Total	3.06 lb	

*M - Manufacturer C - Calculated W - Weighed E - Estimated

UNCOMPENSATED ANGULAR MOMENTUM - LONG TERM

With continuous rotation thru calibration positions 0.375 lb-in-s*
With reversed rotation to and from calibration positions -0-

* Occurs 1.25% of the time. Averages to 0.0007 lb-in-s

ELECTRICAL DRIVE

Drive Efficiency
Size 3.0 in. dia. x 0.5 in. long
Weight 3.2 lb

SELECTION OF FLIGHT SCANNER COMPONENTS

The TOVS/BSU scanner component performance specifications and characteristics have been selected to assure performance demonstrated by the scanner mock-up. Component qualification testing and screening at specified environmental conditions are required to assure a scanner which will meet all flight acceptance tests and provide a high degree of confidence of operating for two years in orbit.

One purpose of the scanner mock-up was to assist in defining components. In addition to verifying scanner dynamic performance, breadboard testing helped determine component sizes. Analysis was also used to achieve the same purpose, so that there was a rational basis for sizing and specifying all components.

Scanner breadboard testing showed that a size-15 stepper motor and size-1C harmonic drive are adequate for the BSU scanner. The motor and system dynamics, and the input inertia were the governing factors in the selection; and the same physical sizes of motor and drive as were used in ITPR are adequate also for the BSU scanner. Motor and harmonic drive specifications are shown in the table.

The motor specification shows a 90°-step, size-15 unit. This is a common configuration, and describes the motor used in mock-up testing. The specified power value of 10 W average power maximum was bettered by 15 percent in testing; and the specified weight by 17 percent.

The harmonic drive unit easily meets specifications. Power and torque capacities are much greater than needed in the application. A specification applied to the harmonic drive which could be met only with difficulty -- if at all -- by alternative devices is that of backlash. The specified value is two minutes of arc. This is achieved by extra tight control of the spline tooth manufacturing processes at USM Corporation, and will be verified for each delivered unit by screening.

The encoder specified is a 7-bit, pin-contact type.* Because the count interval and accuracy requirements are easily met with current technology, the most significant specified values for the encoder are the environmental parameters.

Imposed environmental testing conditions are the same for all scanner components. Some conditions, such as acceleration and vibration, are given as part of the NESS specification. Others, notably temperature, result from the analytical work accomplished as part of the study. The thermal design study predicted temperatures that will occur in various areas of the instrument. Values substantially in excess of the predicted temperature extremes ($31^{o}C$ to $43^{o}C$ operating) are specified for testing. The NESS specification indicates an ambient pressure of 5×10^{-5} torr or less. This value is increased to 10^{-6} torr, since this vacuum can be achieved for testing and results in a more realistic test.

In addition to the considerations discussed above, detailed component specifications will include the necessary workmanship, manufacturing control, traceability, and quality assurance criteria. Detailed component specifications are included in an appendix to this report.

---

* The 7 bits are used to encode the positions in the 72-scene scan line as well as the housing and space look. The resolution of the encoder is 1.125 degrees. Spare positions are used for flagging the neighborhoods of the scan and housing look so that an overshoot cannot confuse the logic.

SUMMARY OF BASIC SOUNDER UNIT SCANNER COMPONENT SPECIFICATIONS

Motor	
Type	Permanent Magnet, 90° stepper, Size 15
Operating Voltage	28 V dc
Power	10 W average power max.
Weight	12 oz.
Speed Reduction Drive	
Type	USM Corporation Harmonic Drive, Size 1C
Weight	6 oz.
Ratio	80:1
Backlash	2 arc minutes
Encoder	
Type	Pin Contact
No. of Tracks	7
Count interval	1.125 degrees
Environmental Specifications - All Components	
Pressure	10^{-6} torr
Temperature	$-25^{\circ}C$ to $+ 70^{\circ}C$
Acceleration	22 G (non-operating)
Vibration	Sinusoidal 10g 5-2000 Hz Random 20 g rms @ 0.2 g^2/Hz 20-2000 Hz

STRUCTURAL PROBLEMS IN THE SCANNER

Analysis has shown that safety factors provide the answers to structural problems in the scanner subassembly. The potential problems were the stress and deflection in the mirror sun-shield and the mirror shaft, stresses in the harmonic drive flexible element, and ball-bearing stresses.

The mirror sun-shield is a thin aluminum cylindrical shell. It is subject to possible stress problems under vibration and acceleration. Analysis shows the maximum stress in the sun shield to be 35,000 lbf/in^2; and the material strength is 70,000 lbf/in^2, giving a strength safety factor of 2.0.

The mirror shaft and bearings are stressed under environmental loading. Accordingly, this area was checked for bending stresses in the shaft and possible vibration overloading of the ball bearings. It was found that the maximum bending stress in the stainless steel shaft is 23,700 lbf/in^2. Since the allowable yield value is 275,000 lbf/in^2, the yield strength safety factor for the scanner shaft is 11.6.

Structural analysis of the scan mirror bearings showed that there was danger of the bearings being overloaded during vibration testing, a condition caused by the growth of the mirror to meet the thermal design. Consequently, the design was changed to show a tandem pair of angular contact bearings at the front of the scanner drive housing (nearest the mirror), and a single bearing at the rear. The highest bearing load under worst vibration conditions is 520 pounds, and the load rating for the tandem pair is 1,310 pounds; therefore the stress safety factor is 2.5 for these bearings.

An area of concern, but one which actually is not a problem, is the flexing member of the harmonic drive. Over the two-year design life of the instrument, this member will undergo 3.3×10^8 cycles of reversed loading as the wave generator rotates inside it. The implications of this are best explored by using the manufacturer's data, which is shown in the figure opposite. Here it can be seen that the operating point is safely below the failure curve, and safety factors are generous.

SCANNER STRESSES AND SAFETY FACTORS

Safety factors are equal to or greater than 2.0 in every case.

Component	Maximum Stress Factors	Rated or Allowable Factors	Safety Factor
Mirror Sunshield	35,000 lbf/in^2	70,000 lbf/in^2	2.0
Mirror Shaft	23,700 lbf/in^2	275,000 lbf/in^2	11.6
Shaft Bearings	520 lb	1,310 lb	2.5
Harmonic Drive Flex Spline	16.4*	60	3.7
Wave Generator - Bearing Life	3.3×10^8	7×10^8 rev	2.1

*Torque Constant - Derived Quantity

1110-102-35

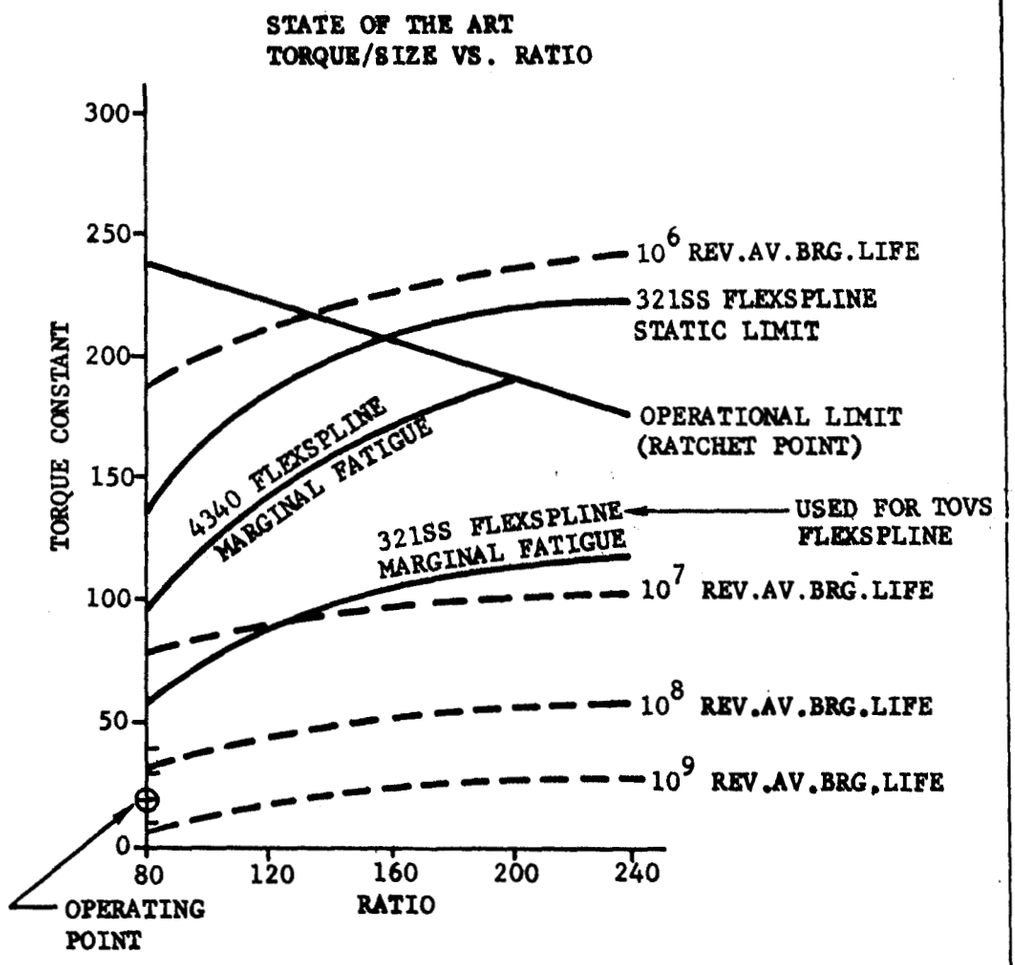

$$\text{TORQUE CONSTANT} = \frac{\text{TORQUE (IN-LB)}}{(\text{PD})^3\ (\text{IN}^3)}$$

WHERE PD = PITCH DIAM (1.4 IN. FOR BSU

$$\text{FATIGUE SAFETY FACTOR} = \frac{60}{16.4} = 3.7$$

$$\text{BEARING LIFE SAFETY FACTOR} = \frac{7 \times 10^8}{3.3 \times 10^8} = 2.1$$

Harmonic Drive Safety Factors

SELECTION OF SCANNER LUBRICANTS

A number of lubricants were considered for the scanner, and the leading candidates are Vac-Kote wet film lubricant, deposited gold, and Krytox grease. Different lubricants and lubrication techniques should be used in the different areas of the scanner mechanism, since the lubrication problems encountered vary.

Because of the variety of mating mechanical parts in the scanner mechanism, a number of lubricants and techniques were examined: silicone oils and greases, Krytox perfluoroalkylpolyether lubricant, Vac-Kote deposited lubricant films, deposited gold metal, polyimide plastic coatings, and diester-based liquid lubricants.

Silicone greases and oils have many successful space applications. Although they have the advantage of a very flat temperature-viscosity curve and low outgassing, their film strength and lubricity properties are poorer than those of other lubricants and they have a known failure mode consisting of the generation of small, glassy particles. This phenomenon is referred to in several reports, and may have contributed to the ITPR scanner failures. Silicone greases and oils should be excluded from consideration until this phenomenon is investigated adequately and the problem is solved.

Krytox lubricants are a series of fluorinated polyethers which have good lubricating properties and good temperature stability. The high temperature viscosity and outgassing properties are not as good as those of the silicones, but these lubricants have been applied successfully in space. In particular, Krytox was used on the Backscatter Ultraviolet (BUV) instrument (a NIMBUS experiment). In that case the grease was "plated" on the metal surfaces by deposition from a solution. This controlled the lubricant thickness so that bearing starting torques were not increased too much at low temperatures.

Vac-Kote is a bonded molybdenum disulfide film. While there are many dry film processes on the market, Vac-Kote has the best history of reliability in space applications. There are two basic types of Vac-Kote--"wet" and "dry." The wet type has a liquid lubricant constituent, in addition to the bonded MoS_2 film, and it is this type that is recommended for the scanner.

Many space mechanisms have been successfully lubricated with deposited films of gold, a technique that is effective when the gold-coated surface runs against a harder metal surface. This lubrication technique is a good candidate attractive for use on the spline mesh.

The preloaded ball bearings that support the mirror shaft are a relatively straightforward bearing application. Their total number of revolutions for two years in orbit is 4×10^6 Vac-Kote film lubricant would be a good choice for these bearings.

The bearings of the motor and wave generator will experience 3×10^8 revolutions during the two-year mission. It is doubtful that bonded-film lubricants would have sufficient life for this application. Therefore, Krytox synthetic liquid lubricants are recommended. Grease plating should be used on motor bearings to avoid torque buildup at low temperatures. A lubricant-impregnated, sintered-nylon reservoir can be put inside the harmonic drive and excess lubricant vapors vented overboard away from the instrument optics.

In the harmonic drive spline mesh, there is a tendency for any particulate matter present to migrate toward the center of the teeth. When liquid lubricants are used, wear-debris particles become trapped in an abrasive paste and wear the teeth badly. Because of this, a dry material of excellent film strength that will prevent the generation of wear particles is needed. Deposited gold is recommended.

Lubrication is required in the encoder and its bearing and for the pins in the pin cage. Krytox oil is recommended for the pins; the bearing should be grease plated with Krytox. Barrier films should be used to prevent oil migration to the encoder contact surfaces.

TABLE I. LUBRICANTS STUDIED

All of these lubricants have been successfully used in space.

• Silicones	- Flat viscosity curve; low outgassing. Has failure mode involving generation of hard, glassy particles.
• Krytox	- Adequate temperature range (-40°C to +230°C); outgassing same as silicones; excellent lubricity and film strength.
• Vac-Kote	- "Wet" and "dry" types. Qualified in many applications. Wear is the only failure mode.
• Gold	- Deposited in films approximately 2×10^{-4} in. thick. High load-carrying ability.

TABLE II. RECOMMENDATIONS

• Mirror Shaft Bearings	- Vac-Kote
• Motor and Wave Generator	- Krytox grease plated, and oil in Nylasint reservoir.
• Harmonic Drive Spline Teeth	- Deposited Gold
• Encoder	- Krytox oil and grease.

NATURE OF SCANNER SUBSYSTEM INTERFACE REQUIREMENTS

The requirements applicable to the interface between the scanner subsystem and the instrument system are: mounting space, adequate mechanical strength and rigidity, optical accuracy, and low thermal resistance.

A mounting surface of appropriate dimensions and flatness must be provided for mounting the scanner. Also, clearance space for the scan mirror and for its beam over the range of look angles is needed, as detailed in the table on the facing page.

In actual instrument operation, the only mechanical stress on the interface is a small torque reaction due to scanner operation. This is so small--about 9 oz-in.--as to be negligible. However, in the launch condition and in environmental testing, considerable stresses are imposed. There are direct tensile, compressive, and shear forces on the joint, as well as bending induced in the scanner mounting web of the housing. The resisting moment necessary at the scanner-to-housing joint is 1500 lb-in. The scanner mounting screws must be sized to have a preload greater than any tensile force that can be imposed on them, including the resisting moment. Dowel pins to positively locate the assembly and take the shear forces are necessary also. These requirements are met with a pattern of three 3/16-inch-diameter bolts torqued to 11.0 in.-lb, and two 3/16-inch diameter pins installed at assembly.

The optical accuracy requirement concerns the pointing accuracy of the instrument's exit beam. The initial installation of the scanner subassembly must be accurate geometrically, and the design must allow it to be repositioned accurately when it is removed and reinstalled. This is achieved by the two 3/16-inch-diameter pins, which also take the shear loads. The pins are installed only after the scanner is aligned and clamped at initial assembly. Thereafter, no alignment is necessary, since the locating pins allow the scanner to be removed and accurately reinstalled as often as desired.

Because the heat of power dissipation in the scanner motor must cross the scanner-to-housing joint, there is a thermal interface requirement. This heat is disposed of, ultimately, at the external radiator panels, and it must follow conductive paths through the housing metal to get there. This heat conduction incurs a temperature drop of about 12°C, leaving an allowable temperature drop at the interface of 36°C, if the motor upper limit of 70°C is not to be exceeded. Since the average power involved is 8.2 W, the maximum allowable thermal resistance at the interface is 4.4°C/W. The design value of 1.0°C/W meets this requirement.

The scanner electrical interface involves the motor and shaft encoder. The motor driver requires an input of programmed pulses from the instrument logic and an input of dc power. Physical connection to the motor driver is through a Cannon MDB-7P connector. The pin-contact encoder is a passive device and requires no power input. Electrical connection to it is also through a Cannon-type multi-pin connector.

SCANNER SUBSYSTEM INTERFACE REQUIREMENTS

• Mounting Surface	-	3 mounting holes on 5-in.-dia. circle; surface flat within 0.005 in.
• Mirror Clearance	-	11.4 in. dia. x 12.0 in. length
• Mirror Beam Size	-	11.4 in. dia.
• Look Angles	-	71 degrees above nadir, anti-sun side
		42 degrees above nadir, sun side
• Resisting Moment of Support Structure	-	1500 lb/in.
• Assembly Features	-	Dowel pins installed in line-reamed holes to permit repeated accurate assembly and disassembly
• Scan Motor Power	-	8.5 W avg.; programmed 10 ms, 28-V pulses
• Thermal Resistance	-	$4.4^{\circ}C/W$, maximum

SECTION 8

INSTRUMENT SEQUENCING AND CONTROL

System Control

System Timing and Control Requirements 8-0
Description of System Timing 8-2

Multiplexer Control

Multiplexer Control Requirements 8-4
Description of Multiplexer Control Logic 8-6
Description of Multiplexer Timing 8-8

ADC Control

ADC Control Requirements 8-10
Description of ADC Control Logic 8-12
Description of ADC Timing 8-14

Scan Motor Control

Evaluation of Scan Motor Excitation Methods 8-16
Performance of the Recommended Excitation Method 8-18
Description of Scan Logic Circuit 8-20
Description of Breadboard Drive Circuit 8-22
Redundant Design of Scan Drive Circuit 8-24
Analysis of Scan Power Requirements 8-26

Chopper Motor Control

Chopper Motor and Excitation Method 8-28
Phase Control of the Chopper Motor 8-30

Other Subsystems

Dual Instrument Mode Control Description 8-32
Formatting Unit Description 8-34
Data Format 8-38
Description of Instrument Commands 8-40

SYSTEM TIMING AND CONTROL REQUIREMENTS

Control of the instrument subsystems is performed by a centralized, synchronous, logic network, denoted as the System Timing and Control Unit.

General: Control and timing logic is required to keep all aspects of the TOVS signal processing in proper synchronism with the TIROS-N Information Processor (TIP), and TOVS scan program, and the optical chopper. The TOVS requires two (2) externally supplied control signals:

- TIP - Master Frame Sync (16 second period)
- S/C Clock - 1248 KHZ signal

Using these signals as a basis, the TOVS system timing and control unit will develop all the necessary instrument control signals. The main control signals and their functions are identified as follows:

a) Integrate, Dump and Hold: Controls the analog data integrators.
b) Advance Multiplexer: Controls the analog multiplexer.
c) Start Conversion: Used to initiate the ADC conversion.
d) Scan Step Rate: Advances the scan mirror.
e) Chopper Rate: Advances the chopper motor.

Description: A block diagram illustrating the Timing and Control unit configuration is shown in Figure A on the adjacent page. Note that three (3) basic functions are performed;

(1) Wave shapers are used to buffer the externally supplied clock (1248KHZ) and master frame sync pulse (MFSP).
(2) A counting register comprised of several stages generates all the necessary frequencies from 1248KHZ to 1/264 HZ.
(3) Logic gates are used to develop the desired control signals by decoding the various counter chain states.

The exact logic structure of the counter stages and associated decoding gates can be synthesized several ways. Care must be exercised to avoid false signals from the decoding gate, due to logic element propagation delays.

Note that the system timing signals have a fixed known relationship relative to each other and are synchronized to the MFSP signal.

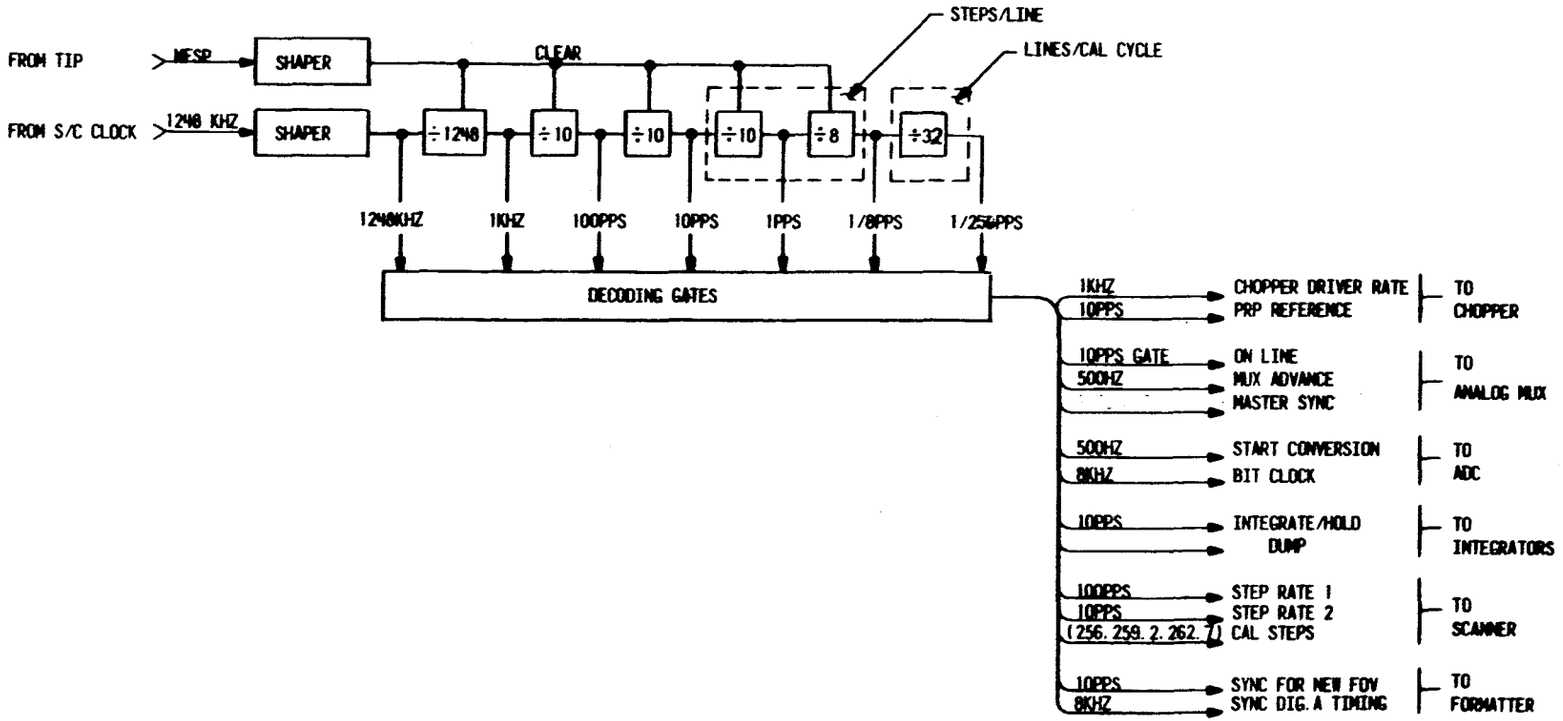

FIGURE A
SYSTEM TIMING
AND CONTROL

DESCRIPTION OF SYSTEM TIMING

A timing diagram is presented to clarify the fundamental instrument control timing requirements.

General: A timing diagram illustrating the phase relation of the key control signals is shown in Figure A. The scan mirror step rate, PRP chopper signal, integrator controls, and data processing signals are identified. Scan steps occur every 100 ms. This interval is subdivided into three (3) segments; 1) 75 ms used for data integration, 2) 18.75 ms used to digitize the 16 data channels and 3) 6.25 ms allocated for dumping the integrators.

Scan Mirror Step: This signal occurs at a 10 pps rate during the normal scan cycle and at a 100 pps rate during the retrace cycle.

PRP Signal: This signal is derived directly from the chopper mechanism and is controlled to maintain phase sync with the integrator control signal. Signal occurs at a 40 Hz rate.

Integrator Controls: Infrared energy integrators perform the integration function for 75 ms, hold the integrated value for a period of 18.75 ms, and are reset to zero during the next 6.25 ms period. A time delay of 31.25 ms is inserted between the scan step signal and the integration period. This dalay allows to scan mechanism to settle to a static value before data processing occurs.

Multiplexer Controls: Analog data will be processed during the 18.75 ms HOLD period. Three signals control the analog multiplexers, i.e., 10 pps ON LINE signal, 500 Hz multiplexer advance signal, and the 1/256 Hz master sync signal.

ADC Controls: The ADC and multiplexer operate in conjunction to digitize the analog data. A start conversion signal (500 Hz, gated) is developed for each sample; plus an 8 kHz bit trial clock.

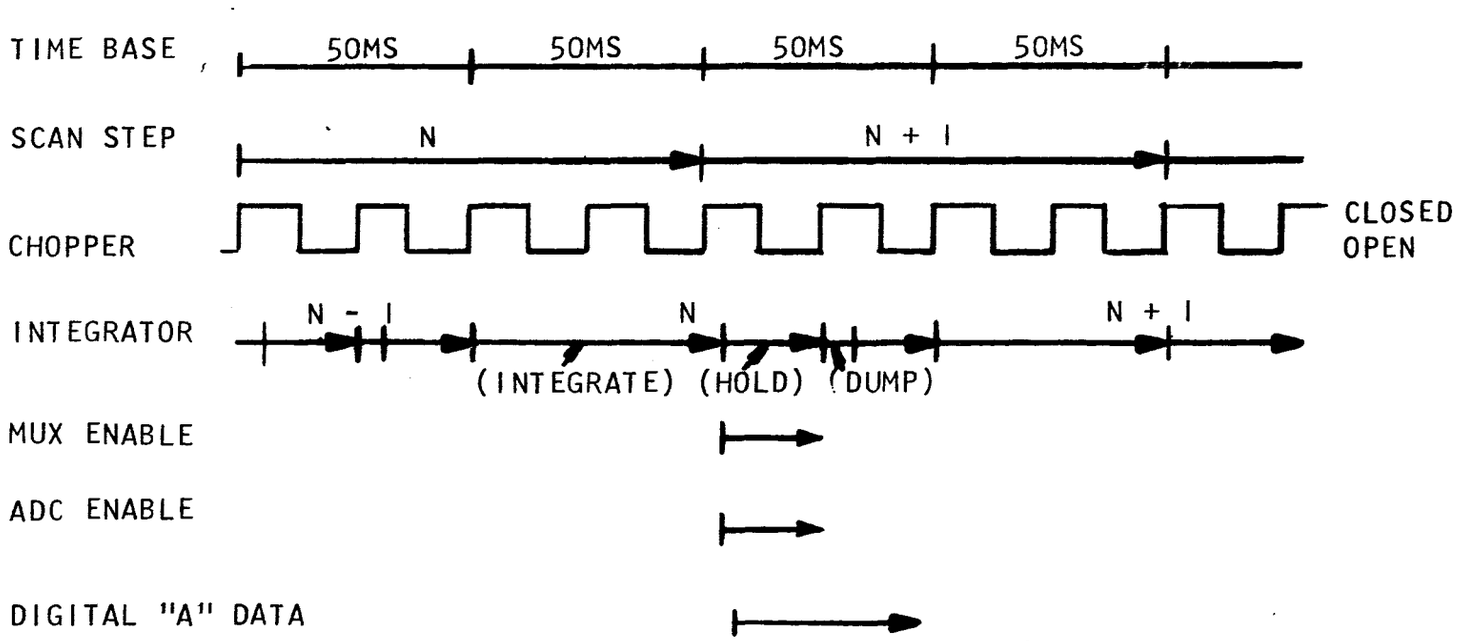

FIGURE A
TOVS SYSTEM TIMING

MULTIPLEXER CONTROL REQUIREMENTS

A logic configuration necessary to control the sequencing of the analog multiplexer is defined. Simple control digital circuitry is used to generate a fixed sampling sequence.

Multiplexer Review: A sequentially addressable, junction FET multiplexer is required to commutate the analog radiation signals, temperature monitor signals and other special analog voltages. A block diagram illustrating the multiplexer configuration is shown on the adjacent page. Note that control logic is required to provide the gate addresses for both the prime and submultiplexers.

Prime Multiplexer Control: The sixteen point prime multiplexer requires an address counter to sequentially scan the input gates. The two level nature of the multiplexer (4 x 4 matrix) allows a natural partition of a four (4) bit binary counter into two sets denoted as $SX_{i/1}^{4}$ and $SY_{i/1}^{4}$. These signals, when translated to compatible voltage levels, directly control the prime multiplexer.

Submultiplexer Control: Submultiplexer control is analogues to that used in the prime multiplexer, however, the twelve (12) point capacity require a different address counter radix. A twelve (12) state address counter is needed. This counter is advanced one count per FOV, or more correctly at a rate of 10 HZ. A data readout cycle is completed every 1.2 second period.

Synchronization: It is essential that the prime multiplexer address counter be synchronized to the TIP's major frame sync signal and the internal TOV's system timing. This requirement means that the address counters must be provided with a reset feature and that the advance rate maintain a fixed phase relationship to the integrate.

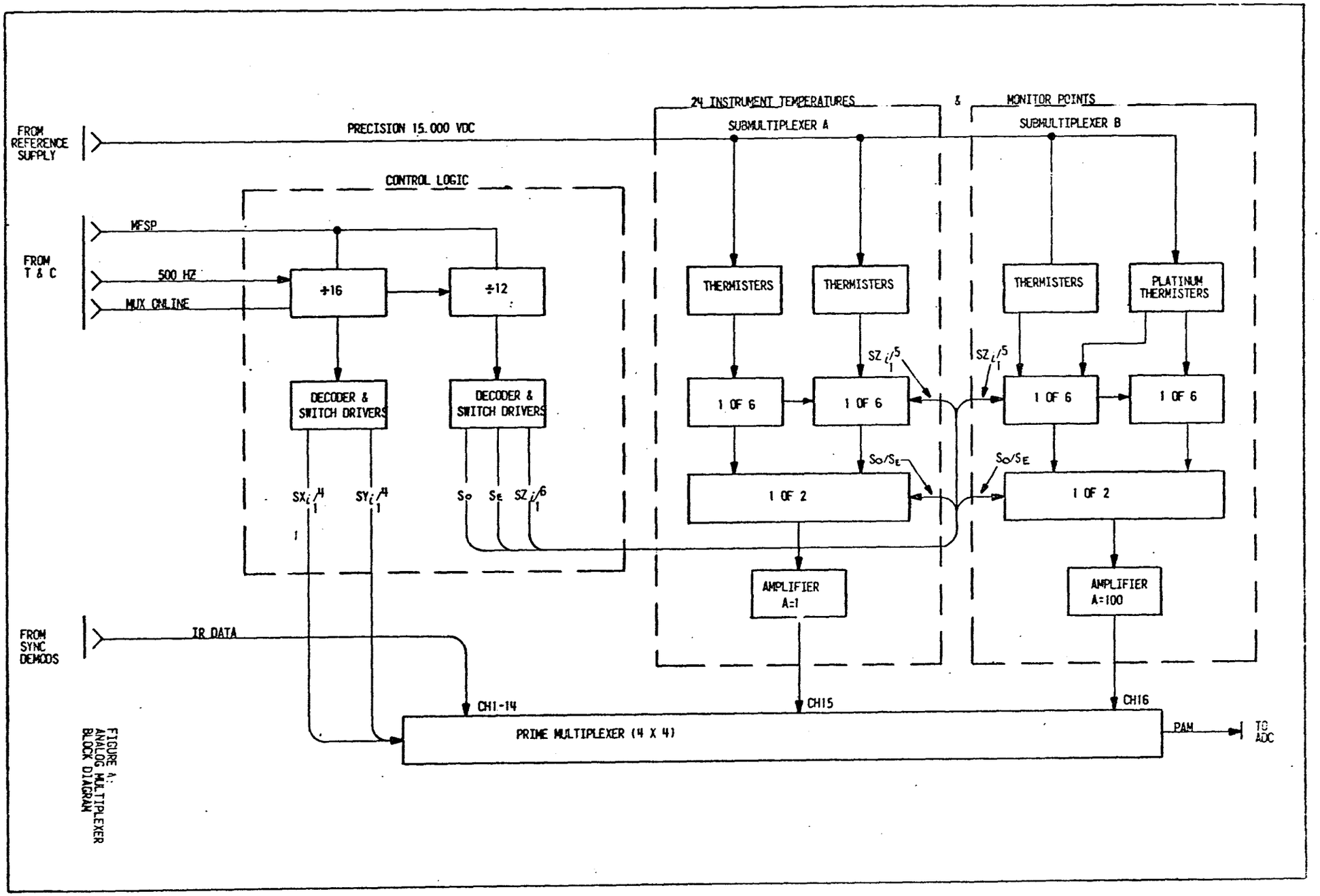

FIGURE 4: ANALOG MULTIPLEXER BLOCK DIAGRAM

DESCRIPTION OF THE MULTIPLEXER CONTROL LOGIC

Multiplexer control signals are developed using simple digital logic circuitry.

General: A simplified logic diagram of the multiplexer control logic is shown in Figure A and consists of prime and submultiplexer address counters, decoding gate and associated switch drivers.

Prime Multiplexer Control Logic: A four (4) bit binary counter is used to furnish the prime multiplexer address. Counter is advanced at a 500 HZ rate when the MUX ON LINE is enabled. Both of these signals are developed in the system timing and control unit, and function to rapidly step the prime multiplexer thru all 16 prime channels after the IR integration period. A reset feature is provided to synchronize the address counter to the TOV's system time. A signal denoted as MASTER SYNC accomplishes this objective.

Two input NAND gates are used to develop a 1 of 4 decoding network. Bits 2^0 and 2^1 form the control signals $SX_i/_1{}^4$; while bits 2^2 and 2^3 form control signals $SY_i/_1{}^4$. The SX_i and SY_i signals provide the matrix drive signal and when applied to 1st and 2nd level analog gates, select 1 of the 16 input gates.

Submultiplexer Control Logic: A divide by twelve counter is used to furnish the submultiplexer address. A two (2) stage configuration is suggested; i.e. a ÷ 2 stage and a ÷ 6 stage. A variety of configuration is available; however, the binary ÷ 2 coupled with a ÷ 6 shift counter yields an efficient decoding structure. The ÷ 2 stage supplies the SO,SE signals to control the 2nd level submultiplexer switches. The ÷ 6 shift counter is decoded into 1 of 6 active signals denoted as $SZ_i/_1{}^6$. Six (6) NAND gates (2 inputs/gate) are used to synthesize the decoder.

The submultiplexer address counter is advanced directly from the prime multiplexer address counter at a 10 HZ rate. Synchronization with the TOVs system time is assured via the reset action of the MASTER SYNC signal.

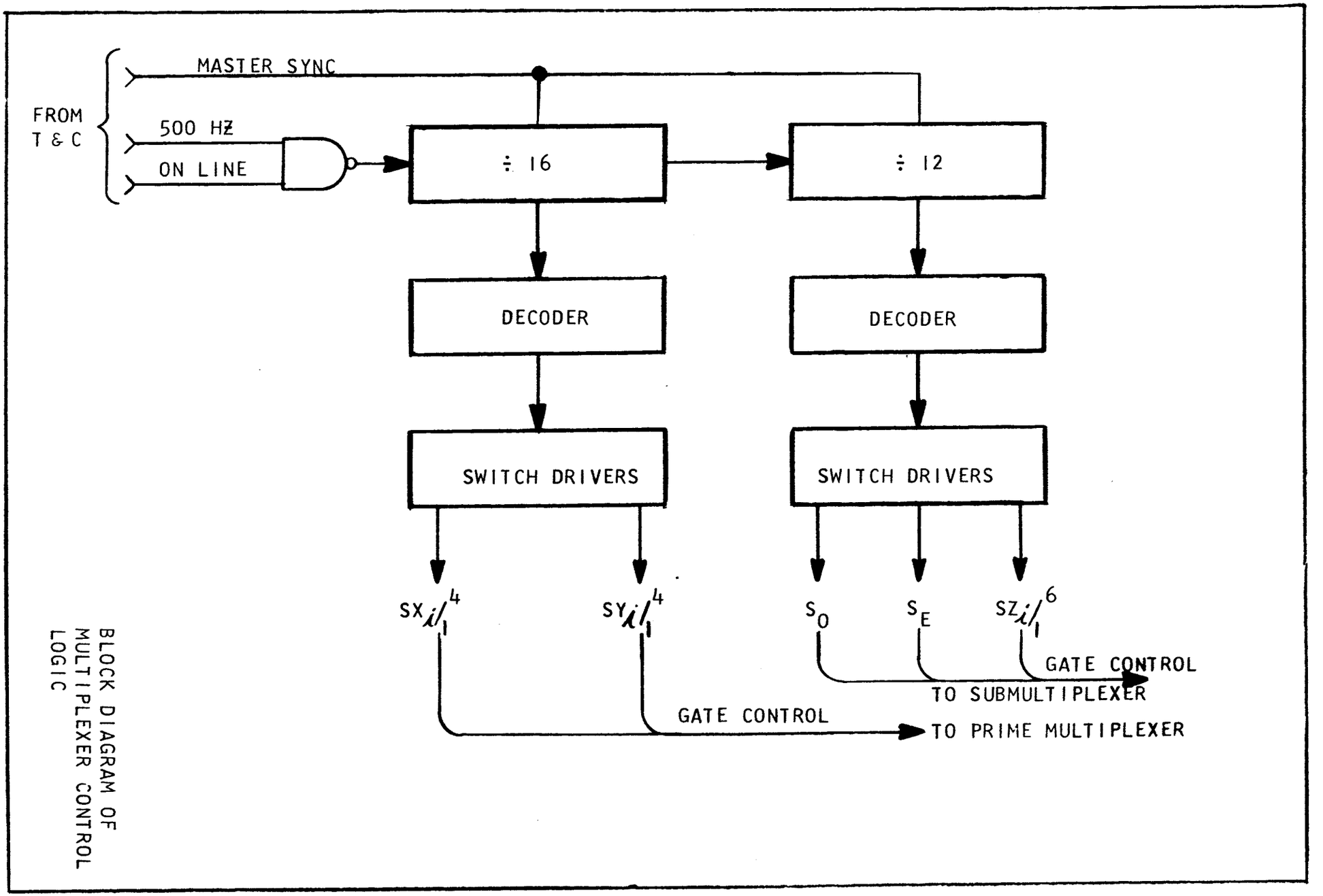

BLOCK DIAGRAM OF
MULTIPLEXER CONTROL
LOGIC

12061-R22 p 7

DESCRIPTION OF THE MULTIPLEXER TIMING

A timing diagram is presented to clarify the multiplexer control signal phase relationships.

General: A timing diagram illustrating the pulse duration and relative phase of multiplexer control signals are shown in Figures A and B. The MASTER SYNC signal, prime and submultiplexer address states, and matrix switch driver signals are identified.

Master Sync Signal: This signal occurs once every 256 seconds and provides the basic reference for the instrument. The leading edge of this 1 ms pulse is the time reference TO. This signal resets both address counters to zero.

Prime Multiplexer Address: The sixteen (16) states of the prime multiplexer address counter are identified. Each state is active for a 2 ms period during each multiplexer ON LINE cycle. This cycle occurs at a 10 HZ rate and is active for a 32 ms period.

The decoded counter states (SX_i and SY_i) are shown to illustrate the relative timing. Each SX_i signal is active for a 2 ms period every 8 ms. Each SY_i signal is active for an 8 ms period every 100 ms (once per FOV).

Submultiplexer Address: The twelve (12) states of the submultiplexer address counter are identified. Each state is active for a 100 ms period and is cyclic every 1.2 seconds.

The decoded switch driver signals are also shown. Signals So and Se correspond to the odd and even number of FOVs and are active for a 100 ms period every 200 ms. Signal SZ_i are active for 200 ms every 1.2 second.

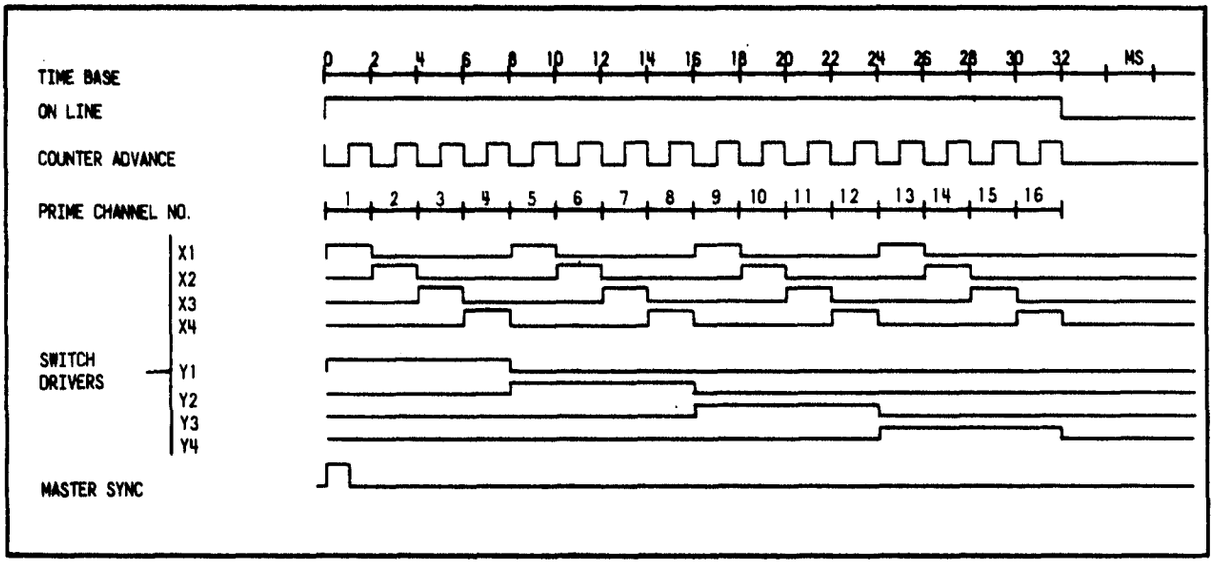

FIGURE A. PRIME MULTIPLEXER TIMING

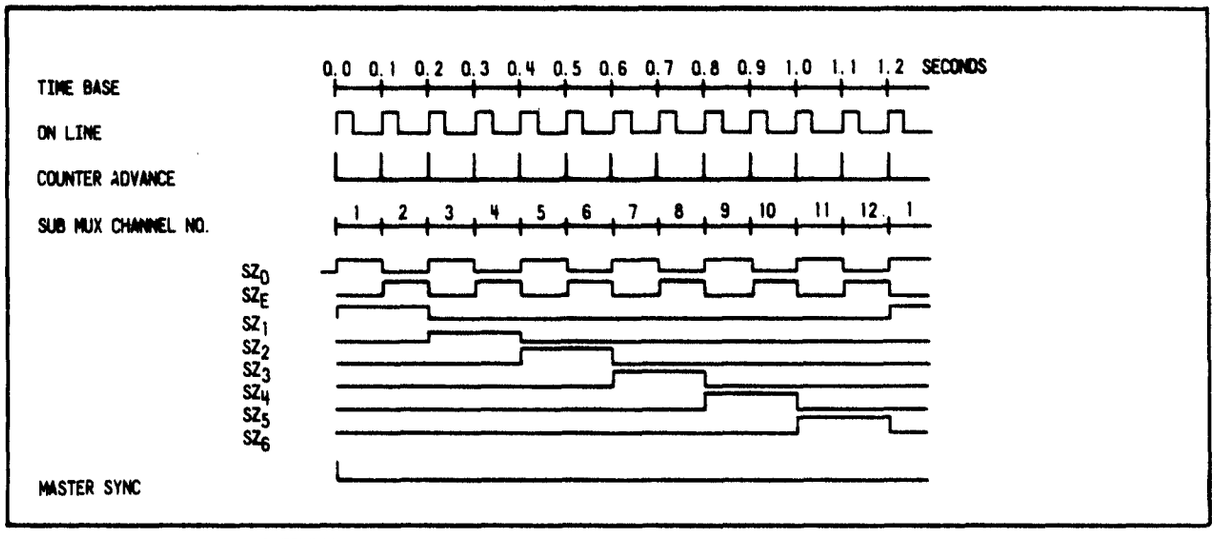

FIGURE B. SUBMULTIPLEXER TIMING

ADC CONTROL REQUIREMENTS

The signals necessary to control the analog to digital converter are identified. Circuit drive requirements and relative timing were considered.

Review of the ADC: A successive approximation, current summing, type of analog to digital converter is recommended for the TOVs. A block diagram illustrating the converter configuration is shown on the adjacent page. Note that logic circuitry is required to control the ladder network, store the partial results, output the digital data and start/stop the conversion process. These functions are performed by the control logic.

Start/Stop Conversion: A control signal obtained from the TOVs system timing and control unit is required to initiate the conversion process. Another signal generated within the control logic is required to denote that the quantization process is completed, and is identified as Conversion Complete signal.

Ladder Control: A twelve (12) bit current ladder is used to establish the binary weighted trail steps. Control requirements for this device can be stated as follows: first, each weighted binary bit must be applied sequentially for one bit period; second, the bit trail signal must be accepted or rejected based upon the decision of the comparator circuit.

Data Storage: A twelve (12) bit data register is required to accumulate the partial results obtained from each bit trail. This device functions in conjunction with the ladder control logic and also serves as a one (1) word buffer register to temporarily store the final encoded value.

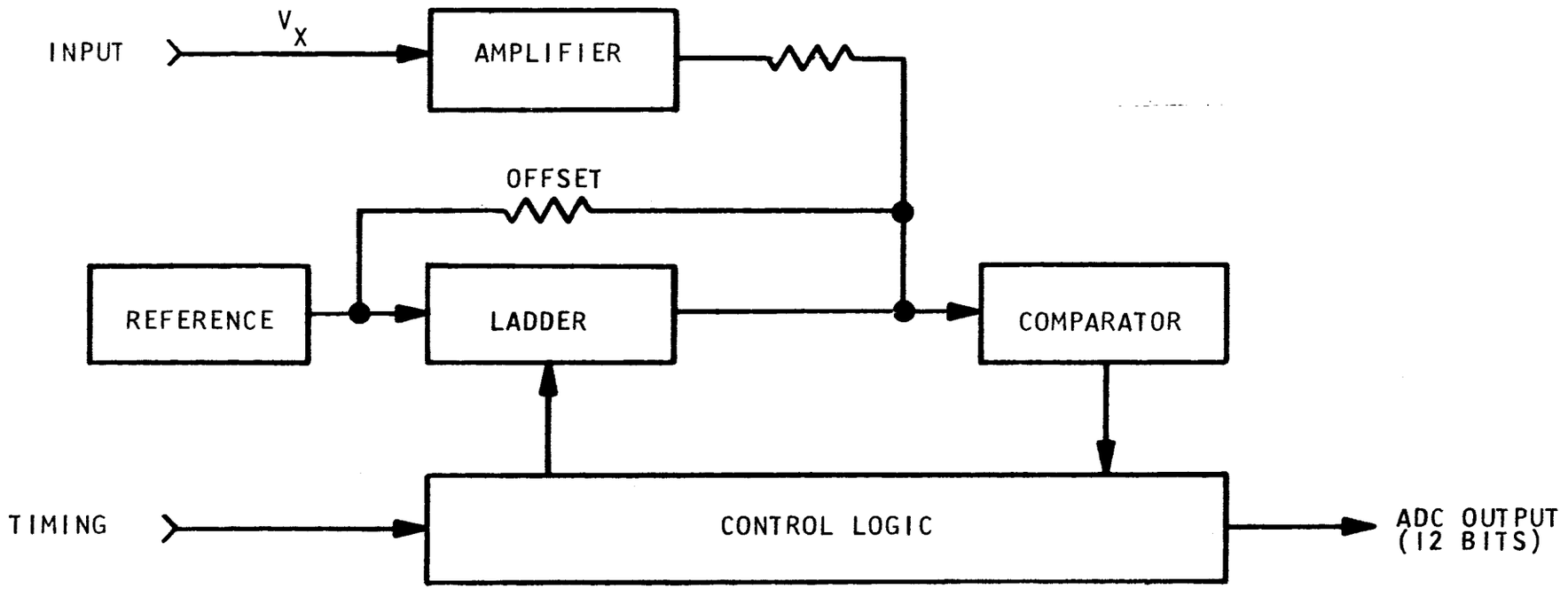

SIMPLIFIED BLOCK DIAGRAM OF THE ADC

13961-829

DESCRIPTION OF THE ADC CONTROL LOGIC

Control of the ADC is performed by well defined, simple, digital logic circuitry.

General: A simplified block diagram of the ADC control logic is shown on the adjacent page and consists of five functional elements. These functions must be performed, however several types of logic structures can be used to implement the control. The structure shown is similar to that employed on the ITPR. Alternate configurations were investigated, but none yielded significant advantages.

Start/Stop Control: The Start Conversion signal obtained from the system T & C unit is used to set the START/STOP flip-flop. This signal initializes the control logic to the state needed to start the conversion process. In particular it performs two functions; i.e., 1) resets the ADC register and 2) enables the trial counter. After the conversion is completed, the start/stop flip-flop is reset by the last trial ring.

Bit Trial Counter: A twelve (12) state counter and associated decoder are used to develop the bit trial signals. A two stage Johnston type shift counter (÷2 and ÷6), a single stage modulo-12 scaler, or a twelve state ring counter are suitable. The ring counter approach is the most simple to implement, however care must be exercised to insure that one and only one active state is possible.

Bit trial signals (T_i) are applied to the ladder driver gates and ADC register. Their purpose is to activate the appropriate ladder current switch and also to select the corresponding bit of the ADC register.

ADC Register: A twelve (12) bit register is used to store the partial results during the conversion cycle. RS, JK or D type logic elements can be used to construct the register; however, two basic capabilities must be provided, 1) a reset to zero capability, and 2) a conditional set based upon the logic AND function of the bit trial signal AND the ACCEPT/REJECT signal.

Register outputs are applied to the ladder driver gates to latch the bit trial steps and also serve as parallel digital data outputs from the ADC.

Comparator Strobe: An ACCEPT/REJECT signal is generated which denotes whether the bit currently being tried is too large or too small. The analog comparator output is gated with the trial clock to develop the desired signal. The exact circuit needed is dependent upon the nature of the ADC register, and can be a simple gate or at most a monostable multivibrator.

Ladder Drive Gates: Logic OR gates are required to control the current ladder switches. Twelve (12) gates of the two input type are needed. One input is furnished by the bit trial signals $T_i/_1^{12}$, while the other is supplied by the ADC register. This gating provides the conditional latching feature necessary to control each bit trial ladder switch.

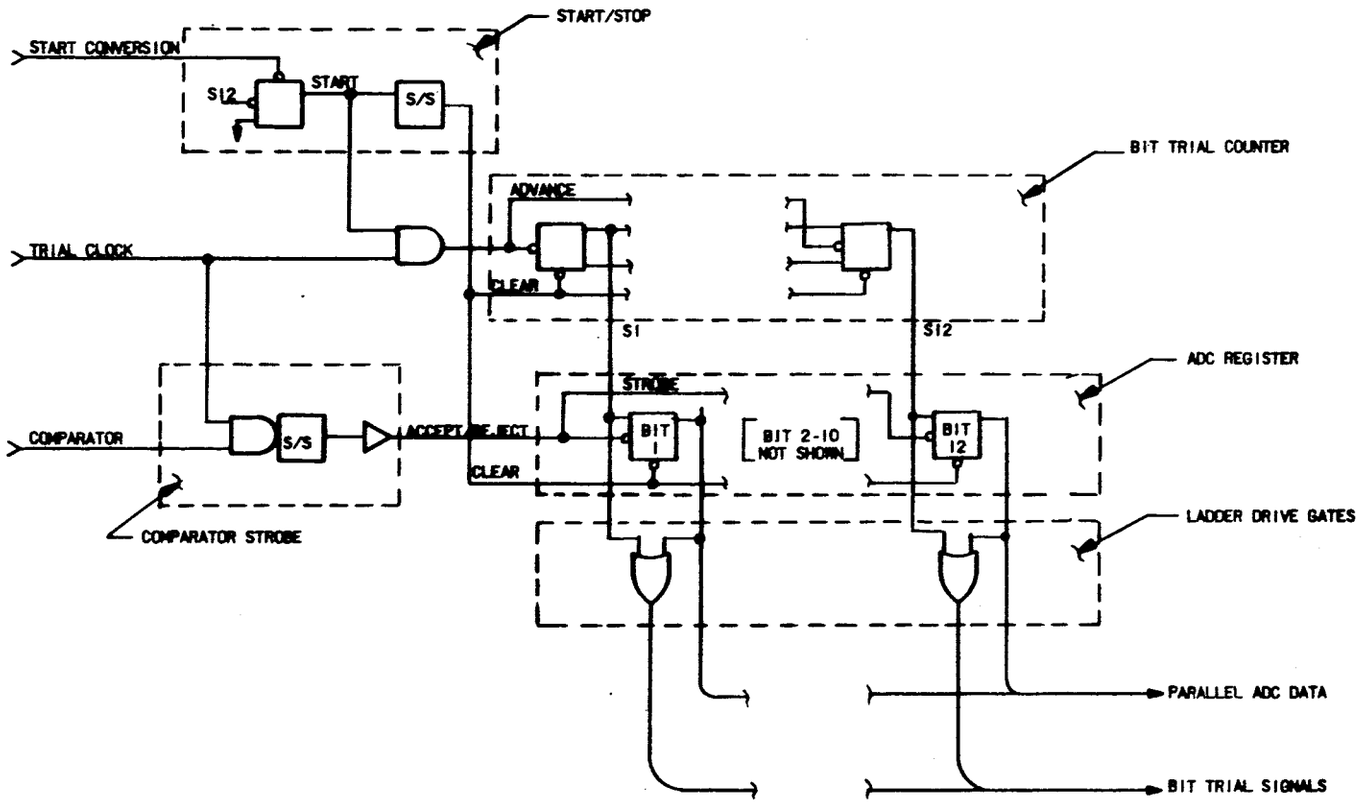

FIGURE A:
ADC CONTROL LOGIC

13961-844

DESCRIPTION OF THE ADC TIMING

A timing diagram is generated and discussed to clarify the ADC control signal timing relationships.

General: A timing diagram illustrating the pulse duration and relative phase relationship of signals used to control the ADC is shown on the adjacent page. The trial clock, start conversion control, ADC register clear, bit trial signals, and conversion complete signals are shown.

Operation of the converter is initiated upon receipt of the START CONVERSION signal. This signal occurs at a 2.0 ms period. Pulse width characteristics are not critical and the duty cycle is optional. This signal will occur once for each analog sample to be digitized.

The CLEAR ADC REGISTER is derived from the leading edge of the START CONVERSION signal and is a 125 μs pulse.

Data Transfer Period: The time period corresponding to window number 16 (T_o + 1.875 thru T_o + 2.00 ms) is allocated for transfer of the ADC data to the formatter logic. Conversion process has been completed and the data is being held static and in parallel form. CONVERSION COMPLETE signal is used to control this transfer operation. This signal has a pulse width of 125 μseconds and occurs during window 16 time period.

A 375 μs period is allocated to permit the ADC and analog multiplexer to settle to a precision value. The bit trail signals start at time T_o + 0.25 ms and are complete by T_o + 1.875 ms. The encoded digital data is available for external use from T_o + 1.875 to T_o + 2.0 ms, at which time the cycle repeats.

Conversion Time: The conversion rate for the ADC has intentionally been kept at a slow rate to provide good accuracy at reasonable power. The basic rate is established by the number of data samples to be digitized during a fixed time interval. For the TOVS, sixteen (16) words must be encoded in 40 ms. This constraint, coupled with the output data rate of 500 HZ/word (max.) yields a range of conversion rates from 400 HZ to 500 HZ. The recommended conversion rates are as follows:

Word Conversion Rate .... 500 SPS (2ms/sample)
Bit Trial Rate .... 8 KHZ (125 μs/Bit)

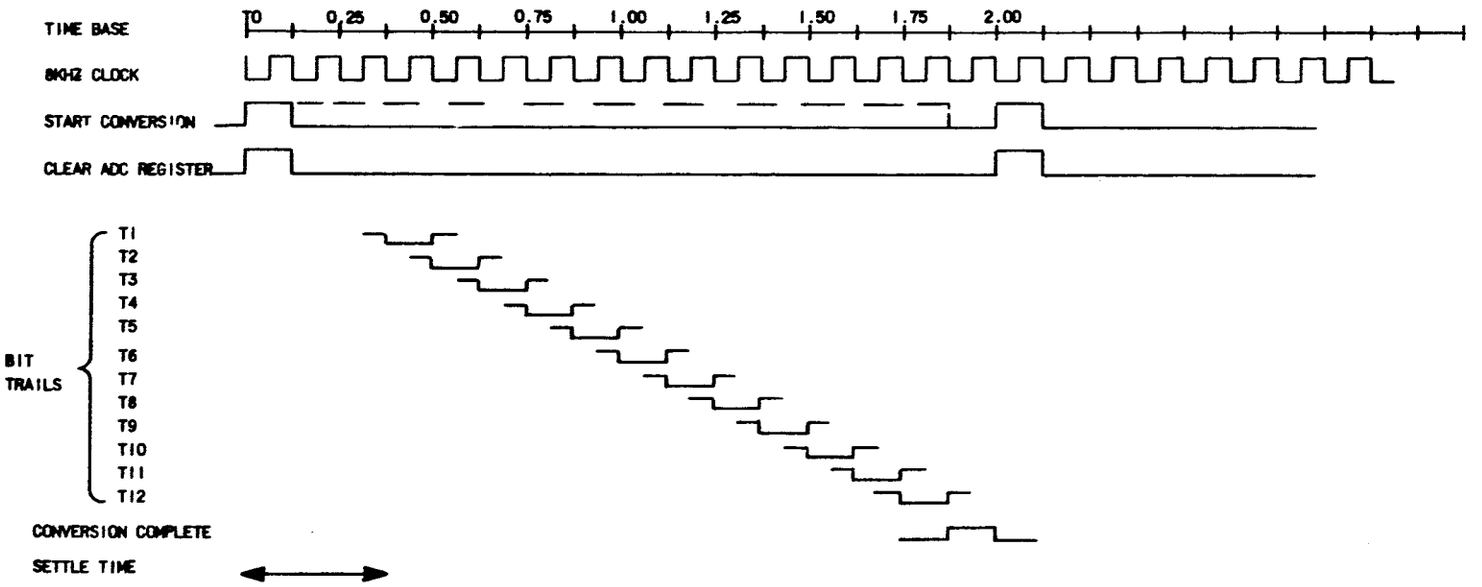

FIGURE A:
ADC TIMING DIAGRAM

EVALUATION OF SCAN MOTOR EXCITATION METHODS

A comparison of stepping motor excitation methods shows that the bipolar single-phase drive method provides a good torque output with moderate consumption and complexity.

Stepping motors provide discrete, incremental rotation in response to a pulsed input applied to the motor windings. Permanent-magnet stepping motors can be driven in several ways. The method for exciting the motor windings affects the efficiency, power consumption, speed, and torque characteristics. Five commonly used excitation techniques were evaluated: (1) unipolar, dual phase; (2) unipolar, single phase; (3) bipolar, dual phase; (4) bipolar, single phase; and (5) series, all windings. Unipolar techniques (1 and 2) provide current flow in one direction through the select excitation winding; while bipolar excitation provides current flow in both directions. Dual-phase excitation implies that two excitation phases are excitated in parallel, while the single phase excitation methods excite only one coil or a series-connected coil.

Significant Characteristics of Excitation Methods - A tabulation of the five excitation methods is shown in the facing table. Power dissipation among the methods varies widely. Assuming Method 1 as a 100% reference, the relative power consumption is 100%, 70%, 50%, 35%, and 25% for Method 1 through 5, respectively.

Comparison of the ampere turns developed by each method affords a measure of the motor performance characteristics. Assuming Method 1 as a 100% reference, the relative values are 100%, 70%, 100%, 70% and 50% for Methods 1 through 5.

An efficiency factor is defined to relate the amount of power required per ampere turn (P/AT). The relative values are 1.4, 1.0, 0.7, 0.5 and 0.35 for Methods 1 through 5. Method 1 is the least efficient for convering power into usable ampere turns; while Method 5 is the most efficient.

Complexity of the drive circuitry required to synthesize the excitation methods was considered. The order is as follows; Method 2, 1, 4, 3 and 5, where Method 2 is the least complex.

Advantages and Disadvantages of Each Method - Method 1 (Unipolar, dual phase) develops the best motor characteristics, but at a high cost in power consumption. This method has the poorest conversion efficiency of all the methods.

Method 2 (Unipolar, single phase) develops good motor characteristics (similar to Method 4) at a reasonable power level. A very simple drive circuit can be used; in fact, this method is employed on the ITPR experiment. Power conversion efficiency is better than Method 1 but poorer than the other methods.

Method 3 (Bipolar, dual phase) develops the same motor characteristics as Method 1 at half the power. Power conversion efficiency is better than that of Methods 1 and 2, but poorer than that of the other methods. The drive circuit is more complex than either Methods 1, 2, or 4.

Method 4 (Bipolar, single phase) develops the same motor characteristics as Method 2 at half the power. Power conversion efficiency is better than that of all but Method 5. Drive circuit complexity is greater than either of the unipolar circuits; but not excessively complex.

Method 5 (all windings) dissipates the least circuit of power and provides the best power conversion efficiency, yet yields the poorest motor performance characteristics. A very complex drive circuit is required to produce the excitation sequence.

GULTON INDUSTRIES, INC.
Data System Division
R. G. Day

COMPARISON OF CANDIDATE MOTOR EXCITATION METHODS

Method	Method 1 Unipolar, Dual Phase	Method 2 Unipolar Single Ø	Method 3 Unipolar Dual Ø	Method 4 Bipolar Single Ø	Method 5 All Windings
Excitation Mode	(A+D) (A+C) (B+C) (B+D)	(A) (C) (B) (D)	(AB+CD) (AB+DC) (BA+DC) (BA+CD)	(AB) (CD) (BA) (DC)	(ABCD) (ABDC) (BADC) (BACD)
(A) Amp-Turns $A.T. = N_t N_t$	$I = \frac{V}{R}$ $\sum AT = NI\phi_1 + NI\phi_2$ $AT = \frac{1.4\ NV}{R}$	$I = \frac{V}{R}$ $\sum AT = \frac{NV}{R}$ $AT = \frac{NV}{R}$	$I = \frac{V}{2R}$ $\sum AT = \frac{2NV}{2R} + \frac{2NV}{2R}$ $AT = \frac{1.4\ NV}{R}$	$I = \frac{V}{2R}$ $\sum AT = \frac{2NV}{2R}$ $AT = \frac{NV}{R}$	$I = \frac{V}{4R}$ $\sum AT = \frac{2NV}{4R} + \frac{2NV}{4R}$ $AT = \frac{0.7\ NV}{R}$
(B) $\sum$ Power $P_t = V_t I_t$	$P_t = V\ I$ $P_t = \frac{2V^2}{R}$	$P_t = V_t I_t$ $P_t = \frac{V^2}{R}$	$P_t = V\ \frac{2V}{2R}$ $P_t = \frac{V^2}{R}$	$P_t = V_t I$ $P_t = \frac{V^2}{2R}$	$P_t = V_t I_t$ $P_t = \frac{V^2}{4R}$
(C) Eff. Factor	$F_1 = \frac{\frac{2V^2}{R}}{\frac{1.4\ NV}{R}}$ $F_1 = \frac{1.4\ V}{N}$	$F_2 = \frac{\frac{V^2}{R}}{\frac{NV}{R}}$ $F_2 = \frac{(1)\ V}{N}$	$F_3 = \frac{\frac{V^2}{R}}{\frac{1.4\ NV}{R}}$ $F_3 = \frac{(0.7)\ V}{N}$	$F_4 = \frac{\frac{V^2}{2R}}{\frac{NV}{R}}$ $F_4 = \frac{(0.5)\ V}{N}$	$F_5 = \frac{\frac{V^2}{4R}}{\frac{0.7\ NV}{R}}$ $F_5 = \frac{(0.35)\ V}{N}$
(D) % Power required Based on F_1 as 100%	Assumed 100% $\%P_1 = 100\%$	$\%\ P_2 = \frac{1.0}{1.4}$ $\%P_2 = 70\%$	$\%P_3 = \frac{0.7}{1.4}$ $\%P_3 = 50\%$	$\%P_4 = \frac{0.5}{1.4}$ $\%P_4 = 35\%$	$\%P_5 = \frac{0.35}{1.4}$ $\%P_5 = 25\%$

PERFORMANCE OF THE RECOMMENDED EXCITATION METHOD

The recommended bipolar single-phase drive method was used in the scanner breadboard and provided the torque needed to meet the retrace and 50 ms requirements with an acceptable power consumption.

Excitation Method 4 (Bipolar, single phase) is recommended for driving the BSU scan motor. A timing diagram illustrating the phasing of the four drive signals (A, B, C and D) is presented in Figure A. A simplified equivalent switching circuit is shown in Figure B. Note that the sequential closure (ground) of switches B, D, A, and C causes current flow through coils AB, CD, BA, and DC, respectively. Motor rotation direction is controlled by theorder of the sequence; i.e., BDAC for one direction, and CADB for the reverse direction.

Motor Response - Data obtained for an actual scan motor using Method 4 excitation verifies the low power consumption; however, the speed response was slightly less than anticipated. This characteristic is due primarily to the fact that the motor winding time constant is doubled in this configuration. Improvements in this characteristic are obtained by applying power for a longer duration.

Excitation for Retrace Cycle - During the retrace portion of the data scan, the motor excitation pulse width will be maintained at 10 ms and the stepping rate will be 100 pps. The breadboard scan mechanism was tested using this drive method to speeds of 115 pps.

Excitation Signals for Drive Cycle - During the data scan, the motor must step and settle within 50 ms, and the step rate must be 10 pps. Various excitation pulse widths and sequences were used to drive the scan mechanism in order to obtain an optimum value. An excitation time of 10 ms followed by a 20-ms off period and a 20-ms on period provided good speed, damping, and power performance characteristics.

1110-102-23

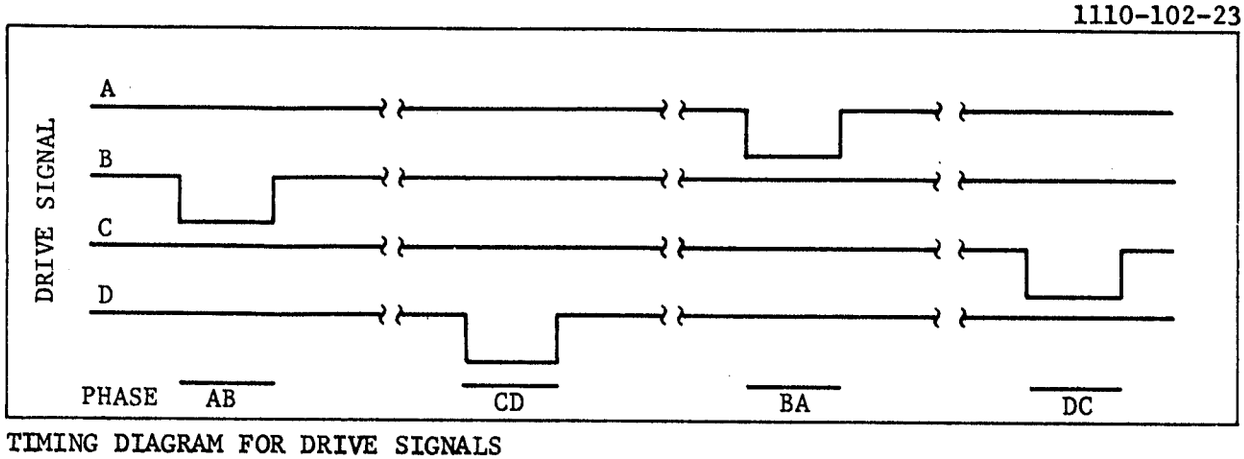

TIMING DIAGRAM FOR DRIVE SIGNALS

1110-102-32

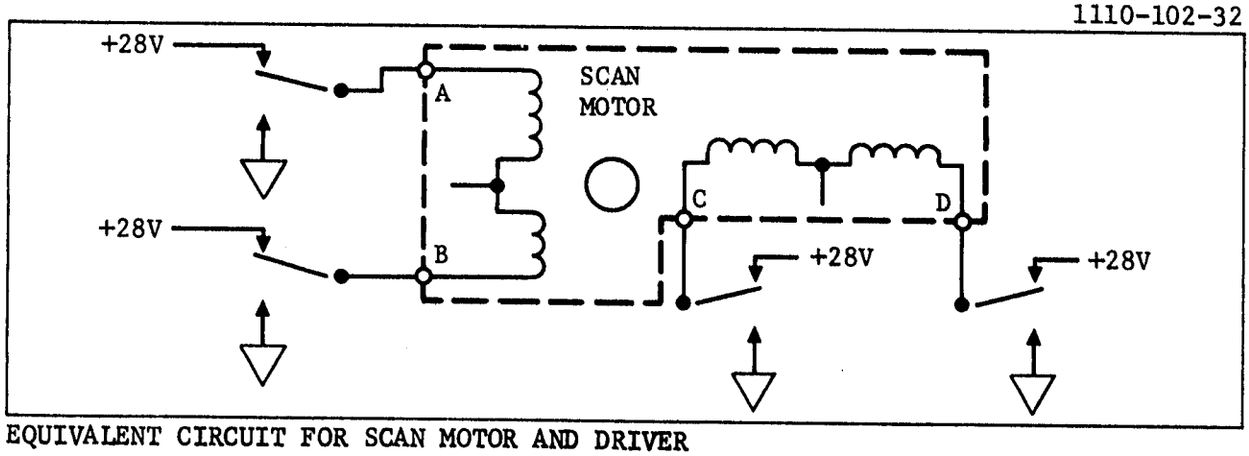

EQUIVALENT CIRCUIT FOR SCAN MOTOR AND DRIVER

DESCRIPTION OF SCAN LOGIC CIRCUIT

The logic required to generate the scan and retrace requires a position counter a two-bit up/down counter to select the motor phase, and a scan-retrace rate selection logic.

Scan Logic - A simplified block diagram of the scan logic is shown in the figure. Logic consists of five basic elements: (1) - 10 step-rate scaler, (2) step-rate selector switch, (3) - 72 position scaler, (4) up/down phase counter, and (5) direction control flip flop.

Circuitry used to synchronize the scan logic is not shown; nor is the logic used to position the scan mechanism at the blackbody or space position. These functions are omitted for clarity purposes; however, their implementation is a simple digital logic network.

Forward scan action is accomplished in 72 steps at a 100-ms step rate. Retrace is performed in a similar manner at a 10-ms step rate. Direction of scan is controlled by the four-state, up/down counter which generates the scan motor drive signal.

Position Counter - A 72-position counter is used to keep track of the FOV. A scan motor position encoder plus the TIP frame sync signal are used to initalize the - 72 scaler to the first FOV and set the scan mode flip flop to the forward direction.

The position counter is advanced one count per step. During the forward scan cycle, an advance rate of 10 pps is maintained until the position counter recycles from a count of 72 back to 0. This action sets the scan mode flip flop to the retrace position, and the advance rate is switched to 100 pps.

Scan Motor Drive Counter - A four-state, up/down counter generates the scan motor excitation signals A, B, C, and D. The direction of scan motor rotation is determined by the order in which the excitation signals are applied; i.e., forward scan requires the sequence BDAC, and retrace requires the sequence CADB.

The up/down counter generates precisely these sequences: where the UP mode corresponds to the forward scan and the DOWN mode corresponds to the retrace. The UP/DOWN mode is controlled directly from the Forward/Retrace flip flop.

Outputs from the UP/DOWN counter are gated with the position counter advance signals to develop the desired scan motor excitation pulse width. During the forward scan, a 30-ms pulse width is used, whereas a 10-ms pulse width is required during retrace.

Scan-Retrace Selector Logic - Selection logic is simply the AND/OR function, which is used to select the scan rate of 100 pps or 10 pps. The scan mode flip flop (Forward/Retrace) acts as the control signal. A prescaler (÷ 10) is employed to develop the 10 pps scan rate frequency directly from the 100 pps. This technique ensures that the proper phased signal is always available.

1110-102-24

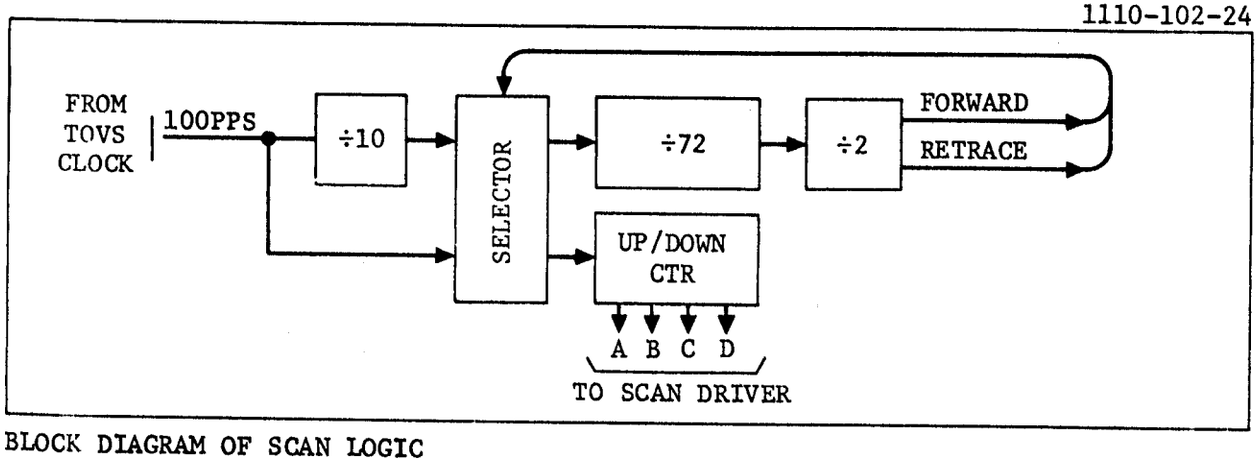

BLOCK DIAGRAM OF SCAN LOGIC

DESCRIPTION OF BREADBOARD DRIVE CIRCUIT

The drive circuit used for the scanner breadboard was a bridge circuit consisting of two complementary switches in a single-pole, double-throw configuration.

Drive Circuit - A drive circuit is required to interface between the scan motor and the scan motor logic. Requirements placed upon the scan motor drive circuit are as follows:

- Sink and supply 700 mA of current to an inductive load.
- Operate from a supply voltage (Vcc) of +28 Vdc.
- Dissipate low power during standby active periods.
- Compatible with low-power logic components.

The selected circuit which meets all these requirements is shown in the figure. Note that the circuit is complementary in nature and acts as a single-pole, double-throw switch, connecting either the 28-Vdc power or the ground bus to the output.

Circuit Description - The scan motor drive circuit uses a Darlington connection (Q1 & Q3) to achieve the high current gain required to buffer the low-power logic drive signal to the high current required by the load. A discrete transistor invertor stage (not shown) is used as a voltage gain to shift from logic levels (5 Vdc max.) to the 28-Vdc drive signal level. Output power transistor Q3 is protected from inductive overshoot by diode CR1. Associated biasing resistor values were selected for a worst-cast analysis. Note that the normal ON condition (output at 28V) is achieved, since the input at terminal (1) is normally near ground.

The lower section of the drive circuit uses an emitter-follower circuit (Q2) to drive the output power transistor (Q4) into saturation. Diode CR4 provides protection against the inductive overshoot. Capacitor C1 ensures that a break-before-make condition exists during turn ON. Input drive signal is obtained from the low-power logic.

A summary of the static transistor parameters illustrate the circuit capa capabilities:

Transistor	$(V_{CE})_{SAT}$,	h_{FE} @	$I_{C(mA)}$	P_D	V_{CEO}
2N2222A	0.3	100	150	0.5	50
2N2907A	0.4	100	150	0.4	60
2N5154	0.2	100	700	11.5	80

The basic power handling transistor is the 2N5154. This device is constructed using the double-diffused planar epitaxial process, and is well suited for this type of application.

Comparison With ITPR Circuit - The drive circuit used on ITPR was essentially a single-pole, single-throw switch used to apply -26 Vdc or open circuit to the output. Component redundancy (series and parallel) was employed for all current handling devices. The table opposite compares the BSU breadboard and ITPR characteristics.

GULTON INDUSTRIES, INC.
Data Systems Division
R. G. Day

COMPARISON OF BSU BREADBOARD WITH ITPR

	ITPR	BSU Breadboard
Drive Method	Unipolar, Single Phase	Bipolar, Single Phase
Switch Type	SPST	SPDT
Load Current	-870 mA	±700 mA, peak
Component Redundancy	Yes	No
Max. Rep. Rate (retrace)	100 pps	100 pps
Power ON/step period	40 ms/400 ms	30 ms/100 ms
Duty Cycle	0.1	0.3
Peak Power	22.5 W	19.6 W
Power/Scan Step (average)	2.25 W	5.88 W
Operating Voltage	-26 Vdc	+28 Vdc
No. of Drivers Required	4	4

1110-102-25

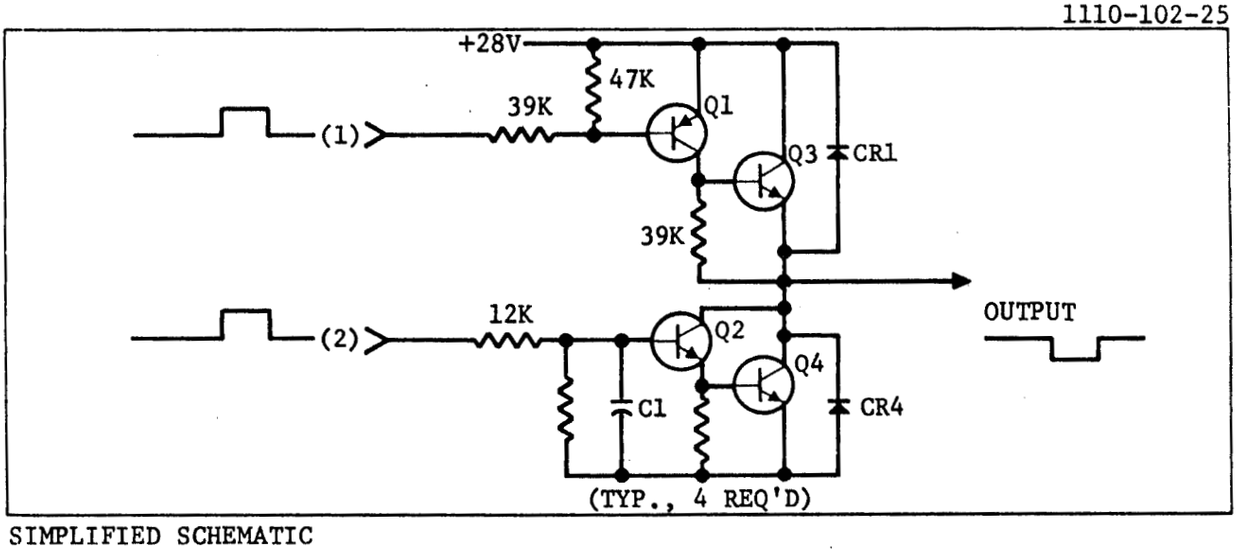

SIMPLIFIED SCHEMATIC
SCAN MOTOR DRIVE CIRCUIT

REDUNDANT DESIGN OF SCAN DRIVE CIRCUIT

Of the methods investigated to achieve component redundancy in the scan drive circuit, the series/parallel was selected because it works whether there is a short or an open component.

Component redundancy can be used to enhance the reliability of the drive circuit. Four types of component redundancy were considered:

Method A: Independent Dual Drive Circuits - A space craft command would be used to select the desired driver.
Method B: Series Redundant Drive Circuits - This circuit will operate properly for single-point failures which result in short circuits between collector and emitter.
Method C: Parallel Redundant Drive Circuit - This circuit will operate properly for single-point failures which result in open circuits between collector and emitter.
Method D: Series/Parallel Redundant Drive Circuit - This circuit will operate properly for single-point failures of either an open or short characteristic.

Figure A is a simplified switching diagram illustrating Methods A, B, and C. Method D is shown in Figure D. A ranking of circuit complexity is as follows:

(1) Least Complex: Method B & C
(2) More Complex: Method A
(3) Most Complex: Method D

Component redundancy Method D is recommended for the BSU scan drive circuit. An implementation of Method D (or B) is shown in Figure C.

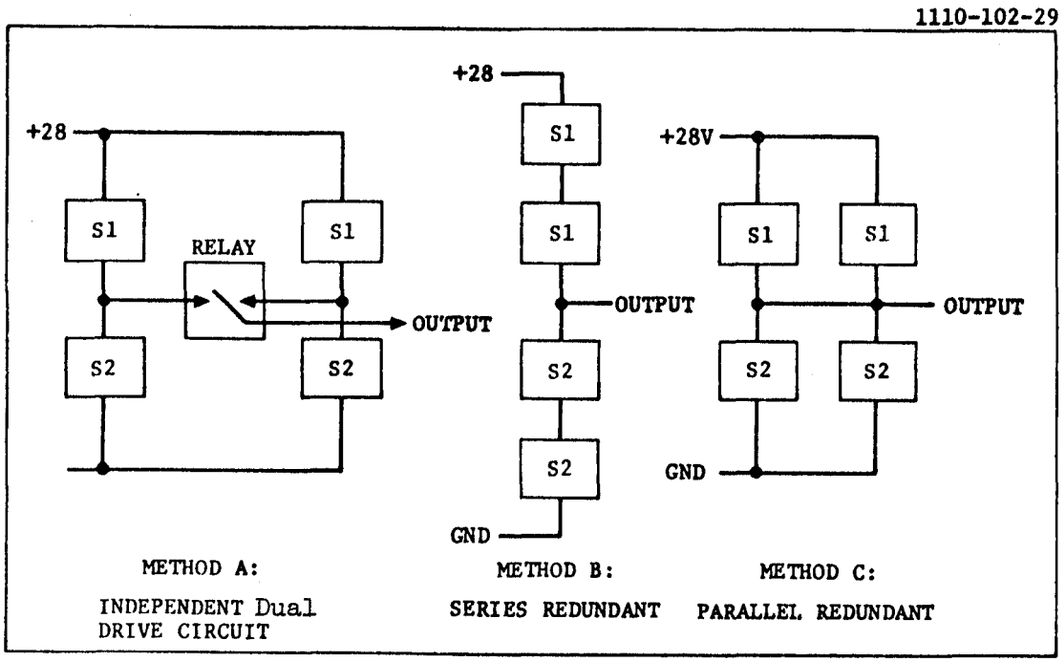

A. COMPONENT REDUNDANCY METHODS

1110-102-28

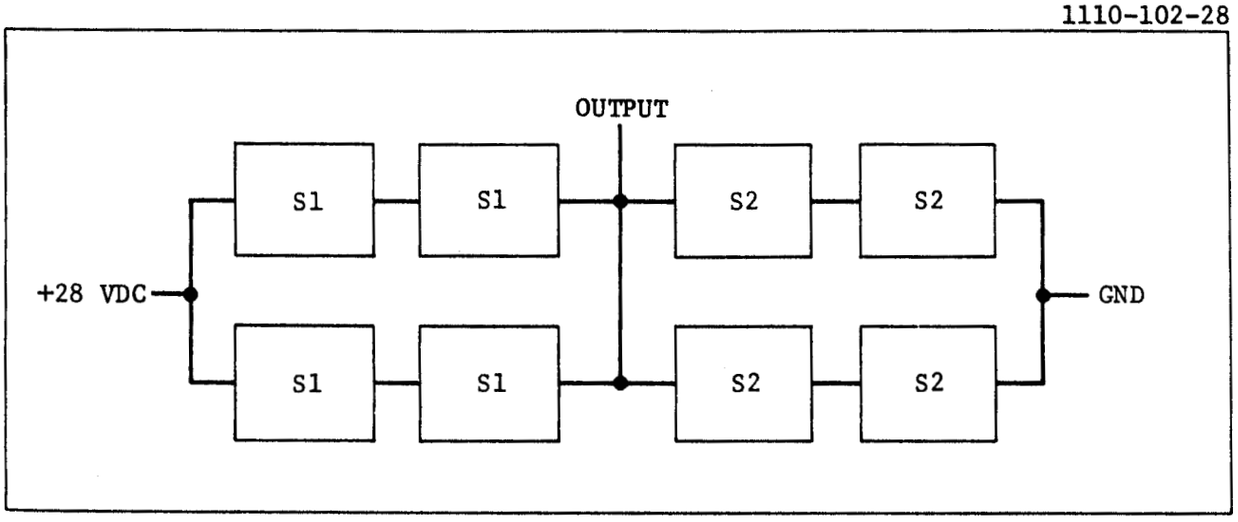

B. METHOD D: SERIES/PARALLEL REDUNDANT

1110-102-30

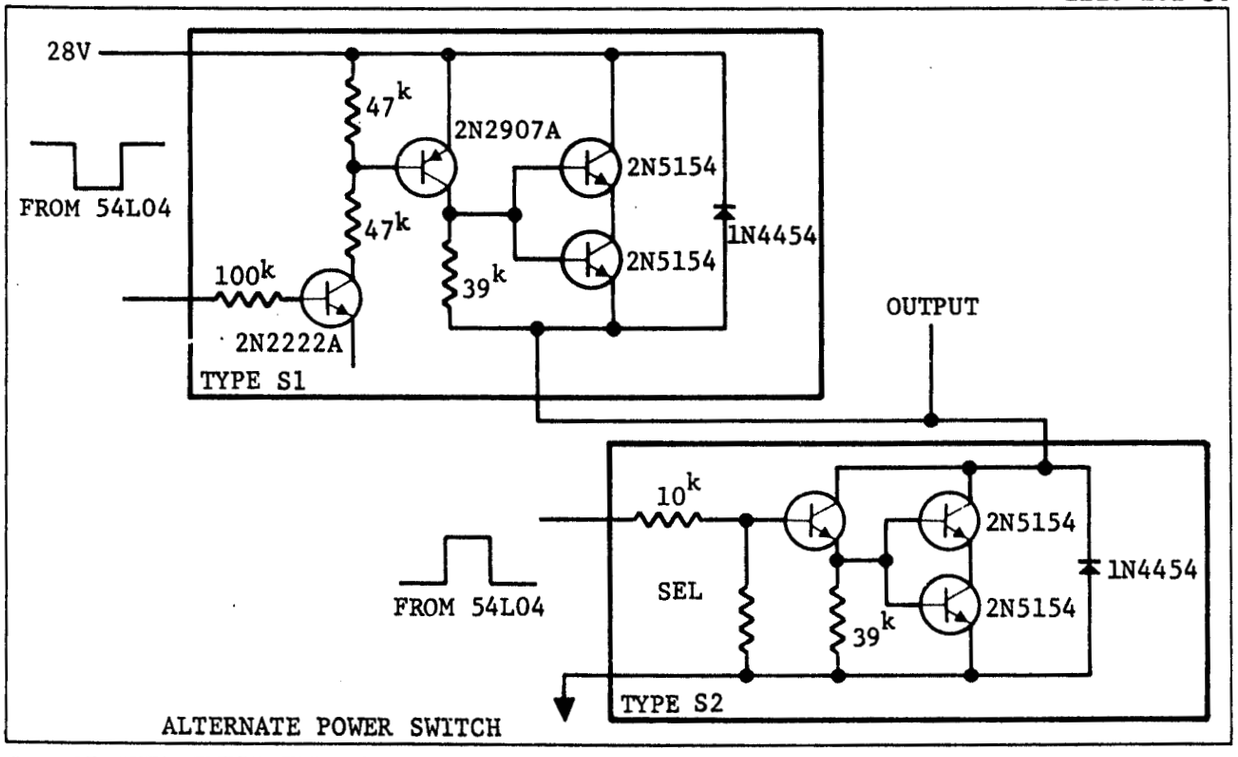

C. CIRCUIT IMPLEMENTATION OF METHOD D

ANALYSIS OF SCAN POWER REQUIREMENTS

The average power required by the scanner is 7.67 W, which because of power supply and drive circuit losses becomes 9.87W at the spacecraft bus. The transient load during step and retrace because of its size and low frequency content, cannot be filtered effectively and will be reflected to the spacecraft.

Power Requirements - Power is dissipated in three (3) functional elements; i.e. 1) scan motor windings, 2) motor excitation drive circuits, and 3) scan mechanism control logic.

Power required to drive Compute Devices motor, Model 15P03 can be computed as a worst case value from $V^2/2R$; where V = 28 V and R = 20 . Secondary effects of back emf and inductance are neglected in order to obtain a limiting value. Peak power dissipated within the motor coil is 19.6 watts.

Power losses within the motor excitation drive circuit amounts to 1.7 W, maximum, peak instantaneous. This loss is due primarily to the motor excitation current flowing through the output driver transistors.

Scan motor control logic dissipates approximately 0.20 W. This is a constant power drain required to keep the scan motor logic active at all times.

Power Dissipation per Cycle - A duty cycle factor is applied to compute the average power required per step; since scan motor power is applied for only 30 msec/step during the scan mode and 10 ms/step during the retrace mode.

The duty cycle factor for the combined scan/retrace cycle is 0.36. This number was obtained from this ratio:

T_1/T_2 where:

T_1 = total time power is applied to motor (2.88 sec)

T_2 = scan/retrace period (8.00 sec)

The average power dissipated per scan/retrace cycle is 7.67 W. A plot of the average power versus time is shown in the visual plan as Figure A.

The power profile required to complete the entire scan cycle (data plus calibration) is shown in Figure B. Thirty-one (31) scan retrace cycles, plus one calibration cycles are completed on a 256 second period. Average power for scan and retrace is 7.67 W, while the average dissipation during the calibration interval is 8.53 W. Combining these values yield as a total of 7.70 W average for the entire scan mechanism and drive circuit.

TOVS BSU Power Supply Effects - TOVS power supply efficiency will effect the actual input power required to drive the scan mechanism. Peak power loads will be directly reflected as current demands from the primary spacecraft power system. Assuming a power conversion efficiency of 78% including drive circuit losses yields an input power of 9.87 W, average. The peak requirements is 27.3 W for as long as 1.24 sec. during the scan return from housing calibration.

Very little power smoothing (averaging) will occur since the power supply filters do not afford sufficient energy storage. Hence, the total load power requirement is reflected directly upon the s/c battery.

1110-102-26

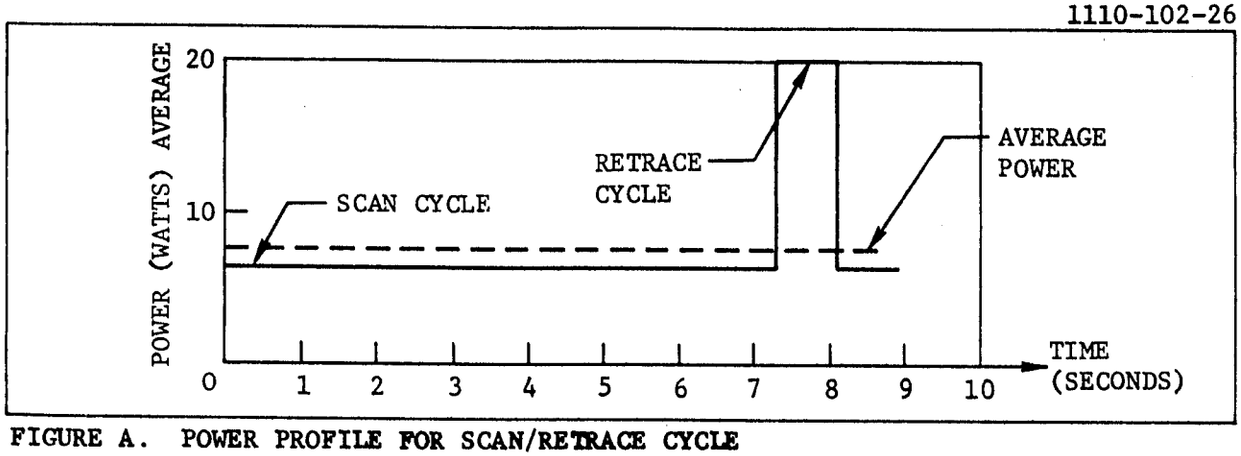

FIGURE A. POWER PROFILE FOR SCAN/RETRACE CYCLE

1110-102-33

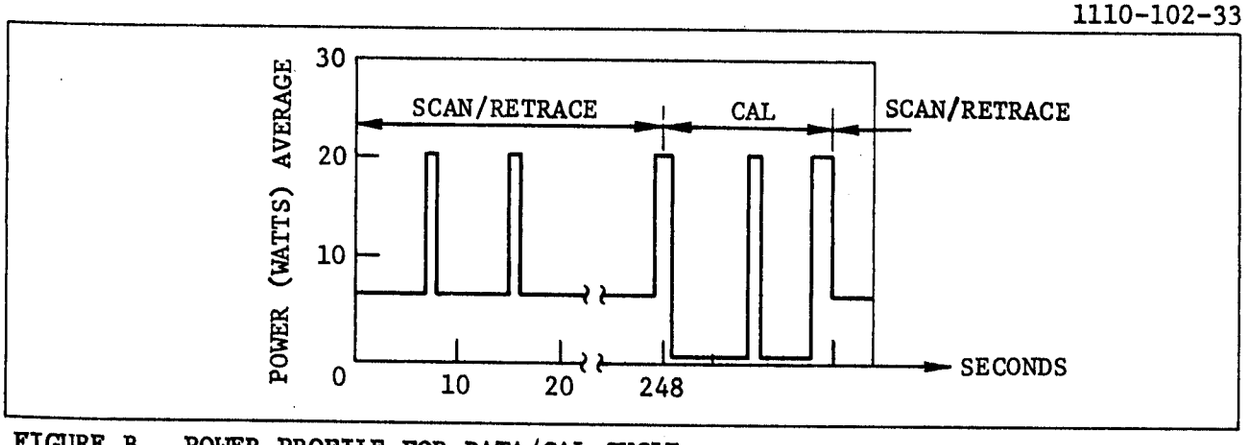

FIGURE B. POWER PROFILE FOR DATA/CAL CYCLE

CHOPPER MOTOR AND EXCITATION METHOD

An A/C synchronous motor driven from a constraint frequency excitation source is recommended as the optical chopper power source.

General: An A/C synchronous motor operates at a constant speed which is independent of the load, but directly proportional to the excitation frequency. This motor can be driven with either a sinusodial or square wave excitation wave form.

Excitation Methods: A two (2) phase excitation signal is required. The signals can be either AC or DC, but they must be 90° out of phase and provide current flow in both directions thru the windings. Four (4) methods were considered:

Method 1: AC, single phase
Method 2: AC, dual phase
Method 3: DC, single phase
Method 4: DC, dual phase

Methods 1 and 2 dissipate the least power within the motor, but requires sinusoidal type drive signals and linear power drive amplifiers. Power savings in the motor are cancelled by the linear power amplifier dissipation and complexity of the sine wave generating circuitry.

Methods 3 and 4 use square wave signals for the motor control. Method 3 uses a single excitation drive and provides a 90° passive phase shift network to develop the other phase.

Recommended Excitation Method: Method 4 is the drive technique used on ITPR and is the recommended approach for the TOV's. This recommendation is based on the simple drive circuit employed, relatively low power consumption, and demonstrated operational performance.

Drive Signal Description: A timing diagram illustrating the phasing of the four drive signals ($\phi 1$, $\phi 2$, $\overline{\phi 1}$, $\overline{\phi 2}$) plus a simplified equivalent switching circuit is shown in the Figure on the adjacent page. Note that signals $\phi 1$ and $\overline{\phi 1}$ are 180° out of phase, causing bidirectional current flow. In like manner, $\phi 2$ and $\overline{\phi 2}$ control the Phase 2 winding. Also note that $\phi 1$ and $\overline{\phi 2}$ are 90° out of phase.

Chopper Motor Drive Circuit: A power switch is required to drive the chopper motor coils. Circuit must be capable of supplying and sinking current (100 mA) to an inductive load.

The bridge type driver circuit used on the scan motor driver is recommended.

Power Requirements: Power is dissipated in three (3) areas; i.e., 1) chopper motor windings, 2) excitation drive circuit, and 3) control logic. The power consumption is as follows:

Motor Windings:	2.75 watts
Drive Circuit:	0.35 watts
Control Logic:	0.15 watts
Total:	3.25 watts, maximum

The power profile is essentially constant, except for a transient which occurs at the driving frequency. The power transient is of short duration, 10 to 20 μs, and occurs when the excitation signal changes states.

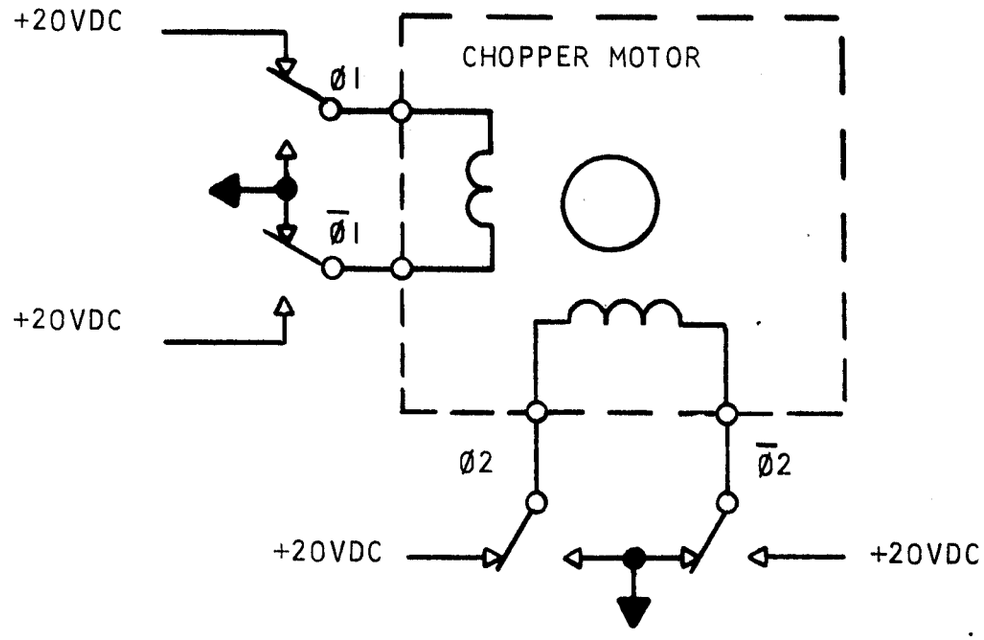

EQUIVALENT CIRCUIT
CHOPPER MOTOR &
DRIVER

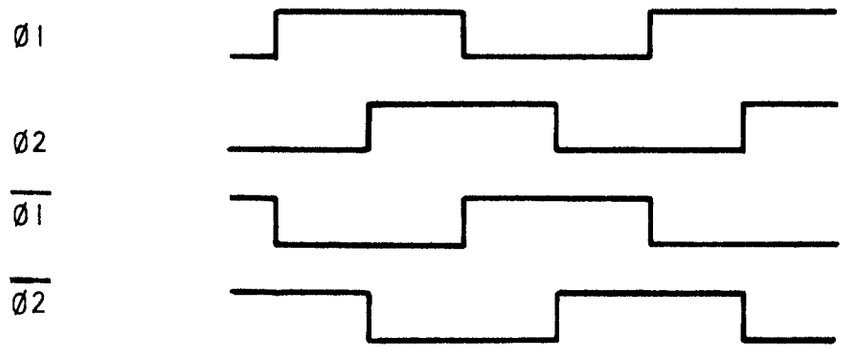

TIMING DIAGRAM
EXCITATION SIGNALS

PHASE CONTROL OF THE CHOPPER MOTOR

A digital phase locked loop is recommended as the means for controlling the chopper motor phase.

Requirement: Due to the limited number of chopper cycles occurring during the dwell period, it is essential that the chopper motor be phase locked to the infrared energy integrator control. This interlock will assure that the integration is synchronized and phased with the basic TOVS system timing, thus tying together the step scan, integration, sampling and digitization processes.

Configuration: A block diagram illustrating the digital phase locked loop is shown in Figure A on the adjacent page. Five (5) functional elements comprise the circuit. A brief description of each elements is as follows:

- Chopper - An optical chopper mechanism powered by an A/C synchronous motor.
- Optical Detector - A circuit used to determine the phase of the chopper wheel, via a light emitting diode and associated detector.
- Phase Comparator - A digital circuit used to determine the phase difference between the electrical PRP reference signal and the actual PRP.
- ÷ N Scaler - A variable length counter used to adjust the drive frequency by I:100 from the nominal value.
- Drive Logic - A digital network which conditions the frequency F2 to drive the chopper motor.

Operation: The loop functions to keep the PRP signal (obtained optically via the mechanical chopper) in phase with the chopper reference clock which is obtained directly from the TOVS system clock. This is accomplished by the action of the variable modulous divider and phase comparator.

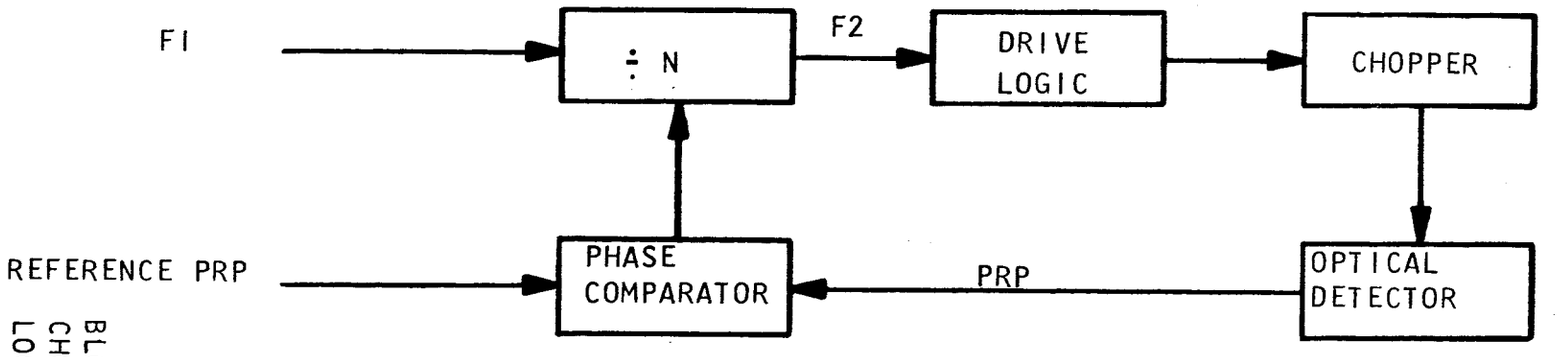

BLOCK DIAGRAM
CHOPPER SYNCHRONIZATION
LOGIC

DUAL INSTRUMENT MODE CONTROL DESCRIPTION

A special operating mode utilizing two (2) TOVs instruments was studied to determine the support requirements when data is obtained from both instruments.

General: Operating conditions required during this mode are summarized below:

a) A unique S/C command will be used to identify the dual operating mode.
b) Both TOVS instruments A and B will be powered and conditioned to gather data at one-half the normal rate.
c) Both TOVS instruments will be controlled to obtain data from the same field of view; $(FOV)_a \equiv (FOV)_b$.
d) TOVS data readout will be performed in the normal manner; i.e., as commanded by the TIP control signals but at a reduced rate.
e) Effective scan rate of TOVS instruments A and B will be reduced to one-half (1/2) the original scan rate to allow the TIP system to maintain its normal data rate.

A simplified block diagram illustrating the relationships of the major subsystems is shown in Figure A. Note that a single S/C command is applied to both $(TOV)_a$, $(TOV)_b$ and TIP to initiate the dual mode operation, also that the TOVS outputs are dedicated to unique TIP channels.

Support Requirements: Dual instrument operating mode imposes requirements upon several spacecraft subsystems including the TOVS, TIP, S/C Command and S/C Power systems. The requirements are listed below:

a) TOVS System: Provide the capabilities described above.
b) TIP System: Provide the data processing capability necessary to alternately address each TOVs instrument.
c) S/C Command System: Provide an unique command to identify the dual instrument mode.
d) Power System: Provide sufficient power to sustain a dual instrument operation. Approximately 55 watts is required to support TOVS A and B during the dual mode.

Scan Mechanism Control: Two (2) major control functions performed by the scan mechanism logic should be provided; i.e.,

a) Scan rate should be reduced from 100 ms/step to 200 ms/step for TOVS A and B.
b) Scan position counters must be synchronized to the same FOV.

One method of implementing these control functions is discussed below. Note that the control function is entirely digital in nature and is a simple logic selection process controlled by the S/C Dual Instrument Command.

Scan Rate Control: A simplified block diagram of the scan logic is shown in Figure A and a timing diagram in Figure B.

Scan rate is selected via the AND/OR logic, as 100 ms/step (normal scan mode) or 200 ms/step (dual instrument mode). A second AND/OR selection network is required for the retrace rates of 10 ms/step and 20 ms/step. Since all the instrument timing signals are derived directly from the S/C clock via digital scalers, the stepping rates for $(TOV)_a$ and $(TOV)_b$ are identical in frequency.

Scan Position Synchronism: A time reference marker is required to synchronize the position address counters for both TOVS A and B.

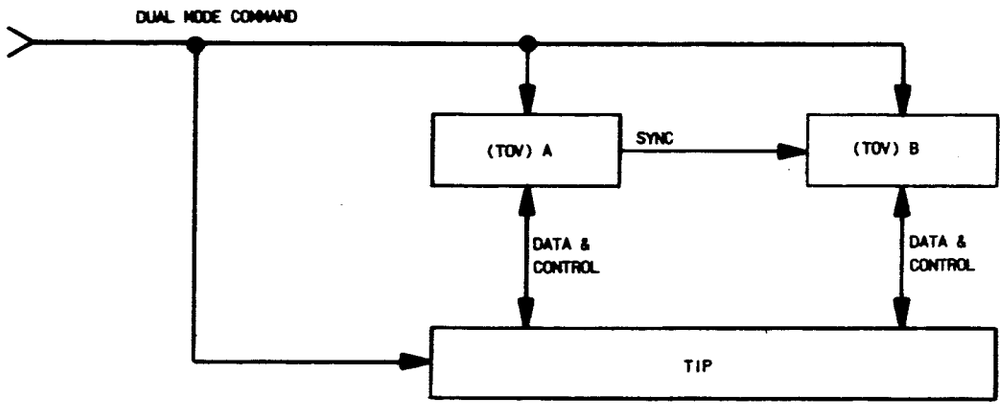

FIGURE A:
BLOCK DIAGRAM OF THE DUAL INSTRUMENT MODE.

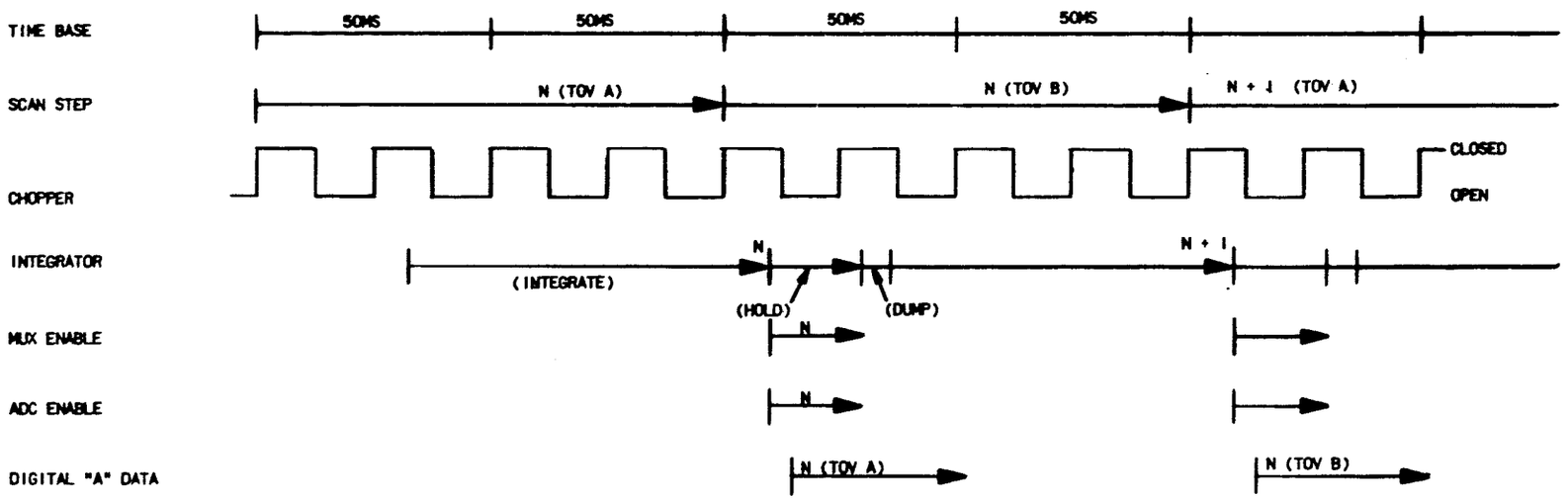

FIGURE B:
DUAL INSTRUMENT TIMING

FORMATTING UNIT DESCRIPTION

Logic circuitry necessary to control the transfer of data from the TOVS instrument to the S/C telemetry information processor is defined. This logic is defined as the Formatting unit.

Data Output Form: All critical data is supplied in serial digital form, similar to NIMBUS digital "A". This data form is recommended to allow the TOVS to use its interval 12-bit ADC in lieu of the TIPs 8-bit converter. Interface signals between the TIP and TOVS are assumed to be similar to those supplied by the VIP.

Buffer Requirements: Interfacing the TOVS instrument with an external data processor was considered from two viewpoints, i.e.,

1) What is the most hardware efficient interface? and
2) What is the most flexible type of interface?

The answer is basically, how much temporary buffer storage is supplied. A minimum of a one (1) word buffer register (16 bits) is necessary and represents the most efficient hardware interface; yet it provides the most strigent requirement on the S/C data processor.

A comparison of three possible interface configurations was conducted and is presented in Table A.

Configuration Description: A simplified block diagram of the formatter unit is shown in Figure B, and illustrates the Method 1 configuration. Methods 2 and 3 are similar, except that the one (1) word buffer register is expanded to a sixteen (16) word capacity.

Logic gates digitally multiplex the data into the storage register, which also acts as a parallel to serial converter. Parity is generated in a serial manner and inserted into the data bit stream via the output selection gates.

ITEM	METHOD 1	METHOD 2	METHOD 3
BUFFER TYPE	Interlaced Load/Unload	Non-Interlaced Load/Unload	Interlaced Load/Unload
CAPACITY	1 Word (16 Bits)	16 Words (256 Bits)	16 Words (256 Bits)
FLEXIBILITY	Least Flexible	More Flexible	Most Flexible
RESTRICTIONS	(1) Requires TOVS and TIP Formats to be synchronized. (2) Requires that 14 TIP Words (adjacent) be readout at a rate of 1 word/2 ms (500 HZ). Readout period is fixed.	(1) Requires that TOVS and TIP Formats to be synchronized. (2) Requires that TOVS Data (16 Words) be readout at any time during a fixed 75 ms period.	(1) Requires that TOVS Data (16 Words) be readout at any time during a 100 ms period
COMPLEXITY	Least Complex	More Complex	Most Complex
VOLUMN ESTIMATE	1.0 (Reference)	1.8	2.0
POWER ESTIMATE	1.0 (Reference)	1.0	1.2
WEIGHT ESTIMATE	1.0 (Reference)	1.1	1.2
AVAILABLE PARTS	(1) Flip-flop register using 54L or CMOS	(1) Multiple register per Method 1. (2) CMOS RAM (3) PMOS RAM (4) PMOS Shift Register	Same as Method 2

TABLE A: BUFFER COMPARISON TABLE

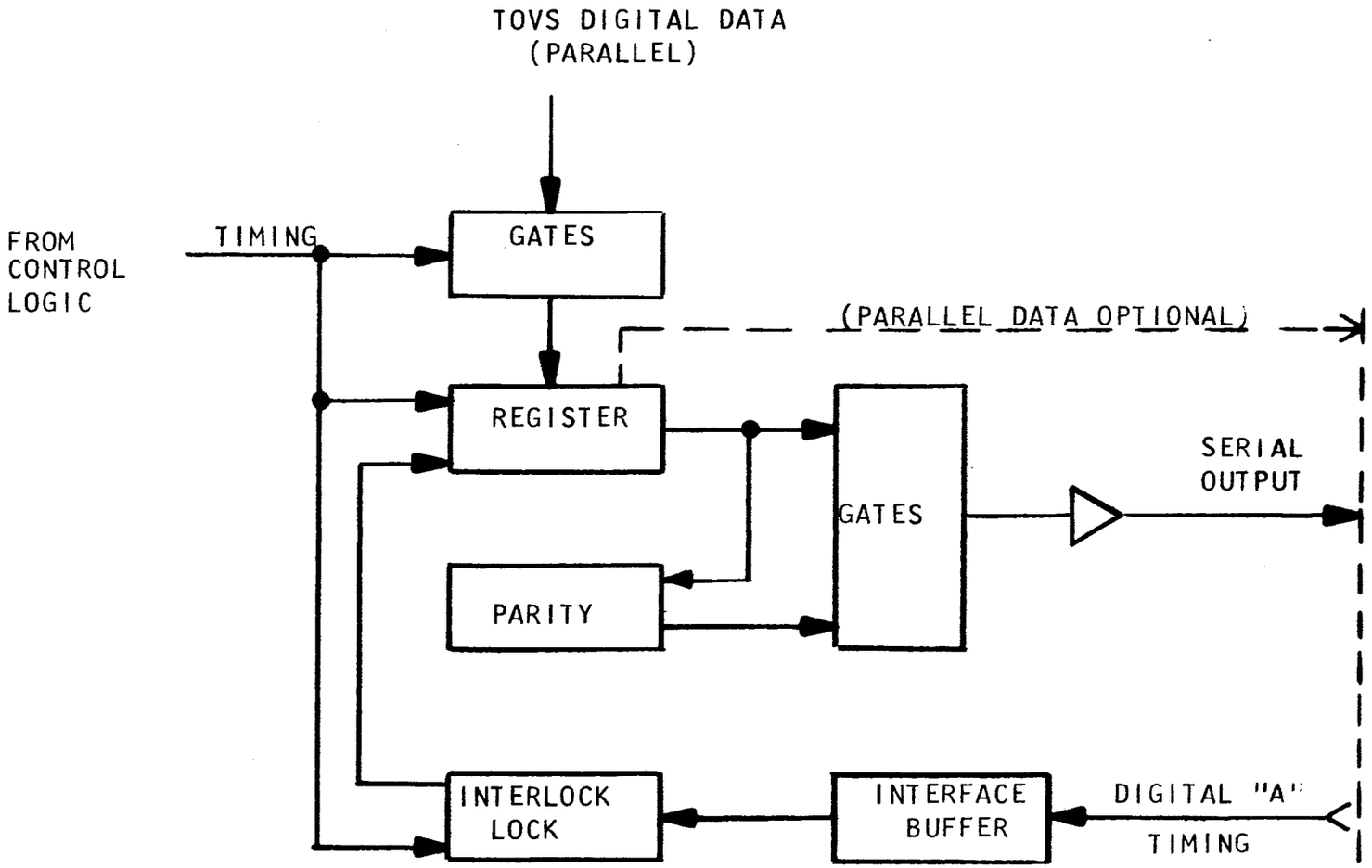

FIGURE B
BLOCK DIAGRAM OF
THE OUTPUT
FORMATTER

DATA FORMAT

The data word length, structure and contents are identified. Data which supports the primary infrared energy measurement is included.

Word Format: A suggested word format diagram is shown in Figure A. The TOVS word is sixteen (16) bits. The word is divided into two (2) fields; Field A consists of bits 9 thru 16 and Field B consists of bits 1 thru 8. Field A bits would be located in TIP word slot N and Field B bits would be packed into word slots N + 1.

A word parity bit is generated and located in bit Position 1. Odd parity is employed.

Bit positions 2, 3 and 4 are used for monitor flags and position data. Recommended discrete bits are tabulated in Figure B.

Bit positions 5 thru 16 are allocated for the digital value of the measurement; where bit 5 is the LSB, bit 14 is the MSB and bit 16 is the sign.

BITS POSITION															
1	2	3	4	5	6	7	8	9	10	11	12	13	14	15	16
P	X	X	X	0	1	2	3	4	5	6	7	8	9	10	S

TOVS DATA

DISCRETE BITS

PARITY

NOTE:
1. TIP Word N, Bits 9 thru 16, TOVS Word Y
   TIP Word N + 1, Bits 1 thru 8, TOVS Word Y
2. 16 TOVS words will be used to process data from 1 FOV
3. 48 bits of discrete data will be inserted into the X X X bit position (See Figure B)
4. Bit position 16 is the MSB and will be shifted to the TIP as the 1st bit.
5. Bit position 1 is the parity bit for the 16 bit TOVS word.

FIGURE A: TOVS WORDS FORMAT

MONITOR	NO. OF BITS
Shaft Angle Encoder	7
FOV Electrical Address	7
Line Number Counter	8
Position Flag P1, Nadir	1
Position Flag P2, Housing	1
Position Flag P3, Space	1
Mode Flag M1, Earth Scan	1
Mode Flag M2, IR Cal.	1
Mode Flag M3, Electrical Cal.	1
Mode Flag M4, Dual Mode	1
PRP Operating Flag	1
Command Monitors	13
Spares	5
TOTAL	48

FIGURE B: RECOMMENDED DISCRETE DATA BITS

Sampling Format: A Recommended Sampling Format is Shown in Figure C Below.

Word No.	Bit Positions		
	1	2 3 4	5 thru 16
1	P	48 Discrete Bits	IR Channel 1
2	P		IR Channel 2
3	P		IR Channel 3
4	P		IR Channel 4
5	P		IR Channel 5
6	P		IR Channel 6
7	P		IR Channel 7
8	P		IR Channel 8
9	P		IR Channel 9
10	P		IR Channel 10
11	P		IR Channel 11
12	P		IR Channel 12
13	P		IR Channel 13
14	P		IR Channel 14
15	P		Temperature Sub Com 1
16	P		Temperature Sub Com 2

FIGURE C: TOVS SAMPLING FORMAT

DESCRIPTION OF INSTRUMENT COMMANDS

TOVs operating modes are directly controlled by thirteen (13) space craft supplied commands.

Command Subsystem: A command subsystem is required to execute the commands obtained from the TIROS-N S/C command system.

TOVS command subsystem is similar to that used on ITPR in that the same type of hardware implementation is recommended.

Command List: A total of thirteen (13) commands are required to control the TOVS. Each of these commands, together with a description of the action, is shown in Table A.

Command Circuitry Description: Magnetic latching relays are recommended as the storage devices for all radiometer commands. A typical command relay is shown in Figure B.

Although the exact spacecraft interface is not defined in the technical specification; it is assumed that the relays will be driven by one (1) MA type line and one (1) MB type line.

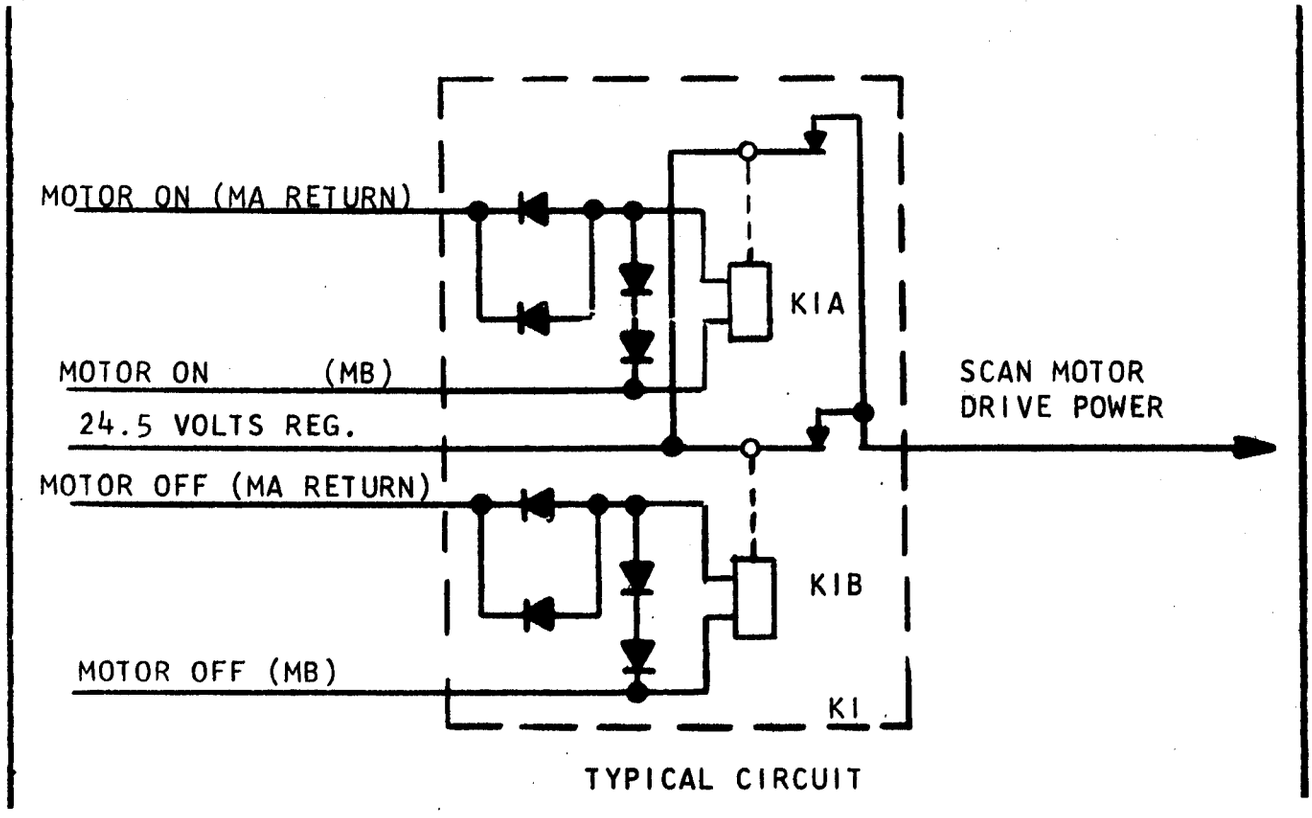

FIGURE B: COMMAND LATCHING RELAY CIRCUIT

TABLE A: TOVS COMMAND LIST

COMMAND	RESPONSE
1. Chopper Motor ON/OFF	Applies/Disconnects power to the chopper motor drive circuit.
2. Electronics ON/OFF	Applied/Disconnects power to all TOVS electronics, causing all channels to become inactive.
3. Scan Drive ON/OFF	Applies/Disconnects power to the scan motor drive circuit.
4. IR Calibrate ON/OFF	Enables/disables the automatic in-flight calibration cycle of space and housing.
5. Electronic Calibration ON/OFF	Enables/disables the electronic calibration of integrator, multiplexer and ADC.
6. NADIR Position ON/OFF	Causes the scan mirror to view the nadir position.
7. Space Position ON/OFF	Causes the scan mirror to view the space position.
8. Housing Position ON/OFF	Causes the scan mirror to view the housing position.
9. Detector Temperature Controller ON/OFF	Applies/disconnects power to the detector temperature controller.
10. Calibration Black Body Heater ON/OFF	Applies/disconnects power to the black body heater.
11. Standby Heater ON/OFF	Applies/disconnects power to the instrument standby heater.
12. Restricted Scan ON/OFF	Causes the scan program to be restricted to 1/2 the normal range.
13. Dual Instrument Mode ON/OFF	Causes TOVS A and B to process data at 1/2 normal rate.

SECTION 9

Design of Power Supply

Instrument Power Subsystem..... 9-0

Section 9 - Design of Power Supply

INSTRUMENT POWER SUBSYSTEM

The combination of a switching type preregulator followed by a dc-dc converter is recommended for maximum efficiency.

This combination has exhibited efficiencies of 70 - 72% for loads in the 25 watt range in both the ITPR and ERB programs. In this design the dc-dc converter is slaved to the system clock when present and free-runs otherwise. This has advantages in terms of the ADC and converter noise spikes.

Total power to signal ground isolation is obtained by means of the converter except for a small amount of capacitive feedthrough. This allows for maximum flexibility in the spacecraft grounding system. A totally enclosed sub-package is required for the power supply. All lines entering and leaving the package should be filtered. Within the instrument a single point grounding system must be set up at the detector signal return point. It is suggested that the scan motor power supply lines be shielded to prevent radiation as much as possible.

The package containing the power supply should communicate thermally with the instrument housing by conduction. It can be considered as virtually a constant source of heat when the instrument is on.

In terms of detail design the area of most difficulty will involve minimizing the turn-on current transient and induced ripple. A relatively high source impedance of 0.3Ω makes a low ripple specification difficult but not impossible to meet. Stiffer filtering requirements are paid for with weight because the chokes needed for low loss LC filtering must pass relatively large dc currents without saturating.

The nature of the scanning requirement results in power variations with time that are considerable. Although the scan power is an average of about 8 watts the peak power is about 3 times that number. The duty cycle during the bulk of the scan period is 30 msec out of every 100 msec. Passive storage on a capacitor allowing for a 10V ΔV during the pulse period requires in excess of 2000 μf. A recharging method consisting of a constant current power supply with a soft voltage limit would be needed to smooth the input current.

It is recommended that scan pattern induced load variations be considered as just that "load variations". They occur at frequencies of 10Hz or less imposing little burden in regulator design directed at a low output impedance. The line drop to the TOVS from the spacecraft power supply should not be added in to the source impedance to the TOVS since voltage drops along it only affect the TOVS.

The current surges caused by the scan motor present a problem that has not been completely resolved. If the motor supply voltage source is taken from the same dc/dc converter as the logic voltages, logic stability during the scan motor pulses must be maintained. The optimum solution may require a separate supply for motor power. This solution suggests itself because the proposed power supply is more tolerant of input voltage variation than load variation.

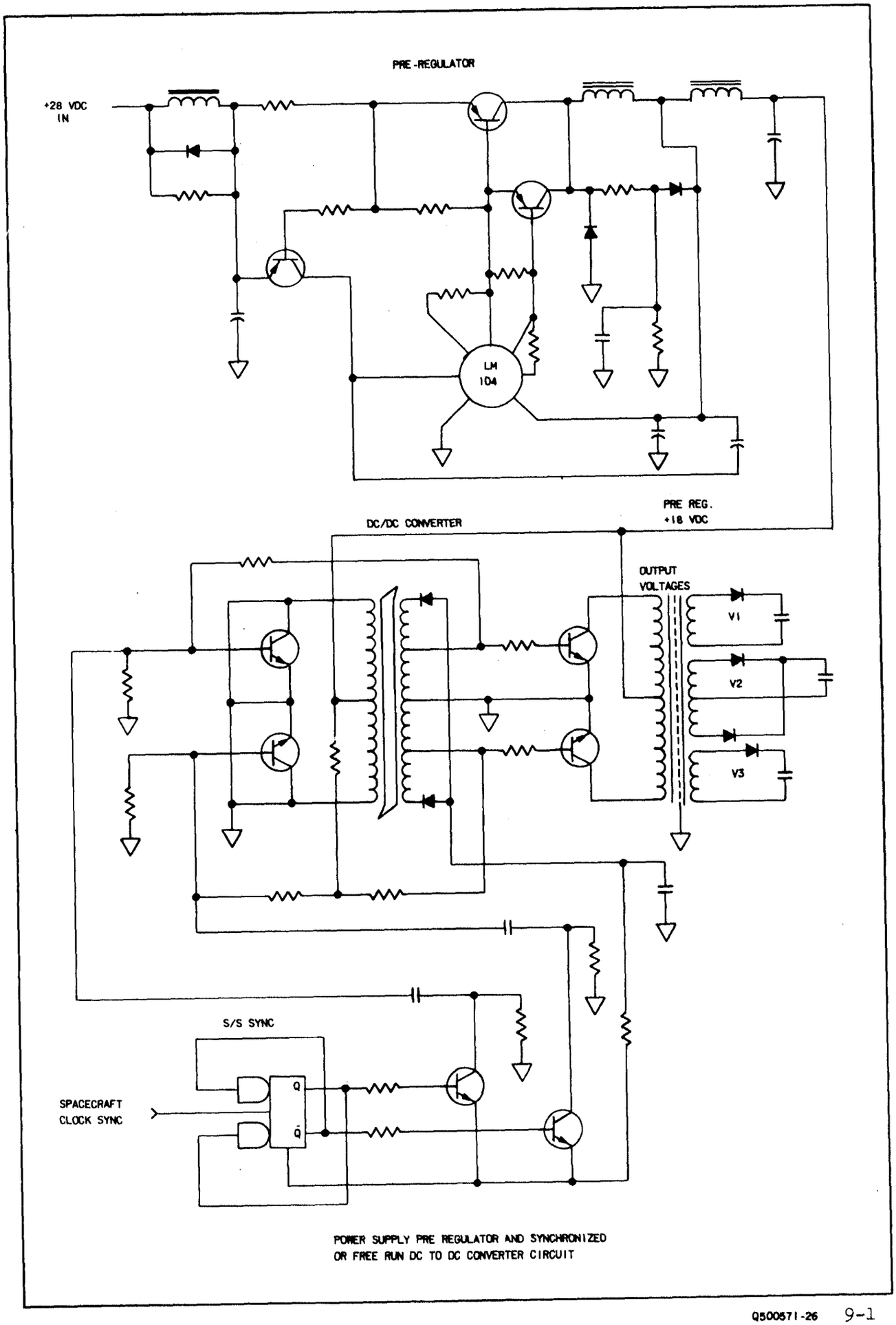

POWER SUPPLY PRE REGULATOR AND SYNCHRONIZED
OR FREE RUN DC TO DC CONVERTER CIRCUIT

SECTION 10
THERMAL ANALYSIS

General Description of Thermal Study 10-0
Summary of Thermal Requirements 10-2
Description of Environmental Constraints 10-4
Highlights of Thermal Design 10-6
Control of Blackbody Temperatures 10-8
Control of Optics Subassembly Temperatures 10-10
Control of Scanner Temperatures 10-12
Description of the Thermal Model 10-14
Summary of Thermal Analysis 10-16
Conclusions of Thermal Study 10-18

GENERAL DESCRIPTION OF THERMAL STUDY

The purpose of the TIROS Operational Vertical Sounder thermal study was to define the approach to thermal control and prove its adequacy with analysis. The analysis of the design shows that adequate control of instrument temperature is attained.

The TIROS Operational Vertical Sounder-Basic Sounder Unit (TOVS-BSU) is a scanning infrared sounder for the TIROS-N spacecraft, which will be launched in 1975. Orbiting the earth daily, the BSU instrument will measure the moisture and temperature of the earth's atmosphere as a function of altitude and cloud cover. The purpose of the BSU thermal study was to define a design approach for thermal control of the instrument and to analyze the approach in detail to determine whether it meets the thermal requirements.

Thermal Related Components - The physical components of the BSU related to the thermal design are listed in Table I. The spacecraft coordinate system defined in Table II is used in discussing thermal control of these components. The instrument is attached to the bottom side of the spacecraft, with the detector optics forward (+X side) and the scanner aft (-X side). The scanner scans in the YZ plane, looking down in the +Z direction at nadir. The sun can irradiate the instrument on the left (-Y) side, on the bottom (+Z) side, and on the front (+X) and rear (-X) sides. The scan motor and scan drive electronics on the -X side are both tied to the scanner web and the dissipated heat from these units must be removed. The housing blackbody assembly is mounted at the top of the structure facing downward. Radiation leaving the assembly must be controlled to maintain a proper instrument energy balance. The scan mirror is located directly beneath the blackbody assembly and must be protected from the sun's influence. The detectors and detector optics are located at the +X end of the instrument and require a very stable environment. The optics baseplate is mounted to the telescope baseplate which, in turn, is mounted to the optics web. The chopper motor and telescope assemblies are fixed to the telescope baseplate, and the design must direct the local energy flow to obtain specified temperature levels of these components. The radiator system straddles the scanner and optics webs, faces the +Y and -Y directions, and ultimately radiates both the dissipated and incident heat loads.

Study Tasks - The thermal design effort depended upon an environmental heating analysis to discover how the sun irradiates various TOVS components at different orbital positions and at different times of the year. Based upon this analysis, a thermal control configuration was designed to meet the temperature control requirements, allowing for the environmental heating effects and the mechanical, optical, and radiometric design constraints of the instrument.

Results of Thermal Analysis - The study obtained the expected thermal performance of TOVS for three extreme conditions in the mission profile. The performance figures obtained are based on transient network analyses of the final TOVS thermal configuration and illustrate the temperature distribution of the instrument for each case. The transient temperatures during two operational cases for several components were also presented. The analyses show that the thermal design goals can be met within the orbital and spacecraft constraints.

TABLE I. MAJOR BSU COMPONENTS AFFECTING THE THERMAL CONTROL DESIGN

The components that influence the BSU energy balance most are the electronics, the motors, and the radiators.

• Scan Motor	- Dissipates heat.
• Scan Drive Electronics	- Dissipates heat.
• Scanner Web	- Conductive link for scan motor and drive.
• Optics Baseplate	- Mounting structure for detector optics.
• Chopper Motor	- Dissipates heat.
• Telescope Baseplate	- Conductive link for chopper motor.
• Optics Web	- Conductive link for all optics subassembly and associated electronics.
• Housing Blackbodies	- Represents large radiating surface.
• Scan Mirror	- Receives direct sun.
• Radiators	- Key element to energy balance.
• Signal Conditioning Electronics	- Dissipates Heat

TABLE II. DEFINITION OF INSTRUMENT AXES

These are the same definitions used on NIMBUS.

Axis	Spacecraft Axis	Direction of Positive Axis
X	Roll	Direction of orbital motion.
Y	Pitch	To right of spacecraft.
Z	Yaw	Down, along local vertical.

SUMMARY OF THERMAL REQUIREMENTS

Three types of thermal requirements impact the BSU thermal design: the agreed spacecraft interface requirements, derived requirements for critical component temperatures, and derived requirements for temperature stabilities which affect radiometric accuracy.

Specified Requirements - The TOVS-BSU must operate in the TIROS spacecraft environment. This environment depends on the nature of the orbit and the agreed-upon spacecraft thermal interface. The implications of the TIROS orbit must be carefully analyzed, because, as can be seen from Table I opposite, the electronic power input alone exceeds the power which can be transferred across the spacecraft interface. The thermal control system must operate within the weight, power, and envelope restrictions given.

Derived Requirements - The TOVS-BSU design study resulted in a number of design decisions. The parameters listed in Table II are the essential derived requirements for the thermal study.

The scanner beam size and look angles determine the size of the cutout in the housing through which heat may be gained or lost by radiation. Certain components, notably the detectors, must remain within the temperature ranges listed. The scan motor, chopper motor, and electronics dissipate the heat shown. There is enough power to control detector and reference blackbody temperatures, but not enough to control the calibration blackbodies.

Radiometric Constraints - Because the BSU measures thermal radiation, it is necessary to keep stable the temperatures of those components that can emit detected radiation.

The design goal chosen was to allow the radiation from each source of error to change between calibrations by no more than the noise equivalent spectral radiance. Because there are a number of sources of radiometric error, this constraint means that a simple linear interpolation between calibrations is necessary to correct for the measured change in instrument gain and offset. (It does not appear feasible to eliminate the need for this interpolation.)

The parameters listed in Table III were derived specifically as follows:

- Because the detector temperature coefficient is about 1%/^{o}C, a shift of 0.1^{o}C corresponds to a gain shift of 0.1%, which is about equal to the noise error in a single measurement of a 330°K blackbody in the most thermally-sensitive channel (Channel 4).
- The reference blackbodies provide a zero for the instrument. The maximum allowable drift was taken to be equal to the noise-equivalent-temperature-difference of $\pm$0.075 degree for channel 4 for a full-scale 330°K scene. A similar criterion was adopted for the calibration blackbody, although change in its temperature is not relevant if correctly measured.
- The scanner, telescope, and chopper mirrors, although polished and gold-coated, do emit detectable radiation. If the effective emissivity is 2%, the detectable temperature change is 3.25%/^{o}C.

TABLE I. SPECIFIED SPACECRAFT AND INSTRUMENT CONSTRAINTS

The design values for weight and power are close to the maximum allowed values.

Maximum Envelope	14 x 24 x 12 in.
Maximum Weight	45 lb
Maximum Input Power	35 W
Orbit: Altitude	906 nmi
Inclination	103 degrees
O'clock Angle	3:00-3:30 pm
Sun Angle	32-57 degrees
Maximum TIROS-BSU Heat Flow	±15 W
Interface Temperature: Min.	+10°C
Max.	+30°C
Calibration Interval	256 s

TABLE II. DERIVED REQUIREMENTS

The following constraints were derived during the design.*

Scanner Beam Diameter:	11.4 in.
Scan Look Angles (nadir = 0°):	-43 to +72 degrees
Detector Temperature (absolute):	35 ±1°C
Scan and Chopper Motor Temperature:	-25 to +70°C
Electronics Temperature:	-25 to +60°C
Total Electronics Power:	15.85 W
Detector Optics Heater:	3.5 W
Scanner Motor Power:	8.17 W
Chopper Motor Power:	7.17 W

*Power figures assumed in the thermal study differed slightly from the final power budget, but the differences do not affect the design or results significantly.

TABLE III. RADIOMETRIC CONSTRAINTS

The following design goals for temperature changes between calibrations were adopted to reduce radiometric calibration corrections.

Detector Temperature:	0.100°C
Blackbody Temperatures:	0.075°C
Mirror Temperatures:	3.25°C

DESCRIPTION OF ENVIRONMENTAL CONSTRAINTS

Environmental factors that constrain the thermal design are primarily solar radiation, albedo, and earth radiation. Of these, solar radiation has the greatest design impact because of the wide variance between the integrated solar flux for the hot and cold cases, and the difficulty in attenuating this difference to meet the specified temperature range.

The nominal sun-synchronous TIROS orbit has an altitude of 906 nm, is inclined at 103 degrees, and has a 3-pm ascending node. These values give an approximate angle of 45 degrees between the sun vector and the negative pitch (-Y) axis. Because of the seasonal variation of the sun vector and the possible increase of the nodal longitude to 3:30 pm, the sun angle can vary between 32 degrees and 57 degrees. Partial shadowing occurs with the larger angle, but with the small angle the spacecraft is illuminated during the entire orbit. These environmental influences are presented in the facing figure, together with energy absorbed from albedo and earth radiation by a second-surface mirror radiator facing the -Y direction.

Albedo - Although the albedo energy input has only minor influence on the -Y surface, it plays a major role in the heating of the scan mirror. When the satellite crosses the equator at 3:00 pm, the albedo input to the scan mirror cavity is 7.6 mW/cm^2, while the solar input just before TIROS enters the shadow on the far side of the earth on November 1 is 17 mW/cm^2.

Earth Radiation - Heating by earth radiation also represents a significant thermal input to the BSU instrument, since three exposed sides of the BSU view the earth with a constant view factor over the entire orbit. The flux on the sides was taken as 3.2 mW/cm^2, while incident radiation to the bottom was taken as 13.5 mW/cm^2.

Temperature Cases - Two temperature cases have been analyzed: (1) the hot case, with a 3:30 pm orbit, a sun angle of 32 degrees, and maximum spacecraft interface temperature; and (2) the cold case, with a 3:00 pm orbit, a sun angle of 57 degrees, partial orbital shadowing (1/2 hour), and minimum interface temperature. The integrated solar flux absorbed on the -Y radiators is 12 mW/cm^2, while the cold-case value is 5.5 mW/cm^2, including the shadowed part of the orbit. The maximum solar energy entering the mirror cavity is 22 W averaged over an orbit in the hot case and 17 W for the cold case. Of this incident radiation, 4.4 W is absorbed for the hot case and 3.4 W for the cold case.

Design Impact Considerations - With this wide variance in environmental heating, careful consideration must be given to the size of radiators, the TIORS-TOVS interface, and the type of thermal coatings used on surfaces (especially those facing the sun).

1110-103-101

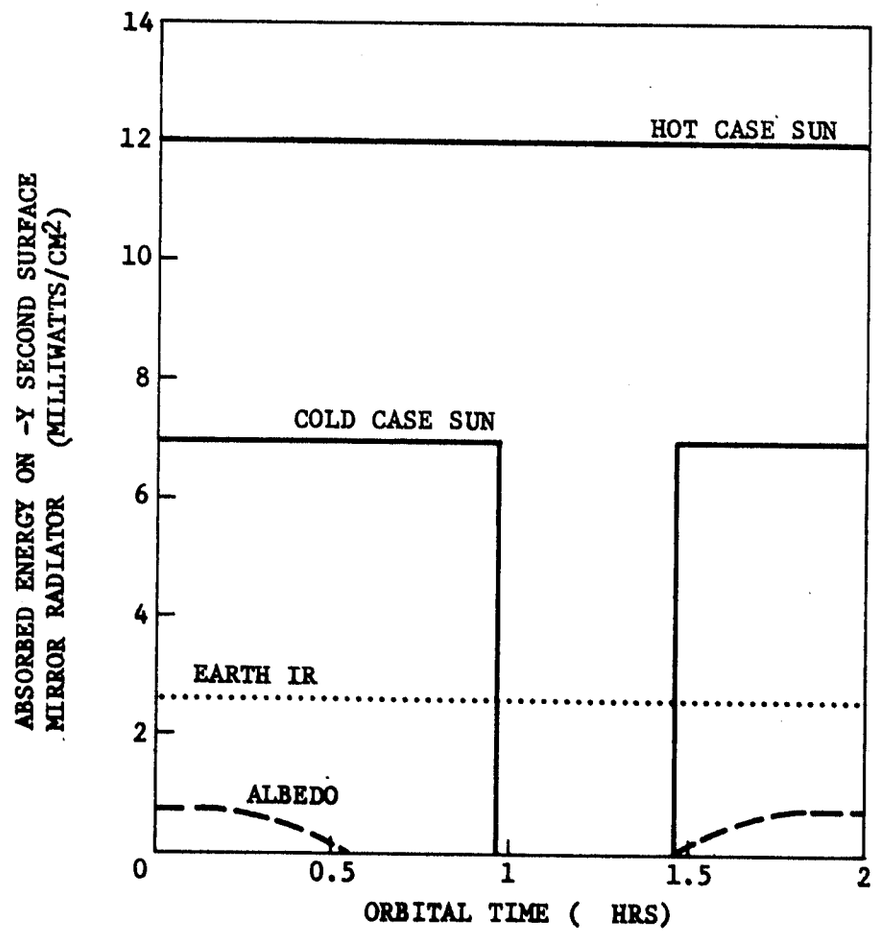

Environmental Heating for TIROS-N Orbit. Seasonal variation of the absorbed solar heating gives an integrated average of 12 mW/cm^2 for the hot case versus 5.5 mW/cm^2 for the cold case.

HIGHLIGHTS OF THERMAL DESIGN

Excessive solar heating of the calibration blackbodies, the scan mirror, and the telescopes is controlled with a sun shield. Instrument temperatures are controlled by a highly-conductive housing and structure, the use of passive radiators to reject heat, and a temperature controller to keep the detectors, filters, and detector optics components at a constant temperature.

The major thermal design considerations for the BSU include meeting stringent temperature stability requirements and preventing non-uniform solar heating of the instrument components. Overall thermal control of the instrument is achieved by reducing the variability of the solar loading with a sun shield and by conductively coupling major components together (thereby using the large thermal inertia for stability) and dissipating excess energy with passive radiators. Fine thermal tuning is accomplished with selective radiative and conductive coupling.

Sun Shield - A sun shield for the scan mirror and the telescopes is positioned directly under the housing blackbody assembly and essentially exchanges energy only by radiation. The sun shield is configured to block a majority of the sun influence on the telescopes, to completely shadow the housing blackbodies, and to radiate the thermal energy of the scan mirror when it is irradiated by the sun. The shield is attached to the rotating mirror.

Conductive Network - The conductive network consists principally of a system of alloy 356 aluminum members cast together to form the BSU housing. Scanner motor dissipated energy flows from the motor housing across an RTV (silicone rubber adhesive) interface into a .70-in. section designated as the scanner mounting web, which is straddled by two 5-in. x .10-in. radiator sections running the length of the instrument. These sections form the structural sides of TOVS and enclose the optics mounting web at the +X end of the instrument.

The temperature controlled optics housing is conductively coupled to the telescope mounting plate with four titanium standoffs which can be trimmed to size to match the environmental influences of the bottom of the TIROS vehicle. Power dissipation from the chopper motor and momentum compensator flows conductively from the motor housing to the telescope mounting plate. The mounting plate, in turn, is conductively coupled to the optics web with RTV. Dissipation from the +X electronics also conductively flows into the optics web and hence into the radiator system. The housing blackbodies are mounted between the radiators and semi-isolated from the structure with six phenolic spacers encasing titanium screws.

To aid in the thermal stability of the optics assembly and the housing blackbody assembly, large beryllium baseplates are used. Beryllium has one of the highest specific heats per unit volume and unit weight of the machineable materials.

Radiators - The passive radiators consist of a 96-in^2 panel covered with second-surface mirrors facing the sun, and a 120-in^2 panel painted with IITRI Z-93 white paint directed in the +Y direction across the bottom of the spacecraft. The size of the radiators can be changed with super insulation masking to accommodate more precise predictions of the temperature of the bottom of the TIROS vehicle.

Although the BSU-TIROS interface heat flow specification is ±15 watts for the cold and hot conditions, the general temperature level of the BSU is cooler than the spacecraft during the hot case, thereby nullifying the heat sink capability of TIROS for this condition. The TIROS-BSU conductance, however, was accepted as 0.35 W/°C in order to heat the instrument during the nonoperational condition. Consequently, the radiator sizes were adjusted to maintain the

detectors at 35°C during the hot case, while keeping the motor temperatures above -25°C during the cold nonoperational case.

HIGHLIGHTS OF THERMAL DESIGN APPROACH

The thermal design depends upon solar heating control, conduction between major components, and localized control of specific subsystems.

- Scan Mirror Sun Shield
  - Controls solar heating on mirror and telescopes.
- Highly Conductive Network
  - Aids thermal inertia, improving temperature stability.
- Passive Radiators
  - Balances energy flow with temperature requirements.
- Proportional Heater on Detector Optics Housing
  - Maintains uniform detector temperatures.
- Large Beryllium Baseplates
  - Aids temperature stability of blackbody assemblies.

CONTROL OF BLACKBODY TEMPERATURES

Blackbody thermal control is achieved with high thermal capacitance, highly-conductive paths between individual bodies, and selective radiative coupling with surroundings.

Because of the transient temperature stability requirement for the blackbodies, the high specific heat of beryllium was used for both the housing reference blackbody assemblies, giving thermal time constants of 0.45 hour and 0.7 hour, respectively.

The reference blackbodies are part of the optics housing and follow the temperature performance of the thermostatically controlled housing. Thermal conductance between the two most distant bodies is about 1.3 W/°C, yielding a maximum temperature difference of 0.5°C.

The housing blackbody assembly is essentially a beryllium plate semi-isolated from the BSU structure with six 3/16-inch titanium screws and phenolic standoffs. Each blackbody consists of a series of V-grooves circularly scribed into the plate and surrounded by a blackened cylinder. The assembly receives heat conductively through the top cover of the BSU, giving the assembly reasonable temperature limits for the hot and cold conditions and relatively stable performance over a given orbit. The temperature differences between the worst two bodies is 1°C.

The impact of the housing blackbody assembly on the gross energy balance of the BSU could be significant because of the total radiating black area of 357 cm^2, which at 300°K could radiate nearly 16 W if entirely exposed to space. However, the energy balance of the scan mirror and sun shield with the environment holds this loss to about 4 watts.

BLACKBODY THERMAL DESIGN DETAILS

These items are important to blackbody thermal control.

- Beryllium baseplates are used for temperature stability and isothermality across assemblies.
- Reference blackbodies are an integral part of the thermostatically controlled optics subassembly.
- Housing blackbodies are semi-isolated from the structure.
- The major influence of the housing blackbodies on the instrument energy balance is controlled with a sun shield.

CONTROL OF OPTICS SUBASSEMBLY TEMPERATURES

Thermal control of the telescope optics is achieved with the aid of a sun shield. Thermal control of the detector optics is achieved by a temperature-controlled baseplate that is thermally coupled to all detector optics elements.

The optics subassembly consists of seven telescopes, the telescope mounting plate, the chopper wheel, and 14 sets of detectors, lenses, and filters. In addition, there are seven sets of reference blackbodies and dichroic mirrors. The physical arrangement of these components is presented in the figure, which also locates the chopper motor.

Telescope Optics Thermal Control - For thermal control, the telescope optics depend upon the scan mirror sun shield to block a majority of the incident solar energy irradiating the system when the satellite passes toward the dark side of the earth. This energy incident on the open telescopes could reach a maximum of 76 mW/cm^2 without the shield. Temperature control of the telescopes depends upon the chopper motor power dissipation and the configuration of the conductive paths between the motor, telescopes, and telescope mounting plate. The present design calls for a 0.4-in. aluminum mounting plate tied to the optics web through an RTV interface, with a minimum contact area of 22 $in.^2$. The telescopes are each bolted to the mounting plate in a circle around the chopper motor assembly. Power dissipated within the motor flows radially outward between the telescopes to the optics mounting flange. Telescope temperatures are predicted to vary from 27 to 32°C during the operational modes. This variation does not lead to a detectable change in mirror emission.

Detector Optics Thermal Control - Detector temperature control is one of the most critical items in the thermal design. It is achieved with the aid of a proportional heater, high conductance paths between detectors, and low radiative coupling with the surroundings. Since the detectors and detector optics are in proximity (as shown in the figure), the thermal benefits of the detector design are passed on to the optics components. These components consist of filters, lenses, reference blackbodies, dichroic mirrors, and the chopper wheel. The chopper wheel is radiatively coupled to the optics baseplate with high emittance coatings, while the other components are in intimate thermal contact with the baseplate.

Elements of the Thermal Design - Because of the three requirements for detector temperature control (35° ±1°C for all orbital cases, 1°C between detectors, and less than 0.1°C change for any detector between calibration), the thermal design is based on a 3.5-W proportional heater bonded circularly to the inside of the optics housing. The housing itself consists of a 1/2-in. thick X 8-in. OD beryllium plate machined very precisely and gold plated to give an extremely low contact resistance with the detectors. The baseplate was sized to give a conductance of 1.32 W/°C between the most distant detector locations, and the interface conductance was taken as 0.057 W/cm^2°C. In order to minimize radiative losses from the detector assemblies, they should be gold-plated and the cabling exiting the detectors should be covered with a single layer of aluminized mylar, and the cables should be thermally grounded to the optics baseplate. With this scheme the radiative worst-case loss from one detector and cable will be less than 0.015 W. The circular layout of the heater, coupled with the highly conductive paths between the detectors, yields a temperature change of less than 1°C between the units. Since the heater is the proportional type and is mounted to a high capacitance plate, the temperature variation over an orbit is predicted to be less than 1°C for the detector assemblies.

The mechanical connection between the optics mounting plate and the telescope mounting plate consists of four titanium standoffs about 0.7 in. on a side and 0.8 in. long. These standoffs can be resized as the temperature influence of the bottom of TIROS becomes more clearly defined.

1110-103-102

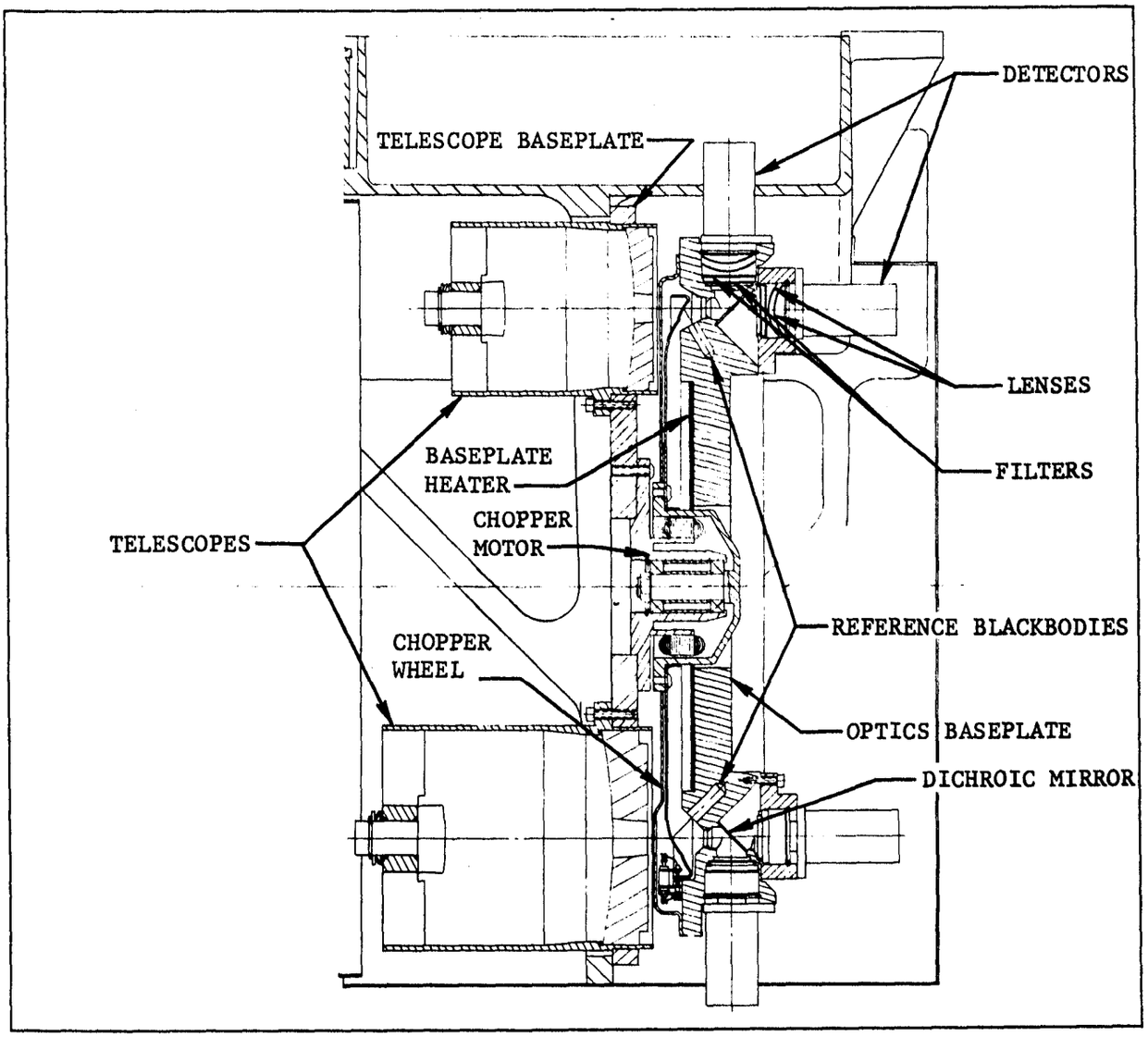

Optics Subassembly. The detectors and detector optics are temperature controlled with a common baseplate heater.

CONTROL OF SCANNER TEMPERATURES

To control the scan mirror and scan motor temperatures, the scan mirror is fitted with a heat shield which aids in the dissipation of absorbed heat from the sun, while the scan motor is tightly coupled to the scanner web so that it generally follows the gross temperature levels of the instrument.

Scan Mirror Temperature Control - The scan mirror receives direct sun, albedo, and earth radiation through a large cutout in the instrument housing. This radiation represents one of the major components of gross BSU energy balance. In order to control the solar heating problem, a sun shield is fixed to the back of the mirror. This sun shield does not entirely shield the mirror, but it almost completely prevents solar radiation from reaching the optics subassembly and completely shields calibration blackbodies on the instrument housing. It also serves as a radiator to reject the solar heat absorbed by the scan mirror, which does not reject the heat well because its gold coating absorbs sunlight but does not emit thermal radiation. The back of the mirror and the inside of the sun shield are painted with a high emittance black paint to help couple the mirror to the shield. The outside of the sun shield is coated with a white paint having low solar absorbency and high infrared emittance.

When TIROS is on the sunlit side of the earth, the shield completely shadows the mirror. During periods when direct sunlight does fall on the mirror, the back of the mirror radiates the sun shield and the shield radiates to space. With this scheme, the mirror temperatures vary from -14°C in the cold case to 5°C in the hot case. The temperature of the sun shield varies from -22°C to -6°C for the same two cases.

Gradients across the mirror are minimized by conduction in the elliptical mirror (5/8-in. thick beryllium) and by the radiative interchange between the back of the mirror and the sun shield. The worst-case gradient between the top and bottom edges of the mirror is calculated to be less than 4°C, which is at the detection threshold of the optical system.

Scan Motor Temperature Control - To prevent overheating, the scan motor is thermally coupled directly to the instrument. The motor housing for the scanner will be custom-made with a large aluminum flange that mates with the scanner web through a thermally-conductive RTV interface of 11 square inches. For the operational modes this will yield motor temperatures about 9°C hotter than the web temperatures.

Thermal Model - The analysis which led to the temperatures quoted above was performed using the thermal model shown in the figure opposite. Major heat inputs to the system are the motor dissipation and solar loading of the scan mirror and the sun shield. The housing blackbody assembly contributes to the energy balance by means of the radiative coupling between it and the sun shield. Other major radiative paths exist between the scan mirror and the sun shield and between the mirror and shield. Conduction between the scan mirror and output shaft and the harmonic drive housing is small, which motivated the use of a monometallic bearing support system to avoid thermal distortions resulting from the possible temperature difference between the drive mechanism and the mirror.

This model does not take account of the internal details of the harmonic drive and scan motor. The motor rotor and wave generator shaft are thermally coupled to the cases only by conduction through lubricant and bearings. The flex spline is tightly coupled to the scan mirror through the output shaft, but only weakly coupled to the harmonic drive case through bearings and the

small contact area of the gears. The omission of these details should not substantially affect the results, since there is little heat generated at the neglected internal nodes.

1110-103-103

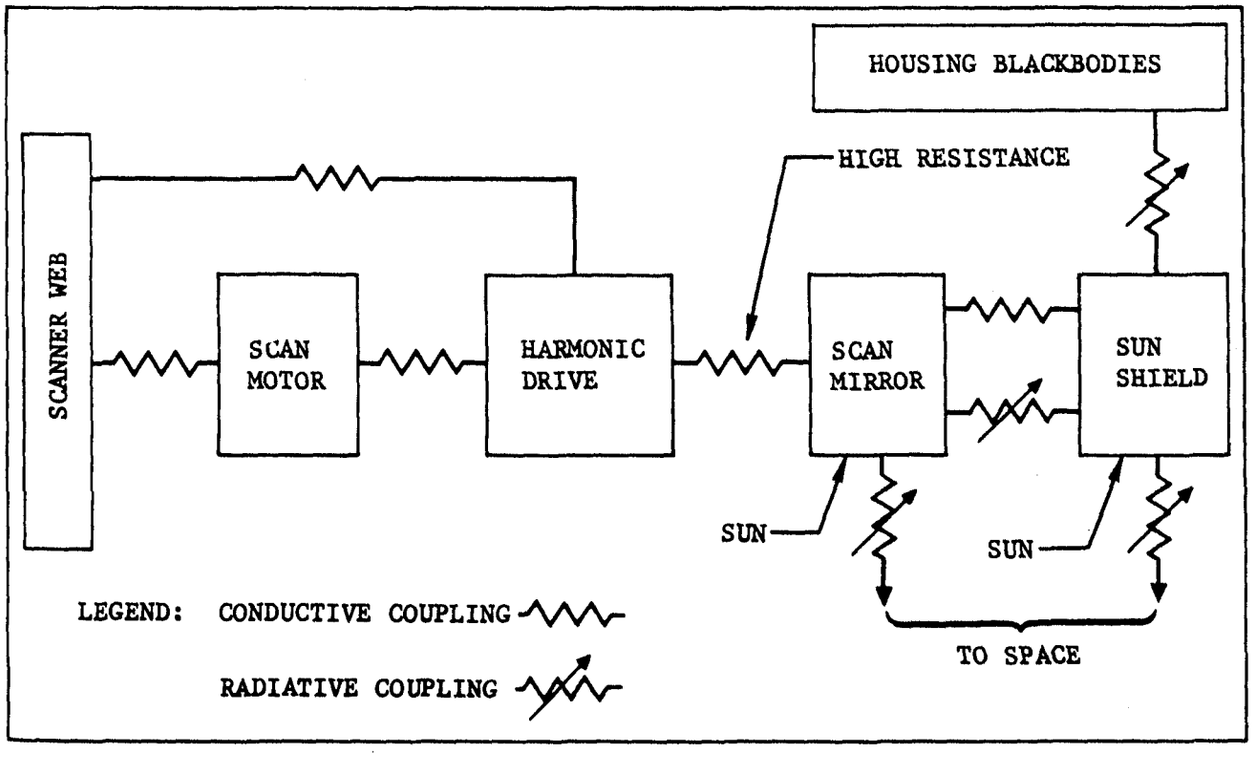

Thermal Network for Scanner. The drive component as well as the scan mirror and shield are thermally decoupled.

DESCRIPTION OF THE THERMAL MODEL

A thermal model with 20 active nodes was used to determine the temperature distribution of the BSU for three cases representing extreme conditions in the TIROS mission.

The thermal model used for determining temperatures consisted of 20 active nodes coupled with 57 conductive and radiative paths. This lumped-parameter network problem was solved with the Beckman heat transfer computer program using an IBM 360-65 computer.

The thermal capacitance of each node was calculated by using the actual weight and material specific heat for each component. Thermal resistances were computed by scaling the BSU design layouts and using the appropriate thermal conductivities. In places where RTV was used to increase the conductance of thermal interfaces, the value of the heat transfer coefficient was taken as 0.014 $W/cm^2 °C$.

The radiative interchange between surfaces was computed when that mode of transfer accounted for at least ten percent of the total heat exchange. View factors were computed from Hamilton and Morgan tables, and emittance values were taken from current surface measurement data.

Electrical heat inputs were taken from the current estimates of power dissipation. Environmental heating influences were taken from the orbital heating values.

The model was run for three extreme transient conditions:

- Nonoperational cold case--sun vector 57 degrees with respect to the -Y face, about half an hour of shadowing, and the spacecraft interface held at 10°C;

- Operational cold case--same boundary conditions but with the BSU activated;

- Operational hot case--sun vector 32 degrees with respect to the -Y face, no shadowing, and the spacecraft interface held at +30°C.

To achieve stabilized conditions for each case, the model was cycled through a number of orbits until the start and end temperatures differed by less than 0.05°C.

The results of this analysis are discussed in the next topic.

NODAL DESCRIPTION OF THERMAL MODEL

The thermal model was restricted to 20 active nodes.

NODE NUMBER	DESCRIPTION	PRINCIPAL MATERIAL
1	Scan Mirror	Beryllium
2	-Y, -X Radiator	Aluminum
3	-Y, +X Radiator	Aluminum
4	Scanner Web	Aluminum
5	Optics Web	Aluminum
6	-X Electronics	Glass Epoxy
7	+Y, -X Radiator	Aluminum
8	+Y, -X Radiator	Aluminum
9	+X Electronics	Glass Epoxy
10	Telescope Baseplate	Aluminum
11	Chopper Motor	Iron and Copper
12	Telescopes	Aluminum
13	Detectors	Aluminum
14	Optics Baseplate	Beryllium
15	Top of Instrument	Aluminum
16	Scan Mirror Shield	Aluminum
17	Scan Motor	Iron and Copper
18	Chopper Wheel	Nickel
19	Harmonic Drive	Stainless Steel
20	Housing Blackbody Assembly	Beryllium
21	Bottom of TIROS	---
22	Space	---
23	Earth	---

+X is in direction of flight
-Y faces the sun

SUMMARY OF THERMAL ANALYSIS

The thermal analysis results verify that the TOVS-BSU design meets the temperature limit specifications and maintains temperature rates of change within the desired limits.

A summary of thermal analysis results is presented in Table I, which lists the predicted thermal performance for selected BSU assemblies. The temperatures are within specification, and the mechanical and electrical constraints are met.

Temperature Ranges - The temperature distribution for the BSU gives an indication of the general operating range of the instrument. The chopper motor, which dissipates about 7 W and is five conductive steps away from the radiators, has the hottest temperature. The scan mirror sun shield, which effectively is only coupled to the instrument by radiation, has the coldest temperature. A typical range for the radiator system is 10 to 22°C, essentially representing a pseudo-sink to which thermal energy from the rest of the instrument flows. The power supply electronics range of 35 to 46°C is an average baseplate temperature and is typical for the other electronic modules.

Temperature Limits - The most critical specific limit is assigned to the detectors; it is 35 ±1°C for all orbital conditions. This requirement is met with the aid of a proportional heater which dissipates about 3.5 W during the cold case. The heater power requirement also meets the allowed power budget. Elements of the detector optics include lenses, filters, dichroic mirrors, reference blackbodies, and the chopper wheel. All these assemblies are closely coupled to the common temperature-controlled optics housing and are within a fraction of a degree of the detector assemblies.

The design limits for the motors are -25 to 70°C. The low temperature requirement is met (not shown in table) during the nonoperational cold case by allowing 12 W of spacecraft heat to flow into the BSU. This heat transfer rate, which is below the 15 W limit specified in the interface specification, is accomplished by balancing the TIROS-BSU conductive interface and the radiator size. The upper temperature limit for the chopper motor is met by increasing the conductance between the motor and radiator by using RTV between the telescope housing and the optics web.

Temperature Rate of Change - To minimize the variation of the radiation background emitting from the optical train and received by the detectors, it is desirable to keep the temperature changes of the optical train to a minimum between calibrations. The temperature rate of change for selected components is listed in Table II and a discussion of these numbers is presented below. Because the blackbodies are high-emittance components, they have the greatest impact on the radiative variance problem. The desired variation between calibrations is 0.075°C for these components, and both the housing blackbodies and reference blackbodies meet the requirement.

The scan mirror and the telescopes have low emittance surfaces and the desired rates of change for these components is 3.25°C between calibrations. This requirement is met for both components. Detector optics elements are tied to the thermally controlled optics housing. The variation for these components is 0.02°C between calibrations, which is within the desired range. The detectors themselves also vary 0.02°C between calibrations which meets the variation requirement imposed on them. In this case, however, the requirement is related to the electronic stability of the detectors, while the other stability requirements are related to background radiation.

Warmup Times and Motor Holding Power - The time required to warm up the instrument until temperatures stabilize to 0.1°C, as well as the power required to hold the scanner and chopper motors at 0°C, is given in Table III.

TABLE I. SUMMARY OF SELECTED BSU TEMPERATURES

The predicted TOVS temperatures are within specified limits.

	Cold Operational (~°C)	Hot Operational (~°C)
Scan Mirror	-14	5
-Y, -X Radiator	10	22
Power Supply Electronics	35	46
Chopper Motor	57	63
Telescopes	27	32
Detectors	35	35
Scan Motor	31	43
Housing Blackbodies	- 1	12
Scan Mirror Sun Shield	-22	- 6

TABLE II. TEMPERATURE RATE OF CHANGE FOR SELECTED BSU COMONENTS

These rates meet the chosen design goals.

	Maximum Rate of Change (°C/Between Calibrations)
Housing Blackbodies	0.067
Reference Blackbodies	0.02
Telescopes	2.9
Scan Mirror	1.2
Detector Optics Elements	0.02
Detectors	0.02

TABLE III. WARMUP TIMES AND MOTOR HEATER POWER

These values were derived using the thermal model.

• Time to warm up:	16 orbits or 32 hours	
• Power required to hold motors at 0°C	Scan Motor:	6.45 W
	Chopper Motor:	2.74 W

CONCLUSIONS OF THERMAL STUDY

The TOVS-BSU thermal design meets the specified goals of temperature limits, rates of change, power requirements, and heat transfer from the spacecraft, as shown by the results of the thermal design analysis.

A thermal math model was used to predict the thermal performance of the BSU for various extremes in the environment. Previous topics of this section provide expected temperature ranges of the various BSU components that were produced by this analysis. This topic compares these expected temperature ranges with the thermal requirements for the instrument.

The detectors, which are mounted on the optics housing, should be maintained at 35 ±1°C in order to give the best electronic response. The expected performance for the detectors is 35°C for both the hot and cold operational cases. Average detector heater power for the cold case is 3.5 W, which meets the power requirement. Heater power for the hot case is about 0.25 W. Detector variance over an orbit is predicted to be less than 0.3°C, with the greatest rate of change less than 0.005°C/min. Both these limits also are well within the detector temperature specifications. Since the reference blackbodies and detector optics are intimately connected to the optics housing, the temperatures of these items are within a fraction of a degree of the detector temperature and, therefore, are within the specifications.

The temperature requirement for the scan mirror is tied only to rates of change between calibrations. The requirement is less than 3.25°C, and the prediction is less than 1.20°C. Since the housing blackbody has a higher emittance, the desirable rate of change is 0.075°C between calibrations. The predicted rate of change is 0.067°C between calibrations, which is considered acceptable since it is small enough to allow accurate radiometric calibration.

The requirements for motor and electronic temperature limits are -25 to 70°C and -25 to 60°C, respectively. The results show that the low temperature requirements are met during the nonoperational cold condition while only drawing 12 W of spacecraft heat vs. the 15-W requirement. It should be emphasized that the low temperatures predicted for the nonoperational cold condition were computed only to show that a nonoperational instrument* can survive and be restarted from the coldest condition. The hot-case temperatures for these components are also predicted to fall within the specified limits.

The analysis has shown that the thermal requirements have been met (see summary tables) and that the instrument constraints of weight and power have been adhered to. In addition, the requirements are met without the use of louvers, external shadow shields, or other active mechanical aids, and without the use of heaters to maintain the temperature of the instrument in the nonoperating condition.

---

* The approach currently being considered is to fly the TOVS-BSU in pairs, with only one in operation at a given time.

TABLE I. THERMAL PERFORMANCE SUMMARY

	Required	Predicted
• Detector	35 ±1°C	35 ±0.03°C
• Motors	-25 to 70°C	-24 to 67°C
• Electronics	-25 to 60°C	-23 to 46°C
• Maximum Heat Flow (TIROS-BSU)	±15 W	12 W (Cold Case) 3 W (Hot Case)
• Maximum Power Dissipation	35 W	35 W

TABLE II. TEMPERATURE VARIATIONS BETWEEN CALIBRATIONS

The total variation of component temperatures during the 256-second interval between calibration is acceptable.

	Temperature Change Required	Temperature Change Predicted
• Detector	0.1°C/256 s	0.02°C/256 s
• Reference Blackbodies	0.075°C/256 s	0.02°C/256 s
• Housing Blackbodies	0.075°C/256 s	0.067°C/256 s
• Scan Mirror	3.25°C/256 s	1.2°C/256 s

SECTION 11
ANALYSIS OF RADIOMETRIC ACCURACY

Method of In-Flight Calibration 11-0
Nature and Impact of Radiometric Requirements 11-2
Statistical Errors in Scene Radiance Determination 11-4
Calculations of Noise Spectral Radiance 11-6
Magnitudes and Correction of Offset and Gain Drifts 11-10

METHOD OF IN-FLIGHT CALIBRATION

Residual offset and gain errors are corrected by a two-point calibration. A space look provides a nominal zero radiance for the determination of instrument offset errors. A view of an on-board calibration blackbody defines the spectral channel gain.

The TOVS-BSU must provide an in-flight, two-point calibration for its radiometers. Calibration is obtained by programming the scan mirror to allow the BSU telescopes to view both space (a nominal 4°K blackbody) and a high emissivity blackbody (at 300°K) which is located in the instrument housing, after every scan grid, or once every 256 seconds. The scan sequence allows time for 24 separate 100-millisecond measurement viewing periods, so that the statistical error in the measurement can be reduced by signal averaging.

The level of radiance from space is much less than the NER_ν for the most sensitive spectral channel. Due to this low radiance, a space view allows the definition of an instrumental zero and, therefore, the offset of the radiometer.

The space view is taken across the bottom of the satellite on the anti-sun side between the satellite instrument package and the outer extent of the earth's atmosphere. Space view is nominally at 70 degrees from nadir, but must be defined as an interface between the BSU and the TIROS-N spacecraft. Radiance from the earth's atmosphere must not lie within the field-of-view (FOV). A space view at 70 degrees from nadir misses the earth's limb by 650 nmi and at 60 degrees by 370 nmi. A scan angle greater than 60 degrees satisfies the above requirement.

A view of the housing blackbody defines the gain of each of the 14 spectral channels based upon the theoretical Planck spectral radiance from that blackbody. The radiant properties of the housing blackbody are critical in the calibration of spectral channel gain. The absolute temperature of the blackbody must be monitored to provide a prediction of the spectral radiant emittance to an accuracy of 1-percent. Variation in temperature between any two portions of the housing blackbody viewed by separate channels from the monitored temperature must correspond to a difference in spectral emittance less than the NER_ν of those channels. These conditions require that the absolute temperature be monitored to within 0.25°C and that channel variations from that temperature do not exceed 0.075°C based upon the NER_ν requirements for channel 4 with a 330°K (worst case).

Calibration measurements are made at the end of each 32-line scan grid; that is, every 256 seconds. Calibration defines the instrument offset and gain errors at the time of calibration. Due to the thermal stability of the detector optics and detector housing, gain errors are not expected to vary significantly between calibrations. The offset errors arising from the emissivity of the scan mirror (and possibly the telescope mirrors), are expected to vary between calibration measurements. The offset errors, however, may be interpolated between calibration measurements inasmuch as the variations are linear to within the NER_ν for all channels.

The design of the housing blackbody is patterned after the design used for the ITPR on the NIMBUS E satellite. The housing blackbody is located directly above the scan mirror and is composed of eight individual blackbodies fabricated on a single plate of beryllium. The individual blackbodies are formed from a series of V grooves whose surfaces are optically blacked with an overcoat of 3M Black Velvet. The individual blackbodies completely fill the FOV of their respective telescopes during calibration. The beryllium blackbody plate is of sufficient mass and is sufficiently well isolated thermally to be thermally stable. A three-point calibration can be obtained by the addition of a heater to the blackbody plate in order to raise its temperature to the third point of calibration.

The temperatures of the individual blackbodies are expected to be uniform to within 0.1°C. Their temperatures are monitored with platinum resistance thermometers to within the temperature equivalent of an NER_ν for each channel which is ±0.075°C, worst case. The blackbody emissivity is calculated as 99.5 percent, based upon a 0.9 emissivity for a specular surface and an apex angle of 30 degrees.

FEATURES OF IN-FLIGHT CALIBRATION

- Space look determines offset.
- Blackbody look determines gain.
- Space look is 70 degrees from nadir on anti-sun side.
- Blackbody is beryllium structure on housing.
- Accurate blackbody temperature monitoring is essential.

NATURE AND IMPACT OF RADIOMETRIC REQUIREMENTS

Extremely accurate radiometric measurements are required to obtain useful atmospheric soundings. The use of accurate in-flight calibration data is required to convert the instrument readings into estimates of scene spectral radiance.

Atmospheric temperature profiles are determined from spectral radiance measurements in a molecular absorption band according to a complex numerical inversion scheme. The high degree of radiometric accuracy required for the determination of atmospheric temperature profiles was emphasized by Wark and Fleming in 1966. Since that time, refinements, extensions of the theory, and allowances for a number of complications have tightened the requirement by only a factor of three from 0.5 to 0.15 mW/m^2-sr-cm^{-1} in the CO_2 band. To attain suitable profiles, it is now considered necessary to achieve the rms accuracies given in Table I. For the most sensitive channel, these allowable errors are about 1000 times less than the full-scale radiance at 330°K blackbody. To achieve such accuracies, it is necessary to consider both random and systematic error sources. A large part of the radiometer design effort has been devoted to the attainment of the specified noise-equivalent spectral radiance, while an equally large part has been devoted to the control of systematic errors from thermal variations and stray light.

As shown in the first equation opposite (Table II), the instrument measures the scene radiance by comparing it to a blackbody reference. The actual output signal is related to the scene radiance not only by a gain parameter but also by an offset which depends on stray light and mirror emissions, and the emission of the reference blackbodies. This background radiation is not negligible. Emission from even the best of mirrors greatly exceeds the detectable threshold, and the reference blackbody itself is warm and has a small, but detectable temperature variation (0.02°C). These effects all appear as an offset; electronic offsets are negligible in comparison. It is therefore essential to provide an in-flight measurement of this offset by means of a space look which establishes an effective zero reference. It is also necessary to check the gain from time to time. While pyroelectric detectors are stable devices when kept at constant temperature, the variations in temperature which occur do lead to detectable changes in gain.

Provided that the radiation received during the space look is really that of deep space at 4°K, the instrument offset is determined by the space look as shown in the second equation. The asterisk indicates that the value of the offset is a statistical estimate because there is a statistical error in the measurement, not only from noise but also from quantization error of the digital output. Similarly, the gain can be estimated from the instrument output when viewing the instrument blackbodies (housing look), using the space look data and the spectral radiance of the calibration blackbodies, as calculated from in-flight temperature measurements. The blackbody radiance is itself subject to both systematic and random noise and quantization.

Finally, the estimated scene spectral radiance in each channel can be calculated from the other measurements and estimates. The radiometric design must reduce the random and systematic error in the final estimate of scene radiance so that it is less than, or at lease close to, the stated design goals. To achieve this objective it may be necessary to interpolate between values of the gain and offset which are measured only at intervals. The fundamental limit on this interpolation is set by the sampling theorem: if detectable changes in the gain and offset occur at frequency f, the frequency of calibrations must be at least 2f, or the results will not only be erroneous but ambiguous.

TABLE I. RADIOMETRIC REQUIREMENTS FOR THE TOVS-BSU

Attainment of these sensitivities is required to attain acceptable soundings.

Description of Specification	Spectral Radiance - mW/m^2-sr-cm^{-1}			
	Ch. 1	Ch. 2	Chs. 3 thru 14	Ch. 11
Maximum noise equivalent spectral radiance	0.003	0.02	0.15	0.5
Relative radiometric error between spectral channels	0.003	0.02	0.15	0.5
Absolute radiometric accuracy Specifications:			±1.0	±1.0
Design Goal:			±0.5	±0.5

TABLE II. REQUIREMENTS TABLE

Symbols for Instrument Response Calculations

All parameters must be determined for each of the 14 channels.

- R = scene radiance
- R_B = calibration blackbody radiance
- R_M = total radiance of mirrors
- R_S = radiance of stray light
- R_R = reference blackbody radiance
- R_C = chopper mirror radiance
- S = instrument output
- S_S = output during space look
- S_B = output during housing look
- G = instrument gain

Equations Determining Response

Blackbody radiance is computed for each channel from Planck's equation, and the measured temperatures. Asterisk indicates statistical temperatures.

Instrument output: $S = G(R + R_M + R_S - R_R - R_C) = GR + S_o$

Estimated offset: $S_o^* = S_S$

Estimated gain: $G^* = (S_B - S_S)/R_B$

Estimated scene radiance: $R^* = (S - S_o^*)/G^* = R_B \dfrac{(S-S_S)}{(S_B-S_S)}$

STATISTICAL ERRORS IN SCENE RADIANCE DETERMINATION

Provision of high digital conversion resolution and the taking of a large number of calibration measurements reduces the total statistical measurement error for each scene to a level nearly equal to error caused by the detector alone.

Random variations in detector output and the finite resolution of the digital system lead to statistical errors in the scene measurements. The calibration data is subject to similar errors.

Equation (1), which was used to determine the scene radiance from the scene and calibration output, was discussed previously and is shown opposite. Each of the values represented by symbols in this equation is subject to random errors. These symbols were defined on the previous page.

The mean-squared error in reducing the data is easily calculated, assuming the errors are small. The result is the second equation which gives the mean-square fractional error in the scene radiance in terms of the fractional errors in measurements of the scene, housing look, space look, and the prediction of blackbody radiance.

The smallest quantization error will be attained if the 4096 levels produced by the analog-to-digital converter span the entire range of signals expected, which corresponds to the radiance from a 330°K blackbody, or about 200 mW/m^2-sr-cm^{-1} in the most sensitive channel. The rms noise equivalent quantization error is obtained by dividing this full-scale signal by 4096 $\sqrt{12}$. The factor $\sqrt{12}$ accounts for the difference between the width of the converter bins and the rms error which, for a uniform distribution of errors of over a band of width W, is $W/\sqrt{12}$.

If the number of successive calibration measurements is N, and the measurements are averaged, the contributions of the calibration measurements to the overall mean-square measurement are reduced by a factor N.

The final expression for the error in measuring the scene radiance is given in equation (3). There are two terms: one resulting from detector noise and quantization error in measurement of the scene, space look, and blackbody radiance, and one from the error in predicting the blackbody radiance. The maximum error resulting from statistical noise sources follows from equation (3) and is given by equation (4).

The first term of equation (3) is a maximum for a scene whose radiance is half-scale. In the worst case, the quantization errors and the errors propagated through the calibration process increase the noise spectral radiance of the detector by only 3 percent. This analysis assumes that only one set of calibration data is used. It can be shown that linear interpolation between two successive calibrations yields the same worst-case error; use of more sophisticated interpolation schemes would reduce the error.

Control of the second term depends on accuracy of measurement of blackbody temperatures. To make the contribution of statistical errors in temperature measurement as small as that of the quantization error in the scene measurement, the temperature must be measured with an error which is small compared to the noise equivalent temperature difference (NETD) in the most sensitive channel. The smallest NETD is 0.075°C in channel 4, assuming a scene temperature of 330°K, so that the blackbody temperature measurement should be made with an rms error less than 0.015°C. If the temperature span of the measurement is 50°C, the 12-bit converter will provide an rms temperature resolution of $50/4096\sqrt{12}$°C, or 0.0035°C. Electronic noise in the measurement will also be negligible because an estimate based on the Johnson noise of a typical platinum resistor predicts a signal-to-noise ratio of 10^8. The statistical errors in the blackbody temperature measurement are therefore negligible.

Equation for Determination of Scene Radiance in Each Channel

The scene spectral radiance is R, the calculated blackbody spectral radiance is R_B; while S, S_S, S_B are the digital output readings for the scene, space look, and housing look.

$$R = R_B (S - S_S)/(S_B - S_S) \tag{1}$$

Equation for Mean-Squared Fractional Error

$$\left(\frac{\Delta R}{R}\right)^2 = \left(\frac{\Delta R_B}{R_B}\right)^2 + \left(\frac{\Delta S}{S-S_S}\right)^2 + \left(\frac{R_B}{R}\right)^2 \left(\frac{S_B-S}{S_B-S_S}\right)^2 \left(\frac{\Delta S_S}{S_B-S_S}\right)^2 + \left(\frac{\Delta S_B}{S_B-S_S}\right)^2 \tag{2}$$

Mean-Squared Error for scene of Radiance R

The number of calibration measurements is N, the noise equivalent spectral radiance from the detector alone is NER_ν, and the ratio of noise equivalent quantization errors to NER_ν is α.

$$(\Delta R)^2 = (NER_\nu)^2 \left\{ 1 + \alpha^2 \left[1 + \frac{1}{N}\frac{R^2}{R_B{}^2} + \frac{1}{N}\left(\frac{R_B-R}{R_B}\right)^2\right]\right\} + (\Delta R_B)^2 \tag{3}$$

Maximum Error Resulting from Statistical Noise Sources

The above error is largest if the scene radiance is half the blackbody radiance ($R/R_B = 0.5$). For $\alpha = 0.20$ and N = 24, the total rms error is only 1.03 times the detector noise. Statistical errors in blackbody radiance predictions are negligible.

$$\Delta R^2 = (NER_\nu)^2 (1 + \alpha^2) (1 + \frac{1}{2N}) = (NER_\nu)^2 (1.03)^2 \tag{4}$$

CALCULATIONS OF NOISE SPECTRAL RADIANCE

An analysis of the sensitivity of the baseline radiometer design shows that the $(NER)_\nu$ design goals are approximated within 40-percent worst-case (channel 2) by an integration for 75 milliseconds (ms). Minor changes in baseline design provide improved performance.

The satisfaction of the BSU radiometric requirements necessitates fulfillment of the spectral channel $(NER)_\nu$ design goals as well as the reduction of spectral radiometric measurements to data essentially free from offset and gain errors. The $(NER)_\nu$ for each of the 14 spectral channels is defined by the following expression:

$$(NER)_\nu = \frac{(NEP)\ \sqrt{\Delta f}}{\pi(\Delta\nu)\ (NA)^2\ A\ T_\nu\ T_T \tau}$$

Where:

$(NER)_\nu$ = the noise equivalent spectral radiance of the source in watts/m^2-sr-cm^{-1}

(NEP) = the detector noise equivalent power in watts/$\sqrt{Hz}$

$\Delta\nu$ = the spectral bandwidth in cm^{-1}

(NA) = the numerical aperture of the telescope measured at the field stop

$\Delta\nu$ = 0.128 for both the 61- and 80-mm OD telescopes

A = the area of field stop in m^2

= $(2.141 \times 10^{-3})^2 = 14.42 \times 10^{-6}\ m^2$ for 61-mm OD telescope

= $(2.815 \times 10^{-3})^2 = 24.90 \times 10^{-6}\ m^2$ for 80-mm OD telescope

T_ν = the spectral transmittance of all optics for the given spectral bandpass

T_T = the transmittance efficiency of the telescope because of secondary mirror and spider obscuration (0.85)

τ = chopping efficiency (0.5)

Δf = noise bandwidth (6.67 Hz)

The calculation of $(NER)_\nu$ values for all channels is based upon the latest NEP data for TGS detectors measured in the study. Spectral transmittance data for the optical elements is based upon state-of-the-art in thin-film coatings. The values used are shown in Table I. This results from a stepping time of 25 ms in a 100-ms scan scene frame time. The chopper is phased to block observation during the 12.5 ms required for settling, thus allowing a maximum integration of signal and a total step-and-settle time of 37.5 ms which can be attained by minor modification of the scanner design.

Table II shows predicted values of $(NER)_\nu$ for several different telescope arrangements. Because the detector noise at the optimum chopping frequency is limited by the loss tangent effect, the detector NEP depends on the detector dimensions, increasing as the square root of the detector area. The first arrangement is the baseline design for the study which places channel 1 on a small telescope. The second arrangement assumes that channel 1 is placed on a larger telescope since attainment of high accuracy in channel 1 is considered particularly critical.

The third arrangement assumes that the numerical aperture of the conservatively designed detector optics is increased to allow a reduction of detector size, and that the telescope diameters have been revised to 87 mm and 56 mm to provide optimum energy balance with detectors of constant detectivity.

TABLE I. SUMMARY OF OPTICAL EFFICIENCIES AND $\Delta\nu$'s USED IN NEW CALCULATIONS
Filter transmittances are based on latest available value

Channel Number	ν Center Frequency (cm^{-1})	ν Frequency Bandwidth (cm^{-1})	T_ν^1 Filter Trans-mittance	T_ν^{11} Mirror and Lens Trans-mittance	T_ν Transmittance of all Optics
1	2700	300	0.76	0.85	0.65
2	2350	50	0.48	0.85	0.41
3	1030	25	0.38	0.85	0.33
4	899	15	0.38	0.88	0.33
5	750	15	0.32	0.88	0.28
6	735	15	0.32	0.88	0.28
7	715	15	0.32	0.88	0.28
8	700	15	0.32	0.88	0.28
9	690	15	0.32	0.88	0.28
10	675	15	0.32	0.88	0.28
11	669	3.5	0.29	0.88	0.26
12	532	25	0.20	0.80	0.16
13	432	25	0.20	0.75	0.15
14	340	25	0.19	0.70	0.13

TABLE II. $(NER)_\nu$ VALUES FOR ALL FOURTEEN CHANNELS
Performance can be improved by reassignment of more critical channels and by a decrease in the detector size by use of faster detector optics.

	ARRANGEMENT #1 (Design Study Baseline) Chan 1 on a Small Telescope Detector Optics NA = 0.4		ARRANGEMENT #2 Baseline Configuration Chan 1 on a Large Telescope Detector Optics NA = 0.4		ARRANGEMENT #3 Revised Configuration Chan 1 on a Large Telescope Detector Optics NA = 0.5	
Channel Number	Tele Size mm Dia	NER_ν $mW/m^2\text{-}sr\text{-}cm^{-1}$	Tele Size mm Dia	NER_ν $mW/m^2\text{-}sr\text{-}cm^{-1}$	Tele Size mm Dia	NER_ν $mW/m^2\text{-}sr\text{-}cm^{-1}$
1	61	0.00377	80	0.00287	87	0.00229
2	80	0.0277	80	0.0277	87	0.0217
3	61	0.0925	61	0.0925	56	0.0844
4	61	0.149	61	0.149	56	0.141
5	61	0.169	61	0.174	56	0.166
6	61	0.169	61	0.174	56	0.166
7	61	0.169	61	0.174	56	0.166
8	80	0.135	80	0.135	87	0.106
9	80	0.135	80	0.135	87	0.106
10	80	0.135	80	0.135	87	0.106
11	80	0.625	80	0.625	87	0.490
12	80	0.141	80	0.141	87	0.111
13	80	0.152	61	0.207	56	0.186
14	80	0.175	80	0.175	87	0.137

For 1.5-mm detector NEP = $9 \times 10^{-11}\ W/\sqrt{Hz}$

For 2-mm detector NEP = $1.2 \times 10^{-10}\ W/\sqrt{Hz}$

BECKMAN INSTRUMENTS, INC.
Advanced Technology Operations
J.O.Maloy; C.F.Dadson; B.D.Henderson

MAGNITUDES AND CORRECTION OF OFFSET AND GAIN DRIFTS

Thermal and orbital analysis of the maximum-weight design shows that variations in component temperatures and stray light result in changes of the instrument offset, which is several times the noise equivalent spectral radiance. A simple linear interpolation between two successive calibrations is required.

Instrument offsets arise not only from the 308°K emission of the blackbodies but also from the emissions of four mirrors. Although the mirrors are highly polished to attain an emissivity in the neighborhood of 1 or 2 percent, this emission still exceeds the specified detectable radiance. Furthermore, sunlight can be scattered from the scan mirror with an efficiency of 1 or 2 percent. Electronic offsets are negligible.

In computing the radiation received by a detector for a given earth-scene radiance, the earth scene is considered to be a uniform extended source having a spectral radiance, N_ν . The radiation then received by that same detector from each of the scan, primary, secondary, and chopper mirror surfaces will be directly proportional to their individual spectral radiances, compared to that of the scene radiance, since they are all uniform extended sources to the remainder of the optical system. The spider mirror radiance must be multiplied by its telescope aperture coverage factor which makes it negligible in comparison to the other mirrors.

The plot shows the relationship between scene radiance and the radiance of optical elements. The abscissa is a linear plot of temperatures from 50°K to 350°K. The ordinate is a 7-decade logarithmic plot of spectral radiance in mW/m^2-sr-cm^{-1}. The fourteen channels' blackbody radiation curves are plotted for their central frequency, showing their spectral radiances for the blackbody temperatures on the abscissa. The specified NER_ν spectral radiances are shown for each channel.

To see the effect of various scan mirror temperatures, the equivalent spectral radiance and temperature for each of the fourteen channels were graphically computed for a scan mirror emissivity of 1 percent at temperatures of both 235°K and 278°K. These temperatures correspond to the observational range of the BSU.

To see the effect of sunlight on the scan mirrors, a 6000°K blackbody radiance was computed for each of the fourteen channels. The solar irradiance of the scan mirror was next computed, and finally the effective scattered radiance of this solar irradiance, assuming the scan mirror to be a 1-percent Lambertian scattered. The figure opposite shows also that the spectral radiance of scan mirror is greater than the NER_ν design goals for channels 1 and 2. This source of error is eliminated by locating the channel 1 and 2 telescopes so they do not view the portion of the scan mirror illuminated by the sun.

Variations in offset between space-look calibrations depend upon variations in the emittances of mirrors and reference blackbodies. For a full-scale source temperature of 330°K, a variation in spectral emittance of 0.15 mW/m^2-sr-cm^{-1} at the wavelength of channel 4 (worst case) corresponds to a temperature difference of 0.075°C for the reference blackbody and 7.5°C for a mirror with a 1 percent emissivity.

The thermal design employs sunshields, radiators, and heavy construction to reduce temperature variations to the minimum values consistent with the weight allowance. It was found possible to control the temperature so that each of the five principal offset sources contributes an error which changes by an amount slightly less than the noise spectral radiance in the most temperature-sensitive channel (channel 4). In the worst case, the total offset changes between calibrations by about twice the noise equivalent spectral radiance. The exact value depends on the value of the mirror emittance attained; the estimate assumes

mirror emissions are 2 percent.

This change is just large enough to require interpolation between offset (space look) measurements. Only a simple linear interpolation is required, using the current and previous calibration measurements, so that data reduction is not complex.

The detector gain has a temperature coefficient of about 1 percent per °C. The detector temperature is actively controlled, but there is some orbital variation of temperature as a result of the finite thermal impedances in the controlled network.

The total variation over an orbit is ±0.3°C, while the change between calibrations is at most 0.02°C. This variation leads to a worst-case error for a 330°K scene of 0.6 mW/m^2-sr-cm^{-1} for the thermal channels (4-14) and small errors in channels 1 and 2 (0.005 and 0.016 mW/m^2-sr-cm^{-1}, respectively. The gain change between calibration is only 0.02 percent. This drift has a smaller effect than the offset drift, and it can be corrected without interpolation.

Because the magnitude of the variations is so small, a linear extrapolation can be used instead of an interpolation to simplify data processing.

1110-104-226

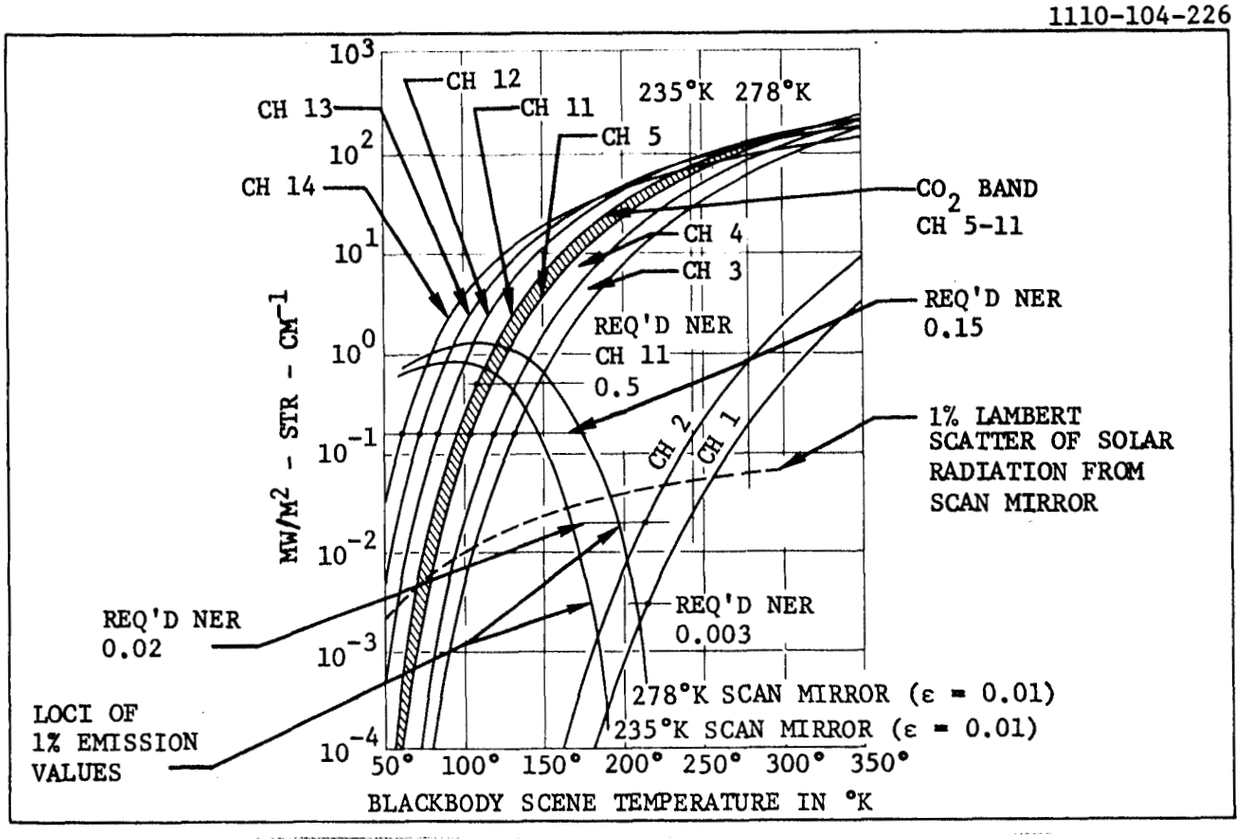

The Curves Show the Offsets from Mirror Emission and Scattering of Sunlight From the Scan Mirror.

SECTION 12
DESIGN OF INSTRUMENT PACKAGE

Assembly of the TOVS Instrument 12-0
Assembly of the Optics Subassembly 12-2
Assembly of the Scanner Subassembly 12-4
Location of Electronic Subassemblies 12-6
Approach to Cabling and Harnessing 12-8
Access for Servicing 12-10

ASSEMBLY OF THE TOVS INSTRUMENT

The TOVS Basic Sounder Unit is organized into six subassemblies which are designed for straightforward noncritical assembly. The subassemblies are self-contained so their assembly and checkout need not be performed on the all-up instrument. Critical fits and adjustments are generally located within the subassemblies so that the top assembly procedure can be simple and straightforward.

A schematic exploded view of the instrument is shown in the facing figure. Here can be seen the relationship of the major subassemblies to the instrument frame and how they are assembled into it. The subassemblies are: scanner, optics, housing blackbodies, electronics, and exterior covers. The removal of the exterior covers, which are simply bolted onto the frame, is straightforward. The scanner subassembly is held in place by three bolts and may be withdrawn as a unit from the bottom. Note that assembly of the scan mirror to its shaft does not have to be accomplished on the completed instrument. The optics subassembly is held in place by four screws, and can be withdrawn from the end of the instrument. Removing the top cover of the instrument gives access to the housing blackbody subassembly. The electronic modules are located in the upper part of the instrument and may also be removed from the top, once the top cover is lifted away.

The instrument subassemblies are, for the most part, complete in themselves. This allows them to be individually assembled and checked out on the bench, reducing the amount of work that must be performed on the completed instrument. Most of the checkout tasks concern the optics subassembly, which must be aligned and radiometrically checked, and the scanner subassembly, whose performance must be verified. To facilitate checkout, all electronics are in separately testable subassemblies.

In order that the top assembly of the instrument may be completed quickly and with a high degree of reliability, it is desirable that no critical functions need be performed at that time. This is achieved with the modular subassembly concept. The primary areas where a good deal of caution is needed are the scanner and the optics subassemblies. In the case of the scanner, a very high degree of concentricity must be maintained between the scanning motor and the harmonic drive components. In the optics subassembly, it is extremely important that the fore optics and the aft optics be aligned, and that all optical axes be parallel. The former is extremely important to radiometric performance (i.e., getting all the energy on the detectors), while the latter has significant impact on achieving operational objectives (i.e., all channels must view the same scene).

The assembly procedure for the top assembly of the instrument is designed to ensure the same setup each time the instrument is assembled and disassembled. The scanner assembly is located by dowel pins in line-reamed holes. The alignment of the two subassemblies relative to each other, when the pin holes are initially put through, is accomplished on the optical bench. The pin arrangement guarantees that subsequent assembly operations will be repeatable every time. A similar concept is used for mounting the housing blackbodies. Also, connectors are used on the electronics so that no soldering or other skilled operation is necessary for their installation and removal.

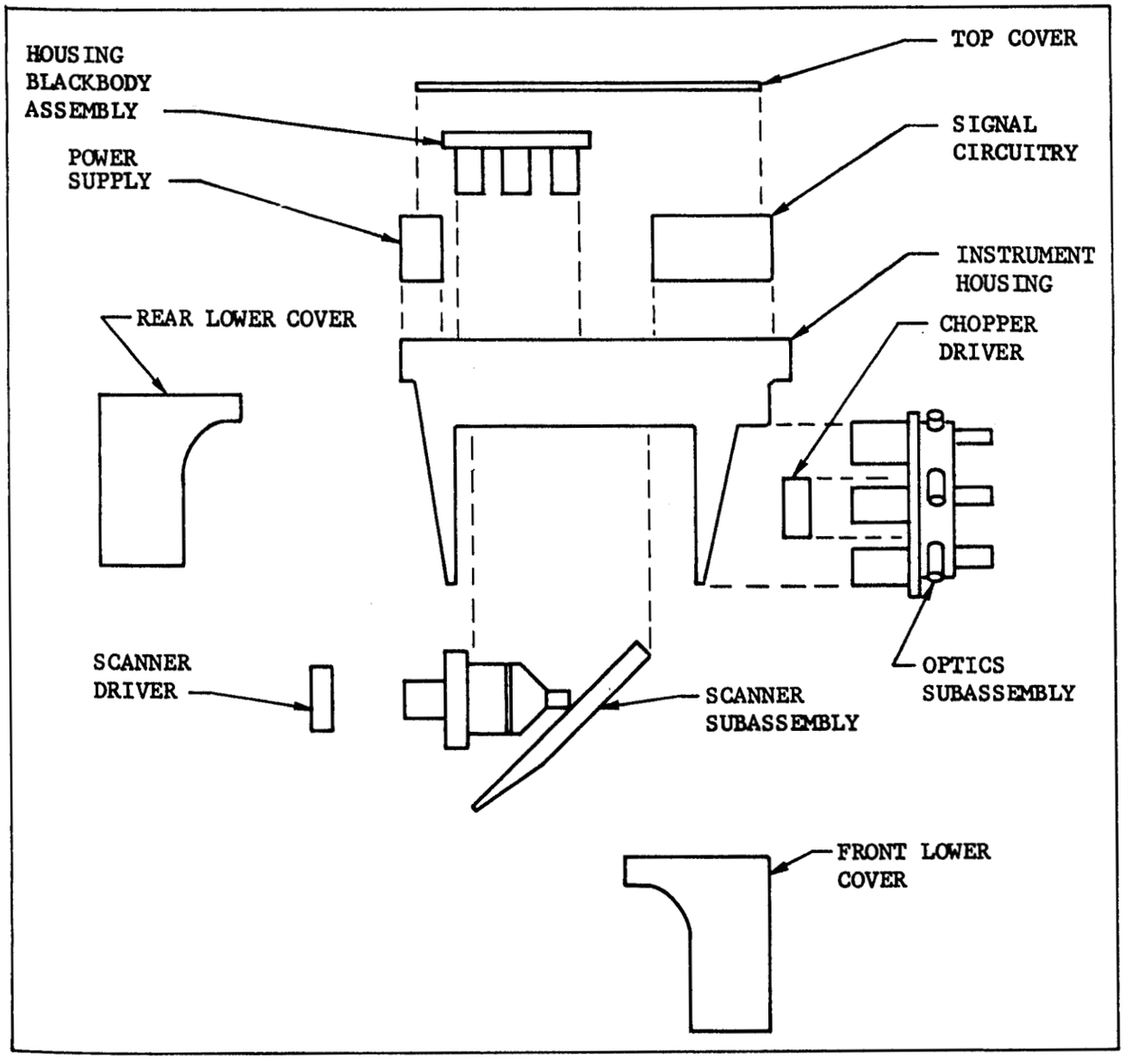

Schematic--TOVS Basic Sounder Unit Assembly

ASSEMBLY OF THE OPTICS SUBASSEMBLY

Like the main instrument, the optics subassembly is made up of independent self-contained parts. It contains all the optical components exclusive of the scan mirror in easily demountable subassemblies.

The optics subassembly (see figure opposite) consists of two sub-parts: (1) the telescopes and telescope mounting plate (the chopper motor is also mounted on the telescope mounting plate), and (2) the aft optics assembly, which includes the optics housing, the aft optics, and the detectors, and which bolts to the telescope mounting plate through a controlled thermal resistance.

The telescope assemblies are preassembled. No adjustment is involved in setting up the telescopes because all important functions are accurately machined. The assembled telescopes are bolted to the telescope mounting plate. They are located by a pilot diameter on the rear of the telescope barrels which fits in holes machined in the telescope mounting plate. The chopper motor is mounted on the telescope mounting plate along with its driver electronics. A heat shield becomes a loose but captive part of this assembly. It is placed over the chopper motor hub and the electro-formed nickel chopper wheel is then mounted to the motor flange. This completes the assembly of the telescope mounting plate and telescopes.

The detector optics assembly proceeds as follows: the preassembled filter housings and lens housings are inserted into the cavities in the optics housing, where they are retained by wave springs and retainer rings. The dichroics are installed in their cavities and retained by the spring clips. The detectors can then be mounted, which completes the assembly of the detector optics portion.

The mating of the aft optics assembly to the telescope mounting plate assembly is one of the more important steps in the assembly process. The optical alignment of the instrument, as well as its thermal performance, are affected by the quality of this interface. The alignment of each telescope with its detector optics channel is accomplished by mechanical alignment during manufacture. For this purpose, precision mandrels are used to locate the detector optics channels relative to the telescope pilot diameters, and the pins which locate the aft optics housing relative to the telescope mounting plate are then installed. This procedure results in alignment to an accuracy of about 0.003 - 0.005 inch. This is adequate since adjustment of the individual detectors can take care of the rest. The thermal requirements of the interface are met in the manner that has been described, by use of thermally resistive spacers. These are assembled dry and torqued accurately in place. At this final step, the outer edge of the captive heat shield is also clamped down, and at this time, the phase reference pickoff assembly also is installed. The optics subassembly is then a completed unit ready for bench checking.

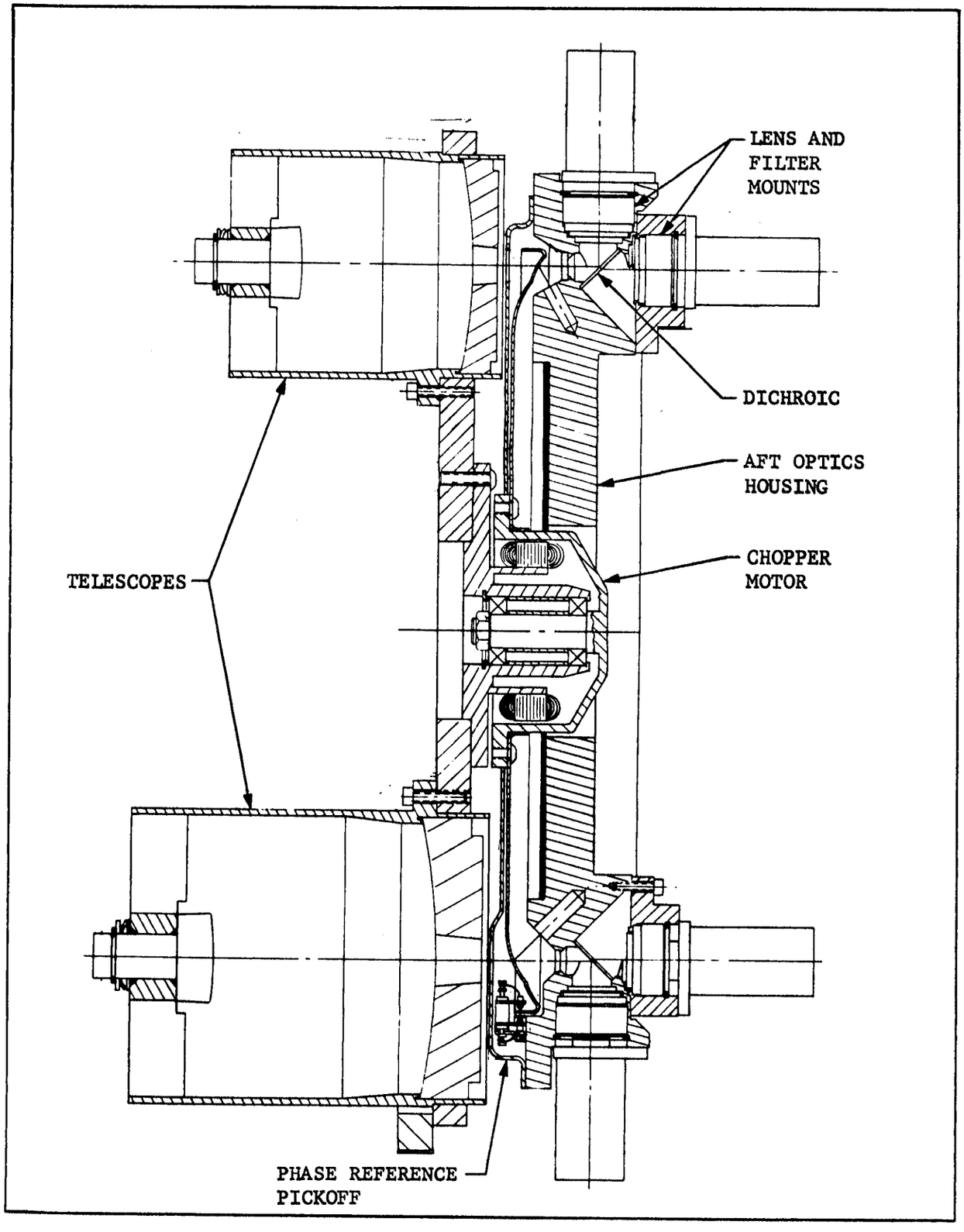

TOVS Optics Subassembly

ASSEMBLY OF THE SCANNER SUBASSEMBLY

The TOVS scanner consists of the scan mirror, shaft, encoder, harmonic drive, and scan motor -- all preassembled into a cylindrical aluminum housing that mates with the instrument frame. The assembly of the scanner drive components follows a logical sequence which yields a preadjusted assembly easily mated to the instrument housing.

The scanner assembly is built around the mirror shaft, which is mounted in the housing on a preloaded duplex pair of ball bearings (see figure opposite). The shaft and bearings are inserted from the front of the scanner housing, and an inner-race retaining nut then may be installed on the threaded portion of the housing and pinned in place, after which the scan mirror is installed on the shaft. It is located by a Woodruff key and retained by a roll pin. The mirror serves to safety the inner-race nut, since the two are in close contact. It should be noted that both the inner race and outer races of the ball bearings are located by precision spacers so that the assembly is not sensitive to the torque applied to either retaining nut. The bearing preload, instead, is determined by the geometry of the spacers.

The shaft encoder next is mounted on the shaft. Since this assembly sits deep down inside the housing, this is a potential trouble spot. However, assembly problems have been averted by making the encoder a preassembled unit rather than a set of components. The preassembled encoder is simply slipped onto the shaft -- it is driven and located by a Woodruff key whose slot is precision-aligned with the mirror's key -- and tightened down with three screws. After the encoder assembly is affixed to the shaft, the pin cage indexing pin is installed from the outside of the housing which serves to locate and immobilize the pin cage. It contains a spring to limit the force that can be applied, making it impossible to excessively load the bearings.

After the encoder is in place, the flex spline member of the harmonic drive is assembled to the shaft with three screws. There is an accurate pilot diameter in the hub of the flex spline to ensure that it is located concentrically. The circular spline member of the harmonic drive is mounted next. It is located by a pilot diameter mating with a diameter in the housing and is seated by six screws.

The scan motor next is bolted up to the assembly. It is located and held concentric by a precision diameter which mates with a diameter in the housing. The motor is made with a large flange on its front end so that good concentricity of the completed assembly can be held. The motor flange is secured with six screws. A light coating of thermal compound is put on the joint before assembly since the motor's heat flows through this joint.

The scanner subassembly is now complete except for the addition of electronics and temperature sensors, and the mirror sunshield. The completed scanner subassembly is slid into place from the bottom of the TOVS instrument and then attached with four screws. Subdrills are provided in the housing at two places for pins which will provide accurate angular orientation (nadir location relative to the instrument). These holes are finish-drilled and reamed, and pins are installed after this adjustment is made. Suitable allowance in the clearance holes for the bolts is made for this.

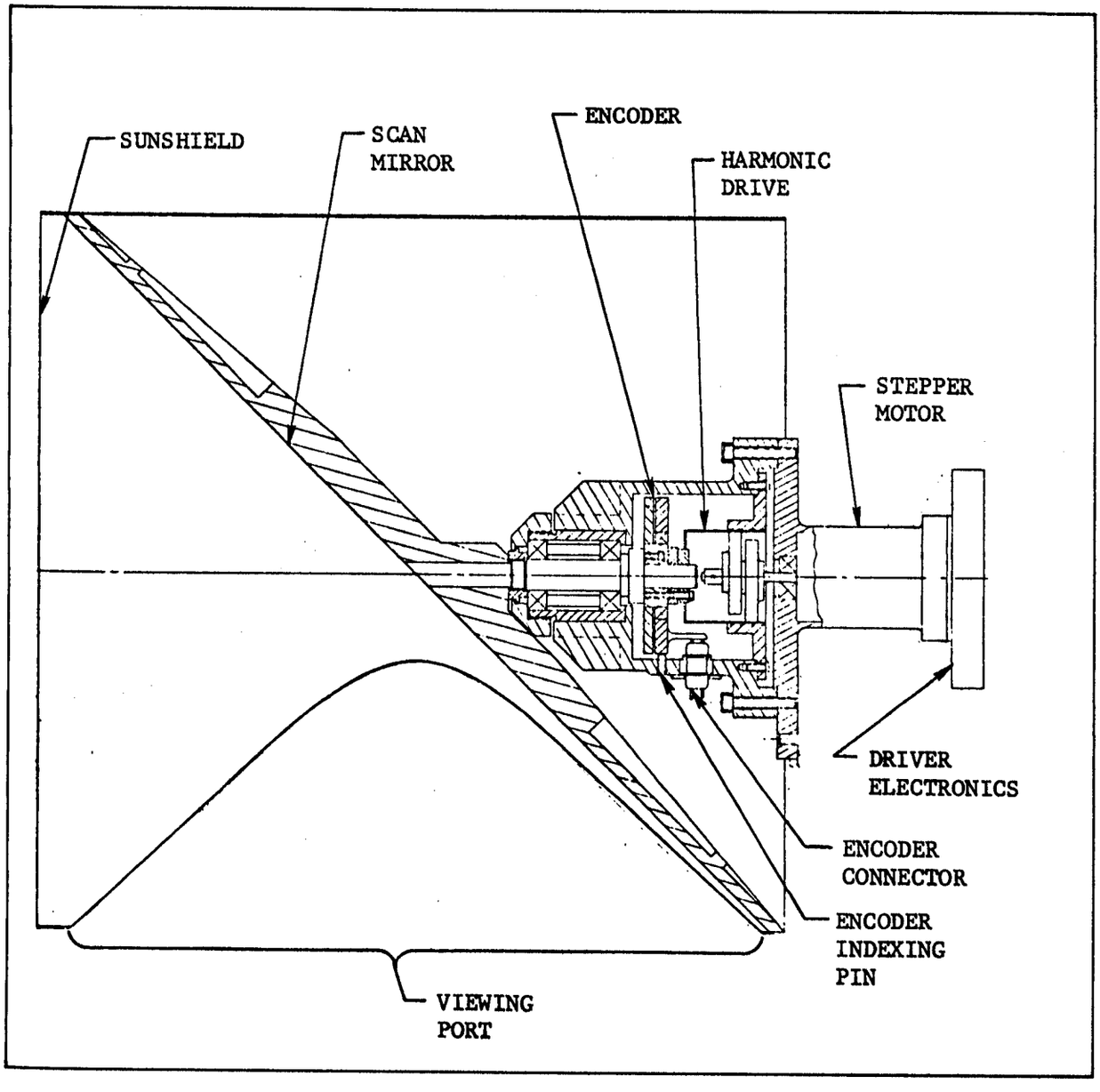

TOVS Basic Sounder Unit Scanner Assembly

LOCATION OF ELECTRONIC SUBASSEMBLIES

The TOVS electronics are organized into modules that are located for optimum function, serviceability, and the enhancement of thermal control. There are five electronics areas: the power supply, the signal circuitry, the scan motor driver, chopper motor drive, and the detector preamplifier.

The power supply module, because of its high currents and interference-generating components, is shielded and located in the upper part of the instrument at the rear end. This module dissipates 6.75 watts of heat; consequently, good thermal contact with the housing is necessary. Since the module is covered with metal shielding, good thermal contact is easily accomplished. The location chosen for the power supply module is close to the instrument's external radiator panels.

The signal processing and control logic circuitry is located in the upper electronics bay area. This circuitry consists of a number of conformally coated boards with attached connectors. A location in the upper part of the instrument directly above the aft optics and also close to the interface connectors helps to minimize lead length from these electronic packages. These circuit boards have perimeter frames of aluminum, which facilitates mounting them and dissipating their heat.

For convenience and ease of wiring, the motor driver circuits are located at their respective motors. This feature allows the driver circuits to be hard wired to the motors, holding down the number of connectors. Dissipation of these circuits is also aided, since they can reject their heat along the same paths as the motors.

To achieve the low noise required, detector and preamplifier circuitry must be integral. This is done by building the detectors and their preamplifiers into single components. These components are mounted in sealed, modular housings on the front of the aft optics assembly. Cables carry the preamplifier signals to the signal processing boards in the electronics area above.

The location of the various electronics modules is shown in schematic form in the facing figure. Generally, to remove an electronics module, it is only necessary to break a connector, remove several mounting screws, and lift the component out.

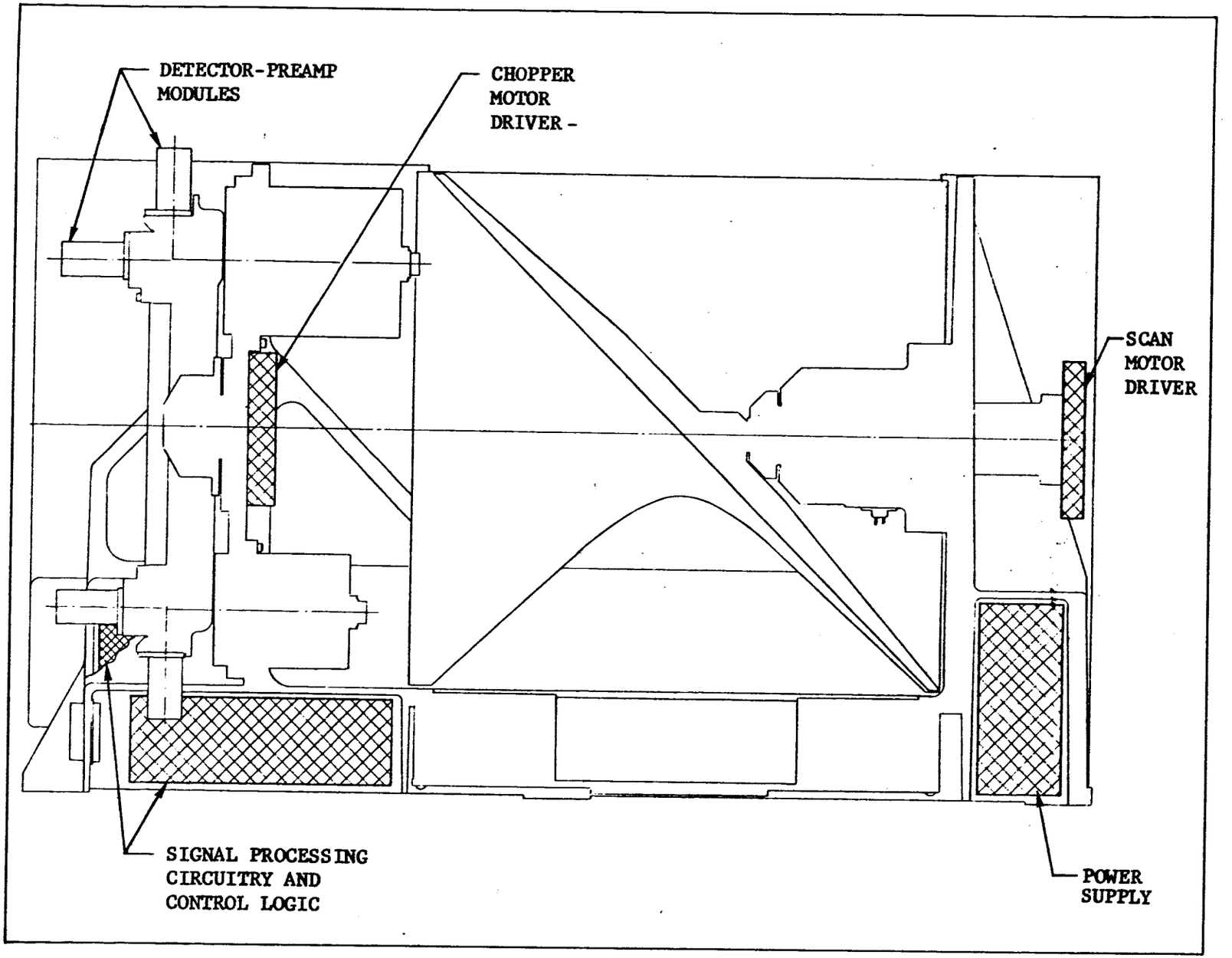

TOVS Basic Sounder Unit Electronics Location

BECKMAN INSTRUMENTS, INC.
Advanced Technology Operations
J.C. Hammond

APPROACH TO CABLING AND HARNESSING

The necessary electrical interconnections in the TOVS instrument are shown in Figure A. Interconnecting the electronics modules presents no great problems -- cable routing and restraining are generally simple.

A number of factors minimize the number of cables and connectors required. The bulk of the signal handling and control logic circuitry is located near the interface electrical connector area, since a large number of conductors must traverse this path. Likewise, this signal circuitry area is close to the detectors so that length and routing of the preamplifier signal cables is manageable. The motor driver circuits are located on their respective motors, which allows the driver-to-motor connections to be made by hard wiring.

There are no connectors at the preamplifier end of the signal cable. The cables enter the upper electronics tray area through a fairly large hole which allows the cables and their connectors on the upper ends to be withdrawn for servicing one or two at a time. The preamplifier signal cables are clamped to the detector-preamplifier housings at one point, then bundled together as they ascend the optics web of the housing. A cable clamp is placed on the bundle at each takeoff point.

Cable runs in the Basic Sounder Unit are shown schematically in Figure B.

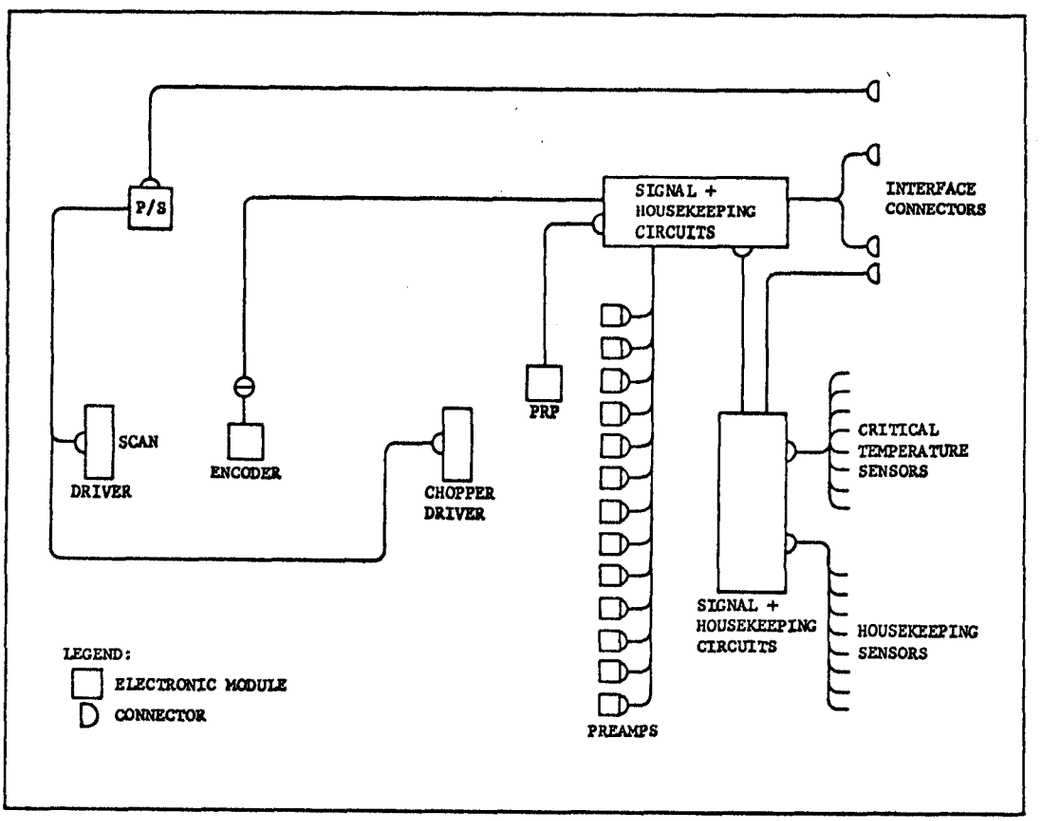

Figure A. TOVS-BSU Electrical Interconnections

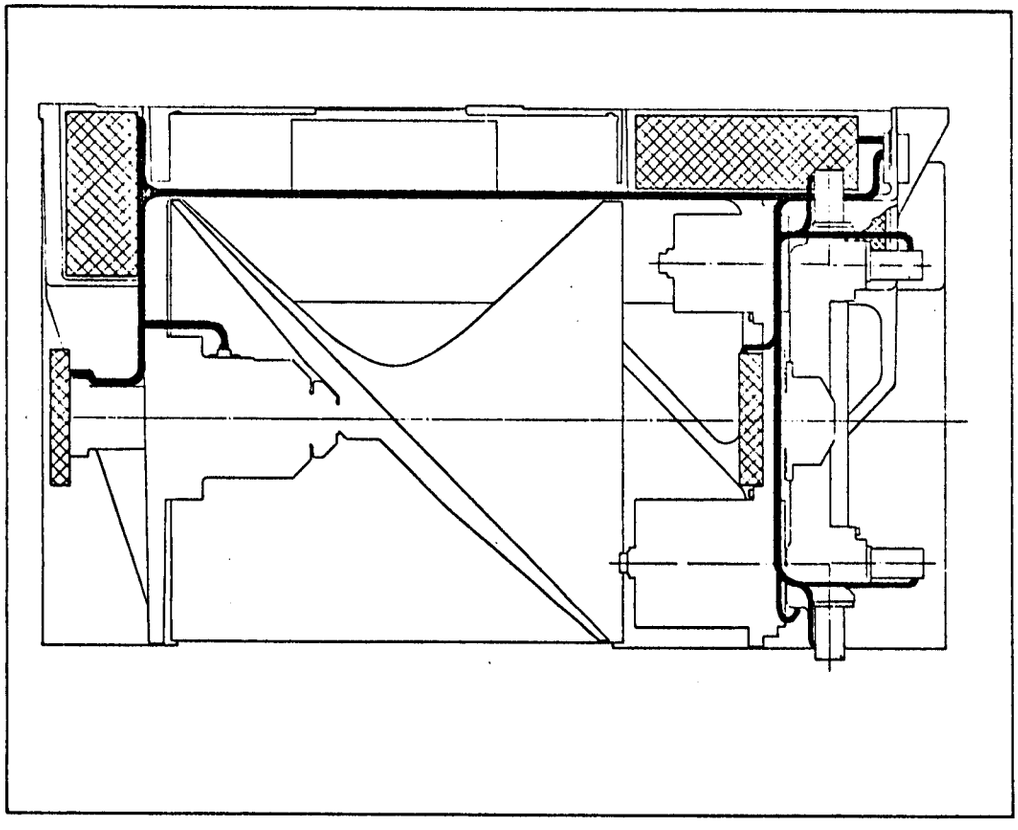

Figure B. Basic Sounder Unit Cable Runs

ACCESS FOR SERVICING

Component servicing is an important consideration for an operational instrument such as the TOVS-BSU. The goal of serviceability has been achieved in the instrument's design in that most components are readily accessible by simply removing a cover.

A number of Basic Sounder Unit instrument components may require some servicing after initial instrument assembly and adjustment. These are listed in the facing table and are discussed below.

Occasional removal of detector-preamplifier housings may be necessary. Access to these is gained by removing the instrument's lower exterior sheet metal cover. The individual detector housings then can be removed by unscrewing their three mounting screws. The upper cover of the instrument also is removed so that the upper end of the signal cable can be disconnected and withdrawn, as has been discussed.

Access to the various electronics modules varies; all can be reached by removing one or the other of the lower covers or the top cover. Extensive use of connectors facilitates removing the electronic modules; also, it should be noted that in-instrument servicing of the electronic modules is not generally necessary. The scanner motor can be easily removed from the aft end of the instrument by removing the mounting screws and unplugging the electrical connector. This can be done with the scanner subassembly either on the instrument or on the bench. Other scan-drive components may be removed from the open end of the scan-drive housing. It is preferable to remove the scanner subassembly in order to do this.

The phase reference pickoff assembly is a self-contained unit mounted at the rim of the chopper wheel. It is readily accessible once the instrument's lower front cover has been removed:

The chopper motor and chopper disc, however, are not so easily reached. The drive electronics and the connections to the motor are readily accessible; however, access to the motor or the disc requires that the optics subassembly be removed and split apart. This is probably the only place in the instrument where good accessibility is not obtained. The chopper motor could have been mounted on the other side of the optics subassembly, as was the case with the ITPR instrument. Then, however, elaborate means would have been necessary to get rid of the motor heat (again as was the case with ITPR). The more straight-forward and lighter thermal design of the BSU chopper outweighs the somewhat more awkward assembly and access situation.

Although there is, in fact, no "routine" servicing required -- the instrument is assembled, adjusted, turned on, and it performs -- experience shows that a certain amount of servicing can be expected. In consideration of this, the BSU design assures that servicing readily can be accomplished.

ACCESS TO TOVS-BSU COMPONENTS

All components are readily accessible with the exception of the Chopper Motor and Disc.

- Detector-Amplifier Housings
  - Removal of lower sheet metal cover.
- Electronics Modules
  - Removal of one of lower covers or the top cover.
- Phase Reference Pickoff Assembly
  - Removal of lower front cover.
- Chopper Motor and Disc
  - Removal of Optics Subassembly is required.

SECTION 13
STRUCTURAL DESIGN OF THE TOVS-BSU

Nature of Structural Requirements 13-0
Approach to Housing Design 13-2
Estimates of Thermal Deflections 13-4

NATURE OF STRUCTURAL REQUIREMENTS

The TOVS instrument is designed to meet the structural requirement for strength, rigidity, and long-term stability. The most critical of these are rigidity and long-term stability.

Strength -- Requirements for simple structural strength relate to the launch environment. The instrument specification requires that strength safety factors be two or better. Because the design is based on rigidity, this is not generally a problem, although a few areas must be examined closely. These include: fatigue strength of the harmonic drive flexible member, stress in bearings in the scanner area, and working stresses in springs. There are no problems in these areas.

Rigidity -- The requirement of rigidity has to do with optical accuracy; that is, maintaining the alignment of optical elements under environmental and operating stresses. The problem areas here are the housing in the vicinity of the scanner subassembly mounting, the optics subassembly mounting, the scan mirror itself, the telescope barrels, and the rotating chopper wheel. Analytical results discussed in the following pages show that the design offers adequate rigidity in these areas.

Long Term Stability -- The instrument must have long-term structural stability to assure that its characteristics will not change under launch stresses, and to guarantee its performance over a two-year life. Designing for stability is primarily a matter of ensuring that stress levels are comfortably low in critical areas. This has been achieved in the design of the TOVS instrument. Some representative stress values and safety factors are shown in the table opposite. In every case, safety factors are 10 or better, indicating a very low level of wholly elastic loading, which is the desired condition.

REPRESENTATIVE STRESS VALUES AND SAFETY FACTORS

	Maximum Stress (psi)	Material Strength (psi)	Safety Factor
Telescope Barrel	51	40000	780.0
Bolts-Optics Subassembly	9500	163000	17.2
Insulating Spacers - Optics Subassembly	378	138000	366.0

APPROACH TO HOUSING DESIGN

The structural requirements of the TOVS instrument are met with a cast aluminum alloy housing whose properties have been carefully analyzed to show that it meets the requirements of strength, rigidity, and stability.

Aluminum alloy A356 was chosen for the material of the housing because of its ability to produce stress-free castings, its good thermal properties, and its easy machinability. It is also a familiar, frequently used, structural material which is a good choice for a long-term application.

The housing design is presented in simplified form in the figure opposite, which shows its basic configuration and important structural features. The design of the housing is based on rigidity. Therefore, strength of the material in the sense of gross yielding is not of concern, with the possible exception of vibration loading. Accordingly, the natural frequencies of the lowest modes of the housing were calculated and compared with the applied vibration spectra. The concern here, of course, is to check the highest stresses that can occur when resonant conditions develop.

The lowest natural frequency found was in the cantilevered scanner web. The lowest mode of this portion of the structure is 2000 Hz, putting it at the upper limit of the test range. Accordingly, it can be concluded that the structure is not responsive to the applied vibration.

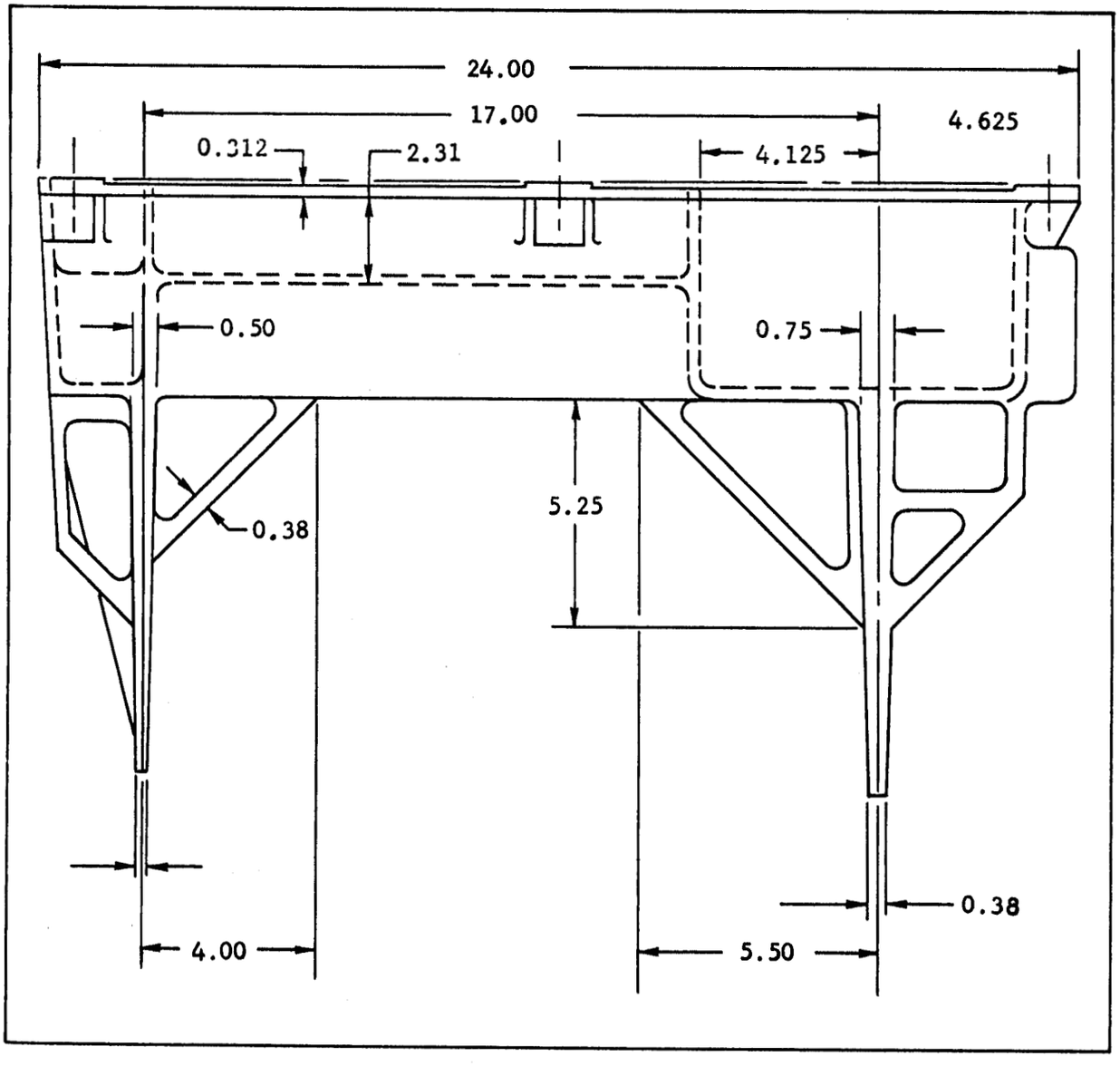

Simplified View - TOVS Structure

ESTIMATES OF THERMAL DEFLECTIONS

Structural deflections caused by temperature gradients in the TOVS instrument were examined to determine whether instrument accuracy would be affected by the predicted temperature changes. The areas considered were the housing, the scanner subassembly, and the optics subassembly.

The deflections found to exist because of temperature gradients in the housing were slight. The areas where gradients may be significant are as follows:

- Vertical gradient - electronics bay area: 6.7°C
- Longitudinal Gradient - scanner web: nil
- Longitudinal Gradient - optics web: nil

The predicted deflections for the electronics bay area vertical gradient is about 0.002 inch. The effect of this is to divert the exit beam of the instrument by about 0.05 degree. Since this error is less than the spacecraft pointing accuracy, and any changes occur very slowly, the effect on instrument performance is negligible.

Obviously, the critical component on the scanner assembly is the scan mirror. The maximum instantaneous gradient that can exist in the mirror is 2.8°C, and analysis shows that this would yield a deflection of 62×10^{-6} inch. This is within the allowable overall flatness tolerance on the mirror, which is 0.0005 inch. Some concern also must be reserved for the possible effect of temperature gradient on the scan mirror shaft bearings, since these are preloaded and loosening or tightening is undesirable. The bearings are installed in a strainless steel cartridge which is pressed into the aluminum scanner housing. This monometallic interface is desirable because of the known tendency of bearings installed directly in aluminum housings to loosen under thermal cycling. Since the maximum gradient between the bearings and the mirror shaft is predicted to be 29°C, no difficulty is anticipated in this area.

The only area in the optics subassembly that is subject to variable deflections from variable temperatures is the telescope barrels, because the remainder of the subassembly (aft optics) is temperature controlled to a fraction of a degree. Bending of the telescope barrels is undesirable in that it leads to defocusing and consequent loss of energy on the detectors. The maximum predicted temperature gradient across the base of a telescope tube (due to chopper motor heat) is 4.5°C. If this gradient is conservatively assumed to exist all along the length of the barrel, an angular deflection of 0.008 degree results. Because of optical doubling, this deflection deviates the beam by 0.016 degree, which is just significant and requires further examination, since the relative pointing accuracy specification is 0.01 degree.

Lengthwise elongation or contraction of the telescope barrels is also undesirable in that this leads to defocusing. The maximum dimensional change that could result because of this effect is 0.0006 inch, which is not significant: it leads to a blurring of less than 1 percent of the beam size.

THERMAL DEFLECTION EFFECTS

A barely significant deflection occurs in the telescope mounting plate; it results from the heat of the chopper motor. This problem requires attention in the detailed design.

- Bending of housing deflects scanner beam by only 0.05 degree.
- Scan mirror bending is acceptable.
- Scanner preload will be stable.
- Telescope pointing may be affected by gradients in mounting plate (less than 0.016 degree).
- Thermal defocusing of telescope is insignificant.

SECTION 14
TOVS/BSU RELIABILITY PROGRAM

Design for Reliability and Production..... 14-1

TOVS/BSU Reliability Program..... 14-5

Expected Reliability of the TOVS/BSU..... 14-7

DESIGN FOR RELIABILITY AND PRODUCTION

The Design for Reliability and Production considered the following: 1) Modular Concept, 2) Ease of Assembly at the Subsystem Level, 3) Producibility, 4) Minimum Parts Count, 5) Optics Reliability, 6) Electromechanical Devices Reliability, 7) Analysis of Failure Mode Prevention, and 8) Redundancy.

One of the major requirements in the design study was the achievement of a reliable design that would not degrade as a function of production. The topics considered are basic to the nature of reliability but are hand-tailored to fit the system being studied.

Modular Concept: Modular construction was one of the main design considerations at the system level. The use of modules will optimize assembly and inspection tasks. Because of the ease of assembly and disassembly, the modular construction also will enhance checkout of the system for localization and isolation of problems during the various phases of system testing.

The following examples illustrate ease of assembly:

- Attachment of the Scan Drive Subassembly to the BSU housing can be achieved by fastening five screws.
- The Blackbody Subassembly can be attached with five screws.
- The Aft Optics Subassembly requires only four screws for attachment.

Ease of Assembly at Subsystem Level: One of the primary considerations in the design of the assemblies and subassemblies at the subsystem level was ease of assembly. For example, through the use of separate, insertable, detector lens housings, the task of assembling the lens elements will be easier to accomplish as compared to the difficult task of inserting the lens elements into seats machined in the Optics Housing Plate. Another example is the simplified dichroic beamsplitter mounting arrangement, whereby the dichroic element can be easily inserted and fastened in place with two spring clips. Also, the entire Optics Subassembly can be detached from the BSU housing by the removal of four screws and a wire harness connector, and the Scanner Subassembly can be detached by the removal of five screws and two wire harness connectors.

Producibility: Another design consideration at the subsystem level was producibility. As an example, the telescope barrels were designed so that the secondary support spider arms will be made integral with the barrel. This will be accomplished in one operation through the use of electrical discharge machining. An added advantage of this approach is that the resulting part will be virtually stress-free and thus more reliable. Another example of enhanced producibility is the use of an insertable cartridge for mounting the Detector Lens Assemblies. The cartridges can be machined easily as compared to the difficult task of machining intricate seats for the lens elements in the large Optics Housing Plate.

Minimum Parts Count: The design principle of using the least number of parts has many advantages, the most important of which is greater reliability. A good example of minimum parts count design as compared to a gear train assembly design is the Harmonic Drive Assembly used in the Scanner Subassembly.

Optics Reliability: The quality of the optical elements used in the BSU will be rigidly controlled by procurement specifications whose provisions have been approved by the Beckman Reliability Department.

For instance, the spherical surfaces of the lenses will be physically tested against test glasses and will be required to match the test glasses to within three fringes spherical, and 1/4 fringe irregularity. The test glass radii will be measured and certified by an independent test laboratory approved by Beckman, prior to lens fabrication.

Environmental tests supervised by Beckman's Quality Assurance Department will be performed on one witness piece from each set of two that represent each material batch and process lot.

The spectral defining optics will be tested for reflectance and transmittance characteristics with a spectrophotometer which has been calibrated by an independent calibration laboratory and the calibration data will accompany the test results obtained from the reflectance and transmittance tests.

Environmental tests will be performed on the spectral defining optic in the same manner as described for the lenses above.

All material used for the optics will be optical grade, polycrystalline, stress-free, fine annealed, and selected for low absorption at the specified spectral wavelength. In addition, all optical elements will be subjected to rigid qualification and screening tests.

Electromechanical Devices Reliability: To obtain reliable space-qualified hardware for the BSU, procurement specifications whose provisions have been approved by the Beckman Reliability Department, have been generated for the Scan Motor, Chopper Drive Motor, Harmonic Drive Assembly, Pin-Contact Shaft Angle Encoder, and Duplex Bearing Sets. Emphasis has been placed on the use of clean room requirements as outlined in Federal Standard No. 2092, and the use of laminal-flow stations for assembly and inspection operations. Special attention has been given to rigid screening and qualification tests, and the selection and testing of space qualified lubricants. In addition, the provisions of NASA Document NHB 5300.4(1C), "Inspection Provisions for Aeronautical and Space System Materials, Parts, Components, and Services," will be imposed on all Beckman suppliers.

The procurement specifications also include the following requirements:

- Submittal of Quality Assurance and Process Control plans by suppliers to Beckman for approval prior to fabrication.
- Source inspection during fabrication at the supplier's facilities by Beckman Quality Assurance personnel.
- Environmental testing.
- Acceptance testing.
- Traceability of material.
- Lot control.
- Insulation resistance measurement and dielectric withstanding voltage tests.

DESIGN FOR RELIABILITY AND PRODUCTION (Continued)

Analysis of Failure Mode Prevention: A detailed FMECA has been performed and the results of that analysis are attached as an appendix to this report. The analysis centers about the prediction of possible failures and results in recommended reliability procedures which will assure the reduction of the probability of such failures.

The probability of instrument failure will be greatly reduced by strict adherence to rigid reliability screening and qualification testing.

Failure of the Scanner Assembly can result from Failure Modes in the Scanner Motor, et al. The probability of failure in the scan motor due to shorted windings, etc..... will be reduced by run-in at elevated temperature prior to acceptance test. In addition, the load presented to the motor is small. The probability of mechanical defects occurring in the Harmonic Drive is also reduced by run-in at elevated temperatures. Redundancy in the shaft encoder allows for normal operation in the event of a loss of one pin. Warpage of the scan mirror can be minimized by stress relieving prior to machining.

The probability of breakage or misalignment of optical components in the telescopes and aft-optics housing can be reduced by testing under simulated launch conditions. Degradation of optical coatings can be minimized by proper handling and environmental testing. The BSU will still operate at 70% of optimum performance in the event of aft-optics heater failure. Redundancy of the temperature sensors minimize the effect of failure.

The probability of failure of the chopper drive motor and angular momentum compensation motor contained in the chopper assembly is minimized by run-in at elevated temperature. Warpage or distortion of the chopper wheel is minimized by stress relieving heat treatment after machining. The gold coating will not be degraded by ultraviolet radiation. The PRP electronic components will be screened for high-reliability.

The coating used for high emissivity of the calibration and reference blackbodies is 3M Black Velvet, which has been proven in many space flight applications. In addition, the manufacturer's recommendation for application will be strictly adhered to in order to prevent surface degradation. The temperature sensors will be mounted in such a fashion as to minimize the probability of lead breakage. Potting of the lead wires will be considered in the final design.

A trade-off exists between reliability and production difficulties, weight and cost. Redundancy, necessary for reliability, must be designed so that cost, simplicity of design, and manufacturing feasibility are all weighed against each other.

Redundancy: The use of redundancy in selected areas should be given due consideration during the actual TOVS/BSU design phase. These areas are merely being pointed out in this section of the study so that they can receive detailed treatment during the design phase of the hardware contract.

1) TIL Diodes - Some degree of redundancy would be beneficial for the TIL diodes. This redundancy should be more than the present considerations, i.e., two TIL diodes in a package.
2) Proportional heaters - Again, some degree of redundancy should be considered for the proportional heaters. This would allow operation in the event of selected failures in the proportional heater circuitry.

TOVS/BSU RELIABILITY PROGRAM

The TOVS/BSU reliability program considered the following: 1) Summary of Failure Modes and Effects, 2) Summary of Special Parts and Devices, 3) TOVS Electronics, and 4) Discussion of Reliability Estimates.

A key element in the TOVS/BSU reliability study was the consideration of the manner in which the multitude of failures that are possible could impact the equipment's performance. The topics considered address the subject of failure modes, effects, and considerations pertaining to the minimization of the impact of these modes and effects.

Summary of Failure Modes and Effects:

TOVS Basic Sounder Unit - The failure Modes, Effects, and Criticality Analysis (FMECA) for the TOVS Basic Sounder Unit can be found elsewhere in this report as an appendix. The FMECA was used as a tool to identify the more probabl and critical failure effects and to initiate trade-off studies for minimizing the probabilities associated with these non-desired failure effects. A glance at the sheets (Forms 13547F1) reveals the more critical failure modes (AeAp is the most critical and EeEp is the least).

Redundancy carries with it attendant increases in volume and weight. At the piece part level on a selected basis, redundancy can be very effective. An example of this is the use of a minimum of 4 Aft-Optics Housing Temperature Sensors. The redundancy affords an inference as to the temperature of the housing at a failed temperature sensor position. Another aspect generated by the FMECA was a chance to review the need for extra pre-conditioning tests. One such case was the plan for acceptance testing for the surface coating of the dichroic mirrors. Of final considerations is the FMECA-generated treatment of the possible mechanical modes of failure. One corrective action item generated was the choice of mounting for the temperature sensors. The lead wires will be stress relieved via design and will be ultimately potted for stress minimization.

TOVS Electronics - Although a formal FMECA is not contained herein for the Electronics, consideration has been given informally to the system-level failure modes and their resultant failure effects. As in the case of the Basic Sounder Unit, the probability of failure modes will be reduced where necessary by consideration of mechanical stress, electrical stress, radiation effects, piece-part level redundancy, and parts count. The first consideration for choice of electronics circuitry was that of previous flight use. An adjunct to standard circuitry is standard parts usage. PPL-12 has been considered in the choice of electronic piece parts. A slight "evolution" of design has been created by the natural "evolution" of the part types contained in PPL-12. This has not brought on undesired effects however, and the designs can still be considered flight qualified.

Previous FMECA's for the SIRS and ITPR instruments will be reviewed to assure that previously-detected undesired failure modes have been treated in proper perspective.

GULTON INDUSTRIES, INC.
Data Systems Divison
J. T. Henderson

Summary of Special Parts and Devices: The scan motor, harmonic drive, encoder, bearings and the chopper motor are a group of subsystem components which do not have devised type reliability data. Normally, the bearings would not be included; however, the loading conditions, total revolutions and lubrications result in a component which is analogous to but not identical to other bearing assemblies.

Each component requires a detailed set of performance specifications as described in Section 7 Selection of Flight Scanner Components. In addition, sufficient engineering and qualification testing must be performed to project two year performance life with better than 0.99 confidence. Thereafter, flight components require production acceptance tests and finally, complete assembly checkout. After environmental tests to assure conformance to in-orbit operational requirements.

TOVS Electronics: With the exception of the detector pre-amp FET the electronics piece parts are virtually all space qualified. The above-mentioned FET will be strictly controlled by Gulton-generated Specification Control Drawings. Gulton is strongly considering the DN1154 currently used on ERB as a candidate for the requirement. This part is currently covered by Gulton's specification DSD-SPEC-E0207. The screening contained in this drawing has been carefully coordinated with NASA for maximum effectiveness. If a different device is selected, similar or more stringent screening will be applied. Gulton is working with Siliconix and T.I. Ltd. on the selection of the exact device to be used. Gulton proposes to use a large-valued resistor (approximately 10^{12} ohms) that has been procured previously for ERB. This part has been subjected to a successful evaluation examination by the NASA GSFC Parts Branch.

Some definite trade offs exist in the logic area between the use of COSMOS and TTL logic. Since it appears that either part type can do the required job, this choice will be deferred until more inputs are available from NASA. For instance the COSMOS RCA line has been conditionally accepted on PPL-12. A year ago this logic line was strongly condemned. Gulton likes COSMOS as a logic series and has had an excellent reliability history with the devices in previous designs.

Discussion of Reliability Estimates:

General - No quantitative estimates of the TOVS relaibility are included in this report. It is felt that the design can be realized via a minimum of space-proven circuits and hardware. The reliability of the unit is of course dependent on the application of reliability and quality programs that insure a maximum in inherent reliability and a minimum of subsequent degradation of this figure via test, manufacturing, and shipment. An integral part of this reliability/quality effort is a parts and materials program. It is the function of this program to insure that the most reliable piece parts available are used for a given function. The design-verification program follows in logical order and has as its purpose the insurance that the ultra-reliable parts are used in a manner that does not degrade their inherent reliability. Stress analyses and FMECA's are but two of the subtasks of this program.

Reliability estimates are relative to the choice of failure rates and therefore derive their best benefit from their use in tradeoff studies. Informal tradeoff studies have been held in conjunction with the electronics and optics design. During the design phase of the instrument such studies should be performed and documented formally.

EXPECTED RELIABILITY OF THE TOVS

The Expected Reliability of the TOVS considered the Reliability Block Diagrams and the detailed Failure Effect Mode and Criticality Analysis of the Optics portion of the TOVS/BSU.

Attention to the possible failure modes and their resultant failure effects can only be obtained via a detailed worksheet and reliability block diagrams. These items are treated in the following section.

GULTON INDUSTRIES, INC.
Data Systems Division
J. T. Henderson

EXPECTED RELIABILITY OF THE TOVS

Introduction

The subject Failure Mode, Effect, and Criticality Analysis (FMECA) Report for the Basic Sounder Unit of the TIROS Operational Vertical Sounder (TOVS) is submitted in accordance with the requirements of Gulton DSD Drawing No. 13961-900, dated 5/9/72.

Gulton DSD Forms 13547F1, Failure Effect Analysis, have been used and are a part of this report.

Purpose

The purpose of this report is to present a detailed analysis of possible ways the Basic Sounder Unit can fail, and to define the effects of these assumed failures on the performance of the equipment.

Summary

Since the Primary Units assemblies will channel the field-of-view radiant flux to Gulton's electronic system for level measurements, any failure modes within these assemblies that result in any loss of radiant flux will degrade the accuracy of the TOVS mission objective. However, through the use of adequate design factors, the likelihood of failure will be very small.

Discussion

The Reliability Logic Block Diagram for the Primary Unit is presented in Figure 1. The Primary Unit Housing and each of the assemblies are described below.

Primary Unit Housing

The housing is basically a box casting with provisions for mounting the Scanner Assembly, Fore and Aft Optics Assembly, Chopper Assembly and Calibration Blackbody Assembly. It also includes attachment points to support the instrument to the TIROS Spacecraft, and the provisions for interface electrical connectors.

Scanner Assembly

The function of the scanner assembly is to perform a continuous cross-course scan centered on the sub-orbital track. The scan consists of 72 instantaneous fields of view (IFOV) which cover a total scan-angle of 40.5° on either side of the sub-orbital track. Coverage on the earth's surface varies from 33 km x 33 km at the sub-orbital track, to 47.5 km x 80 km at the end of the scan. The scanner assembly also permits the optics assembly to look at space and the calibration blackbodies for calibration.

The scanner assembly consists of a scan motor, harmonic drive, pin-contact shaft angle encoder, and scan mirror.

Force and Aft Optics Assembly

The function of the fore and aft optics assembly is to gather radiant energy from the scene and calibration sources and focus it on the detectors.

The assembly contains seven Cassegrainian telescopes. Four have objective diameters of 80 mm, and three have 61 mm objective diameters. The assembly also contains seven dichroic beam-splitters, 14 sets of bandpass/blocking filters, 14 sets of detector lenses, and at least four platinum resistance temperature sensors. Each telescope is shared by two optical channels, with separation being accomplished by the dichroic beamsplitters.

An aft-optics heater will be utilized to provide heat so that the aft-optics components (detectors, filters and chopping reference blackbody surfaces) will meet the performance specifications.

Chopper Assembly

The chopper assembly consists of the chopper drive motor, angular momentum compensation motor, phase reference pickup (PRP), and chopper wheel. The chopper drive motor will rotate at 600 rpm.

The chopper wheel chops the incoming beam of radiant energy, and also images the chopping reference blackbody surfaces during the off cycle of the cyclic chopping waveform. When in the field-of-view, the reference blackbody temperature is sensed by the detector.

The angular momentum compensation motor's design will be similar to the chopper motor's design but will probably rotate at 1200 rpm and in the opposite direction. Since there is no need for a shaft-output from the angular momentum compensation motor, it can be of a closed construction, providing good retention of lubricant and lubricant vapors.

The phase reference pickup (PRP) is used to synchronize the chopping cycl with the scanning cycles. This is accomplished by using a light source (GaAsdiode) whose output is first channeled through a 0.005-inch hole and is then interrupted by reference apertures in the chopper wheel. The interrupted lightbeam is then received by the phase pickup amplifier portion of the PRP which uses a phototransistor with associated circuitry which synchronizes the signal demodulators.

Calibration Blackbody Assembly

The function of the calibration blackbody assembly is to provide an array of black fields-of-view for the telescopes to view for the purpose of calibration.

The blackbodies are essentially light traps which simulate the action of a perfect absorber when viewed from their open ends. This effect is a result of their geometry, and is heightened by their optically black finish. The blackbodies are contained in a thermally massive metal block to attenuate temperature fluctuations. The block is instrumented with platinum resistance temperature sensors so that its temperature is known for calibration purposes

Figure 1. Reliability Logic Block Diagram - TOVS PRIMARY UNIT

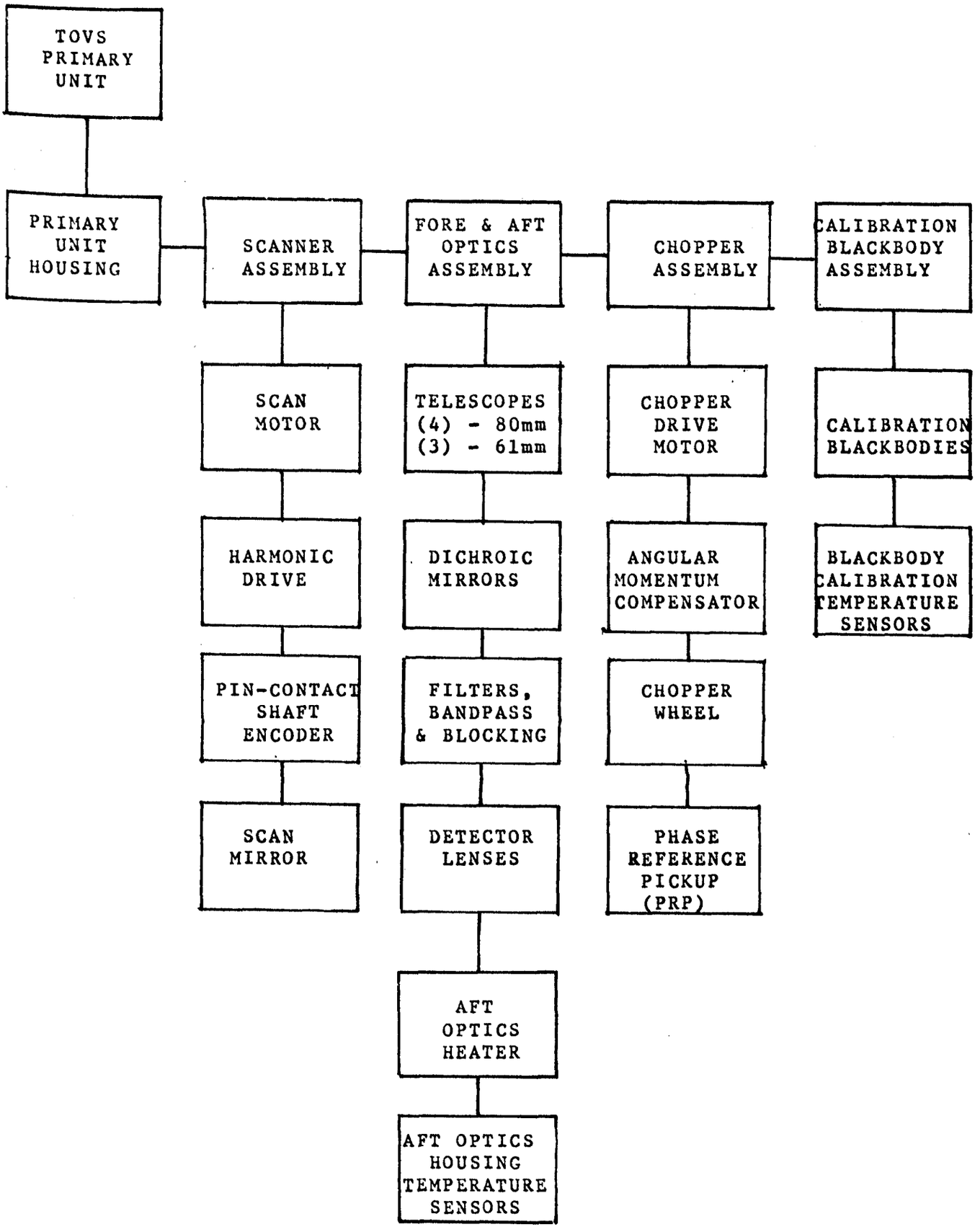

NOTES:

FAILURE MODE: O=Open, S=Short, D=Drift, CS=Set F/F, CR=Reset F/F
C1=Constant "1" Level, CO=Constant "0" Level, G=Gate Failure
+ = Either Mode, NO=No Output, EO=Erroneous Output
DETECTABILITY: Y=Yes, P=Possibly, N=No
ALTERNATE MODE(S) OF OPERATION: N=None, D=Operate with Degradation
CORRECTIVE ACTION: R=Replace Unit

NOTES:

CRITICALITY/PROBABILITY FAILURE MODE ASSIGNMENTS (X_e & X_p)
A_e = 75% degraded to catastrophic
B_e = 50% to 75% degraded
C_e = 25% to 50% degraded
D_e = negligible to 25% degraded
E_e = no effect
A_p = 20% + of possible failures
B_p = 5-20% " " "
C_p = .5-5% " " "
D_p = .05-.5% " " "
E_p = < .05% " " "

Issue Date January 1971
Rev. ___ Date ___
Preliminary (X)
Final Issue ( )
Prepared by J. Rosenbaum, ATO

FAILURE EFFECT ANALYSIS

Gi GULTON INDUSTRIES INC.
DATA SYSTEMS DIVISION

Contract GI No. ___
TOVS Basic Sounder Unit
Circuit ( )
Subsystem (X)
System ( )
Drawing No. ___
Code No. ___

ITEM	REF DESIG.	FUNCTION	FAILURE MODE	DETECT-ABILITY	FAILURE EFFECT	ALTERNATE MODE OF OPERATION	CORRECTIVE ACTION	X_e	X_p	REMARKS
TOVS Basic Sounder Unit	N/A	The Basic Sounder Unit consists of: 1) Basic Sounder Unit Housing 2) Scanner Assembly 3) Fore and Aft Optics Assembly 4) Chopper Assembly 5) Calibration Black-body Assembly Functions of the above items are noted on the following sheets.	N/A	N/A	N/A	N/A	N/A	N/A	N/A	

13547F1

NOTES:
FAILURE MODE: O=Open, S=Short, D=Drift, CS=Set F/F, CR=Reset F/F
C1=Constant "1" Level, CO=Constant "0" Level, G=Gate Failure
+ = Either Mode, NO=No Output, EO=Erroneous Output
DETECTABILITY: Y=Yes, P=Possibly, N=No
ALTERNATE MODE(S) OF OPERATION: N=None, D=Operate with Degradation
CORRECTIVE ACTION: R=Replace Unit

NOTES:
CRITICALITY/PROBABILITY FAILURE MODE ASSIGNMENTS (X_e & X_p)
A_e = 75% degraded to catastrophic
B_e = 50% to 75% degraded
C_e = 25% to 50% degraded
D_e = negligible to 25% degraded
E_e = no effect
A_p = 20% + of possible failures
B_p = 5-20% " " "
C_p = .5-5% " " "
D_p = .05-.5% " " "
E_p = < .05% " " "

Issue Date January 1972
Rev. ___ Date _____
Preliminary (X)
Final Issue ( )
Prepared by J. Rosenbaum, ATO

FAILURE EFFECT ANALYSIS
GULTON INDUSTRIES INC.
DATA SYSTEMS DIVISION

Contract GI No. _____
TOYS Basic Sounder Unit
Circuit ( )
Subsystem (X)
System ( )
Drawing No. _____
Code No. _____

ITEM	REF DESIG.	FUNCTION	FAILURE MODE	DETECT-ABILITY	FAILURE EFFECT	ALTERNATE MODE OF OPERATION	CORRECTIVE ACTION	X_e	X_p	REMARKS
Basic Sounder Unit Housing	N/A	To attach the BSU to the TIROS Spacecraft, to provide a rigid structure for alignment of the Fore & Aft Optics, and to house the Scanner Assembly, Chopper Assembly and the Calibration Blackbody Assembly.	1) Housing develops large crack.	Y	Will cause misalignment of optics, thus rendering the BSU inoperative.	N	R	A_c	E_p	Housing design will incorporate an adequate safety factor, and the housing will be subjected to X-ray examination to insure that the likelihood of its cracking will be very remote.
			2) One of mounting points breaks loose.	N	BSU Housing will have one less attachment point to support the BSU to the spacecraft (TIROS). The effect would be variable, from no effect, to possible local yielding of casting.	D	Repair mounting point	D_e	D_p	Since the housing has redundant attachments, the failure of one point would most probably have no effect on mission. If yielding does occur, it may result in optical misalignment.

13547F1

NOTES:
FAILURE MODE: O=Open, S=Short, D=Drift, CS=Set F/F, CR=Reset F/F
C1=Constant "1" Level, CO=Constant "0" Level, G=Gate Failure
+ = Either Mode, NO=No Output, EO=Erroneous Output
DETECTABILITY: Y=Yes, P=Possibly, N=No
ALTERNATE MODE(S) OF OPERATION: N=None, D=Operate with Degradation
CORRECTIVE ACTION: R=Replace Unit

NOTES:
CRITICALITY/PROBABILITY FAILURE MODE ASSIGNMENTS (X_e & X_p)
A_e = 75% degraded to catastrophic
B_e = 50% to 75% degraded
C_e = 25% to 50% degraded
D_e = negligible to 25% degraded
E_e = no effect
A_p = 20% + of possible failures
B_p = 5-20% " " "
C_p = .5-5% " " "
D_p = .05-.5% " " "
E_p = < .05% " " "

Issue Date January 1973
Rev. ___ Date ___
Preliminary (X)
Final Issue ( )
Prepared by J. Rosenbaum, ATO

FAILURE EFFECT ANALYSIS
GULTON INDUSTRIES INC.
DATA SYSTEMS DIVISION

Contract GI No. ___
TOVS Basic Sounder Unit
Circuit ( )
Subsystem (X)
System ( )
Drawing No. ___
Code No. ___

ITEM	REF DESIG.	FUNCTION	FAILURE MODE	DETECT-ABILITY	FAILURE EFFECT	ALTERNATE MODE OF OPERATION	CORRECTIVE ACTION	X_e	X_p	REMARKS
Scanner Assembly	N/A	The function of the scanner assembly is to view earth, to view space and to view a housing blackbody reference for calibration. The assembly is made up of the scan motor, harmonic drive, pin-contact shaft encoder, and scan mirror.	N/A	N/A	N/A	N/A	N/A	N/A	N/A	For the components below, X_e is at the BSU level, and X_p is at the Scanner Assembly level.
Scan Motor	N/A	Provides power to harmonic drive for driving the scan mirror to achieve 1.125° steps.	1) No output due to open or shorted motor windings.	Y	Scan mirror cannot be driven through its 1.125° steps.	N	R	A_e	B_p	The load presented to the motor will be small; the motor will be run-in for a minimum of 168 hours at 70° ±2°C prior to acceptance tests; and the motor will be subjected to rigorous screening and qualification tests.
			2) No output due to failure of bearing.	Y	Scan mirror cannot be driven through its 1.125° steps.	N	R	A_e	B_p	
			3) Inadequate torque output due to degrdation of motor performance characteristics.	Y	Scan program cannot be reliably and reproducibly achieved.	D	R	B_e	C_p	

13547F1

NOTES:
FAILURE MODE: O=Open, S=Short, D=Drift, CS=Set F/F, CR=Reset F/F
CI=Constant "1" Level, CO=Constant "0" Level, G=Gate Failure
+ = Either Mode, NO=No Output, EO=Erroneous Output
DETECTABILITY: Y=Yes, P=Possibly, N=No
ALTERNATE MODE(S) OF OPERATION: N=None, D=Operate with Degradation
CORRECTIVE ACTION: R=Replace Unit

NOTES:
CRITICALITY/PROBABILITY FAILURE MODE ASSIGNMENTS (X_e & X_p)
A_e = 75% degraded to catastrophic
B_e = 50% to 75% degraded
C_e = 25% to 50% degraded
D_e = negligible to 25% degraded
E_e = no effect
A_p = 20% + of possible failures
B_p = 5-20% " " "
C_p = .5-5% " " "
D_p = .05-.5% " " "
E_p = < .05% " " "

Issue Date _____
Rev. ___ Date January 1973
Preliminary (X)
Final Issue ( )
Prepared by J.Rosenbaum, ATO

FAILURE EFFECT ANALYSIS
GULTON INDUSTRIES INC.
DATA SYSTEMS DIVISION

Contract GI No. _____
TOVS Basic Sounder Unit
Circuit ( )
Subsystem (X)
System ( )
Drawing No. _____
Code No. _____

ITEM	REF DESIG.	FUNCTION	FAILURE MODE	DETECT-ABILITY	FAILURE EFFECT	ALTERNATE MODE OF OPERATION	CORRECTIVE ACTION	X_e	X_p	REMARKS
Harmonic Drive	N/A	Drives the scan mirror to achieve 1.125° steps.	Fails to operate due to defective flexible spline, circular spline, or wave generator.	Y	Scan mirror cannot be driven through its 1.125° steps.	N	R	A_e	C_p	Harmonic drive will be run-in for a minimum of 168 hours at 70° ±2°C prior to acceptance tests; and the harmonic drive will be subjected to rigorous screening and qualification tests.
Pin-Contact Shaft Angle Encoder	N/A	Resolves the exact position of the scanner in the optical field.	1) Failure of one pin-contact.	N	Negligible.	N/A	N/A	E_e	C_p	The loss of only one pin-contact would have no effect on the function of the encoder due to the redundancy of pin-contacts.
			2) Failure of two pin-contacts on the same track.	P	Loss of scan position information.	D	R	A_e	D_p	The encoder will be subjected to stringent acceptance tests to assure low probability of failure.
Scan Mirror	N/A	Views earth, views space, and views a housing blackbody reference for calibration.	1) Scan mirror becomes warped or distorted.	P	Fields of view do not fully coincide.	D	R	D_e	E_p	Scan mirror will be stress relieved by heat treatment after machining, to prevent subsequent warping.
			2) Scan mirror reflective coating becomes degraded.	P	Degradation of sensitivity of the scanner assembly.	D	R	D_e	D_p	Gold will be used for the reflective coating since it is not subject to degradation by ultraviolet radiation.

13547F1

NOTES:
FAILURE MODE: O=Open, S=Short, D=Drift, CS=Set F/F, CR=Reset F/F
C1=Constant "1" Level, CO=Constant "0" Level, G=Gate Failure
+=Either Mode, NO=No Output, EO=Erroneous Output
DETECTABILITY: Y=Yes, P=Possibly, N=No
ALTERNATE MODE(S) OF OPERATION: N=None, D=Operate with Degradation
CORRECTIVE ACTION: R=Replace Unit

NOTES:
CRITICALITY/PROBABILITY FAILURE MODE ASSIGNMENTS (X_e & X_p)
A_e = 75% degraded to catastrophic
B_e = 50% to 75% degraded
C_e = 25% to 50% degraded
D_e = negligible to 25% degraded
E_e = no effect
A_p = 20% + of possible failures
B_p = 5-20% " " "
C_p = .5-5% " " "
D_p = .05-.5% " " "
E_p = < .05% " " "

Issue Date January 1973
Rev. ___ Date ___
Preliminary (X)
Final Issue ( )
Prepared by J. Rosenbaum, ATC

FAILURE EFFECT ANALYSIS
GULTON INDUSTRIES INC.
DATA SYSTEMS DIVISION

Contract GI No. ___
TOVS Basic Sounder Unit
Circuit ( )
Subsystem (X)
System ( )
Drawing No. ___
Code No. ___

ITEM	REF DESIG.	FUNCTION	FAILURE MODE	DETECT-ABILITY	FAILURE EFFECT	ALTERNATE MODE OF OPERATION	CORRECTIVE ACTION	X_e	X_p	REMARKS
Fore and Aft Optics Assembly	N/A	The function of the optics assembly is to channel (by frequency) the radiant flux from the field-of-view so that the level of radiation can be measured by electronics. The assembly is made up of the Telescopes, Dichroic Mirrors, Bandpass/Blocking Filters, Detector Lenses, Aft Optics Heater and Aft Optics Housing Temperature Sensors.	N/A	N/A	N/A	N/A	N/A	N/A	N/A	For the components below, X_e is at the BSU Level, and X_p is at the Fore and Aft Optics Assembly level.
Telescopes (7)		The seven telescopes channel the radiant flux to the detectors.	1) Primary or secondary mirror breaks (during launch) on one telescope.	Y	BSU is degraded in function by loss of two of its channels.	D	R	D_e	C_p	Primary and secondary mirror designs will be qualified for simulated launch conditions.
			2) One telescope becomes misaligned during launch.	P	Loss of accuracy of radiant flux level measurements on two channels of the BSU.	D	Replace or Repair.	D_e	C_p	Mechanical design of telescopes will be qualified for simulated launch conditions.

13547F1

NOTES:
FAILURE MODE: O=Open, S=Short, D=Drift, CS=Set F/F, CR=Reset F/F
CI=Constant "1" Level, CO=Constant "0" Level, G=Gate Failure
+ = Either Mode, NO=No Output, EO=Erroneous Output
DETECTABILITY: Y=Yes, P=Possibly, N=No
ALTERNATE MODE(S) OF OPERATION: N=None, D=Operate with Degradation
CORRECTIVE ACTION: R=Replace Unit

NOTES:
CRITICALITY/PROBABILITY FAILURE MODE ASSIGNMENTS (X_e & X_p)
A_e = 75% degraded to catastrophic
B_e = 50% to 75% degraded
C_e = 25% to 50% degraded
D_e = negligible to 25% degraded
E_e = no effect
A_p = 20% + of possible failures
B_p = 5-20% " " "
C_p = .5-5% " " "
D_p = .05-.5% " " "
E_p = < .05% " " "

Issue Date January 1973
Rev. ___ Date ___
Preliminary (X)
Final Issue ( )
Prepared by J. Rosenbaum, ATO

FAILURE EFFECT ANALYSIS
GULTON INDUSTRIES INC.
DATA SYSTEMS DIVISION

Contract GI No. ___
TOVS Basic Sounder Unit
Circuit ( )
Subsystem (X)
System ( )
Drawing No. ___
Code No. ___

ITEM	REF DESIG.	FUNCTION	FAILURE MODE	DETECT-ABILITY	FAILURE EFFECT	ALTERNATE MODE OF OPERATION	CORRECTIVE ACTION	X_e	X_p	REMARKS
Telescopes (Continued)			3) Primary or secondary mirror surface becomes degraded on one telescope.	P	Degradation of sensitivity of two channels of the BSU.	D	R	D_c	C_p	Gold will be used for the reflective coating since it is not subject to degradation by ultraviolet radiation.
Dichroic Mirrors (7)	N/A	The seven dichroic mirrors split the radiant flux into two beams and direct the separate beams into the two detectors associated with each telescope.	Degradation of surface coating of one dichroic mirror.	P	Degradation of sensitivity of two channels of the BSU.	D	R	D_c	D_p	Surface coating will be subjected to acceptance tests covering the environmental conditions that may be encountered in operation, to reduce the probability of degradation.
Bandpass/ Blocking Filters (28)	N/A	The fourteen bandpass filters each allow a specified band of frequencies to pass through while attenuating all other frequencies.	Degradation of one bandpass filter surface.	P	Degradation of sensitivity of one channel of the BSU.	D	R	D_c	D_p	(Same as above)
		The fourteen blocking filters block out frequencies from the UV to approximately 50 micrometers.	Degradation of one blocking filter surface.	P	Degradation of sensitivity of one channel of the BSU.	D	R	D_c	D_p	(Same as above)
Detector Lenses (14 sets)	N/A	The fourteen sets of detector lenses focus the radiant flux onto the detector elements.	Degradation of surface coating of one set of lenses.	P	Degradation of sensitivity of one channel of the BSU	D	R	D_c	D_p	(Same as above)

13547F1

NOTES:
FAILURE MODE: O=Open, S=Short, D=Drift, CS=Set F/F, CR=Reset F/F
C1=Constant "1" Level, CO=Constant "0" Level, G=Gate Failure
+=Either Mode, NO=No Output, EO=Erroneous Output
DETECTABILITY: Y=Yes, P=Possibly, N=No
ALTERNATE MODE(S) OF OPERATION: N=None, D=Operate with Degradation
CORRECTIVE ACTION: R=Replace Unit

NOTES:
CRITICALITY/PROBABILITY FAILURE MODE ASSIGNMENTS (X_e & X_p)
A_e = 75% degraded to catastrophic
B_e = 50% to 75% degraded
C_e = 25% to 50% degraded
D_e = negligible to 25% degraded
E_e = no effect
A_p = 20% + of possible failures
B_p = 5-20% " " "
C_p = .5-5% " " "
D_p = .05-.5% " " "
E_p = < .05% " " "

Issue Date January 1973
Rev. ___ Date ___
Preliminary (X)
Final Issue ( )
Prepared by J. Rosenbaum, ATO

FAILURE EFFECT ANALYSIS
GULTON INDUSTRIES INC.
DATA SYSTEMS DIVISION

Contract GI No. ___
TOVS Basic Sounder Unit
Circuit ( )
Subsystem (X)
System ( )
Drawing No. ___
Code No. ___

ITEM	REF DESIG.	FUNCTION	FAILURE MODE	DETECT-ABILITY	FAILURE EFFECT	ALTERNATE MODE OF OPERATION	CORRECTIVE ACTION	X_e	X_p	REMARKS
Aft-Optics Heater	N/A	To provide heat to the Aft-Optics components (detector lenses, filters, dichroic mirrors and chopping reference black-body surfaces) so that they will meet the performance specifications.	1) Heating element fails due to open.	Y	Degradation of operation of the Aft-Optics components due to loss of heat.	D	R	C_c	C_p	Primary Unit will operate at approximately 70% of optimum performance if heater fails.
			2) Heating element changes resistance value.	N	Negligible.	N/A	N/A	E_c	C_p	Temperature controlling circuit will compensate for resistance value changes.
Aft-Optics Housing Temperature Sensors (at least four)	N/A	The temperature sensors monitor the temperature of the aft-optics housing (which contains the chopping reference black-body surfaces).	One temperature sensor fails to open due to broken lead wires.	Y	Loss of degree of confidence in performance of instrument.	D	R	D_c	D_p	Due to the redundancy afforded by the use of at least four temperature sensors in the housing, the temperature of the housing at the failed temperature sensor's position could be inferred.

13547F1

NOTES:
FAILURE MODE: O=Open, S=Short, D=Drift, CS=Set F/F, CR=Reset F/F
CI=Constant "1" Level, CO=Constant "0" Level, G=Gate Failure
+ = Either Mode, NO=No Output, EO=Erroneous Output
DETECTABILITY: Y=Yes, P=Possibly, N=No
ALTERNATE MODE(S) OF OPERATION: N=None, D=Operate with Degradation
CORRECTIVE ACTION: R=Replace Unit

NOTES:
CRITICALITY/PROBABILITY FAILURE MODE ASSIGNMENTS (X_e & X_p)
A_e = 75% degraded to catastrophic
B_e = 50% to 75% degraded
C_e = 25% to 50% degraded
D_e = negligible to 25% degraded
E_e = no effect
A_p = 20% + of possible failures
B_p = 5-20% " " "
C_p = .5-5% " " "
D_p = .05-.5% " " "
E_p = < .05% " " "

Issue Date January 1973
Rev. ___ Date ___
Preliminary (X)
Final Issue ( )
Prepared by J. Rosenbaum, ATO

FAILURE EFFECT ANALYSIS
GULTON INDUSTRIES INC.
DATA SYSTEMS DIVISION

Contract GI No. ___
TOVS Basic Sounder Unit
Circuit ( )
Subsystem (X)
System ( )
Drawing No. ___
Code No. ___

ITEM	REF DESIG.	FUNCTION	FAILURE MODE	DETECT-ABILITY	FAILURE EFFECT	ALTERNATE MODE OF OPERATION	CORRECTIVE ACTION	X_e	X_p	REMARKS
Chopper Assembly	N/A	1) The function of the chopper motor assembly is to chop the radiant flux from the field-of-view. The chopped radiant flux is then processed by electronics to define signal level. 2) The chopper also images a blackbody reference during the off cycle of the cyclic chopping waveform. The assembly is made up of the chopper drive motor, angular momentum compensator, chopper wheel and phase reference pickup (PRP).	N/A	N/A	N/A	N/A	N/A	N/A	N/A	For the components below, X_e is at the BSU Level, and X_p is at the Chopper Assembly level.
Chopper Drive Motor	N/A	Drives the chopper wheel.	1) No output due to electrical failure.	Y	(1) Chopper wheel fails to chop radiant flux to be provided to the detectors. (2) Chopper wheel fails to image blackbody reference.	N	R	A_e	B_p	The chopper drive motor will be run-in for a minimum of 168 hours at 70° ±2°C prior to acceptance tests; and the motor will be subjected to rigorous screening and qualification tests.
			2) No output due to bearing failure.	Y	(1) Chopper wheel fails to chop radiant flux to be provided to the detectors. (2) Chopper wheel fails to image blackbody reference	N	R	A_e	B_p	

13547F1

NOTES:
FAILURE MODE: O=Open, S=Short, D=Drift, CS=Set F/F, CR=Reset F/F
CI=Constant "1" Level, CO=Constant "0" Level, G=Gate Failure
+=Either Mode, NO=No Output, EO=Erroneous Output
DETECTABILITY: Y=Yes, P=Possibly, N=No
ALTERNATE MODE(S) OF OPERATION: N=None, D=Operate with Degradation
CORRECTIVE ACTION: R=Replace Unit

NOTES:
CRITICALITY/PROBABILITY FAILURE MODE ASSIGNMENTS (X_e & X_p)
A_e = 75% degraded to catastrophic
B_e = 50% to 75% degraded
C_e = 25% to 50% degraded
D_e = negligible to 25% degraded
E_e = no effect
A_p = 20% + of possible failures
B_p = 5-20% " " "
C_p = .5-5% " " "
D_p = .05-.5% " " "
E_p = < .05% " " "

Issue Date January 1973
Rev. ___ Date ___
Preliminary (X)
Final Issue ( )
Prepared by J. Rosenbaum, ATO

FAILURE EFFECT ANALYSIS
GULTON INDUSTRIES INC.
DATA SYSTEMS DIVISION

Contract GI No. ___
TOVS Basic Sounder Unit
Circuit ( )
Subsystem (X)
System ( )
Drawing No. ___
Code No. ___

ITEM	REF DESIG.	FUNCTION	FAILURE MODE	DETECT-ABILITY	FAILURE EFFECT	ALTERNATE MODE OF OPERATION	CORRECTIVE ACTION	X_e	X_p	REMARKS
Angular Momentum Compensator	N/A	Rotates in the opposite direction of the chopper assembly and thus compensates for the angular momentum generated by the rotation of the chopper assembly.	1) No output due to electrical failure.	P	Instrument would go out of specification with regard to Angular Momentum.	D	R	D_e	B_p	The angular momentum compensator device will be run-in for a minimum of 168 hours at 70° ±2°C prior to acceptance tests; and the device will be subjected to rigorous screening and qualification tests.
			2) No output due to bearing failure.	P	Instrument would go out of specification with regard to Angular Momentum.	D	R	D_e	B_p	
Chopper Wheel	N/A	1) Chops the radiant flux input to the detectors.	1) Chopper wheel becomes warped or distorted.	P	Loss of accuracy of radiant flux level measurements.	D	R	D_e	C_p	Chopper wheel will be stress relieved by heat treatment after machining, to prevent subsequent warping.
		2) Also images a black-body reference during the off cycle of the cyclic chopping waveform.	2) Surface degradation of reflecting surface used to image the black-body reference.	P	Loss of accuracy of radiant flux level measurements.	D	R	D_e	C_p	Gold will be used for the reflective coating since it is not subject to degradation by ultraviolet radiation.
Phase Reference Pickup (PRP)	N/A	Synchronizes chopping and scanning cycles.	No output due to electrical failure.	Y	Loss of data correlation between channels.	N	R	A_e	E_p	The PRP electronic components will be screened and selected for high reliability; therefore, the probability of failure will be very low.

NOTES:
FAILURE MODE: O=Open, S=Short, D=Drift, CS=Set F/F, CR=Reset F/F
Cl=Constant "1" Level, CO=Constant "0" Level, G=Gate Failure
+ = Either Mode, NO=No Output, EO=Erroneous Output
DETECTABILITY: Y=Yes, P=Possibly, N=No
ALTERNATE MODE(S) OF OPERATION: N=None, D=Operate with Degradation
CORRECTIVE ACTION: R=Replace Unit

NOTES:
CRITICALITY/PROBABILITY FAILURE MODE ASSIGNMENTS (X_e & X_p)
A_e = 75% degraded to catastrophic
B_e = 50% to 75% degraded
C_e = 25% to 50% degraded
D_e = negligible to 25% degraded
E_e = no effect
A_p = 20% + of possible failures
B_p = 5-20% " " "
C_p = .5-5% " " "
D_p = .05-.5% " " "
E_p = < .05% " " "

Issue Date [illegible]
Rev. ___ Date ___
Preliminary (X)
Final Issue ( )
Prepared by J. Rosenbaum, ATO

FAILURE EFFECT ANALYSIS
GULTON INDUSTRIES INC.
DATA SYSTEMS DIVISION

Contract GI No. ___
TOVS Basic Sounder Unit
Circuit ( )
Subsystem (X)
System ( )
Drawing No. ___
Code No. ___

ITEM	REF DESIG.	FUNCTION	FAILURE MODE	DETECT-ABILITY	FAILURE EFFECT	ALTERNATE MODE OF OPERATION	CORRECTIVE ACTION	X_e	X_p	REMARKS
Calibration Blackbody Assembly	N/A	The function of the Calibration Blackbody Assembly is to provide the primary upscale calibration reference point. The assembly is made up of seven calibration blackbodies and will contain at least four platinum resistance temperature sensors.	N/A	N/A	N/A	N/A	N/A	N/A	N/A	For the components below, X_e is at the BSU Level, and X_p is at the Calibration Blackbody Assembly level.
Calibration Blackbodies (7)	N/A	The calibration blackbodies act as light traps which simulate the action of perfect absorbers when viewed from their open ends.	Degradation of black surface on one calibration blackbody.	P	Calibration error depending upon the degree of surface degradation.	D	Repaint surface of blackbody.	D_e	E_p	The surface coating will be "3M" Black Velvet paint, which has been used for space applications before, and has proven to be exceptionally reliable. In addition, all precautions and tests recommended by the manufacturer will be taken to prevent surface degradation from taking place.
Blackbody Calibration Temperature Sensors (at least four)	N/A	Sense the temperature of the calibration blackbody assembly for calibration purposes.	One temperature sensor fails due to broken lead wires.	Y	Loss of degree of confidence in performance of instrument.	D	R	D_e	D_p	The type of mounting used for the temperature sensors will be designed to eliminate the probability of stress on the lead wires. Potting of the lead wires will be considered for the final design.

13547F1

LIST OF APPENDIXES

Appendix 1 - Radiation Effects on the TIROS Spacecraft Electronics

Appendix 2 - Outline of Interface Integration Data Between the Basic Sounding Unit of the TOVS Instrument and the TIROS-N Spacecraft

Appendix 3 - Harmonic Analysis of TIROS Sounder System, a Self Documenting Math Model Program

Appendix 4 - Design Study of Dichroics

Appendix 5 - TOVS Immersed Detector Study

APPENDIX 1

Radiation Effects on the TIROS Spacecraft Electronics

Introduction

Many of the reports on this subject lately all purportedly based on the same or similar data, seem to have almost no correlation. Some get lost in confusing irrelevant conversions, and many seem to miss some physical effects that would alter their conclusions drastically. We will try to cover the subject clearly and concisely, hoping to explain our rationale as we go, but without getting mired in detail. Where it seems appropriate, some basics of the subject will be mentioned, as they may be points missed by other reports.

Radiation Sources and Effects

Van Allen radiation is a cloud of electrons and protons trapped by the earth's magnetosphere. The particles continually drift between the southern and northern extremities of the magnetic field lines, with a slight longitudinal drift, forming a toroidal configuration not unlike a "class ring", so if there is a preferred direction of spacecraft incident radiation, it is front-to-back or sideways, rather than up or down.

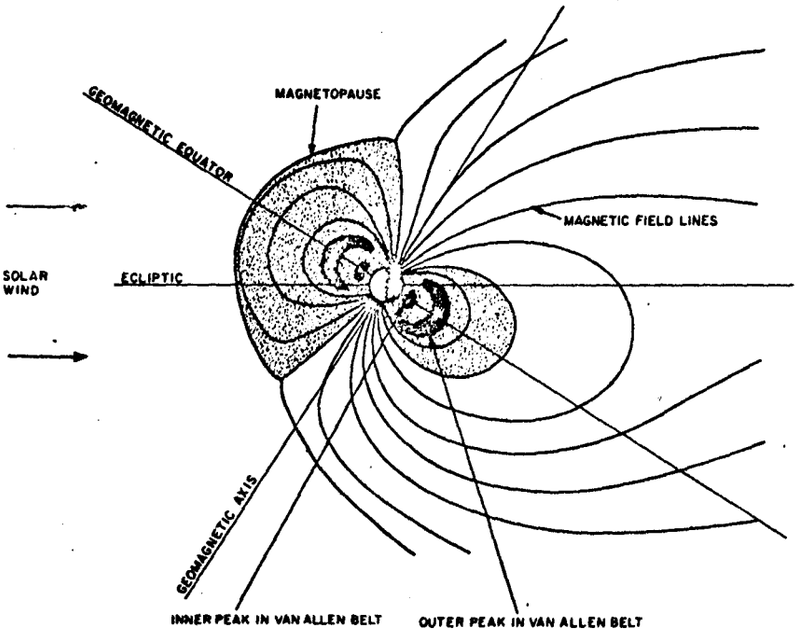

Contour plot of magnetosphere showing Van Allen belts (after L. J. Cahill, Jr., Scientific American, March 1965, p. 59).

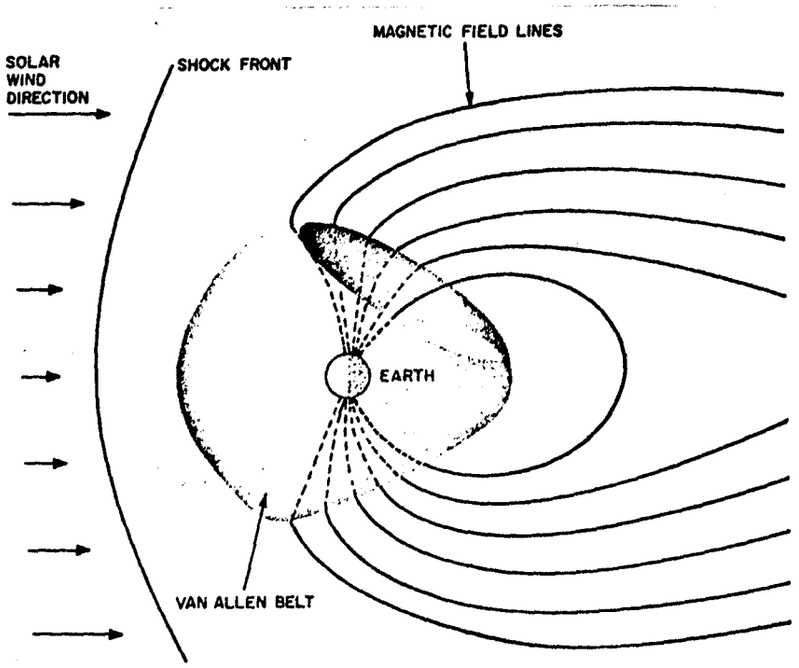

Three-dimensional view of magnetosphere (after L. J. Cahill, Jr., Scientific American, March 1965, p. 66).

The protons are of high average energy and difficult to shield against, but likewise difficult to "see" because they pass through electronics as easily as spacecraft structure. In the highest gain, poorest shielded channels of the ITPR, single event noise spikes occur a maximum of a few times per second as the spacecraft passes through the South Atlantic anomolie. The flux levels here approximate those expected in the TIROS orbit in the inner Van Allen belt. These few events per second translate to maybe a hundred particles/cm^2-sec of a "just-right" energy, i.e. protons fast enough to penetrate the shielding of the spacecraft and slow enough to deposit energy in a detector or semi conductor (>45MeV). The proton count is insufficient to cause any permanent degradation, the resultant noise is easily subtracted by iterative data routines, and it appears that little can be done about them anyway. Cosmic particle flux (90% protons and 10% alphas) is about 2 particles/cm^2 - sec, resulting in about one millirad/hr. The "Cosmic Ray" count is then a percent or two of the expected Van Allen proton count, is undistinguishable except possibly in time of occurence, and can likewise be ignored for this discussion.

The average energy of Van Allen belt electrons allow shielding (< 5 MeV) because such a medium energy electron expends its energy by ionizing the spacecraft skin materials. This results in a secondary ionization. Bremsstrahlung is X-ray production caused by the braking or stopping of these electrons, and is the principle radiation of interest, as non-bremsstrahlung producing electrons (>5 MeV) would resolve themselves as did the protons.

Using Stassinopoulos data of TIROS-N radiation predictions, and Peter Cook's energy bin conversions, it is noted that the 1971 predictions and 1972 predictions differ in spectrum, but the sums of the bremsstrahlung

conversions are almost identical, so that most experiments and predictions based on the earlier data are no less valid. The principle difference is the energy shift downward, the 1971 data had only about 1% of the 4.5×10^9 MeV/cm^2 day remsstrahling production in the <0.5 MeV electron bin, the new data has about 80% <0.5 MeV. The significance is that the electron to bremsstrahlung conversion is complete, through almost any portion of the instrument package.

Using the worst-case electron fields estimated by E.G. Stassinopoulos and the bremsstrahlung environment calculated by Peter Cook, the conversion compares very favorably to other work in this area by Fultz and Hansen, the flux in the detector package is:

a) average flux - 5.21×10^4 photon MeV/cm^2 sec.
b) peak flux - 7.2×10^5 photon MeV/cm^2 sec.

The predominant beta flux intensity is in the 0.5-4.5 MeV range. The average bremsstrahlung energy associated with these electron energies is approximately 1 MeV. Therefore the relation to Rads is:

a) average dose - 9.4×10^{-2} Rads/hr.
b) peak dose - 1.3 Rads/hr.

At this point a discussion of the expected effects from these fields is in order.

When nuclear radiation interacts with semiconductors, changes are produced in the properties of these materials. The changes are of two types, permanent effects and ionization effects. Effects of the permanent type involve displacement of lattice atoms from their lattice site, and include lattice parameter, stored energy, mobility, electrical conductivity, carrier lifetime, electron paramagnetic resonance, optical absorption,

thermal conductivity, etc. Ionization effects are the manifestations of free electrons produced by the radiation interacting with atomic electrons, and are usually transient phenomena. Those effects called permanent may also appear transient, as in many cases the displacements are unstable and the material may anneal. Self annealing is a function of temperature, so operating devices will tend to heal more quickly than idle devices.

It has been shown that lifetime degradation in silicon, assuming no annealing begins at about 10^{12} defects/cm^3, which requires about 10^{11} protons/cm^2, 10^{13} electrons/cm^2, or 10^{15} γMeV/cm^2. Assuming the worst case ITPR data, it would take about three years to acquire 10^{10} protons in a 2mm square detector, one order of magnitude less than that required for permanent effects to begin. The electrons are completely stopped, statistically, and any remaining would constitute less threat than the protons. In three years about 10^{14} γMeV/cm^2 have accumulated, using peak dose rates and Stassinopoulos' new uncertainty factor of two. This integrated energy flux is again an order of magnitude lower than that required for permanent effects to show up, if there were no annealing.

The effects to be noted then, are the transient phenomena produced by the protons above 45 MeV, about which we can do little except subtract these transients from data, and the X-ray induced noise.

Predicted Effects

Assuming the density of triglycene sulfate to be about that of silicon, and using the bremsstrahlung flux as before, and using a sensitivity of $S_{si} = 5 \times 10^{-15}$ amperes per cm^3 MeV for TGS, the predicted detector noise for the average flux is 2.25 millivolts, after 40 Hz chopping and an amplifier gain of 9,475. The detector noise for the peak flux is expected to be 31 millivolts at the amplifier output using the same sensitivity for the FETs. The amplifier contribution is predicted as 0.65 mv for the average flux and 4.48 mv for the peak flux.

Because of the many uncertainties in these predictions, an experiment was designed to try to simulate the bremsstrahlung environment for irradiation of sample systems to verify these expectations.

Bremsstrahlung Radiation Experiment

The source chosen to most closely duplicate the TIROS bremsstrahlung is a CO_{60} source. The CO_{60} spectrum is two lines, at 1.173 MeV and 1.333 MeV. This spectrum very closely approximates the average 1 MeV spectrum of the expected bremsstrahlung. The continuous emission of a CO_{60} source is obviously closer to reality than a pulsed source, and the data may be leisurely taken, interpreted and retaken if necessary, because the dose rate is relatively constant. An additional advantage is the availability of a CO_{60} source. We located a source belonging to the DOD adjacent to Kirtland Air Force Base, that was made available to the Department of Commerce for these tests at no cost. This source is 2500 curies, and is housed in a large bunker that is continuously monitored. Weekly computer updates indicate the dose rate at any point in the room. The minimum dose rate at the point in the room farthest from the source, at full extraction from its pig is 28 R/hr. Dosimeters placed in the quarter inch thich walled aluminum box that was built to house the experiment, indicated 10 R/hr at full extraction. We obtained repeatable readings of 1 R/hr and 0.1 R/hr at partial extractions of the source from the pig.

The experiment design is shown in the attached drawing. The differential scope input was to cancel out noise picked up in the cable, but was found to be unnecessary.

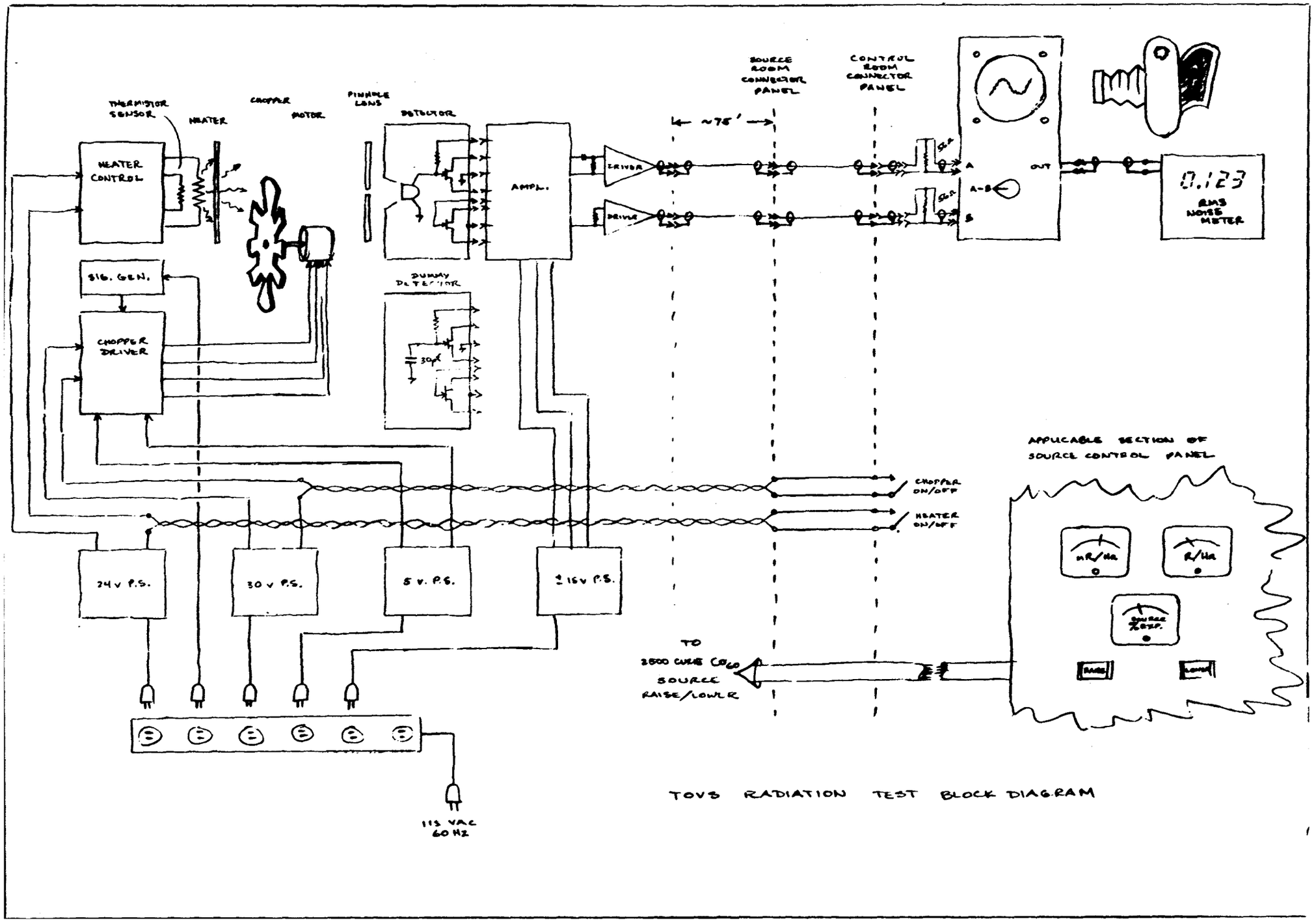

TOVS RADIATION TEST BLOCK DIAGRAM

Conclusions

The explanations should be preceded by a statement that the RMS readings were difficult to measure to better than $\pm$ 10%.

Some general trends are readily apparent from the data:

1. The experimental data roughly agrees with the predicted data, almost within the experimental error.

2. The noise at 0.1 R/hr tends to be slightly higher than predicted.

3. The noise at 1 R/hr tends to be slightly lower than predicted.

4. Noise measurements at 10 R/hr clearly show a non-linear noise to radiation relationship, in our favor.

5. The zero radiation noise tends to be lower following a test.

The explanation for 2 and 5 is probably the activation of surface states on the various components. Since no high-temperature spec. was required of any of these tested devices, other than some of the MIL spec. FETS employed in the amplifier, the surface conditions were probably not closely controlled, and as has been shown, a high temperature spec. device has in general, a lower surface state noise under radiation. The radiation tends to neutralize the surface charges, and might possibly result in a lower ambient noise.

The explanation for 3 and 4 is probably the fact that the devices exhibit a non-linear relationship of increased conductivity to output that was not taken into account in the predictions due to our looking for worse case conditions.

Experiment Results (cont'd)

Detector	Amplifier Output: Experimental RMS Noise (mv) 0 -∞Hz	20-60Hz	30-50Hz	Predicted RMS Noise (mv) 0-∞Hz	Comments on 50° source signal (100x noise)
Barnes #2					
(before) 0 R/Hr	38.7	--	--	x	
--	--	--	--	--	
1 R/Hr	45.16	--	--	$\sqrt{x^2 + 31.0^2 + 9.0^2} = 50.4$	N/C
--	--	--	--	--	

Experiment Results

Detector		Amplifier Output: Experimental RMS Noise (mv) 0-∞Hz	20-60Hz	30-50Hz	Predicted RMS Noise (mv) 0-∞Hz	Comments on 50°C source signal (100xnc[redacted]
Dummy						
(before)	0 R/Hr	12.0	6.5	6.72	$\sqrt{\chi^2 + 0.65^2} = 12.02$	N/A
	0.1 R/Hr	11.3	8.0	7.16	$\sqrt{\chi^2 + 9.0^2} = 15.0$	N/A
	1 R/Hr	17.0	8.87	9.0	--	
(after)	0 R/Hr	11.0	6.1	6.0		
Barnes #1 X-ray poled						
(before)	0 R/Hr	22.6	--	--		
	0.1 R/Hr	24.2	12.9	11.0	$\sqrt{\chi^2 + 2.25^2 + 0.65} = 22.72$	N/C
	0.5 R/Hr	24.2	14.5	12.32	--	N/C
	1 R/Hr	25.8	16.13	13.47	$\sqrt{\chi^2 + 31.0^2 + 9.0^2} = 39.4$	Pertur[redacted] slight[redacted]
(after)	0 R/Hr	21.0	12.0	10.0	--	
Mullard #1						
(before)	0 R/Hr	15.16	8.7	6.72		
	0.1 R/Hr	18.1	10.3	7.84	$\sqrt{\chi^2 + 0.33^2 + 0.65^2} = 15.18$	N/C
	0.5 R/Hr	18.55	10.3	8.5	--	N/C
	1 R/Hr	18.1	9.68	8.5	$\sqrt{\chi^2 + 4.57^2 + 9.0^2} = 18.21$	N/C
	10 R/Hr	17.74	10.3	8.96	--	N/C
(after)	0 R/Hr	16.13	8.7	7.4	--	
Barnes #4						
(before)	0 R/Hr	25.8	--	--		
	0.1 R/Hr	32.26	--	--	$\sqrt{\chi^2 + 2.25^2 + 0.65^2} = 25.9$	N/C
	1 R/Hr	45.16	--	--	$\sqrt{\chi^2 + 31.0^2 + 9.0^2} = 41.32$	N/C
	10 R/Hr	115.4	--	--	--	Pertur[redacted] slightly ~5%
(after)	0 R/Hr	22.6	--	--	--	

The explanation for 1 on the previous page is probably our good data from Peter Cook, W. F. Lindsay and other excellent sources.

Our conclusion is that there is about a 20% noise increase due to inner Van Allen belt bremsstrahlung. Possibly by selecting detectors, a somewhat lower percentage may be achieved. Also, shielding will not help sufficiently to be worth the space and weight. We are stopping all $<$5 MeV electrons with the present estimate of 0.24 inches of aluminum, plus the detector housing, and more shield will not appreciably attenuate the bremsstrahlung nor the $>$45 MeV protons, within any reasonable limits on thickness and weight. The present configuration using a higher Z materiel in the detector/preamp package, brass, about 0.125 thick, within the average 0.24 inch aluminum structure, is close to an ideal compromise.

REFERENCES

Stassinopoulos, E.G.	"Van Allen Belt Radiation in TIROS/TOS/ ITOS Spacecrafts"; Goddard Space Flight Center, X-641-71-413 (Sept. 1971)
Stassinopoulos, E.G.	"Predicted Trapped Particle Radiation Levels for TIROS-N"; Goddard Space Flight Center, X-601-72-429 (Nov 1972)
Cook, Peter	TIROS-N, TOVS: "Pyroelectric Detector Radiation Shielding"; Memo to S. Anderson, U. S. Dept Commerce, NOAA (Aug. 1971)
Lindsay, W. F.	"Fast Transient High Intensity Gamma-Ray Solid State Detectors"; Univ. Calif. L.R.L. UCRL 6298 (May 1961)
Kuckuck, R. W. et al	"Response Functions of Sensitivity of Double Diffused Silicon Detectors in High Gamma Dose Rate Fields"; Nuclear Science, V-NS-13 #1, IEEE Transactions pp 111-119 (Feb. 1966)
Dickinson, W. C. (Ed.)	"Detector Handbook"; U. of C. L. R. L. UCRL-50176 (Aug. 1967)
Berry, Peter F.	"Gamma Ray Attenuation Coefficients"; Nucleonics, p. 62 (June 1961)
Oleson, H. L.	"Radiation Effects on Electronic Systems"; Plenum Press, N.Y. (1966)
Fultz S & Hanson N.	"Cross Sections and Spectra for Negative Electron Bremsstrahling"; U. of C. L.R.L., UCRL-6099 (Nov 1960)
Watts, J. W. Jr.	"Electron and Bresstrahling Penetration and Dose Calculation"; NASA, TN-D-6385 (June 1971)
Naber, J. A.	"Radiation Effects in Semiconductors used as Infrared Detector Materials"; Proceeding of the Special Meeting on the Physics of Detectors, U of Mich. Willow Run Lab. (Aug 1972)

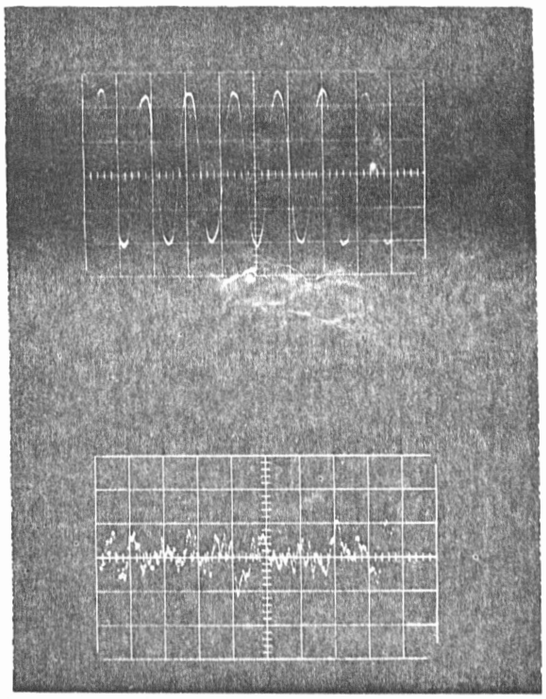

Barnes Detector #1 before radiation. Amplification is 9,475. Top trace is an an alternate 50° C source and 25° C black body, 2 v/cm, 40 hz. The bottom trace is the noise at 0.05 v/cm.

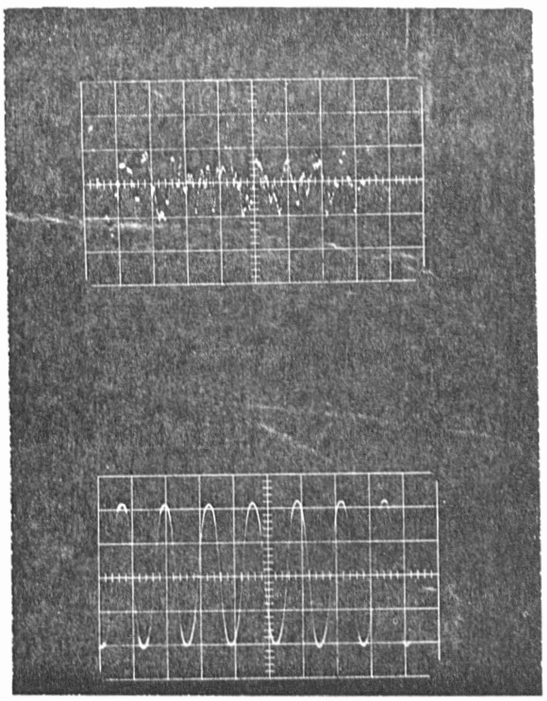

At 0.1 R/hr, otherwise as above.

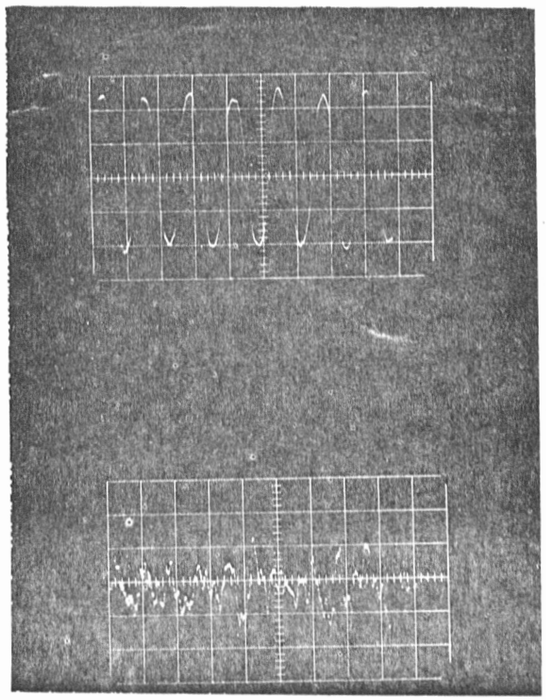

At 1 R/hr, otherwise as above.

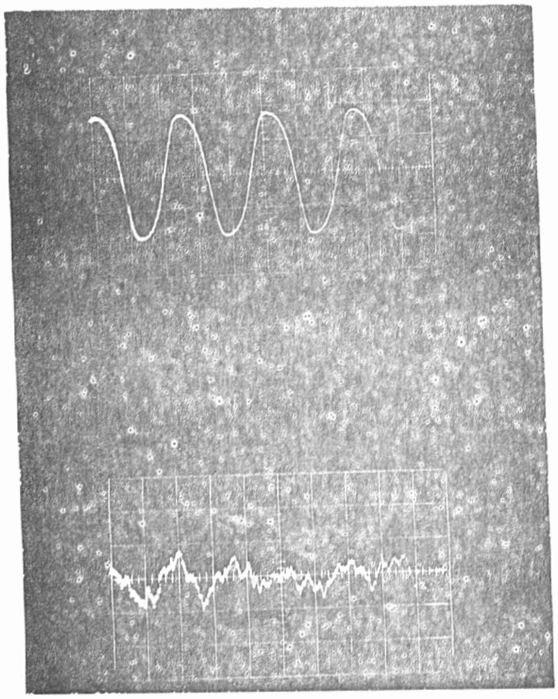

Mullard Detector #1 before radiation.
All parameters as for Barnes Detectors.
Loss of high frequencies on 40 Hz signal is different cable loading.

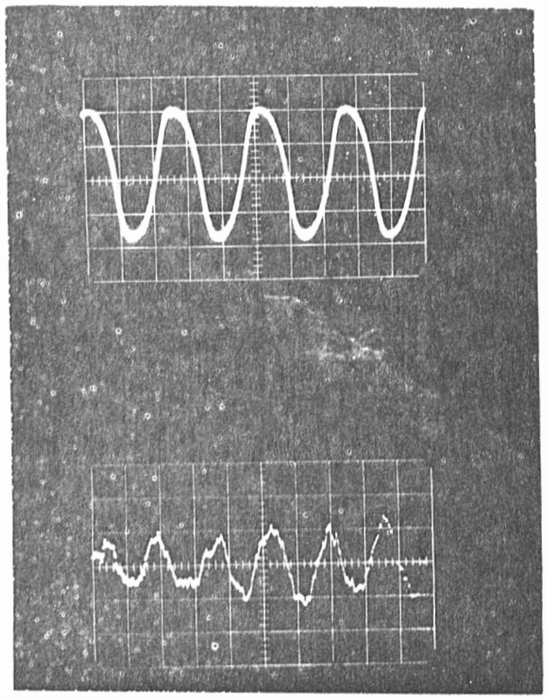

At 0.1 R/hr, otherwise as above.

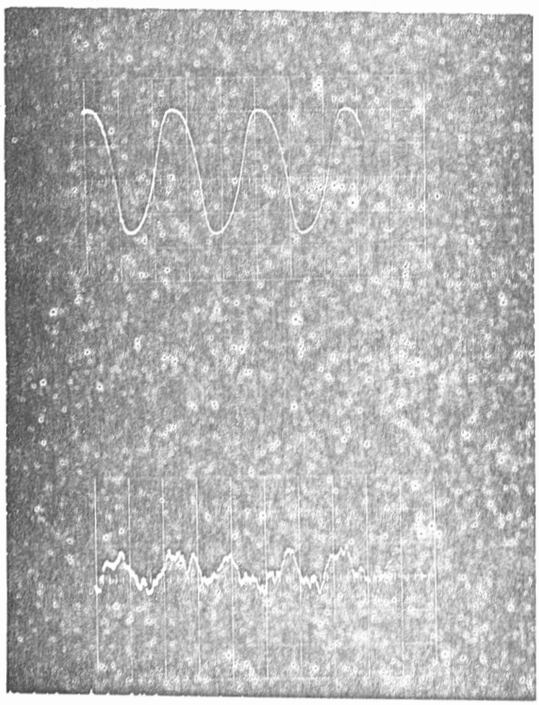

At 1 R/hr, otherwise as above.

APPENDIX 2

OUTLINE OF INTERFACE INTEGRATION DATA BETWEEN THE BASIC SOUNDING UNIT OF THE TOVS INSTRUMENT AND THE TIROS-N SPACECRAFT

1.0 General
- 1.1 System Definition
- 1.2 Brief Description of System Components

2.0 Mass Property Data
- 2.1 Weight Budget Table
- 2.2 Residual Angular Momentum Table
- 2.3 Residual Translational Momentum Table

3.0 Mounting Definition

4.0 Mechanical and Thermal Interface
- 4.1 Thermal
- 4.2 Radiation Susceptability, Reliability and Shielding

5.0 Power Interface & Budget

6.0 Description of Instrument Commands

7.0 SSU System Interface

8.0 Special or Unique Operational Requirements
- 8.1 Additional Ground Support
- 8.2 Special Test Equipment

9.0 TOVS Instrument Measurement List

1.0 General

1.1 System Definition

The TIROS Operational Vertical Sounder is a major experiment for the TIROS-N spacecraft. It is a multi-spectral scanner to provide sufficient information on atmospheric radiances to obtain temperature profiles on a global basis. The TOVS is two separate packages, the Basic Sounding Unit and the Stratospheric Sounding Unit. The BSU is a 14-channel, cross-course, scanning radiometer with an FOV of about 1.125° and IR spectral channels from 3.8 μm to 30 μm. The SSU is being supplied by the UK.

The BSU will have a separate detector for each channel and utilize Cassegrainian fore-optics and refractive after-optics. The instrument will use a programmed object scan mirror, a 40 Hz earth-chopper reference reflective chopper, and doped triglycine sulfate (TGS) pyroelectric detectors having a locked-in polarization.

The preamplifiers will be integral parts of the detector packages.

The instrument will utilize either bi-polar analog-to-digital- conversion with 11 bit resolution, or unipolar 12 bit resolution, and an accuracy of $\pm 0.02\%$. The data will be formatted in 16 bit words containing parity, polarity, and several identifiers for input to the Low Rate Data Processor (LRDP). Scan control will be achieved via a stepping motor encoder, stepping to discrete positions. The calibration sequence mode will be in addition to the normal earth scan mode. The scan will be synchronized to the LRDP.

1.2 System Components

1.2.1 Scanning Mirror and Drive Mechanism

The scanning mirror sweeps in a sawtooth pattern, with the ramp composed of 72 discrete transverse dwell steps providing 81° coverage.

The scanning mirror turns the optical path from swept vertical to the spacecraft direction-of-flight axis and into the collector optics.

1.2.2 Optics

The optical system includes the objective telescopes, field-defining apertures, dichroic mirrors, interference filters, and field lenses. There are eight optical systems, essentially identical except for bandpass and the two telescope diameters. Each system employs a spherical-primary/spherical-secondary, gold-surface, Cassagranian-type objective telescope. In the focal plane of the objective is an aperture plate to define the field-of-view. The spectral bandwidth definition and colinearization of two detectors per telescope is then accomplished with dichroic beam splitters and bandpass filters. The multi-element field lens then focuses the objective lens secondary onto the detector element, collecting all available system energy and providing an effective system f number of .7.

1.2.3 Chopper

The copper raises the lower limit of the noise bandwidth, improving the signal-to-noise ratio of the absolute radiation measurement. The chopper is of the chopper-mirror type, minimizing emissivity effects of the chopper blade and providing a blackbody background reference level. The blackbody

reference is constructed with a geometric wedge in the structural mass, which is focused on the detectors by constructing the chopper blade with a toroidal, spherically concave reflecting surface. The combination provides an effectively large geometric blackbody with a small aperture, giving an extremely stable reference in a minimum space. The chopper is placed so as to chop all channels simultaneously with a 50-50 duty cycle, driven with a multi-pole, brushless, synchronous motor. The chopping frequency is 40 Hz.

1.2.4 Detectors

The 14 detectors are uncooled pyroelectric devices.

1.2.5 Analog Circuitry

The 14 channels of analog circuitry each receive the low-level ac signal from a detector and amplify, demodulate, and integrate the signal to provide a dc output voltage linearly proportional to the detector's incident energy for each target resolution element.

1.2.6 Digital Circuitry

The analog data is serialized by an analog multiplexer into an analog-to-digital converter. The associated registers, addressers, and output buffers provide the processed digital data in a format compatible with the spacecraft's LRDP and ground data-processing systems.

1.2.7 Control Circuitry

The scanning mirror, chopping wheel, multiplexers, gates, calibration signals, etc., are all synchronized and controlled by the control logic in sync with the spacecraft master-clock.

1.2.8 Auxiliary Circuitry

In addition, various temperature measurements and other selected analog signals are amplified and encoded, the spacecraft power is regulated and and converted to the subsystem requirements, and system control commands are accepted and decoded.

2.0 Mass Property Data

2.1 Weight Budget Table: Primary Module Subsystem Weight Budget

Subassembly	Weight (pounds)
Housing	13.5
Scanner Assembly (with driver)	7.31
Housing Blackbodies	1.2
Fore Optics Assembly	6.71
Aft Optics Assembly	4.92
Chopper Assembly	0.84
Covers	
Baffle Tubes	0.3
Lower Covers	0.9
Top Cover	.43
Electronics	6.8
Hardware	0.4
Connectors	.8
Cabling	.8
TOTAL	44.91

2.2 Residual Angular Momentum Table

Source	Axis	In-Oz-Sec
Scan Mirror	Roll	0
Chopper	Roll	10
None	Pitch	0
None	Yaw	0

2.3 Residual Translational Momentum Table

Source	Direction	In-Lb-Sec	Ins. from S/C Ctr. of Rotation
None	---	0	---

3.0 Mounting Definition

The contractor shall be responsible for mounting and aligning the BSU to the spacecraft. Master female drill jigs shall be provided as GFE to enable the contractor to drill the appropriate mounting holes. The contractor shall furnish appropriate bolts, washers, spacers, and thermal grease as may be specified by the instrument contractor. Alignment surfaces will be provided on each BSU to permit alignment of the instruments to the spacecraft. Alignment of these surfaces must be accomplished to within $\pm 0.50^{\circ}$ of the spacecraft axes with a measurement accuracy to within $\pm 0.25^{\circ}$.

Mounting of all instruments to the spacecraft must be accomplished in a manner which shall permit the instruments to have completely clear (free from any obstruction) fields-of-view for any viewing angle normal to the operation of the instruments. This specifically includes the ± 40.5 degree scans of each instrument normal to the sub-satellite crack and a clear view of the nil radiation for a space view calibration ($\sim 4^{\circ}K$). The space view of each instrument is obtained by viewing space at 90° to the sub-satellite track if the instrument is mounted on the side away from the sun. This angle may be decreased to 70°, within instrumental configuration limits, to permit flexibility of spacecraft placement if the instrument is mounted on the side toward the sun, but it must be identical for each instrument and must not view any portion of the earth's atmosphere or

other area containing higher radiometric contributions than what be achieved by directly viewing space.

4.0 Mechanical and Thermal Interface

4.1 Thermal

The spacecraft/BSU mounting surface temperature range shall be limited to a nominal 20°C plus or minus 10°C and isothermal within 0.5°C. Maximum rate of change shall be limited to 0.005°C per second. Minimum contact area between the BSU and spacecraft mounting surface is 8 square inches.

The BSU thermal dissipation to the spacecraft shall be 15 watts maximum during all instrument loading conditions including periods of exposure to solar heating.

Minimum temperature of a non-operating BSU shall be 0°C with a maximum of 15 watts thermal sink loading under all conditions, including time period when the spacecraft is in earth's shadow.

4.2 Radiation Susceptability, Reliability and Shielding

There should be an equivalent mass between any detector/preamp, and the outside of the spacecraft, of 0.25 ins of aluminum and 0.125 ins of copper or brass, the brass being closest to the detector to give a graded mass type of absorption. This shielding should limit the detector/amplifier noise, in a 0.1 R/hr Bremsstrahlung environment, to $\leq$20% increase over background, and there should be no performance degradation at 2.3×10^4 R integrated dose.

The detector and FET geometrics, noise characteristics and cleanliness are all factors in the radiation noise produced. The smaller geometry, and pure material and cleaner produced units produce lower radiation induced noise.

5.0 Power Interface & Budget

The average power required by the TOVS instrument is 29.6 watts, average; supplies from the 28VDC S/C power system.

Power Budget

Power requirements of the various instrument subsystems are identified and presented in Table A. Two values are shown for the scan mechanisms due to the uncertain status of the Angular Momentum Compensation (AMC) motor.

The total average power requirement without AMC is 29.6 watts, and with AMC in 34.3 watts. Load variations will occur, due to the scan motor power gating and scan pattern. Refer to the systems report ANALYSIS of SCAN POWER REQUIREMENTS for detailed information.

In the dual mode, per instrument, the power requirement is 24.83 watts, 29.53 watts with AMC. In the off mode, $0^{o}C$, the power requirement is 9.19 watts.

TABLE A POWER REQUIREMENTS

Subsystem	Item	Watts
System Timing & Control	Logic	0.50
	Buffers (Input)	0.10
	Subtotal	0.60
Command	Latching Relays	0
	Relay Drivers (1)	-
	Subtotal	0
Scan & Chopper Motors	AMC Motor	3.50
	Chopper Motor (AMC motor)	3.50
	Scan Motor	7.25
	Motor Drive Circuits (Scan & Chopper)	0.85
	Logic	0.50
	PRP	0.25
	Subtotal (with AMC)	12.35
	Subtotal (with AMC)	15.85
Electronics	AMP Regulators (±15v)	1.05
	Amplifiers & Detectors (50 w/CH)(1)	0.70
	Sync Demod & Integrators (50 w/CH)(1)	0.70
	Analog Multiplexer	0.40
	A/D Converter	0.95
	A/D Calibrator	0.20
	Control Logic	0.20
	Subtotal	4.20
	(1)Est per RMM (2-16-73) 10 VDC Analog Section	
Temperature Monitors & Control	Housing Temperature Monitors (TMs)	0.10
	Platinum Bridges Monitor	0.20
	Temperature Control Circuit & Load	3.50
	Subtotal	3.80
Telemetry Output Buffers	Mode & Position Flags	0.10
	Command Monitors	0.10
	Misc. Buffers	0.10
	Subtotal	0.30
Power Supply	Preregulator, Filter,	7.15
	DC/DC Converter	(8.35)
	15 Vdc Regulator, Precision	0.70
	Subtotal	7.85
		(9.05)
	TOTAL INPUT POWER	29.6
	TOTAL INPUT POWER (w/AMC)	(34.3)

6.0 Description of Instrument Commands

TOVs operating modes are directly controlled by thirteen (13) space craft supplied commands.

Command Subsystem: A command subsystem is required to execute the commands obtained from the TIROS-N S/C command system. TOVS command subsystem is similar to that used on ITPR in that the same type of hardware implementation is recommended.

Command List: A total of thirteen (13) commands are required to control the TOVS. Each of these commands, together with a description of the action, is shown in Table A.

Command Circuitry Description: Magnetic latching relays are recommended as the storage devices for all radiometer commands. A typical command relay is shown in Figure B.

Although the exact spacecraft interface is not defined in the technical specification; it is assumed that the relays will be driven by one (1) MA type line and one (1) MB type line.

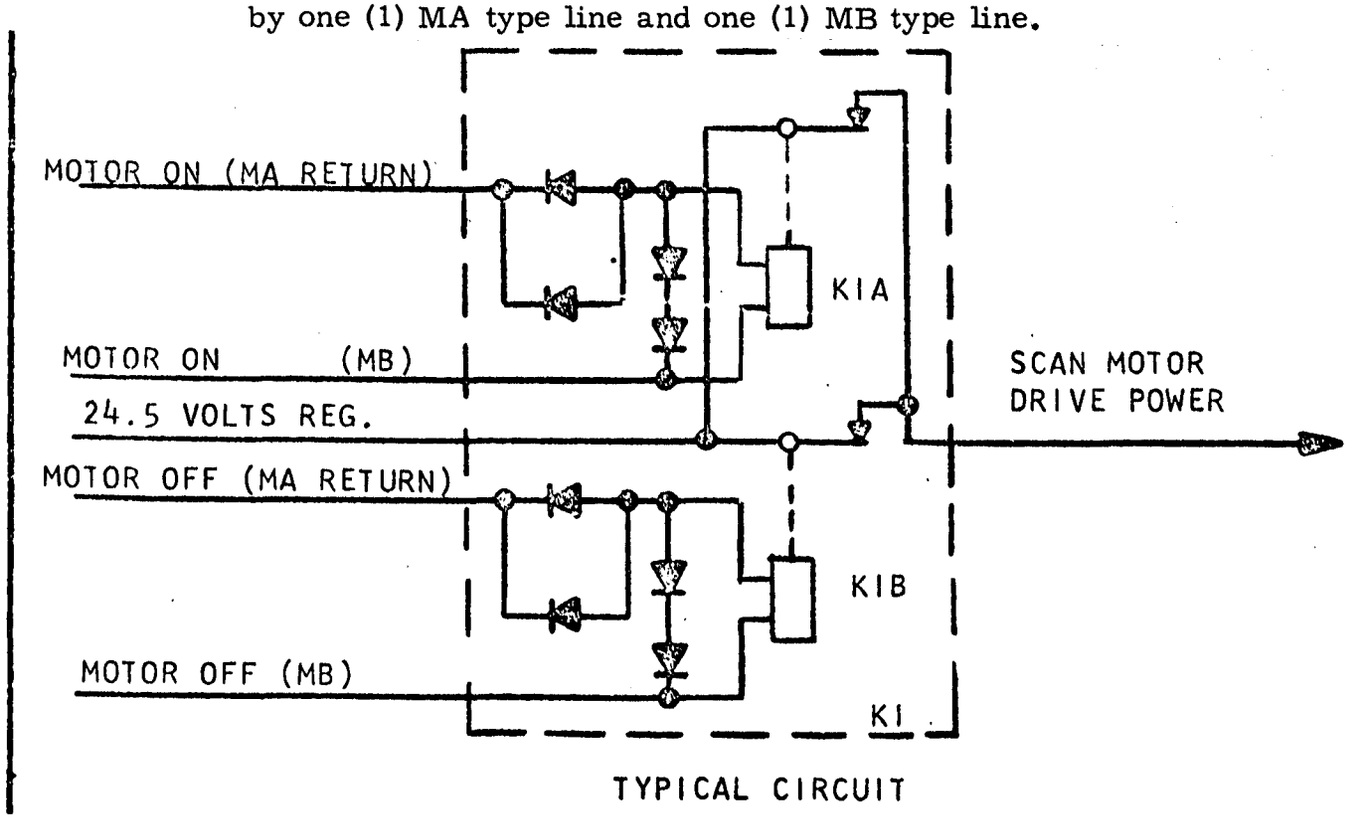

FIGURE B: COMMAND LATCHING RELAY CIRCUIT

TABLE A: TOVS COMMAND LIST

COMMAND	RESPONSE
1. Chopper Motor ON/OFF	Applies/Disconnects power to the chopper motor drive circuit.
2. Electronics ON/OFF	Applied/Disconnects power to all TOVS electronics, causing all channels to become inactive.
3. Scan Drive ON/OFF	Applies/Disconnects power to the scan motor drive circuit.
4. IR Calibrate ON/OFF	Enables/disables the automatic in-flight calibration cycle of space and housing.
5. Electronic Calibration ON/OFF	Enables/disables the electronic calibration of integrator, multiplexer and ADC.
6. NADIR Position ON/OFF	Causes the scan mirror to view the nadir position.
7. Space Position ON/OFF	Causes the scan mirror to view the space position.
8. Housing Position ON/OFF	Causes the scan mirror to view the housing position.
9. Detector Temperature Controller ON/OFF	Applies/disconnects power to the detector temperature controller.
10. Calibration Black Body Heater ON/OFF	Applies/disconnects power to the black body heater.
11. Standby Heater ON/OFF	Applies/disconnects power to the instrument standby heater.
12. Restricted Scan ON/OFF	Causes the scan program to be restricted to 1/2 the normal range.
13. Dual Instrument Mode ON/OFF	Causes TOVS A and B to process data at 1/2 normal rate.

7.0 Stratospheric Sounding Unit (SSU) System Interface

The SSU, to be provided by the British Meteorological Office, will be a four (4) channel filter radiometer utilizing carbon dioxide cells for selective absorption. The technique was originally developed for the Selective Chopper Radiometer (SCR) flown on Nimbus 4. It consists of measuring the radiation transmitted by two cells, each containing different path-lengths of carbon dioxide. Behind the CO_2 cell is a narrow band-pass filter, and a light pipe which converges the radiation onto a pyroelectric detector.

Interface to the SSU will consist of the 160 Hz LRDP interface clock and a .003125 Hz major frame sync pulse. There is no interface between the BSU and the SSU.

8.0 Special or Unique Operational Requirements

8.1 Additional Ground Support

Unique Ground Support Equipment

Bench Check Units

One (1) complete Bench Check Unit (BCU) for the BSU shall be delivered to the spacecraft contractor as GFE with the engineering model of each instrument. The BCU is defined as the equipment necessary to exercise the engineering model, prototype model, or flight models for functional tests. It provides all inputs to the sensor identical to those in the spacecraft system and is equipped to record all output data, sensory and housekeeping, for evaluation purposes. An additional output is provided on each BCU to interface to a digital tape recorder.

Radiation Stimuli (Targets)

(1) Ambient

One (1) pair of ambient radiation stimuli (each pair shall be identical) shall be furnished to the S/C contractor as CFE for the BSU. These stimuli shall be utilized by the spacecraft contractor for all ambient testing of the instruments. A control panel (standard 19 inch relay rack mountable) complete with

cabling will also be provided as GFE with each set of stimuli equipment.

(2) Thermal-Vacuum

One (1) pair of thermal-vacuum radiation stimuli (each pair shall be identical) shall be furnished to the 8/0 contractor as OFE for the BSU. These stimuli shall be utilized by the S/C contractor for all thermal-vacuum testing of the instruments. A control console complete with cabling will also be provided as GFE with each set of stimuli equipment.

8.2 Special Test Equipment

The spacecraft contractor shall be responsible for furnishing the following:

(a) Gaseous nitrogen (dry) to permit purging of the BSU prior to and during any ambient test.

(b) Cooling water, tubing, and necessary connections to heat sink BSU scan motor during ambient testing.

(c) Cooling water, tubing, and necessary connection to heat sink ambient radiation stimuli for the BSU.

(d) All necessary vacuum wall penetrations to operate thermal-vacuum radiation stimuli for the BSU (thermocouple and power).

(e) Liquid nitrogen including supply lines and appropriate connections to operate thermal-vacuum radiation stimuli for the BSU.

(f) Cooled radiator plate to adequately cool BSU scan motor during vacuum testing.

(g) All necessary fixturing to mount thermal-vacuum radiation stimuli for the BSU. To facilitate alignment between the radiation stimuli and their respective units, locating pins and mating holes (or equivalent means) will be provided on the instruments and their stimuli equipment.

9.0 TOVS Instrument Measurement List

A list of all the data developed within the instrument is tabulated, together with a description of the data source and processing requirements.

Parameters: A list of the parameters required to support the TOVS instrument is documented in TABLE A: TOVS Measurements List.

Note that a total of 67 Analog signals and 53 bilevel signals are recommended. A portion of these signals are processed internally via the TOVS ADC; while the balance is available for direct input to the TIP or for use as test points.

Types of Data: Data generated within the TOVS instrument is supplied in the following forms:

- Digital "A" Data: This is the primary source of instrument data and consists of the infrared energy measurements and supporting information.
- Digital "B" Data: This is monitor type data consisting of bilevel logic signals. It is not essential for instrument operation, but does contain value status information.
- Analog Data: A few analog type monitor points are recommended to evaluate the instrument performance.

Data Destination: Data is available for processing or monitoring at three (3) locations; i.e., (1) internally within the TOVS, (2) externally via the S/C information processor, or (3) for externally monitoring as test points. Some redundancy is employed, not for data security reasons, but to accommodate the data processing format.

Primary Instrument Data: The primary output for the TOVS instrument data is via the serial digital output defined as Digital "A" data. All processing necessary to develop this data form is accomplished internally, however, externally generated control signals are required to initiate data readout.

TABLE A: TOVS MEASUREMENT LIST

PARAMETER	QTY	DATA TYPE	DATA SOURCE	CHARACTERISTIC	DATA DESTINATION			REMARKS
					TOVS	TIP	TEST PT	
1. IR DATA CHANNELS	14	A	INFARED RADIATION	DIGITAL ENCODED 12 BITS	14			PRIME DATA
2. SCAN MIRROR POSITION	7	BL	SHAFT ANGLE ENCODER (SAE)	DIGITAL ENCODED 7 BITS	7			POSITION DATA
3. SCAN STEP ADDRESS	7	BL	FOV POSITION COUNTER	DIGITAL SIGNAL 7 BITS	7			
4. SCAN LINE NUMBER	8	BL	LINE NUMBER COUNTER	DIGITAL SIGNAL 8 BITS	8			
5. POSITION FLAG, P1, NADIR	1	BL	DECODED SAE POSITION		1	1	1	POSITION FLAG
6. POSITION FLAG, P2, HOUSING	1	BL			1	1	1	
7. POSITION FLAG, P3, SPACE	1	BL			1	1	1	
8. MODE FLAG, M1, EARTH SCAN	1	BL	CONTROL LOGIC		1	1	1	MODE FLAG
9 MODE FLAG, M2, IR CAL	1	BL			1	1	1	
10. MODE FLAG, M3, ELECTRICAL CAL	1	BL			1	1	1	
11. MODE FLAG M4, DUAL INSTRUMENT	1	BL			1	1	1	
12. PRP OPERATING FLAG	1	BL	PRP CIRCUIT		1	1	1	STATUS
13. VOLTAGE MONITORS	1	A	TOVS POWER SUPPLY	5 VDC, FULL SCALE	1	8		
14. COMMAND MONITORS	13	BL	COMMAND REGISTER	ON/OFF	13	13		
15. TEMPERATURE MONITORS, TM1-TM7	7	A	HOUSING BLACK BODY	PLATINUM WIRE (0.05°C)	7			PRIME DATA
16. TEMPERATURE MONITORS, TM8-TM15.	8	A	REFERENCE BLACK BODY	THERMISTOR (0.1°C)	8			
17. TEMPERATURE MONITORS, TM16-TM23	8	A	DETECTOR MOUNTING PLUG		8			
18. TEMPERATURE MONITORS, TM24	1	A	POWER SUPPLY CIRCUITRY			1		HOUSEKEEPING
19. TEMPERATURE MONITORS, TM25	1	A	PRP CIRCUITRY			1		
20. TEMPERATURE MONITORS, TM26	1	A	SCAN DRIVE CIRCUITRY			1		
21. TEMPERATURE MONITORS, TM27	1	A	ADC CIRCUITRY			1		
22. TEMPERATURE MONITORS TM28	1	A	DETECTOR RING TEMP. CONTROLLER			1		
23. TEMPERATURE MONITORS, TM29-TM45	17	A	TOVS HOUSING & MOTORS			17		
24. KEY CONTROL SIGNALS	10	BL	SYSTEM LOGIC	DIGITAL SIGNALS			10	ESTIMATE
TOTALS:								
ANALOG CHANNELS (A)	67	—	—	—	37	30		
BILEVEL CHANNELS (BL)	53	—	—	—	43	21	18	

APPENDIX 3

Harmonic Analysis of TIROS Sounder System, a Self Documenting Math Model Program.

The model input is set-up as two single valved scenes of differing radiance, a continuing dull input being the special case of zero difference. The transition between the two scenes approximates the scan mirror step-and-settle by a sinusoid from the one scene value to the second, in 37 milliseconds. For purposes of scene 1 initial wave shape, scene 2 final wave shape, and scene integration, odd scenes are assumed equal and even scenes are assumed equal. In other words, the two single valued scenes are assumed endlessly repetitious. The Forier Series representation is: $A_i \sin nwt, w = 2\pi . 5$ Hz.

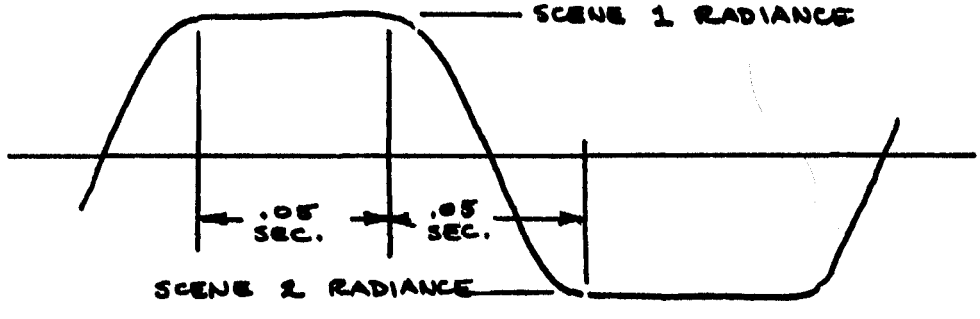

The chopper is similarly an alternating almost-square wave, the transition being the time that the chopper blade traverses the beam envelope. Since the blade is square cut and the beam is circular, this transition is also a sinusoid. The chopping operation is of the half wave type and can be written as: $\frac{Ao}{2} + \sum B_i \sin nwt, \; w = 2\pi f_{chopper}$

The chopper output alternates between the input scene value and the "black body" reference value. The output of a 40 HZ chopper, with the "black body"

reference value half-way between scenes 1 and 2 values would be:

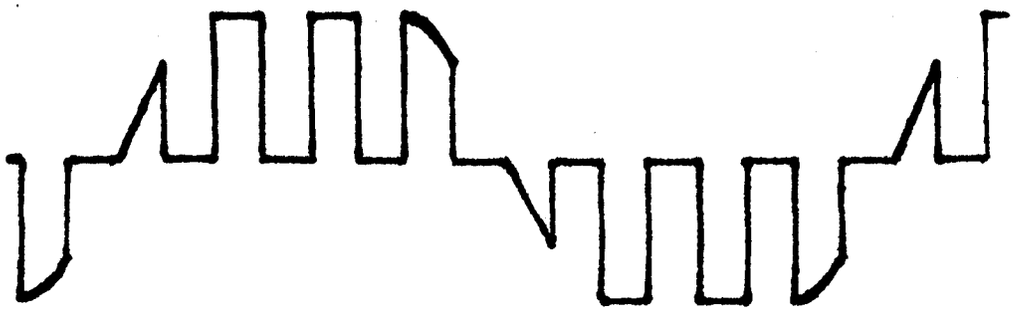

The chopper frequency may be any multiple of ten cycles. The chopper is synchronized with the scan mirror, and as the time of a scene is .1 second, there is always an integral number of chop cycles per scene.

The harmonic content of the detector scene may be represented by the product of the input scene and the chopper. Ai and Bj are the appropriate sum-and-difference Fourier coefficients, for instance, at 25 Hz the first harmonic of a 40 Hz chopper, 40 Hz, would combine with the third scene harmonic, 3 times 5 Hz, and also the zero harmonic of the chopper would combine with the fifth scene harmonic, 5 times 5 Hz, for a net amplitude of $R(A_3 B_1 \& A_5 B_0)/2$.
Other comginations also yield 25 Hz, for instance (3 x 40 Hz) - (19 x 5 Hz), but the values are negligible and therefore not included. The selection of useful terms is determined on the basis of harmonic combinations up to the ninth harmonic of each component. The actual coefficient values were computed by resolving plots of the desired input wave-shapes by G. E. 's FORIER*** program.

The program initializes itself by asking for several inputs.

WHAT ARE THE RELATIVE RADIANCES OF SCENE 1, 2, & THE B. B. ?

The "relative" implying a dimensionless relationship to each other, such

as typing 1, 1, 0 would imply that scenes 1 and 2 have the same relative radiance (maybe full scale) and the blackbody some radiance much less. 1, -1, 0 might imply + and - full scale scene radiances, with the black-body half way between. 1, .5, -.5 would imply scene 1 was twice the radiance of scene 2, and both above the black body radiance by the indicated ratio. If one has a balanced wave form, such as 1, -1, 0, there is no d.c. component. A dull scene such as 1, 1, -1 has no a.c. component. The scenes before and after the requested scenes 1 and 2 are assumed to be cyclicly repetitious at a 5 Hz rate, or continuous d.c. in the "dull" scene case. Any numbers will be accepted and used in computations, 1's and 0's will provide the easiest comparisons, but 100, .005 or any real number may be used. Insert commas between the numbers.

WHAT ARE THE DETECTORS ELEC. & THERMAL T.C.'S?

This asks for the electrical and thermal time constants, in that order. For instance typing 1, .1 will be understood as a 1 second electrical time constant and a 0.1 thermal time constant. Insert a comma between the two numbers.

WHAT IS THE CHOPPER FREQ. IN 10'S OF Hz?

WHAT IS THE PHASE OF THE CHOPPER RELATIVE TO THE SCENE EDGE?

The chopper frequency is set-up to compute in even multiples of 10 Hz, i.e. 10, 20, 30, 80, 100, etc., so the question is asked for the multiplier only. A 4 is interpreted as your desiring a 40 Hz chopping frequency, an 8 as 80 Hz, 100 as 1 kHz, etc. The phase is 0 to 360° where 0° is the start of an "open" and 180° is the start of a "closed" chop cycle.

WHAT IS THE MAX. FREQ. OF INTEREST, UP TO 1000 Hz?

This is a useful input to limit computation time.

After absorbing this much data the computer goes ahead and tabulates:

THE HARMONIC CONTENT OF THE DETECTOR INPUT IS--

FREQUENCY	AMPLITUDE	PHASE DEG.
X	XXX.XXXXX	XXX.XXXXX
XX	XXX.XXXXX	XXX.XXXXX

THE HARMONIC CONTENT OF THE AMPLIFIER INPUT IS--

FREQUENCY	AMPLITUDE	PHASE DEG.
X	XXX.XXXXX	XXX.XXXXX
XX	XXX.XXXXX	XXX.XXXXX

The detector input calculations are merely mixing the input scene and the chopper. The input scene is assumed flat for the center .063 seconds and varying sinusoidally for .037 seconds between each scene, during the mirror transition time. The chopper wave form is assumed flat for all except that portion of time that a blade edge is in the optical path, and during that time to vary sinusoidally from the scene to the blackbody radiance, or the reverse. The computation is of the form of the Forier Series, R(Ao/2) for the d.c. component, and $R\sum(AnBm + ApBq)$ for the magnitude of the a.c. components, where R is the radiance multiplier, Ax and Bx are the coefficients for the scene and chopper, and n, m, p and q are appropriate harmonics.

The amplifier input calculations alternate the signals according to the detector's time constants by the formula $X\ in/\sqrt{2\pi fT_2)^2 + 1}\ \sqrt{(1/2\pi fT_1)^2 + 1}$,

and shift the phase by Φ in $-\tan^{-1} 2/\pi f T_2 + 90 - \tan^{-1} 2/\pi f T_1$.

This data is printed out on the teletype if an affirmative answer was given to:

DO YOU WANT INTERMEDIATE RESULTS, YES OR NO?

Otherwi e, the program merely stores the answers and continues to ask for circuit parameters.

The program then plots a generalized amplifier pass-band with a second low-end knee.

ASSUMING A RESPONSE FOR THE AMPLIFIER SIMILAR TO --

```
A - - - - X X X X X X
          X I         I X
        X   I         I   X
      X     I         I     X
     XI     I         I       X
    X I     I         I         X
   X  I     I         I           X
- - - - - - - - - - - - - - - - - - - - - - - - - - - -
0     1     2         3             HZ
```

WHAT ARE THE FREQUENCIES AT POINTS 1, 2, & 3?

Insert commas between the three numbers, as before on multiple entries. The fall-off from F_2 Hz to F_1 Hz is 6 db/octave, as is the fall-off from F_3 Hz upwards. The fall off from F_1 Hz down is an additional 6 db/octave "A" may be any convenient value, as it is merely a linear multiplier, and the amplifier never "saturates". The amplifier output is calculated according to X in $(1/\sqrt{1 + (F_1/f)^2} \times 1/\sqrt{1+(F_2/f)^2} \times 1/\sqrt{1+(f/F_3)^2} \times$ 'A', where F1, F2, F3 and 'A' are as defined above, f the frequency of interest, and Xin the input amplitude. The phase shift is:
Φ in $-(\tan^{-1} (f/F_3))+(90-\tan^{-1}(f/F_1)) + (90-\tan^{-1} (f/F_2))$, where Φ in is the

input phase shift at f. The amplifier output is tabulated:

THE HARMONIC CONTENT OF THE AMPLIFIER OUTPUT IS --

FREQUENCY	AMPLITUDE	PHASE DEG.
X	XXX.XXXXX	XXX.XXXXX
XX	XXX.XXXXX	XXX.XXXXX

The signal at this point resembles a triangular wave of the fundamental frequency of the chopper with phase shift at the points of scene change. In order to reconstruct the 5 Hz scene we full-wave demodulate the signal at the chopper frequency. The relative phasing between the chopper and the demodulator is important, as the frequency component amplitudes are directly proportional to the cosine of the phase difference. The optimum demodulator phase is then approximately that phase that the chopper frequency would have been shifted through the system thus far, or that angle $\pm 180^{\circ}$. The program has inserted the chopper frequency into the system automatically, and kept track of its phase even though it may not have normally been a waveform constituent. It now uses this information to predict the optimum phase for the demodulator.

The program then types:

THE OPTIMUM DEMOD. PHASE SHIFT IS AROUND ___ DEGREES.

WHAT PHASE SHIFT WOULD YOU LIKE TO TRY?

Any phase shift, $0^{\circ} \leq \Phi \leq 360^{\circ}$, may be inserted, and the program will proceed accordingly.

THE HARMONIC CONTENT OF THE DEMOD. OUTPUT IS --

FREQUENCY	AMPLITUDE	PHASE DEG.
X	XXX.XXXXX	XXX.XXXXX
XX	XXX.XXXXX	XXX.XXXXX

This computation is $\sum$ Xn Bm/2 cos ($n\Phi n$ - Φ prp) for the amplitude, where m and n are the harmonic subscripts for all the constituent sums and differences, and the phase shift is Φ in + (Φ chop - Φ prp) f/2F.

The program then asks:

WHAT IS THE TIME CONST. OF THE LO-PASS FILTER?

If a "0" is typed in, the program skips to the integrator, if any value is typed in, it computes and tabulates:

THE HARMONIC CONTENT OF THE FILTER OUTPUT IS --

FREQUENCY	AMPLITUDE	PHASE DEG.
X	XXX.XXXXX	XXX.XXXXX
XX	XXX.XXXXX	XXX.XXXXX

According to X in / $\sqrt{(T_f\, 2\pi f)^2 + 1}$, and the phase shift as Φin - $\tan^{-1} T_f\, 2\pi f$.

The program asks:

ABOUT HOW MANY INTERACTION INTERVALS OVER SCENES 1 and 2?

This may be any number up to 300, but the program will round to the nearest multiple of 20, with a minimum of 20. The integration is continuous, but this number controls the interval listing, and the number of plot points.

The program then computes and tabulates the integrator input waveform amplitude, and output integral:

THE INTEGRATOR OUTPUT, AT THE END OF "INCREMENT", IS --

INCREMENT	INTEGRAL	INT. INPUT
.XXXXX	XXX.XXXXX	XXX.XXXXX

The integral is $B_1 X_{dc}/2 + \sum^{\infty}\sum^{\infty} x_f/w\ (\cos n\,\Phi_f\ (\sin(wt+Z) - \sin wt)$

$- \sin n\,\Phi_f\ (\cos\ (wt + Z) - \cos wt))$, and the input amplitude is

$\sum X_f \cos\ (wt - \Phi_f)$. The variable Z is the integration time.

The program then asks:

WOULD YOU LIKE A PLOT, YES OR NO?

A property typed yes will cause the program to plot:

```
        MINUS                ZERO                PLUS

0            +            0  I         X
0.1            +                          X  0
0.2              +          I      X        0
0.3              +          I               0       X
0.4                +        I           X   0
 .                          .
 .                          .
 .                          .
 .                          .
1.2          X            0  I         +
 .
 .
 .
```

WHERE "0" IS THE SCENE INPUT,

"X" IS THE INTEGRATOR INPUT,

"+" IS THE INTEGRATOR OUTPUT

and "*" IS AN X & + SUPERPOSITION.

The I's are merely a "zero" line.

Any other input to the plot question will cause the program to ask:

WOULD YOU LIKE TO:

1. START OVER;
2. CHANGE THE CHOPPING FREQUENCY;
3. CHANGE THE AMPLIFIER PASS-BAND;
4. CHANGE THE DEMOD. PHASE SHIFT;
5. CHANGE THE LO-PASS FILTER;
6. CHANGE THE INTEGRATION INTERVAL;

OR

7. QUIT?

Typing in the appropriate number will return you to the applicable input question in the program, saving all other previous inputs and resultant calculations. The "start over" saves some computer time over the 7 (quit) and "RUN" program restart, because on subsequent time through, the amplifier pass-band is not re-plotted, as well as saving the compile time. The program simply types:

ASSUMING THE AMPLIFIER RESPONSE AS BEFORE --

WHAT ARE THE FREQUENCIES AT POINTS 1, 2 & 3?

After accepting the new input to the restart question, the program will proceed normally through all following steps.

Det. Input

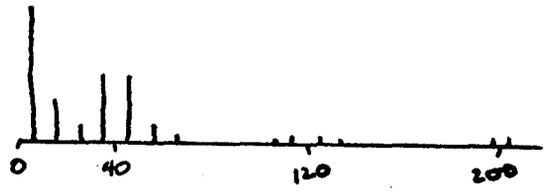

Amp Input

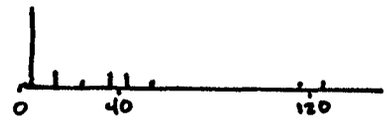

Amp. Output

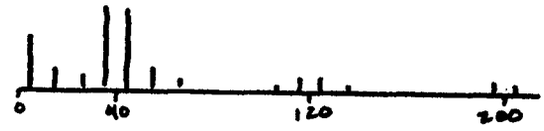

Demod. Output

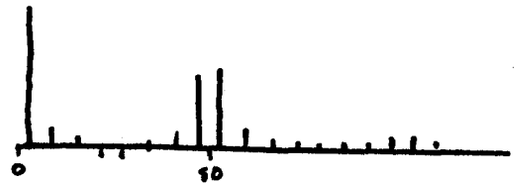

Int. Output

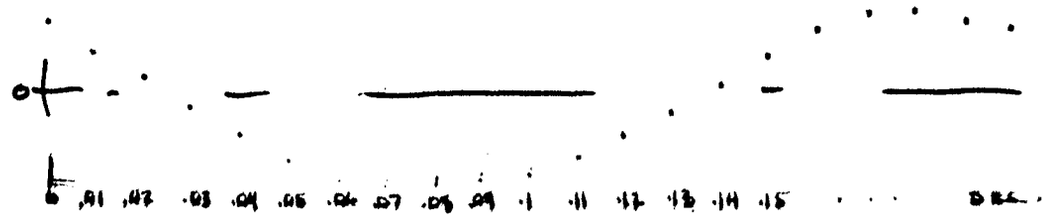

Plots of harmonic content of sounder system signals at progressive steps through system.

Full scale alternating scene input

40 Hz chopping frequency

Pyroelectric detector with 1 SEC. ELEC. T.C. & 0.1 SEC. THERM. T.C.

Amp rolloffs at 20, 40 & 200 Hz, x 1000 amplification

Demod. phase shift optimized for 0° chopper phase.

Integration interval .05 sec.

A typical run is as follows:

We start by asking for intermediate results in order to see the effects of the various stages of the system.

We then ask for alternating scenes above and below the black body radiance.
The detectors time constants were inserted as one second electrical and tenth second thermal.
The chopper speed is 40 Hz and zero phase shift relative to the scene edge. For economy of the listings we limit the frequencies to <240 Hz.

```
TIRØS      10:25MST     01/18/73

      HARMØNIC ANALYSIS ØF TIRØS SØUNDER SYSTEM

WØULD YØU LIKE INTERMEDIATE RESULTS, YES ØR NØ ? YES

WHAT ARE THE RELATIVE RADIANCES ØF SCENE 1, 2 & THE B.B. ? 1,-1,0

INCØRRECT FØRMAT--RETYPE IT
? 1,-1,0

WHAT ARE THE DETECTØR'S ELEC. & THERMAL T. C.'S ? 1,.1

WHAT IS THE CHØPPER FREQ. IN 10'S ØF HZ. ? 4

WHAT IS THE CHØPPER PHASE RELATIVE TØ THE SCENE EDGE,
'0' IS THE START ØF ØPEN, '180' IS START ØF CLØSED CYCLE ? 0

WHAT IS THE MAX. FREQ. ØF INTEREST, UP TØ 1000 HZ ? 240
```

THE HARMONIC CONTENT OF THE DETECTOR INPUT IS -

FREQUENCY	AMPLITUDE	PHASE DEG.
5	.59495	78.75000
15	.13167	56.25000
25	.09272	33.75000
35	.37310	11.25000
45	.37610	168.75000
55	.07722	146.25000
65	.01102	123.75000
75	-.00396	101.25000
85	-.00266	78.75000
95	.00428	56.25000
105	.02852	33.75000
115	.11760	11.25000
125	.11760	168.75000
135	.02352	146.25000
145	.00348	123.75000
155	-.00133	101.25000
165	-.00104	78.75000
175	.00199	56.25000
185	.01200	33.75000
195	.06000	11.25000
205	.06000	168.75000
215	.01200	146.25000
225	.00178	123.75000
235	-.00068	101.25000

THE HARMONIC CONTENT OF THE AMPLIFIER INPUT IS -

FREQUENCY	AMPLITUDE	PHASE DEG.
5	.18037	8.22996
15	.01389	332.91453
25	.00589	307.75741
35	.01695	284.11416
45	.01329	80.97824
55	.00223	58.07333
65	.00027	35.29293
75	-.00008	12.58727
85	-.00005	349.92999
95	.00007	327.30580
105	.00036	304.70526
115	.00163	282.12221
125	.00150	79.55144
135	.00028	56.99301
145	.00004	34.44177
155	-.00001	11.89714
165	-.00001	349.35793
175	.00002	326.82319
185	.00010	304.29221
195	.00049	281.76440
205	.00047	79.23931
215	.00009	56.71656
225	.00001	34.19582

ASSUMING A RESPØNSE FØR THE AMPLIFIER SIMILAR TØ -

```
A - - - - - X X X X X X
          X I         I X
        X   I         I   X
      X     I         I     X
     XI     I         I       X
    X I     I         I         X
   X  I     I         I           X
  ----------------------------------
  0   1      2         3          HZ
```

WHAT ARE THE FREQUENCIES AT PØINTS 1, 2, & 3 ? 20,40,200

WHAT VALUE SHØULD I USE FØR 'A' ? 1E3

THE HARMØNIC CØNTENT ØF THE AMPLIFIER ØUTPUT IS -

FREQUENCY	AMPLITUDE	PHASE DEG.
5	5.42423	83.63853
15	2.91853	342.66072
25	2.41909	201.15409
35	9.54496	251.90475
45	8.85784	38.35050
55	1.63686	8.04808
65	.20884	339.78166
75	-.06708	312.86633
85	-.04030	286.88791
95	.05838	261.58278
105	.28973	236.77610
115	1.31277	212.34790
125	1.19404	8.21331
135	.21796	344.31079
145	.02955	320.59472
155	-.01035	297.03056
165	-.00747	273.59177
175	.01322	250.25756
185	.07364	227.01153
195	.34167	203.84045
205	.31775	.73365
215	.05922	337.68236
225	.00819	314.67933
235	-.00292	291.71850

The optimum demodulator phase shift is calculated from the shift that the 40 Hz chopper frequency would have experienced through the system:

```
THE ØPTIMUM DEMØD. PHASE SHIFT IS ARØUND 324.61 DEGREES.
WHAT PHASE SHIFT WØULD YØU LIKE TØ TRY? 324.61134

THE HARMØNIC CØNTENT ØF THE DEMØD. ØUTPUT IS :-
```

FREQUENCY	AMPLITUDE	PHASE DEG.
5	-5.97994	173.63853
15	-.24655	72.66072
25	-.89677	21.15409
35	.13070	341.90475
45	.11461	308.35050
55	-.91972	278.04808
65	-.51678	249.78166
75	-2.46387	222.86631
85	-3.24948	196.88792
95	.18266	171.58278
105	.00702	146.77610
115	-.50928	122.34790
125	-.52778	98.21331
135	-.01559	74.31080
145	-.19501	50.59472
155	.23950	27.03056
165	.32270	3.59177
175	.09256	340.25756
185	.13560	317.01153
195	.09701	293.84045
205	.09443	270.73365
215	.13782	247.68237
225	.06733	224.67933
235	-.01284	201.71851

```
WHAT IS THE TIME CØNST. ØF THE LØ-PASS FILTER ? 0
```

Had we chosen 144.61°, the numbers would have been identical, except for sign.

We inserted no lo-pass filter for this run.

ABØUT HØW MANY INTEGRATIØN INTERVALS ØVER SCENES 1 & 2 ? 80

WHAT IS THE INTEGRATIØN TIME IN SECØNDS ? .05

THE INTEGRATØR ØUTPUT, AT THE END ØF 'INCREMENT', IS -

INCREMENT	INTEGRAL	INT. INPUT
.00000	.16842	10.90088
.00250	.13615	8.43235
.00500	.11449	4.33821
.00750	.10833	.82105
.01000	.11091	2.16172
.01250	.09490	8.20180
.01500	.05973	7.60772
.01750	.03529	3.28983
.02000	.02798	1.69825
		.....
.09750	-.19128	-3.71693
.10000	-.16842	-10.90088
.10250	-.13615	-8.43234
.10500	-.11449	-4.33819
.10750	-.10833	-.82104
.11000	-.11091	-2.16174
.11250	-.09490	-8.20181
.11500	-.05973	-7.60771
.11750	-.03529	-3.28988
.12000	-.02798	-1.69825
.12250	-.01439	-5.73685
.12500	.02325	-8.55329
.12750	.06406	-4.40096
.13000	.08263	-1.07888
.13250	.09025	-.68895
.13500	.10119	-1.82443
.13750	.12873	-2.84602
.14000	.16782	-.84009
.14250	.18551	.60999
.14500	.18570	-.52307
.14750	.18745	-.38661
.15000	.20571	2.28884
.15250	.22346	2.94744
.15500	.23418	1.26937
.15750	.23981	-1.21595
.16000	.24680	-1.52174
.16250	.25728	4.01734
.16500	.26489	5.85499
.16750	.26785	2.27849
.17000	.27048	.51969
.17250	.27412	4.30527
.17500	.27462	9.94153
.17750	.26832	7.53194
.18000	.26143	4.10008
.18250	.25778	2.09508
.18500	.25238	5.06057
.18750	.23751	12.38267
.19000	.20861	12.00469
.19250	.19023	2.82983
.19500	.18932	-1.58591
.19750	.19128	3.71696
.20000	.16842	10.90088

WOULD YOU LIKE A PLOT, YES OR NØ ? YES

```
                MINUS                ZERØ                PLUS
0                                    I  O                +     X
0.0025                               I        O +    X
0.005                                I       X+ O
0.0075                               IX        +  O
0.01                                 I  X      +     O
0.0125                               I        +      X
0.015                               0I   +        X
0.0175                               0  + X
0.02                                 0 +X
0.0225                              0I+        X
0.025                              + I        O      X
0.0275                        +      I      X        O
0.03                         +       I X            O
0.0325                      +        IX             O
0.035                       +        I  X            O
0.0375                   +           I    X O
0.04                +               0IX
0.0425            +                 X0
0.045             +                 0 X
0.0475            +                0IX
0.05            +          X       I      O
0.0525         +            X      I                O
0.055        +                   X I               O
0.0575       +                     I X             O
0.06       +                       I X              O
0.0625    +            X           I      O
0.065     +         X             0I
0.0675  +                    X     0
0.07    +                         X0
0.0725  +              X          0I
0.075   +  X                       I      O
0.0775  +          X               I              O
0.08      +                X       I          O
0.0825    +                   X    I          O
0.085       +            X          I      O
0.0875  X  +                        I  O
0.09    X  +                        0
0.0925        +          X          0
0.095         +                     0  X
0.0975        +        X            0
0.1         X     +          0      I
0.1025        X    + 0               I
0.105              0 +X              I
0.1075           0  +              XI
0.11            0     +      X      I
0.1125          X      +             I
0.115            X         +        I0
0.1175                  X +         0
0.12                    X+ 0
0.1225             X          +I0
0.125           X    0             I +
0.1275        0          X         I     +
0.13          0              X I        +
0.1325        0                XI        +
0.135         0              X  I        +
0.1375              0 X       I          +
```

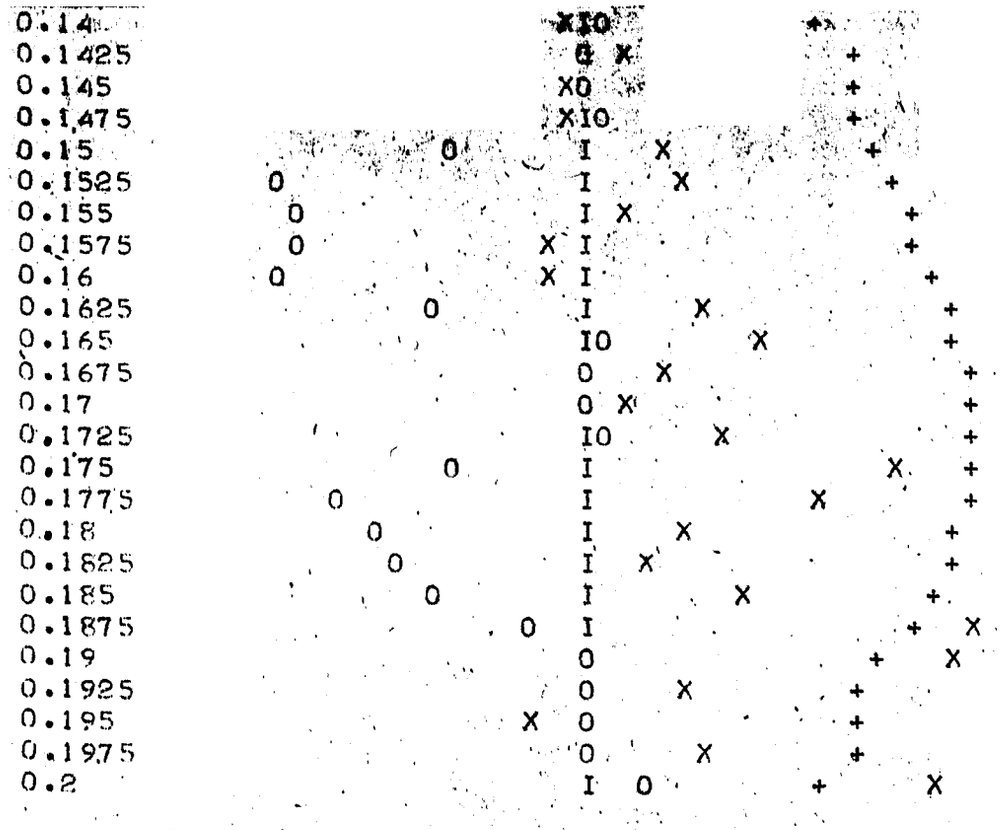


```
WHERE 'O' IS THE CHØPPED INPUT,
      'X' IS THE INTEGRATØR INPUT,
      '+' IS THE INTEGRATØR ØUTPUT,
  AND '*' IS AN X & + SUPERPØSITIØN.

WOULD YØU LIKE TØ :
    1. START ØVER;
    2. CHANGE THE CHØPPING FREQUENCY;
    3. CHANGE THE AMPLIFIER PASS-BAND;
    4. CHANGE THE DEMØD. PHASE SHIFT;
    5. CHANGE THE LØ-PASS FILTER;
    6. CHANGE THE INTEGRATIØN INTERVAL;
 ØR 7. QUIT ? 2

WHAT IS THE CHØPPER FREQ. IN 10'S ØF HZ. ? 4

WHAT IS THE CHØPPER PHASE RELATIVE TØ THE SCENE EDGE,
'0' IS THE START ØF ØPEN, '180' IS START ØF CLØSED CYCLE ? 90
```

The D.C. level would have been about 0.264, so was overshot by less than 4% and had the "read" position been chosen judiciously a condition of virtually no scene-to-scene cross-talk is possible. On the ITPR program the optimum integration start and stop times were found to be at the chopper quadrature points.

Another pass through, this time identical in all respects to the last plot, except the integrate time is chosen as 0.075 seconds.

ABØUT HØW MANY INTEGRATIØN INTERVALS ØVER SCENES 1 & 2 ? 80

WHAT IS THE INTEGRATIØN TIME IN SECØNDS ? .075

THE INTEGRATØR ØUTPUT, AT THE END ØF 'INCREMENT', IS -

INCREMENT	INTEGRAL	INT. INPUT
.00000	-.23048	-12.38262
.00250	-.18270	-12.00476
.00500	-.15393	-2.82987
.00750	-.15104	1.58593
.01000	-.14617	-3.71691
.01250	-.10704	10.90088
.01500	-.05847	-8.43237
.01750	-.02955	-4.33820
.02000	-.01802	-.82104
.02250	-.00766	-2.16173
.02500	.02680	-8.20180
.02750	.08219	-7.60774
.03000	.11392	-3.28982
.03250	.11944	-1.69824
.03500	.12795	-5.73684
.03750	.16758	-8.55329
.04000	.20984	-4.40099
.04250	.23188	-1.07888
.04500	.23975	-.68894
.04750	.24473	-1.82443
.05000	.26431	-2.84602
.05250	.29080	-.84009
.05500	.30415	.61000
.05750	.30876	-.52307
.06000	.31924	-.38661
.06250	.33599	2.28884
.06500	.34600	2.94745
.06750	.34637	1.26938
.07000	.34809	-1.21596
.07250	.35564	-1.52174
.07500	.35921	4.01733
.07750	.35053	5.85499
.08000	.33944	2.27850
.08250	.33675	.51967
.08500	.33363	4.30526
.08750	.31275	9.94152
.09000	.28198	7.53196
.09250	.26373	3.10009
.09500	.25783	2.09506
.09750	.25445	5.06056
.10000	.23048	12.38264
.10250	.18270	12.00473
.10500	.15393	2.82985
.10750	.15104	-1.58593
.11000	.14617	3.71694
.11250	.10704	10.90088
.11500	.05847	8.43235
.11750	.02955	4.33818
.12000	.01802	.82103
.12250	.00766	2.16174
.12500	-.02680	8.20181
.12750	-.08219	7.60773

WØULD YØU LIKE A PLØT, YES ØR NØ ? YES

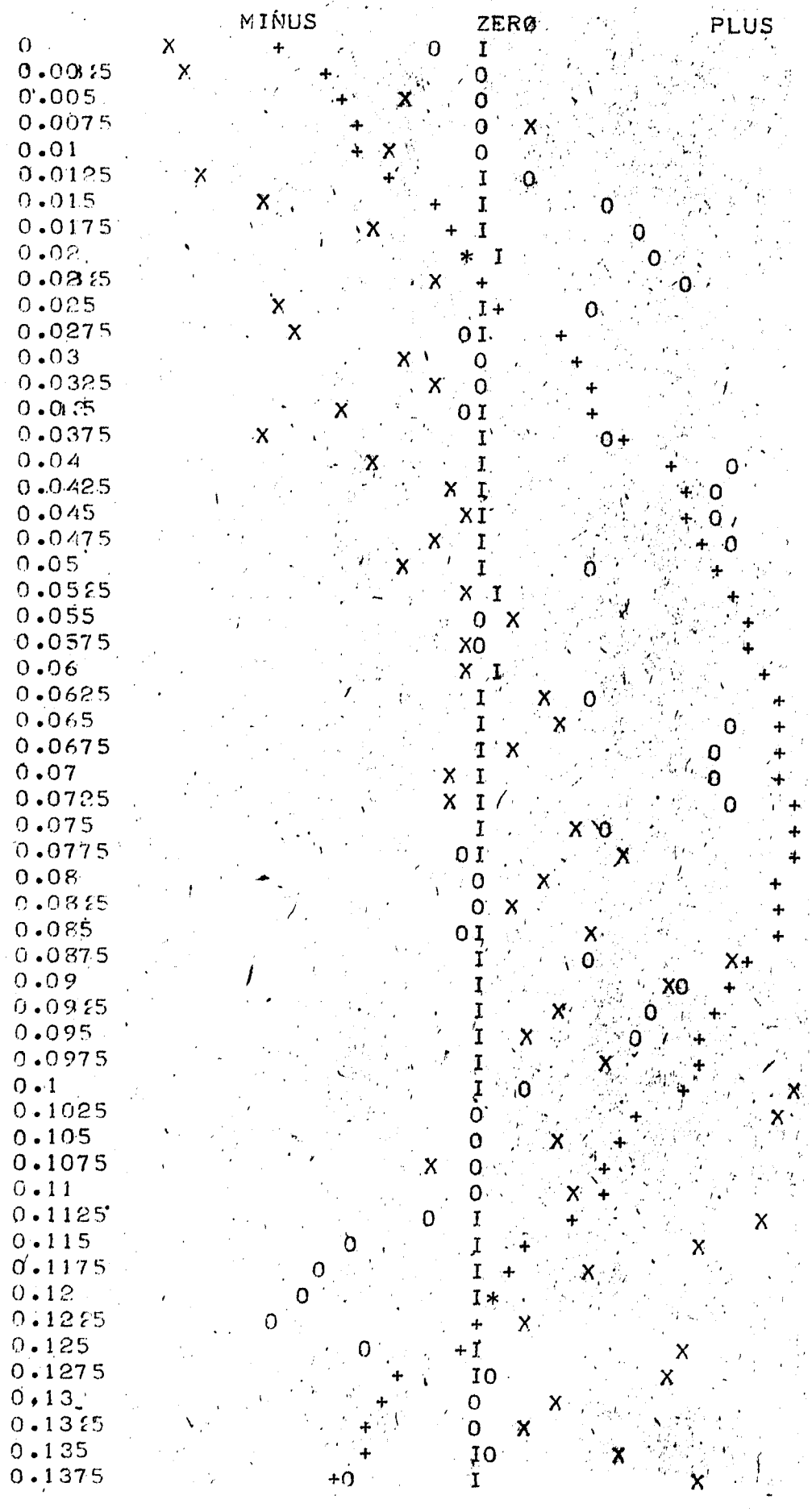

Then a pass to determine the D.C. level one would achieve with equal scene radiances.

```
WØULD YØU LIKE INTERMEDIATE RESULTS, YES ØR NØ ? NØ

WHAT ARE THE RELATIVE RADIANCES ØF SCENE 1, 2 & THE B.B. ? 1,1,0

WHAT ARE THE DETECTØR'S ELEC. & THERMAL T. C.'S ? 1,.1

WHAT IS THE CHØPPER FREQ. IN 10'S ØF HZ. ? 4

WHAT IS THE CHØPPER PHASE RELATIVE TØ THE SCENE EDGE,
'0' IS THE START ØF ØPEN, '180' IS START ØF CLØSED CYCLE ? 180

WHAT IS THE MAX. FREQ. ØF INTEREST, UP TØ 1000 HZ ? 400

ASSUMING THE AMPLIFIER RESPØNSE AS BEFØRE -

WHAT ARE THE FREQUENCIES AT PØINTS 1, 2, & 3 ? 20,40,200

WHAT VALUE SHØULD I USE FØR 'A' ? 1E3

THE ØPTIMUM DEMØD. PHASE SHIFT IS ARØUND 144.61 DEGREES.
WHAT PHASE SHIFT WØULD YØU LIKE TØ TRY? 144.61

WHAT IS THE TIME CØNST. ØF THE LØ-PASS FILTER ? 0

ABØUT HØW MANY INTEGRATIØN INTERVALS ØVER SCENES 1 & 2 ? 0

WHAT IS THE INTEGRATIØN TIME IN SECØNDS ? .075

THE INTEGRATØR ØUTPUT, AT THE END ØF 'INCREMENT', IS -

      INCREMENT          INTEGRAL          INT. INPUT

      .00000             .35465            7.62225
      .01000             .35465            1.10461
      .02000             .35465            -.33427
      .03000             .35465            3.8
```

Demonstrating only slightly over 1% overshoot, or scene-to-scene cross-talk, and again that an optimal "read" time may be chosen.

APPENDIX 4

OPTICAL COATING LABORATORY, INC.

DESIGN STUDY OF DICHROICS

Gulton Industries

Gulton Purchase Order 02663
OCLI Work Order 14-7416-760

OPTICAL COATING LABORATORY, INC.
2789 GIFFEN AVE., SANTA ROSA, CALIFORNIA, U.S.A. • TELETYPE 510-744-2083 • PHONE (707) 545-6440

GULTON INDUSTRIES

DESIGN STUDY OF DICHROICS

Per Para. 4.7.e of Spec. DSD-SPEC-E0253

Gulton Purchase Order 02663
OCLI Work Order 14-7416-760

February 9, 1973

By
N. deLeuze

Norman C deLeuze

Written by
Norman C. deLeuze
Project Engineer

Frederick K Crosher

Approved by
Frederick K. Crosher
Manager, Product Engineering

TABLE OF CONTENTS

I. INTRODUCTION

II. SINGLE SURFACE DICHROIC COATING PERFORMANCE

III. SINGLE SURFACE ANTI-REFLECTION COATING PERFORMANCE

IV. SUBSTRATE PERFORMANCE

V. OVERALL ABSORBING PERFORMANCE OF FILTERS FOUR AND SIXTEEN

VI. f/NUMBER EFFECTS

VII. ITPR FILTER INFORMATION

SECTION I. INTRODUCTION

I. INTRODUCTION

This report is organized into five sections which include the performance calculations for dichroic filters two through seven as shown in Table 1 of DSD-SPEC-E0253. Also included is additional information requested by Gulton concerning the substrate and dichroic beamsplitter theoretical performance for the ITPR program. A summary of the calculations made for each coating is shown in Table 1 in this section. Further discussion of each calculation is included in the appropriate section.

The filters are designed for a single incidence angle of 45°, and the design calculations are shown in Sections II and III. Since both the coating materials used and the substrate are absorbing to varying degrees over the wavelength range of interest, absorbing calculations are included where possible. A conservative estimate of the overall performance can be made for high transmitting filters by multiplying the transmittance for each plane of polarization for one surface by the same value for the other surface, and multiplying this by the substrate internal transmittance. Overall absorbing transmittance has been calculated on the computer for filters number four and seven as shown in Section V.

The effect of using the designs in an f/4 system has also been calculated, and the results presented in Section VI.

The Beckman IRIZ Infrared Spectrophotometer has f/10 optics, and the theoretical comparison of the filter performance in an f/4 and an f/10 systems is included. The performance at 0° and 45° incidence angles is also included, since spectrophotometer measurements are not reliable at high angles of incidence.

It should be noted that a Perkin-Elmer 180 Spectrophotometer has been recently installed at OCLI, and is currently undergoing testing. This spectrophotometer has f/4 optics, and may improve our capability for measurements at angle. However, our current capabilities require spectral acceptance at 0°, with 45° measurements made for information, if requested.

TABLE 1

CALCULATION SUMMARY BY FILTER NUMBER

SECTION	CALCULATION	SINGLE SURFACE							TWO SURFACE
		ABSORPTION					ABSORBING		ABSORBING
		Collimated 45°, 0°	f/10 45°, 0°		f/4 45°, 0°		Collimated 45°, 0°		45°
II	Dichroics	2 - 7					4-7		
III	Anti-Reflection	2 - 7 (2 MLAR + 1 SLAR)					2-7 (2 MLAR +1 SLAR)	2-7 (2 MLAR +1 SLAR)	
IV	Substrate							2-7	
V	Overall								4
VI	f/Number		2-5	2-5	2-5	2-5			
VII	Dichroic								

SECTION II. DICHROIC

II. SINGLE SURFACE DICHROIC COATING PERFORMANCE

There are two sets of computer generated curves in this section and one set of hand plotted curves made from the computer printout. The first set of computer generated curves shows the theoretical non-absorbing s-plane, p-plane and average transmittance for all six of the dichroic filters (numbers two through seven) at 45° incidence. The second set shows the performance of the same filters at 0° incidence. The third set of four curves (hand plotted) shows the absorbing performance of filters four through seven at 45° incidence, using the best available coefficients of absorption for the coating materials.

Absorption coefficients were not available for the materials used in filters number two and three, but absorption will be less than filters four through seven in the transmitting region.

The coatings requiring performance above 15μm (filters number two and three) will be less durable than those used in filters number four and seven, but all of the coatings will meet the requirements of the specification.

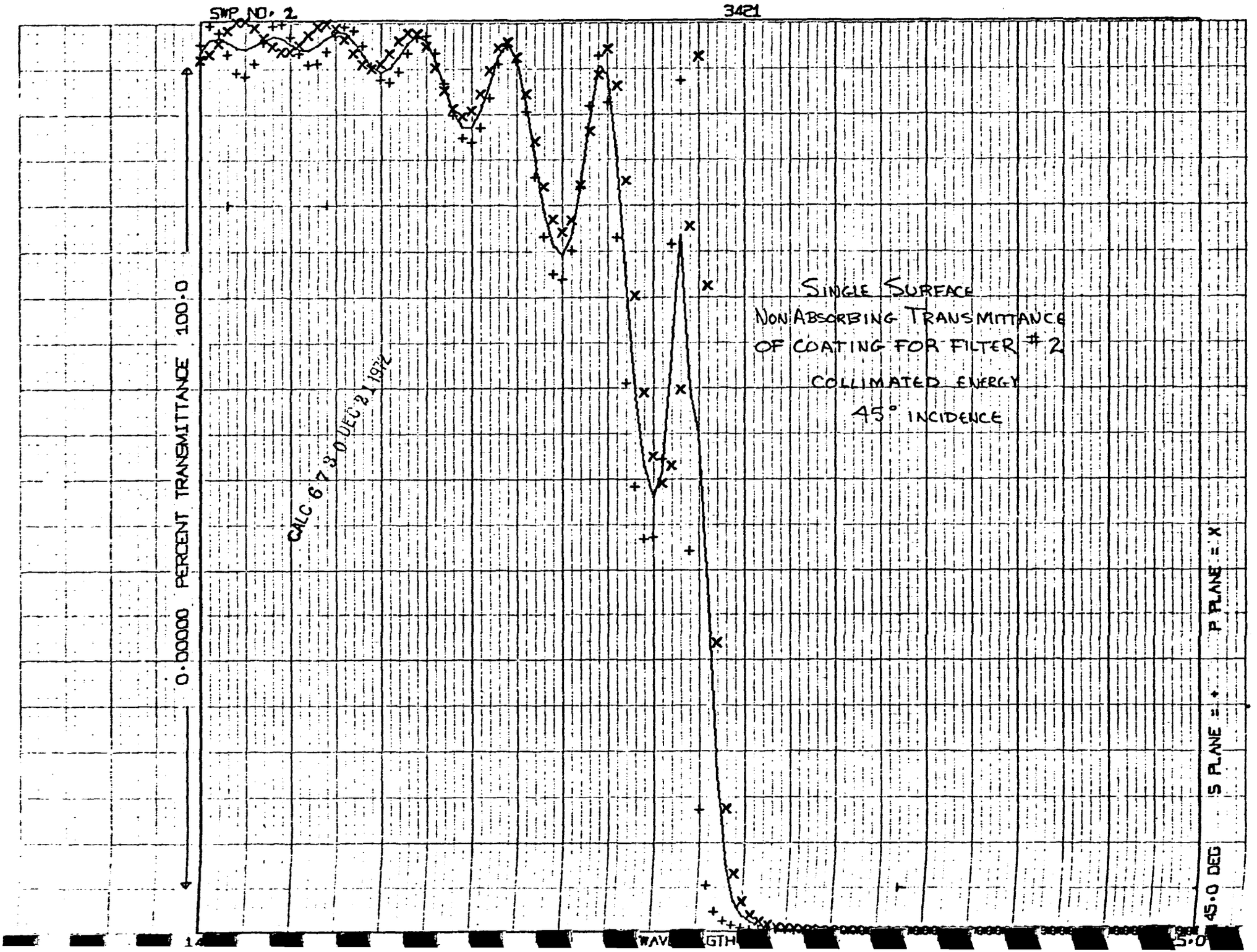
SWP NO. 2
3421
SINGLE SURFACE
NON ABSORBING TRANSMITTANCE
OF COATING FOR FILTER # 2
COLLIMATED ENERGY
45° INCIDENCE
CALC 67.3 0 DEC 21 1972
100.0
0.00000 PERCENT TRANSMITTANCE
WAVELENGTH
45.0 DEG
S PLANE = +
P PLANE = X

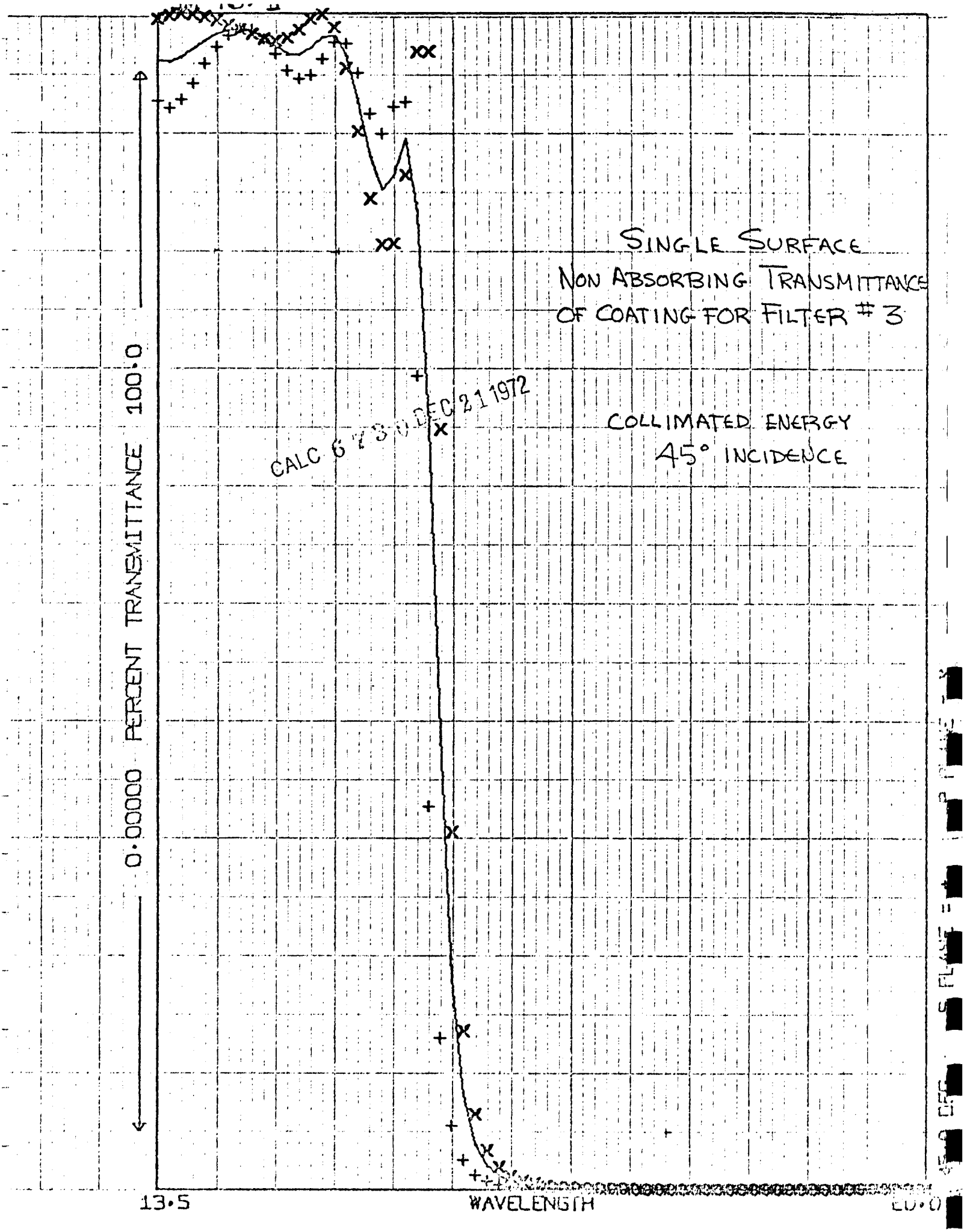
SINGLE SURFACE
NON ABSORBING TRANSMITTANCE
OF COATING FOR FILTER # 3
COLLIMATED ENERGY
45° INCIDENCE
CALC 6 73 0 DEC 21 1972
0.00000 PERCENT TRANSMITTANCE 100.0
13.5
WAVELENGTH

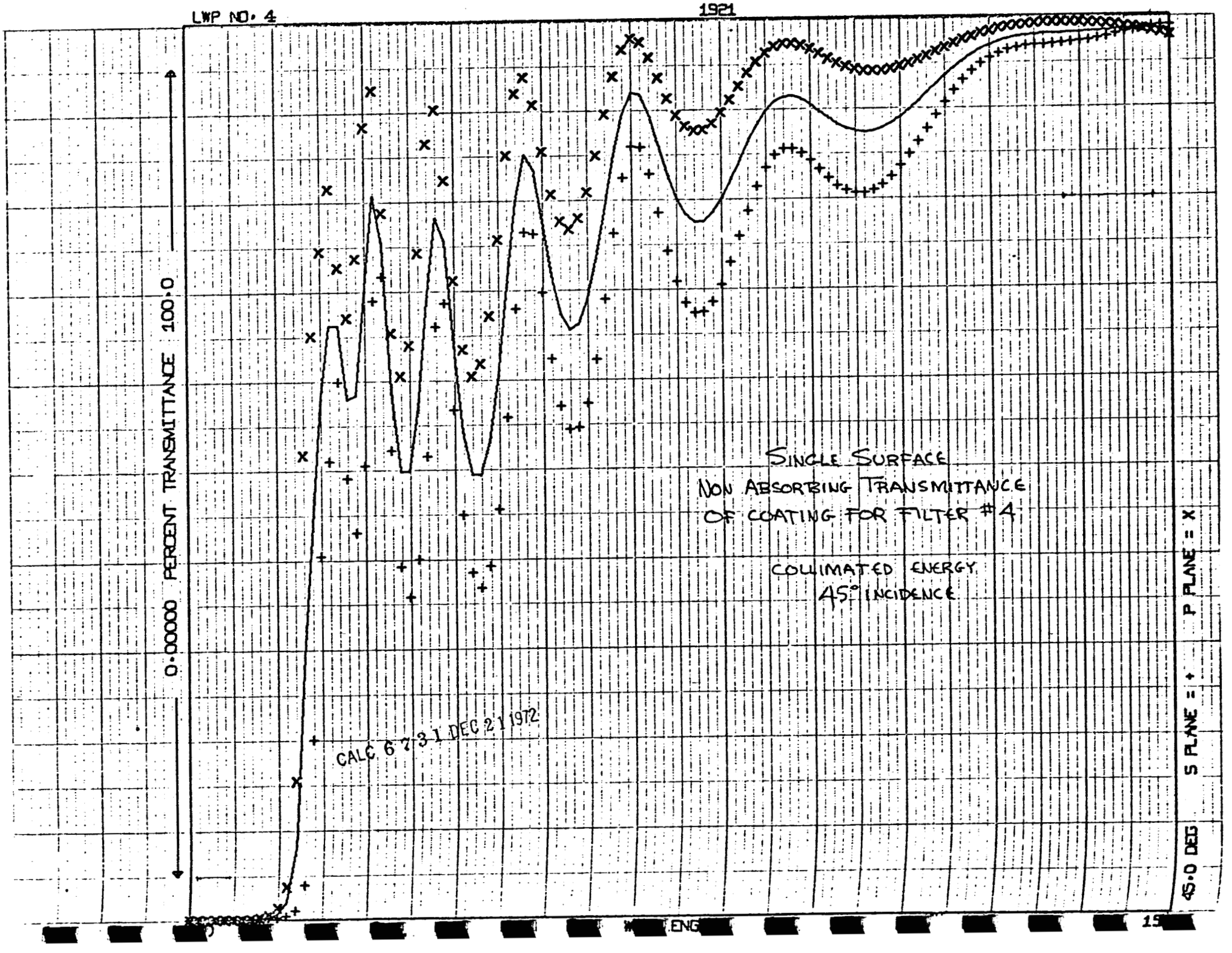
LWP NO. 4
1921
0.00000 PERCENT TRANSMITTANCE 100.0
SINGLE SURFACE
NON ABSORBING TRANSMITTANCE
OF COATING FOR FILTER #4
COLLIMATED ENERGY
45° INCIDENCE
CALC 6 7 3 1 DEC 21 1972
45.0 DEG
S PLANE = +
P PLANE = X
ENG
15

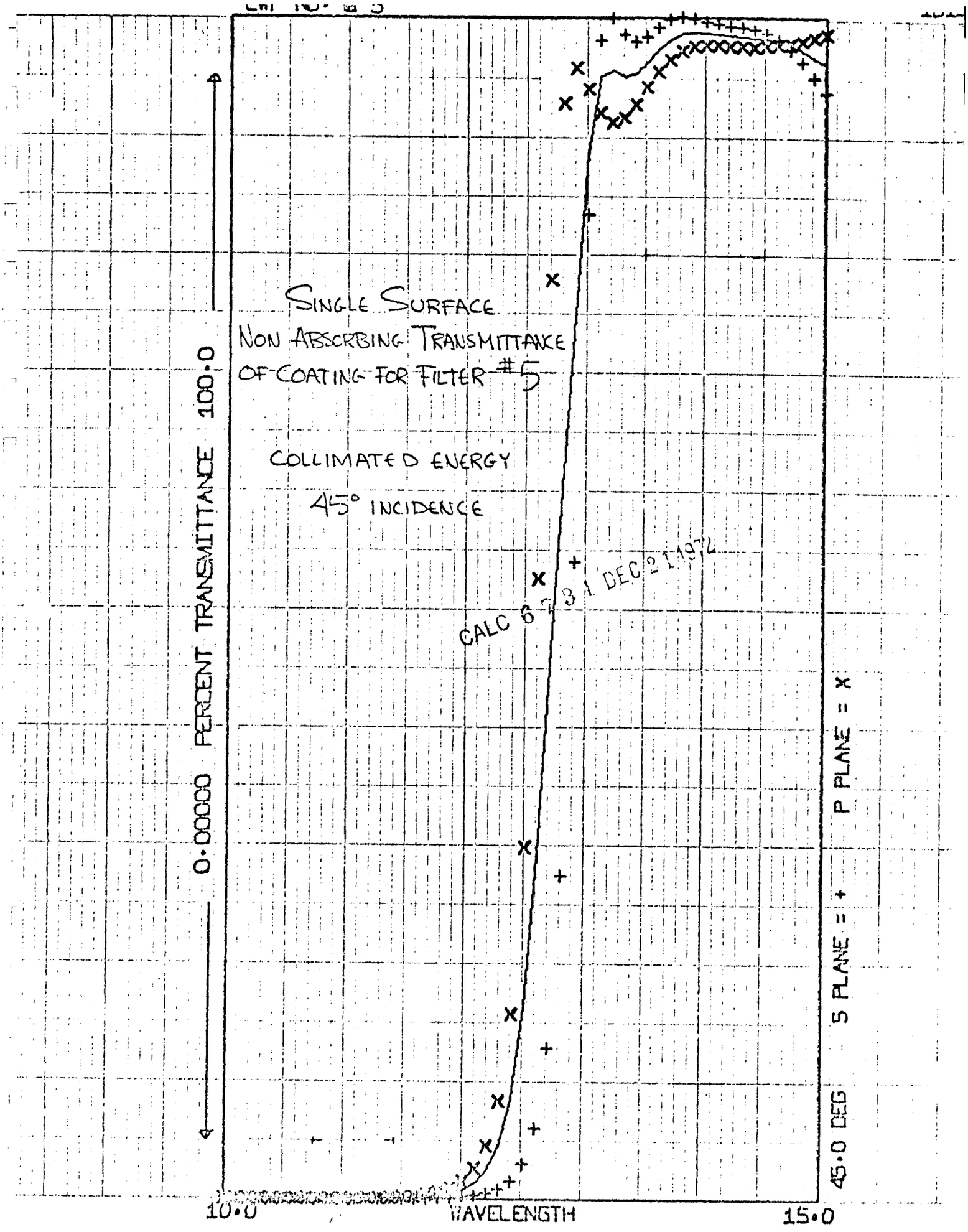
SINGLE SURFACE
NON ABSORBING TRANSMITTANCE
OF COATING FOR FILTER #5
COLLIMATED ENERGY
45° INCIDENCE
CALC 6 31 DEC 21 1972
0.00000 PERCENT TRANSMITTANCE 100.0
10.0
WAVELENGTH
15.0
45.0 DEG
S PLANE = +
P PLANE = X

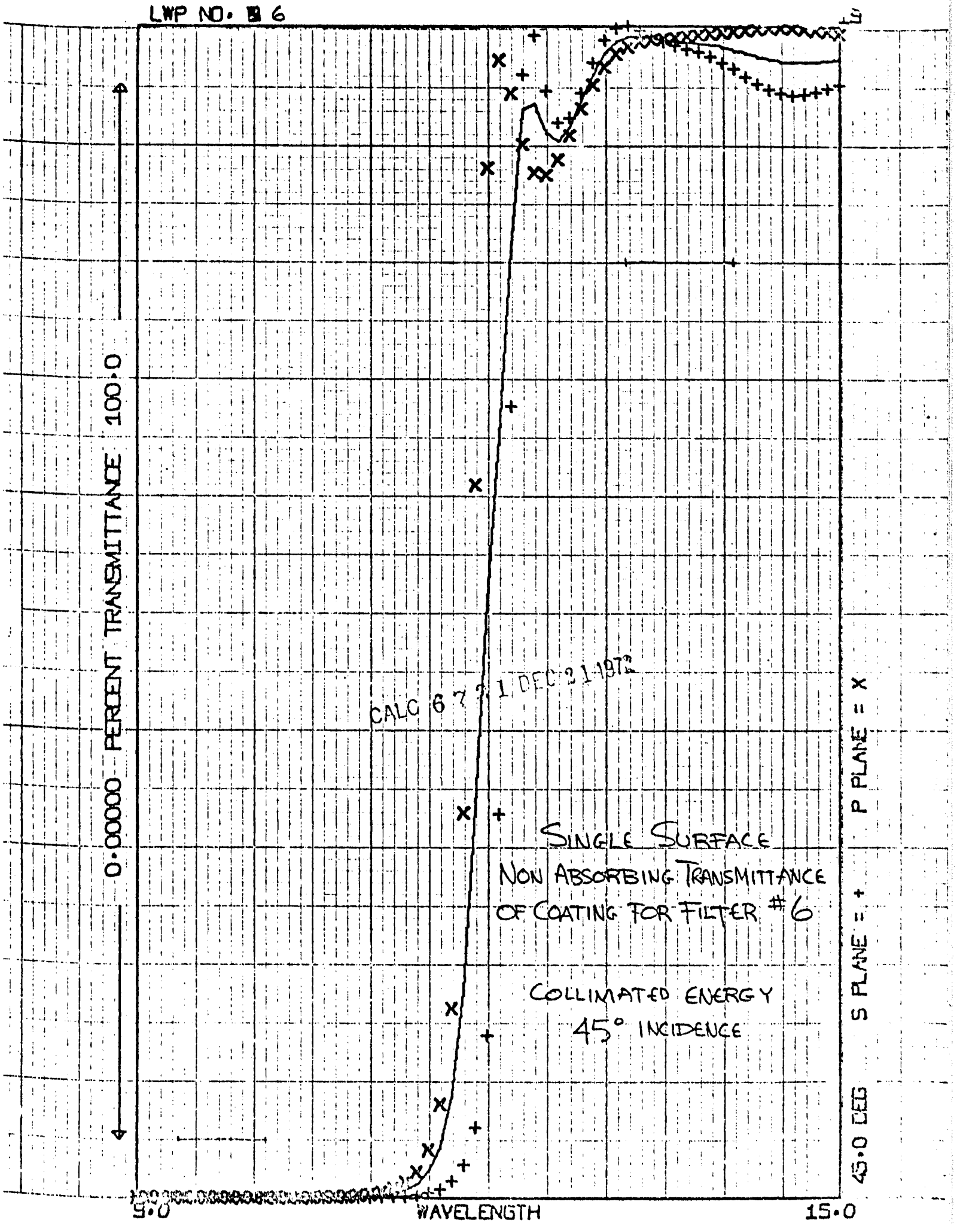
LWP NO. B 6
0.00000 PERCENT TRANSMITTANCE 100.0
9.0
WAVELENGTH
15.0
45.0 DEG
S PLANE = +
P PLANE = X
CALC 6 ? ? 1 DEC 21 1972
SINGLE SURFACE
NON ABSORBING TRANSMITTANCE
OF COATING FOR FILTER #6
COLLIMATED ENERGY
45° INCIDENCE

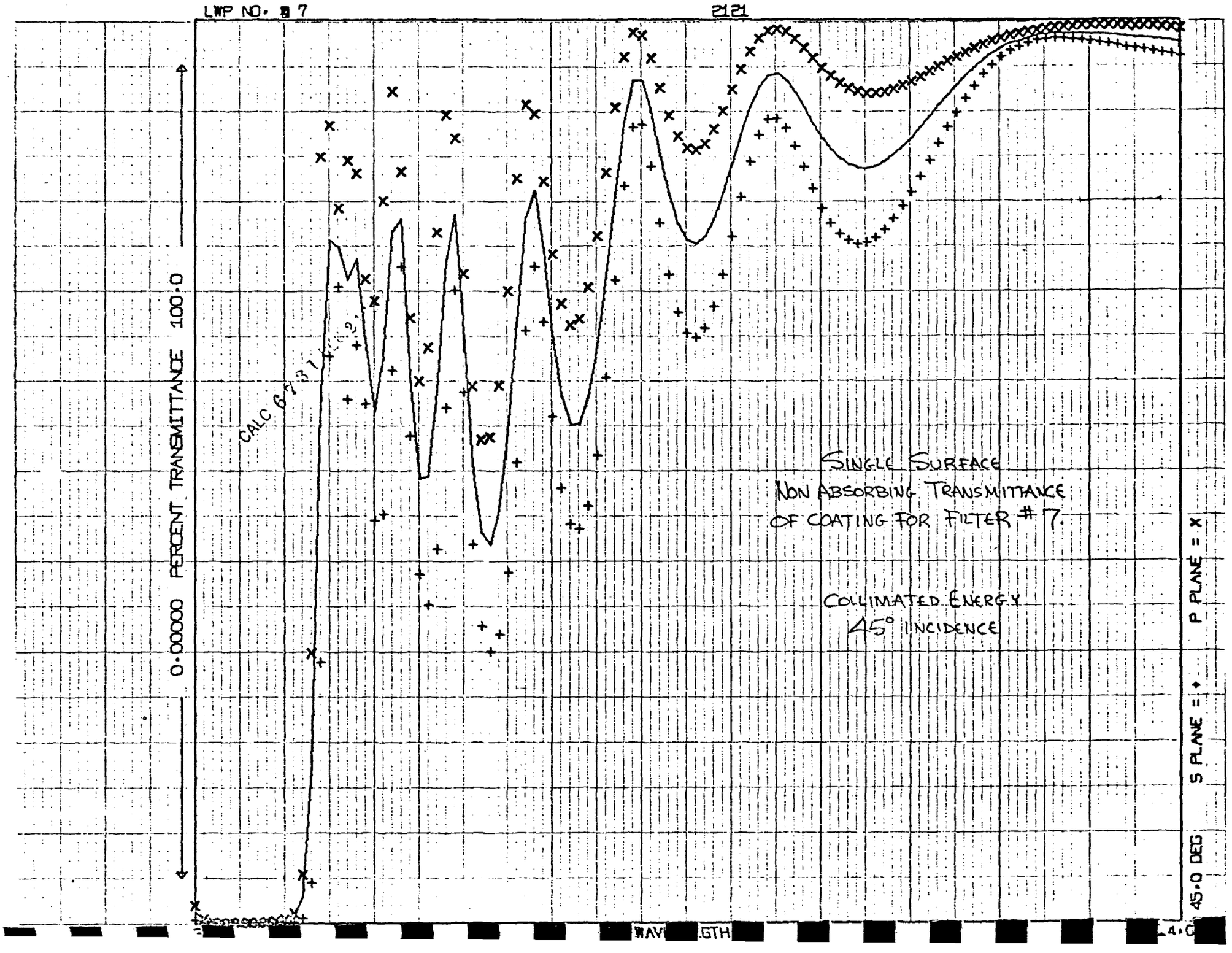
LWP NO. 7
2121
0.00000 PERCENT TRANSMITTANCE 100.0
CALC 6/31
SINGLE SURFACE
NON ABSORBING TRANSMITTANCE
OF COATING FOR FILTER # 7.
COLLIMATED ENERGY
45° INCIDENCE
P PLANE = X
S PLANE = +
45.0 DEG
WAVELENGTH

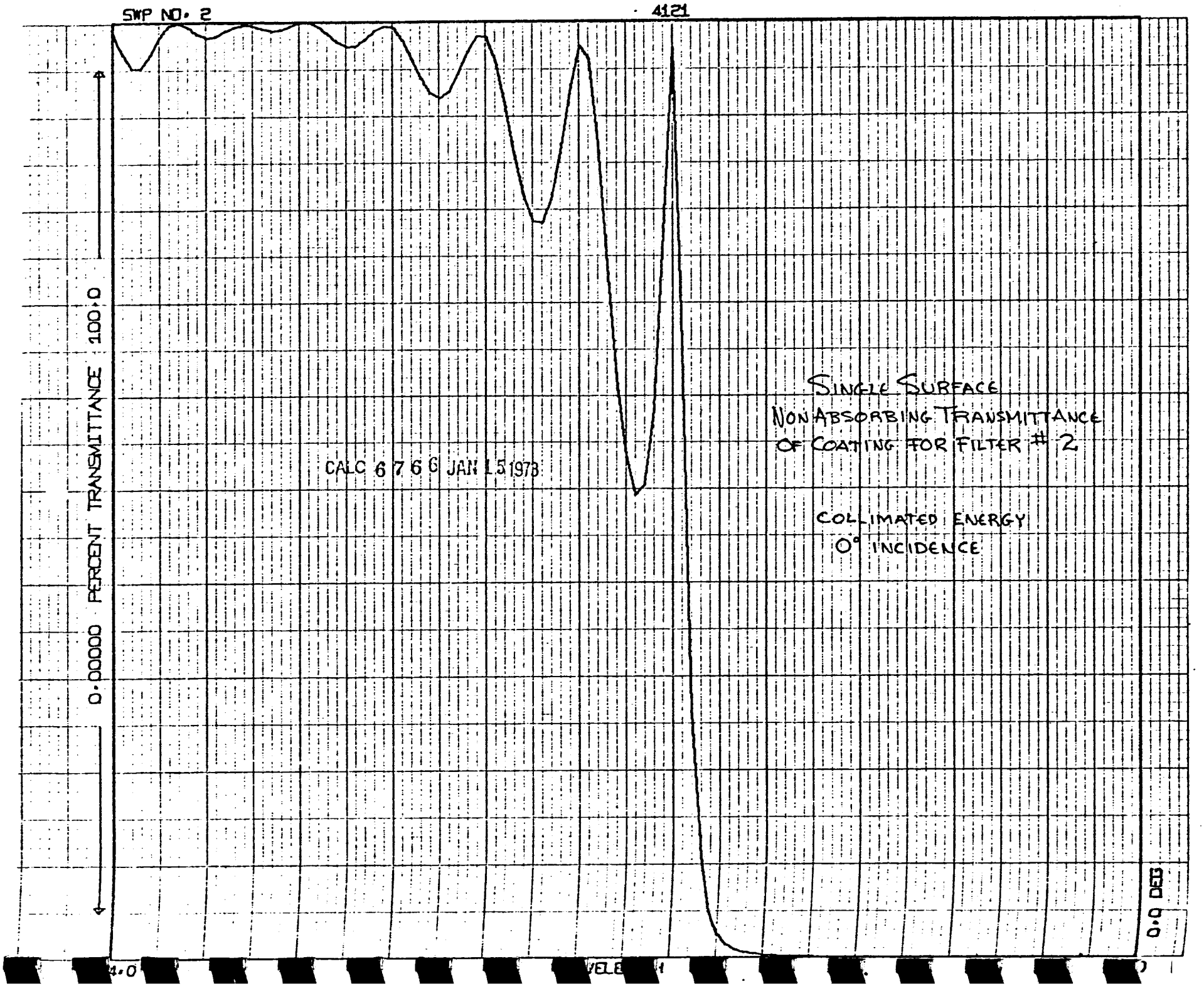
SWP NO. 2
4121
0.00000 PERCENT TRANSMITTANCE 100.0
CALC 6 7 6 6 JAN 15 1973
SINGLE SURFACE
NONABSORBING TRANSMITTANCE
OF COATING FOR FILTER # 2
COLLIMATED ENERGY
0° INCIDENCE
0.0 DEG

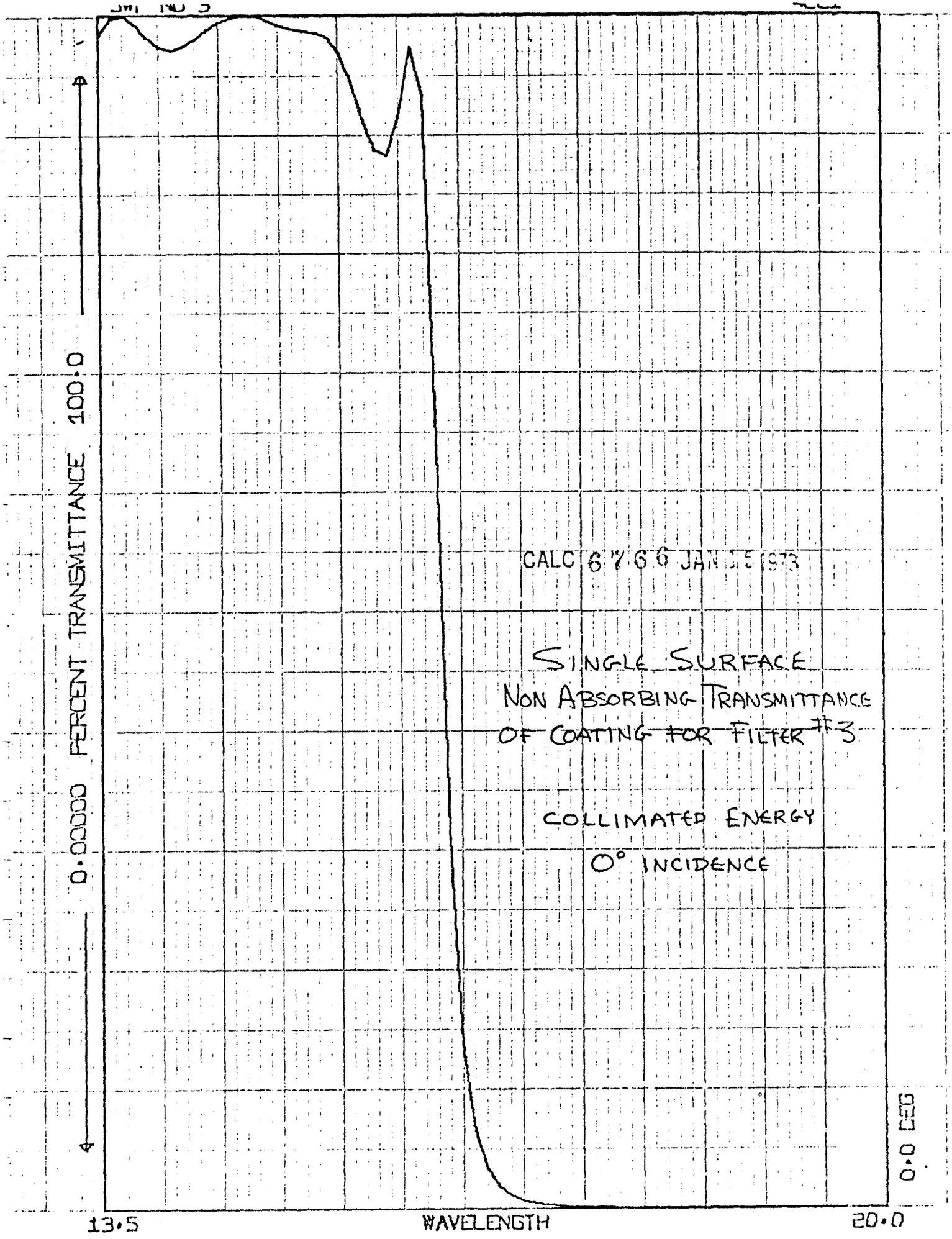
PERCENT TRANSMITTANCE
100.0
0.00000
13.5
WAVELENGTH
20.0
0.0 DEG
CALC 6 7 6 6 JAN 15 1973
SINGLE SURFACE
NON ABSORBING TRANSMITTANCE
OF COATING FOR FILTER #3
COLLIMATED ENERGY
0° INCIDENCE

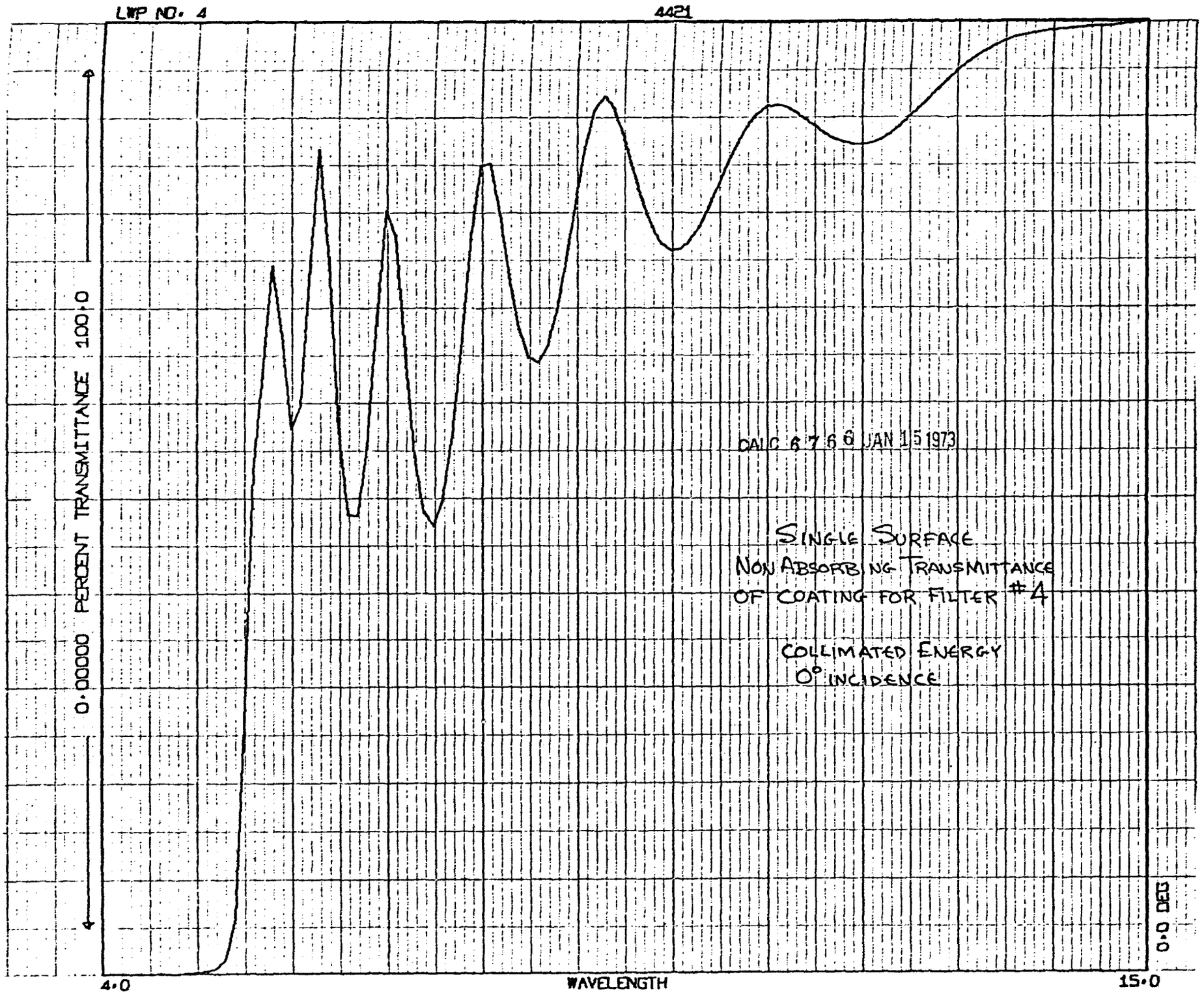
LWP NO. 4
4421
100.0
PERCENT TRANSMITTANCE
0.00000
DALC 6 7 6 6 JAN 15 1973
SINGLE SURFACE
NON ABSORBING TRANSMITTANCE
OF COATING FOR FILTER #4
COLLIMATED ENERGY
0° INCIDENCE
0.0 DEG
4.0
WAVELENGTH
15.0

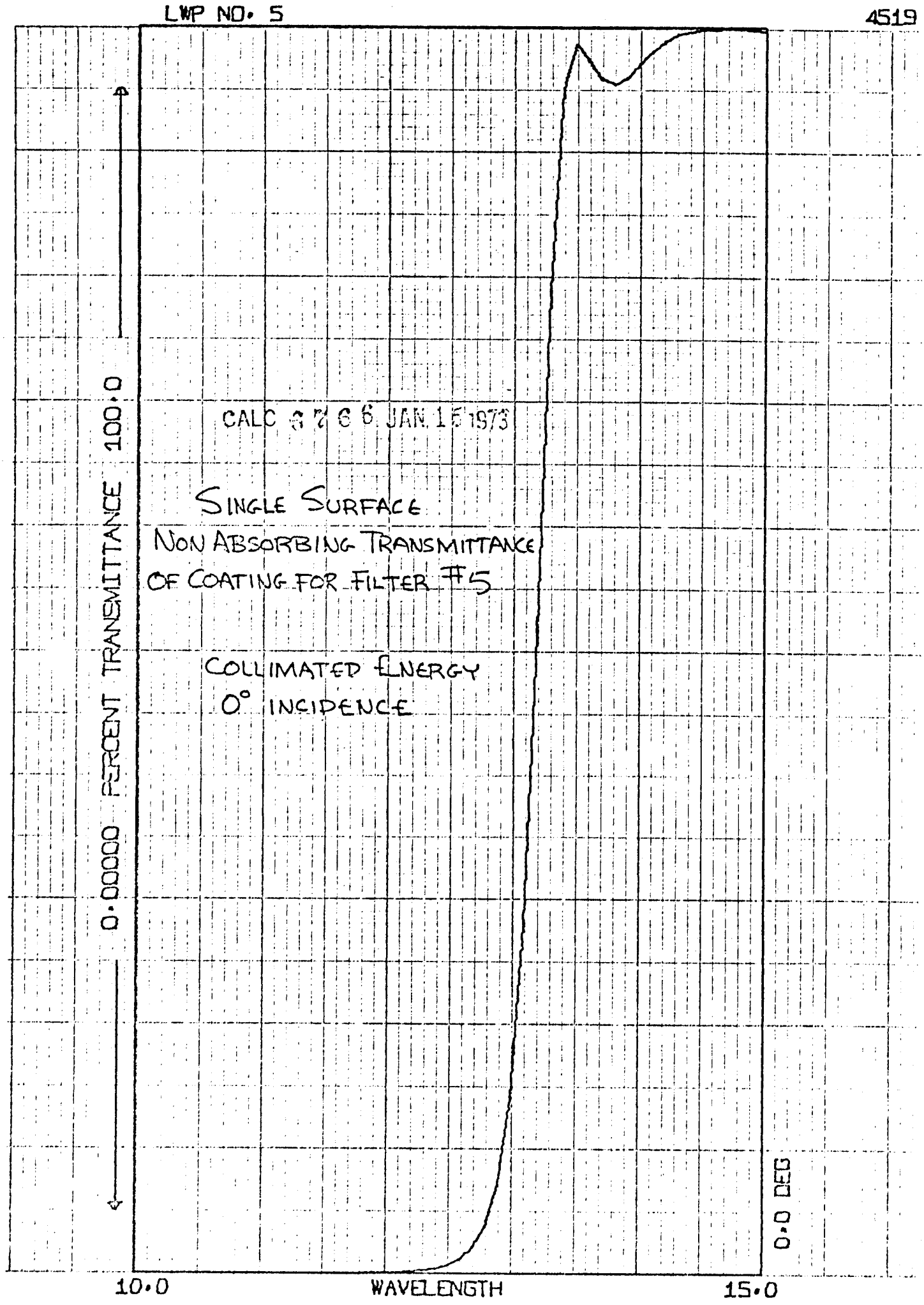
LWP NO. 5
4519
CALC 3 7 6 6 JAN 15 1973
SINGLE SURFACE
NON ABSORBING TRANSMITTANCE
OF COATING FOR FILTER #5
COLLIMATED ENERGY
0° INCIDENCE
100.0
PERCENT TRANSMITTANCE
0.00000
0.0 DEG
10.0
WAVELENGTH
15.0

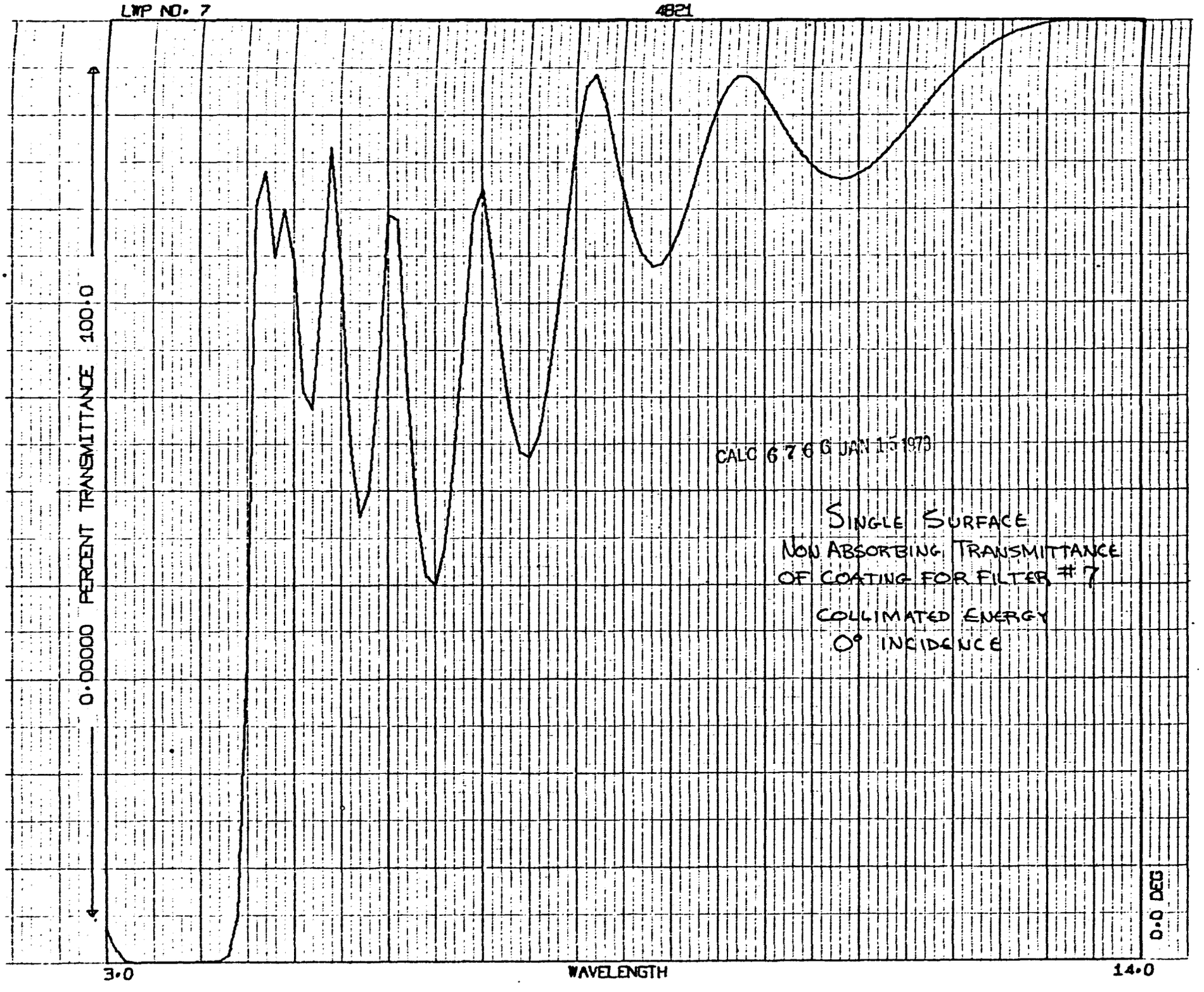
LWP NO. 7
4821
100.0
PERCENT TRANSMITTANCE
0.00000
CALC 6 7 6 6 JAN 15 1973
SINGLE SURFACE
NON ABSORBING TRANSMITTANCE
OF COATING FOR FILTER # 7
COLLIMATED ENERGY
0° INCIDENCE
0.0 DEG
3.0
WAVELENGTH
14.0

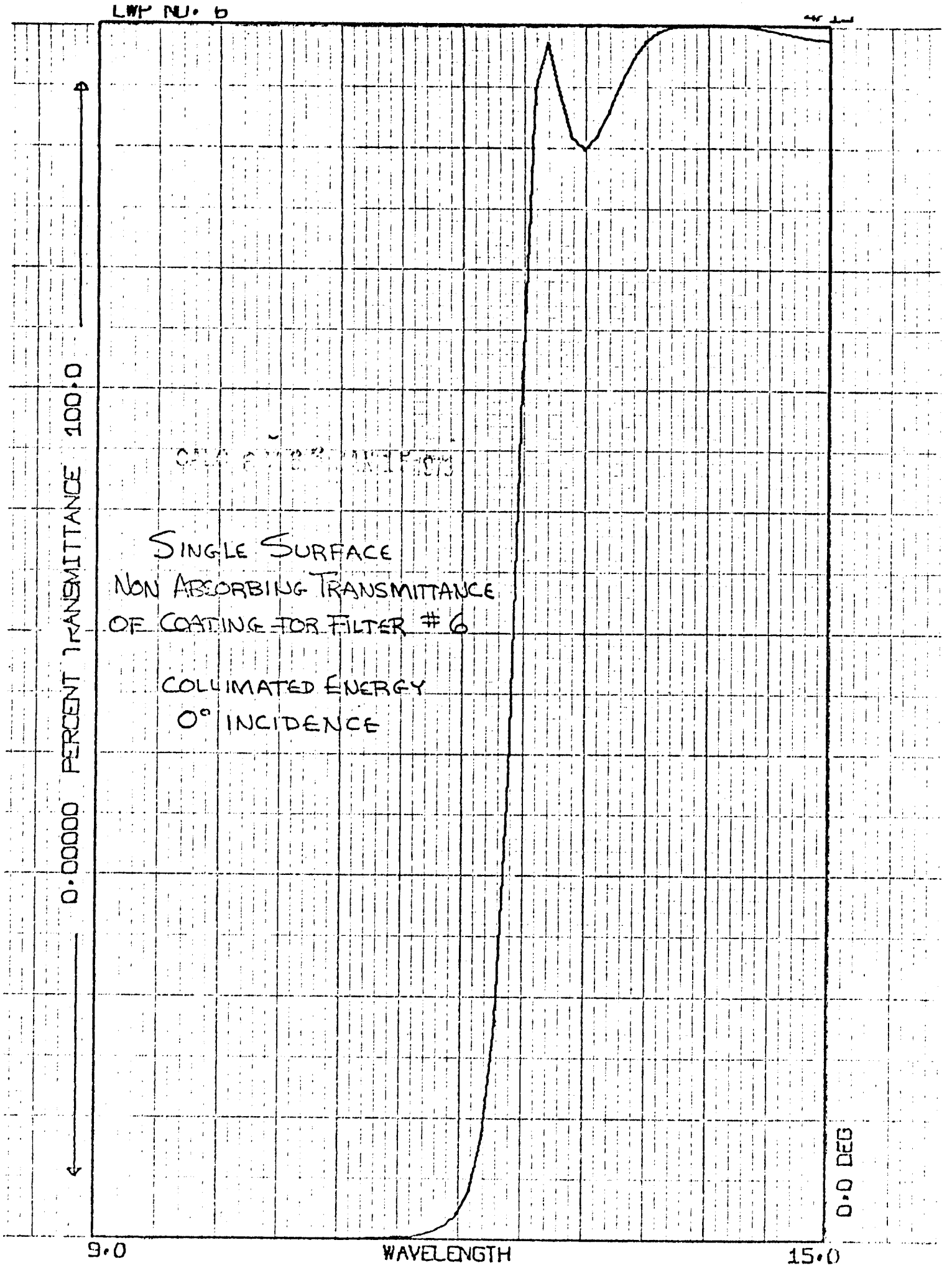
LWP NO. 6
SINGLE SURFACE
NON ABSORBING TRANSMITTANCE
OF COATING FOR FILTER #6
COLLIMATED ENERGY
0° INCIDENCE
PERCENT TRANSMITTANCE
100.0
0.00000
9.0
WAVELENGTH
15.0
0.0 DEG

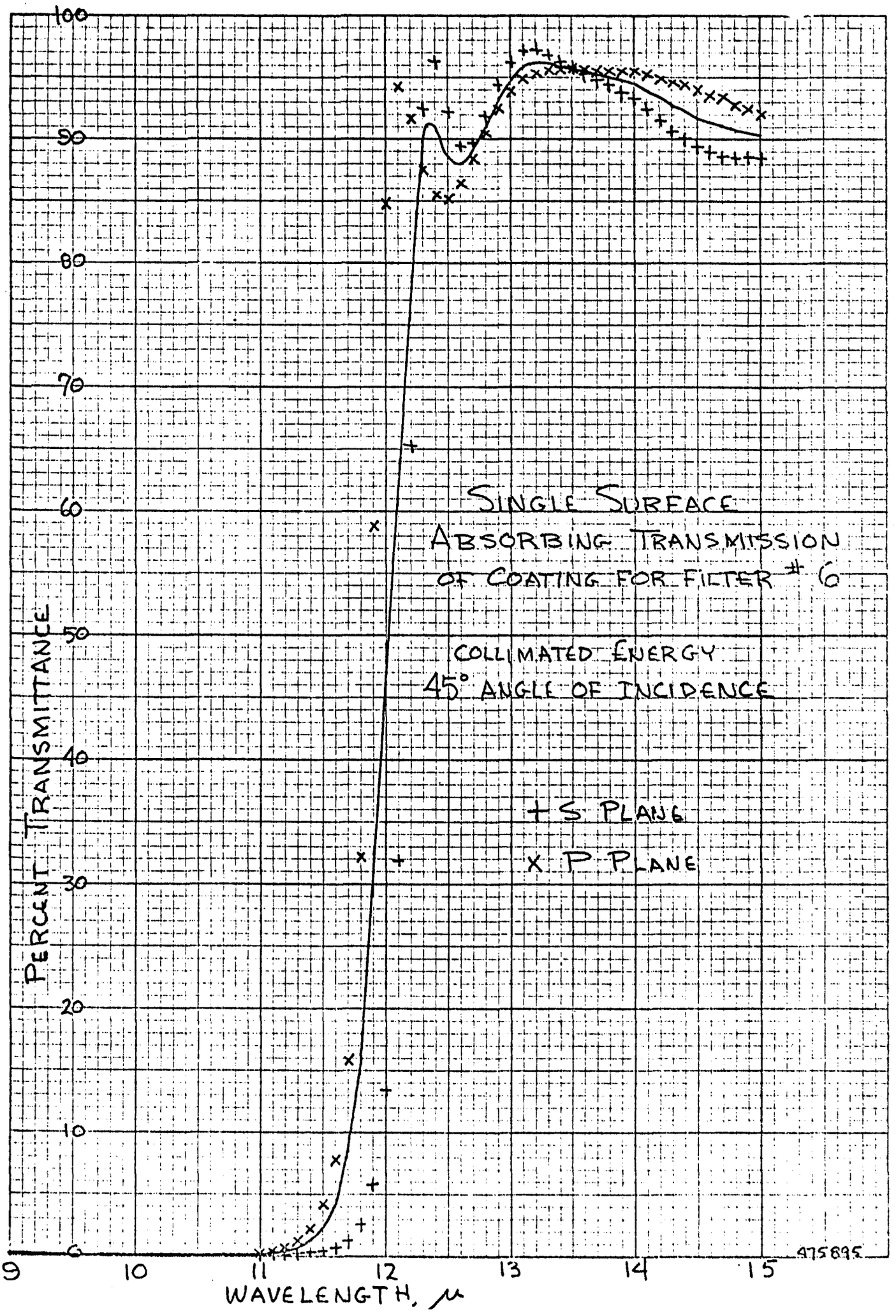

K+E 7 X 10 INCHES KEUFFEL & ESSER CO.

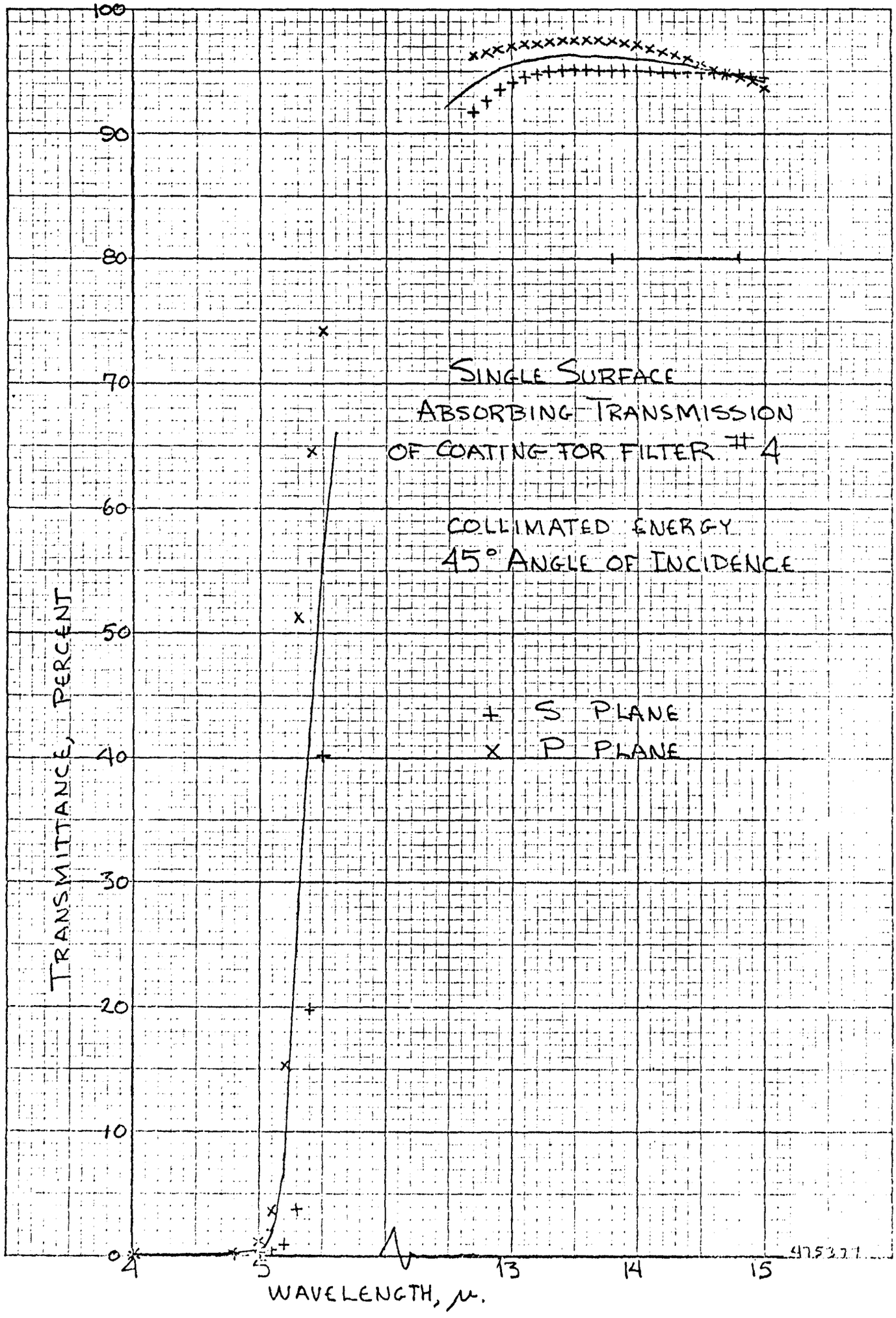

KEUFFEL & ESSER CO.
MADE IN U.S.A.

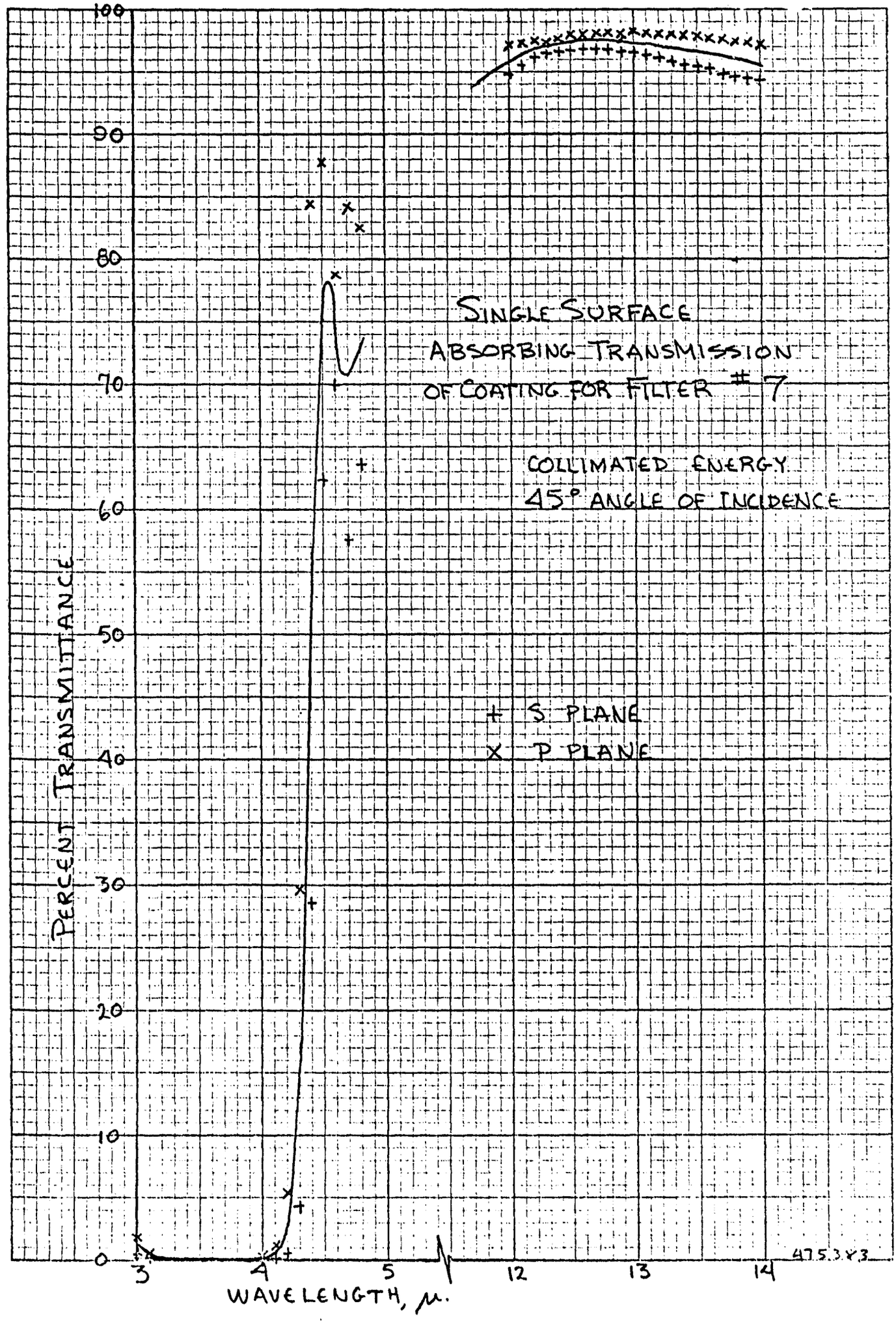
SINGLE SURFACE
ABSORBING TRANSMISSION
OF COATING FOR FILTER # 7
COLLIMATED ENERGY
45° ANGLE OF INCIDENCE
+ S PLANE
× P PLANE
PERCENT TRANSMITTANCE
WAVELENGTH, μ.
100
90
80
70
60
50
40
30
20
10
0
3
4
5
12
13
14
475.3x3

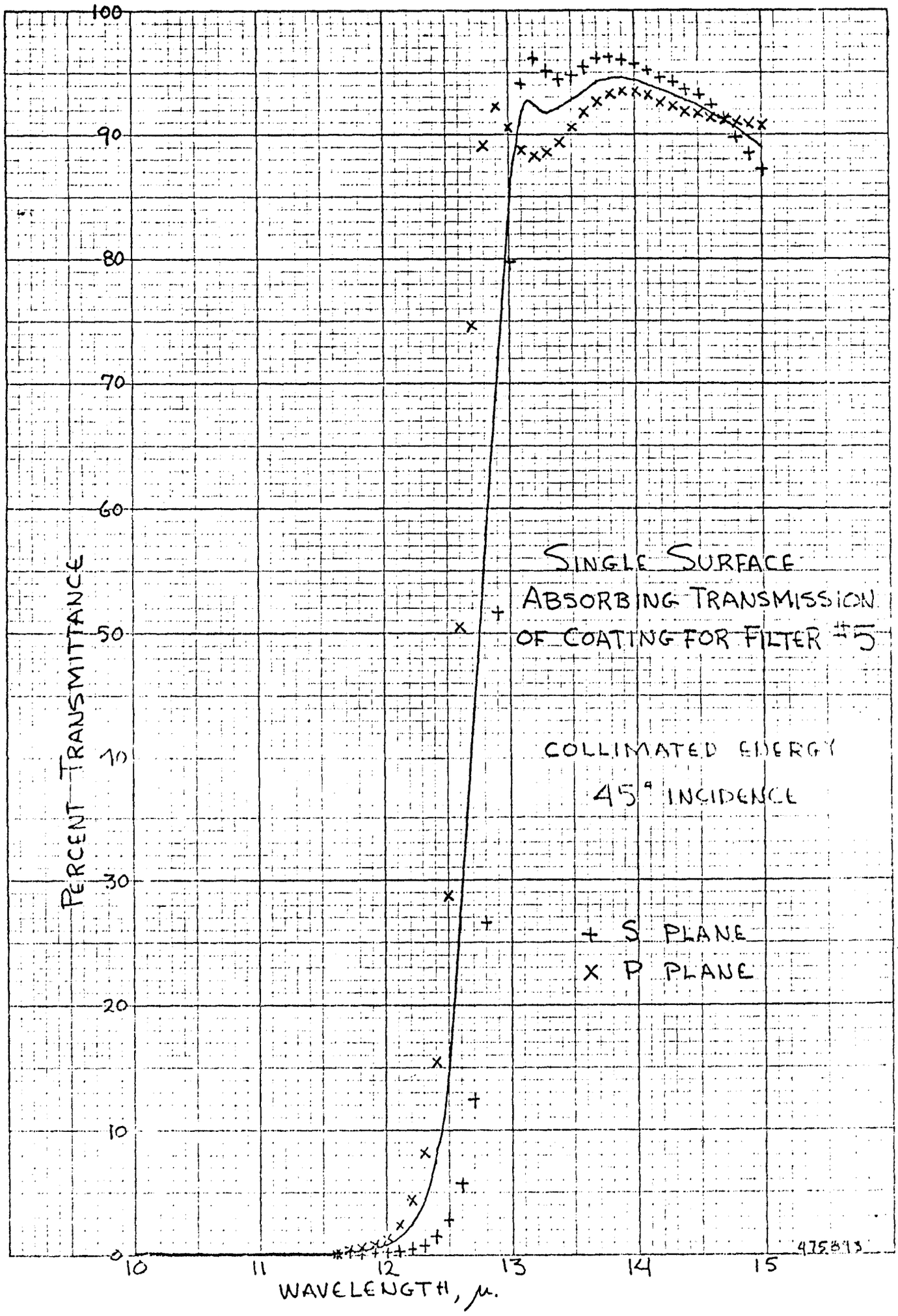
SINGLE SURFACE
ABSORBING TRANSMISSION
OF COATING FOR FILTER #5
COLLIMATED ENERGY
45° INCIDENCE
+ S PLANE
× P PLANE
PERCENT TRANSMITTANCE
WAVELENGTH, μ.
100
90
80
70
60
50
40
30
20
10
0
10
11
12
13
14
15
475893

SECTION III. ANTI-REFLECTION

III. SINGLE SURFACE ANTI-REFLECTION COATING PERFORMANCE

To eliminate back surface reflection in the region where the filter is transmitting, an anti-reflection coating must be applied. Three potential designs are shown in this section; a single layer and two multilayer coatings. One of the multilayer coatings (MLAR 1) is a very simple design in which polarization can only be reduced by narrowing the transmitting region. However, a more sophisticated design (MLAR 3) maintains the wide transmitting region and also minimizes polarization. Both absorbing and non absorbing calculations have been made for 0° and 45° angles of incidence.

One unsuccessful attempt was made to effect a reversal of the planes of polarization on MLAR 1. Apparently this is not readily accomplished with simple designs, although the coating could be shifted to longer or shorter wavelengths to make use of the reversed polarization where this occurs in the design. For instance, MLAR 1 could be used with LWP #6, by shifting the MLAR to shorter wavelengths so that the polarization crossover at 14.9μ on the MLAR was located at 13.5μ. This is a 9.5% shift to shorter wavelengths, which would result in a very good polarization match of the two coatings, and a nearly unpolarized transmitted energy from 13.2 to 14.1μ (760-710 cm^{-1}).

Note that all of these coatings can be shifted to longer or shorter wavelengths, with nearly identical <u>non-absorbing</u> performance.

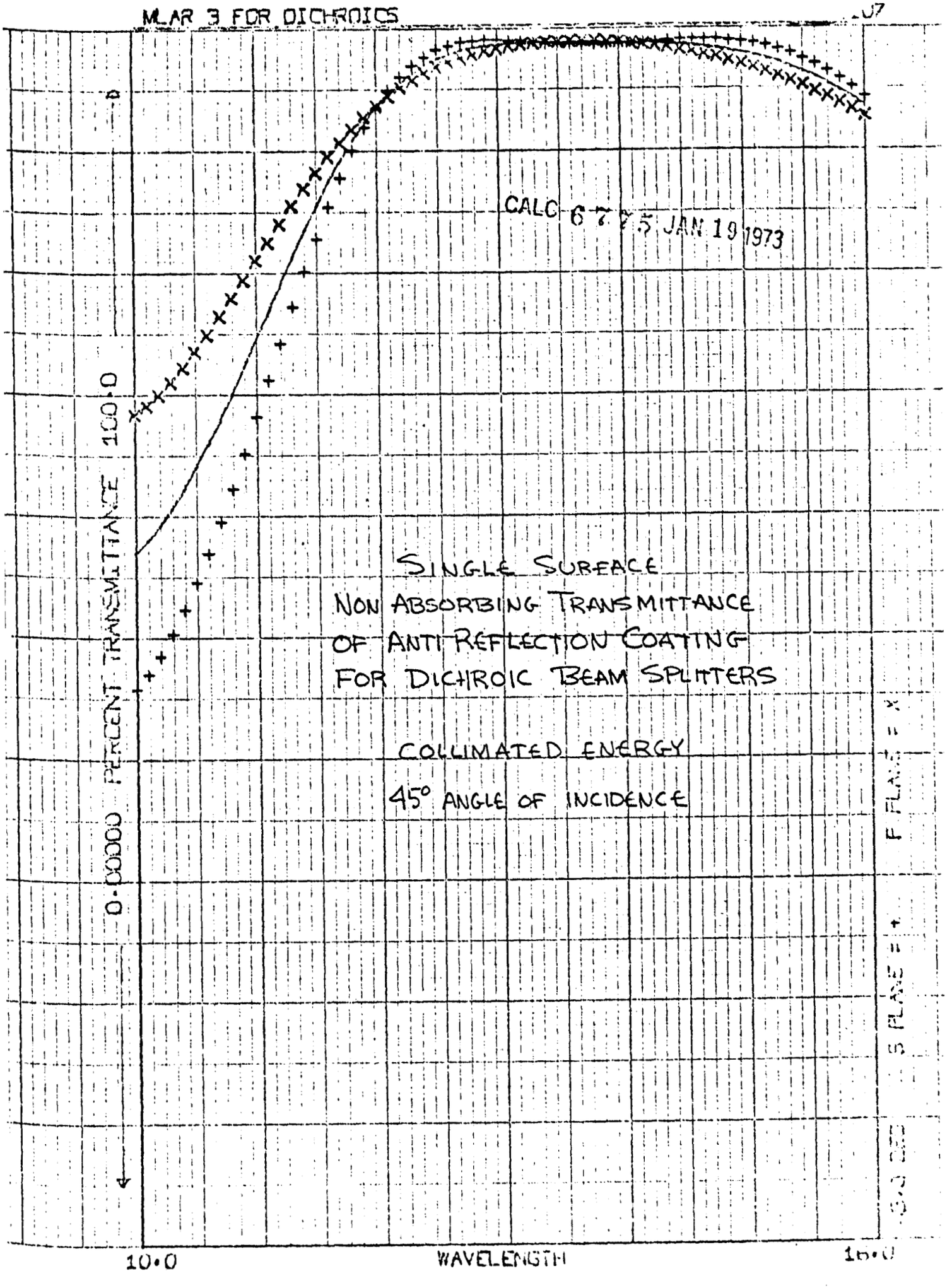
MLAR 3 FOR DICHROICS
CALC 6 7 5 JAN 19 1973
SINGLE SURFACE
NON ABSORBING TRANSMITTANCE
OF ANTI REFLECTION COATING
FOR DICHROIC BEAM SPLITTERS
COLLIMATED ENERGY
45° ANGLE OF INCIDENCE
100·0
PERCENT TRANSMITTANCE
0·00000
10·0
WAVELENGTH
S PLANE = +
P PLANE = X

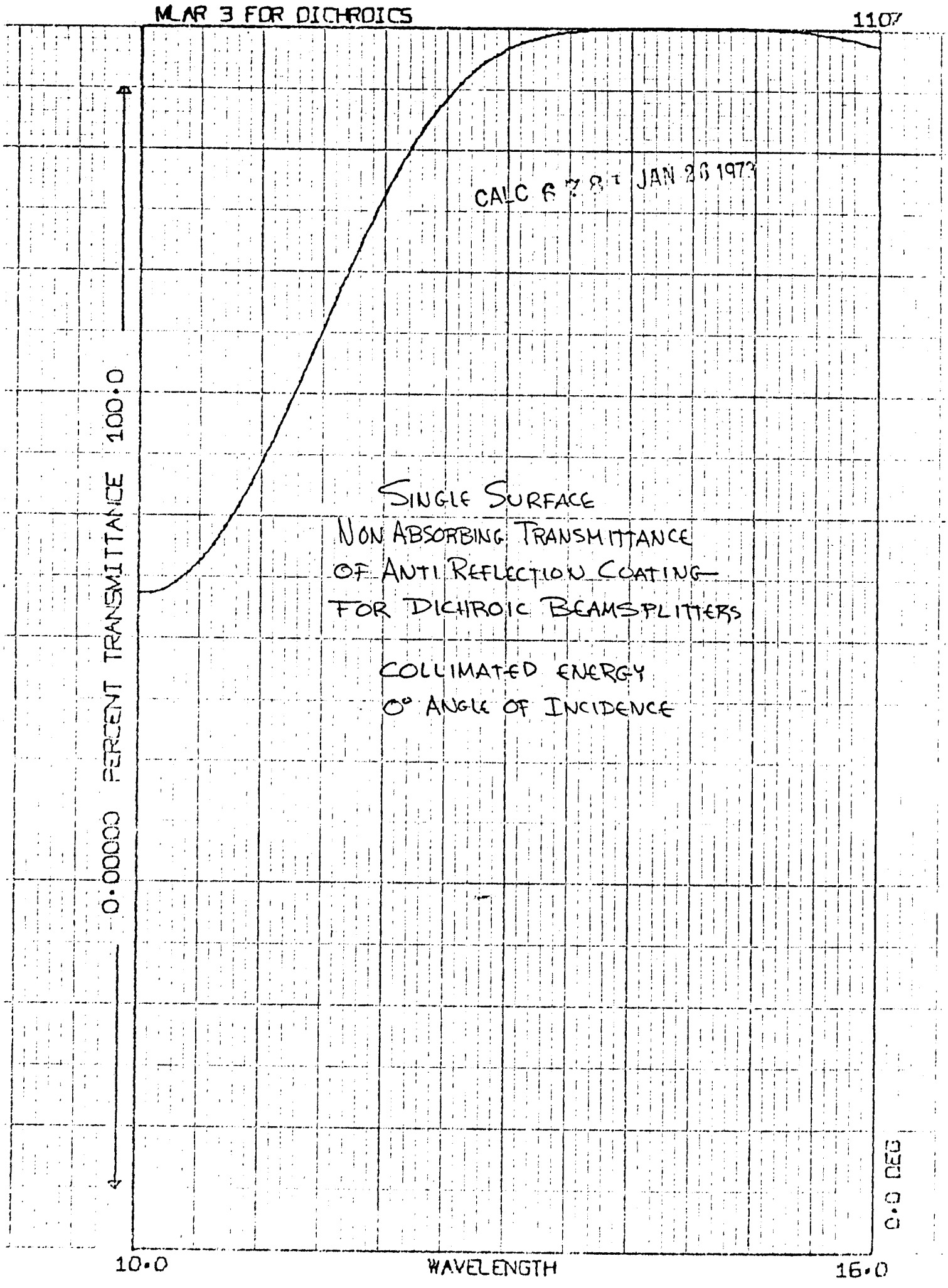
MLAR 3 FOR DICHROICS
1107
CALC 6 7 8 1 JAN 26 1973
SINGLE SURFACE
NON ABSORBING TRANSMITTANCE
OF ANTI REFLECTION COATING
FOR DICHROIC BEAMSPLITTERS
COLLIMATED ENERGY
0° ANGLE OF INCIDENCE
PERCENT TRANSMITTANCE
100.0
0.00000
10.0
WAVELENGTH
16.0

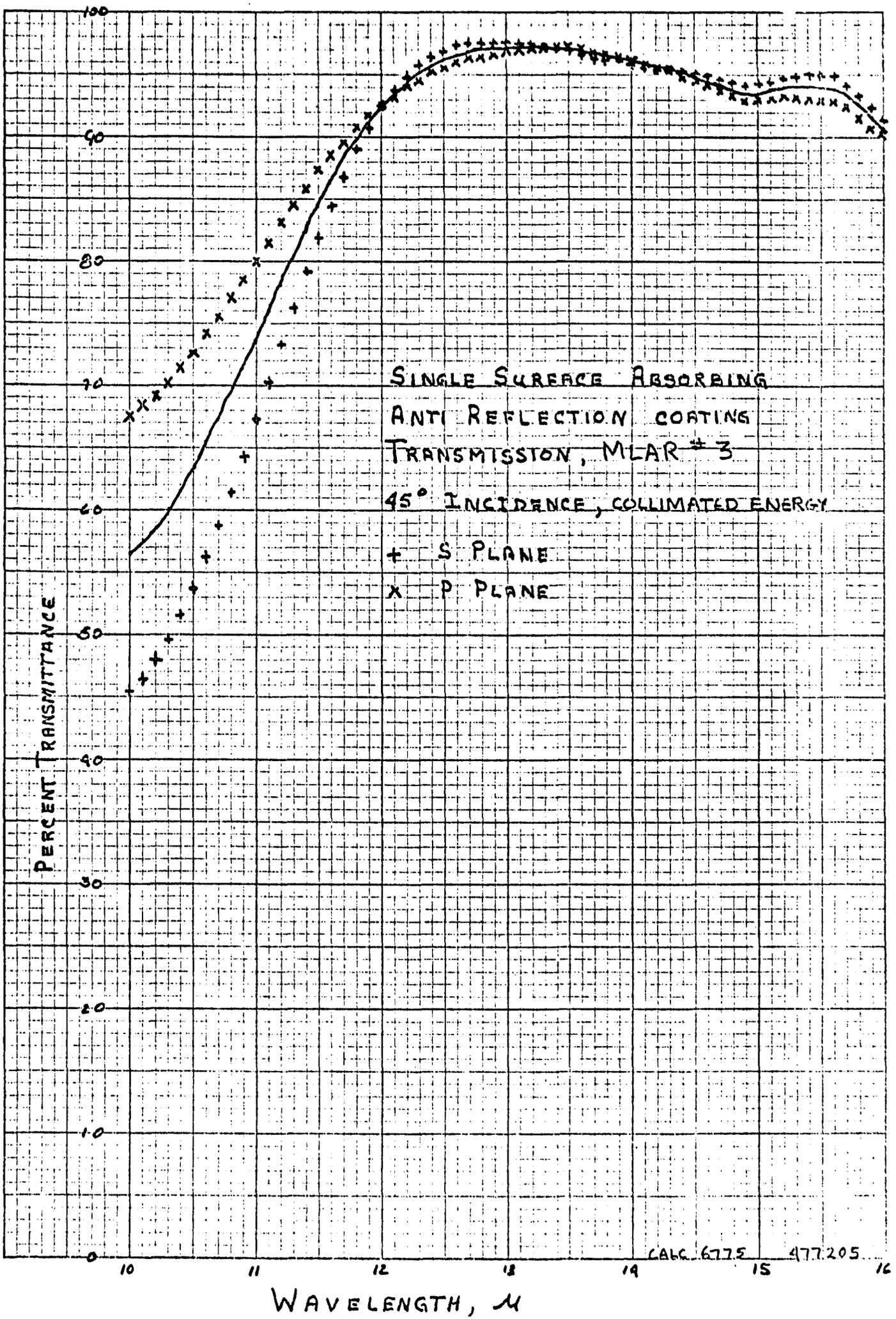

KEUFFEL & ESSER CO.
7 X 10 INCHES
MADE IN U.S.A.

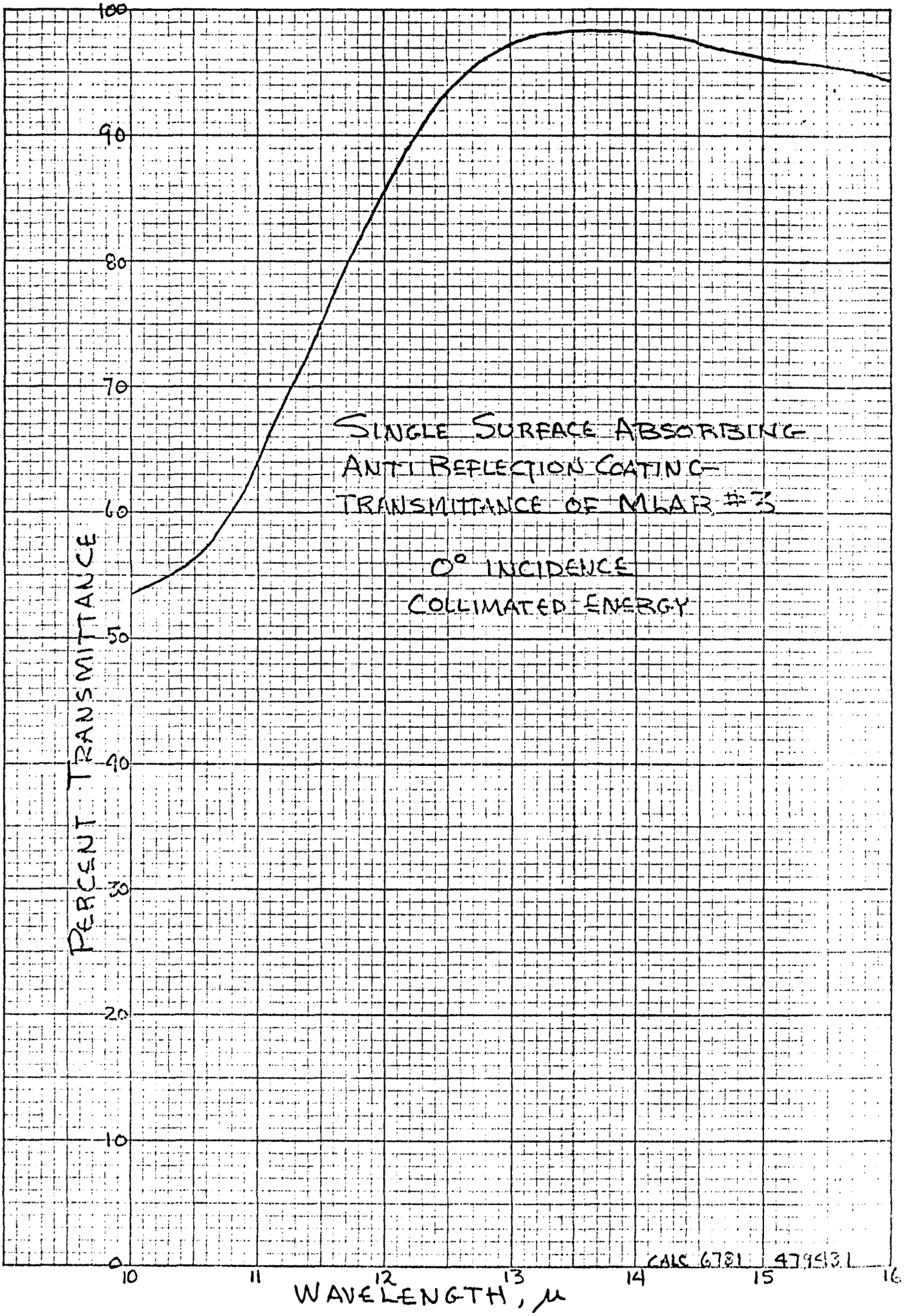

K+E 10 X 10 TO THE INCH 46 0782
7 X 10 INCHES MADE IN U.S.A.
KEUFFEL & ESSER CO.

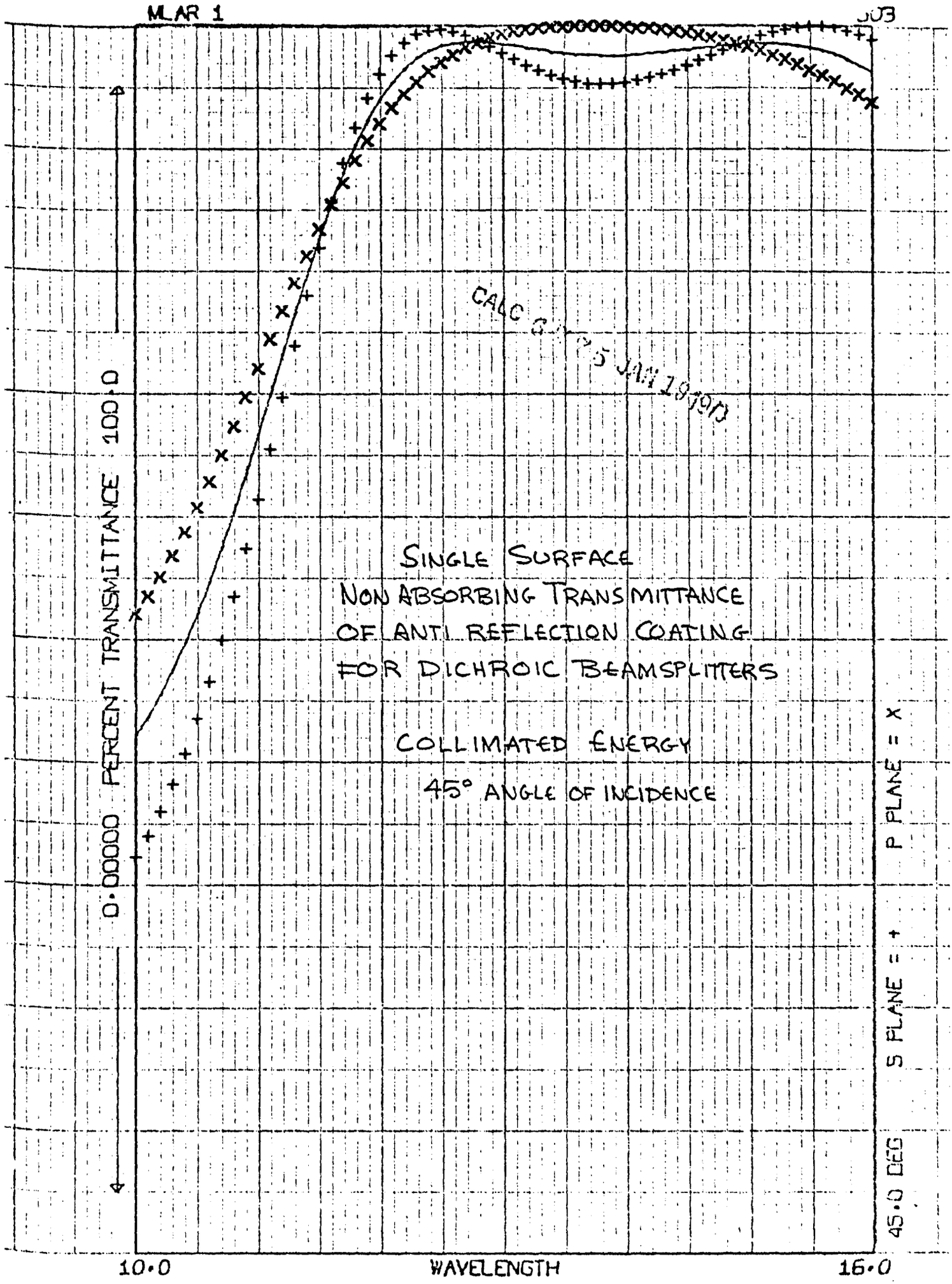
MLAR 1
CALC 25 JAN 1990
SINGLE SURFACE
NON ABSORBING TRANSMITTANCE
OF ANTI REFLECTION COATING
FOR DICHROIC BEAMSPLITTERS
COLLIMATED ENERGY
45° ANGLE OF INCIDENCE
100.0
PERCENT TRANSMITTANCE
0.00000
10.0
WAVELENGTH
16.0
P PLANE = X
S PLANE = +
45.0 DEG

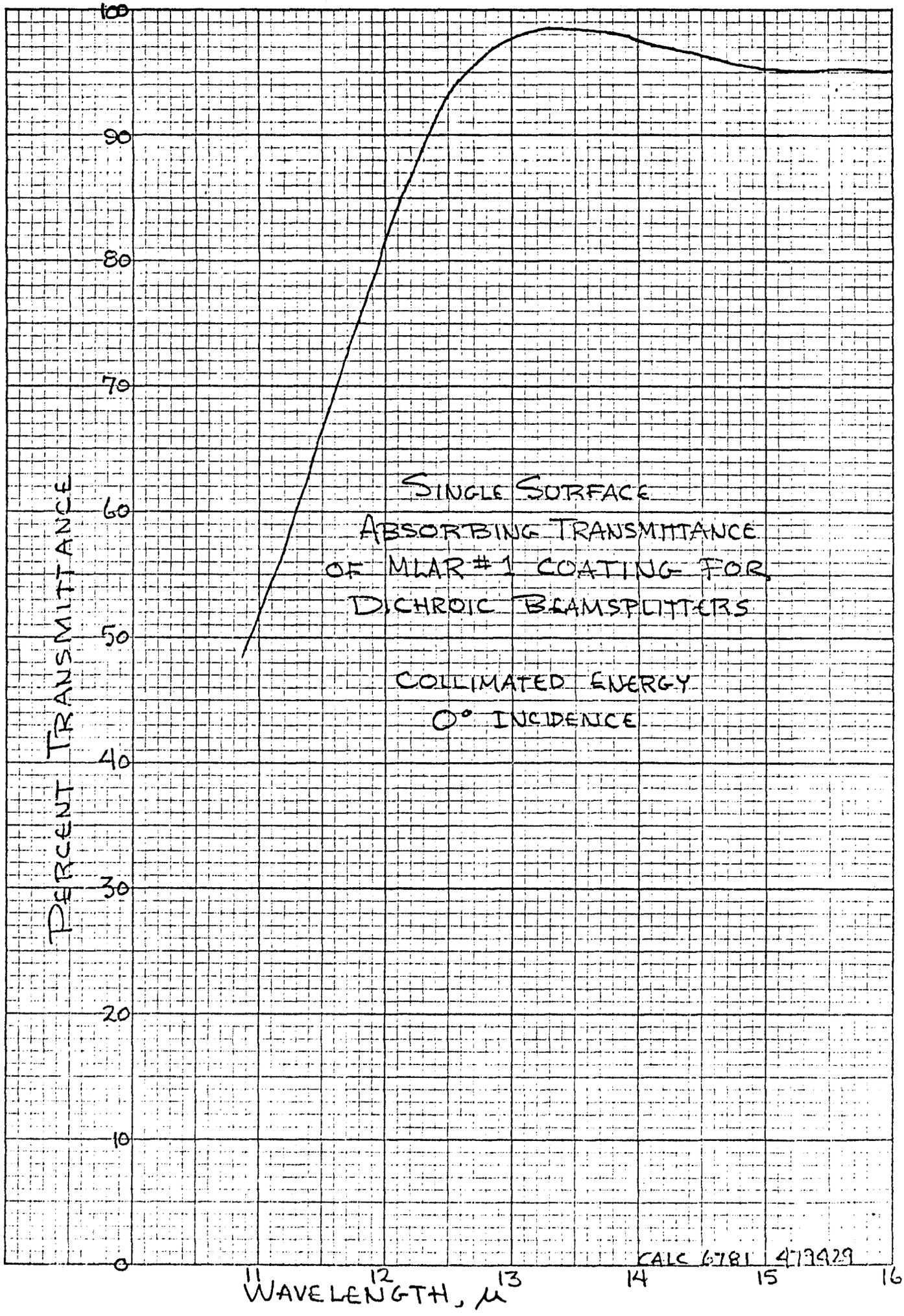

K&E 10 X 10 TO THE INCH 46 0782
7 X 10 INCHES MADE IN U.S.A.
KEUFFEL & ESSER CO.

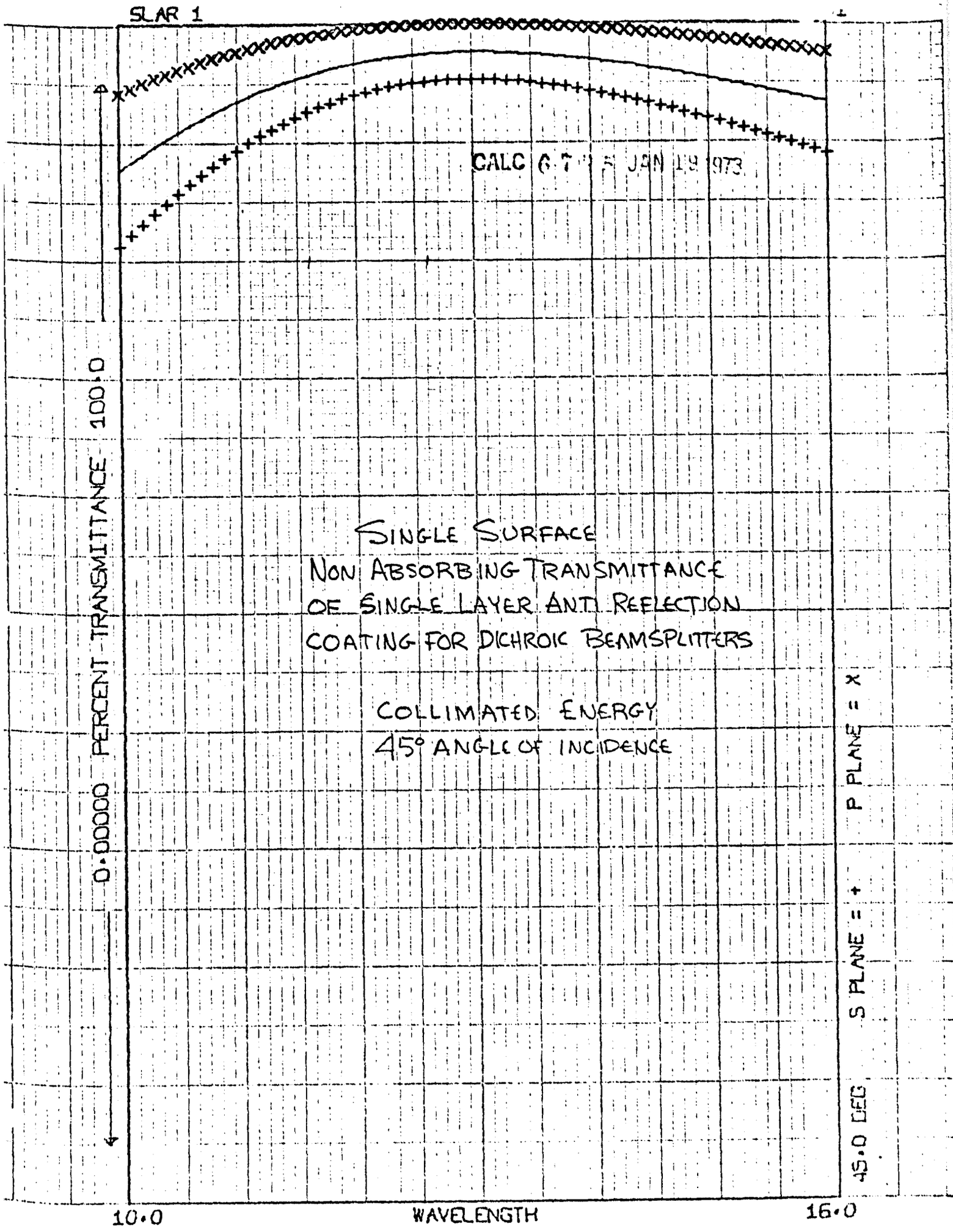
SLAR 1
CALC 6 7 5 JAN 19 1973
100.0
PERCENT TRANSMITTANCE
0.00000
SINGLE SURFACE
NON ABSORBING TRANSMITTANCE
OF SINGLE LAYER ANTI REFLECTION
COATING FOR DICHROIC BEAMSPLITTERS
COLLIMATED ENERGY
45° ANGLE OF INCIDENCE
P PLANE = X
S PLANE = +
45.0 DEG
10.0
WAVELENGTH
16.0

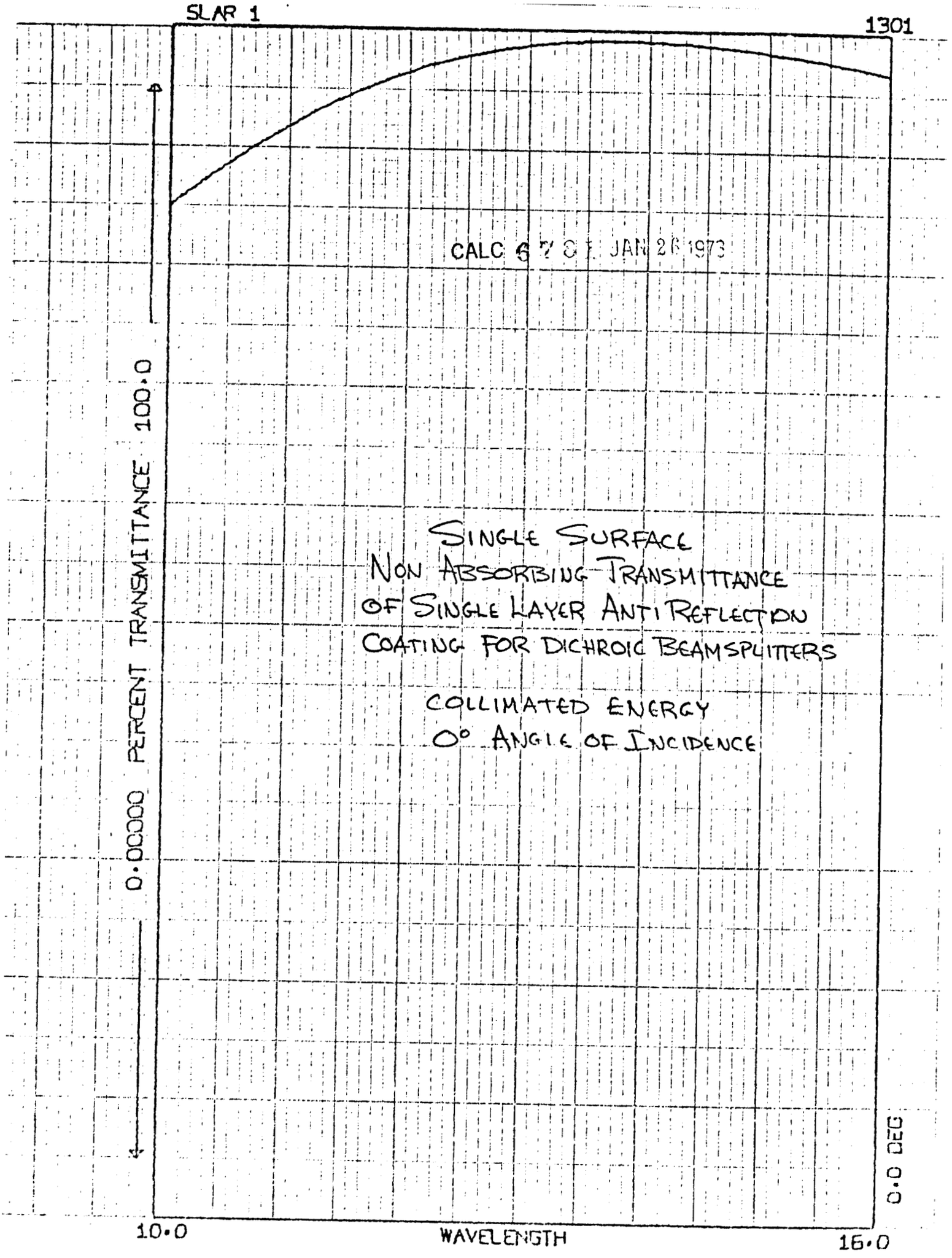
SLAR 1
1301
CALC 6 7 8 1 JAN 26 1973
SINGLE SURFACE
NON ABSORBING TRANSMITTANCE
OF SINGLE LAYER ANTI REFLECTION
COATING FOR DICHROIC BEAMSPLITTERS
COLLIMATED ENERGY
0° ANGLE OF INCIDENCE
100.0
PERCENT TRANSMITTANCE
0.00000
0.0 DEG
10.0
WAVELENGTH
16.0

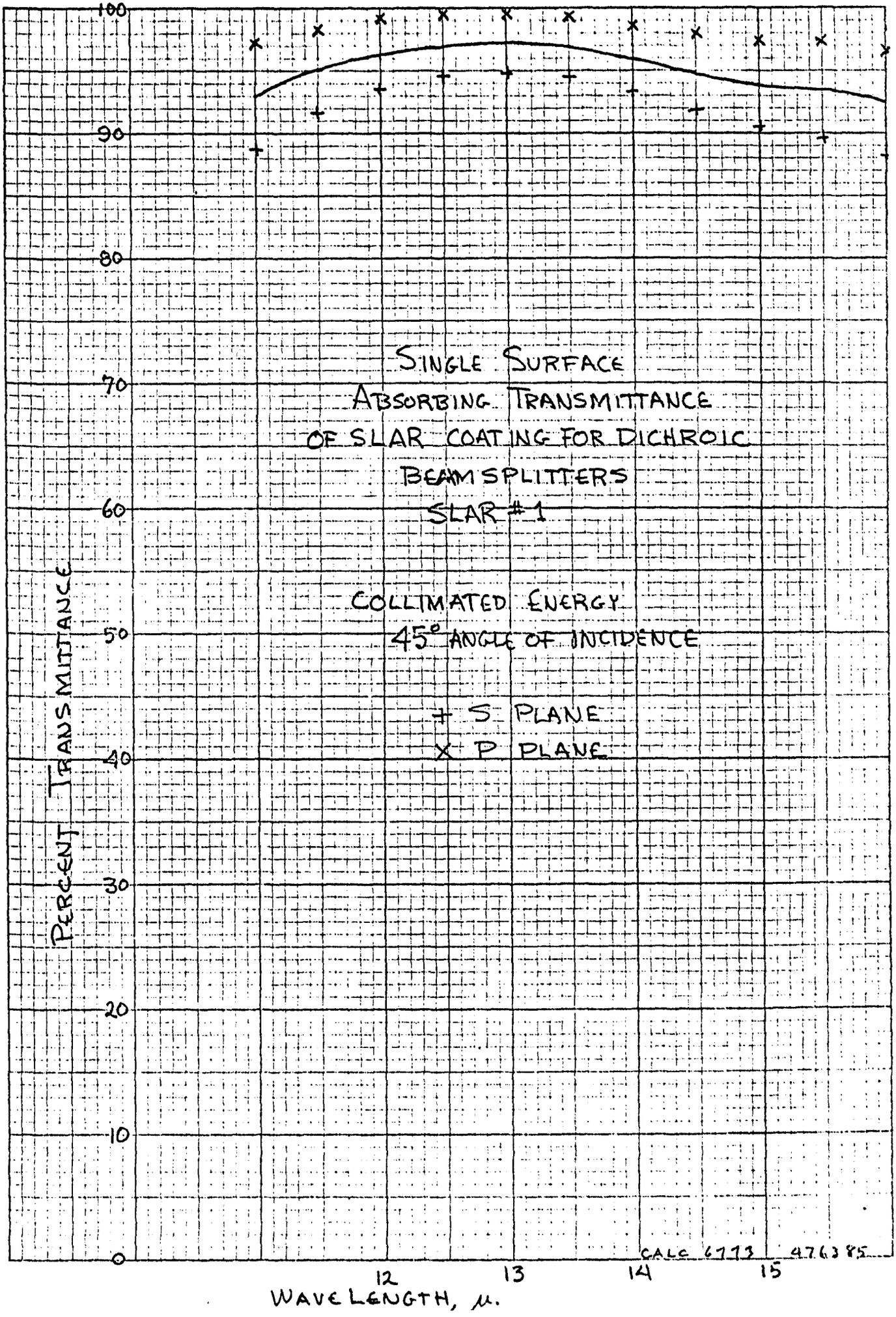

KEUFFEL & ESSER CO.

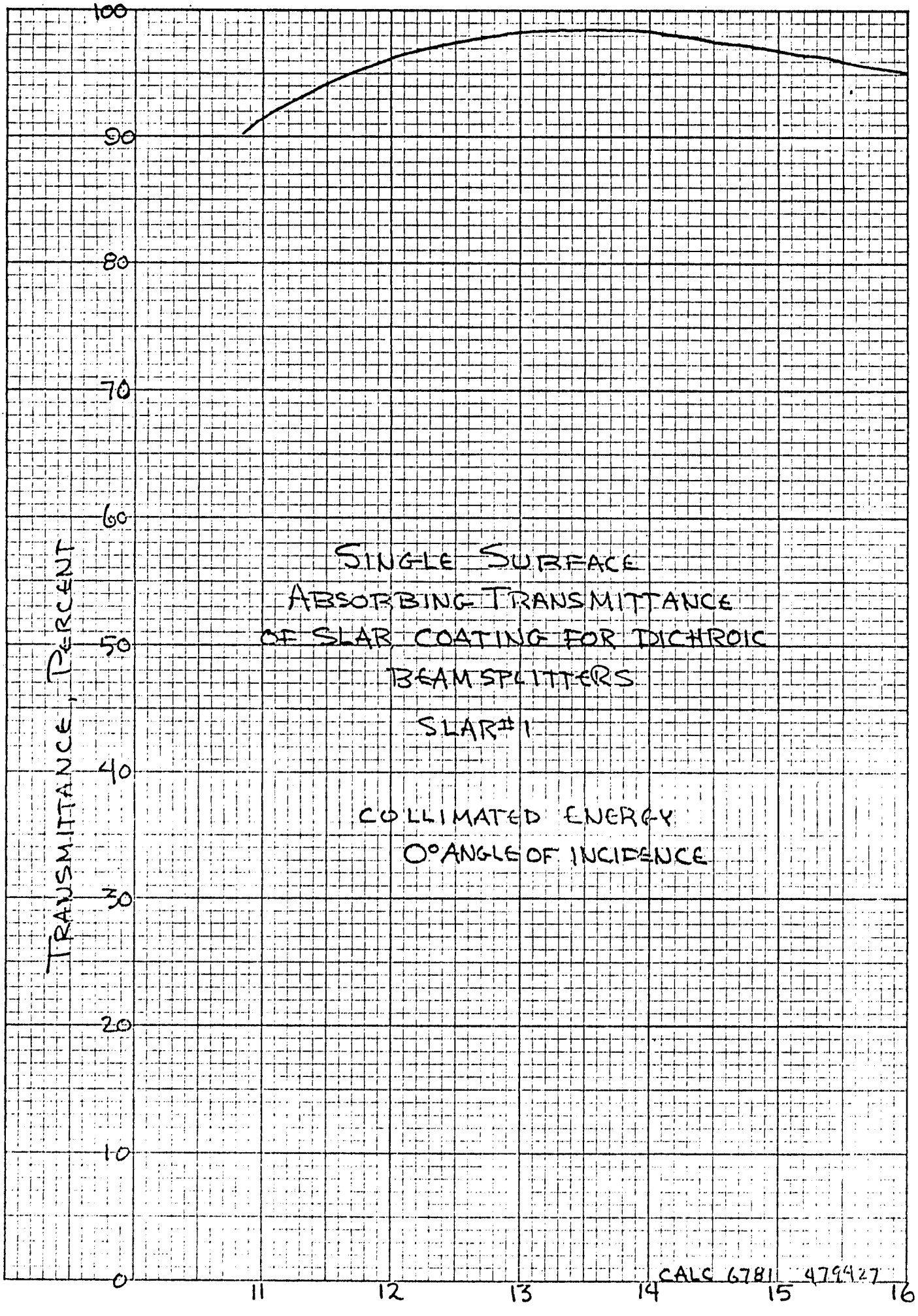

K&E 10 X 10 TO THE INCH 46 0782
7 X 10 INCHES MADE IN U.S.A.
KEUFFEL & ESSER CO.

SECTION IV. SUBSTRATE

IV. SUBSTRATE PERFORMANCE

The two curves in this section show the transmittance of germanium substrate. The first curve has been hand plotted from spectrophotometer scans of uncoated germanium substrate. Germanium has an index of refraction of 4.0, so that each surface reflects 36%. Transmittance through an uncoated non-absorbing element would be 47%, however germanium has some absorption in the transmitting range of the dichroic beamsplitters. Curves are presented to show this effect and the effect of reducing substrate thickness.

The second curve, which shows the "Internal Transmittance of Germanium", is the maximum transmittance that can be achieved for the actual measured transmittance shown on the first figure. Surface reflectance has been reduced to zero for this curve.

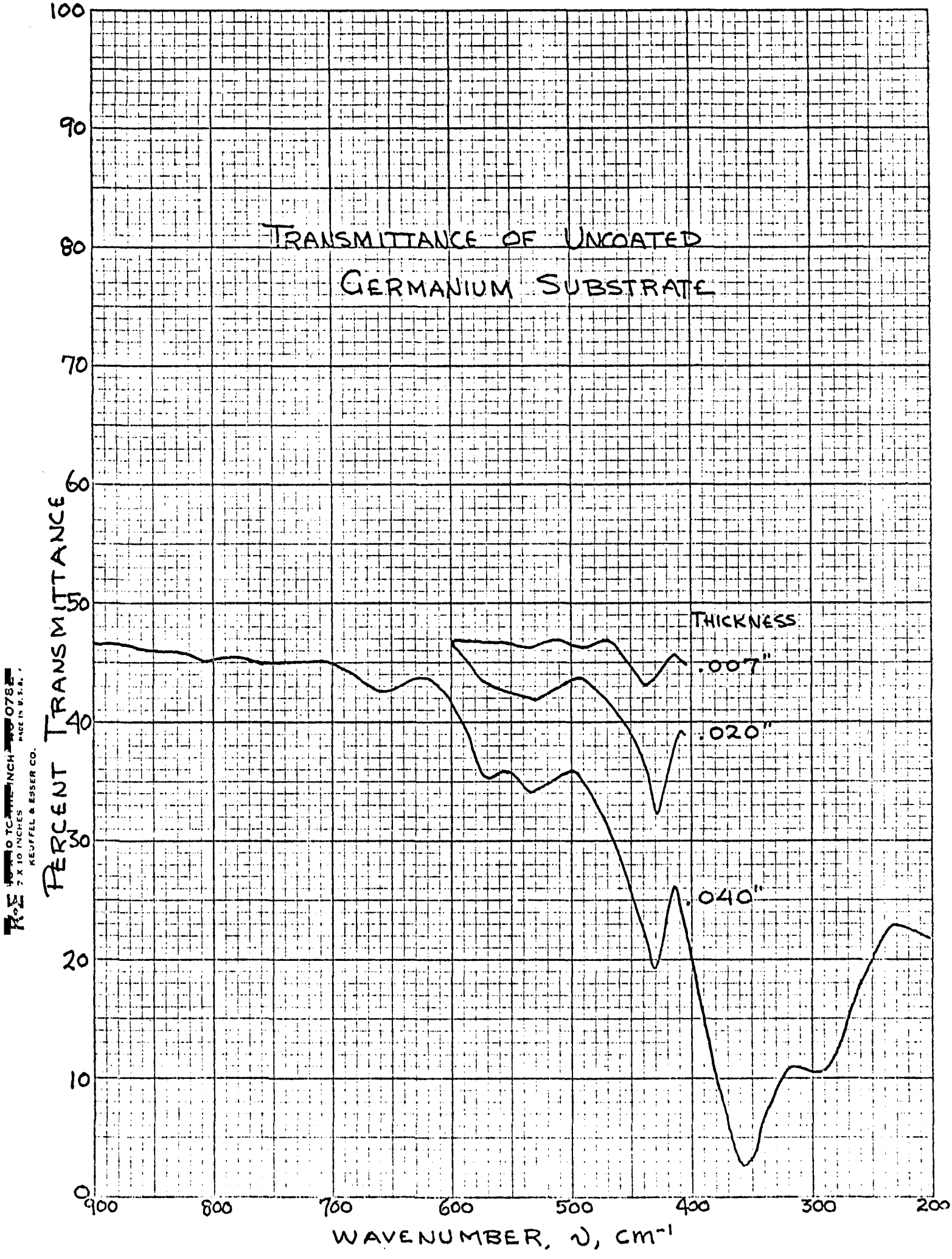
TRANSMITTANCE OF UNCOATED
GERMANIUM SUBSTRATE
THICKNESS
.007"
.020"
.040"
PERCENT TRANSMITTANCE
WAVENUMBER, ν, cm⁻¹
100
90
80
70
60
50
40
30
20
10
0
900
800
700
600
500
400
300
200
KEUFFEL & ESSER CO.
MADE IN U.S.A.

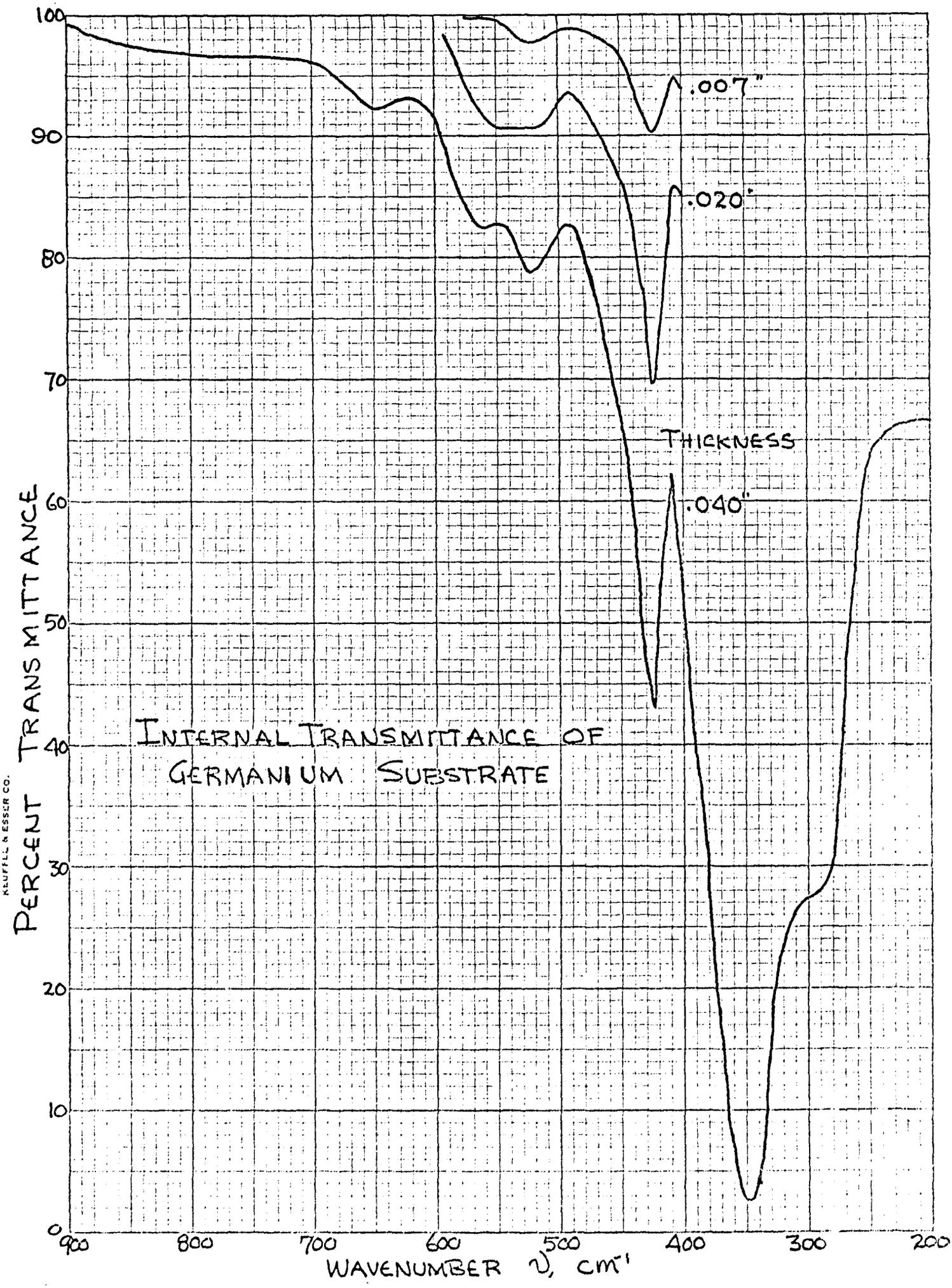

K&E 10 X 10 TO THE INCH 46 0782
7 X 10 INCHES MADE IN U.S.A.
KEUFFEL & ESSER CO.

SECTION V. OVERALL PERFORMANCE

V. OVERALL ABSORBING PERFORMANCE OF FILTERS FOUR AND SEVEN

Sample calculations of the overall absorbing transmittance of two filters has been calculated at both 0° and 45° incidence, and the computer plots are included in this section. The calculation for LWP #4 was inadvertently calculated to only 9μ, rather than 4μ. However, since this is a time consuming calculation, and the high reflecting region is not significantly polarizing, it was not re-calculated.

The two filters presented will provide information on the overall performance compared to approximate estimates made from single surface calculations. It appears that a flatter transmittance response over the wavelength range of interest could be achieved by shifting the MLAR to longer wavelengths, to take advantage of the transmission increasing with increasing wavelength in the lower region of the high transmitting band. There is also a possibility of slight modifications to the LWP design to achieve an overall flatter response if required.

The dependent variable on the ordinate is 0-100% transmittance, and the independent variable on the abscissa is wavelength (microns). The first plot covers the 9-15μ wavelength range, with a spacing of 1μ/inch.

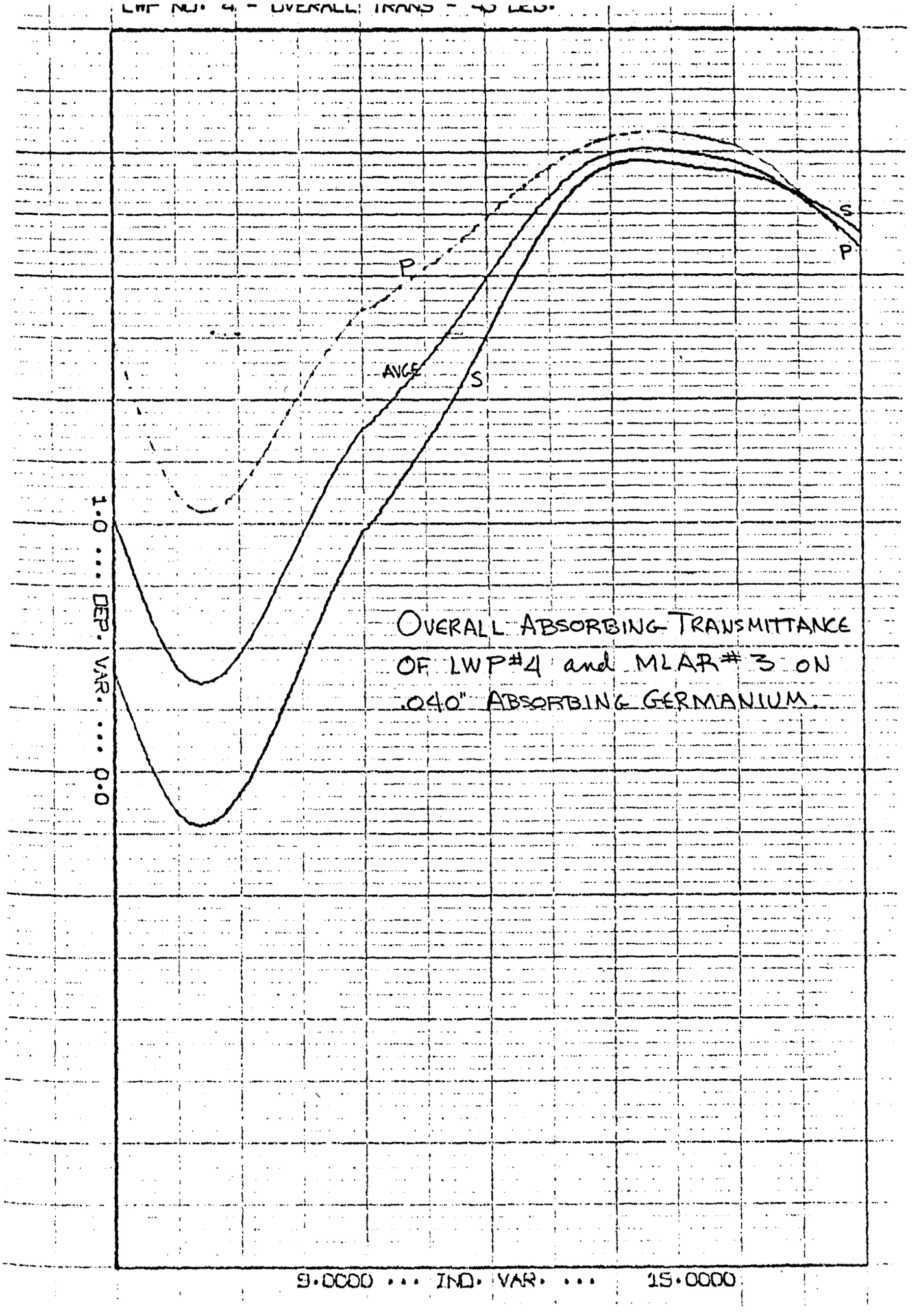
LWP NO. 4 - OVERALL TRANS - 40 DEG.
P
AVGE
S
S
P
1.0 ... DEP. VAR. ... 0.0
9.0000 ... IND. VAR. ... 15.0000
OVERALL ABSORBING TRANSMITTANCE
OF LWP#4 and MLAR# 3 ON
.040" ABSORBING GERMANIUM.

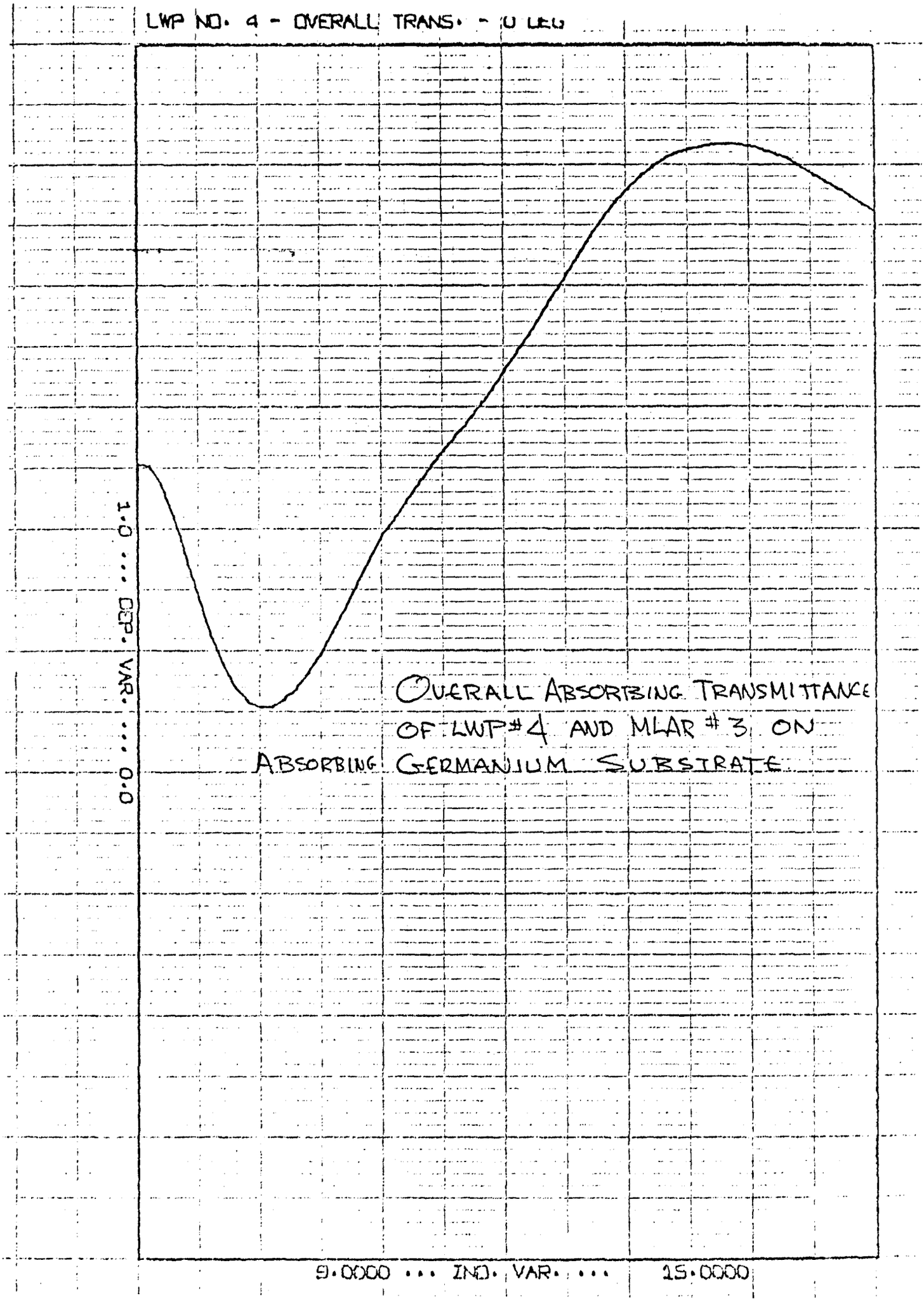
LWP NO. 4 - OVERALL TRANS. - 0 DEG
1.0 ... DEP. VAR. ... 0.0
9.0000 ... IND. VAR. ... 15.0000
OVERALL ABSORBING TRANSMITTANCE
OF LWP #4 AND MLAR # 3 ON
ABSORBING GERMANIUM SUBSTRATE

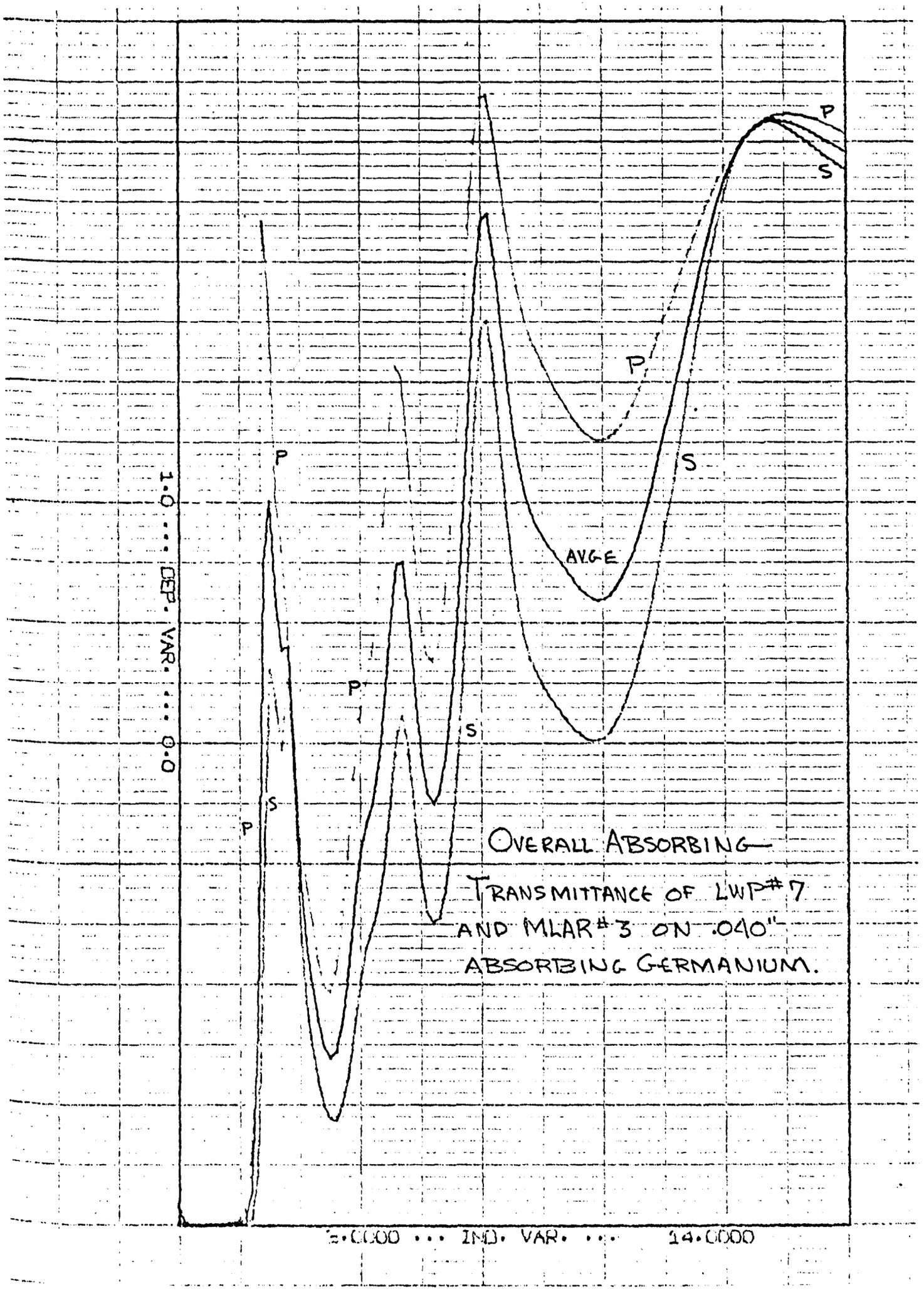
P
S
P
S
P
S
P
S
P
S
AVG-E
1.0 ... DEP. VAR. ... 0.0
=.0000 ... IND. VAR. ... 14.0000
OVERALL ABSORBING—
TRANSMITTANCE OF LWP#7
AND MLAR#3 ON .040"
ABSORBING GERMANIUM.

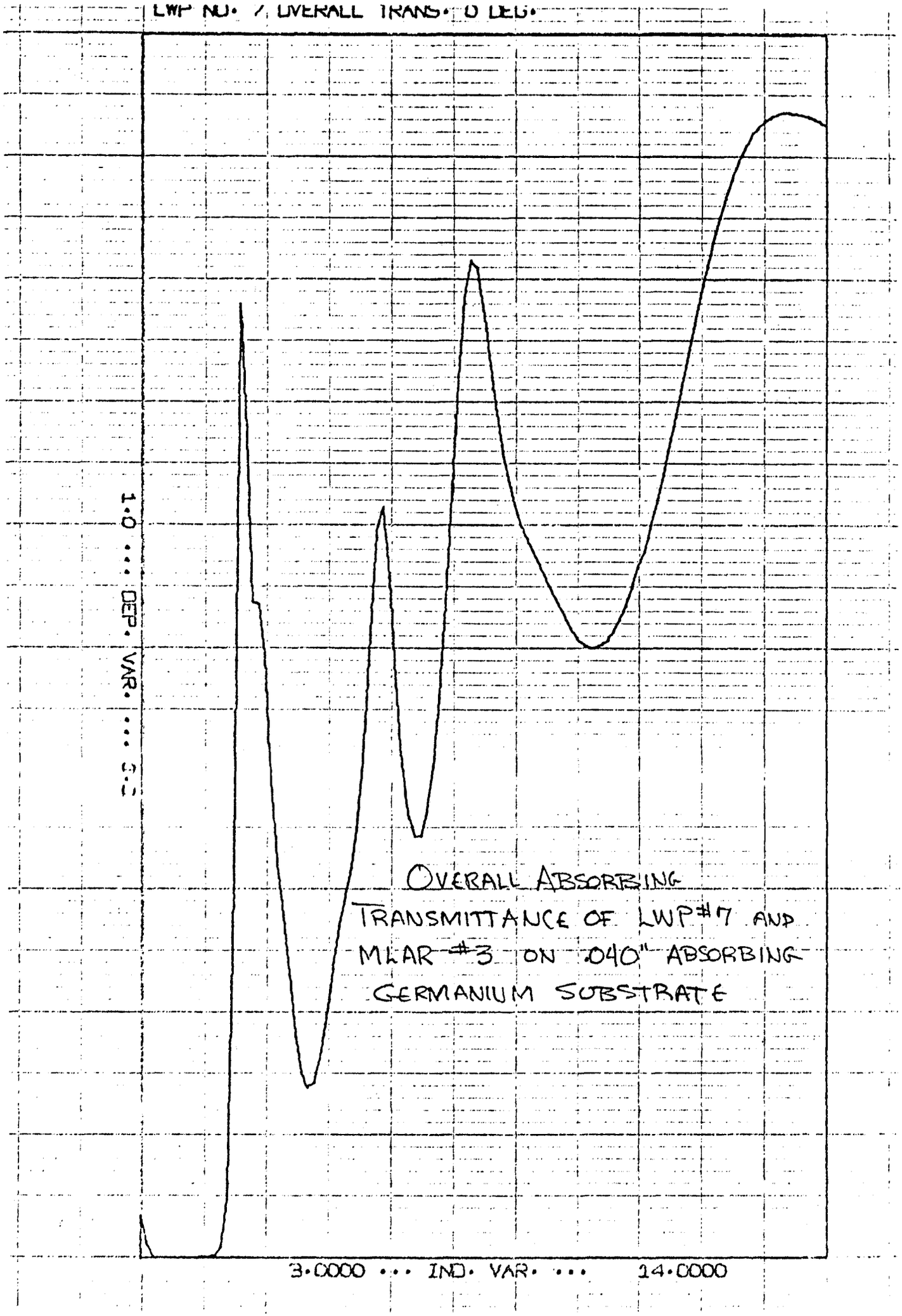

OVERALL ABSORBING TRANSMITTANCE OF LWP #7 AND MLAR #3 ON .040" ABSORBING GERMANIUM SUBSTRATE

SECTION VI. f/NUMBER EFFECTS

VI. f/NUMBER EFFECTS

Four filters (numbered two through five) were selected as representative for calculating the effect of f/number on filter overall performance. Calculations were made for each filter at 0° and 45° incidence, with an f/4 and an f/10 lens focusing an image of a point source at infinity on the filter.

The primary conclusion which can be drawn from these calculations is that there is very little effect of f number in the regions of interest. There is a slight shift to lower wavelengths as the angle of incidence is increased, but in relatively flat response regions as are important in the dichroics, this is of minor significance.

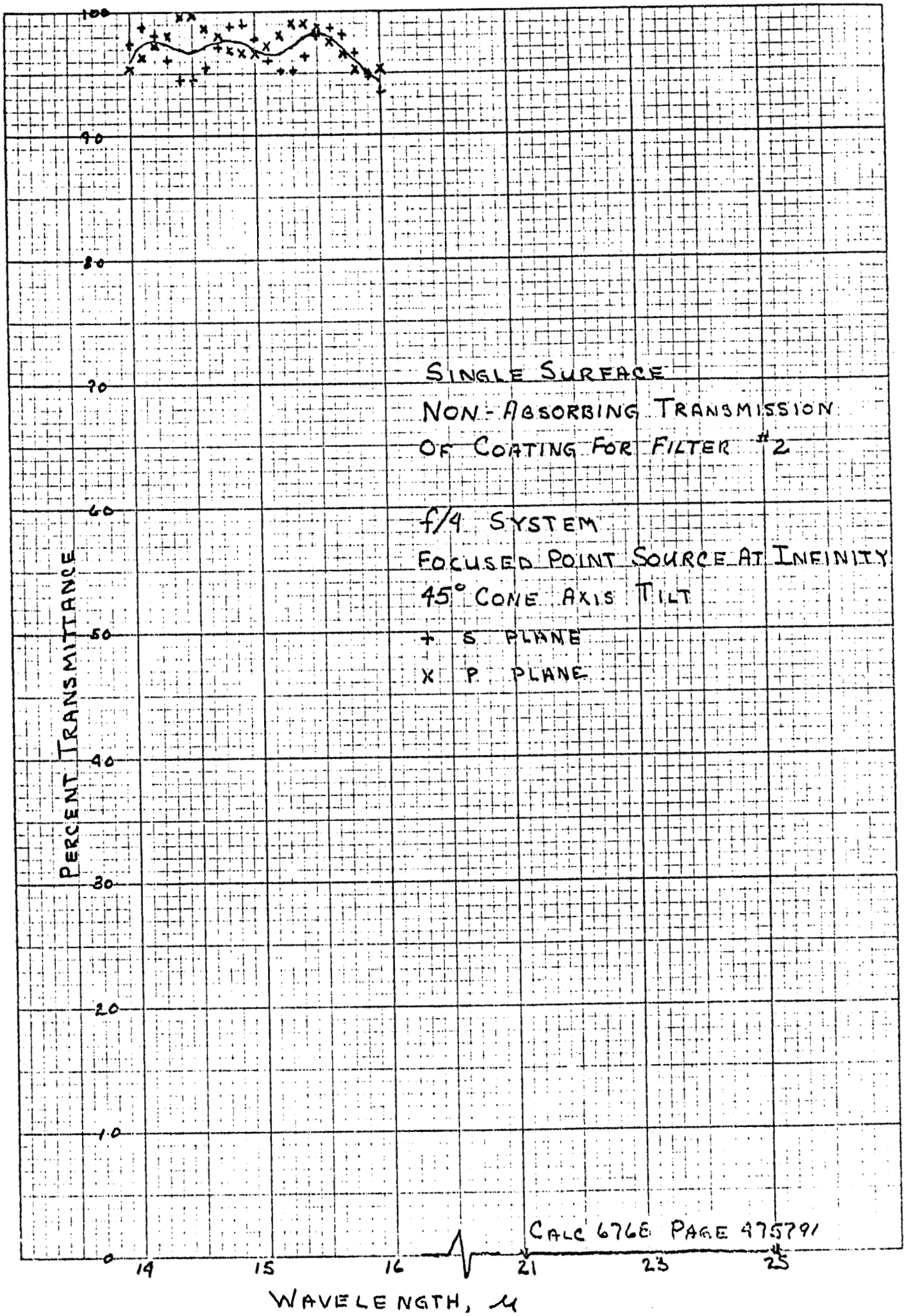
SINGLE SURFACE
NON-ABSORBING TRANSMISSION
OF COATING FOR FILTER #2
f/4 SYSTEM
FOCUSED POINT SOURCE AT INFINITY
45° CONE AXIS TILT
+ S PLANE
X P PLANE
PERCENT TRANSMITTANCE
100
90
80
70
60
50
40
30
20
10
0
14
15
16
21
23
25
WAVELENGTH, μ
CALC 676E PAGE 475791

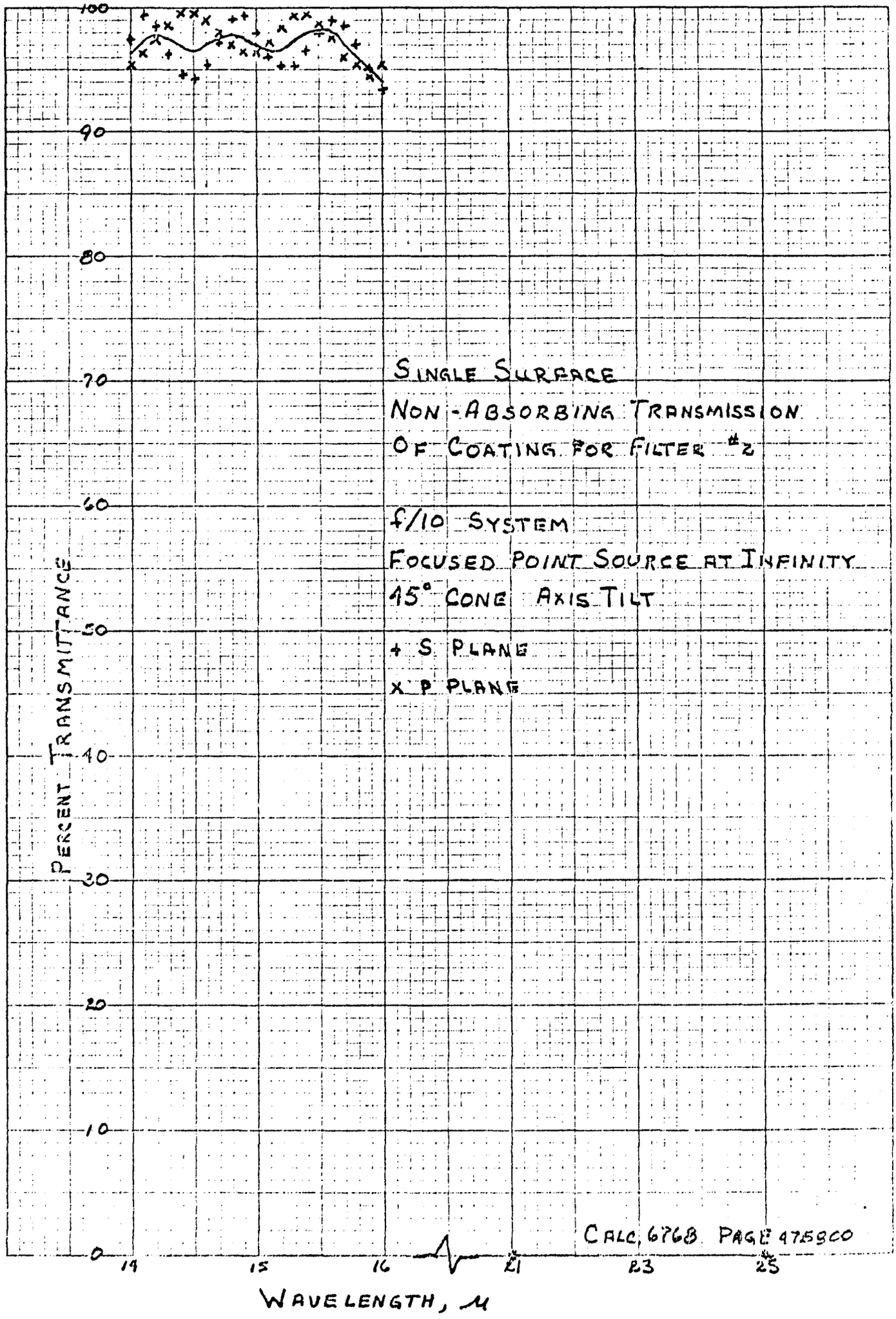
SINGLE SURFACE
NON-ABSORBING TRANSMISSION
OF COATING FOR FILTER #2
f/10 SYSTEM
FOCUSED POINT SOURCE AT INFINITY
45° CONE AXIS TILT
+ S PLANE
x P PLANE
PERCENT TRANSMITTANCE
100
90
80
70
60
50
40
30
20
10
0
14
15
16
21
23
25
WAVELENGTH, μ
CALC. 6768 PAGE 475900

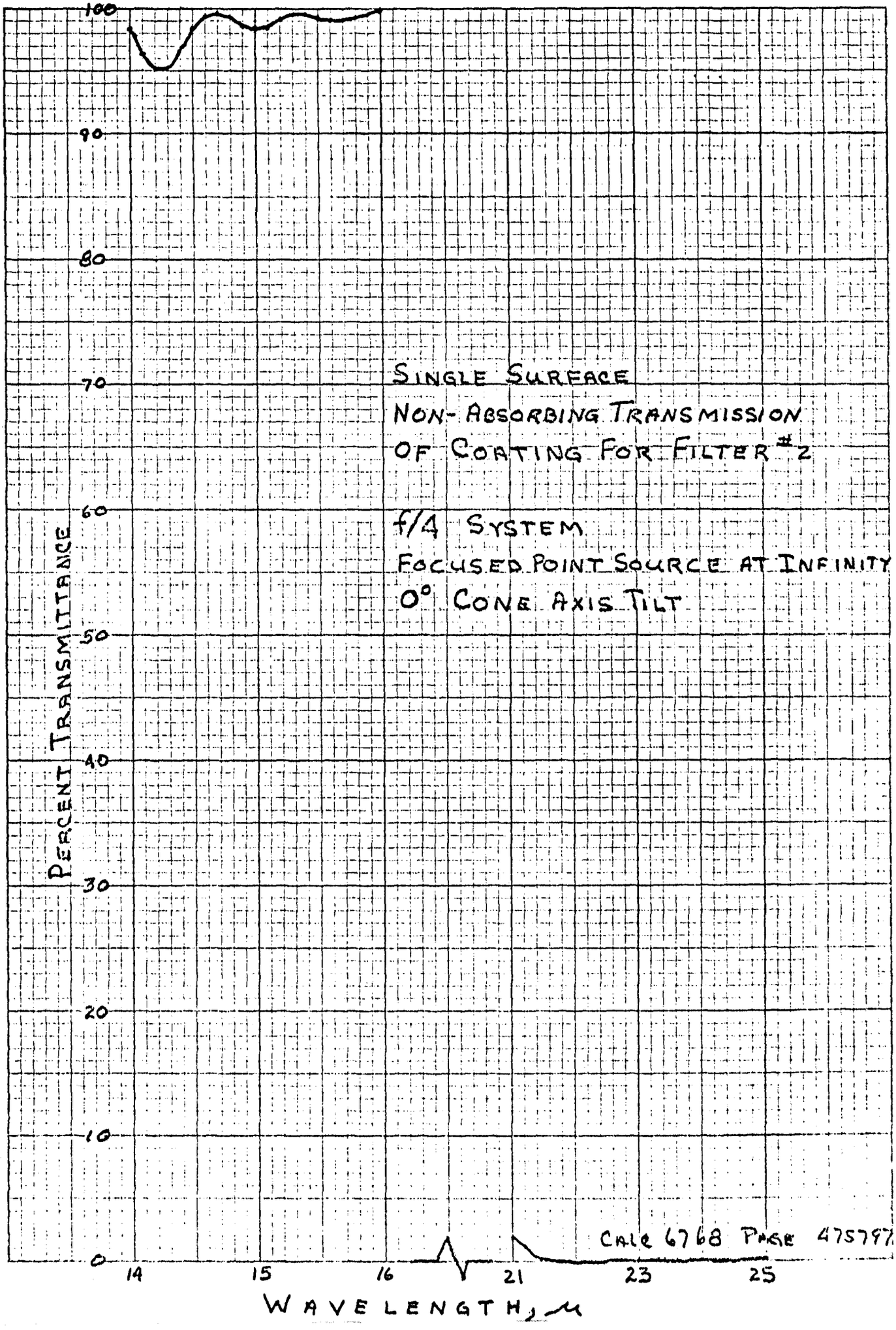

KEUFFEL & ESSER CO.

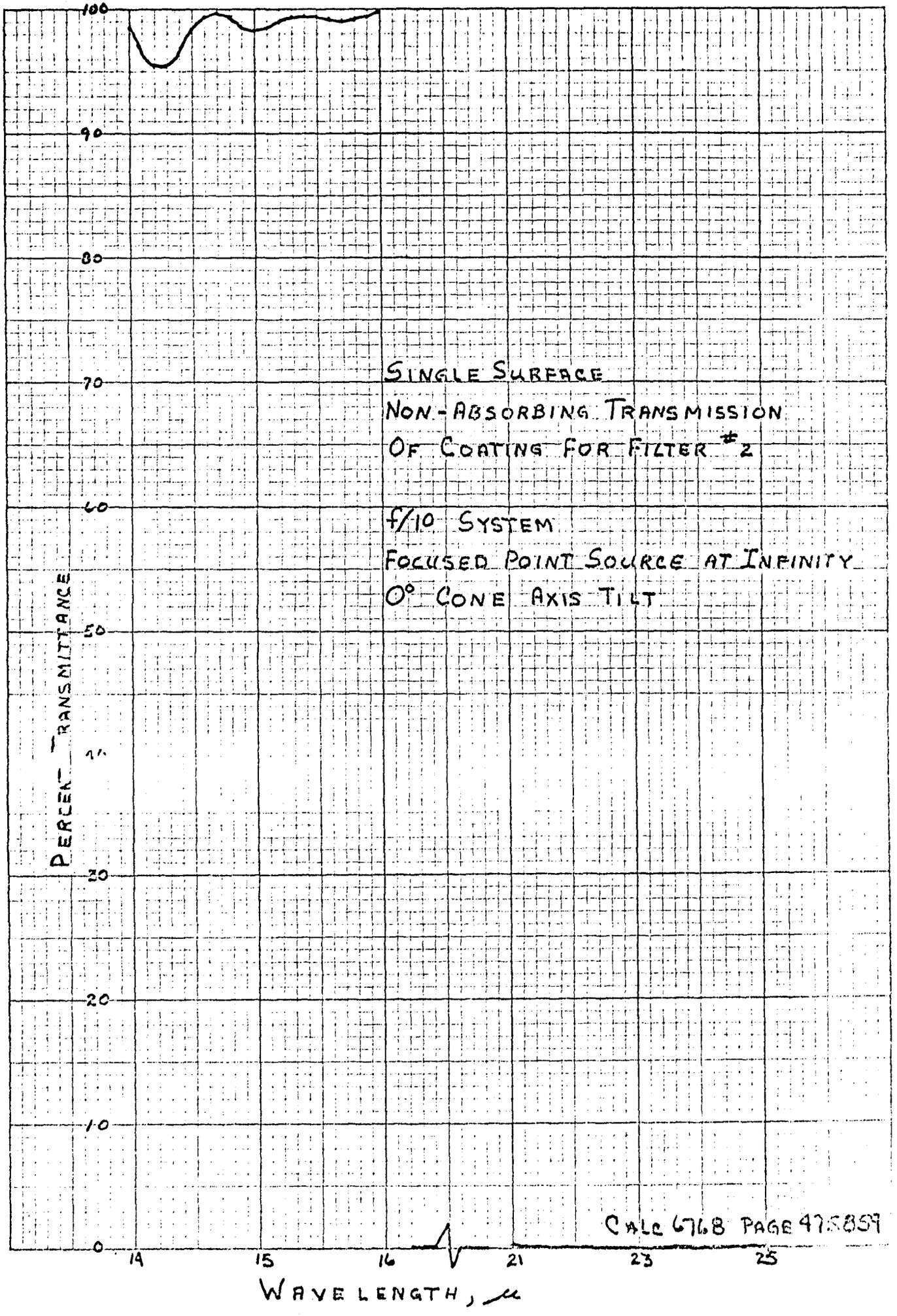

K&E 10 X 10 TO THE INCH 7 X 10 INCHES KEUFFEL & ESSER CO.

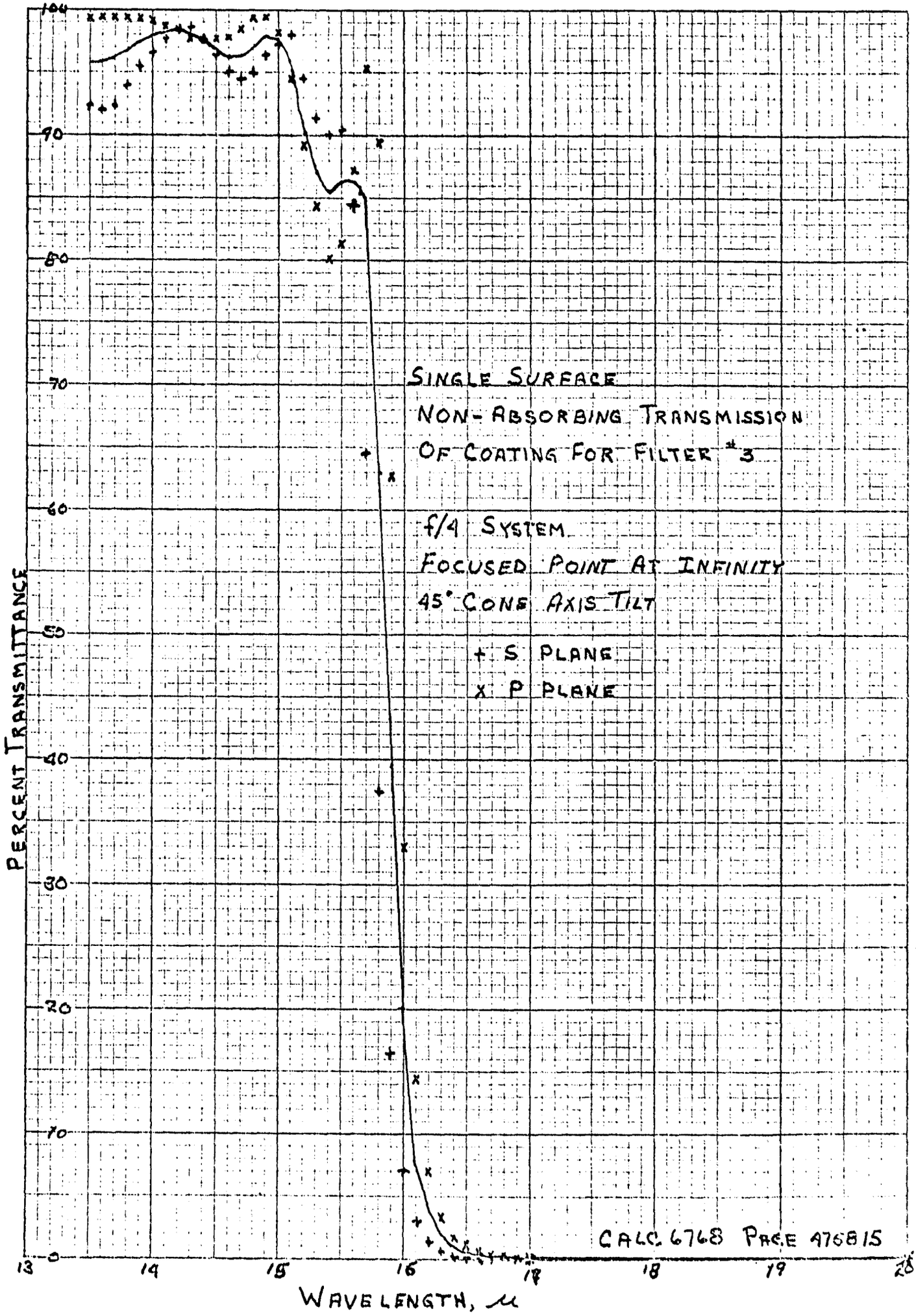

KEUFFEL & ESSER CO.

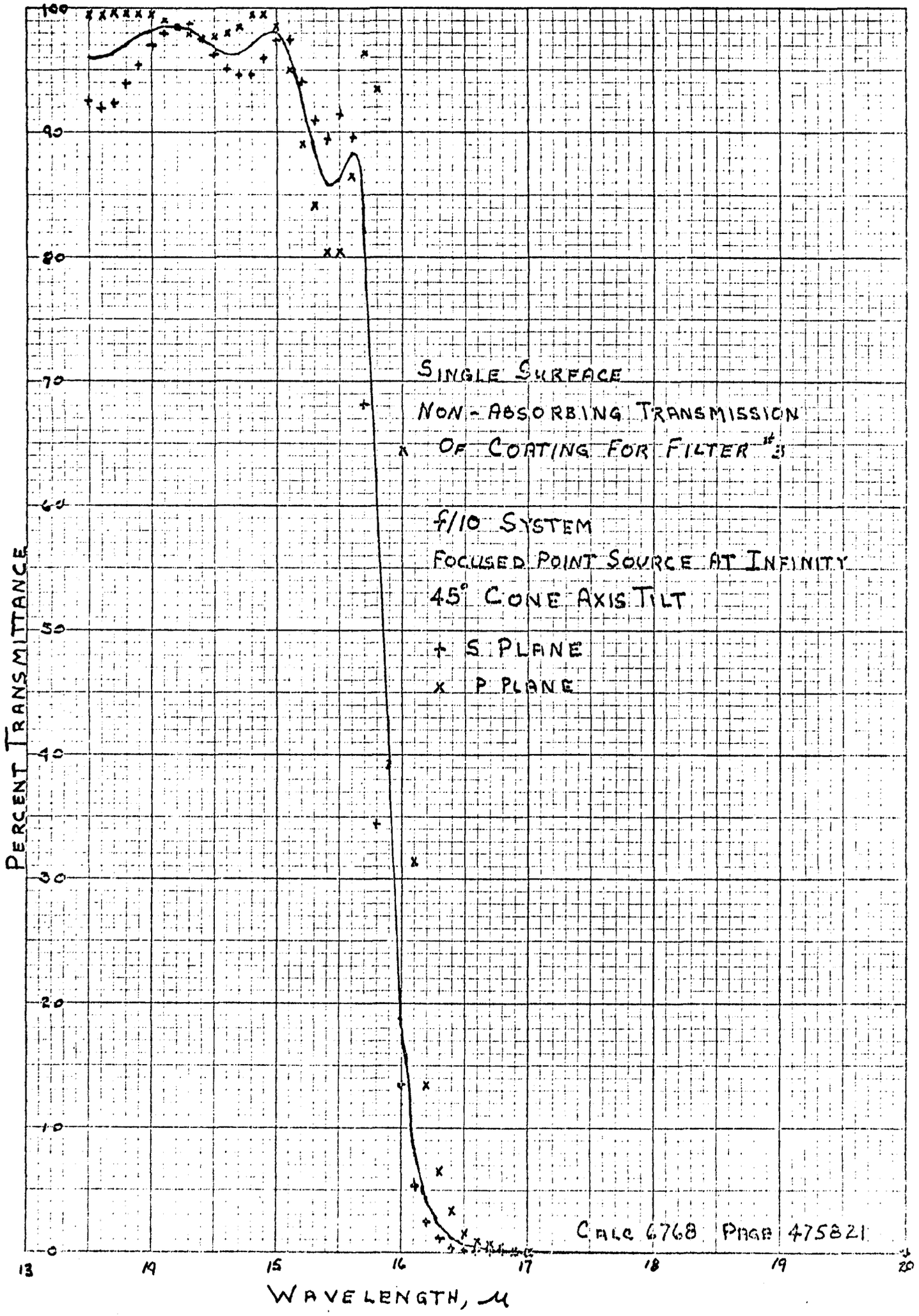

10 X 10 TO THE INCH 46 0782
KEUFFEL & ESSER CO.

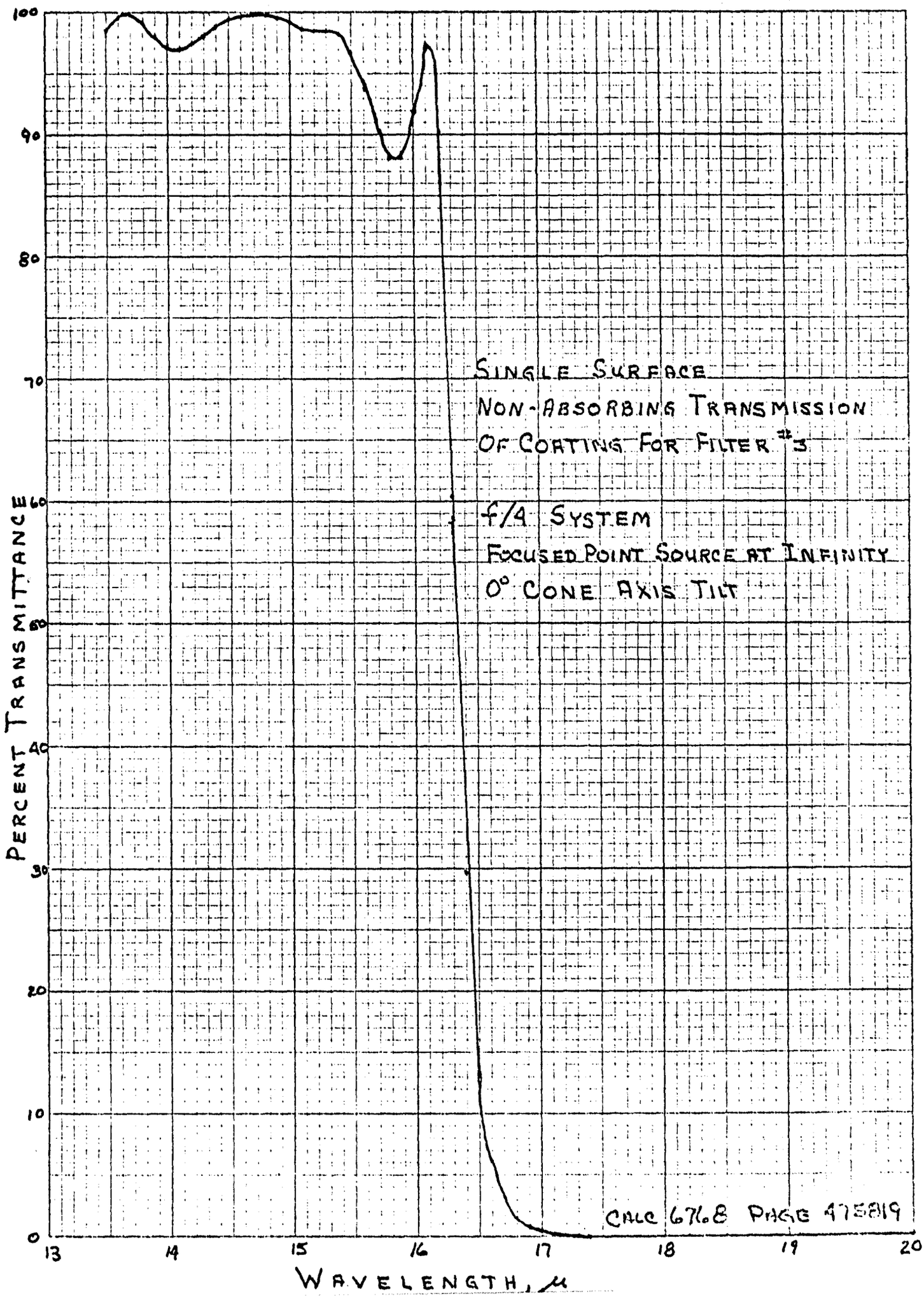

K&E 10 TO [redacted] INCH [redacted] 078
7 X 10 INCHES MADE IN U.S.A.
KEUFFEL & ESSER CO.

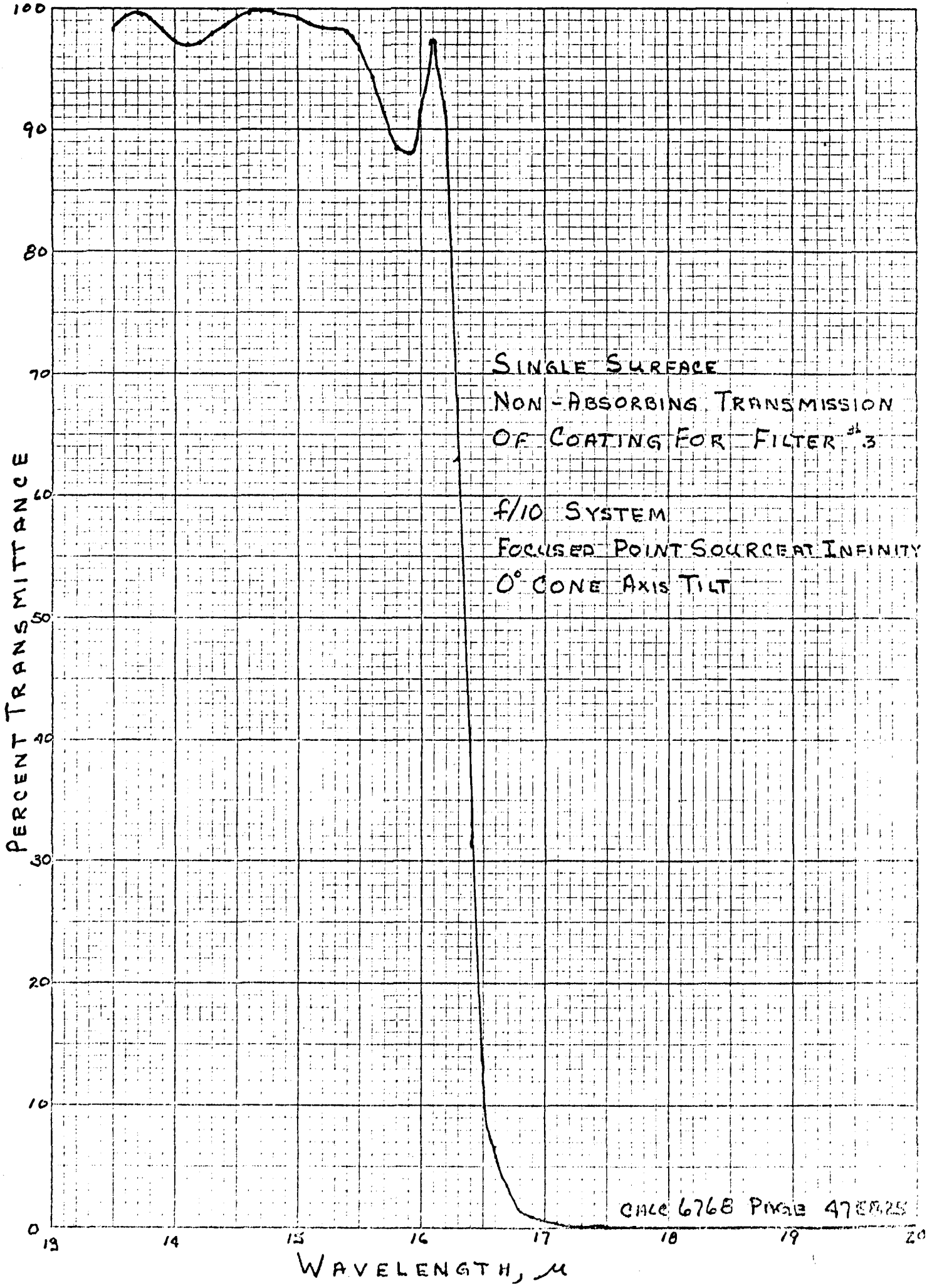

K&E 10 X 10 TO THE INCH 46 0782
7 X 10 INCHES
KEUFFEL & ESSER CO.

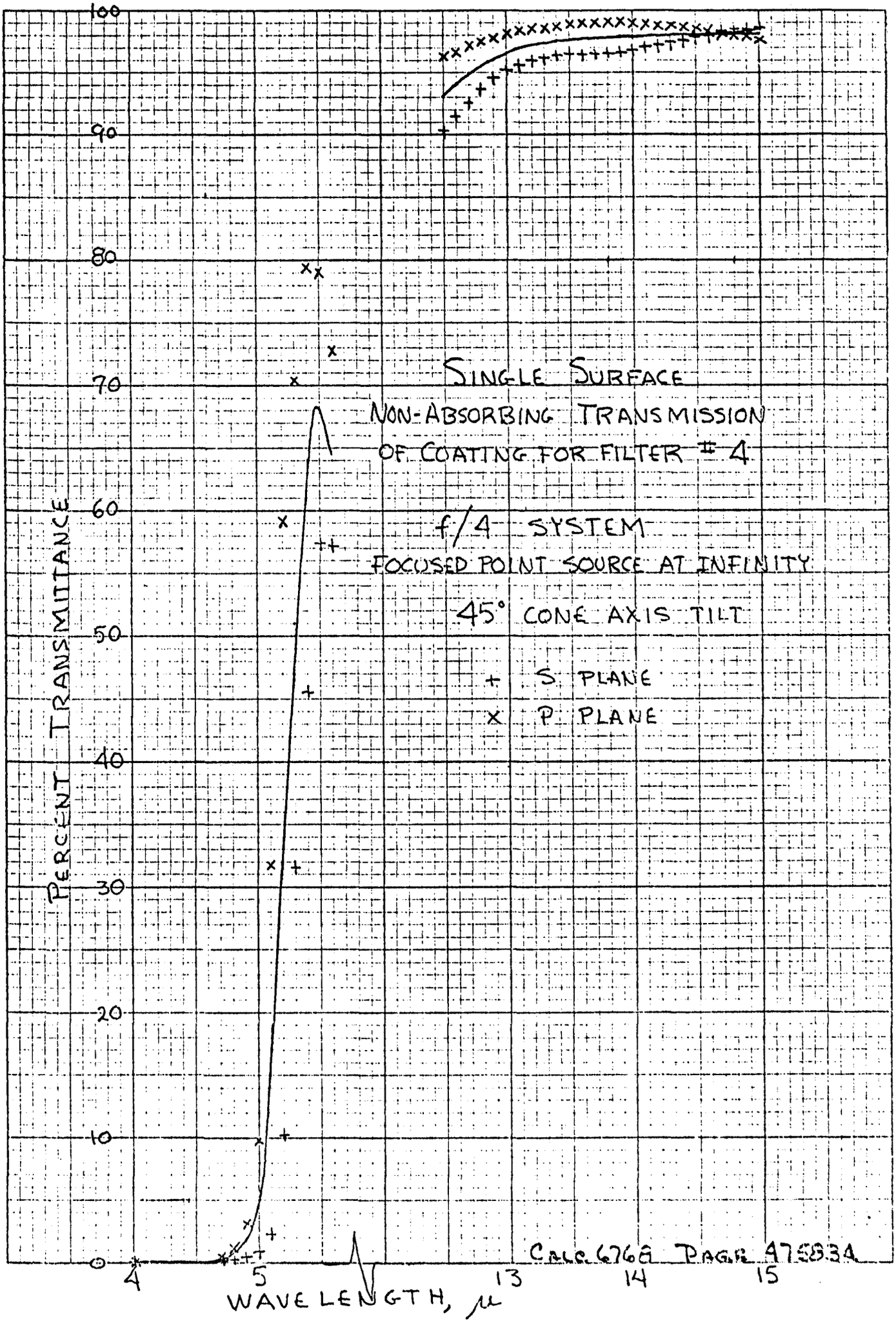

KEUFFEL & ESSER CO.

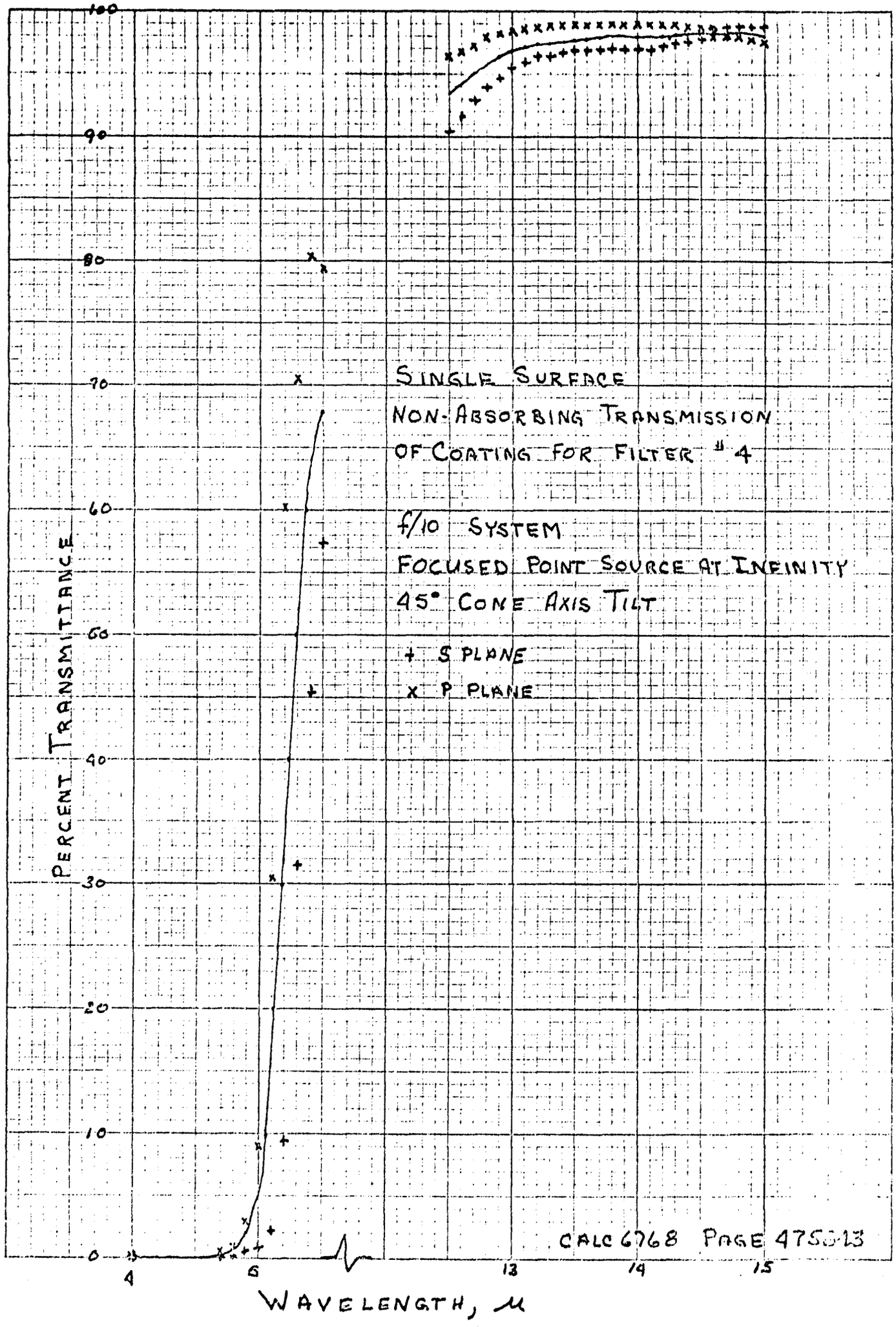

10 X 10 TO THE INCH 46 0782
KEUFFEL & ESSER CO.

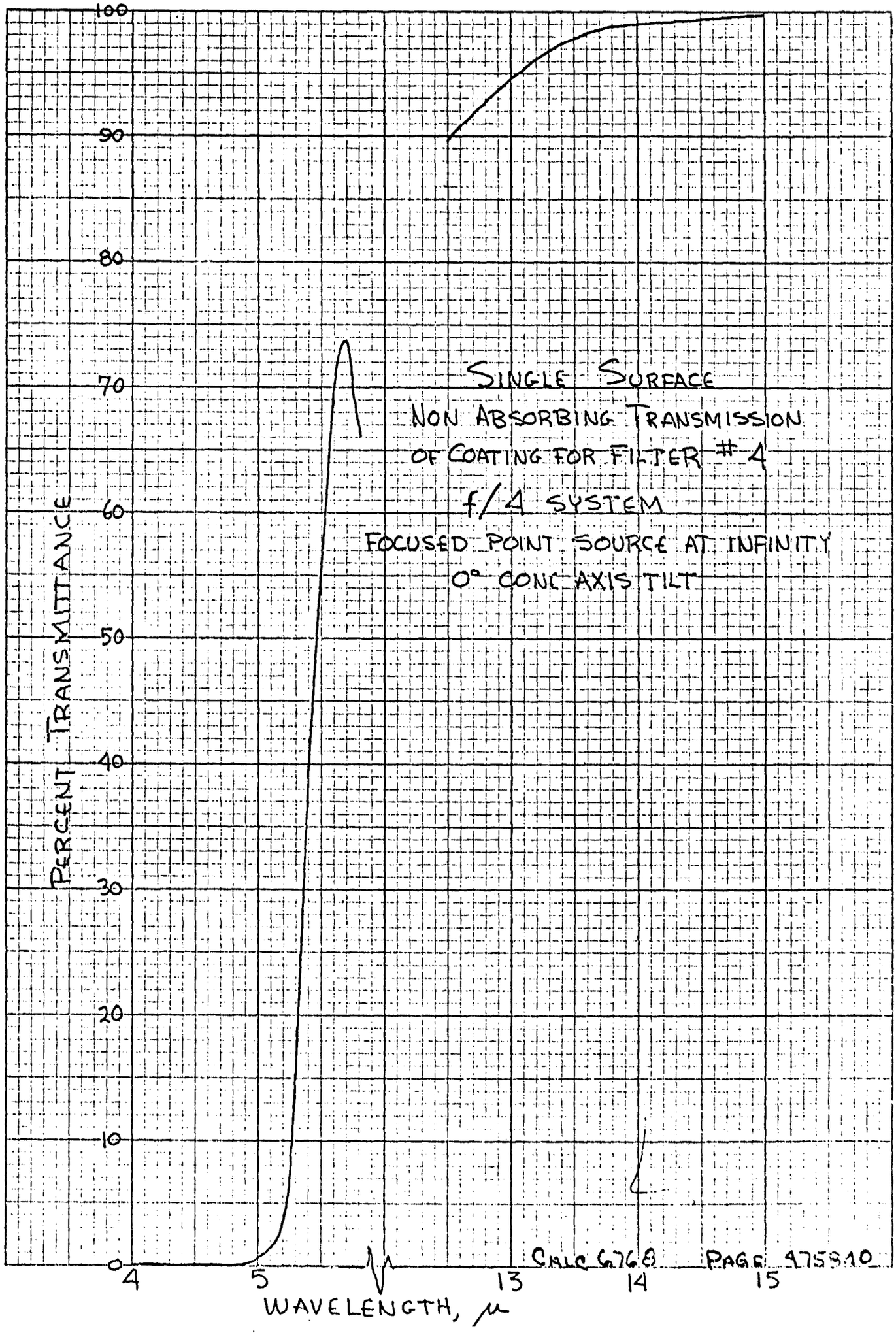

CALC 6768 PAGE 475810

KEUFFEL & ESSER CO.

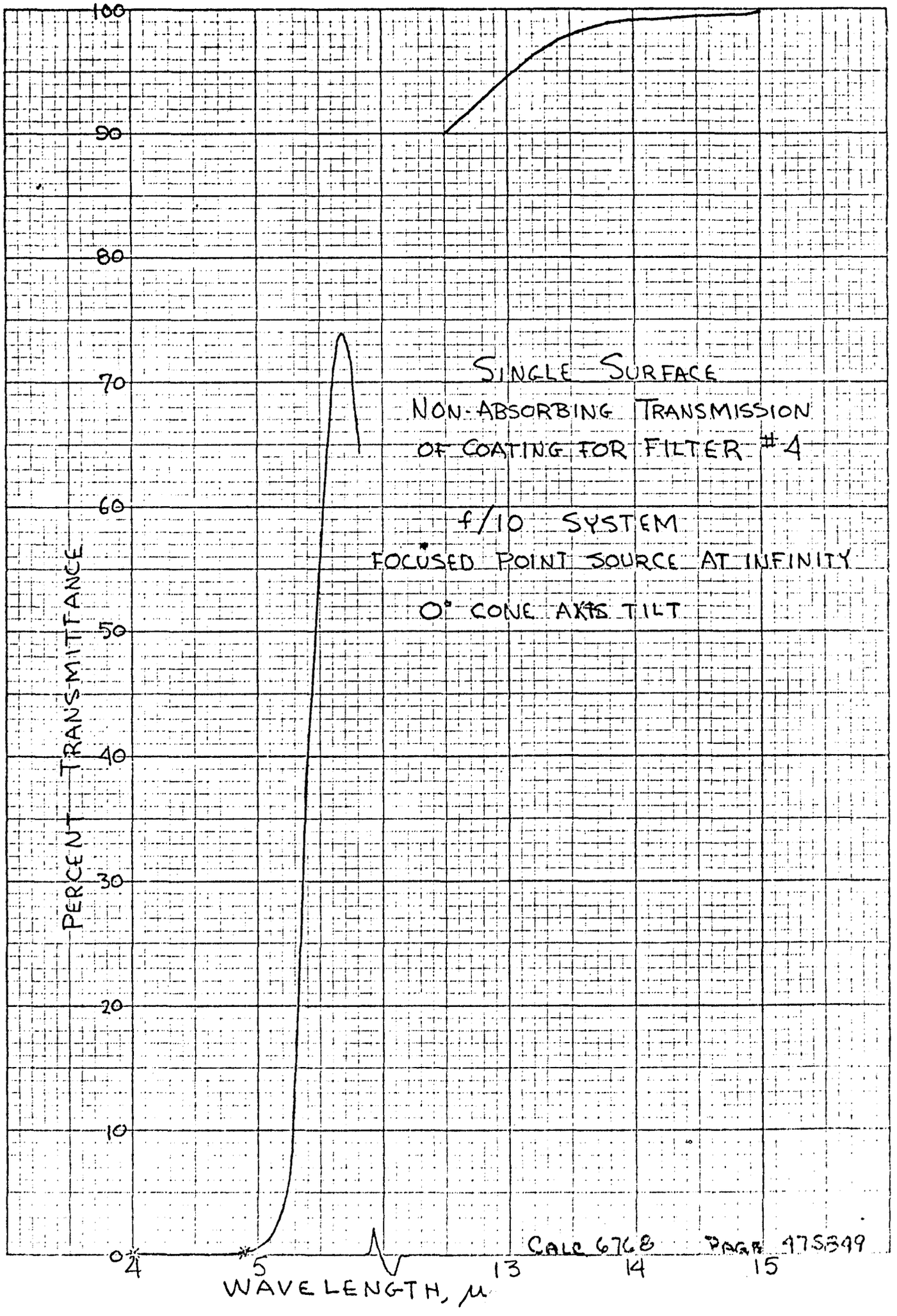

K&E 10 X 10 TO THE INCH 46 0782
7 X 10 INCHES MADE IN U.S.A.
KEUFFEL & ESSER CO.

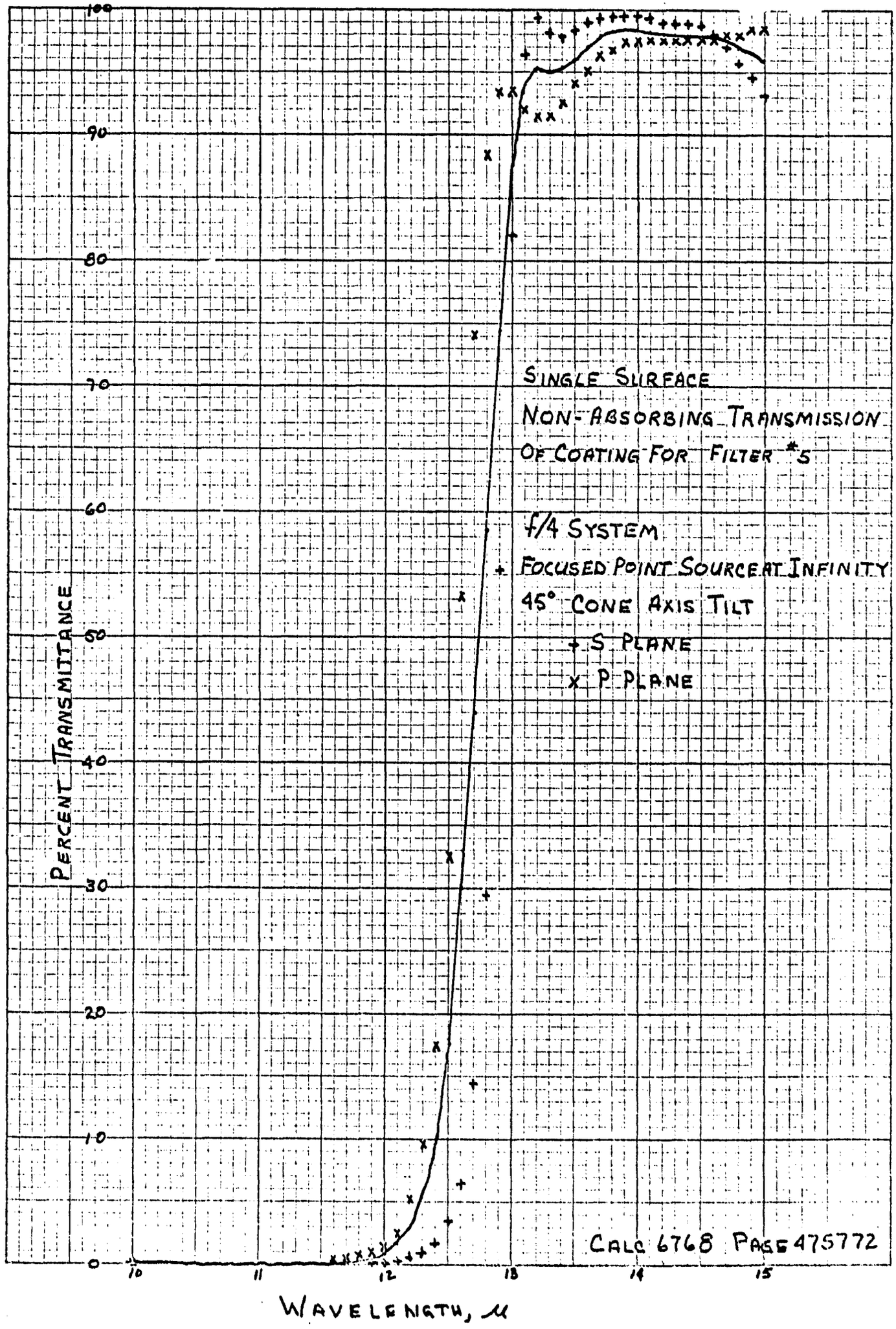

10 X 10 INCHES 7 X 10 INCHES 07 INC MADE IN U.S.A. KEUFFEL & ESSER CO.

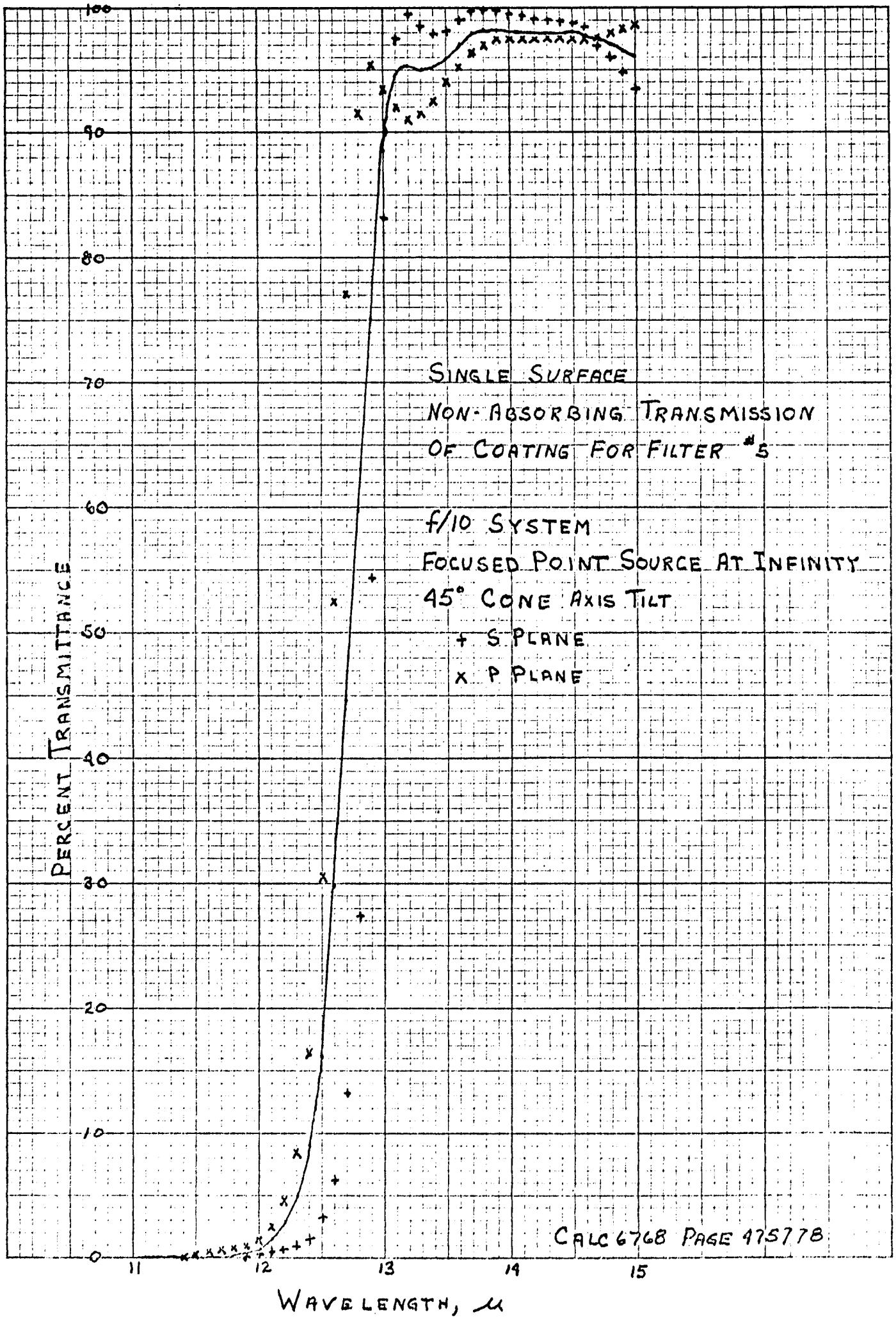

K&E 10 X 10 TO THE INCH 46 0782
7 X 10 INCHES
KEUFFEL & ESSER CO

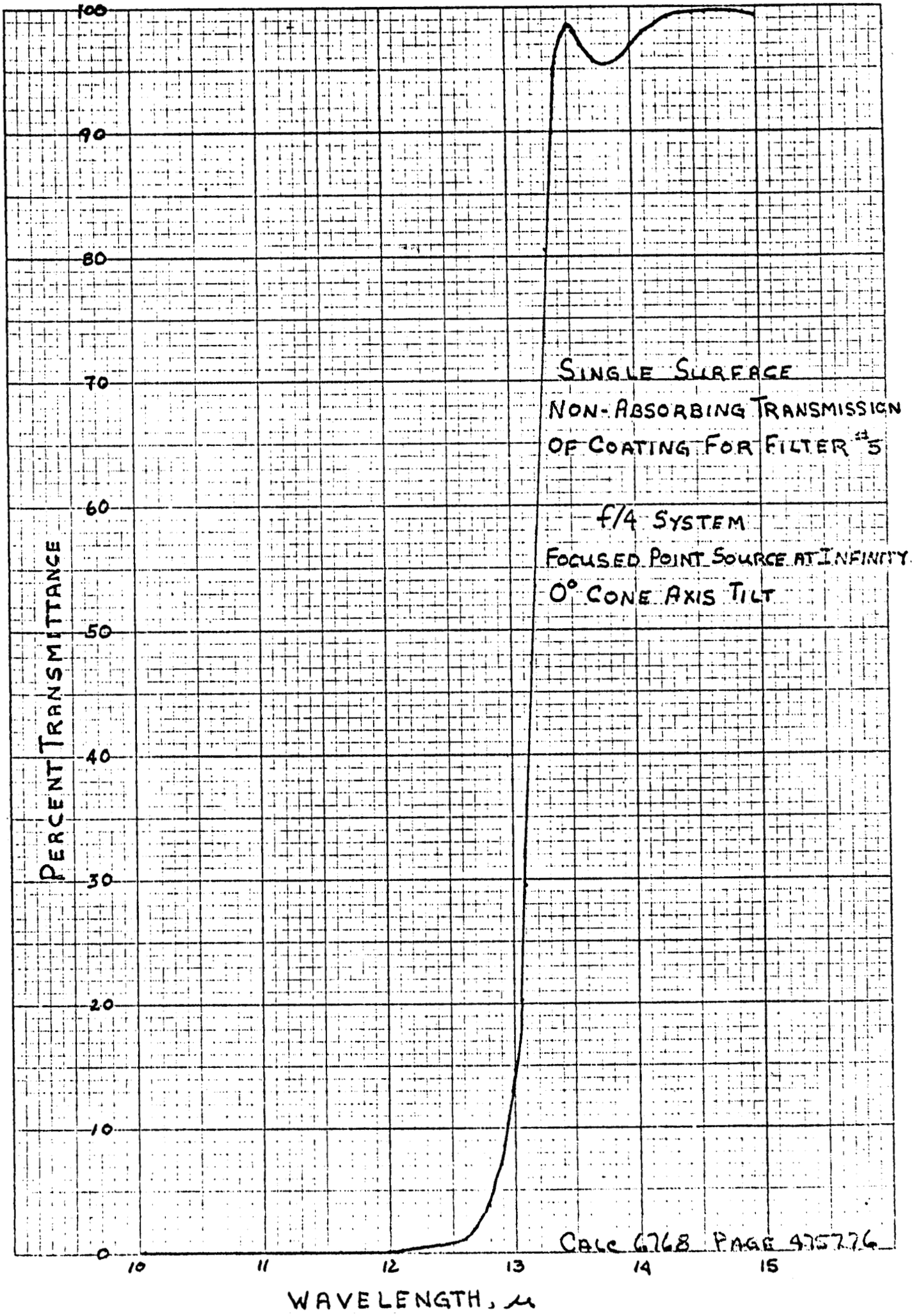

KEUFFEL & ESSER CO.
7 X 10 INCHES
MADE IN U.S.A.

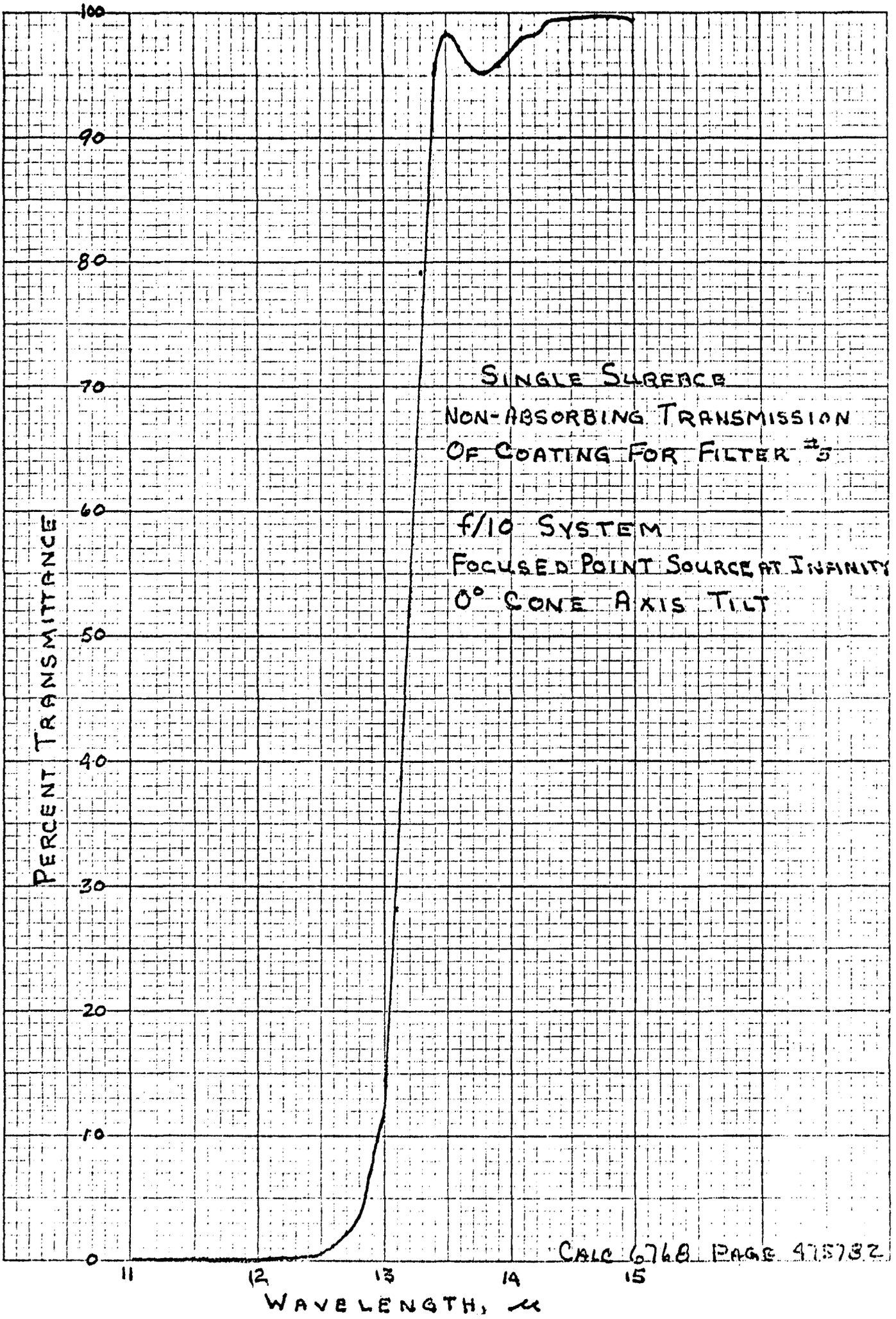

K+E 10 X 10 TO THE INCH 46 0782
7 X 10 INCHES MADE IN U.S.A.
KEUFFEL & ESSER CO.

VII. ITPR FILTER INFORMATION

The information requested on the ITPR filters has been included in this section. The first table shows the substrates and thickness of each of the filter elements, and the dichroic beamsplitter. The next two figures show the computer plotted theoretical transmittance of the ITPR dichroic beamsplitter, at 45° and at 0° incidence.

The back surface of the beamsplitter was coated with a single layer coating, and indications are that it was probably centered at a somewhat longer wavelength (perhaps 13μm). The performance of the single layer coating in Section III was calculated with a center at 13μm, so overall performance for this combination can be estimated. The transmission range of the dichroic is from 10.6 to 11.6μ, and it is apparent that the greatest net polarization will occur at the shorter wavelength, where both the anti-reflection coating and the dichroic have the highest transmission in the P plane. Extrapolating the anti-reflection curve somewhat, the transmittances are

Plane	Dichroic	Anti-Reflection	Combination
S	93.6	85.5	80.0
P	98.8	95.7	94.5

so that a theoretical 15% spread between the two planes of polarization did exist at 10.6μ. It should, however, have been less at all other wavelengths, and could have been reduced substantially by proper choice of anti-reflection coating, if this had been a requirement.

SECTION VII. ITPR FILTERS

ITPR FILTERS

Channel	Element 1	Element 2
1	.040" Ge	.040" Sapphire
2	.040" Ge	.030" Irtran 2
3,4,5	.040" Ge	.069" Irtran 4
6	.030" Ge	.069" Irtran 4
7	.030" Si	.069" Irtran 6
Dichroic	.040" Ge	--

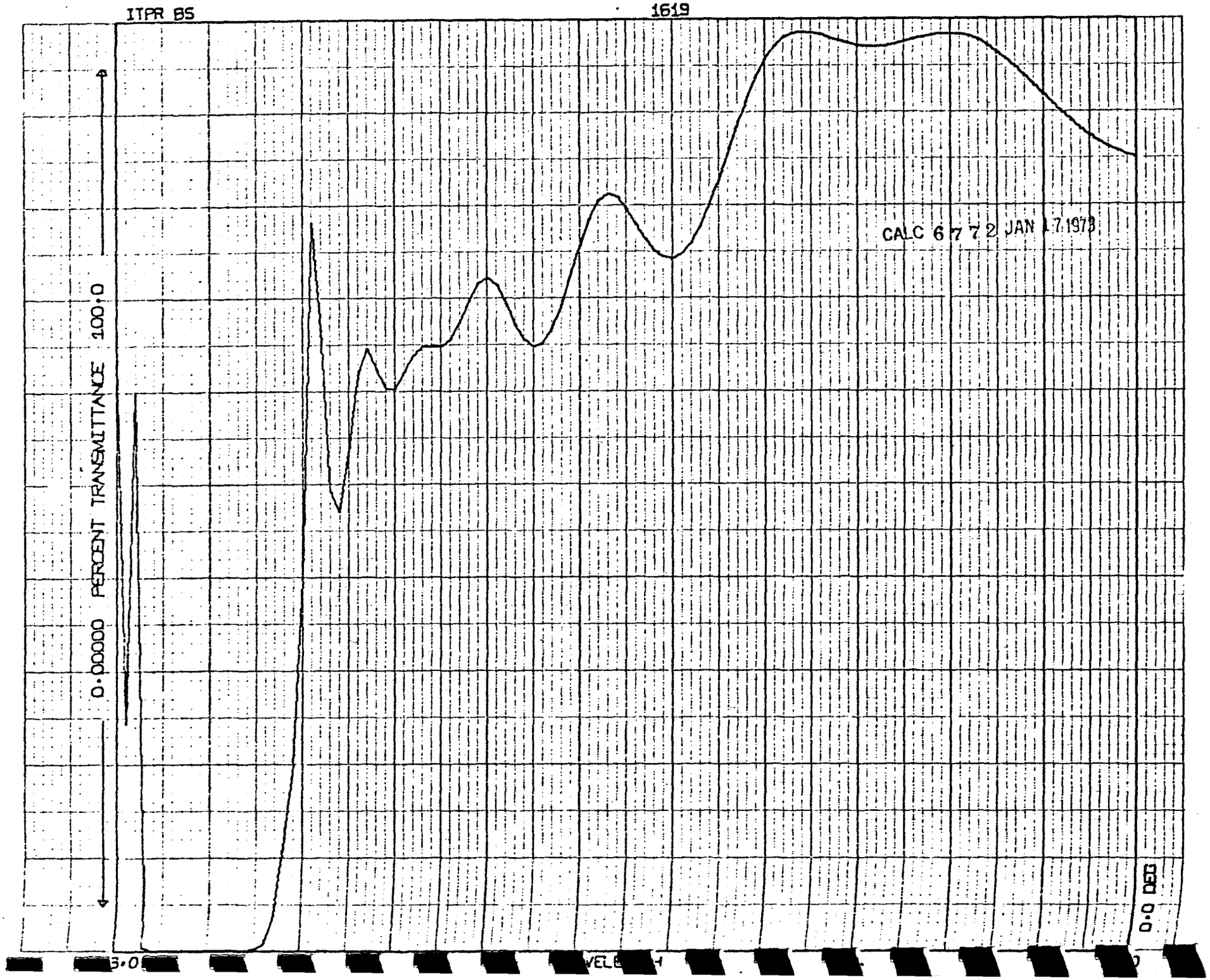
ITPR BS
1619
CALC 6 7 7 2 JAN 17 1973
0.00000 PERCENT TRANSMITTANCE 100.0
3.0
0.0 DEG

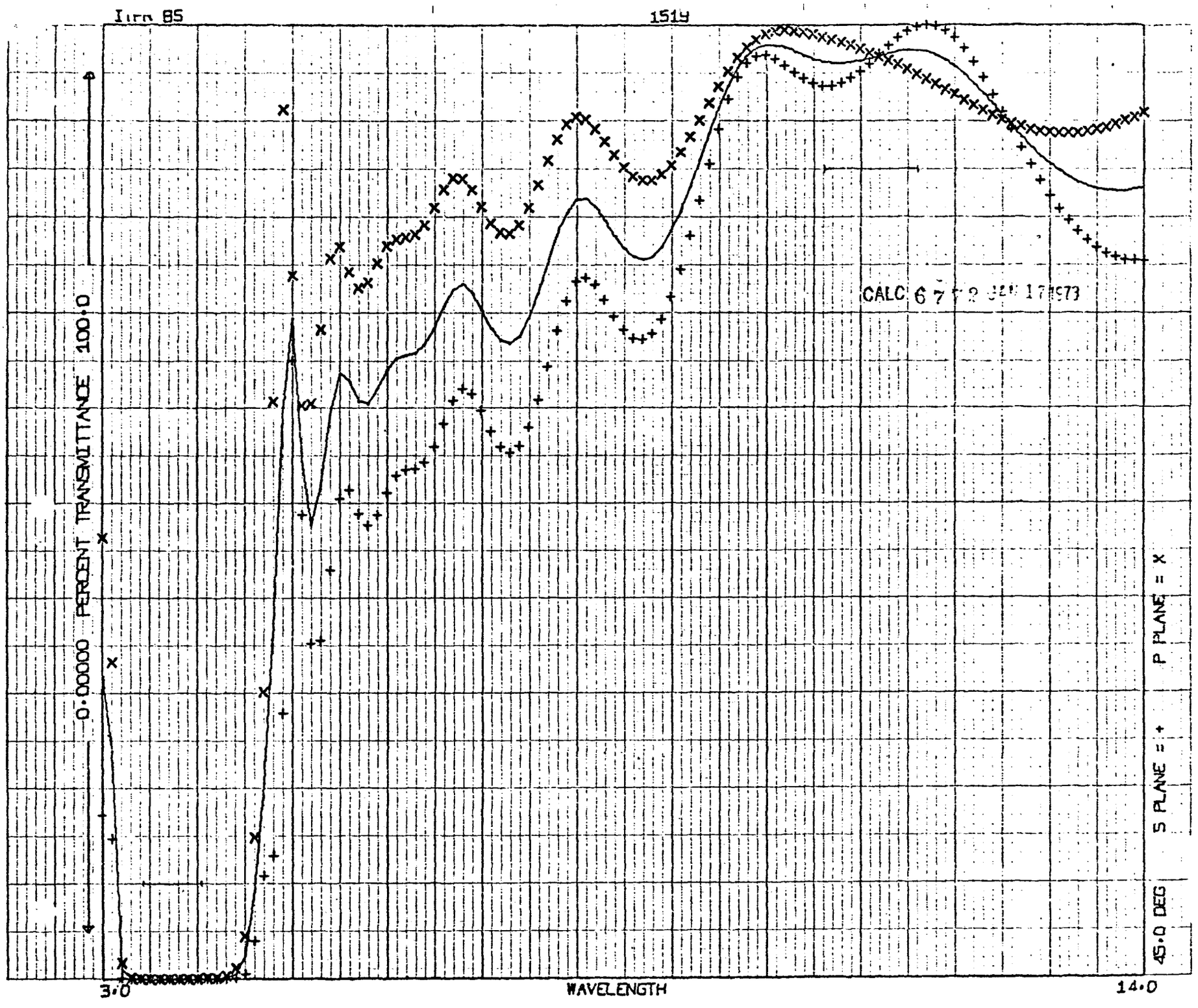
Ilrn 85
1514
CALC 6 7 2 JAN 17 1973
0.00000 PERCENT TRANSMITTANCE 100.0
3.0
WAVELENGTH
14.0
45.0 DEG
S PLANE = +
P PLANE = X

APPENDIX 5

TOVS IMMERSED DETECTOR STUDY

TECHNICAL REPORT RK-154

laser precision corp.... making light work

FIVE WEST WHITESBORO STREET • YORKVILLE, NEW YORK 13495 • TELEPHONE 315/797-4449

December 28, 1972

TOVS IMMERSED DETECTOR STUDY

TECHNICAL REPORT RK-154

TOVS IMMERSED DETECTOR STUDY

TECHNICAL REPORT RK-154

I. Introduction and Summary:

This report summarizes the major results of the work performed under Gulton Industries, Data Systems Division Purchase Order #02023. The aim of this effort has been to demonstrate the feasibility of using immersion techniques to produce high performance pyroelectric detectors for use in the Tiros Operational Vertical Sounder.

The specific tasks undertaken were intended first to reveal the general characteristics of immersed pyroelectric detectors, and second, to shed some light on the optimum choice of detector material and the degree of performance enhancement to be expected.

It was found that immersed pyroelectric detectors generally perform as expected theoretically. Hemispherical immersion leads to effective element area n_L^2 times the actual area, where n_L is the lens index of refraction (4.04 for Germanium). The angualr field of view is $2\sin^{-1}(n_D/n_L)$ where n_D is the detector element index. The immersion process does lead to some sacrifice in low frequency performance. This is due to heat sinking by the immersion medium which causes a decrease in the thermal time constant.

The most extensive experiments were carried out using LPC's kT-4000 detector material. This material has the advantage of being rugged, non-hygroscopic, and thermally very stable. Although the results have followed the theory quite closely, practical fabrication problems have so far prevented us from achieving, in a single detector, all of the very stringent requirements envisioned for TOVS. An immersed kT-4000, mated to a current mode preamp-

lifier, is being delivered to Gulton.

Theoretically, the greatest performance enhancement should occur when immersion is used with detector materials whose performance is limited by capacitance and hence voltage noise rather than by the pyroelectric coefficient. For example, several double oxide crystals have pyroelectric coefficients which are considerably higher than either TGS or the kT-4000. These materials, however, have very high dielectric constants so that their voltage responsivity is rather limited. Immersion can reduce the required detector area by a factor of typically sixteen. Thus, we might expect an increase in voltage responsivity by this factor, obviating the limitations of amplifier voltage noise.

To test the effects of immersion on a high dielectric constant material, we constructed a number of immersed detectors using SBN (50/50). The theoretical reduction in effective capacitance did occur. However, the results were compromised by general performance variability and by an anonalous increase in dielectric loss over that measured for unimmersed SBN detectors.

The limited scope of the present effort has prevented the study of the many other detector materials whose performance may be enhanced by immersion. However, material property measurements reported in the open literature suggest that a number of attractive candidates exist, both in the double oxide and the order-disorder families. These materials offer fertile ground for further development efforts.

Our work has demonstrated the general attractiveness of immersion for use in radiometric instruments such as TOVS. We believe that a reasonable probability exists that a sufficiently high performance immersed kT-4000 detector can be produced if further attention is devoted to solving the practical fabrication problems. In addition, investigation of additional materials offers the possibility of an even greater improvement in performance.

II. The Requirements:

The most critical TOVS channels occur at 3.8 and 4.3 microns. These require an NEP of 7.5×10^{-11} W/Hz$^{\frac{1}{2}}$ when used with a 3" telescope. The required effective detector diameter is 2.0mm with a 70° field-of-view or about 2.5mm with a 60° field-of-view. The assumed chopping frequency is 50Hz.

The necessary NEP can be obtained, for example, with a current responsivity of 4 μA/W and a total noise level of 3×10^{-16} A/Hz$^{\frac{1}{2}}$. If we assume a hand picked FET preamplifier with a current noise level of 2×10^{-16} A/Hz$^{\frac{1}{2}}$ we will need a combined loss tangent and voltage noise contribution of less than 2×10^{-16} A/Hz$^{\frac{1}{2}}$. The function of immersion is to minimize the required detector element area and hence capacitance in order to minimize the effects of voltage and loss tangent noise.

III. kT-4000 Experiments:

A. General Discussion:

We have constructed a number of immersed kT-4000 type detectors using both hemispherical and hyperhemispherical Germanium lenses. kT-4000 was chosen for the bulk of the experiments because of its excellent electrical and mechanical properties. These allow the greatest possible freedom in experimenting with immersion techniques and in studying the effects of immersion on detector behavior. In addition, measurements made on unimmersed detectors indicate that it might be possible to meet the program requirements with this material. If so, its superior ruggedness and stability would give it an advantage over unimmersed TGS.

Selected unimmersed kT-4000 detectors have yielded current responsivities of greater than $r_i = 3$ μA/W and loss tangents of less than 1×10^{-3}. Neglecting strays, the capacitance is given by $C = 8.3\ r_i\ A$(pf) where A is the electrode area in mm^2.

Theoretically a Germanium immersed kT-4000 should have a linear magnification factor of 4.04 and a field-of-view of 66°. The main cause of any departure from the performance of unimmersed detectors is the heat sinking at the front surface due to contact with the immersion medium. As a result of this heat sinking it was assumed at the outset that a front surface black coating could not be used. Thus all of the detectors constructed utilized a metallic semitransparent front electrode.

kT-4000 material is transparent at 3.8 and 4.3 microns. Thus, it was necessary to blacken the rear detector surface to compensate for the fact that the semitransparent electrode is only 30% to 40% absorbing. For the present experiments a convenient carbon black was used having a resistance of 20 to 30 kilohms/square. The resulting series resistance is a voltage noise source and will contribute to the measured loss tangent. It is clear that this effect can be eliminated in future work either by finding a more conductive black or by depositing a metallic electrode on top of the black.

B. Experimental Results:

As an example of the typical results obtained wtih immersed kT-4000 detectors, we list below the characteristics of detector IA-2C.

PROPERTIES OF DETECTOR IA-2C (Ser:466)

Current Responsivity

4.0 μ (extrapolated estimate)	2.0 μ A/W
1.8 to 3.4 μ band	1.85 μ A/W
700°K black body	1.64 μ A/W
10.6 μ laser	1.55 μ A/W

Effective Diameter	1.7mm
Capacitance	9 pf
Loss Tangent (at 1kHz)	0.004
Angular FOV	65°
Thermal Response Time	3 msec.
Leakage	$>10^{13}$ ohms

Figure 1 is the transmission curve supplied by the vendor for the lens coating used. Since only one side was coated the measured values must be divided by 0.65 to obtain the properties of the coating itself.

Measurements of r_i were made under the three conditions indicated. Extrapolation to the region of peak lens transmission was hampered by the lack of transmission data below 2.5 or beyond 8.3 microns. However, the value 2.0 μ A/W is reasonable.

Immersed detectors with metallic rear electrodes have given current responsivities of over 3.0 μ A/W at 10.6 microns. High responsivity is more difficult to achieve with a carbon coating because of the difficulty of handling the thin crystals without the added strength of the metal. The highest responsivity obtained to date with the carbon coating was 2.7 μ A/W.

The intended active area diameter was 2.0 millimeters. The area of this unit was inadvertantly reduced, however, during the masking process. A plot of linear aperture response is given in Figure 2. Figure 3 is a plot of response versus incidence angle.

As mentioned above the measured loss tangent includes a contribution due to the series resistance of the rear surface coating. Lower values are achievable.

The thermal response time of this unit is quite short. This parameter tends to decrease with increasing r_i since this requires a reduction in crystal thickness. However, the relationship varies considerably. This is at least partly due to the fact that r_i also depends on electrode properties, while

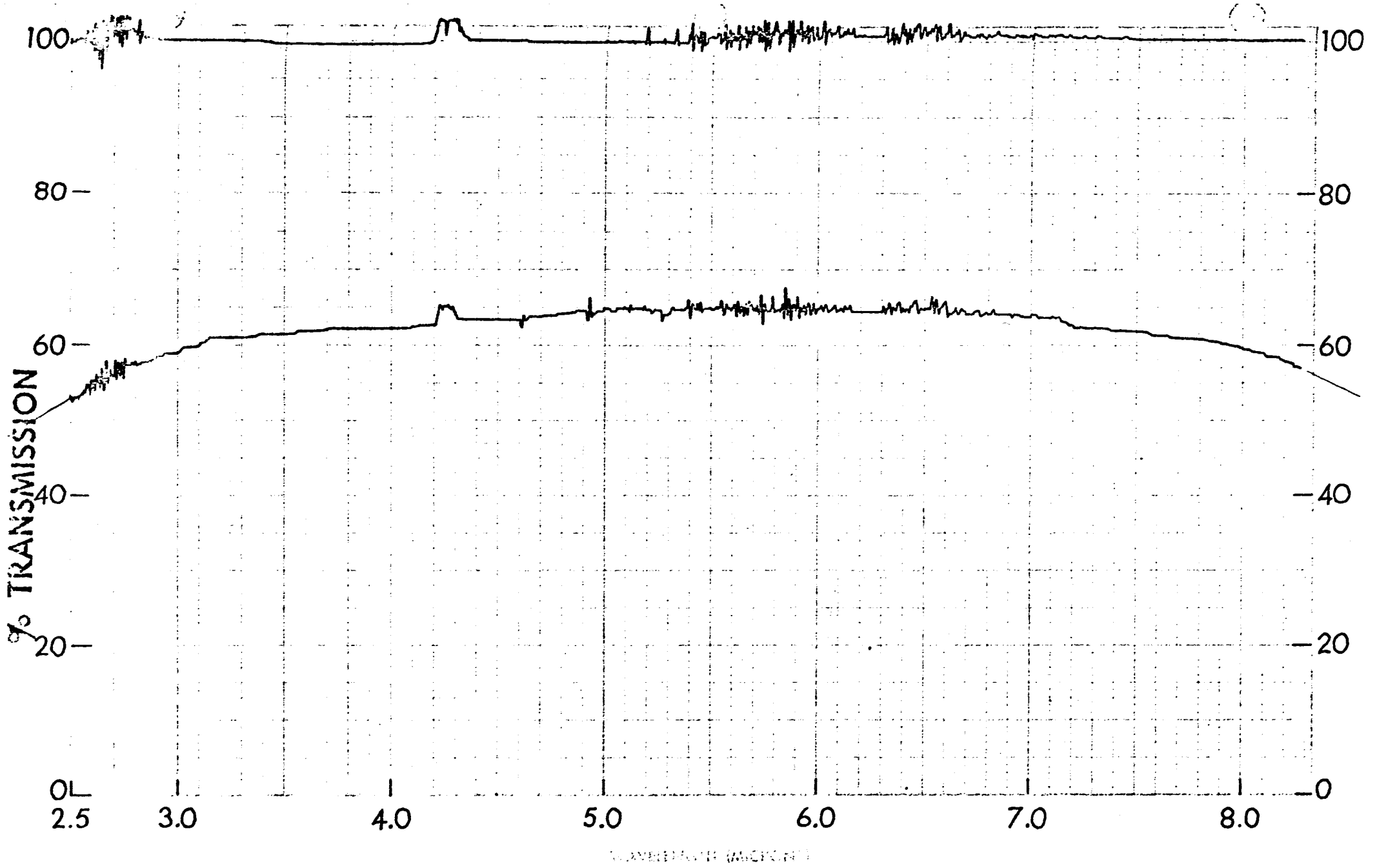

Laser Precision
10814

1pc. Germanium
coated on convex surface
for A.R. from 3 to 8 μ
peaked @ 4.5 μ.

E.S.
9-25-72

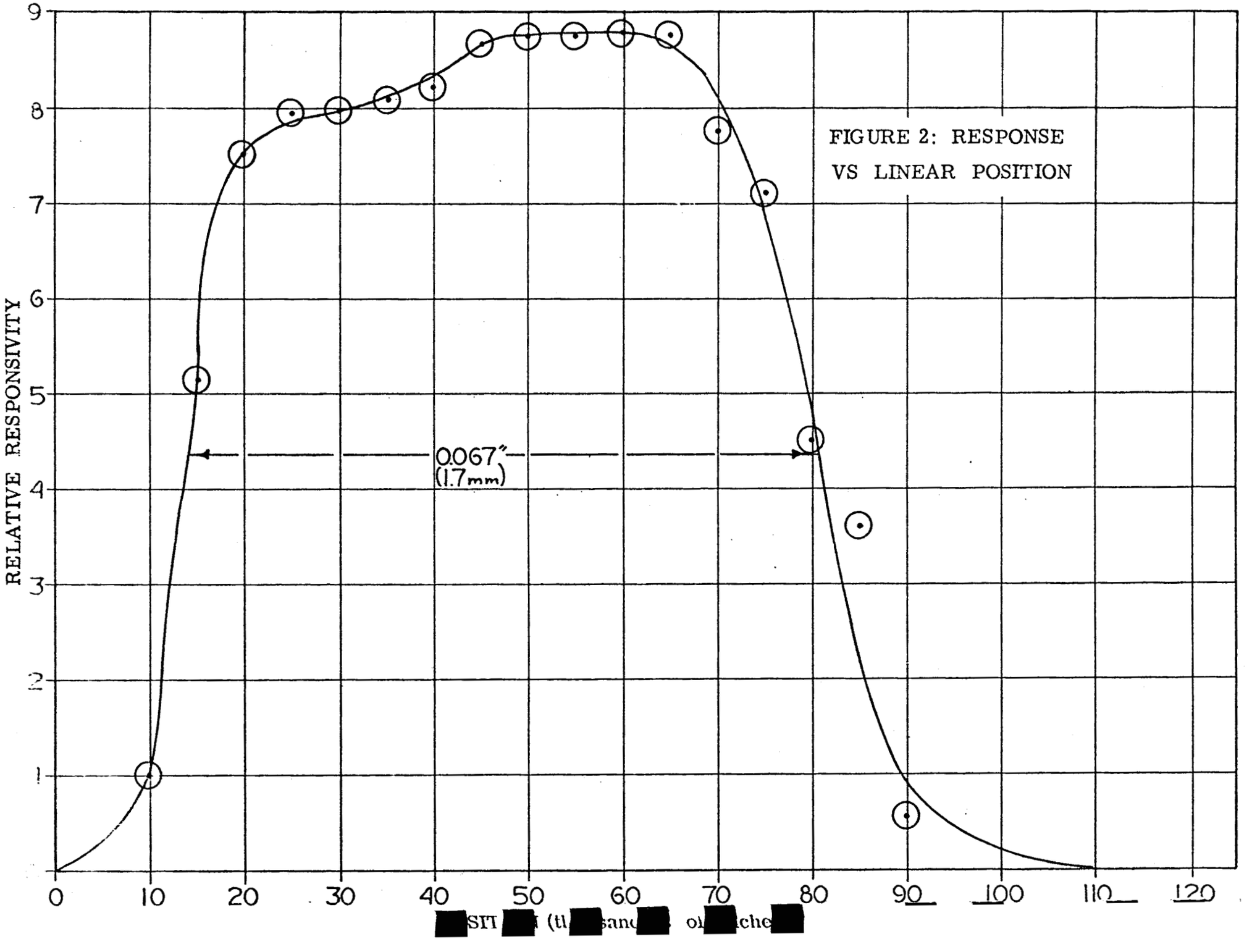
FIGURE 2: RESPONSE
VS LINEAR POSITION
RELATIVE RESPONSIVITY
0.067"
(1.7mm)
0
10
20
30
40
50
60
70
80
90
100
110
120
1
2
3
4
5
6
7
8
9
[redacted]SIT[redacted] (th[redacted]sand[redacted] of[redacted]che[redacted]

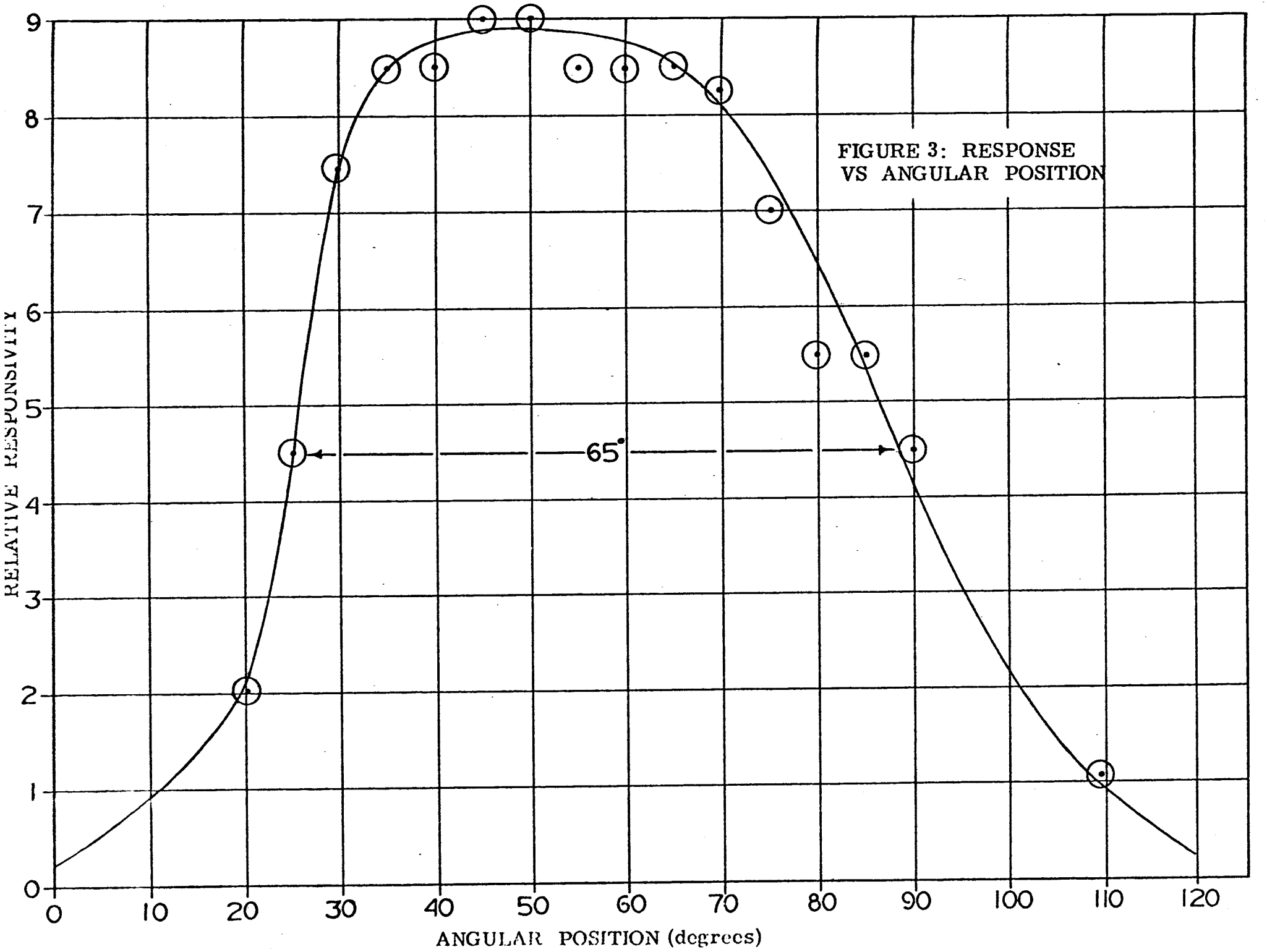
FIGURE 3: RESPONSE
VS ANGULAR POSITION
65°
RELATIVE RESPONSIVITY
ANGULAR POSITION (degrees)
0
1
2
3
4
5
6
7
8
9
0
10
20
30
40
50
60
70
80
90
100
110
120

response time depends on the thickness of the index matching layer. For example, one metal backed detector with $r_i = 2.0\ \mu$ A/W at 10 μ exhibited a response time of 8 msec.

IV. SBN Experiments:

Considerable effort was expended during the program to build a high performance immersed detector using SBN (50/50). The rational behind this stemmed from the very high current responsivity obtainable with SBN and from the fact that some workers had reported loss tangents well under 1%.

A considerable number of SBN detectors were constructed, some conventional and some immersed. The conventional detectors were somewhat variable in their behavior, but in many cases exhibited current responsivities in the range of 5 to 8 μ A/W. Measured loss tangents were typically 3% to 5% for the most sensitive detectors and as low as 1.4% for relatively thick detectors.

Discussions with workers who had done extensive research with SBN indicated that loss tangents as low as 0.3% can be obtained by the use of a specialized surface preparation and electrode deposition procedure. Unfortunately, the tooling costs associated with this procedure are beyond the scope of the present effort.

The behavior of the immersed SBN detectors was even more erratic than that of the conventional devices, exhibiting variability with time as well as from unit to unit. In particular the loss tangents ranged all the way from 5% to 20%. Measurements of a function of frequency indicated that these values corresponded to actual dielectric loss rather than series or parallel resistance.

Our experiments have indicated the possibility of using immersion with SBN, but have revealed some rather unexpected and troublesome behavior. Further work in this direction would require more effort than allowed by our program.

A number of other materials exist which have pyroelectric coefficients of a similar magnitude to SBN. Furthermore, isolated measurements, reported in the literature have indicated loss tangents low enough for the present program. Considerable experimentation will be required, however, to determine whether any of these materials exhibit all of the required properties.

V. Conclusions and Recommendations:

Our major conclusions are listed below:

(1) The immersion process leads to the anticipated reduction in required element area and yields the theoretical field-of-view.

(2) Immersed kT-4000 detectors show some promise but will require the development of special tooling and fabrication procedures in order to achieve the sensitivity required by the critical channels.

(3) Immersed SBN detectors presented several problems which may or may not be solvable.

We believe that efforts to develop a more highly sensitive immersed kT-4000 detector should be continued. In addition, immersion should be evaluated with a much greater variety of detector materials, both double oxide and order-disorder, in order to establish the combination of material and structure yielding the optimum overall performance. In the materials area, an effort should be made to determine the minimum loss tangents achievable with the various highly sensitive double oxide materials. Likely candidates exist, for example, in the $PbTiO_3/PbZ_rO_3$ family.

Clearly, the present program has only scratched the surface both in determining the appropriate materials for immersion and in optimizing the

immersion process itself. However, the advancements made an this program have been sufficient to indicate the very attractive potential of the approach. As a result, Laser Precision intends to maintain a continuous although necessarily limited in-house effort in this area.